esa WPP-108
May 1996

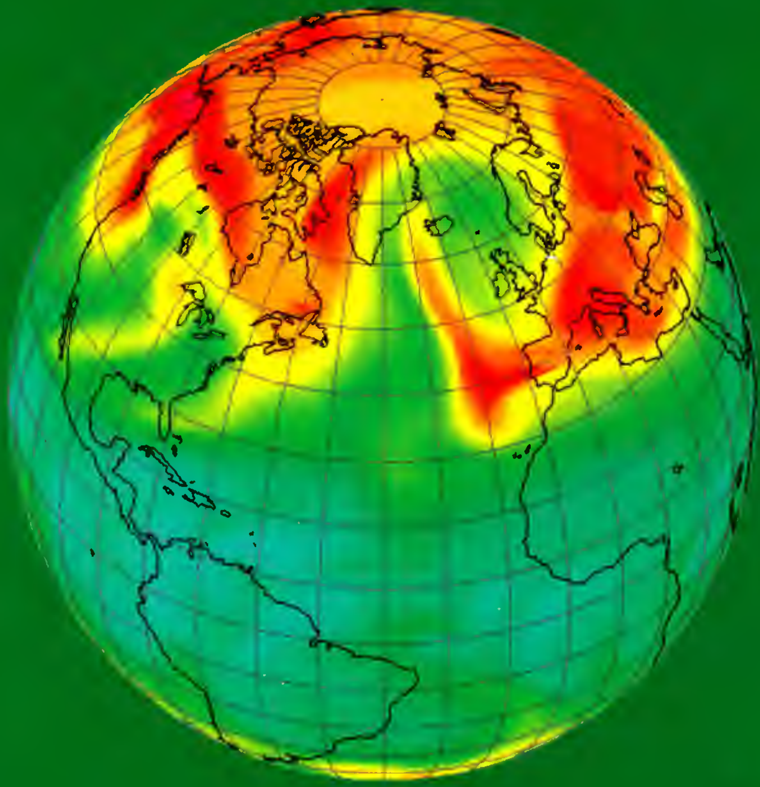

GOME
Geophysical Validation Campaign

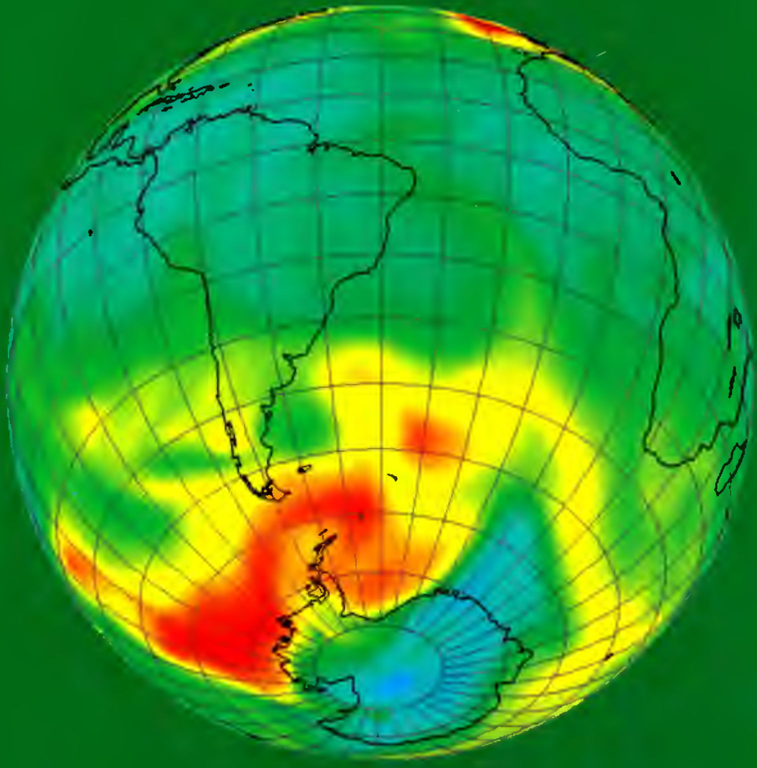

Final Results
Workshop Proceedings

ESA-ESRIN, Frascati, Italy
24-26 January 1996

esa wpp-108
April 1996

GOME Geophysical Validation Campaign

Final Results Workshop Proceedings

ESA/ESRIN, Frascati, Italy,

24-26 January 1996

Cover picture: *Total ozone column in the atmosphere at the Poles on 14 December 1995, 00 UT, as derived from GOME measurements on 11, 12 and 13 December* (Courtesy of Ankie Piters, KNMI).

GOME Validation Campaign Manager:

Evert Attema
ESA/ESTEC
Postbus 299
2200 AG Noordwijk
The Netherlands

Workshop Proceedings Compiled by:

Peter Fletcher and Freda Lodge
Remote Sensing Applications Consultants
Mansfield Park
Medstead,
Alton, Hampshire
GU34 5PZ UK

Disclaimer

This document is published inthe ESA WPP (Workshop Preliminary Proceedings) series. This is an informal series and the documents do not necessarily carry the full authority of the formal ESA publication series. Such documents are intended for issue to workshop participants and as working documents. Some papers in the ESA WPP series may be selected for editing and inclusion in a formal ESA publication at a later date.

There is no formal distribution of ESA WPP publications; distribution is arranged by the workshop organisers.

CONTENTS

CONCLUSIONS AND RECOMMENDATIONS

OVERVIEW OF THE GOME GEOPHYSICAL VALIDATION CAMPAIGN

20 July 1995 to 26 January 1996

A. Hahne[1] & P. A. Fletcher[2]

[1] GOME Project Manager, ESA/ESTEC, Postbus 299, Noordwijk 2200 AG, The Netherlands
[2] Secretary to the GOME Geophysical Validation Campaign, Remote Sensing Applications Consultants, Alton, GU34 5PZ, UK

1. Introduction

During the early stages of the GOME programme, it was recognised that the geophysical validation of the data products derived from the sensor would be a major exercise, requiring support from the scientific community. Therefore, two years prior to launch, a special scientific sub-group of the GOME Science Advisory Group was established. Its role, as the GOME Validation sub-group, was to assist the Agency in the initial planning and preparation for the geophysical validation programme. Following the evaluation of the ERS-2 Announcement of Opportunity (AO), twenty groups had their proposals accepted for the geophysical validation of GOME. Of these, a selected group of Principal Investigators (PI's) took over the task of preparing for the geophysical validation campaign. In parallel, the sub-groups responsible for "Calibration and Characterisation" and "Data Processing and Algorithm Development" continued with their work.

2. GOME Validation Campaign

In late August 1994, a first GOME Validation PI Meeting was held at ESTEC. The objective was to develop a campaign plan derived from the successful responses to the ERS-2 AO. The duration of the campaign, and also the GOME commissioning phase, was to be 6 months, and at the end of this period a statement was to be produced describing the performance of GOME according to the validation activities which had been carried out. In order to help co-ordinate the campaign, an "Experimenters Handbook" was compiled which was distributed in February 1995.

Certain constraints were imposed on the validation campaign because of developments still in progress relating to data supply and processing. The constraint relating to data supply was that only the Kiruna Ground station would be able to provide GOME data within the time scale of the campaign. This had the effect of limiting the coverage readily available from GOME, to 10 out of 14 orbits. During the validation period therefore, GOME data would not be available for much of the Pacific, Australasia, most of Asia and part of Antarctica. The constraint on data processing for the validation campaign, was that GOME ozone profiles would not be available.

The campaign involved the validation of level 1 and level 2 products, supplied as ESA data products by DLR, the location of the GOME data processor. Priority validation requirements for level 1 was to be irradiance and radiance measurements and for level 2, measurement of total column ozone. The level 1 products were to be validated primarily by comparing the measurements with those from other spaceborne sensors, such as SOLSTICE onboard UARS, TOMS, SBUV/2 and SSBUV as well as some balloon flights. Level 2 products were to be validated using ground based sensors including: Dobson/Brewer, the SAOZ network, the SCUVS/2 network and also satellite and balloon borne sensors.

3. NILU Data Centre

It was agreed that the validation campaign required a central facility to hold and help disseminate data from GOME, as well as data from instruments producing correlative data measurements and analysis reports. The NILU facility in Lillestrøm, Norway, was asked to perform this function. NILU was already established as a data centre for other campaigns associated with research into the atmosphere, particularly EASOE and SESAME. The majority of GOME participants were already users of the NILU Data Centre, which significantly reduced the time for NILU to become established as part of the GOME validation campaign. Before participants were granted access to NILU, it was necessary for them to sign data protocol agreements for GOME data, other data held by NILU and for ECMWF meteorological data, where applicable. In practice, level 2 products were supplied by DLR to NILU via electronic transfer and the larger volume level 1 products were sent directly to the appropriate groups on CD-ROM.

4. Functional Testing

On 21 April 1995, ERS-2 was launched with GOME onboard. After the satellite had achieved its nominal state and orbit, the main instruments were progressively switched on over a period of two weeks, without any problems.

GOME subsequently underwent a number of functional tests of the various sub-systems. In order to allow sufficient time for the outgassing of the Focal Plane Assemblies, however, the Peltier coolers were not activated during this initial period.

The switch-on of the coolers, and the first performance assessment, occurred about one month after launch. This was followed by a period of thorough functional and performance evaluation, during which the instrument was operated in its various modes and with different settings (e.g. integration times, scanner angles etc.). During a third period, the individual settings were combined with the initial operating "time lines" in order to prepare for routine operations. Other exercises were conducted which involved stepping through a variety of different swath widths and integration time combinations.

Whilst the GOME instrument was being checked out, the ground segment element at Kiruna was commissioned, enabling GOME data to be extracted from the downlinked telemetry stream and forwarded via BDDN to DLR. The BDDN link was made available for the period of the validation campaign. At this time DLR completed its preparations for incorporating the "key calibration data" resulting from the pre-flight calibration campaign at TPD.

5. Early Conclusions

During the early part of the commissioning phase, various issues arose which, to varying degrees, had some bearing on the progress of the validation campaign.

5.1 Because the satellite and the instruments, as well as the data handling and transmission sub-system, were being commissioned at the same time, some interruptions to GOME operations were experienced. In particular the Scatterometer commissioning lead to rather frequent outages of GOME because of unintended payload switch-offs, the need for payload resynchronisation and data loss due to minor disruptions in data transmission.

5.2 Several parameters of the GOME instrument which had been assumed to be stable, or to stabilise after a short period, did not actually behave as expected. Consequently, key data had to be re-calculated and updated in the processor, necessitating some re-processing of data.

5.3 Early in the commissioning phase it was recognised that the air mass factors then used in the processor, were based on a too simplistic approach and did not take into account for example, spherical geometry, nor multiple scattering. Implementing the necessary modifications by way of multi-parameter look-up tables, took time and delayed the start of data supply.

5.4 With the atmosphere being so variable in space, time and composition, and also being affected by parameters such as surface albedo and cloud cover, the geophysical validation exercise remains a complex task. In order to be meaningful, many parameters have to be considered and measured with an accuracy comparable to the expected accuracy of the data products resulting from the sensor's data.

5.5 At least one conclusion was already obvious prior to the Final Results Workshop: the geophysical validation of data products from an ambitious spaceborne sensor has to be a continuos process and does not stop at a certain point in time. Even so, within a compressed time scale, the validation campaign provided the means whereby a provisional statement could be made as to the accuracy and precision of the products from GOME.

6. Final Results Workshop

The first data were released to the campaign participants during September 1995. As a result sufficient products had been delivered for the GOME Validation Campaign Final Results Workshop to take place on 24 to 26 January 1996, in Frascati, Italy. The papers in this document were written in support of the Workshop presentations. The GOME performance statement, as of January 1996, is presented at the end of the Proceedings.

GOME Operations during Validation Campaign

J. Callies, C. Caspar, A. Lefebvre and A. Hahne

Earth Observations Projects Department
ESA/ESTEC
Noordwijk, NL

Abstract
An overview about GOME operation during the commissioning/validation phase is given. The time covered range from 13.6.1995 to 31.1.1996. The operational timelines for the instrument operation are presented and anomalies are reported . Solutions for the loss of ground coverage at 0.375 seconds and the dark signal fluctuations in channel 1A have been identified and are described.

1. Introduction

In chapter 2 GOME operations are summarised for the optimisation phase of the commissioning phase. This phase was covering 13.6.1995 to 19.7.1995.
This is followed by a summary of the ESOC reports given to the project between 13.6.1995 and 8.7.95. In case of problems/anomalies cross references are made between both.

For the geophysical validation timelines are presented. The influence of integration times shorter than 1.5 seconds on the ground pixel size are discussed and a S/W solution is presented. This is followed by a listing of the reported anomalies and the list of the cooler switchings.
The report finishes with the presentation of the solution to the dark signal anomaly of channel 1A.

2. GOME operations in the optimisation phase of the commissioning phase (13.6.1995 - 19.7.1995)

The following tables give an overview about the operation of GOME during the optimisation phase. The operation in this phases is in line with the GOME operations plan during commissioning phase (ER-TN-ESA-GO-0346).

The 1. column defines the performed activity. The 1.st information gives the swath width varying form static (0 km) to 960 km. The 2.nd information gives the integration time of channel of channel 1B to 4 for a sun zenith angle below 75 degree. For more details about timelines see chapter 3. It is followed by the date of operation, the name of the timeline (see ER-TN-ESA-GO-0434 for details), and the duration of the timeline. The next 2 columns give the start and end date and defines the number of repetitions of this timeline. The last column is reserved for additional remarks (e.g. highlights problems, changes to plan).

The following table summarises the operation with different swath widths and integration times between 13.6. - 19.7.1995.

Table 1: Swath width statistics

Swath width	number of days (10 orbits in Kiruna visibility)	integration time in channel 1B to 4 for SZA <75 deg
nadir static	2	0.375s , 1.5 s
120 km	4	0.375 s
	1	0.75 s
	1	1.5 s
240 km	1	0.375 s
	1	0.75 s
	1	1.5 s
360 km	1	0.375 s
	1	0.75 s
	1	1.5 s
480 km	4	0.375 s
	1	0.75 s
	1	1.5 s
960 km	11	0.375 s
	1	0.75 s
	1	1.5 s

GOME operation in optimisation phase (I)

Optimisation phase	date of operation	timeline	day of year	duration of timeline	start date	end date	number of repetition of this timeline	remark
nadir static 0.375s	13.6.95	GMNNOT11	164	1	L + 53	L + 53	10	
120 km swath “”	14.6	GMNNOT12	165	1	L + 54	L + 54	10	
240 km swath “”	15.6	GMNNOT13	166	1	L + 55	L + 55	10	
360 km swath “”	16.6	GMNNOT14	167	1	L + 56	L + 56	10	
480 km swath “”	17.6	GMNNOT15	168	1	L + 57	L + 57	10	
960 km swath “”	18.6	GMNNOT16	169	1	L + 58	L + 58	10	IT’s corrupted
120 km swath 0.75s	19.6	GMNNOT17	170	1	L + 59	L + 59	10	IT’s corrupted
240 km swath “”	20.6	GMNNOT18	171	1	L + 60	L + 60	6	IT’s corrupted
960km swath 0.375s	20.6	GMNNOT16	171	1	L + 60	L + 60	2	
960km swath “”	21.6	GMNNOT16	172	1	L + 61	L + 61	10	
120 km swath 0.75s	22.6	GMNNOT17	173	1	L + 62	L + 62	10	
240 km swath “”	23.6	GMNNOT18	174	1	L + 63	L + 63	10	
360 km swath “”	24.6	GMNNOT19	175	1	L + 64	L + 64	10	
480 km swath “”	25.6	GMNNOT21	176	1	L + 65	L + 65	10	
960 km swath “”	26.6	GMNNOT22	177	1	L + 66	L + 66	10	

GOME operation in optimisation phase (II)

Optimisation phase	date of operation	timeline	day of year	duration of timeline	start date	end date	number of repetition of this timeline	remark
960 km swath 0.375	27.6.95	GMNNOT16	178	1	L + 67	L + 67	4	
Sun Calibration	27.6.	GMNSOT11	178	1	L + 67	L + 67	2	
Calibration TL	27.6	GMNCAT11	178	1	L + 67	L + 67	5	
960 km swath 0.375	27.6	GMNNOT16	178	1	L + 67	L + 67	3	
960 km swath	28.6	GMNNOT16	179	1	L + 68	L + 68	6	
Sun Calibration	28.6	GMNSOT11	179	1	L + 68	L + 68	1	
960 km swath	28.6/29.6	GMNNOT16	179/180	1	L + 68	L + 69	12	
Sun Calibration	29.6	GMNSOT11	180	1	L + 69	L + 69	1	
960 km swath	29.6/1.7.	GMNNOT16	180/183	1	L + 69	L + 72	30	no SOT on 30.6 + 1.7 due to thruster operation
Sun Calibration	2.7.	GMNSOT11	183	1	L + 72	L + 72	1	
960 km swath	2.7./3.7.	GMNNOT16	183/184	1	L + 72	L + 73	12	
Sun Calibration	3.7.	GMNSOT11	184	1	L + 73	L + 73	1	
nadir static 1.5 s	3.7./4.7.	GMNNOT23	184/185	1	L + 73	L + 74	14	no SOT on 4. + 5.7.
120 km swath “”	4.7./5.7	GMNNOT24	185/186	1	L + 74	L + 75	14	“”
240 km swath “”	5.7./6.7	GMNNOT25	186/187	1	L + 75	L + 76	12	“” failure on 6.7
	6.7.	GMNSOT11	187	1	L + 76	L + 76	1	failure on 6.7.

SOT - Solar Observation Timeline
TL - timeline

GOME operation in optimisation phase (III)

Optimisation phase	date of operation	timeline	day of year	duration of timeline	start date	end date	number of repetition of this timeline	remark
	6.7./7.7.	failure	187/188	1	L + 76	L + 76	12	DDHU failure
	7.7.	failure	188	1	L + 77	L + 77	1	DDHU failure
nadir static 0.375s	7.7./8.7.	GMNNOT11	188/189	1	L + 77	L + 78	12	wrong commanding
Sun Calibration	8.7.	GMNSOT11	189	1	L + 78	L + 78	1	
480 km swath 1.5s	8.7./9.7.	GMNNOT27	189/190	1	L + 78	L + 79	12	
Sun Calibration	9.7.	GMNSOT11	190	1	L + 79	L + 79	1	
960 km swath 1.5s	9.7./10.7.	GMNNOT28	190/191	1	L + 79	L + 80	12	
Sun Calibration	10.7.	GMNSOT11	191	1	L + 80	L + 80	1	
960 km swath 0.375s	10.7./11.7	GMNNOT16	191/192	1	L + 80	L + 81	12	
Sun Calibration	11.7.	GMNSOT11	192	1	L + 81	L + 81	1	
960km swath 0.375s	11.7./12.7	GMNNOT16	192/193	1	L + 81	L + 82	12	
Sun Calibration	12.7.	GMNSOT11	193	1	L + 82	L + 82	1	
960km swath 0.375s	12.7./13.7	GMNNOT16	193/194	1	L + 82	L + 83	12	
Sun Calibration	13.7.	GMNSOT11	194	1	L + 83	L + 83	1	
480km swath 0.375s	13.7./14.7	GMNNOT15	194/195	1	L + 83	L + 84	12	
Sun Calibration	14.7.	GMNSOT11	195	1	L + 84	L + 84	1	
480km swath 0.375s	14.7./15.7	GMNNOT15	195/196	1	L + 84	L + 85	12	
Sun Calibration	15.7.	GMNSOT11	196	1	L + 85	L + 85	1	
480km swath 0.375s	15.7./16.7	GMNNOT15	196/197	1	L + 85	L + 86	12	

DDHU - Digital Data Handling Unit of GOME

GOME operation in optimisation phase (IV)

Optimisation phase	date of operation	timeline	day of year	duration of timeline	start date	end date	number of repetition of this timeline	remark
Sun Calibration	16.7.	GMNSOT11	197	1	L + 86	L + 86	1	
120km swath 0.375	16.7./17.7	GMNNOT12	197/198	1	L + 86	L + 87	12	
Sun Calibration	17.7.	GMNSOT11	198	1	L + 87	L + 87	1	
120km swath 0.375	17.7./18.7	GMNNOT12	198/199	1	L + 87	L + 88	12	
Sun Calibration	17.7.	GMNSOT11	198	1	L + 87	L + 87	1	
120km swath 0.375	17.7./18.7	GMNNOT12	198/199	1	L + 87	L + 88	12	
moon calibration	18.7.		199	1	L + 88	L + 88	1	10:42:56 UTC
moon calibration	18.7.		199	1	L + 88	L + 88	1	12:22:33 UTC
moon calibration	18.7.		199	1	L + 88	L + 88	1	14:02:15 UTC
moon calibration	18.7.		199	1	L + 88	L + 88	1	15:42:02 UTC
960km swath 0.375	18.7./19.7	GMNNOT16	199/200	1	L + 88	L + 89	12	
Sun Calibration	19.7.	GMNSOT11	200	1	L + 89	L + 89	1	

2.1 Summary of ESOC reporting

13.6.1995 day 164
GMNNOT11 was activated 10 times starting at 07.20.33 UTC

14.6.1995 day 165
GMNNOT12 was activated 10 times starting at 06.48.55 UTC

15.6.1995 day 166
GMNNOT13 was activated 10 times starting at 07.57.53 UTC

16.6.1995 day 167
GMNNOT14 was activated 10 times starting at 07.26.15 UTC

17.6.1995 day 168
GMNNOT15 was activated 10 times starting at 06.54.37 UTC

18.6.1995 day 169
GMNNOT16 was activated 10 times starting at 08.03.35 UTC

19.6.1995 day 170
GMNNOT17 was activated 10 times starting at 07.31.58 UTC

20.6.1995 day 171 **(operations were not according to the planned operations)**
GMNNOT18 was activated 6 times starting at 07.00.20 UTC
The timeline was stopped. A DDHU dump was taken, the GOME was switched off due to S/W corruption (integration time were showing 0 sec)
GOME was switched on at 20:20 UTC
GMNNOT16 was activated 2 times starting at 20.25.07 UTC

21.6.1995 day 172
GMNNOT16 was activated 10 times starting at 08.09.19 UTC

22.6.1995 day 173
GMNNOT17 was activated 10 times starting at 07.37.41 UTC

23.6.1995 day 174
GMNNOT18 was activated 10 times starting at 07.06.04 UTC

24.6.1995 day 175
GMNNOT19 was activated 10 times starting at 08.15.03 UTC

25.6.1995 day 176
GMNNOT21 was activated 10 times starting at 07.43.26 UTC

26.6.1995 day 177
GMNNOT22 was activated 10 times starting at 07.11.49 UTC

27.6.1995 day 178
GMNNOT16 was activated 4 times starting at 01.38.24 UTC
GMNSOT11 was activated 2 times starting at 08.20.48 UTC
GMNCAT11 was activated 5 times starting at 11.42.00 UTC
GMNNOT16 was activated 3 times starting at 20.05.00 UTC

28.6.1995 day 179
GMNNOT16 was activated 6 times starting at 01.06.47 UTC
GMNSOT11 was activated 1 times starting at 11.10.23 UTC
GMNNOT16 was activated 7 times starting at 12.50.59 UTC

From 29.6.95 (day 180) GOME operations was commanded with the Mission Planning System. (TML1 will be activated 13 times and TML2 1 time every day.) For the activation times see the DMOP file available from ESRIN.

A manoeuvre was executed in the night between day 180 and 181, consequently, the GMNSOT11 activation on day 181 and 182 was replaced by a GMNNOT16 activation.

7.7.95 day 188 **(operations were not according to the planned operations)**
During the recovery of GOME on 7.7.95, the GMNNOT26 was loaded, but was straight away erased by the GMNNOT11 due to a timeline loading error.

8.7.95 day 189 **(operations were not according to the planned operations)**
Consequently the GMNNOT11 was activated until 8.7.95 TML2 activation time instead of GMNNOT26, at which point it was replaced by the GMNNOT27.

3. Timelines of the Validation Phase

During the geophysical validation the following timelines have been used:

GMNNOT16 - nominal nadir observational timeline with 960 km swath and different integration time scenarios around the orbit. Activation 13 times per day.

GMNSOT12 - nominal solar calibration timeline (like GMNNOT16, but including the solar calibration window). Activation once per day.

GMNSPT13 - south polar observational timeline (like GMNNOT16 and special south pole scanning (+/- 4.393 deg) (used between 9. Sept. 95 and 12. Oct. 95)

GMNSPT14 - south polar observational timeline (like GMNNOT16 and special south pole scanning (+/- 4.393 deg) (used between 13. Oct 95 and 20. Nov. 95). The change was necessary due to the timing of the south pole view.

GMNSPT15 - south polar observational timeline (like GMNNOT16 and special south pole scanning (+/- 4.393 deg) (used between 29. Nov. 95 and 20. 1. 96).

GMNCAT11 - calibration timeline. Activation every 28th day of a month (e.g. 28.7., 28.8. etc). Timeline is 5 times repeated.

GMNMOO12 - moon calibration of 16.8.95. The timeline was executed for 4 consecutive orbits 1682 to 1685 (13:43.44 - 20:26:08). A moon calibration is performed on the night side only. It was tried to operate GOME on the dayside as under normal conditions, but with a reduced set of integration times. Therefore the instrument performance at high solar zenith angle are reduced. During the last orbit (1685) GOME was in fixed nadir pointing. A sun calibration has been performed in orbit 1684. Due to DDHU anomaly all channel 2 data are corrupted for this moon calibration.

GMNMOO13 - moon calibration of 13./14.11.95. The timeline was executed for 8 consecutive orbits 2958 to 2964 (17:07 - 14.11.95 4:51). A moon calibration is performed on the night side only. It was tried to operate GOME on the dayside as under normal conditions, but with a reduced set of integration times. Therefore the instrument performance at high solar zenith angle are reduced. A sun calibration has been performed in orbit 2960.

3.1 Impact of integration times shorter than 1.5 sec on ground pixel size

During the engineering commissioning phase it was discovered, that with the nominal integration times of 1.5 seconds and high scene albedos saturation can occur in the visible channels. As a consequence the integration times for some part of the orbit were reduced to 0.375 seconds. This leads to a smaller ground pixel size. Due to the limited data rate of GOME, integration times of shorter than 1.5 seconds also lead to a loss of ground coverage. E. g. an integration time of 0.375 seconds means that a ground pixel of 320*40 km^2 (for 30 degree swath and 1.5 second integration time) is shortened to 80 *40 km^2.Looking at the ground pixel of 320*40 km^2 in flight direction (from left to right or east to west for descending orbit) the first three quarters of the ground pixel are not transmitted to ground, while the last quarter is downlinked. This concept is shown in figure 1.

3.1.1 Co-adding Patch

Shorter integration times than 1.5 seconds are not only creating a loss of ground coverage, but also reducing the signal to noise ratio for low albedo scenes and increase the ground pixel aliasing error.
In order to overcome these problems ESTEC developed a S/W patch enabling the Digital Data Handling Unit (DDHU) of GOME to perform an averaging operation in the affected channels (2 to 4).

This averaging mode performs a dynamic co-adding of the 4 readings acquired at 0.375 seconds, and transfers the average every 1.5 seconds to ground. Furthermore, in case of low signals, the co-adding is performed but the averaging process is trimmed to the result of the addition in order to optimise the signal resolution.

The patch has been developed, and tested on the GOME flight spare on -ground in the 2. half of 1995 and is now expected to be uplinked in February 1996 by ESOC.

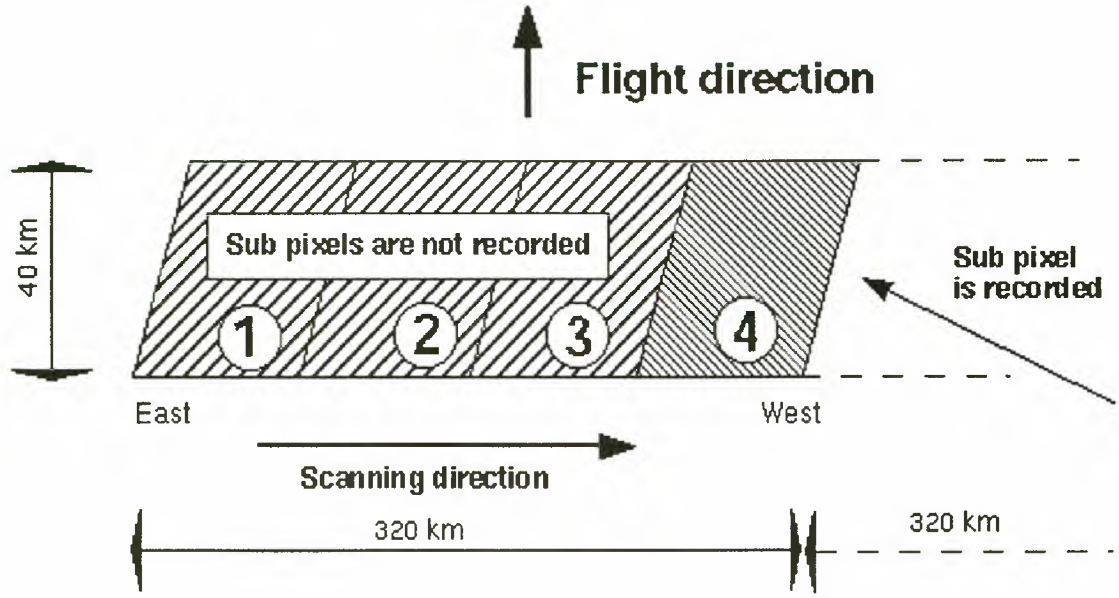

Figure 1: Breakdown of one ground pixel of the 960 km swath for descending orbit

GMNNOT16

mode	time *	SZA	band 1A	band 1B	band 2A+B	Band 3+4	# of
	(s)	(deg)	(s)	(s)	(s)	(s)	CMD's
	duration	SZA tag.	240-307 nm	307-312 nm	311-400 nm	400-790nm	
dark signal	400	start	12	0.375	0.375	0.375	2
nadir scan 30 deg	260	100	60	6	6	6	2
"	180	85	60	1.5	1.5	1.5	1
"	2480	75	12	0.375	0.375	0.375	1
		...					
"	180	75	60	1.5	1.5	1.5	1
"	260	85	60	6	6	6	1
dark signal		100	scan mirror to dark current position				
"	1000		60	6	6	6	1
"	900		60	1.5	1.5	1.5	1
dark signal	370		60	6	6	6	1
sum	6030						11

* The duration is given as an estimate only.

start means begin of timeline at SZA = 90 deg - 580 sec
SZA - Sun Zenith Angle
CMD - MacroCommand Words

GMNSOT12

mode	time	SZA	band 1A	band 1B	band 2A+B	band 3	band 4	# of
	(s)	(deg)	(s)	(s)	(s)	(s)	(s)	CMD's
	duration	SZA tag	240-307 nm	307-312 nm	312-400 nm	400-605 nm	600 - 790 nm	
dark signal	120	start	6	6	1.5	0.375	0.09375	2
wave cal	120		6	6	1.5	0.375	0.09375	1
dark signal	220		1.5	0.75	0.75	0.75	0.75	1
sun cal	240	95	1.5	0.75	0.75	0.75	0.75	1
wave cal	120		6	6	1.5	0.375	0.09375	1
nadir scan 30 deg	2460	75	12	0.375	0.375	0.375	0.375	2
		...						
	180	75	60	1.5	1.5	1.5	1.5	1
	180	85	60	6	6	6	6	1
dark signal	1000		60	6	6	6	6	1
	900		60	1.5	1.5	1.5	1.5	1
	390		12	0.375	0.375	0.375	0.375	1
DDHU memory dump (1)	100							13
sum	6030							26

GMNCAT11

mode	time	orbit	band 1A	band 1B	band 2A+B	band 3	Band 4	# of
	(s)		(s)	(s)	(s)	(s)	(s)	CMD's
	duration		240-307nm	307-312 nm	312-405 nm	400-605nm	600-790 nm	
dark sig.	600	start	6	6	1.5	0.375	0.09375	2
wave cal	600	day	6	6	1.5	0.375	0.09375	1
FPN	150	day	0.09375	0.09375	0.09375	0.09375	0.09375	1
FPN	150	day	0.1875	0.1875	0.1875	0.1875	0.1875	1
dark sig.	300	day	3.0	3.0	3.0	3.0	3.0	1
LED meas.	300	day	3.0	3.0	3.0	3.0	3.0	1
wave cal	600	day	6	6	1.5	0.375	0.09375	1
dark signal	240	day	24.0	24.0	24.0	24.0	24.0	1
LED meas.	240	day	24.0	24.0	24.0	24.0	24.0	1
wave cal	592	day	6	6	1.5	0.375	0.09375	1
dark sig.	120	night	6	6	1.5	0.375	0.09375	1
	870	night	288	288	288	96	96	1
wave cal	120	night	6	6	1.5	0.375	0.09375	1
diffus cal	12	night	0.09375	0.09375	0.09375	0.09375	0.09375	1
	870	night	288	288	288	96	96	1
wave cal	12	night	0.09375	0.09375	0.09375	0.09375	0.09375	1
	120	night	6	6	1.5	0.375	0.09375	1
dark sig.	134	night	6	6	1.5	0.375	0.9375	1
sum	6030							19

FPN - Fixed Pattern Noise Mode
LED - Light Emitting Diode Mode
diffus cal - Characterisation of the GOME internal diffuser

GMNSPT13

mode	time	SZA	band 1A	band 1B	band 2A+B	Band 3+4	# of
	(s)	(deg)	(s)	(s)	(s)	(s)	CMD's
	duration		240-307 nm	307-312 nm	312-400 nm	400-790 nm	
dark signal	400	start	12	0.375	0.375	0.375	2
nadir scan 30 deg	260	100	60	60	60	60	1
	180	85	60	6	6	6	1
	2247	75	12	0.375	0.375	0.375	1
		...					
	122	75	60	1.5	1.5	1.5	1
s-pole scan	66		60	1.5	1.5	1.5	2
s-pole scan	315	85	60	6	6	6	1
dark sig.	1000		60	6	6	6	1
	900		60	1.5	1.5	1.5	1
	525		60	6	6	6	1
sum	6024						12

GMNSPT14

mode	time	SZA	band 1A	band 1B	band 2A+B	Band 3+4	# of
	(s)	(deg)	(s)	(s)	(s)	(s)	CMD's
	duration		240-307 nm	307-312 nm	312-400 nm	400-790 nm	
dark signal	400	start	12	0.375	0.375	0.375	2
nadir scan 30 deg	260	100	60	60	60	60	1
	180	85	60	6	6	6	1
	2370	75	12	0.375	0.375	0.375	1
		...					
s-pole scan	107		12	0.375	0.375	0.375	2
s-pole scan	350		60	1.5	1.5	1.5	1
s-pole scan	248		60	6	6	6	1
dark signal	1000		60	6	6	6	1
	900		60	1.5	1.5	1.5	1
	200		60	6	6	6	1
sum	6015						12

GMNSPT15

mode	time	SZA	band 1A	band 1B	band 2A+B	Band 3+4	# of
	(s)	(deg)	(s)	(s)	(s)	(s)	CMD's
	duration		240-307 nm	307-312 nm	312-400 nm	400-790 nm	
dark signal	400	start	12	0.375	0.375	0.375	2
nadir scan 30 deg	260	100	60	60	60	60	1
	180	85	60	6	6	6	1
	2270	75	12	0.375	0.375	0.375	1
		...					
s-pole scan	195		12	0.375	0.375	0.375	2
s-pole scan	370		60	1.5	1.5	1.5	1
s-pole scan	258		60	6	6	6	1
dark signal	1000		60	6	6	6	1
	900		60	1.5	1.5	1.5	1
	180		60	6	6	6	1
sum	6013						12

GMNMOO12

mode	time	SZA	band 1A	band 1B	band 2A+B	Band 3+4	# of
	(s)	(deg)	(s)	(s)	(s)	(s)	CMD's
	duration	SZA tag.	240-307 nm	307-312 nm	311-400 nm	400-790nm	
orbit 1682							
dark sig.	400	start	12	0.375	0.375	0.375	2
nadir scan 30 deg	3376	100	12	0.375	0.375	0.375	2
dark sig	962	100	12	12	12	12	1
moon (84.98 deg)	600		12	12	12	12	1
orbit 1683							
nadir scan 30 deg	3388	100	12	0.375	0.375	0.375	2
dark sig		100	12	12	12	12	1
moon (84.65 deg)	600		12	12	12	12	1
orbit 1684							
wave cal	240		6	6	1.5	0.375/ 0.09375	1
dark sig	464		6	6	1.5	0.375/ 0.09375	1
wave cal	70		6	6	1.5	0.375/ 0.09375	1
dark sig	70		1	0.75	0.75	0.75	1
sun cal	190		1	0.75	0.75	0.75	1
nadir scan 30 deg	3076		12	0.375	0.375	0.375	2
dark sig	1084		12	12	12	12	1
moon (83.86 deg)	600		12	12	12	12	1
orbit 1685							
nadir scan 30 deg	3388		12	0.375	0.375	0.375	2
dark sig	1083		12	12	12	12	1
moon (83.05 deg)	600		12	12	12	12	1
orbit 1686							
nadir fixed	3388		12	0.375	0.375	0.375	1
dark sig	2280		12	0.375	0.375	0.375	1
sum	30200						28

GMNMOO13

mode	time	SZA	band 1A	band 1B	band 2A+B	Band 3+4	# of
	(s)	(deg)	(s)	(s)	(s)	(s)	CMD's
	duration	SZA tag.	240-307 nm	307-312 nm	311-400 nm	400-790nm	
orbit 2958							
dark sig.	400	start	12	0.375	0.375	0.375	2
nadir scan	3379	100	12	0.375	0.375	0.375	2
dark sig	151	100	12	12	12	12	1
moon (82.92 deg)	2495		12	12	12	12	1
orbit 2959							
nadir scan	3390	100	12	0.375	0.375	0.375	2
moon (84.65 deg)	883		12	12	12	12	1
orbit 2960							
dark sig	240		6	6	1.5	0.375/ 0.09375	1
wave cal	240		6	6	1.5	0.375/ 0.09375	1
dark sig	1264		6	6	1.5	0.375/ 0.09375	1
wave cal	70		6	6	1.5	0.375/ 0.09375	1
dark sig	70		1	0.75	0.75	0.75	1
sun cal	190		1	0.75	0.75	0.75	1
nadir scan	3079		12	0.375	0.375	0.375	2
moon (82.59deg)	2646		12	12	12	12	1
orbit 2961							
nadir scan	3390		12	0.375	0.375	0.375	2
moon (82.23 deg)	2645		12	12	12	12	1
orbit 2962							
nadir scan	3390		12	0.375	0.375	0.375	2
moon (81.80 deg)	2646		12	12	12	12	1
orbit 2963							
nadir scan	3390		12	0.375	0.375	0.375	2
moon (81.29 deg)	2646		12	12	12	12	1
orbit 2964							
nadir scan	3390		12	0.375	0.375	0.375	2
moon (81.29 deg)	2005		12	12	12	12	1
sum	42000						29

4. Anomalies
This chapter describes the main anomalies experienced and continues with a list of gaps in the level 0 data due to these anomalies.

4.1 Payload Synchronisation
One problem is linked to the resynchronisation of the satellite clock (Payload (PL) synchronisation). Every time this activity is performed, the GOME timeline has to be interrupted and be restarted at the beginning of the next orbit
The synchronisation was needed more often during a test period of an other instrument, therefore this anomaly occurs more often in July - September.

4.2 Single Event Upsets (SEU)
Radiation particle penetrating the GOME shielding can cause bitflips in the DDHU memory. In case they hit a sensitive part of the software, GOME operations can be strongly affected. Due to the fact that the GOME S/W is copied at every switch on from EEPROM into RAM, a SEU in the RAM is recoverable by a GOME switch off.
In one case (2.8.1995) a SEU in the DDHU let the values of 6 GOME temperature sensors go to 0. These values were surveilled by ATSR and therefore GOME was switch off by ATSR.

4.3 List of datagaps due to anomalies
The following list contains the datagaps which are present in the data due to known anomalies.

26.7.95 PL synchronisation TL stopped at
20:07 next activation 23:15 UTC
28.7.95 PL synchronisation TL stopped at
10:44 next activation 14:13 UTC
29.7.95 PL synchronisation
10:26 next activation 12:04 UTC
31.7.95 PL synchronisation
15:53 next activation 17:35 UTC
31.7.95 PL synchronisation
19:18 next activation 20:54 UTC

2.8.95 15:17 - 21:15 UTC GOME switch off by ATSR surveillance
9.8.95 14:28 - 19:28 UTC PL anomaly, GOME switched off
11.8.95 11:56 - 13:34 UTC
16.8.95 05:42 until 18.8.95 11:20 channel 2 data are corrupted
17.8.95 17:01 - 18:41 UTC
18.8.95 08:14 - 11:20 UTC GOME switch off due to DDHU anomaly
24.8.95 08:21 - 10:08 UTC

5.9.95 PL synchronisation TL stopped at
10:25 next activation 11:46
5.9.95 PL synchronisation TL stopped at
17:04 next activation 18:43 UTC
6.9.95 07:16 -15:39 UTC satellite fine pointing mode (no yaw steering)
7.9.95 19:19 - 21:00 UTC

15.9.95 PL synchronisation TL stopped at
08:30 next activation 09:52
15.9.95 PL synchronisation TL stopped at
21:40 next activation 23:17

16.9.95 PL synchronisation TL stopped at
09:38 next activation 13:24

24.9.95 01:53 - 11:51 IDHT anomaly

26.9.95 PL synchronisation TL stopped at
16:04 next activation 17:27
28.9.95 PL synchronisation TL stopped at
23:11 next activation 00:51 (29.9)
29.9.95 PL synchronisation TL stopped at
11:11 next activation 12:35
30.9.95 PL synchronisation TL stopped at
14:42 next activation 15:25
30.9.95 PL synchronisation TL stopped at
19:43 next activation 20:27

10.10.95 PL synchronisation TL stopped at
10:37 next activation 11:51

23.10.9510:00 - 25.10.95 12:20 GOME anomaly on science data (integration time of channel 2 corrupted)

24.10.95 PL synchronisation TL stopped at
11:23 next activation 12:53

2.11.95 PL synchronisation TL stopped at
8:26 next activation 09:49

21.11.95 Padded data frames are reported between 16:15 and 19:50.

23.11.95Padded data frames are reported between 15:40 and 17:10.

27.11.95 Padded data frames are reported between 12:00 and 13:30.

12.12.95 PL synchronisation TL stopped at 12:28 next activation 13:56

22.12.95 ATSR anomaly TL stopped at 6:19 next activation 20:29 (until 4.1.96 every 7.5 second frame 19+20 of the GOME data packet are missing)

18. 1.96 AMI recovery causes a GOME switch off between 11:30 and 17:54

24.1.96 ERS 2 depointing anomaly, GOME was switched off at 09:10. GOME was switched on at 29.1.96 15:26.

30.1.96 13:26 - 16:35 GOME dump mode testing in preparation of the patch

4.4 Cooler switching
The switching of the GOME coolers is of importance for the stability of the etalon structures, therefore a list of cooler switching in this period is provided.

Due to cooler switching the detectors were not in cooled mode on

30.5.95 timeline with warm detector cooler off: 08:20, detectors warmed up to 263K, cooler on: 08:40.

6.6.95 timeline with warm detector, detectors were cooled again at 9:40
cooler off:07:40, cooler on: 09:40, detectors warmed up to ? (no data available due to IDHT problem)

20.6.95 GOME switching due to DDHU problem, cooler off: 17:15, detectors warmed up to 263K, cooler on: 20:23.

7.7.95 GOME off, due to DDHU problem cooler off: 6.7. 15:00, detectors warmed up to 250 K, cooler on 7.7. 11:00

17.7.95 GOME off, due to cooler anomaly, cooler off on 16.7. 11:53, detectors warmed up to 263 K, cooler on 17.7. 13:30

2.8.95 GOME switching due to ATSR surveillance cooler off: 02.08. 15:20, detectors warmed up to 260 K, cooler on 02.08. 19:50

9.8.95 GOME switching due to ERS2 Payload anomaly, cooler off: 14:30, detectors warmed up to 258K, cooler on:19:30.

18.8.95 GOME switching due to DDHU anomaly (SEU) cooler off: 8:14, detectors warmed up to 273K, cooler on: 9:59.

25.10.95GOME switching due to DDHU anomaly (SEU) cooler off: 10:50, detectors warmed up to 267K, cooler on: 12:20.

22.12.95 GOME switching due to ATSR anomaly, cooler off: 6:19, detectors warmed up to 259 K, cooler on 20:29

18.1.96 GOME switching due to AMI recovery anomaly, cooler off: 11:30, detectros warmed up to 264K, cooler on 17:54

24.1.96 GOME switching due to depointing anomaly, cooler off: 09:10, detectors warmed up to 263K, cooler on at 29.1.96 15:26

30.1.96 GOME switching due to dump mode testing, cooler off: 13:26, detectors warmed up to 264K, cooler on at 16:35

4.5 Dark signal fluctuations in channel 1A
An anomaly in the behaviour of the dark signal of band 1A was discovered. The dark signal fluctuations are in the order of 6 %, which corresponds at an integration time of 12 seconds to an absolute change of about 10 binary units. Due to the low light levels in this UV channel, even small fluctuations do affect the radiance/irradiance measurements.
Further analysis of the fluctuations had been performed at ESTEC and have been reported in the report 'GOME Dark Signal Characterisation'.
The report concludes that the fluctuations is mainly due to cross talk with the peltier cooler control loop. A method to predict the fluctuations from the numerical output of the peltier control loop has been defined and tested. The tests revealed that the correction method provides very good results, setting the residual noise level below 2 binary units, which means an improvement of a factor of five.
This correction method will be implemented in the GOME data processing system at DLR.

5 Conclusions

GOME operation during the commissioning /validation phase was successful. No major anomaly occured. The rate of single event upsets is as predicted for the ERS 2 orbit.

For the problem of saturated detector pixels and the correlated gaps in ground coverage due to the short integration time a DDHU S/W solution has been defined and tested on-ground. A test of this modification in-orbit is still outstanding.

The dark signal fluctuation in channel 1A related to a crosscoupling with peltier cooler operation can be corrected for in the ground processing. Implementation has still to be done.

References

ER-TN-ESA-GO-0346
GOME Operations Plan during the ERS-2 Commissioning Phase

ER-TN-ESA-GO-0434
GOME Test Timelines

ER-RP-ESA-GO-0472
GOME Operations Report during Commissioning Phase

ER-TR-ESA-GO-0467
GOME FS S/W F.5 Test Report and Co-adding/Cluster Modes Description

ER-TN-ESA-GO-0473
GOME Dark Signal Characterisation

VALIDATION OF IN-ORBIT CALIBRATION OF GOME

Roel Hoekstra, Carina Olij, Erik Zoutman, Marco Le Kluse
TNO Institute of Applied Physics (TPD)
2600 AD Delft, The Netherlands
Jörg Callies
ESA/ESTEC
2200 AG Noordwijk, The Netherlands

Abstract
During the in-orbit validation of GOME the changes in the instruments performance were monitored. An update of the calibration functions that have changed from the pre-flight to the in-flight situation i.e. the radiance response function and the polarisation sensitivity function is generated. This update reflects the in-orbit situation of GOME on July 2 1995. Changes of the instrument since that date are thus not reflected in the calibration functions and have to be accounted for in future updates.

Introduction
TPD has undertaken the pre-flight calibration of GOME. The aim of this pre-flight calibration was to determine all instrument characteristics that are needed in order to be able to transform the raw GOME in-orbit data into level 1 data (i.e. atmospheric radiance, solar irradiance and atmospheric albedo as a function of wavelength). Figure 1 shows a diagram for the processing of raw data into physical quantities and other refined products. The starting point here is the raw data in binary units per pixel and PMD signals. With a proper wavelength calibration this will be converted into binary units as a function of wavelength. With a proper polarization calibration the influence of instrument polarization properties is removed, yielding binary units corrected for polarisation as a function of wavelength. From this the data can be further processed into three different level 1 products:
a) Earth Radiance (in $W.cm^{-2}.sr^{-1}nm^{-1}$) as a function of wavelength; for this the radiance calibration is necessary.
b) Solar irradiance (in $W.cm^{-2}nm^{-1}$) as a function of wavelength; for this the radiance calibration and the BRDF calibration of the on board calibration unit are necessary.
c) Atmospheric Albedo (in sr^{-1}). For this the BRDF of the on board calibration unit is necessary.
To remove the influence of the spectral resolution from the final data a calibration of the spectral profile is needed.
From this can be concluded that the primary calibration functions are:

- wavelength calibration
- polarisation calibration
- spectral radiance calibration
- calibration of the BRDF

Because of the crucial importance of the BRDF the reflectance of the on board diffuser is monitored during the entire lifetime of GOME.
The serious time constraints for GOME forced us to the approach to do the pre-flight calibrations to a large extent with GOME outside a vacuum environment. Results from additional thermal vacuum tests and analyses had to be used in order to arrive at the in-flight calibration functions for GOME.
The objectives of our investigations during the in-orbit validation of GOME were:

- to check possible instrument changes between pre-flight and in-orbit phase;
- to check in-orbit instrument stability;
- to update calibration functions in order to describe as closely as possible the in-orbit GOME performance;
- to validate GOME level 1 results by inter-comparison of observed radiances and irradiances with observations from other instruments;

Additionaly the radiance, irradiance and BRDF standards that have been used for the GOME pre-flight calibration have been validated by inter-comparing them with the standards used by NASA for SBUV and SSBUV.

Results
<u>Wavelength calibration</u>
The GOME spectral calibration is obtained by the use of the internal calibration lamp (Pt/Cr/Ne-lamp) which

gives sufficient spectral lines in each channel. The TPD procedure for spectral calibration as used during pre flight calibrations leads to an accuracy of the wavelength scale of approximately 0.04 pixels. The spectral resolution obtained in-orbit and during the TV test pre flight are listed in table 1.
The wavelength calibration scale obtained in-orbit and the one obtained pre-flight in vacuum with the same temperature are identical within 0.1 pixels.
During several orbits the calibration lamp was operated continuously. This enabled us to monitor the shift of spectral lines due to the temperature fluctuations over an orbit. In figure 2 the results of this measurement are shown. In this figure the position of the spectral line on the detector array relative to the position at the start of the measurement is shown in time. The fluctuation of the spectral line position is superimposed on a slope. The latter is due to the spectral lamp warming up the optical bench. The in-orbit wavelength scale variations over one orbit are at maximum 0.03 pixels peak to peak. Long term drifts observed in-orbit are less than 0.04 pixels over a period of 6 months for identical phases of orbits.

Stability of etalon structures and dichroic features

Since May 30 1995 GOME measures the solar irradiance on a regular basis. Assuming that the solar irradiance corrected for the varying distance from Earth to the sun is constant, these measurements can be used to investigate the radiometric stability of the instrument. The Reticon detectors show a so-called etalonning effect, which is not stable when ice is condensed onto the cooled detector. It was anticipated that the almost perfect vacuum conditions in-orbit would render the etalon structure stable after some time. Indeed it was observed that this is the case. Directly after cooling the FPA detectors a rapid shift of the etalon structure is observed. This rapid shift is followed by a slower shift, which after 7 days of cooling changes less than 1%. In figure 3 the changing etalon structure is shown. In this figure two sun measurements are divided. Changes of the etalon structure result in a ratio that differs from 1. The difference in the time that the detectors have been cooled is given in the legend. For simplicity only channel 2 is shown. The top graph shows the etalon structure change between a measurement after 1 day cooling and a measurement after 48 days in which a remaining etalon structure of more than 6% can be observed. The bottom graph shows the difference between a measurement after 7 days cooling and a measurement after 48 days cooling, in which less than 1% remaining etalon can be observed. A small wavelength mismatch between wavelength calibration of the measurements results in remaining noise like spectral features on the ratios of the irradiances. After the occasional warming up of the detectors the etalon structure reaches in general a different stable situation, which makes it necessary to update the radiometric response function after every cooler switch-off. This occurs a few times per year.
The dichroic features that are present in channel 3 and 4 are known to shift as the dichroic outgasses. This shift was indeed observed and a correction to the applicable calibration functions (radiometric response and polarisation sensitivity) is applied. The correction consists of eliminating the pre-flight dichroic features and replacing them with the in-flight dichroic function. In figure 4 the result of this correction for the radiance response function is shown. Small shifts of less than 1% per month were still observed after the correction was applied suggesting that the outgassing of the dichroic was not yet complete which makes it necessary to update these calibration functions once per month until the outgassing is complete.
For the GOME level 1 products absolute Earth radiance and absolute solar irradiance the position of the etalon structures and the position of the dichroic features must be known. For Sun normalized radiance or Albedo the position of the etalon and dichroic features are not important as long as they do not change between the solar irradiance and the Earth radiance measurement. In figure 5 the change that occurs in a time interval of one day, which is the maximum time interval between an irradiance and radiance measurement in-orbit in the presently used time lines, can be observed. At the time of the measurements the detector had been continuously cooled for seven days. Remaining etalon features of at maximum 0.2% peak to peak can be observed in the ratio. The noise like features in this graph are caused by small differences in the wavelength calibration of the two measurements.

Solar irradiance

The comparison of the level 1 irradiance as produced by GOME with other instruments showed an initial deviation of up to 18% as can be seen in figure 6.
The irradiance is calculated as:

$$Irradiance = \frac{S_{GOME}}{RADRESP \times f_2 \times BRDF(ez, az) \times SMDEP(17.15^{\circ})} \qquad (1)$$

With:

- S_{GOME} GOME irradiance signal in BU/s, dark signal subtracted;
- Radresp Radiance response function in key data;
- f_2 Overlap correction in the key data;
- BRDF() BRDF function of the CU for the current

elevation and azimuth angie;

-SMDEP Scan mirror dependence of polarization properties for the sun viewing angle.

From this formula can be concluded that only the BRDF, the scan mirror dependence and the radiance response function can be responsible for the change in irradiance (f_2 is only applied to the overlap regions). Based on the results of the inter-comparison of the radiance calibration between NASA and TPD (see figure 7) there was confidence in the pre-flight radiance calibration. Also the BRDF of the calibration unit has been proven to be consistent within 3% by dividing the radiance and the irradiance calibration of GOME. Since the only major difference between pre-flight calibration and in-flight measurement was the vacuum condition in-flight (pre-flight only the FPA's were evacuated) the thermal vacuum (TV) test data was re-analyzed. The ratio of in-air and in-vacuum measurements during this TV test showed a similar change of radiance response although the magnitude of the change was less. In figure 8 this change observed during the TV test can be seen. The different TV test levels TV2, TV8 and TV14 are all in vacuum at 20°C. The difference between TV14 and TV2 is the time in vacuum. The duration of the TV test is too short to reach a stable situation for the so-called air to vacuum effect. This explains the difference in magnitude, maximal 7% during TV test and 18% in-flight. The square dots in the same figure 8 presents the ratio of the PMD signals during the same TV test levels. The PMDs are affected to a lesser degree compared with the channels.

Thorough investigation of this phenomenon suggested that a small change due to outgassing of the many anti-reflection coatings in GOME has changed the radiometric response function.

The calibration lamp is the only light source that is measured both in- and pre-flight. Based on measurements of the internal calibration lamp a correction to the radiometric response was derived. In figure 9 the ratio of the lamp spectra in-flight and pre-flight compared to the ratio of irradiances from GOME and SOLSPEC proves that the same shape of the air to vacuum effect is observed. The absolute scaling of the air to vacuum effect can be obtained from this lamp output ratio by taking into account the change of lamp output from pre-flight to in-flight. The PMD signals can be used to correct for this change in lamp output. In figure 10 the result of the air to vacuum correction can be seen. The deviation after this correction is only a few percent w.r.t. SOLSTICE and SSBUV observations. With this correction an updated absolute radiometric response is obtained for the data of 02-07-1995.

Apart from the above described update of the radiance response a long term change is observed in the irradiance response of GOME in-orbit, shown in figure 11. In this figure the average change per day of solar irradiance signals between July 2 and November 28 1995 is shown. For reliable radiance and irradiance measurements this effect has to be accounted for.

Diffuser reflectance

The internal calibration lamp of GOME can be observed directly by GOME and via the internal diffuser. The ratio of these two measurements enables us to monitor the on board diffuser.

The light from the calibration lamp via the diffuser has a very low intensity resulting in a high relative noise. Because of this the possible degradation of the diffuser can not yet be observed. This means that the diffuser degradation over a period of 3 months is less than 4%.

Key data versions

The calibration functions or key data of GOME have been updated a number of times since the pre-flight calibration. Since March 1995, eight versions have been delivered. In the following a brief description of the versions is given:

• Version 0 of the key data set reflects the so-called "at TPD" situation. That is, the key data is valid for ambient pressure and room temperature.

• Version 1 reflects the so-called "in vacuum" situation. The version 0 key data is corrected for the overlap regions, etalon structure, and dichroic features, using the TV test data.

• Version 2, the last 20 pixels of the radiance response function are added to version 1.

• Version 3 the wavelength grid of version 2 of the key data set is translated to a "vacuum" wavelength grid using the Edlen formula.

• Version 4 of the key data corrects the "at TPD" key data (version 0) for the "in orbit" situation (correcting overlap regions, etalon structure, and dichroic features), using the sun observation of July 2nd, 1995.

• Version 5 is as version 4, but with the wavelength grid set to a vacuum wavelength grid using the 1966 Edlen formula.

• Version 6 differs from version 5 in:

The overlap correction function (f2) is recalculated.

The overlap correction function (f2) is set to zero for low/zero signal regions (start of channel 2 and 4).

Additional pixels in channel 1 are added to the radiance response function.

• Version 7 differs from version 6 in:

The overlap correction function (f2) is again recalculated.

Stray light figures as computed during the pre-flight phase are added to key data set.

• Version 8 contains the radiance response function that is corrected for the air to vacuum effect as described above.

Conclusions and recommendations

Observations:

The performance of GOME in orbit has changed with respect to the pre-flight calibrations on several points. The in-flight situation of the instruments performance is reflected by the key-data version 8. Changes with respect to these key-data of more than 1% makes an update of the key-data necessary on the following points:

Etalon effect: The in-flight etalon structure differs from the preflight etalon structure, which affects mainly the radiance response function. The latest key-data version (version 8) has been updated to reflect the in-flight situation of July 2 1995. After every cooler switch-off a new etalon structure is formed however, which makes an update of the key-data functions necessary. The first 7 days after a cooler switch-off the rapid etalon shift makes it necessary to update the etalon structure every day.

Dichroic features: The in-flight dichroic features differ from the pre-flight situation, which affects the radiance response function and the polarization properties of GOME. The latest key-data version (version 8) has been updated to reflect the in-flight situation of July 2 1995. A shift of the dichroic features of less than 1% per month is observed after July 2 1995, which makes an update of the key-data once per month necessary.

Air to vacuum effect: Comparisons of the GOME absolute irradiance with observations of other instrument showed a difference due to an air to vacuum change of the instruments radiance response. The latest key-data version (version 8) has been updated for this effect to reflect the in-flight situation of July 2 1995.

BRDF: No significant changes in the diffuser reflectance has been observed. The BRDF of the on-board diffuser must be monitored using the diffuser reflectance measurement every month. The BRDF function must be updated when a change of more than 1% is observed in the diffuser reflectance.

Long term degradation: A change of at maximum 0.05% per day of the Solar irradiance sensitivity is observed. This effect can be caused by a degradation of the calibration unit and/or a change in the instruments radiance response. No correction for this effect is included in the latest key-data version.

Consequences for level 1 products:

Albedo: Since the changes of the etalon structure and dichroic features affects the Earth radiance measurement in the same way as it affects the solar irradiance, they cancel out in the albedo. A degradation of the on-board calibration unit however affects only the solar irradiance and thus affects the albedo.

Absolute radiance and irradiance: The calibration functions are determined for July 2 1995, which makes the absolute radiance and irradiance products valid for this date. Due to a changed etalon structure caused by several instrument switch-offs and a slightly shifted dichroic structure, data after July 2 1995 will show residual etalon structures and dichroic features when the radiance response function and polarisation sensitivity function without further update after July 2 are applied to these data. Frequent monitoring of the instruments performence and updates of the key data are therefore necesarry during the entire lifetime of GOME.

References

1. A. Hahne e.a., "GOME a new instrument on ERS-2", ESA bulletin, Vol. 73, p.p. 22-29, 1993.
2. A. Hahne e.a., "Calibration of the GOME Instrument for ERS-2, ESA Journal Vol. 18, p.p. 1190128, 1994.
3. R. Hoekstra e.a., "Calibration and Validation of ozone monitoring space instruments", Proceedings of 45th congress of the international astronautical federation, October 9-14, 1994, Jerusalem.
4. G.H. Mount e.a., "Compact far ultraviolet emission source with rich spectral emission 1150-3100 Å". Applied Optics, Vol. 16 No. 3, 1977, pp. 591-595.
5. J.Z. Klose e.a., "Characterization of a Pt-Ne hollow cathode spectral line source", Applied Optics, Vol. 29, No. 19, 1990, pp. 2951-2959,
6. J.E. Sansonetti, e.a., "Atlas of the Spectrum of a Platinum/Neon Hollow-Cathode Reference lamp in the Region 1130-4430 Å, J. Res. Natl. Inst. Stand. Technol. vol. 97, 1, 1992.
7. C. Smorenburg e.a., "Absolute Radiometric Calibration Facility, Parijs, Sept. SPIE 1995.
8. D.F. Heath, e.a., "Comparability of Spectral Radiance Calibrations of Large Aperture Earth Observating Instruments Based Upon Diffuse Reflective Panels and Internally Illuminated Spherical Integrator Techniques", Space Optics 1994: Earth Observation and Astronomy, Proc. EUROPTO, SPIE vol. 2209, 148-159, 1994.
9. D.F. Heath, Z. Wei, W.K. Fowler, V.W. Nelson, J. Butler and E. Hilsenrath, "Comparisons of UV Spectral Radiance Calibrations of SBUV-2 Type Ozone Monitoring Instruments and Traceability to NIST", Ultraviolet Technology V, SPIE Proc. vol. 2282, 313-323, 1994.
10. Article Nature in preparation. (DONALD HEATH)
11. D.F. Heath e.a., "Spectroradiometric calibration and validation of space instruments used to derive

long term changes in stratospheric ozone using the solar backscattered ultraviolet radiation technique, SPIE vol. 2318, pp.174-187, 1994.

12. J.W. Walker e.a., "A Technique for Improving of the Calibration of Large-Area Sphere Source", Calibration of Passive Remote Obser-ving Optical and Microwave Instrumentation, Prov. Soc. Photo-Opt, Instrum. Eng., vol. 1493, pp. 224-230, 1991.
13. J.T. McLean e.a., "Radiance Calibration of Spherical Integrators, "Optical Radiation Measurements II, Proc. Soc. Photo-Opt. In-strum. Eng., vol. 1109, pp. 114-121, 1989.

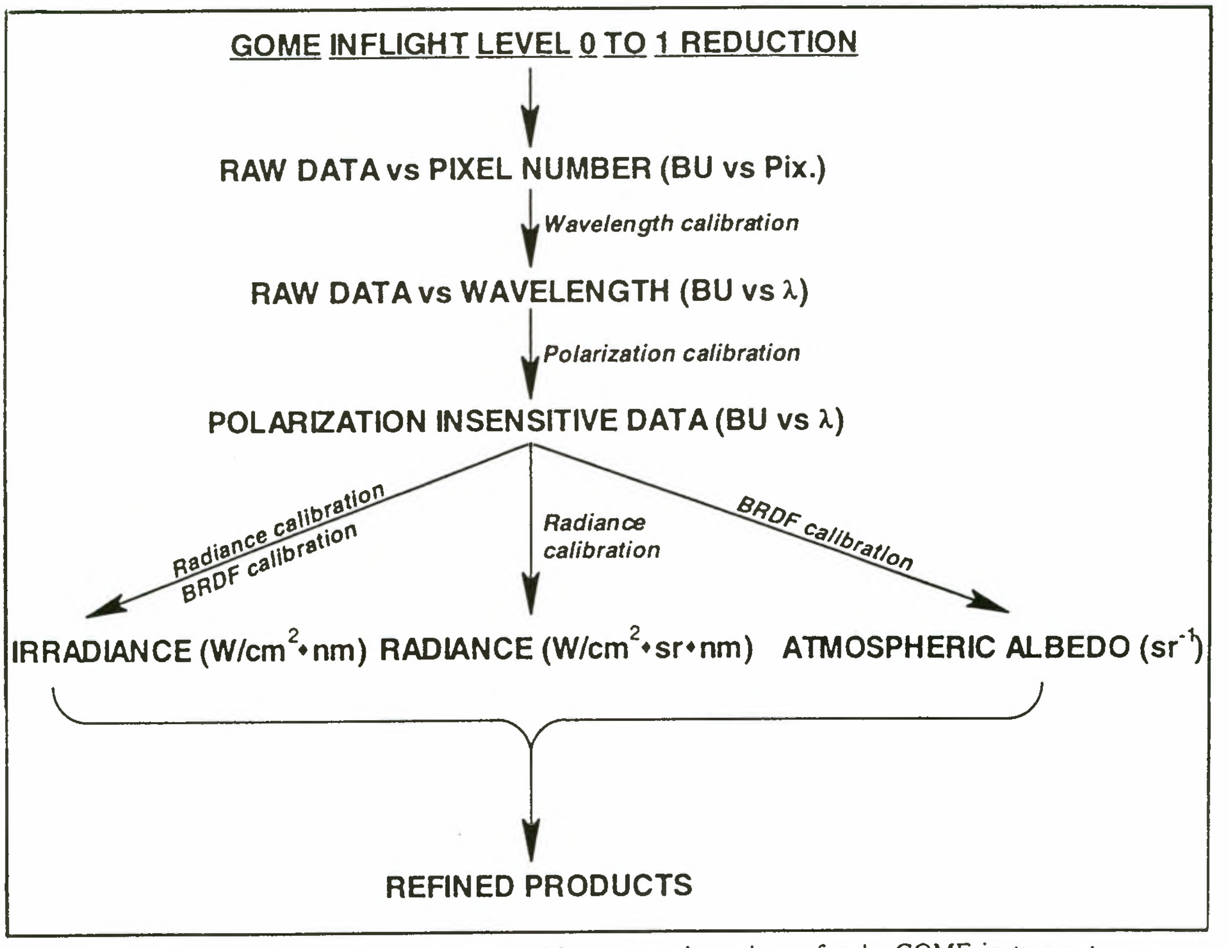

Figure 1: Level 0 to 1 data (digital to physical quantities) processing scheme for the GOME instrument

	Spectral resolution in-flight		Spectral resolution TV-test	
	[pix]	[nm]	[pix]	[nm]
Channel 1	1.6	0.18	1.7	0.19
Channel 2	1.5	0.17	1.5	0.17
Channel 3	1.4	0.28	1.4	0.28
Channel 4	1.5	0.30	1.6	0.32

Table 1: The spectral resolution of GOME in-flight and pre-flight during the TV test (in vacuum)

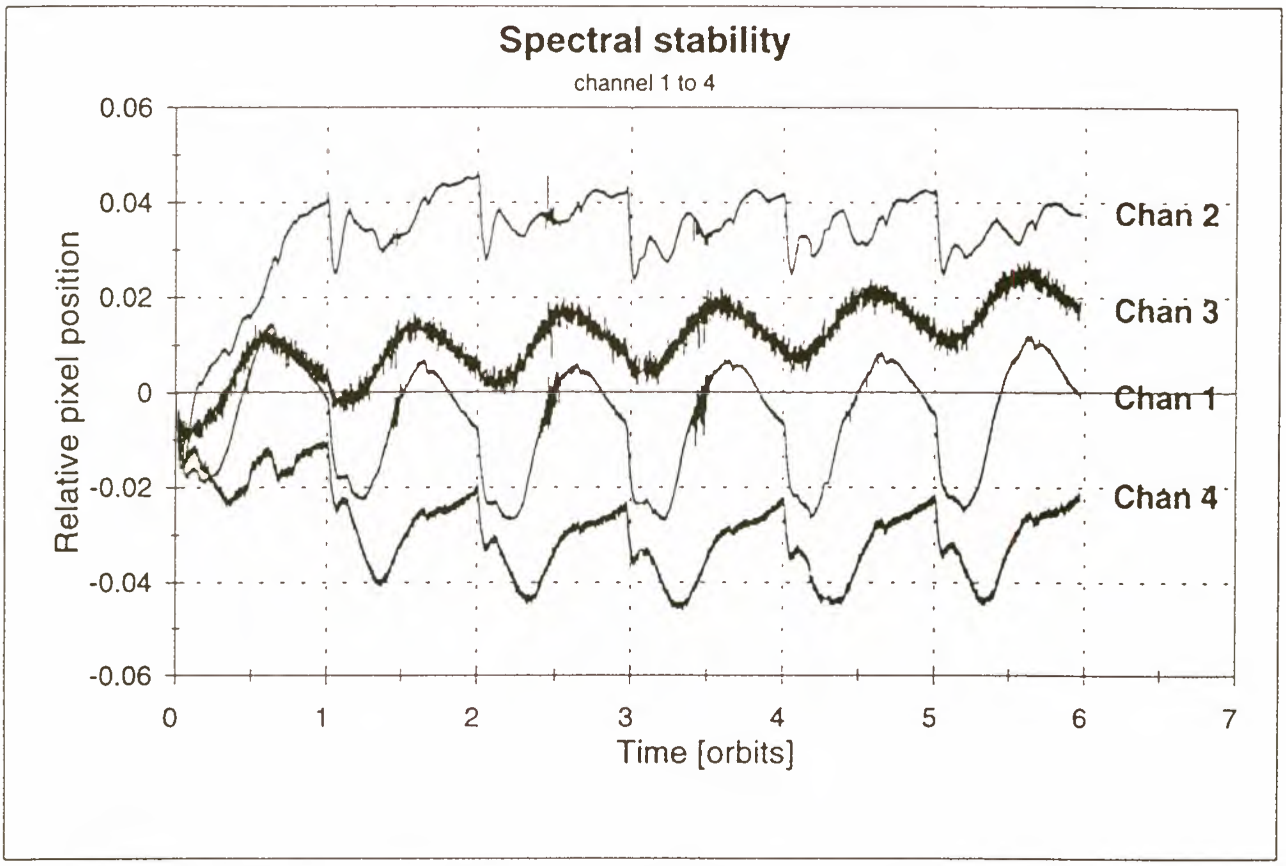

Figure 2: Relative spectral line positions of a line in the middle of all GOME channels during several orbits, with a 0.5° temperature fluctuation. The higher noise on the channel 3 is due to a lower line intensity of the used line in channel 3. Between orbits 2 and 4 a higher noise is seen on all lines, which is caused by the SAA (South Atlantic Anomaly). Just after the out of eclipse point (change of orbital number) a large temperature gradient is seen, resulting in a fast pixel position change, which is best seen in channel 2 .

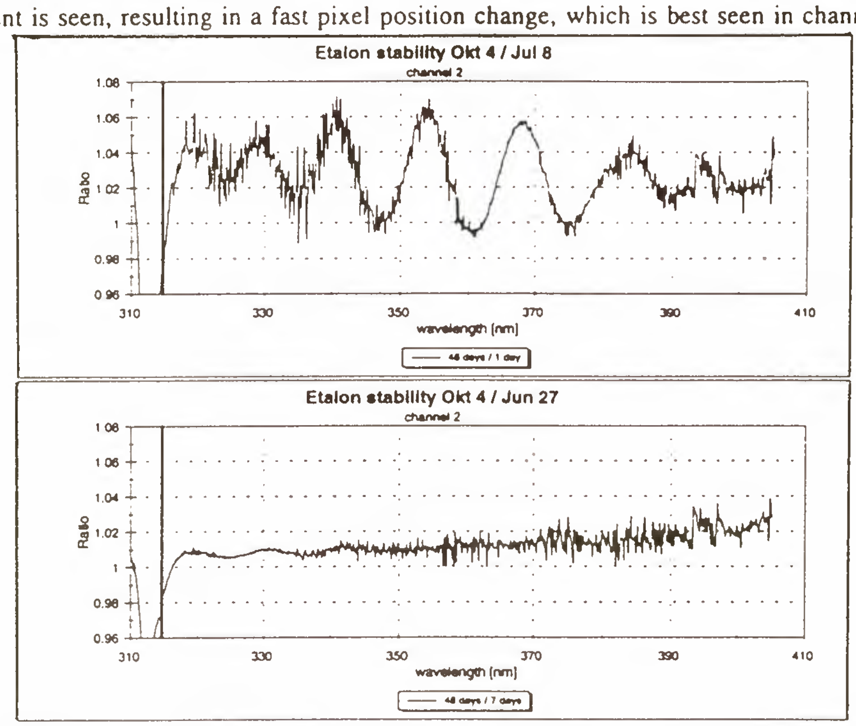

Figure 3: The etalon stability w.r.t. the later sun measurement of October 4, showing a large etalon after 1 day cooling the detectors and an almost disappeared etalon after 7 days cooling

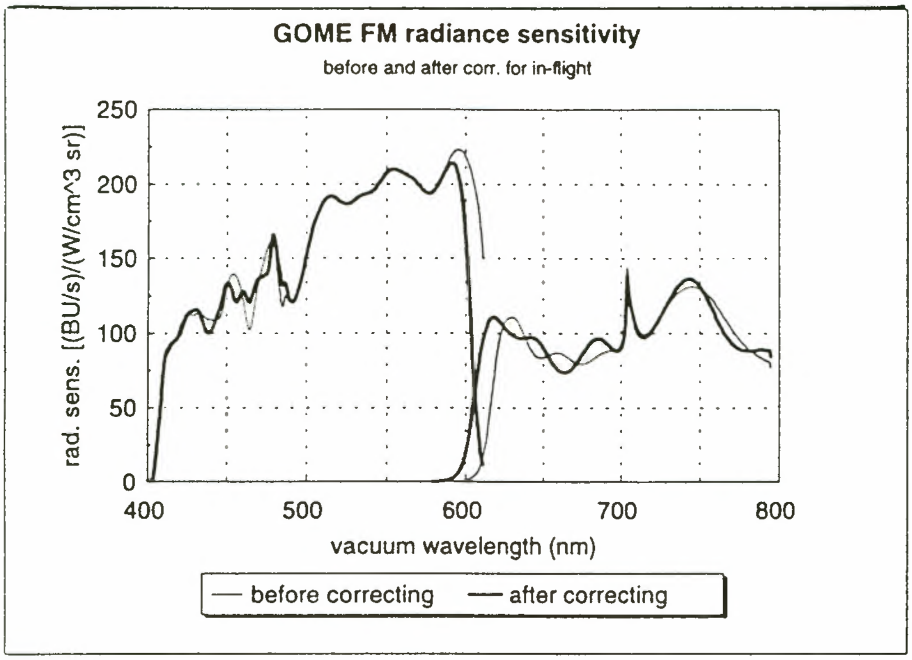

Figure 4: GOME radiometric sensitivity pre-flight (before correction) and in-flight (after correction) in channel 3 and 4. The correction is for the outgassing of the dichroic.

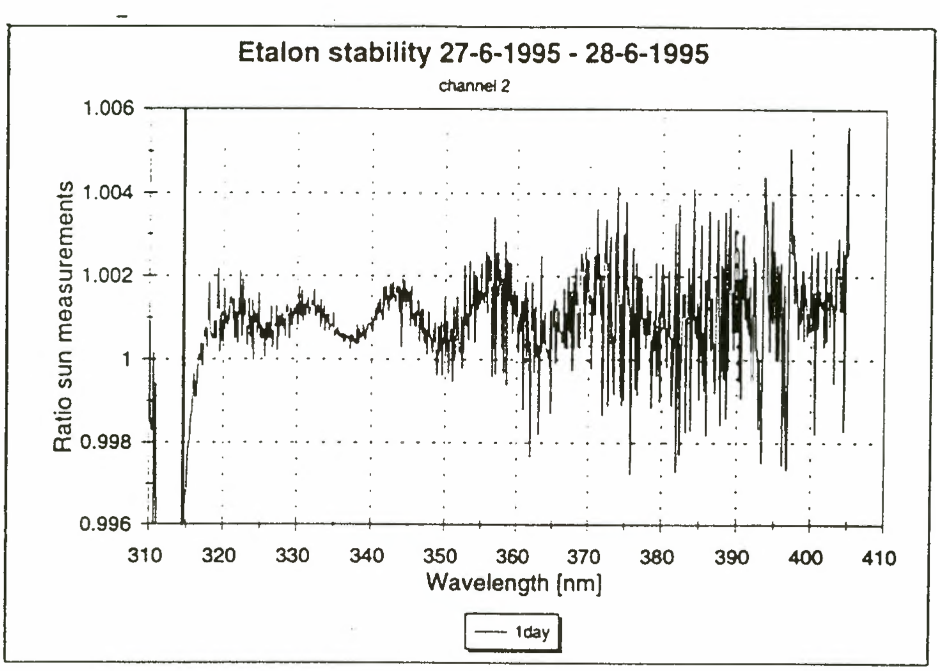

Figure 5: Short term etalon stability, between two sun measurements at two consecutive days, after the detectors have been cooled for 7 days

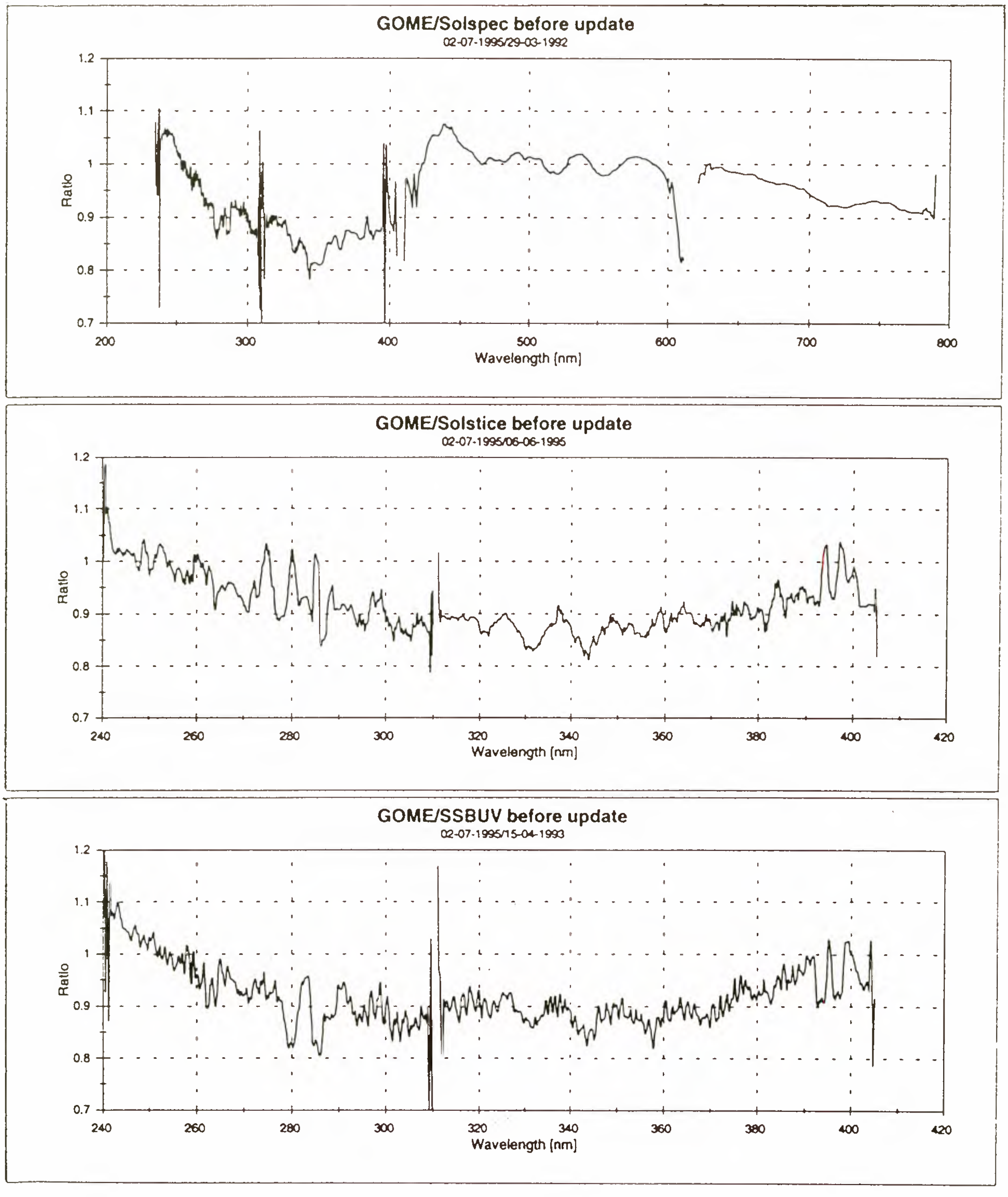

Figure 6: Comparisons of GOME absolute solar irradiance (02-07-1995), calculated with the pre-flight determined absolute radiometric response, with the SOLSPEC (29-03-1992), SOLSTICE (06-06-1995) and SSBUV (15-04-1993) absolute solar irradiance

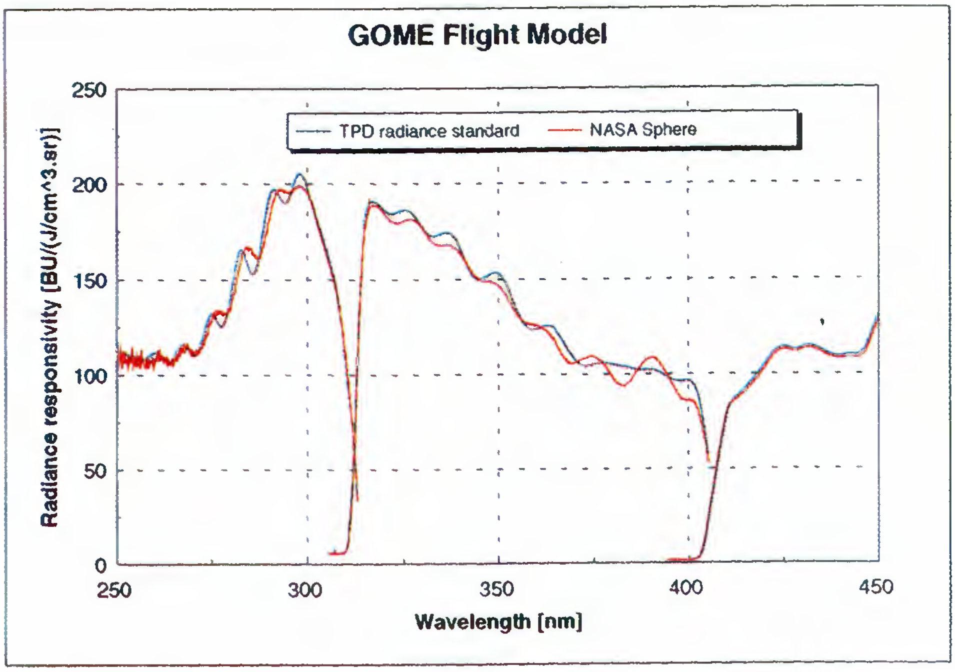

Figure 7: Comparison of TPD radiometric standard with the NASA standard, measured both pre-flight on the GOME instrument, showing no significant differences in the absolute radiometric response calibration.

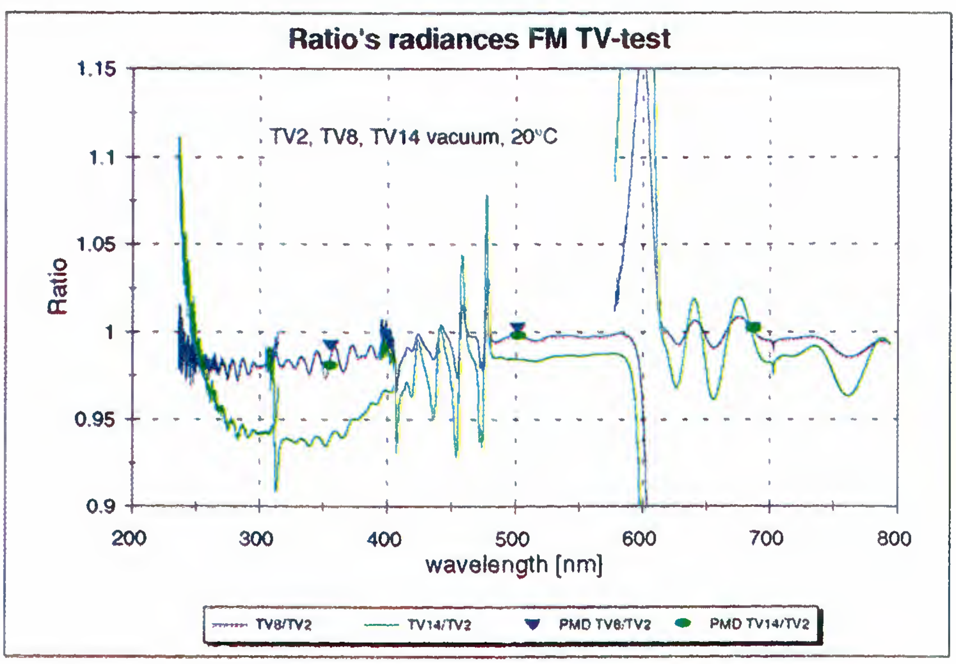

Figure 8: Ratio of the pre-flight in vacuum (TV test) measured radiances, with the air/vacuum effect building up from TV2 (1 day vacuum) to TV14 (10 days vacuum)

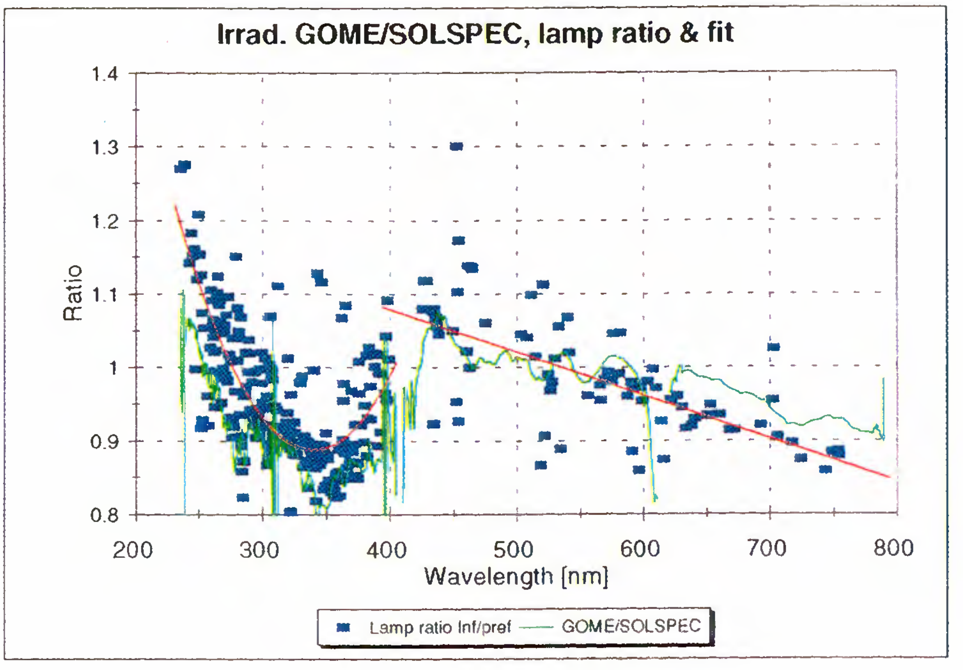

Figure 9: The red line represents the fitted curve through the spectral line ratios (blue dots), which is the change from air to vacuum. The green line represents the ratio of the irradiance measured by GOME with the irradiance measured by SOLSPEC. The difference observed in the ratio GOME/SOLSPEC can thus be explained by the difference caused by the air to vacuum effect.

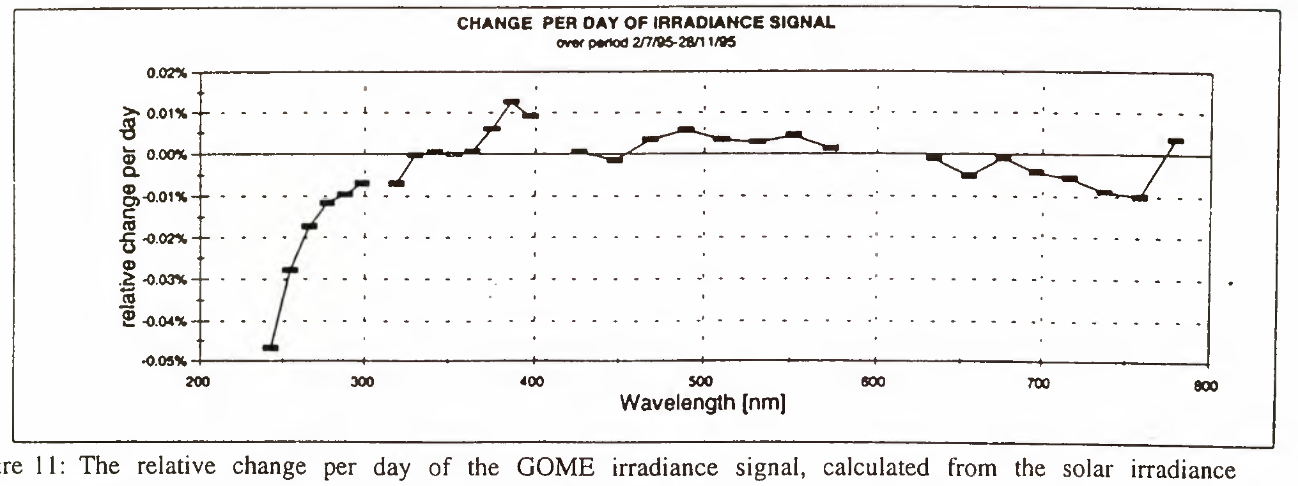

Figure 11: The relative change per day of the GOME irradiance signal, calculated from the solar irradiance measurements of 28-11-1995 and 02-07-1995

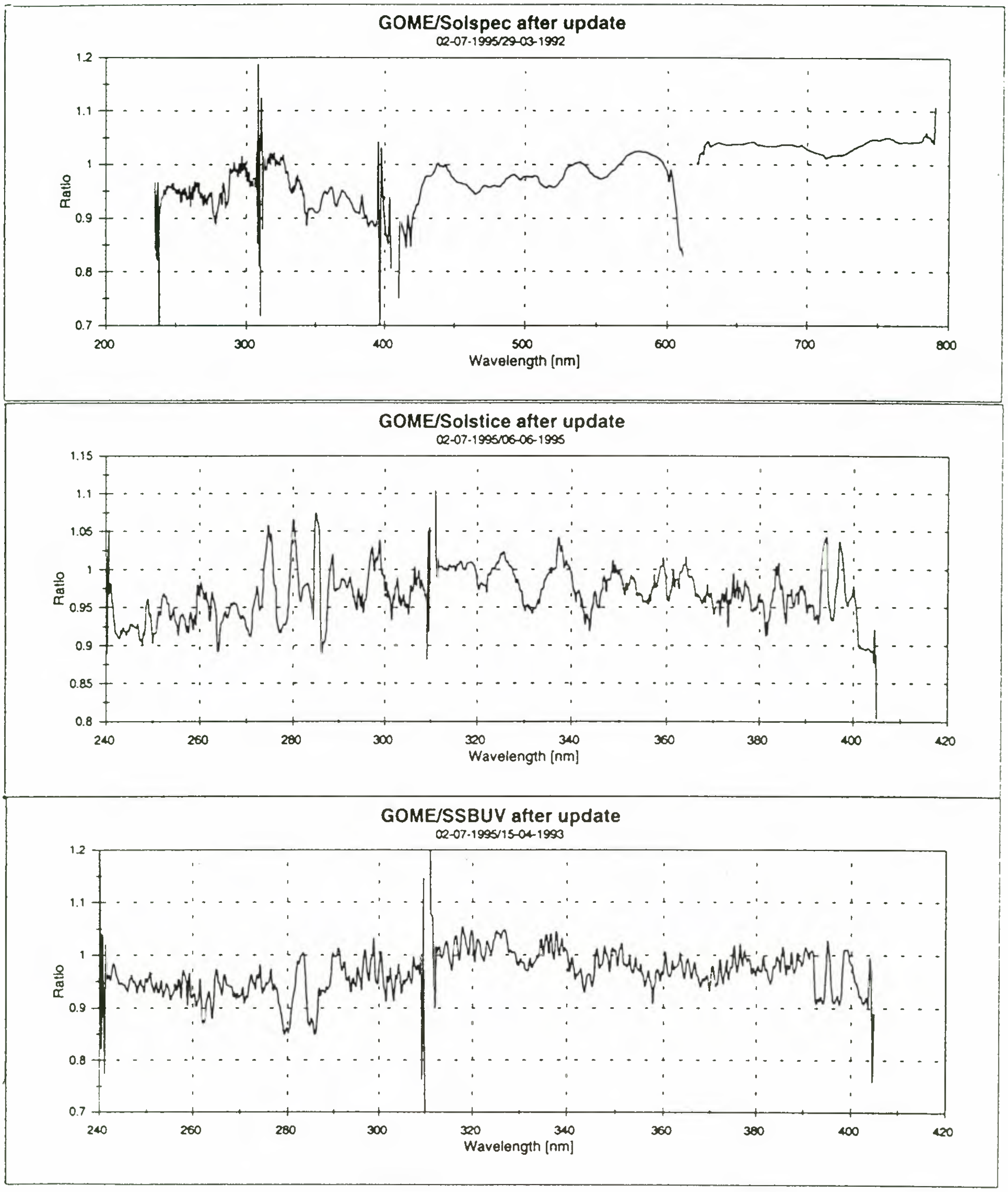

Figure 10: Comparison of the GOME absolute solar irradiance (02-07-1995) with SOLSPEC, SOLSTICE and SSBUV after correcting the absolute radiometric response for the air/vacuum effect with the lamp ratios..

GOME DATA PROCESSOR CONFIGURATION DURING COMMISSIONING PHASE

W. Balzer, D. Loyola, B. Aberle, E. Mikusch, T. Ruppert, C. Schmid, R. Spurr, W. Thomas, M. Wolfmüller

Deutsche Forschungsanstalt für Luft– und Raumfahrt
Deutsches Fernerkundungsdatenzentrum
82230 Oberpfaffenhofen, Germany

(e–mail: balzer@dfd.dlr.de, loyola@dfd.dlr.de)

Abstract

The Global Ozone Monitoring Experiment (GOME) is a new atmospheric chemistry instrument on–board the ERS–2 satellite launched in April 1995. The GOME is designed to measure a range of atmospheric trace constituents, with particular emphasis on the global ozone distribution.

The German Remote Sensing Data Center (DFD) plays a major role in the design, implementation and operation of the GOME Data Processor (GDP), the ground segment for the GOME sensor.

In this paper the configuration of GDP during the commissioning phase and the recommendations for the next release of GDP are presented.

1. INTRODUCTION

Major components of the GDP are the complete GOME data archive, the Level 0 to 1 processing chain, the total ozone column retrieval process (level 1 to 2 processing), and image processing for the generation of higher level products.

In the next sections a brief description of the different processing steps is done. Then the status of the production system and a summary of the data computed with this system are given. The recommendation for the next releases of GDP and the results reached with the multiple–scattering correction tables are also presented. Finally, Level 3 products generated by DFD are shown.

2. LEVEL 0 TO 1 PROCESSING

Raw GOME data are converted to "calibrated radiances" during the Level 0 to 1 processing by the application of a series of calibration algorithms. Calibration parameters are calculated and stored on a regular basis from in–flight observations of darkness, the calibration lamp, internal LED and sun measurements. Data from pre–flight instrument calibration, the so called KeyData, are also required.

The output of this step are earth–shine spectra and sun spectrum delivered as level 1 product.

3. LEVEL 1 TO 2 PROCESSING

The level 1 to 2 processing derives the total columns of ozone and other trace gases based on the level 1 product. This step comprises three main algorithms.

The Initial Cloud Fitting Algorithm (ICFA) is used to determine the fractional cloud cover of the pixel scene. ICFA utilizes measurements close to and within the well–known O_2 A–band around 760 nm. The average transmittance through this band defines a relationship between cloud–top height and fractional cloud cover.

The Differential Optical Absorption Spectroscopy (DOAS) algorithm is used for the retrieval of atmospheric trace gas effective slant column amounts from moderately high–resolution spectral data in the UV and visible regions of the spectrum. DOAS involves the least–squares fitting of measurement spectra to a set of reference spectra. GOME represents the first application of this technique to passive remote sensing instruments in space. The first operational DOAS algorithm will focus on the retrieval of total columns of ozone.

The output of DOAS are fitted slant columns of atmospheric absorbers, e.g. O_3, which must be converted to geometry–independent vertical columns by division with an appropriate Air Mass Factor (AMF). These are derived from radiative transfer simulations. The AMF represents the enhancement of the absorption of a given trace gas due to slant paths of incident light in the atmosphere. In the operational processing the single–scattering AMF is calculated in real time only but combined with a multiple–scattering correction factor using pre–calculated look–up tables.

4. PRODUCTION SYSTEM STATUS

During the commissioning phase the level 0 to 1 processor version 0.5 and 0.6 and the Level 1 to 2 processor version 1.20 and 1.21 were used to produce products for validation purposes. The entries in table 1 and 2 describe the production system status for the time period of the validation campaign.

Version 0.5 released October, 25th 1995
KeyData version 7.0 Polarization correction of band 1a using an averaged p7 Error values calculated using one average KeyData factor per channel Adds the flag '–w' (write the calibration data) to the extracting program Geolocation of ground pixels disagree with the ESA propagator
Version 0.6 released November, 28th 1995
Performance–tunning improvement of ~15% Simplification and better log messages handling

Table 1 : Release Notes Entries of Level 0 to 1 Processing used during geophysical validation campaign

Version 1.20 released October, 27th 1995
AMF multiple–scattering correction molecules: O_3, NO_2 solar zenith angle: <75deg windows: UV(325–335nm) only no intensity correction
Version 1.21 released November, 13th 1995
AMF multiple–scattering correction windows: UV(325–335nm) and VIS (510–560nm) Option for ground albedo in escape function correction computation of cloud–top reflectance (ICFA)

Table 2 : Release Notes Entries of Level 1 to 2 Processing used during geophysical validation campaign

5. DATA PROCESSED FOR GEOPHYSICAL VALIDATION

Two Geophysical Validation processing periods were defined by the GOME Validation PI's, where GOME data was processed by GDP and the corresponding level 1 and level 2 were distributed via CDs and/or via ftp server. These validation periods where selected taking into account the availability of ground or balloon data for periods of 3 or more consecutive days

The first Geophysical Validation processing period is shown in table 3 . The data was distributed via CDs and our ftp server. The processing was started October 27 and the following GDP version was used:

- Level 0 to 1 version 0.5
- Level 1 to 2 version 1.20

Period	Days	Processed	Distributed
July 23 to 25	3	✓	✓
August 25 to 27	3	✓	✓
September 15 to 17	3	✓	✓
October 5 to 7	3	✓	✓
October 29 to 31	3	✓	✓
TOTAL	15		

Table 3 : First Validation Period

The second Geophysical Validation processing period is shown in table 4 . The processing was started December 5 and the following GDP version was used:

- Level 0 to 1 version 0.6
- Level 1 to 2 version 1.21

Due to performance reasons the DOAS visible window was changed from 510–560nm to 425–450nm at November 27th 1995.

Period	Days	Processed	Distributed
July 22	1	✓	ftp
August 29 to 31 This period contains 14 orbits per day (Exabyte data) for the global maps	3	✓	✓
September 1 to 3	3	✓	✓
September 4 to 9	6	✓	✓
September 20 to 23	4	✓	✓
September 27 to October 4 No level 0 data available for September 29	7	✓	✓
October 11 to 13	3	✓	✓
October 22 to 25	***No Processing Possible*** The Level 0 to 1 processing found inconsistencies with the IT of Channel 2 due to a GOME Single Point Event problem		
December 11 to 13	3	✓	✓
TOTAL	30		

Table 4 : Second Validation Period

GOME data from November 9 to 11 was processed with the same configuration of the second validation period. The processing was part of an internal GDP–DMS test, DMS is the Data Management System used at the D–PAF.

Additional GDP Level 0 to 1 processing was done for the 28^{th} of each month (calibration timeline) and one day before each period (sun calibration).

Table 5 shows some statistics on the product sizes and processing times needed by GDP. One day calculations are done using a basis of 14.3 orbits per day.

	Level 0	Level 1	Level 2
One GOME orbit product size	≈ 32 Mb	≈ 14.5 Mb	≈ 0.7 Mb
One day GOME data production size	≈ 450 Mb	≈ 207 Mb	≈ 10 Mb
One GOME orbit processing time	–	≈ 15 minutes	≈ 35 minutes using 36 proces-sors
One day GOME data processing time	≈ 30 minutes Screen-ing per Exabyte (10 or-bits)	≈ 3 hours 40 min-utes	≈ 8 hours 30 min-utes

Table 5 : Processing Statistics

6. RECOMMENDATIONS FOR NEXT RELEASE

As a result of the subgroup meetings which took place during the commissioning phase various recommendations for the next release of GDP were made.

The following recommendations were made for the Level 0 to 1

- Use the ESA orbit propagator instead of the DLR–VENI propagator because there are discrepancies in the calculated ground pixels geolocation
- Correct for dark current oscillations in band 1a due to the Peltier switching on and off which causes a FPA cross–talk problem
- Flag the reflectivity jumps checking the channel–to–channel discontinuities at 600 nm.
- Generation of Sun and Moon products

There are also some open issues for the Level 0 to 1

- Generate a new set of In–flight KeyData parameters which consider Etalon problems, Eta changes from pre–flight to in–flight, etc.
- Polarization Correction
  - The overlapping regions are not working properly
  - No Polarization correction done for pixels with IT > 1.5s
  - Further analysis and off line tools are needed to develop a better algorithm

The Level 1 to 2 processing recommendations are summarized in Table 6

In parallel to the operational production the development system is being continuously improved to implement these recommendations. The right part of table 6 shows the current status of this effort.

Sub-system	Feature	C	I	T
ICFA	Database of O_2 A–band spherical template trans-mittances	✓	✓	✓
DOAS	General structure for the selection of reference spectra of different sources	✓	✓	✓
	Individual convolution and smoothing of cross–sec-tions	✓	✓	
	Fourier smoothing for measurement and refer-ence spectra	✓	✓	
	Exclusion of sun from lin-ear fitting	✓	✓	
DB lib	Reference spectra GOME FM: O_3, NO_2, RING	✓	✓	
	Reference spectrum Har-wood/Jones: NO_2	✓	✓	
AMF	Extended multiple–scatter-ing correction table (solar zenith angles up to 92deg, latitudinal and seasonal variation)	✓		
ICFA	Enhanced cloud–top pres-sure derivation from ISCCP data base	✓		
For–mat	Extension of geophysical parameters	✓		
	Addition of cloud clearing algorithm results	✓		

Table 6 : Level 1 to 2 Processing Recommendations for Next Release (C=Coded, I=Implemented, T=Tested)

7. MULTIPLE–SCATTERING CORRECTION TABLES

As an example of an important feature for the next release, the extension of the multiple–scattering correction tables is explained in more detail. These tables were introduced first in version 1.20 and improved in version 1.21 (see Table 2). However these calculations were performed with plan–parallel geometry, thus the correction factors were valid for solar zenith angles less than 75deg only.

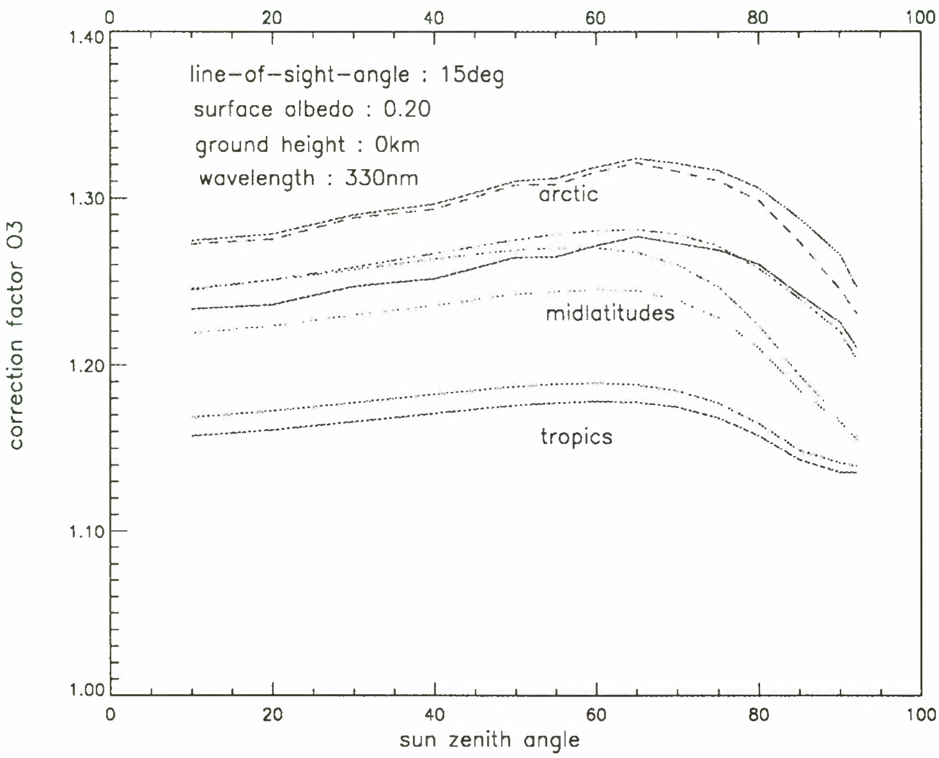

Figure 1 : Multiple–scattering Correction Factors for mid–latitude autumn/winter conditions

New lookup–tables are created for the next release using GOMEtran++ Version 2.0 capable to simulate radiative transfer in a spherical atmosphere. Therefore the correction factors are available now up to a solar zenith angle of 92deg. Additionally, latitudinal and seasonal variations are included. In table 7 the parameter variations are depicted.

Parameter Name	Parameter Values	Number
Wavelengths	330, 437, 520	3
Solar Zenith Angles	10, 20, 30, 40, 50, 55, 60, 65, 70, 75, 80, 85, 90, 92	14
Line–of–Sight Angles	0, 5, 10, 15, 20, 25, 30, 35	8
Albedo	5, 20, 30, 50, 75, 95	6
Ground altitude	0.0, 0.5, 1.0, 2.0, 3.0, 4.0, 5.0, 6.0, 7.0	9
Geographical latitude	+85, +50, +35, +10, –10, –35, –60, –85	8
Season	spring/summer, fall/winter	2
Aerosol content in planetary boundary layer	maritime (+85,–60,–85) or rural (other lat.)	1

Table 7 : Multiple–scattering Correction Table Parameters

Figure 1 shows an example of the variation of correction factors for ozone as a function of the solar zenith angle for different latitude zones. It is clearly shown, that the impact of different ozone content in different latitude zones on the calculated correction factors could not be neglected.

A distinct improvement of the results of the current operational processor is estimated due to the implementation of the recommendations made by the subgroup meetings.

8. LEVEL 3 PRODUCTS

Level 3 products are also generated at DFD in addition to the Level 1 and Level 2 products. The Level 3 products are obtained mapping ozon level 2 data to standard global geophysical grids.

Different products are planed; a tree days global coverage, a daily Europe product and daily polar coverage. Figure 2 shows total column ozon global coverage for November 9 to 11 in rectangular projection. Figure 3 is a polar–stereographic projection of south pole total column ozon for November 9.

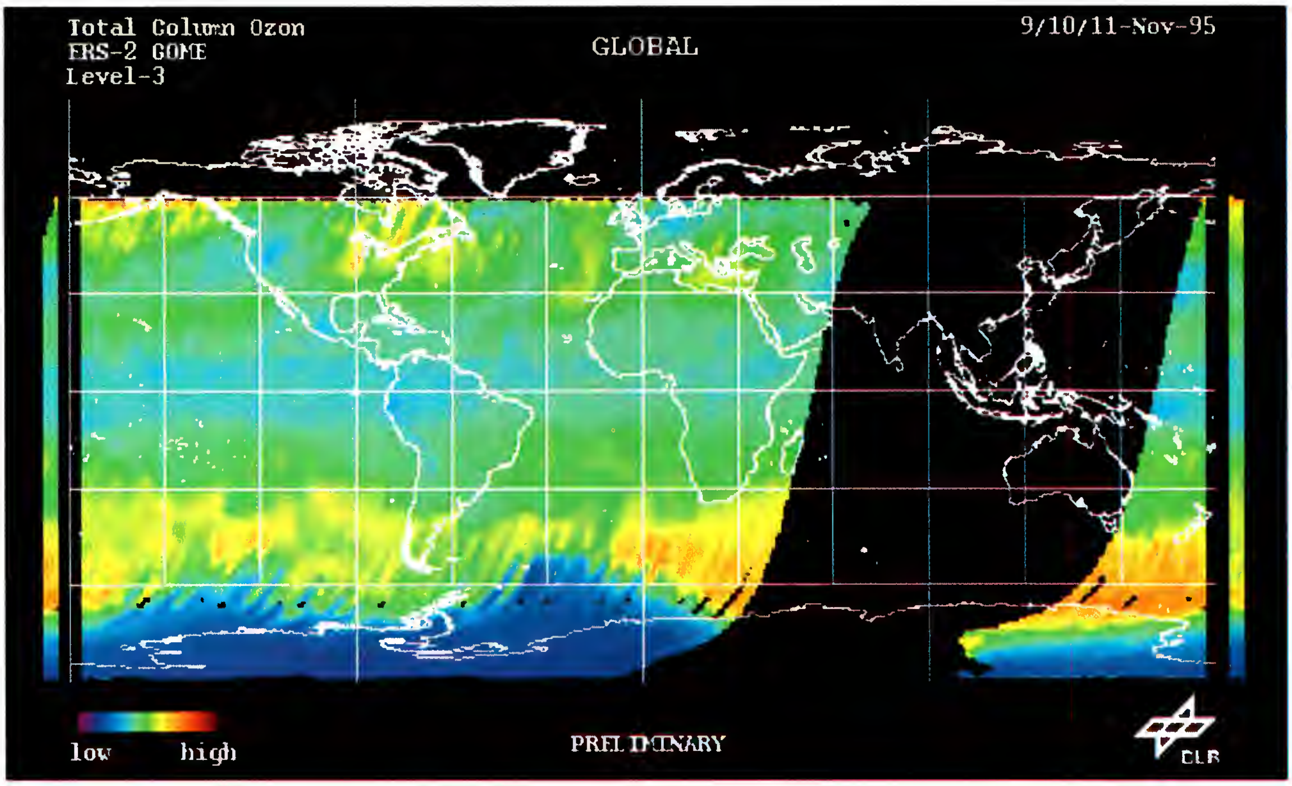

Figure 2 : Level 3 Product — Total column ozon global coverage

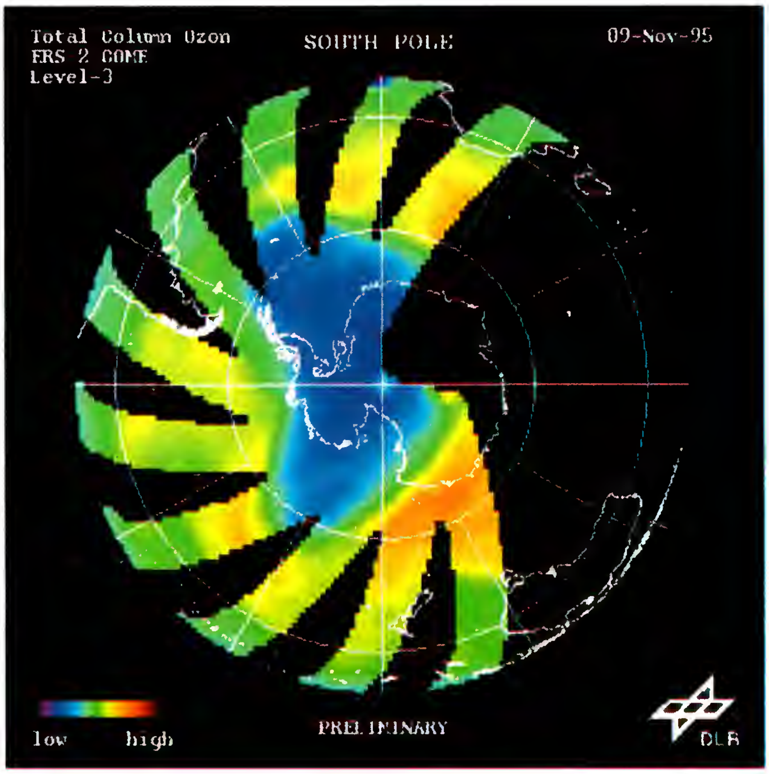

Figure 3 : Level 3 Product — Total column ozon pole daily map

9. CONCLUSIONS

For GOME Geophysical Validation purposes a total of 49 days with ca. 430 Orbits of GOME data that has been processed at the DLR. The data processed cover all kind of scenarios where the GDP level 0 to1 and GDP level 1 to 2 processors have demonstrated his stability and robustness.

In parallel to the data processing for the validation periods an enormous amount of processing for the multiple scattering correction tables has been conducted. This table was calculated twice. In summary an amount of about 9000 hours of processing time was used (this is continuously 1 year of processing divided on several processors).

10. ACKNOWLEDGEMENTS

It has to be noted that the implementation of the GOME data processor was made possible by the Deutsche Agentur für Raumfahrtangelegenheiten (DARA) which financed most of this work.

Furthermore, the help and cooperation of all agencies and scientist was very appreciated. Most notable are the ESA project team at ESTEC (A. Hahne, J. Callies, C. Caspar), J. Burrows and his colleagues, K. Chance, P. Stammes and many others.

VALIDATION OF IRRADIANCE, RADIANCE AND POLARISATION MEASUREMENTS (LEVEL 1 PRODUCTS)

Validation of GOME polarisation and radiance measurements

P. Stammes[1], D.M. Stam[1,3], R.B.A. Koelemeijer[1], and I. Aben[2]

[1] Royal Netherlands Meteorological Institute (KNMI)
P.O. Box 201, 3730 AE De Bilt, The Netherlands

[2] Space Research Organization Netherlands (SRON)
Sorbonnelaan 2, 3584 CA Utrecht, The Netherlands

[3] Faculty of Physics and Astronomy, Vrije Universiteit
De Boelelaan 1081, 1081 HV Amsterdam, The Netherlands

Abstract

The accuracy of radiance measurements of the Earth by GOME on board ERS-2 depends on the correction for the polarisation sensitivity of the instrument. The polarisation measurements of the Earth by GOME needed to perform this correction have been validated by comparison with polarised radiative transfer calculations.

It has been found that the fractional polarisation measurements of the Polarisation Measuring Devices (PMDs) are consistent and overall correct (for systematic and random polarisation errors, see Aben et al., this issue). The overlap polarisations are strongly deviating, and should not be used in the polarisation-correction scheme.

The radiance measurements show jumps from channel to channel. This is most probably due to the serial read-out of the spectral detector arrays, which causes a varying scene over a spectral channel. Radiance jumps will especially occur over inhomogeneous (e.g. partially cloudy) scenes.

1 Introduction

The Global Ozone Monitoring Experiment (GOME) on board the ERS-2 satellite has been designed to measure column densities and, possibly, profiles of trace gases and aerosols in the Earth's atmosphere (ESA, 1993). The primary measurements performed by GOME are, however, spectral radiance measurements of the Earth from about 240 to 790 nm with a high spectral resolution. The spectral radiance, which is called a level 1 data product, is the basis of all derived information on atmospheric composition, e.g. trace gas column densities, which are called level 2 data products. Therefore, the accuracy of the measured radiance should be as high as possible. Since GOME is sensitive to polarisation (mainly due to its scan mirror and gratings), its radiance measurements must be corrected for the polarisation of the incoming light, because atmospheric radiation is in general polarised. To this purpose, GOME measures the polarisation with three broad-band Polarisation Measuring Devices (PMDs) and three narrow-band channel-overlaps. These polarisation measurements are intended to be used in the polarisation-correction part of the GOME data processing.

The aim of the work presented here is, firstly, to validate the polarisation measurements, and, secondly, to validate the radiance measurements by GOME. Since there was no other polarisation measuring satellite instrument available during the GOME validation phase, which took place in the second half of 1995, the validation approach was indirect by using radiative transfer calculations. The validation approach consisted of: (a) checks on the consistency of the GOME data; (b) comparison of GOME data with results from single scattering theory; (c) comparison of GOME data with multiple scattering results using the Doubling-Adding KNMI (DAK) model.

Part of the validation work was an error analysis of the PMD measurements, based on special geometries along the GOME orbit. This work is described separately in this issue by Aben et al. (1996). Another part, discussing various instrumental effects relevant for polarisation and radiance calibration, is described in this issue by Slijkhuis (1996).

The structure of this paper is as follows. In Section 2 the GOME data used for validation are briefly described. In Section 3 the DAK model is introduced. The polarisation validation is reported in Section 4 and the radiance validation in Section 5. Conclusions are given in Section 6.

2 Description of GOME data

2.1 Overview

Technical information about the GOME instrument and data processing can be found in the GOME Users Manual (ESA, 1995). Here a few relevant details are given. ERS-2 is in a sun-synchronous polar orbit with an equator-crossing time of 10.30 AM (local solar time of the descending node). GOME measures the Earth's radiation by scanning perpendicular to the flight direction from East to West in 4.5 s, and doing an integration every 1.5 s. This leads to three ground pixel types: East (E), Nadir (N), and West (W). The backscan of 1.5 s also involves an integration, which leads to the Backscan (B) pixel. The swath width can in principle be varied between 120 and 960 km; in the validation phase it was 960 km. The integration time (IT) in the validation phase was only 0.375 s instead of the planned 1.5 s, leading to a size of 80×40 km^2 (across×along track), for the E, N, and W pixels, and a size of 240×40 km^2 for the B pixel. The nadir angles of the viewing directions for the centres of these pixels are, at satellite altitude (about 780 km): −13.9° (E), 6.6° (N), 27.3° (W), and −23.5° (B), where the minus sign denotes the eastern side of the nadir direction.

GOME observes the Sun and the Earth in four spectral channels, encompassing the range from about 240 to 790 nm, with 0.2 to 0.4 nm resolution. Each channel is a 1024-element diode-array (Reticon). The dispersion is performed by means of a predisperser prim and gratings. The present radiance validation has been limited to data of spectral channel 1B (307–315 nm), channel 2 (311–405 nm), channel 3 (394–611 nm), and channel 4 (578–794 nm). Here the total ranges are given, which are larger than the useful ranges.

The GOME level 1 data product contains a sun irradiance spectrum in W/(m^2 nm), measured once per day, and an Earth radiance spectrum in W/(m^2 nm sr) for each ground pixel, with the corresponding solar and viewing geometries and geolocation. The polarisation measurements can be found in the level 1 data using an option in the extraction software of the GOME Data Processor (GDP). We used data from 22 and 23 July 1995, which were processed with GDP versions 1.43 and 1.55, respectively.

2.2 Polarisation measurements

GOME measures the polarisation of the incoming light by measuring the radiance of two perpendicularly polarised components of the incident light. This is sufficient to correct for the polarisation sensitivity of the instrument. The polarisation measurements from the three broad-band PMD detectors follow from a combination of the PMD signals with the signals from the spectrally integrated spectral channels. The polarisation measurements from the channel overlaps (OVL) follow from a combination of the signals at the end of one channel and the beginning of the next, using the fact that these have different polarisation sensitivities. The spectral ranges and effective wavelengths of the PMD and OVL polarisation measurements are listed in Table 1. (The polarisation in overlap 2 is in fact missing due to too low sensitivity.)

Table 1: Spectral ranges and effective wavelengths λ_e of the GOME polarisation measurement points in spectral order. The theoretical value p_7 is also listed. PMD=Polarisation Measuring Device, OVL=channel overlap (channel i/channel j).

p point	range (nm)	λ_e (nm)	remark
p_7	240–300	$\leq$300	theory
OVL 1 (1B/2)	311–315	313	
PMD 1	300–400	350	
OVL 2 (2/3)	(394–405)	–	low sens.
PMD 2	400–600	490	
OVL 3 (3/4)	578–611	605	
PMD 3	600–800	700	

The incident radiation has a radiance I which can be regarded as the sum of the radiances of two perpendicularly polarised beams, I_p and I_s, where the subscript p means parallel to the slit direction (equal to the flight direction) and s means perpendicular to it. The polarisation quantity in the GOME level 1 data is the so-called fractional polarisation along the flight direction, denoted by p and defined as $p = I_p/I$. We may write down two alternative formulations for p in more usual polarisation quantities:

$$p = (1 - Q/I)/2 \quad (1)$$
$$p = (1 - P\cos 2\chi)/2, \quad (2)$$

where $P = \sqrt{Q^2 + U^2}/I$ is the degree of linear polarisation and $\chi = \frac{1}{2}\arctan(U/Q)$ is the direction of polarisation ($0^\circ \leq \chi < 180^\circ$). I, Q and U are the Stokes parameters as defined by e.g. Van de Hulst (1957); the plane of reference chosen here is the local meridian plane, containing the local nadir and the viewing direction. Note that unpolarised light has $p = 0.5$. The more p is deviating from 0.5, the larger the degree of polarisation (assuming that the direction of polarisation remains unchanged).

In addition to the six polarisation measurement points, there is a so-called seventh polarisation point, denoted by p_7, which is determined from theory assuming single scattering by molecules (Stammes, 1994a). From extensive multiple scattering calculations with DAK it has been found that this assumption holds for $\lambda < 300$ nm if there is not a high aerosol loading in the stratosphere. The seventh point p_7 is calculated from Eq. (2) by assuming that the degree and the direction of linear polarisation are due to single scattering (s.s.) by molecules. $P_{s.s.}$ and $\chi_{s.s.}$ only depend on the viewing and solar geometry, so p_7 can be calculated straightforwardly in the GOME data processing (cf. Stammes, 1994a).

2.3 Polarisation-correction

In order to derive the radiance I (level 1 data) from the measured signal S (level 0 data in counts/s), the GDP performs two main calibration steps: (1) polarisation correction by transforming the polarised signal S_{pol} into an unpolarised signal S_{unpol}, and (2) radiance calibration by transforming S_{unpol} into I. We here give the main polarisation correction formula, to indicate how the GOME polarisation measurements are used in the data processing:

$$S_{unpol} = S_{pol}\, \frac{1}{2}\, \frac{1+\eta}{p(1-\eta)+\eta}, \tag{3}$$

where η is the polarisation sensitivity ratio of the GOME instrument, which is strongly wavelength-dependent (see, e.g., ESA, 1995, Fig. 6.4-2).

The above formula must be applied to the signal at each array detector wavelength. This means that the p data points, including p_7, must be interpolated in λ (see Spurr, 1994).

3 Radiative transfer model

The radiative transfer model DAK used here for validation purposes, is an application of the doubling-adding method to polarised radiative transfer in the Earth's atmosphere. The doubling-adding method is an accurate method to solve multiple scattering in a plane-parallel atmosphere (Van de Hulst, 1980). The extension of the method to include polarisation has been described by De Haan et al. (1987). The DAK model consists of an atmospheric shell around a doubling-adding radiative transfer kernel (Stammes, 1994b).

Before we will consider the actual polarisation measurements of GOME, we first show in Fig. 1 the expected spectral behaviour of the fractional polarisation p, as calculated with DAK for a simple case. Figure 1 shows $p(\lambda)$ for nadir view of a clear sky atmosphere, containing only molecules and ozone, with a Lambertian surface albedo $A_g = 0.05$. The solar zenith angle has three values: 30°, 60°, and 75°, and the relative azimuth between viewing and solar direction is assumed to be 0°. Note that the line $p = 0.5$

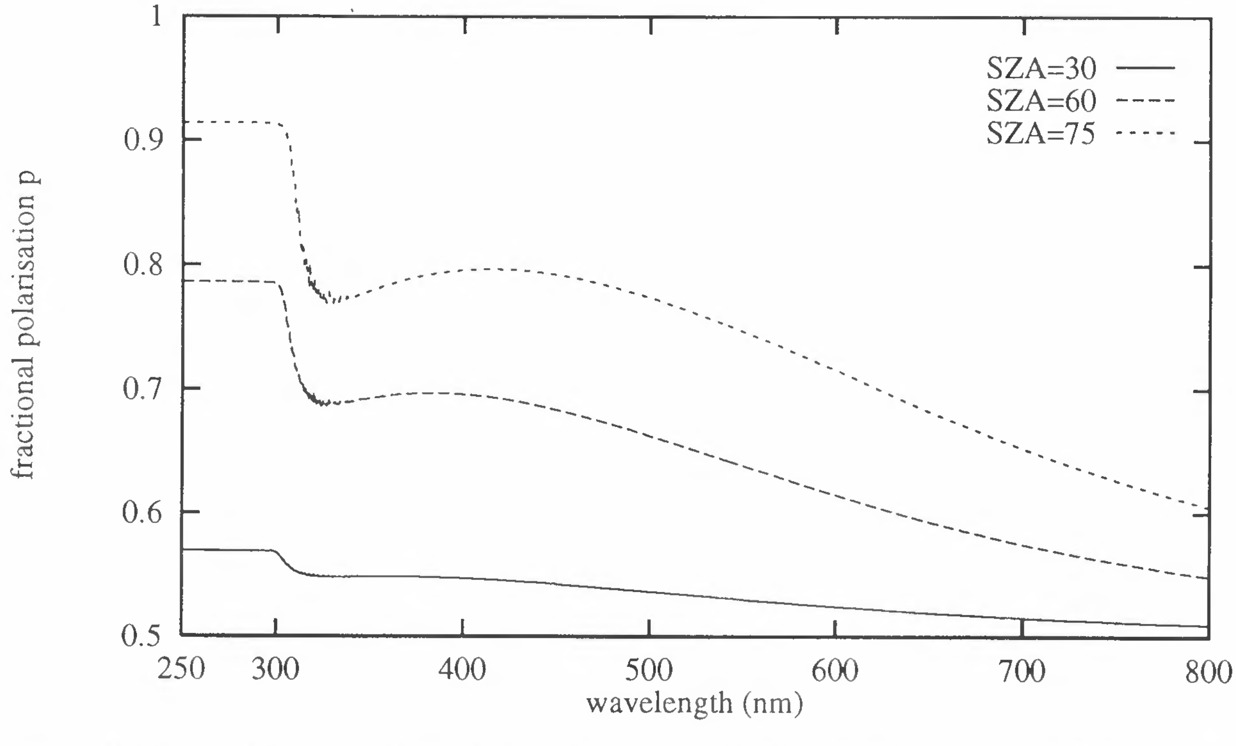

Figure 1: Fractional polarisation $p(\lambda)$ as calculated by the DAK model for nadir view and three solar zenith angles (SZA); the relative azimuth is 0° (solar direction in the plane of scanning). Atmospheric model: Mid-Latitude-Summer, with only molecular scattering and ozone absorption; no aerosol or clouds present. Surface albedo is 0.05.

denotes unpolarised light, or polarised light having $\chi = 45^o$ or 135^o. The behaviour of $p(\lambda)$ is flat below about 300 nm, then steeply falls off until about 320–330 nm, and is rather smoothly rising and then decreasing at the larger wavelengths. The small wiggles around 320 nm are due to the ozone Huggins bands. When aerosol is added to the atmosphere the general behaviour of p does not change much, but in general p becomes closer to 0.5. When the surface albedo is increased, the drop of p in the UV becomes steeper, and p becomes closer to 0.5 (i.e. unpolarised light) at the larger wavelengths. It should be noted that in this figure the single scattering polarisation value p_7 would be indistinguishable from p at 290 nm.

4 Polarisation validation

We will first give an impression of the GOME polarisation measurements by considering the variation of p along an orbit. Next we will look into the polarisation measurements of a selected pixel, and compare those with model results.

4.1 Polarisation along an orbit

As an example of the PMD polarisation measurements, Figure 2 shows p versus latitude on 23 July 1995, orbit 1337 (pixels 1 to 1200, Nadir type). This part of the orbit was entirely above the Atlantic Ocean (see the PMD cloud image in Koelemeijer et al., 1996, this issue). In this case the scene is simple: clear and cloudy sky above a dark ocean. The three PMD curves follow each other nicely, and, apart from the peaks, they approximately follow the shape of the theoretical curve of p_7. The curves for p_7 and the PMDs are in the correct spectral order for a low sun (latitude below about 30° S): p_7 has the largest deviation from 0.5, then PMD1, PMD2, and PMD3. PMD3 usually has the largest peaks, which may occur due to clouds or aerosol in the boundary layer, or surface reflection. PMD1 is less affected by these effects, because it is more sensitive to molecular scattering than PMD3. Generally, the PMD polarisation measurements show reasonable values and behaviour along the orbit. For other orbits we found a similar behaviour.

The corresponding OVL1 and OVL2 polarisation measurements of this orbit are very poor: of the considered 1200 groundpixels OVL1 yielded only 5 (strongly deviating) data points, whereas OVL2 yielded no data points at all (which was expected). On the other hand, OVL3 yielded about 1000 data points, of which the Nadir pixel values are shown in Fig. 3. However, these overlap polarisation data cannot be trusted, since their variability is unphysically large. A similar behaviour of the overlap polarisation measurements was found for other orbits.

4.2 Polarisation for a selected pixel

As an example of the GOME spectral polarisation measurements for one pixel, we chose a cloudless pixel measured on 22 July 1995, orbit 1322, over the North Sea. This pixel was cloudless according to the Meteosat image close to the time of overpass and the GOME level 2 cloud product. Figure 4 shows the three PMD polarisation points and p_7 together with DAK calculations of $p(\lambda)$. In the calculations the albedo of the (Lambertian) sea surface was varied. One of the calculations was done for a spectrally dependent albedo measured on the North Sea (Althuis and Shimwell, 1994); the others were done for a constant albedo. Clearly, even small albedo changes have an appreciable influence on the polarisation of a clear pixel. Without aerosol the correct spectral behaviour could not be reproduced; the largest deviations occurred for the sea albedo case and the $A_g = 0$ case. The addition of aerosol, of maritime type in the boundary layer and background type for free troposphere and stratosphere, led to a much improved fit. Here the aerosol was assumed to be polarising according to Mie theory and to have a total aerosol optical thickness of 0.13 at 550 nm. From this and similar analyses we conclude that the GOME polarisation measurements of clear ocean pixels can be well interpreted in terms of a realistic sea surface albedo and aerosol parameters.

5 Radiance validation

Next the GOME radiance measurements were investigated. Only data from channels 1B to 4 ($\lambda \geq 307$ nm) with IT=0.375 s were considered; data from channel 1A ($\lambda < 307$ nm), which has a longer IT, were neglected. Furthermore, the part of channel 3 between 405 and 416 nm has been omitted, because of an anomalously steep spectral behaviour due to instrument calibration problems.

For atmospheric studies a more useful quantity than the radiance is the reflectivity R, which is defined as π times the Earth's radiance I divided by the solar irradiance at the top-of-the-atmosphere (TOA), and can be written as:

$$R = I/(\mu_0 F) \tag{4}$$

where πF is the solar irradiance perpendicular to the solar direction (as measured by GOME) and μ_0 is the cosine of the solar zenith angle.

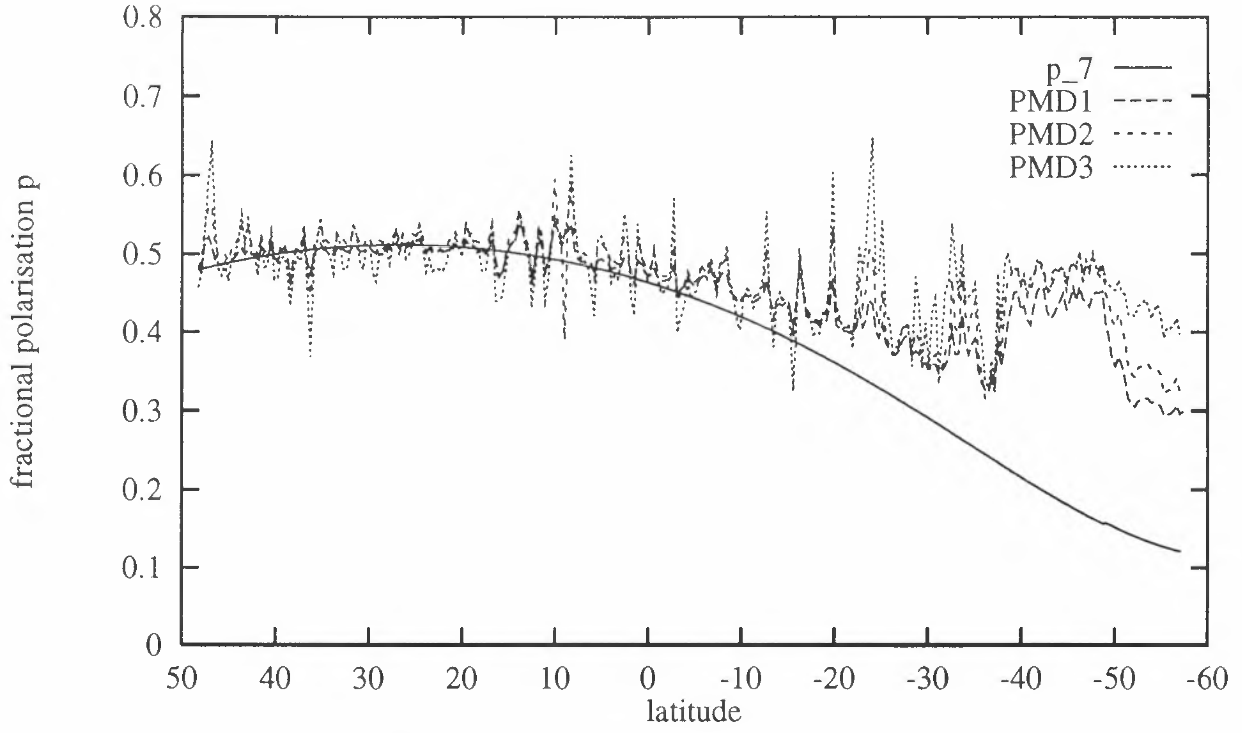

Figure 2: Fractional polarisation p as a function of latitude (+=North, −=South) as measured by the GOME PMDs on 23 July 1995, orbit 1337. Only nadir pixel data are shown. The curve of the theoretical value p_7 is also given. All pixels were above the Atlantic Ocean.

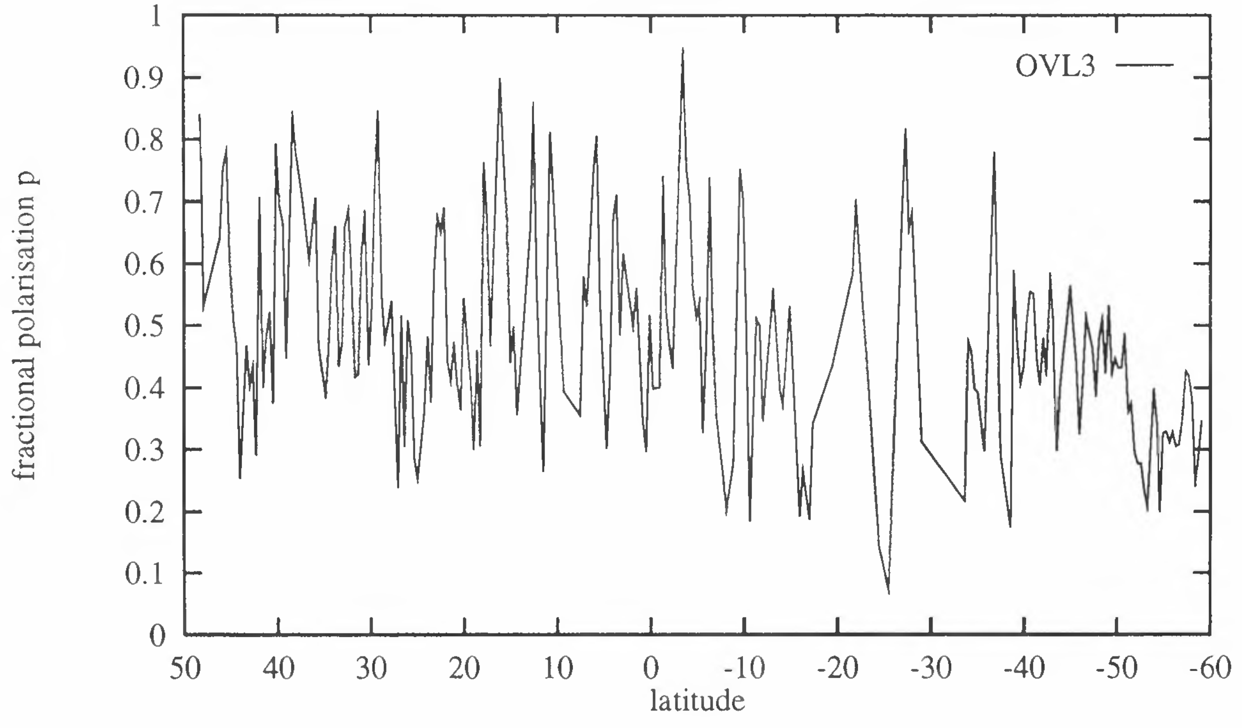

Figure 3: Same as Fig. 2, but for the OVL3 fractional polarisation.

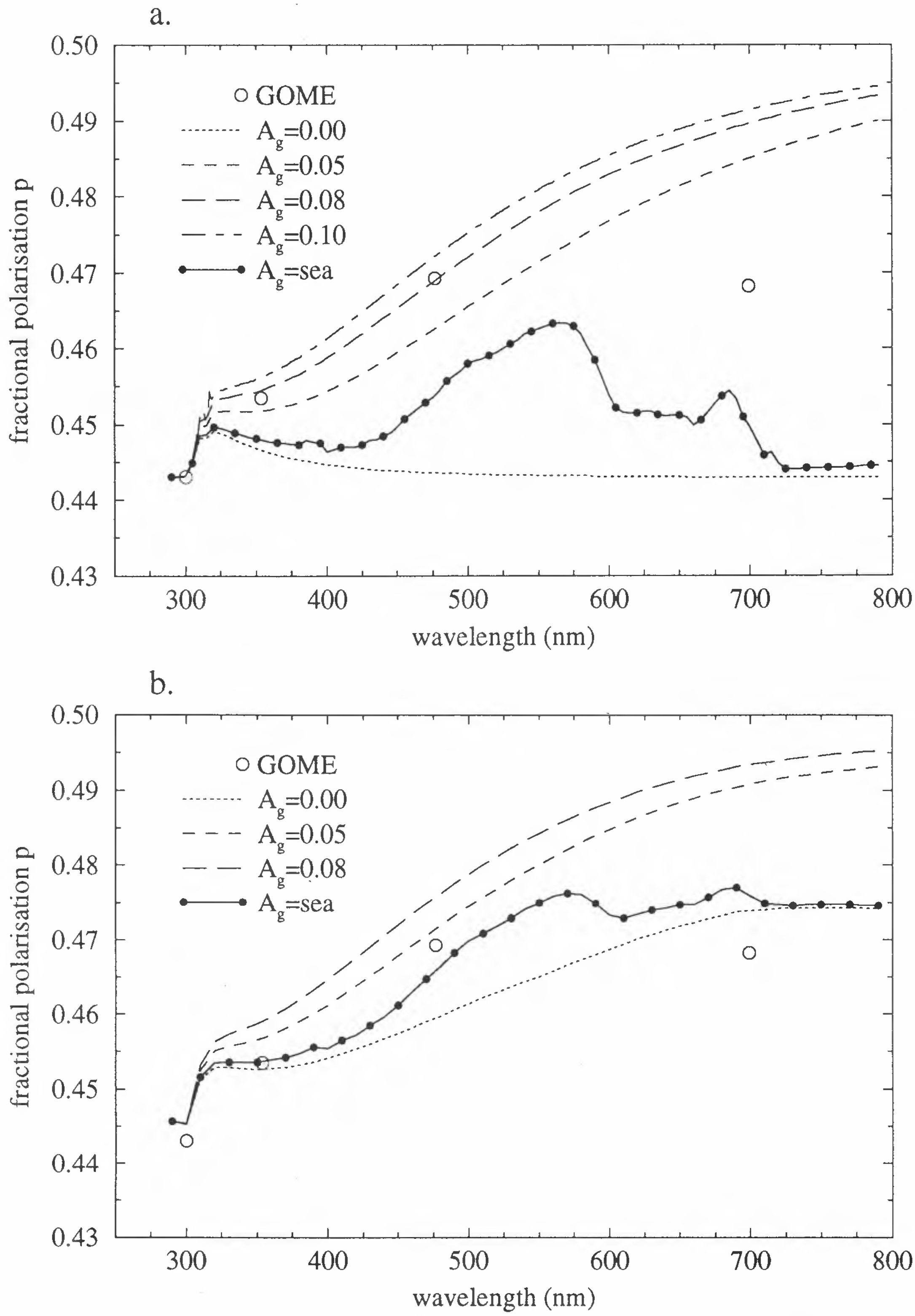

Figure 4: Spectral behaviour of the fractional polarisation p of a cloudless pixel on the North Sea as measured by the GOME PMDs together with calculated curves from the DAK model. p_7 is shown as a GOME data point. Data belong to pixel 785 (W) of orbit 1322 on 22 July 1995. Location: 55° N, 2° E; SZA=35°. (a) Calculations without aerosol (only molecular scattering, ozone absorption, and sea reflection). The sea albedo, A_g, is varied; A_g =sea denotes a spectrally dependent sea albedo. (b) Calculations include maritime aerosol in the boundary layer and background upper tropospheric and stratospheric aerosol; total aerosol optical thickness is 0.13 at 550 nm.

5.1 Occurrence of jumps

Reflectivity spectra for various scene types were investigated. Spectra of clear pixels over ocean and land looked generally as expected, but the spectra of some cloudy pixels showed jumps between the spectral channels. In Fig. 5 the spectra of two "normal" cloudy pixels over land are shown. This is the expected spectral shape for a cloudy scene: a flat, "white" reflectivity spectrum. Note the numerous gaseous absorption features, e.g. the steep rise below 300 nm due to the ozone Huggins band, the broad depression around 600 nm due to the ozone Chappuis band, the oxygen B-band at 687 nm, the water vapour band around 720 nm, and the deep oxygen A-band at 761 nm. As an example of spectra with jumps, Fig. 6 shows the spectra of two other cloudy pixels over land. Here the reflectivities measured by spectral channels 2 and 3 do not match going from 405 to 416 nm, and those measured by channels 3 and 4 do not match around 605 nm. Channel-to-channel continuity of R is of course a basic requirement for the GOME data. A further investigation showed that these channel-to-channel jumps occurred frequently and not only for cloudy (i.e. high reflectivity) scenes. As an illustration of this, Fig. 7 shows the jumps at 605 nm for orbit 1337 (the first 1200 pixels), expressed as the ratio of the reflectivities of channels 3 and 4 at 605 nm. A ratio of 1 means no jump. Apparently, jumps occur all over the orbit and in both directions. They reach in this case as high as 40–80 %.

5.2 Explanation of jumps

An extensive investigation was performed to find the cause of these reflectivity jumps. Correlations with other measurements and parameters were investigated, and some suggested explanations could be excluded:
(1) The solar irradiance spectrum did not show significant jumps, so the cause was the Earth's radiance spectrum.
(2) The GDP level 0–1 data processing did not show bugs. This was found by comparing measured GOME level 0 data (uncalibrated counts) with calculated level 0 data, as generated by the GOME Instrument Simulator (Slijkhuis, 1995) using level 1 radiances as input.
(3) An error in the key data, especially in the η-function, would cause a systematic jump, which is not found. It is known that the η-function suffers from an uncertainty, especially in the overlap regions, due to the fact that it was not measured in vacuum. Systematically deviating reflectivities in the overlaps between channels 1B and 2 (around 313 nm) and between channels 2 and 3 (around 400 nm) are indeed observed. However, the observed jumps are not limited to the overlap regions, but cover a large spectral range.
(4) No correlation of the jumps was found with the PMD p measurements, nor the p_7 value, nor the reflectivity at 755 nm (i.e. no correlation with scene brightness).
(5) The jumps at OVL2 correlated with the jumps at OVL3.
(6) A strong correlation was found between the jump at 605 nm and the OVL3 polarisation, which is illustrated by Fig. 8. This suggests that both problems, the radiance jumps and the unreliable overlap polarisations, have the same cause.

The most probable explanation of the jumps, which was suggested by TPD and ESTEC, is the *serial read-out* of the array channels. Each Reticon array is read out serially, with a time difference of 0.094 s between the first and last diode; different channels are read-out simultaneously (details are given by Callies and Lefebvre, 1996). This means that, for a 960 km swath, the scenes seen by the first and last diodes are shifted 20 km across-track in the forward scan (80 km in the backscan). For ground pixels of 80 km across-track (240 km backscan) due to the 0.375 s integration time, this is a 25 % scene difference. This can introduce large radiance differences caused by e.g. broken clouds or surface inhomogeneities. The scene differences can be most clearly seen at the overlaps, where the last diodes of one array are compared to the first diodes of another array. The serial read-out also explains the erratic overlap polarisations: if the radiances at the end of one channel and the start of the next do not belong to the same scene, then the measured overlap polarisation is useless. An observation which supports the above explanation of the jumps, is that over homogeneous scenes, such as the Sahara or fully cloud covered areas, no jumps or only small jumps are found. For example, the small jumps in Fig. 7 for pixel number > 1000 hold for the cloudy region at the lower end of orbit 1337, as shown in the PMD image of Koelemeijer et al. (1996, this issue).

The jumps will probably be reduced when the integration time of channels 1B to 4 is increased to 1.5 s, by means of co-adding four pixels of 0.375 s integration time in-orbit.

6 Conclusions

The GOME polarisation and radiance measurements have been validated by means of consistency checks, comparisons with single scattering theory, and comparisons with the polarised radiative transfer model DAK. The conclusions and recommendations that have been reached are given below in two parts.

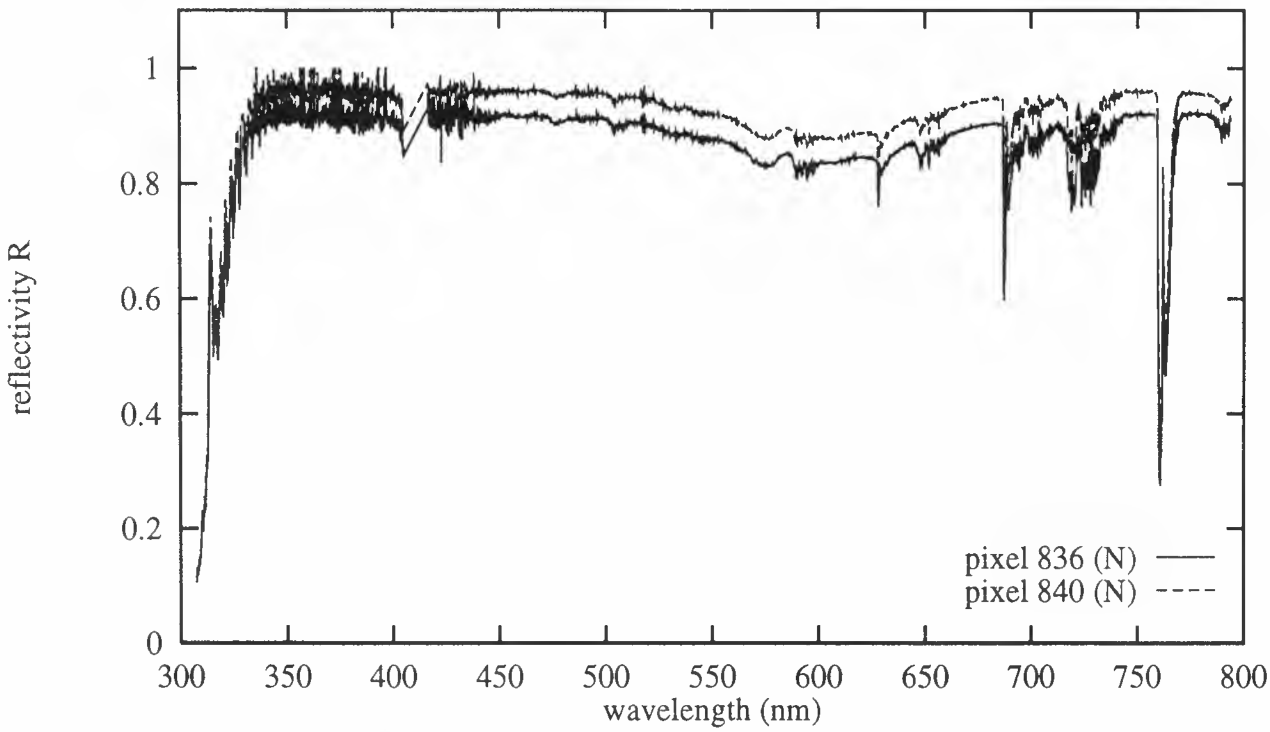

Figure 5: Spectral reflectivity of two adjacent cloudy pixels over land. Date: 22 July 1995, pixels 836 and 840 (N) of orbit 1322. SZA=31°. Location: 50° N, 5° E (Belgium).

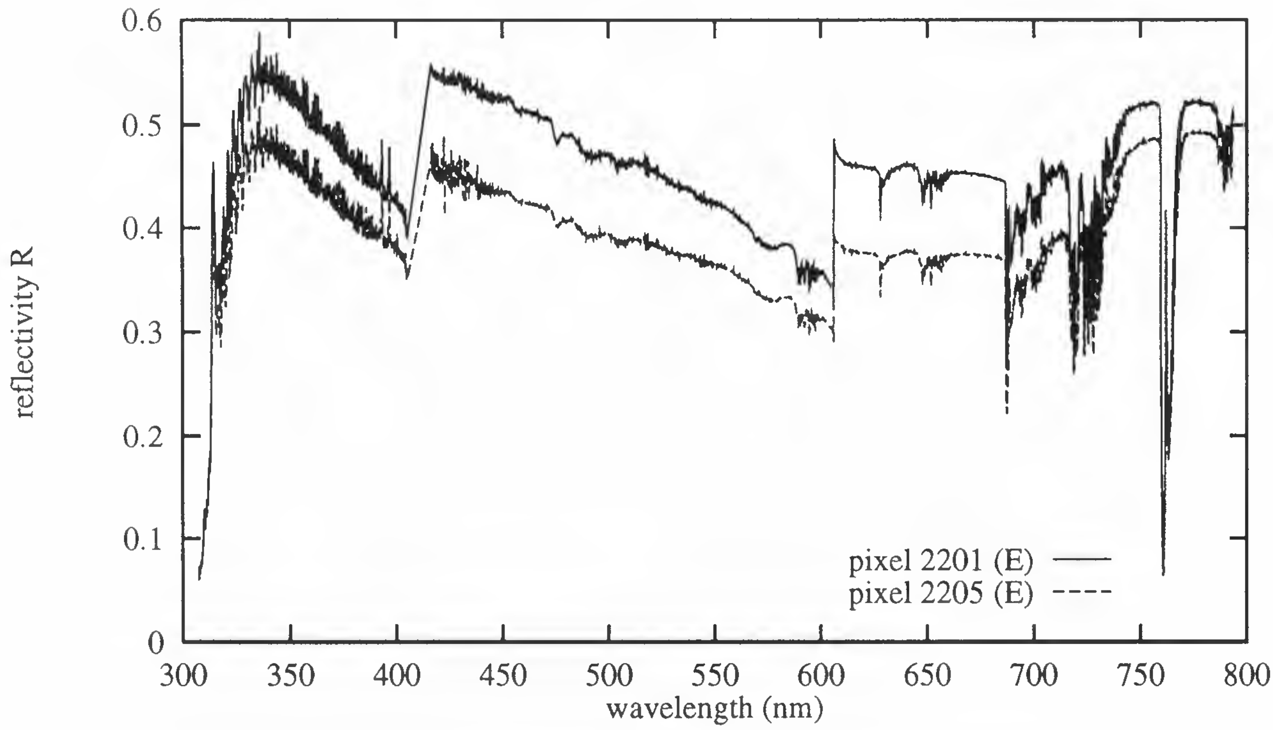

Figure 6: Spectral reflectivity of two adjacent cloudy pixels over land. Date: 23 July 1995, pixels 2201 and 2205 (E) of orbit 1335. SZA=30°. Location: 48° N, 16° E (Middle-Europe).

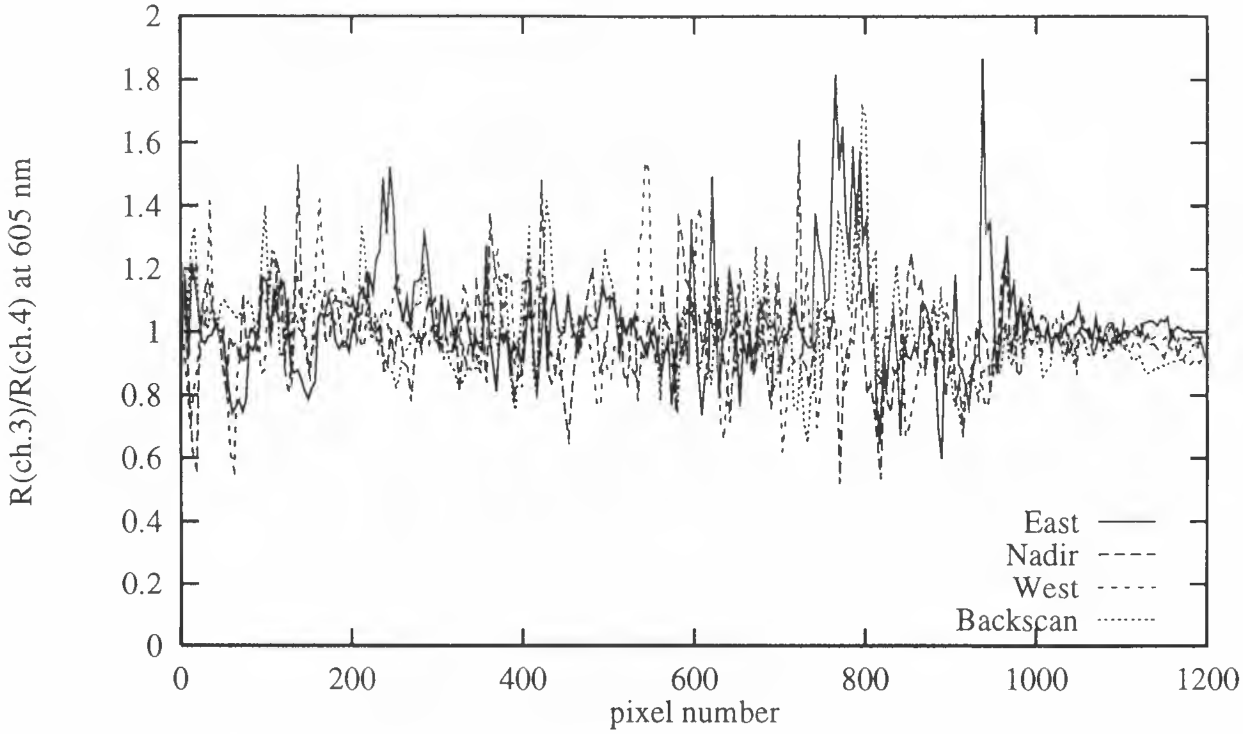

Figure 7: Reflectivity jumps between channels 3 and 4 at 605 nm, defined as R(channel 3)/R(channel 4), for the first 1200 ground pixels of orbit 1337 on 23 July 1995 (same orbit as shown in Figs. 2 and 3). The four curves belong to the four pixel types.

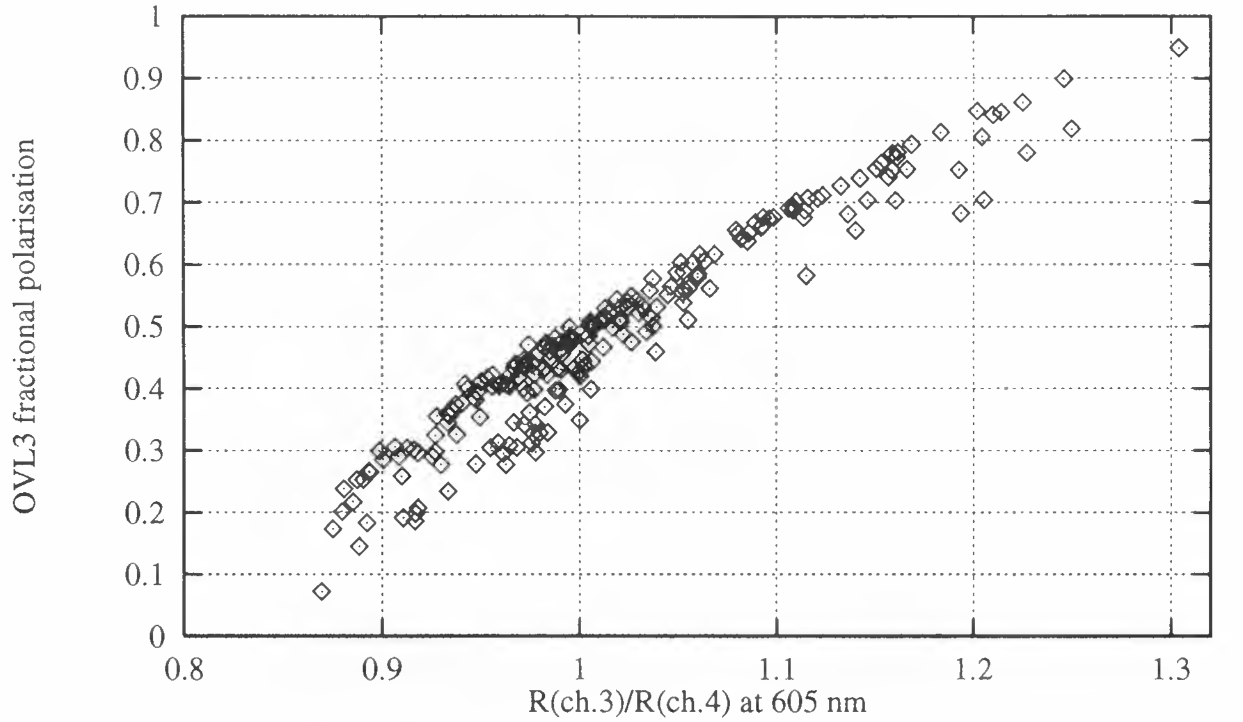

Figure 8: Correlation between the reflectivity jumps at 605 nm and the OVL3 fractional polarisations for the nadir pixels of Fig. 7.

6.1 Polarisation validation

1. The fractional polarisations measured by the PMDs are overall consistent with single and multiple scattering models.
2. The calculation of the theoretical fractional polarisation, p_7, is being performed correctly.
3. The OVL1 fractional polarisation is almost always absent or strongly deviating.
4. The OVL3 fractional polarisation is often deviating from the PMD2 and PMD3 values, and attains sometimes unphysical values. The problem with the overlap p-values is strongly correlated with the channel-to-channel radiance jumps (see below).
5. On the basis of an analysis involving pixels with a special geometry (so-called $\cos 2\chi_{s.s.} = 0$ points), systematic and random errors on the p-values of the PMDs were found. These errors are reported and discussed in this issue by Aben et al. (1996).
6. Polarisation correction of the GOME radiances should be performed on the basis of the three PMD p-values and p_7. The overlap polarisations should not be used.

6.2 Radiance validation

1. At the overlaps of the channels 2, 3, and 4 often jumps in the radiance (or reflectivity) occur, which may be tens of percent. The jumps at OVL3 are strongly correlated with the p values of OVL3.
2. The main cause of these jumps is the difference in scene observed by the detector diodes at either side of the overlap due to the serial read-out of the four diode-array detectors. It takes 0.094 s between the read-out of the first and the last diode of an array. This is 1/4-th of the integration time of 0.375 s used in the GOME validation phase. Hence the diodes at the end of one channel and at the beginning of the next, share only 75 % of their field-of-views. In case of inhomogeneous scenes (e.g. cloudy scenes) large jumps in reflectivity may occur. For homogeneous scenes (e.g. Sahara) it has been observed that the jumps are smaller. A secondary cause is the difference in instantaneous field-of-view between detector pixels. This has been noted in the on-ground calibration, and during solar observation (see Slijkhuis, 1996).
3. Apart from the jumps, the reflectivity spectra are qualitatively correct. Many spectral features can be discovered, e.g. those of trace gases, vegetation, soil, aerosols, clouds, and Ring effect.
4. For spectral studies involving a large GOME wavelength range, or spectral studies needing absolutely calibrated radiances, spectra should be checked for jumps. This is a check for spectral integrity.

Acknowledgements

The work presented here was performed in the framework of GOME validation project NL-109. ESA and DLR (Oberpfaffenhofen) have kindly provided help with using the GOME data and processing software. Discussions with J.F. de Haan, J.W. Hovenier, and W.J. Knibbe of Vrije Universiteit Amsterdam and S. Slijkhuis of SRON are gratefully acknowledged. The work was partly funded by Space Research Organization Netherlands (SRON) through project EO-009.

References

Aben, I., M. Dobber, D.M. Stam, P. Stammes, 1996, "Error analysis of polarisation measurements by GOME", this issue

Althuis, W., and Shimwell, 1994, "Interpretation of remote sensing imagery for suspended matter monitoring in Coastal waters", EARSeL workshop on Remote sensing, GIS and Coastal Zone Management, 24-26 October 1994, Delft, The Netherlands

Callies, J., Lefebvre, A., 1996, "GOME PMD reading timing", Fax of 11 Jan. 1996, Ref. LTP/0271/JC-uu, ESTEC, Noordwijk

De Haan, J.F., P.B. Bosma, and J.W. Hovenier, 1987, "The adding method for multiple scattering calculations of polarized light", Astron. Astrophys. **183**, 371–391

ESA, 1993, *GOME Interim Science Report*, ESA SP-1151, ESA/ESTEC, Noordwijk

ESA, 1995, *GOME Users Manual*, ESA SP-1182, ESA/ESTEC, Noordwijk

Koelemeijer, R.B.A., P. Stammes, A.J. Feijt, A.C.A.P. van Lammeren, 1996, "First validation of GOME cloud observations", this issue

Slijkhuis, S., 1996, "GOME instrument properties affecting the calibration of radiance and polarisation", this issue

Slijkhuis, S., 1995, "GOME/SCIAMACHY Instrument Simulation Software", Report GO/SCIA-IS-TR01, SRON, Utrecht

Spurr, R., 1994, "GOME level 0 to 1 algorithms description", Report ER-TN-DLR-GO-0022, Issue 3A, DLR/DFD, Oberpfaffenhofen

Stammes, P., 1994a, "The seventh point polarisation algorithm", Internal Report, KNMI, De Bilt

Stammes, P., 1994b, "Errors in UV reflectivity and albedo calculations due to neglecting polarisation", SPIE Proceedings Vol. 2311, *Atmospheric Sensing and Modeling*, 227–235

Van de Hulst, H.C., 1957, *Light scattering by small particles*, J. Wiley & Sons, New York (also: Dover, 1981)

Van de Hulst, H.C., 1980, *Multiple Light Scattering, Tables, Formulas, and Applications, Volume 1 and 2*, Academic Press, New York

ERROR ANALYSIS OF POLARISATION MEASUREMENTS BY GOME

I. Aben[1], M.R. Dobber[1], D.M. Stam[2] and P. Stammes[2]

[1)] Space Research Organization Netherlands (SRON)
Sorbonnelaan 2, 3584 CA Utrecht, The Netherlands

[2)] Royal Netherlands Meteorological Institute (KNMI)
P.O. Box 201, 3730 AE De Bilt, The Netherlands

ABSTRACT

At defined locations along the GOME orbit the geometrical conditions are such that the fractional polarisation, which is measured by GOME, can be predicted from the illumination and viewing geometry only. Deviations from this predicted value at these locations are used to assess the systematic and random errors of the polarisation measurements of the Earth by GOME. Only PMD polarisation measurements are considered, as the polarisation measurements obtained from the spectral overlap regions are not considered reliable at present. The analysis is applied separately to data corresponding to large ground pixels of size 40 x 80 km^2 (along x across track) and to small ground pixels of size 52 x 2 km^2.

The systematic errors in fractional polarisation determined in this way are less than 0.02, thus less than a few percent. The resulting relative error in the radiances will be of similar magnitude. The systematic errors deduced for the two different sizes of ground pixels are very similar and suggest the need for out-of-band straylight correction for PMD 1 and PMD 2.

Furthermore, it is shown that the random errors in fractional polarisation for the large ground pixels are 1 to 2 orders of magnitude larger than those obtained for the small ground pixels. This is due to variation of the illumination and viewing geometry, and scene across the ground pixels. Such a variation is clearly more pronounced for the larger ground pixels. The random errors for the small ground pixels are the worst for PMD 3 but are still less than 1 %. This observed random error for PMD3 is most likely related to assumptions concerning the out-of-band straylight correction used in the level 0→1 polarisation correction algorithm.

An orbit propagator was used to derive the variation of geometrical parameters across ground pixels. Single scattering theory for molecules was then used to determine variations across ground pixels of the polarisation characteristics of atmospheric light at short wavelengths ($\lambda \leq 300$ nm) as observed by GOME.

1. INTRODUCTION

GOME has been designed to measure accurately the Earth's radiance from 240 to 790 nm. However, GOME is a polarisation-sensitive instrument and the atmospheric spectrum of the Earth is in general polarised. To correct for its polarisation-sensitivity, GOME measures the polarisation in six wavelength bands by means of three Polarisation Measuring Devices (PMDs) and by using the three polarisation-sensitive spectral overlap regions. The wavelength bands covered by the three PMDs are for PMD 1 : 295 - 397 nm, for PMD 2 : 397 - 580, and for PMD 3 : 580 - 745 nm. The spectral overlap regions are defined around the cross-over-points where the signals from the two channels are equal. For channel 1-2 overlap the cross-over-point is at λ = 313.4 nm and for channel 3-4 overlap at λ = 606.5 nm. There is no cross-over-point for the spectral overlap of channel 2-3 [*ESA*, 1995]. A seventh polarisation point, p_7, is calculated in the GOME data processing from single Rayleigh scattering by molecules and only depends on the illumination and viewing geometry. This single scattering assumption is valid for atmospheric light in the UV ($\lambda \leq 300$ nm) [*Stammes*, 1994a]. An interpolation scheme is used to reproduce the polarisation curve across the entire wavelength range of GOME [*DLR*, 1995].

This paper presents an analysis to assess the systematic and random errors of the polarisation measurements by GOME and thus validates these measurements. The analysis is based on the identification of locations along the GOME orbit where the polarisation measurements can be predicted based on the illumination and viewing geometry alone.

The method used to assess these errors will be explained in the next section. The errors obtained for data corresponding to different ground pixel sizes are then summarized. A discussion on possible causes for the observed systematic and random errors is presented thereafter. Finally, a suggestion is made which could improve the PMD 1 and PMD 2 polarisation measurements.

2. ANALYSIS METHOD

The amount of circularly polarised light reflected by the Earth's atmosphere is negligible [*Coulson*, 1988], and therefore only linearly polarised light needs to be considered. Linearly polarised light can be described by the Stokes parameters I, Q and U. The Stokes parameters are defined, relative to any reference plane, as follows [*Van de Hulst*, 1957] :

$$I = I_{0^\circ} + I_{90^\circ} \qquad (1)$$
$$Q = I_{0^\circ} - I_{90^\circ} \qquad (2)$$
$$U = I_{45^\circ} - I_{135^\circ} \qquad (3)$$

where I is the total intensity and Q and U fully represent the linear polarisation. In Eq. (1) - (3) the angles denote the direction of the transmission axis of a linear polariser, relative to the reference plane.The degree of linear polarisation P is given by [*Van de Hulst*, 1957; *Stammes*, 1994a] :

$$P = (Q^2 + U^2)^{1/2}/I \qquad (4)$$

The direction of polarisation χ relative to the reference plane is :

$$\chi = 1/2 \arctan(U/Q) \qquad (5)$$

In the following, we choose the local meridian plane as the reference plane, i.e. the plane of the local zenith and the viewing direction.

For polarisation correction purposes, GOME only measures the fractional polarisation p, which is defined as the ratio of the radiance polarised along the entrance slit of GOME to the total radiance. The fractional polarisation p is related to P and χ as follows :

$$p = 1/2\,(1 - P \cos 2\chi) \qquad (6)$$

Both parameters P and χ, and thus p, are in principle wavelength-dependent. However, extensive multiple scattering calculations with the polarisation radiative transfer model Doubling-Adding KNMI (DAK) [*Stammes*,1994b] have shown that in general χ can be well approximated by its single scattering value, $\chi_{s.s.}$. This is illustrated in Figure 1, where χ is shown as a function of wavelength for arbitrary ground pixels along GOME orbit 1335, and thus for varying geometries. The single scattering value $\chi_{s.s.}$ can be calculated directly from the illumination and viewing geometry [*Stammes*, 1994a], the Sun-Earth-satellite geometry. The degree of polarisation P, however, is a quantity which can vary drastically with wavelength and scene. Therefore, p can vary also with wavelength and scene.

Fortunately, at defined locations along the GOME orbit the geometrical conditions are such that $\cos 2\chi_{s.s.}$ is exactly zero. From Eq.(6) and the approximation of χ by $\chi_{s.s.}$, it is clear that at these locations the fractional polarisation p should be equal to 0.5 independent of P, thus for all wavelengths and for any atmospheric condition. When the measured p deviates from 0.5 at these locations, this deviation implies an error in the estimate of p. Results of an analysis based on this principle will be presented in the next section.

3. RESULTS

Here results of the $\cos 2\chi_{s.s.}=0$ analysis are given for polarisation measurements of a number of GOME orbits. Only the PMD polarisation measurements are considered in this study, because the polarisation measurements determined from the spectral overlap regions are presently not reliable. First the behaviour of $\cos 2\chi_{s.s.}$ is considered.

In Figure 2 the value of $\cos 2\chi_{s.s.}$ is shown along orbit 1335 of July 23, 1995, as a function of geographical latitude for east, nadir and west pixels. The theoretical fractional polarisation values p_7 (the seventh point) for this orbit are shown in Figure 3. The pixels at the locations where $\cos 2\chi_{s.s.}=0$, correspond to the locations in Figure 3 where $p_7=0.5$. The integration time for these pixels is 0.375 s and the size of the ground pixel is 40 x 80 km^2. The jumps in $\cos 2\chi_{s.s.}$ around 48^0 S and above 70^0 N are due to a stepwise increase in integration time for large solar zenith angles. The backscan pixels are not considered as they are larger than the other pixels.

The $\cos 2\chi_{s.s.}=0$ analysis was first applied to all the available orbits of July 23, 1995. Here 44 pixels were identified to fulfil the $\cos 2\chi_{s.s.}=0$ condition. The corresponding 44 fractional polarisation measurements for each PMD are plotted in Figure 4. The average deviation of these measurements from p=0.5 (i.e., the systematic error) and their spread (i.e., the random error)

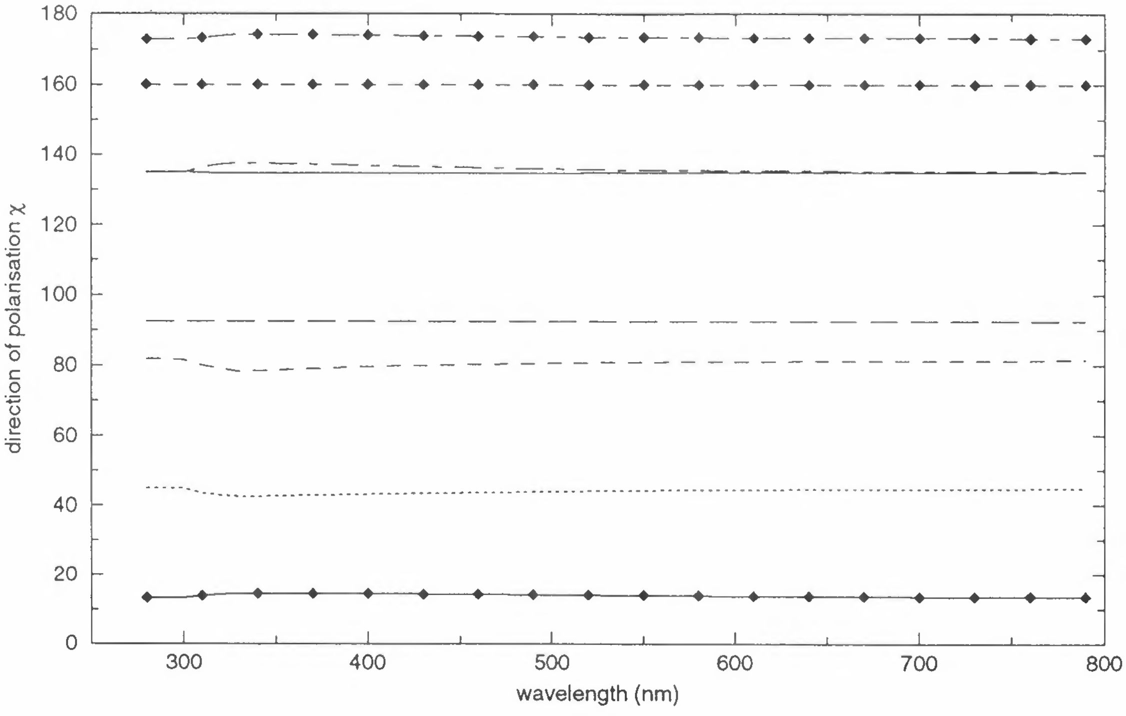

Figure 1 Direction of polarisation χ as a function of wavelength for a number of arbitrary GOME geometries along orbit 1335 July 23, 1995. All calculations were performed for a Midlatitude Summer profile [*McClatchey et al.*, 1972] and a surface albedo of 0.

Table 1
Systematic and random errors in fractional polarisation p for all orbits of July 23, 1995.

	PMD 1	PMD 2	PMD 3
systematic error	0.005	0.018	-0.003
random error (1 σ)	0.01	0.025	0.06

are tabulated in Table 1.
To study the most homogeneous ground pixels, the same analysis was done for the orbits where the scan mirror was fixed in the nadir position. This is called the nadir static mode. The data obtained in this mode are from July 3, 1995. The integration time is 1.5 s and the size of the ground pixels is 52 x 2 km^2 (this results from the IFOV of 2.87^0 * 0.14^0 [*ESA*, 1995] and the satellite velocity of 7.5 km/s with respect to the surface). Due to the longer integration time a large number of spectra from this dataset were saturated and could not be used in this analysis. Only 13 measurements for each PMD were used, which are shown in Figure 5. The deviation and spread obtained for these measurements are tabulated in Table 2.

Table 2
Systematic and random errors in p for the nadir static orbits of July 3, 1995.

	PMD 1	PMD 2	PMD 3
systematic error	0.007	0.012	-0.004
random error (1 σ)	0.0002	0.0002	0.003

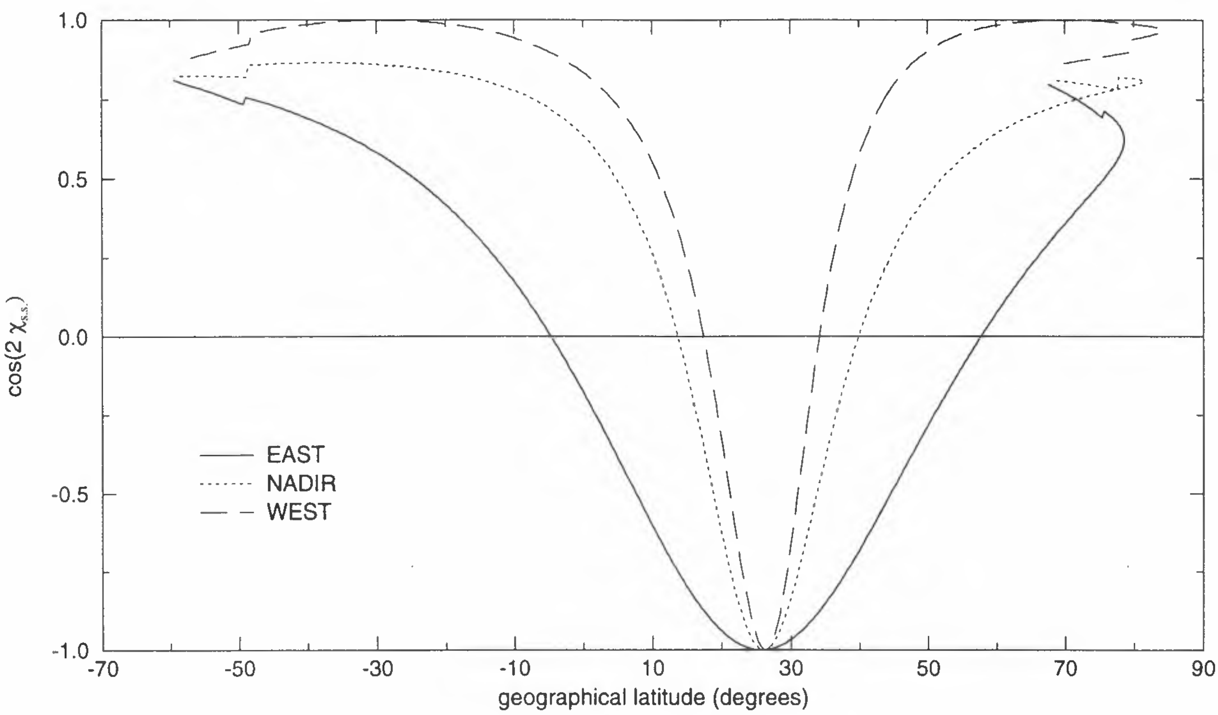

Figure 2 $\cos 2\chi_{s.s.}$ along orbit 1335 July 23, 1995.

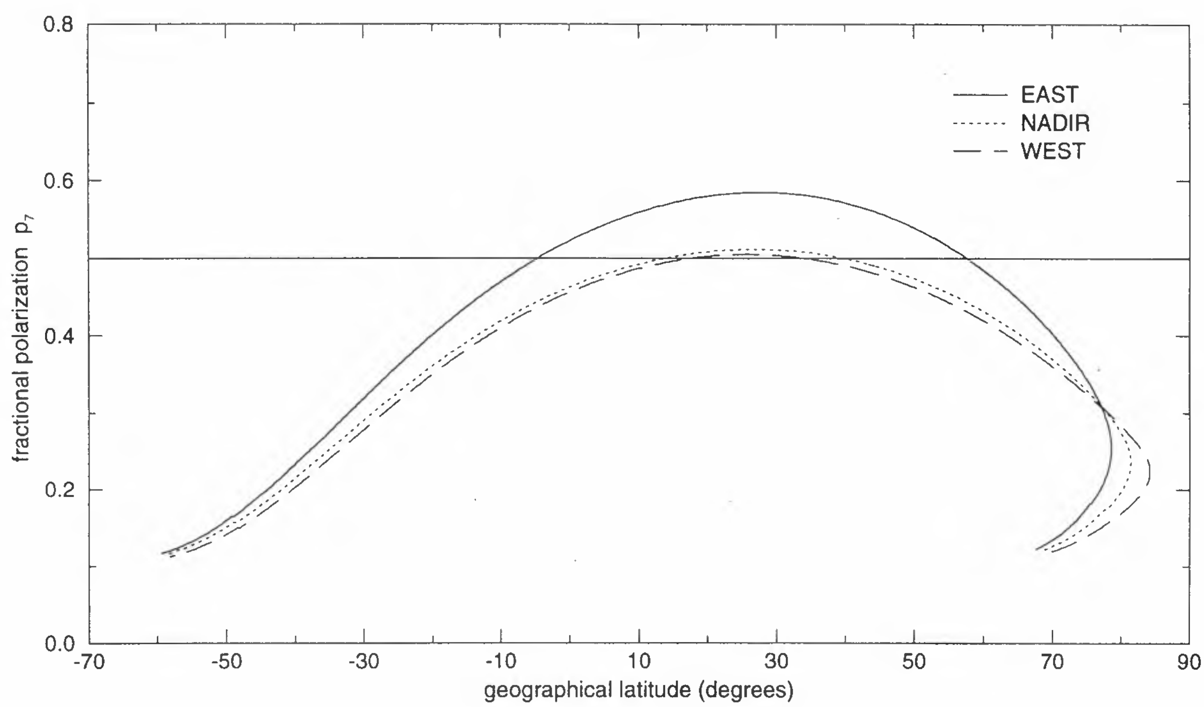

Figure 3 Fractional polarisation p_7 along orbit 1335 July 23, 1995.

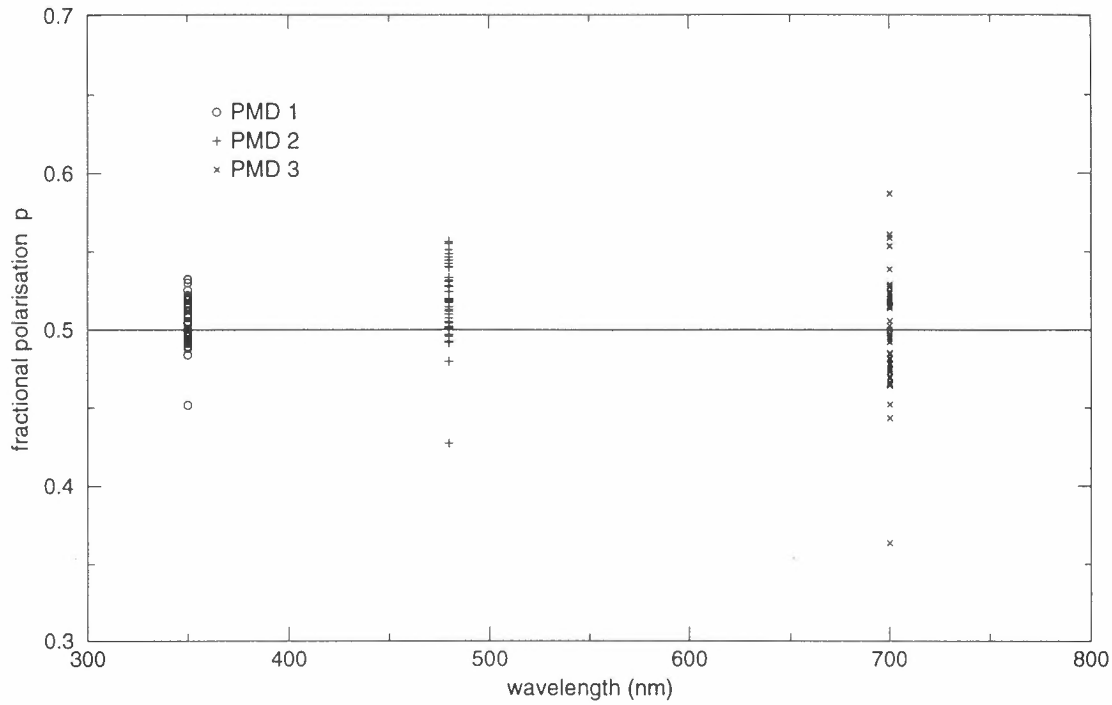

Figure 4 Fractional polarisation p measured by GOME July 23, 1995, at the $\cos 2\chi_{s.s.}=0$ locations.

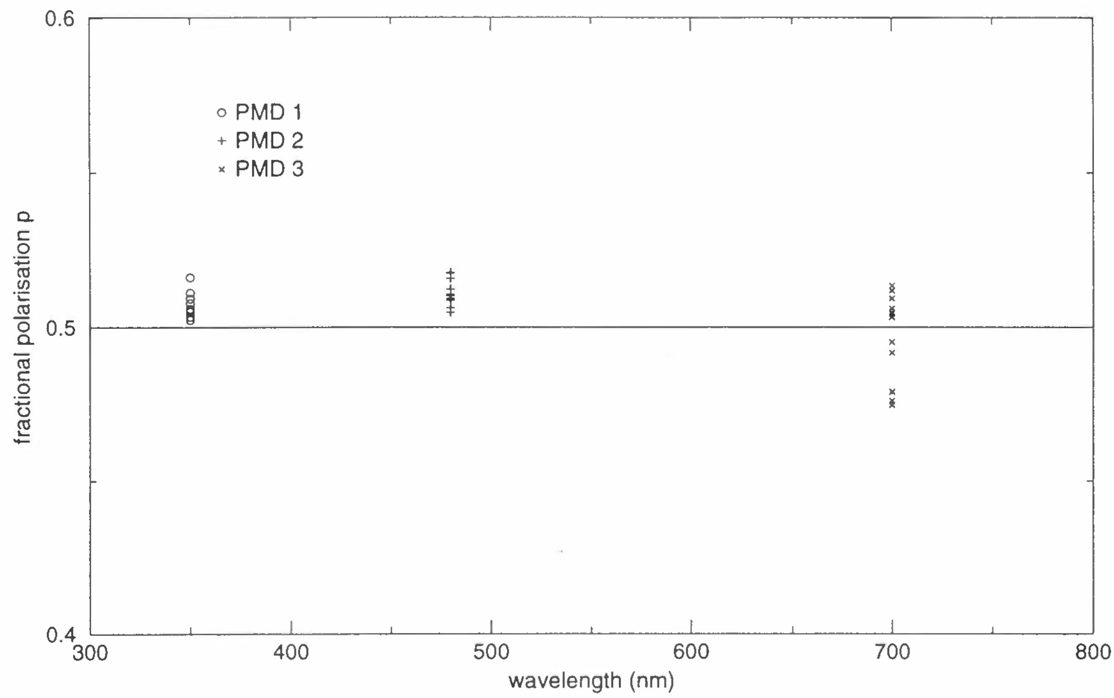

Figure 5 Fractional polarisation p measured in nadir static mode by GOME July 3, 1995, at the $\cos 2\chi_{s.s.}=0$ locations.

It can be concluded that for both datasets the systematic errors are largest for PMD 2 and the random errors are largest for PMD 3.

4. DISCUSSION OF ERRORS

Systematic errors

The systematic errors for the fractional polarisation p, as determined in the present paper, are less than a few percent (relative errors). The effect of these systematic errors on the systematic errors of the polarisation corrected Earth spectral radiances are of the same order of magnitude.

The systematic errors deduced for the large and small (static) ground pixels are very similar. This suggests that this error is not caused by phenomena related to the size of the observed scene or its inhomogeneity. Systematic errors as found in the present study, could suggest a slight misorientation of the main polarisation axes of the PMDs relative to the corresponding spectral channels. The measurements by TPD [*TPD*, 1994a] however, show no evidence to confirm this statement.

Furthermore, it was known that the DLR processing software used in this analysis produced slightly incorrect geolocation information [*DLR*, 1996]. However, the error introduced by this small effect should be similar for all three PMDs. Furthermore, this geolocation information was correct for the nadir static orbits. It is therefore concluded that the slightly incorrect geolocation information is not the cause for the observed systematic errors.

More likely, out-of-band straylight, which is not corrected for PMD 1 and PMD 2, causes the observed systematic deviations. The PMD out-of-band straylight measurements by TPD [*TPD*, 1994b; *TPD*, 1995] showed that the PMDs are sensitive to light beyond 790 nm. The correction for this out-of-band straylight is deduced from the GOME measurement of the solar spectrum and is based on the fact that the solar spectrum is known to be unpolarised. It is assumed that this correction is also appropriate when measuring an unpolarised Earth spectrum. The polarisation of a given PMD is then assumed to take the same (constant) value in the out-of-band straylight region [*DLR*, 1995]. This estimate is most appropriate for PMD 3, which has a wavelength range adjoining the straylight region beyond 790 nm. The correction for out-of-band straylight turns out to be by far the largest for PMD 3, where this correction reduces the value of the fractional polarisation with ~ 17 % [*Aberle,* 1996]. Although slight correction factors are found for PMD 1 and PMD 2 [*Slijkhuis*, 1996], no out-of-band straylight correction is applied for PMD 1 and PMD 2.
It is concluded from this analysis that the out-of-band straylight correction for PMD 3 works quite well for cases where $p = 0.5$. The remaining systematic error in p is less than 1 %. Application of the out-of-band straylight correction to PMD 1 and PMD 2 is expected to result in a decrease of their systematic errors, as suggested by this analysis.

Random errors

Differences observed between the random errors obtained for large and small (static) ground pixels are explained by two phenomena. The first reason is the variation of geometrical parameters across the ground pixels. Using an orbit propagator the variation in solar zenith angle, relative azimuth and view zenith angle was calculated along and across the GOME track. In Figures 6 and 7 the variations in $\cos 2\chi_{s.s.}$ and p_7 are shown for July 23, 1995 at 50^{0}N. Each rectangle in these figures represents a 40 x 40 km pixel; the arrow denotes the GOME flight direction. From these figures it is clear that the variation in $\cos 2\chi_{s.s.}$ and p_7 across track is much larger that the variation along track. It can thus be concluded from these figures that the effect of variation in $\cos 2\chi_{s.s.}$ is negligible for the observations made in nadir static mode, but could be important for the observations in scanning mode.

The second contribution to the random errors for larger ground pixels is due to the higher probability of observing an inhomogeneous scene. This introduces errors through the level $0 \rightarrow 1$ polarisation correction algorithm, which is based on the assumption of observing homogeneous scenes. Both effects are less severe in the case of observations in nadir static mode. This is clearly reflected in the results obtained in this study. The random errors for the large ground pixels are 1 to 2 orders of magnitude larger than those obtained for the small (static) ground pixels.

It was recognized that due to sequential readout of the array pixels the first and last array pixel of the spectral channels observe a somewhat shifted scene [*Stammes et al.*, 1996]. For the ground pixels of size 40 x 80 km^2 the scenes of the first and last array pixel are shifted by about 20 km across track. This could give rise to an error

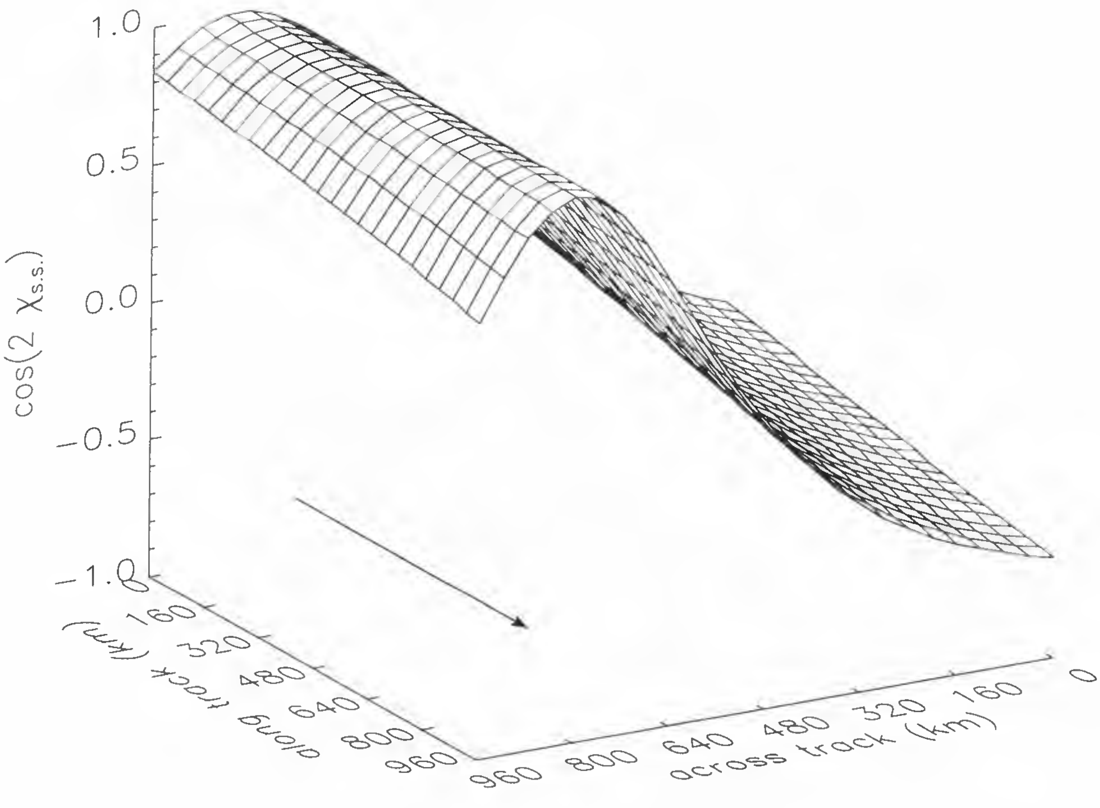

Figure 6 $\cos 2\chi_{s.s.}$ along and across the GOME track for July 23, 1995, at 50⁰N.

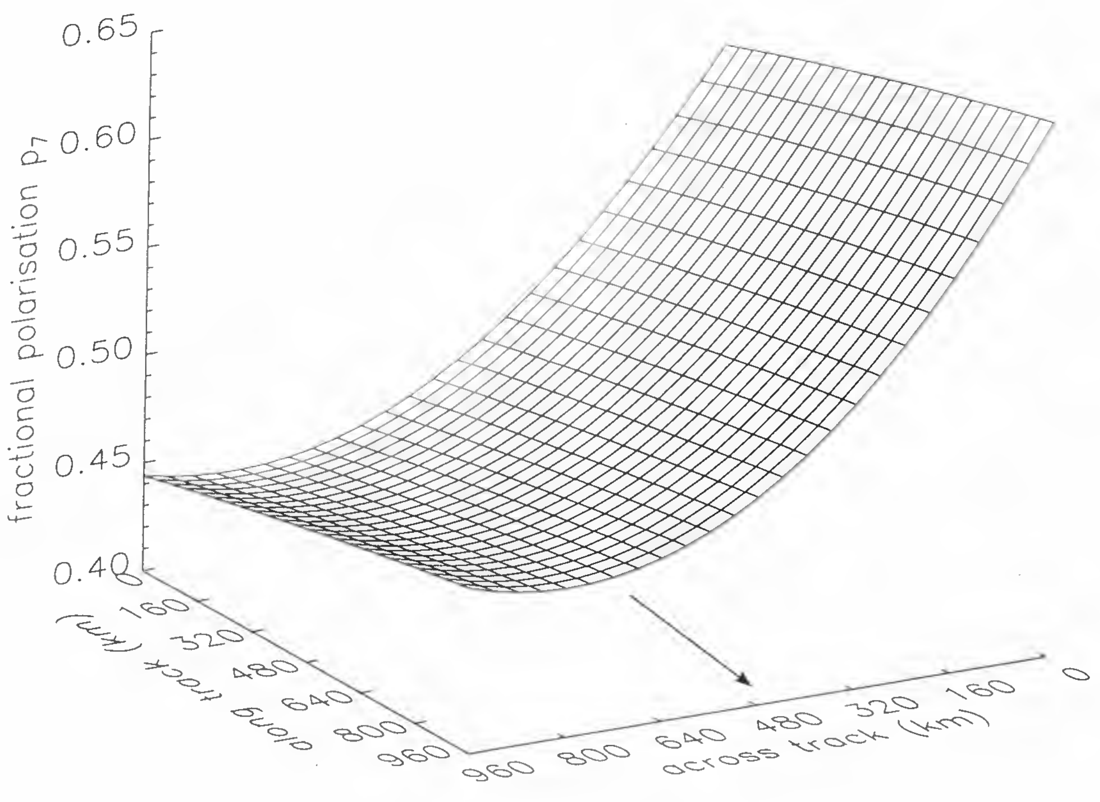

Figure 7 p_7 along and across the GOME track for July 23, 1995, at 50⁰N.

in the PMD polarisation measurements. However, for the data obtained in nadir static mode the two scenes are shifted by only 0.7 km along track, which will not influence the polarisation measurements.

In the case of the nadir static ground pixels, the random error obtained for PMD 3 is one order of magnitude larger than the random errors obtained for PMD 1 and PMD 2. One explanation for the spread in p is based on atmospheric scattering considerations. Scattering in the atmosphere by molecules, aerosols, and clouds and reflection by polarising surfaces, is capable of changing the direction of polarisation χ. However, this change of χ has a wavelength dependence which suggests the largest variations for PMD 1.
The observed large random error in the fractional polarisation for PMD 3 could more likely be related to the out-of-band straylight correction. This correction assumes that the out-of-band straylight correction for an unpolarised Earth spectrum is equal to the correction for the solar spectrum and independent of the actually observed spectrum. It is possible that for instance the presence of clouds or varying water absorption influences the amount of out-of-band straylight. As the out-of-band straylight correction is largest for PMD 3, the error introduced by this effect will be most pronounced for PMD 3.

5. CONCLUSIONS

The $\cos 2\chi_{s.s.}=0$ analysis presented here has proved to be a useful diagnostic to assess the systematic and random errors in the fractional polarisation measured by GOME. Therefore, the effect of future processing software updates for GOME should be evaluated by means of this analysis. Preferably, it should be applied on data obtained with GOME operated in the nadir static mode to avoid complications introduced by the effect of measuring across (inhomogeneous) large ground pixels.
It is concluded that the PMD measurements of fractional polarisation p considered in this study are accurate to within a few percent. This is considered adequate for the purpose of the polarisation correction of the radiances.
It is concluded that the out-of-band straylight correction for PMD 3 works quite well for cases where p=0.5. Furthermore, improvements for PMD 1 and PMD 2 are anticipated after application of a correction for the out-of-band straylight.

ACKNOWLEDGEMENTS

The work presented here was performed in the framework of GOME validation project NL-109. Discussions with Dr. S. Slijkhuis are gratefully acknowledged. The DLR-team is acknowledged for their assistance on software and level 0 → 1 algorithm issues.

REFERENCES

Aberle, B., 1996, DLR, private communication.

Coulson, K.L., 1988, "Polarisation and intensity of light in the atmosphere", A. Deepak Publ., Hampton (VA).

DLR, 1995, Report ER-TN-DLR-GO-0022, "GOME level 0→1 algorithms description".

DLR, 1996, 9th GOME Calibration and Characterisation Committee Meeting, 8 Jan. 1996, Oberpfaffenhofen, Germany.

ESA, 1995, SP-1182 ESA, "GOME Users manual".

McClatchey, R.A., R.W. Senn, J.E.A. Selby, S.E. Volz, J.S. Garing, 1972, "Optical properties of the atmosphere", 3rd edition Report AFCRL-72-0497, U.S. Air force Cambridge Research Labs.

Slijkhuis, S., 1996, "GOME instrument properties affecting the calibration of radiance and polarisation", this issue.

Stammes, P., 1994a, "The seventh point polarisation algorithm", Internal report, KNMI, De Bilt.

Stammes, P., 1994b, "Errors in UV reflectivity and albedo calculations due to neglecting polarisation", SPIE Vol. 2311, Atmospheric Sensing and Modelling , pp. 227 - 235.

Stammes, P., D.M. Stam, R.B.A. Koelemeijer, I.Aben, 1996, "Validation of GOME polarisation and radiance measurements", this issue.

TPD, 1994a, Report TPD-ERS-GO-MIR-28, "Polarization properties of GOME FM".

TPD, 1994b, Report TPD-ERS-GO-TN-96, "Out of band straylight in the GOME PMD channels".

TPD, 1995, Report TPD-ERS-GO-MIR-29, "Straylight measurements of GOME FM".

Van de Hulst, H.C., 1957, "Light scattering by small particles", J. Wiley & Sons, New York.

GOME instrument properties affecting the calibration of radiance and polarisation

S. Slijkhuis

Space Research Organisation Netherlands,
3584 CA Utrecht, NL

Abstract

During the GOME validation period a number of instrumental effects were noticed, which potentially limit the accuracy of the radiance and polarisation calibration. This paper describes three such effects.

Time delay between detector pixel readouts, and small misalignenments in field-of-view of the various detectors, may affect the spectral radiance in case of scene noise. This shows up most clearly as 'jumps' in radiance between the channels. In the measurement mode used sofar, intensity 'jumps' of up to 20% were observed.

Spectral intensity oscillations observed in channels 3 and 4 (400-790 nm) during solar calibration may interfere with trace gas absorptions on the 10^{-3} level.

Stray signals in the polarisation measuring detectors potentially limit the accuracy of atmospheric polarisation retrieval, and the associated corrections to the radiance calibration.

1. Introduction

In a study of the GOME 'level 0' data from solar calibration measurements, a few instrument anomalies were noticed. These are related to field-of-view of the main channels detectors, which record the spectrum from 240-790 nm, and to spectral oscillations in these channels. It was also noticed that the Polarisation Measurement Devices (PMDs) measure more signal than expected from ground-calibration data. This difference in signal is often referred to as 'PMD straylight', but its origin (whether it is straylight or not) is not known.

The GOME 'level 1' data (calibrated radiances) often show 'jumps' in intensity between the various channels (see e.g. the paper of P. Stammes in these proceedings). This is generally attributed to the fact that different detector pixels, especially those in neighbouring channels, 'see' a different ground scene. Other possible causes which have been suggested are errors in the polarisation retrieval, and errors in the on-ground polarisation-sensitivity calibration. In the next Section it is shown that the latter effects are not the (main) cause for the 'jumps'.

2. Intensity jumps

An example of an intensity 'jump' is given in Figure 1. This shows a GOME radiance spectrum (ground pixel 2201 on orbit 1335) normalised to the sun. The jumps at 400 and 600 nm, between channels 2/3 and 3/4, are clearly visible.

The spectrum is calibrated for 'unpolarised light'. To obtain the finally calibrated radiance, this spectrum needs to be multiplied by the so-called 'polarisation correction factor'.

This wavelength dependent 'polarisation correction factor' includes the polarisation sensitivity of the GOME instrument, and the 'polarisation fraction' which is a number between 0 and 1 indicating which fraction of the atmospheric radiance is polarised parallel to the spectrometer's entrance slit.

The polarisation correction factor is given by

$$c_i = \frac{1}{2} \cdot \frac{1 + \eta_i}{p_i(1 - \eta_i) + \eta_i}$$

where subscript i refers to each of the 3584 channel detector pixels; η_i denotes the polarisation-sensitivity of the instrument; p_i denotes the polarisation fraction, as retrieved from the PMD signals.

In the following we investigate if the jumps can be explained by errors in η, by errors in the retrieved p, or by field-of-view effects.

Sensitivity for p

The numbers written in Fig 1 above the channel overlaps indicate the values of p which are needed to eliminate the jumps after polarisation correction, (given the η of the calibration data).

The GOME 'level 1' dataproduct gives $p \approx 0.55$. From the appearance of the spectrum it follows that p cannot be far from 0.5, otherwise we would clearly see the polarisation features of the dichroics in the Channel 3/Channel 4 overlap at 600 nm. To eliminate the jump, a polarization fraction of 0.77 would be needed in the 3/4 overlap, which seems unrealistically high in view of the 'unpolarized' appearance of the spectrum. In overlap 2/3 we would need $p > 1$ which is unphysiscal.

Therefore, a wrong retrieval of p doesn't seem to be the cause of these jumps.

Sensitivity for η

For $p = 0.5$ the polarization correction factor is 1.0 regardless of η (by definition). Even for $p = 0.77$ as needed to close the 3/4 gap in Fig 1, a 20% change in η leads only to a 6% change in retrieved p (at this particular wavelength). Because of this insensitivity to changes in η, it is unlikely

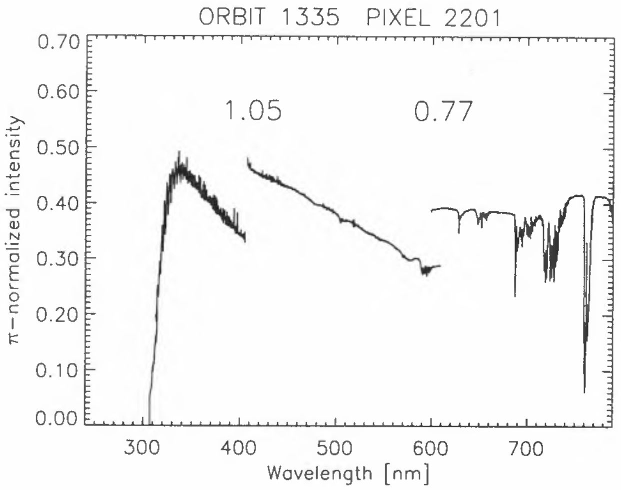

Fig. 1. Example of a GOME 'uncorrected' radiance spectrum (see text) showing intensity jumps

that the jumps are caused by errors in η.

Field-of-view effects

There appear to be two effects why the detector pixels in the overlap of one channel do not see the same ground pixels as those in the other channel.

1. across satellite track: 'synchronisation' error, pixels are read out with a time delay.
2. along track: 'detector alignment' error, as suggested by the behaviour of the signal during sun calibration (see below); and a 'field-of-view (FOV) size' error, i.e. different detector pixels have different size of FOV as determined during on-ground calibration

Synchronisation errors

All four channel detectors are read out simulataneously, but there is a time delay of 91.6 μs between each detector pixel within a channel. The pixel at the long-wavelength end of each channel is read out first, and the pixel at the short-wavelength end of each channel is read out after 1024× 91.6= 93.75 ms. The difference in ground scene between the first pixel of a channel and the last pixel of a channel is dependent on the speed by which the scanner mirror moves.

In the present GOME observation mode, this difference in ground scene between the two ends of a channel amounts to 20 km. It is clear that e.g. cloud cover can drastically vary over such a distance. In the current observation mode the 20 km correspond to a quarter of a ground pixel, hence large differences in radiance can be expected due to differences in illumination across the scene ('scene noise').

Detector alignment error

This effect is derived from analysis of a Sun calibration sequence. Sun calibration starts at the dark side of the orbit, just before sunrise. While the sun rises and moves through the field-of-view of the instrument (using the viewport over the on-board diffuser) a spectrum is taken every 1.5 seconds. About 20 spectra are recorded while the sun moves into the FOV, ~ 40 while the sun is completely in the FOV, and another ~ 20 while the sun disappears from the FOV.

We analyse the relative changes of the Sun spectrum while the Sun starts moving into the FOV. To this end a time series is made of the ratio of each spectrum with the Sun spectrum when the Sun is fully in the FOV. What we expect is a spectrally flat ratio, which increases in intensity at every timestep the sun moves further inside the FOV.

What we actually see is shown in Figure 2. The time steps are increasing from low to high signal ratios. Apart from the wiggles on the spectra which can be ignored for this purpose (like the channel overlaps which show as vertical bands), Figure 2 shows that the long-wavelength part of channel 2, pixels 1000-1500, see the sun significantly before channels 3 and 4 do (disregard channel 1, since it has an integration time different from the other channels). In the sequence where the Sun moves out of the FOV, exactly the opposite behaviour is observed.

From an instrument point of view, this can be explained if the detector of channel 2 is slightly misaligned with the dispersion direction in the focal plane.

From the atmospheric science point of view, it suggests that there is a difference in the ground scene observed across channel 2. If this FOV effect during sun calibration corresponds to a similar effect in scanning mode (which still needs to be confirmed since the respective light paths in the instrument are not completely equal), the misalignment translates to a diffence in ground pixel of ~ 0.7 km for the begin of channel 2, and ~ 1.4 km for the end of channel 2.

FOV size error

The various channel detector pixels and PMDs have slightly different sizes of along-track FOV, as determined from ground calibration. If we take the FOV of the PMDs as standard (~ 36 km ground coverage), then the channel detectors have the following differences in ground coverage (based on GOME Users Manual):

Channel 1	+1.8 to +2.1 km
Channel 2	-0.3 to +0.3 km
Channel 3	+0.6 to +3.1 km
Channel 4	+2.1 to +2.5 km

Note the large difference within channel 3: the pixels near 400 nm have a ~ 6% smaller FOV than those near 600 nm. The difference between channels 2/3 and channels 3/4 in the overlap regions is ~ 2% in FOV or ~ 0.7 km in ground coverage.

3. Spectral intensity oscillations

Low-amplitude spectral intensity oscillations have been observed during Sun calibration measurements. These oscillations can be visualized using the same analysis technique as used in the detector alignment error analysis.

We take a sequence of Sun spectra, but this time in the central part of the calibration time sequence. The average of these spectra would be used as 'the Solar Calibration Spectrum' for that particular day.

Figure 3 shows the ratio of successive spectra, normalised on the 'median' spectrum i.e. the spectrum exactly in the middle of the time series. Due to a well-known

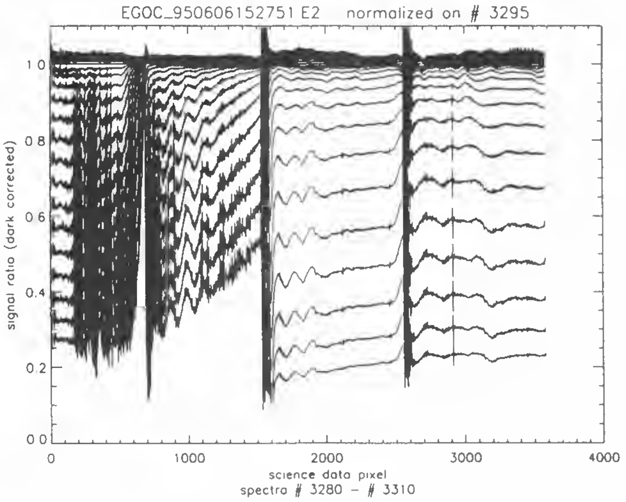

Fig. 2. Sequence of solar calibration spectra while the Sun enters the FOV. Spectra are ratioed with 'full sun' spectrum. Pixel numbering increases from start of channel 1 to end of channel 4

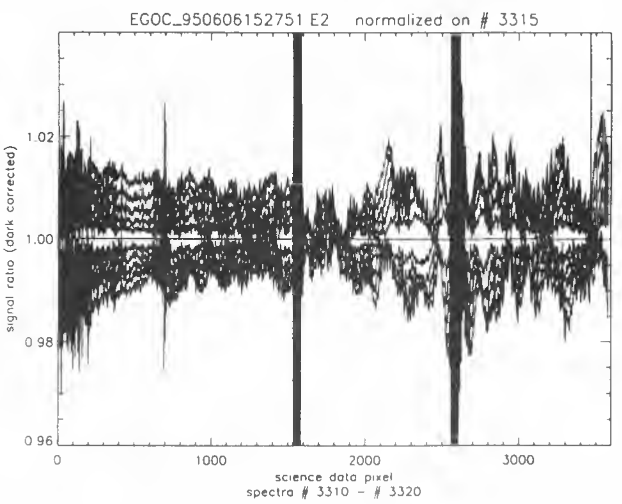

Fig. 3. Similar to Fig. 2, but solar spectra are taken from the central part of the calibration sequence, see text

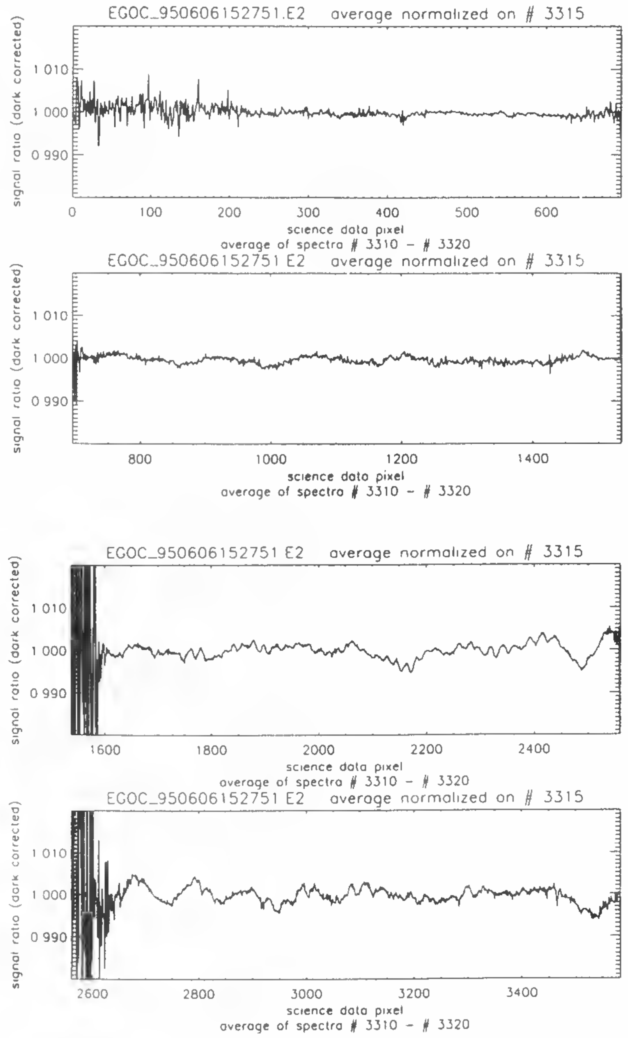

Fig. 4. Signal ratio of the 'average' with the 'median' solar calibration spectrum. From top to bottom: channel 1 to channel 4

and calibrated dependence of sun diffuser efficiency on the solar elevation angle, we would expect a series of flat spectral ratios, with intensity slightly increasing on each 1.5 second timestep.

However, we see oscillations on the spectral intensity, with amplitudes of up to 2%. The oscillation pattern is fairly symmetrical (in time) around the 'median' spectrum, but not quite.

This raises the question: what is the 'best' Solar Calibration Spectrum. Is it the average of the spectra, or should we take the 'median' where the Sun is in the center of the FOV?

The ratio of 'average' to 'median' Solar spectrum is shown in Figure 4.

Based on random noise levels as calculated by the GOME Instrument Simulation Software we expect random variations of 0.0006 (0.06%) for signal levels as in channels 2,4, and variations of 0.0025 (0.25%) for signal levels as in channel 1 below science pixel 150.

From Fig. 4 we see that in channels 1 and 2, the pixel-to-pixel variation is more or less as expected from the Instrument Simulation results. However, in channel 1 there is a small but systematic difference of spectral slope (about 0.2% over the channel). In channel 2 there are wiggles with a wavelength of $\sim$ 150 pixels and a peak-to-peak amplitude of 0.3%.

In channels 3 and 4 the situation is significantly worse. The wiggles with wavelength of 100–200 pixels have peak-to-peak amplitudes of 0.5–1%, but there are also wiggles with wavelengths of $\sim$ 20 pixels and amplitudes of 0.3%.

In Section 5 the possible impact on trace gas retrieval is discussed.

4. PMD stray signal

If the polarisation state of the light entering GOME is known, then it is possible to calculate the ratio of main channel signal to PMD signal, using the on-ground calibration of the instrument's polarisation sensitivity.

This situation exists in Sun measurements, since the Solar irradiance is virtually unpolarised.

Using the Solar calibration spectrum from the GOME 'level 1' data product, the PMDs appear to measure more signal than expected from on-ground calibration. We find the following signal excess:

```
PMD 1 (300-400 nm)    + 0.5%
PMD 2 (400-600 nm)    + 2.5%
PMD 3 (600-800 nm)    +16.5%
```

The estimated calculation accuracy is $\sim 1\%$.

A small part of the discrepancy for PMD 3 can be attributed to the fact that this PMD is known to be sensitive for wavelengths above the main channel limit of 790 nm. However, calculations using the GOME Instrument Simulation Software indicate that this should not account for more than 3%.

During the on-ground calibration it was established that there is some near-infrared stray light in the PMDs, but measurements suggested that this should mostly affect PMD 1.

The reason for the discrepancy is not yet found.

5. Discussion

The largest effects on the GOME radiance calibration are currently due to the 'readout synchronisation error'. This causes detector pixels at one end of a channel array to see a FOV which is 1/4 ground pixel shifted across-track compared to the what detector pixels at the other end of a channel array see. Variations in ground scene illumination thus lead to variations in spectral intensity.

This error will be drastically reduced when a new 'co-adding' observation mode is implemented. This will reduce the FOV shift to 1/16 ground pixel, or $\sim$ 6% of the FOV. The error then becomes comparable with other FOV effects in the along-track direction.

Note that the FOV effects of the main channel array detectors are not just a matter of intensity calibration, but affect the consistency in atmospheric sampling of one spectral region compared another.

A pure intensity calibration effect does occur because of mismatch in FOV between PMDs and main channels. Here, variations in ground scene illumination can lead to an error in retrieved polarisation, and hence an error in 'polarisation correction'.

Other potential errors in 'polarisation correction' are due to the PMD stray signal problem, and to the fact that the polarisation fractions, which are established at 3 wavelength points, must be interpolated/extrapolated over the whole spectral range of GOME.

For an error analysis on polarisation fractions, see the paper by I. Aben in these proceedings.

The effect of the spectral intensity oscillations on the absolute radiance calibration is negligible compared to uncertainties in the radiance calibration parameters. Sofar, the effect has only been seen in solar calibration measurements.

The aim of the solar calibration is to enable calculation of the Earth's albedo (which contains all tracegas and atmospheric scatterers information) from the measured Earth shine spectrum.

For trace gas retrieval using the BUV technique, the small amplitude of the oscillations causes negligible deviations in absolute albedo. The same holds for e.g. aerosol retrieval.

For the DOAS technique, where a high spectral resolution is essential, the oscillations with wavelength 100-200 pixels are probably not interfering significantly with the trace gas absorptions; they probably can be divided out in the polynomial which is always used to normalize the absorptions. However, the oscillations with wavelength $\sim$ 20 pixels in channel 3 and 4 cannot be removed this way. Their amplitude of 0.3% can potentially interfere with (especially the weaker) trace gas absorption spectra.

Further study is needed to see if this interference indeed occurs. If it does, techniques should be developed to remove the effect of oscillations from the spectral albedo.

References

I. Aben et.al., 1996, "Error analysis of polarisation measurements by GOME", these proceedings.

W. Balzer, R.D.J. Spurr, 1995, "GOME level 0 to 1 Algorithms Description", DLR report ER-TN-DLR-GO-0022.

F. Bednarz (ed.), 1995, "GOME Users Manual", ESA Pub. SP-1182

GOME calibration team, 1994, "GOME FM Calibration Results Review"

S. Slijkhuis, 1995,"GOME/SCIAMACHY Instrument Simulation Software", SRON report GO/SCIA-IS-TR01.

P. Stammes et.al., 1996, "Validation of GOME polarisation and radiance measurements", these proceedings.

O_2 *A* BAND STUDIES FOR CLOUD DETECTION AND ALGORITHM IMPROVEMENT

K. Chance

Harvard-Smithsonian Center for Astrophysics
Cambridge, MA, USA

Abstract

Detection of cloud parameters from space-based spectrometers can employ the vibrational bands of O_2 in the $b^1\Sigma_g^+ \leftarrow X^3\Sigma_g^-$ spin-forbidden electronic transition manifold, particularly the $\Delta v = 0$ *A* band. The GOME instrument uses the *A* band in the Initial Cloud Fitting Algorithm (ICFA). The work reported here consists of making substantial improvements in the line-by-line spectral database for the *A* band, testing whether an additional correction to the line shape function is necessary in order to correctly model the atmospheric transmission in this band, and calculating prototype cloud and ground template spectra for comparison with satellite measurements.

1. SUMMARY OF NEW LABORATORY MEASUREMENT DATA

The new measurements incorporated into the present work are from Ritter [1986] and Ritter and Wilkerson [1987] (together, RW). They include improved measurements of line intensities, giving an overall band intensity that is 15% larger than the previous measurements that are the source of the parameters in the current HITRAN listing [Miller *et al.*, 1969; Rothman *et al.*, 1992]. It is worth noting that the uncertainties in Miller *et al.* [1969] are given as 4%, while those of RW are 2%. The level of disagreement (arguably just a bit worse than 2σ) is an indication of how difficult these seemingly straightforward measurements actually are. RW also include self-broadening measurements of the linewidths, which are on the average 8% smaller than the current air broadening values in HITRAN (the HITRAN values actually come from measurements in the *B* band [Giver *et al.*, 1974], which were substituted for *A* band widths for lack of specific *A* band measurements (see Kuze and Chance [1994]). The RW measurements are made at 294 K, for lines up to $P29P29$ in the P branch and $R27R27$ in the R branch, except for the $R21Q22$ and $R25R25$ lines, which are blended together. The measurements also include air broadening studies for a selection of 5 lines. They find "roughly a 3% increase in broadening for air over pure O_2," although their Table II appears to indicate more like a 2% increase. Their 3% is adopted here, with a 2% uncertainty. The temperature dependence of the self broadening was measured for 24 lines, from $P29P29$ through $R5R5$, over the temperature range +100 to -20° C. The temperature coefficient, n, for the pressure broadening coefficients, determined for the ensemble of lines measured, is 0.76(5), where $(\gamma(T) = \gamma(T_0) \times (T_0/T)^n)$. This compares with the $\overline{n} = 0.72$ that can be obtained from the very limited data set assembled in Chance *et al.* [1991].

Estimated (2σ) final uncertainties for the measurements are:

1. Intensity: 2%; directly from the RW band strength.
2. Pressure broadening coefficients: 2%; from 294 K individual line uncertainties (small), plus the N_2/O_2 correction (the dominant term).
3. n: 7%; directly from measurements, $\overline{n} = 0.76(5)$. This corresponds to less than 2% uncertainty in the broadening coefficient for the range of temperatures encountered in the lower and middle atmosphere. The root-sum-square of the various error terms in pressure broadening is 3%.

The data measured by Ritter and Wilkerson can be extended to provide updated coefficients for use in cloud determination to replace the ones currently included in HITRAN [Rothman *et al.*, 1992], which were shown by Kuze and Chance [1994] to be insufficiently accurate for satellite-based cloud detection.

Processing of the Ritter and Wilkerson data to provide a more complete data set is accomplished as follows:

1. Pressure broadening coefficients for the lines omitted due to interference are replaced by those with the same N', N'': $R21Q22$ and $R25R25$ are replaced by $R21R21$ and $R25Q26$.

2. O_2 pressure broadening coefficients measured by RW are multiplied by 1.03, to give air broadening. Coefficients for lines measured by RW in the $v = 0 \leftarrow 0$ band are also applied to the respective lines in the $v = 1 \leftarrow 1$ hot band and the $v = 0 \leftarrow 0$ band of $^{18}O^{16}O$. Hitran lines not measured by RW are multiplied by 1.03 / 1.09009 = 0.94488, where 1.09009 is the average ratio of the RW measurements to the HITRAN coefficients.

3. The isotopic abundances are taken to be the those used in HITRAN, so that $^{16}O_2$ is 99.52% and $^{18}O^{16}O$ is 0.40%.

4. Intensity values for the three sub-bands are calculated starting with the 294 K band strength of RW, correcting the hot band by the Boltzmann factor of the band origin (1556.385 cm^{-1}) and the minor isotopic band by the appropriate isotopic ratio. The line intensities are translated to 296 K by explicitly calculating the rotation-spin partition functions using the term values from HITRAN and correcting for the RW approximation for the 294 K partition function of the major band.

5. In order to calculate individual line intensities, to supplement the measured ones, it is necessary to use the appropriate intensity formulas, which take into account the spin-rotation and spin-spin interactions [RW; Watson, 1968]. For the $v = 0 \leftarrow 0$ band of $^{16}O_2$ measured by RW the molecular constants from Albritton *et al.* [1973] are used, to be consistent, although better constants are now available from Mizushima *et al.* [1984] (and references cited therein). These latter constants are used to calculate the individual line intensities for the $v = 1 \leftarrow 1$ band of $^{16}O_2$ and the $v = 0 \leftarrow 0$ band of $^{18}O^{16}O$.

The final database derived from these calculation is available from the author via ftp.

2. TESTING OF LINE SHAPES, INCLUDING LINE NARROWING COEFFICIENTS

RW determined that the data as measured under laboratory conditions at high spectral resolution ($< 10^{-4}$ cm^{-1}) were fitted better by including narrowing of the line core (Dicke narrowing) in the line shape function. Several line shapes were tested, including the Galatry line shape [Galatry, 1961]. It was found that all of the tested line shapes which included line narrowing provided superior fits to those using the Voigt profile, and that all were equivalent, to within experimental uncertainty. The Galatry profile was adopted for the bulk of the work because of the relative simplicity in implementing it [Varghese and Hanson, 1984]. RW found that all of the lines in the O_2 A band can be reasonable described by a line narrowing coefficient of 0.0145 cm^{-1} atm^{-1} (see RW for the exact definition of the coefficient in terms of the Galatry profile). An improved method for generating Galatry line profiles, employing the fast Fourier transform (FFT), has since been developed by Ouyang and Vargese [1985] (OV). These authors have distributed a version of their FFT computer code, which was used in the present study for investigation of the effect of line narrowing on the atmospheric O_2 absorption. In order to use the code, it was necessary to update it and streamline it somewhat. The FFT routine used in the code is from the International Mathematical and Statistical Library (IMSL); however, calls were to an outdated version of IMSL, which is no longer supported at our institution (nor, presumably, at most others). Therefore, the code was updated to IMSL Version 10. The updated version of the Galatry line profile code is available from the author via ftp. Implementation of this code and atmospheric investigation for the O_2 A band proceeded as follows:

1. The OV code was compared in the Voigt limit against our standard Voigt subroutine (based upon algorithm 363 of the Collected Algorithms from CACM), which has an accuracy of 10 significant figures, for the case where the Lorentz half-width at half-maximum is 3.0 times the Gaussian half-width at $1/e$ intensity. The maximum disagreement was 0.13%; the maximum disagreement relative to the line center intensity was 0.06%. This was accepted as validation that the OV code can be properly used to assess the importance of line narrowing on the atmospheric O_2 spectrum.

2. Comparisons were made using the OV code with and without line narrowing for cases corresponding to the O_2 A band at 5 and 10 km altitudes in the atmosphere, using pressure and temperature values from the US Standard Atmosphere [1976]. In the 5 km case, the maxi-

mum relative error in the line shapes is 1.8%; differences go to <1% by 2.9 Gaussian 1/e widths from line center. In the 10 km case, the maximum relative error is 2.4%; differences go to <1% by 2.5 Gaussian 1/e widths from line center. In both cases, the integral of differences over the line shapes is zero to within the accuracy of the single precision calculations. In the atmosphere, these differences will be in the saturated central parts of the lines for all but the weakest lines. Differences greater than 1% are all within 0.02 GOME pixel (for example) so they will not be visible in the spectra. Thus, the effect of line narrowing should be totally negligible, and we should be able to simply use the Voigt profile for satellite-based cloud correction.

3. SAMPLE O_2 *A* BAND CLOUD CORRECTION TEMPLATES FOR GOME

For initial comparisons with the GOME satellite data sample ground and 400 mbar cloud template spectra are calculated using a 16-layer atmosphere based upon the U.S. Standard Atmosphere [1976] and employing Version 5 of the GOME key data for wavelength calibration and for the GOME compound hyperbolic slit function:

$$y = \frac{a_1^2}{(x-x_0)^2 + a_0^2} + \frac{a_2^2}{(x-x_0)^4 + a_0^2} + \frac{a_3^2}{(x-x_0)^6 + a_0^2},$$

where y is the normalized spectral response and x is the spectral position in pixel number. The current slit function values are $a_0 = 0.7334$, $a_1 = 0.0756$, $a_2 = 0.4689$, and $a_3 = 0.5589$. The calculations are made for a solar zenith angle of 60° and a viewing angle of 22°, for a total (typical) path multiplier of 3.07853, as initially used in the Initial Cloud Fitting Algorithm (ICFA) of GOME. Figure 1a is the sample ground template, *i.e.*, the measured spectrum for light reflected back from ground level (1013.25 mbar). Figure 1b is the sample template for reflection from a cloud surface at 400 mbar. Figure 1c compares the shapes of the two templates to provide some feeling for the information available in distinguishing the relative level of light penetration from satellite spectra.

4. REFERENCES

D. L. Albritton, W. J. Harrop, and A. L. Schmeltekopf, Resolution of the discrepancies concerning the optical and microwave values for B_0 and D_0 of the $X^3\Sigma_g^-$ state of O_2, *J. Molec. Spectrosc.* **46**, 103-118, 1973.

K. V. Chance, W. A. Traub, K. W. Jucks, and D. G. Johnson, On the use of O_2 spin-rotation lines for elevation angle calibration of atmospheric thermal emission spectra, *Int. J. IR and MM Waves* **12**, 581-588, 1991.

L. Galatry, Simultaneous effect of Doppler and foreign gas broadening on spectral lines, *Phys. Rev.* **122**, 1218-1223, 1961.

L. P. Giver, R. W. Boese, and J. H. Miller, Intensity measurements, self-broadening coefficients, and rotational intensity distribution for lines of the Oxygen B band at 6880 Å, *J. Quant. Spectrosc. Radiat. Transfer* **14**, 793-802, 1974.

A. Kuze and K. V. Chance, Analysis of cloud-top height and cloud coverage from satellites using the O_2 *A* and *B* bands, *J. Geophys. Res.* **99**, 14,481-14,491, 1994.

J. H. Miller, R. W. Boese, and L. P. Giver, Intensity measurements and rotational intensity distribution for the oxygen A band, *J. Quant. Spectrosc. Radiat. Transfer* **9**, 1507-1517, 1969.

M. Mizushima, L. R. Zink, and K. M. Evenson, Rotational structure of $^{16}O_2$, $^{16}O^{17}O$, and $^{16}O^{18}O$ ($X^3\Sigma_g^-$) from laser magnetic resonance spectra, *J. Molec. Spectrosc.* **107**, 395-404, 1984.

X. Ouyang and P. L. Varghese, A reliable and efficient program for fitting Galatry and Voigt profiles to spectral data on multiple lines, *Appl. Opt.* **28**, 1538-1545, 1989.

K.J. Ritter, A high resolution spectroscopic study of absorption line profiles in the A-band of molecular oxygen, Ph.D. Thesis, University of Maryland, 1986.

K.J. Ritter and T.D. Wilkerson, High-resolution spectroscopy of the oxygen *A* band, *J. Molec. Spectrosc.* **121**, 1-19, 1987.

L. S. Rothman, R. R. Gamache, R. H. Tipping, C. P. Rinsland, M. A. H. Smith, D. C. Benner, V. M. Devi, J.-M. Flaud, C. Camy-Peyret, A. Perrin, A. Goldman, S. T. Massie, L. R. Brown, and R. A. Toth, The HITRAN molecular database editions of 1991 and 1992, *J. Quant. Spectrosc. Radiat. Transfer* **48**, 469-507, 1992.

"U.S. Standard Atmosphere Supplements, 1976," U.S. Government Printing Office, Washington, DC.

P. L. Varghese and R. K. Hanson, Collisional narrowing effect on spectral line shapes measured at high resolution, *Appl. Opt.* **23**, 2376-2385, 1984.

J. K. G. Watson, Rotational line intensities in $^3\Sigma - ^1\Sigma$ electronic transitions, *Canad. J. Phys.* **46**, 1637-1643, 1968.

5. ACKNOWLEDGEMENTS This research was supported by NASA grant NAGW-2541.

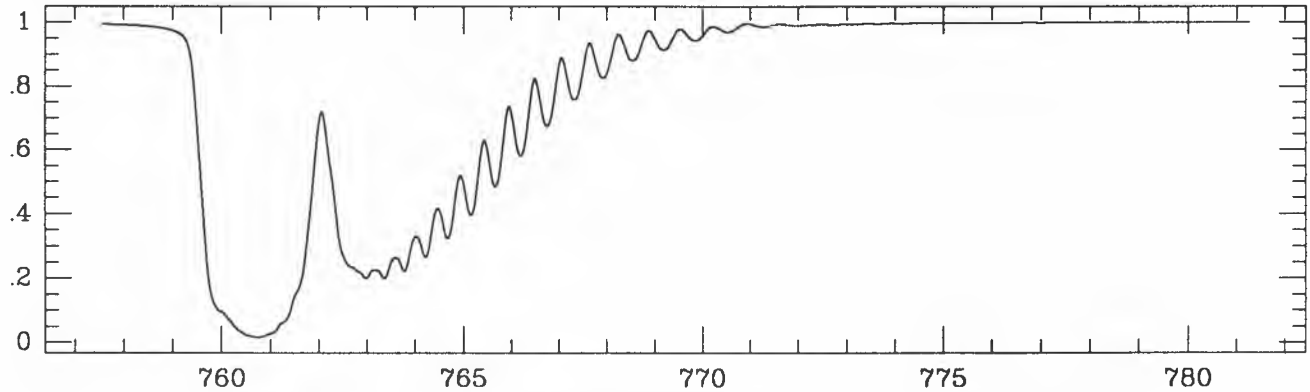

Figure 1a. Ground template convolved with GOME slit function

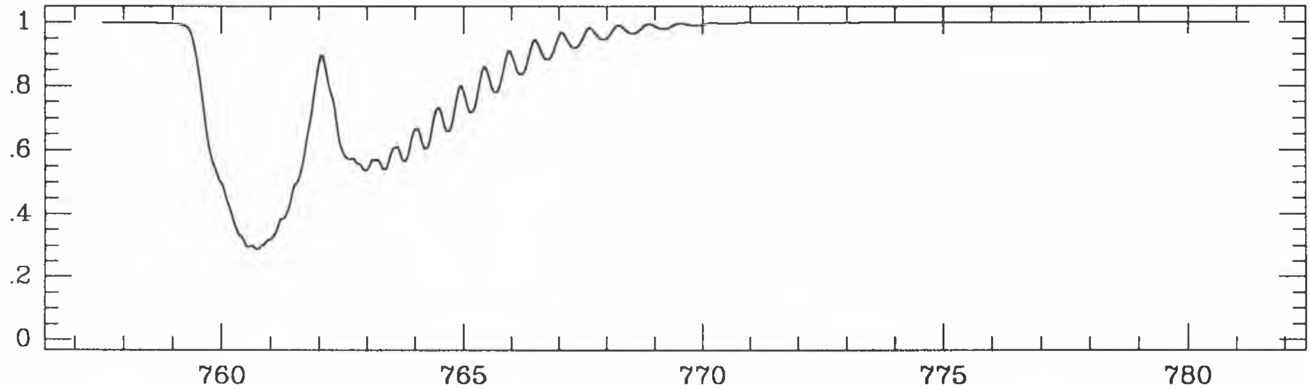

Figure 1b. Cloud template convolved with GOME slit function

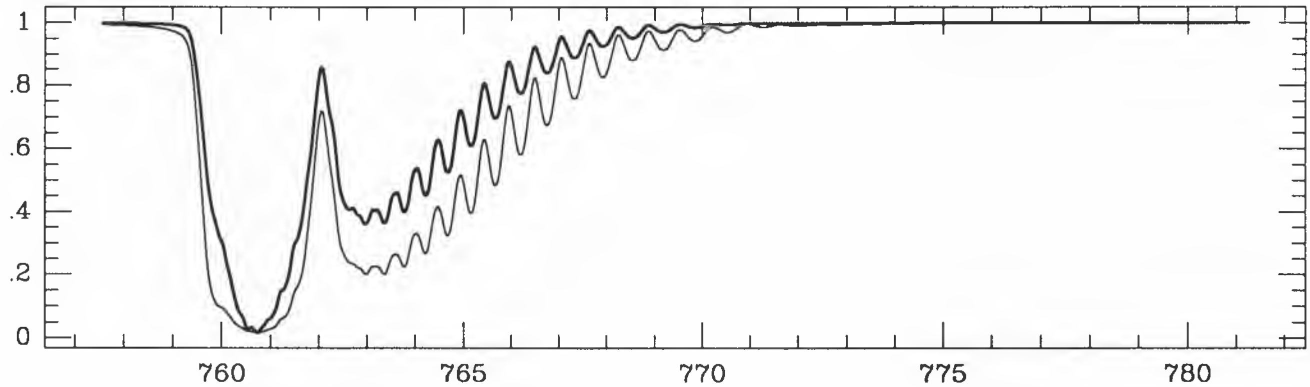

Figure 1c. Cloud vs. ground shape comparison

RING EFFECT STUDIES: RAYLEIGH SCATTERING, INCLUDING MOLECULAR PARAMETERS FOR ROTATIONAL RAMAN SCATTERING, AND THE FRAUNHOFER SPECTRUM

K. Chance and R.J.D. Spurr

Harvard-Smithsonian Center for Astrophysics
Cambridge, MA, USA

Abstract
Improved parameters for the description of Rayleigh scattering in air and for the detailed rotational Raman scattering component for scattering by O_2 and N_2 are presented for the wavelength range 200-1000 nm. These parameters enable more accurate calculations of bulk molecular scattering and of the "Ring effect" for a variety of atmospheric radiative transfer and constituent retrieval applications. A solar reference spectrum with accurate absolute vacuum wavelength calibration, suitable for convolution with the rotational Raman spectrum for Ring effect calculations, has been produced and is briefly described. The solar-rotational Raman convolved product is available for fitting of atmospheric spectra.

1. INTRODUCTION

The phenomenon that has come to be known as the "Ring effect" was first noted by Grainger and Ring [1962] as a filling in (broadening and reduction of depth) of solar Fraunhofer lines when viewed from the ground in scattered sunlight. Various processes have been proposed as contributing to the effect including scattering with fluorescence from aerosols and from the ground [Noxon and Goody, 1965; Hunten, 1970]. The predominance of molecular scattering as the major cause was established by Kattawar *et al.* [1981], who analyzed the Ring effect contributions from rotational Raman scattering and inelastic Rayleigh-Brillouin scattering. The Rayleigh-Brillouin contribution arises from the Doppler effect due to relative motion of the atmosphere with respect to the observer, with contributions from thermal motions, winds and, particularly, acoustic waves. The situation is nicely defined by Young [1981]: "To summarize: molecular scattering consists of Rayleigh scattering and vibrational Raman scattering. The Rayleigh scattering consists of rotational Raman lines and the central Cabannes line. The Cabannes line is composed of the Brillouin doublet and the central Gross or Landau-Placzek line. None of the above is completely coherent. The term 'Rayleigh line' should never be used." Note that the vibrational Raman contribution results in lines so widely separated from the frequency of the incoming light that they are not normally considered part of the "Ring effect" even though in recent applications the Ring effect has developed a somewhat broader definition that includes substantial interfering structure in observations, rather than the initial effect which was limited to broadening of partially-resolved lines.

The Ring effect has become more important in recent years with the increase in ultraviolet and visible spectroscopic observations of the Earth's atmosphere from the ground [Solomon *et al.*, 1987; Fish and Jones, 1995] and from satellites [Chance *et al.*, 1991a; Burrows *et al.*, 1993; Joiner *et al.*, 1995; Joiner and Bhartia, 1995]. In order to retrieve abundances of trace species from many such observations it is necessary to take the Ring effect into account. Methods have been developed to do so by pragmatic means, by measuring the polarization of scattered sunlight [Solomon *et al.*, 1987] and by modeling of the effect directly from molecular scattering processes [Fish and Jones, 1995; Joiner *et al.*, 1995]. It has been proposed to use the Ring effect with selected Fraunhofer lines (in particular, the CaI h and k lines) to determine cloud parameters in conjunction with satellite-based observations of O_3 [Joiner and Bhartia, 1995]. Joiner *et al.* [1995] also determined that the contribution to the Ring effect from the Rayleigh-Brillouin scattering process is negligible for most geometries used in satellite observations. For the European Space Agency's Global Ozone Monitoring Experiment (GOME) and the upcoming SCanning Imaging Absorption spectroMeter for Atmospheric CHartographY (SCIAMACHY), as well as proposed future space-based atmospheric monitoring which emphasize tropospheric measurements, the use of visible bands of O_2, in particular the 762 nm A band, for determination of cloud parameters is being developed [Kuze and Chance, 1994]. The Ring effect has a substantial influence on such observations and work is underway in our institution to refine and model the effects. In this case, the effect is due to inelastic scattering in molecular absorption lines themselves, rather than in the solar Fraunhofer lines. Similar effects have been noted for the detailed retrieval of trace species including O_3 and NO_2 [Solomon *et al.*, 1987; Fish and Jones, 1995; J.P. Burrows, private communication, 1995].

The present work is part of an ongoing effort to quantify the Ring effect for atmospheric radiative transfer modeling, with application to satellite- and ground-based measurements, and to apply it to particular cases such as the detailed absorption in the O_2 bands. Much of previous modeling work has relied on the development of molecular parameters for N_2 and O_2 by Penney *et al.* [1974] (e.g., Bussemer [1993], Fish and Jones [1995]; Joiner *et al.* [1995]) with one study updating the dynamic polarizability anisotropies as developed by Bates [1994] (Joiner *et al.* [1995]). Previous work has largely ignored the complication of the rotational Raman spectrum of O_2 caused by the electronic spin angular momentum in the $^3\Sigma_g^-$ ground state and the issue of pressure broadening of the rotation Raman lines. In this publication we update the molecular parameters and the scattering with respect to the solar Fraunhofer spectrum using the best currently available laboratory and field data and theoretical studies of which we are aware. This provides: An updated expression for Rayleigh scattering by air; expressions for the wavelength-dependent polarizability anisotropies of O_2 and N_2; accurate Placzek-Teller coefficients (the state-dependent factors in the line intensities) for O_2 rotational Raman lines; a tentative set of pressure broadening coefficients for the O_2 and N_2 rotational Raman lines; A solar reference spectrum for convolution with calculated Ring cross sections; and a convolved Fraunhofer-rotational Raman source spectrum for fitting of atmospheric spectra. The tables and spectra are not included here due to size limitations. They are available from the authors.

2. RAYLEIGH SCATTERING

To examine the detailed Rayleigh and rotational Raman scattering properties, including their relative intensities and the scattering phase functions, we begin with Table I of Kattawar *et al.* [1981]. This table describes the relative intensities and angular behavior for the Rayleigh-Brillouin and rotational components, and their sum, for various input polarizations, including unpolarized light (the predominant contribution for most atmospheric observations where single scattering is the major contributor to the Ring effect). For unpolarized light the depolarization ratios (defined in each case as the ratio of the horizontally-polarized component to the vertically-polarized component at 90° scattering angle) may be determined directly. Table I of Kattawar *et al.* [1981] is reproduced here as Table 1, with the addition of the depolarization ratios, for the three cases: Rayleigh-Brillouin (the central Cabannes component, C); rotational Raman (the wings, W); and the sum of the two (R, for Rayleigh). The phase functions for scattering may also be derived for each case. They are given here normalized over solid angle to 1.

$$\begin{aligned}
\Phi_0^C &= \frac{3}{160\pi}\left[\frac{(180+13\epsilon)+(180+\epsilon)\cos^2\theta}{18+\epsilon}\right] \\
\Phi_0^W &= \frac{3}{160\pi}(13+\cos^2\theta) \qquad (1)\\
\Phi_0^R &= \frac{3}{80\pi}\left[\frac{(45+13\epsilon)+(45+\epsilon)\cos^2\theta}{9+2\epsilon}\right]
\end{aligned}$$

In each case, the phase function is given in terms of the *respective* depolarization ratio ($X = C, W, R$)

$$\Phi_0^X = \frac{3}{8\pi}\left[\frac{(1+\rho_0^X)+(1-\rho_0^X)\cos^2\theta}{2+\rho_0^X}\right]. \quad (2)$$

The Rayleigh scattering cross section at standard temperature (273.15 K) and pressure (1 atmosphere) is given by

$$Q_R = \frac{32\pi^3(n-1)^2 F_K}{3N_0^2\lambda^4} \quad (3)$$

where n is the index of refraction, F_K is the King correction factor (King [1923]), N_0 is Loschmidt's number (2.686763×10^{19} cm^{-3}), and λ is the wavelength. The King correction factor is given by

$$F_K = 1 + 2\left(\frac{\gamma}{3\overline{\alpha}}\right)^2 = \frac{6+3\rho_0^R}{6-7\rho_0^R} \quad (4)$$

where γ is the anisotropy of the polarizability and $\overline{\alpha}$ is the average polarizability. The average polarizability can be determined from

$$|\overline{\alpha}|^2 = \frac{(n-1)^2}{4\pi^2 N_0^2}. \quad (5)$$

3. MOLECULAR PARAMETERS

3.1 Rayleigh scattering cross sections

The major source of improved data for the index of refraction of air (and of O_2 and N_2) versus wavelength, the King correction factors, and the anisotropies of the polarizabilities) is Bates [1984]. He presents a comprehensive review of both measurements and theoretical calculations to derive a data set that is demonstrated to be better than 1% for all data and parameterizations presented here.

Bates' [1984] Table 1 gives refractive indices, Rayleigh scattering cross sections, and King correction factors versus wavelength for air from 200-1000 nm. The index of refraction data are fitted here to an Édlen-type expression to better than 0.1% for all values:

$$(n_{air} - 1) \times 10^4 = \\ 0.7041 + \frac{315.90}{157.39 - \sigma^2} + \frac{8.4127}{50.429 - \sigma^2} \tag{6}$$

where σ (μm^{-1}) = $1/\lambda$ (μm). The Rayleigh cross sections are reproduced to better than 1% by the expression

$$Q_R \times 10^{24}(\mathrm{cm}^2) = \\ \frac{3.9993\times10^{-4}\sigma^4}{1-1.069\times10^{-2}\sigma^2-6.681\times10^{-5}\sigma^4}. \tag{7}$$

The King factor and depolarization for any choice of wavelength within the 0.2-1.0 μm range can be accurately determined from the previous two equations.

3.2 Polarizability anisotropies

The previous expansions are for air, including standard amounts of Ar and CO_2. For rotational Raman cross sections we will limit the calculations to O_2 and N_2. Bates gives segmented representations for the indices of refraction of O_2 and N_2 versus wavelength and expansions for the respective King correction factors. Tables giving the King correction factors, values of $\sqrt{\epsilon}$, where $\epsilon = (\gamma/\overline{\alpha})^2$, index of refraction $\overline{\alpha}$, and γ for O_2 and N_2 are available from the authors. From these data γ_{O_2} is determined to better than 1% over this wavelength range by

$$\gamma_{O_2} \times 10^{24} = 0.07149 + \frac{45.9364}{48.2716 - \sigma^2} \tag{8}$$

and γ_{N_2} to much better than 1% by

$$\gamma_{N_2} \times 10^{25} = -6.01466 + \frac{2385.57}{186.099 - \sigma^2}. \tag{9}$$

These equations should be considered merely as phenomenological fits over the particular wavelength range, rather than trying to attach physical importance to (for example) the negative value of the constant term in the N_2 equation. Extrapolation to outside the 0.2 - 1.0 μm range should be considered perilous.

3.3 Basic spectroscopy

The ground state of O_2 is $^3\Sigma_g^-$; it has significant electronic structure in both its magnetic dipole rotational and rotational Raman spectra. Rotational Raman spectra of both O_2 and N_2 have previously been approximated by simple expansions in the lowest rotational parameters (for positions) and by using T/c_2B_0 for the rotational partition functions. Very precise data are now available for the term energies, allowing line positions and Boltzmann factors to be accurately and rapidly calculated. The use of term values from the current HITRAN listing [Rothman *et al.*, 1992] allows for calculations of lines positions to 0.0001 cm^{-1} accuracy and highly accurate statistical partitioning. Tables including the quantum numbers and term energies for O_2 and N_2 up to states allowing for partitioning to better than 0.01% accuracy and Boltzmann factors (with nuclear spin degeneracies, g_N) are available from the authors.

3.4 Placzek-Teller coefficients

Cross sections for rotational Raman scattering are given by

$$Q^W_{N,N'}(\mathrm{cm}^2) = \\ \frac{256\pi^5}{27(\lambda')^4}\gamma^2 f_N c_{PT}(N, J, N', J'), \tag{10}$$

where f_N is the fractional population in the initial state. The quantum state-dependent factors $c_{PT}(N, J, N', J')$ are commonly known as "Placzek-Teller coefficients" from the initial derivations [Placzek and Teller, 1933]. These factors are given for a molecule in a Σ electronic state with one electronic spin angular momentum, in a Hund's case b coupling scheme (electron spin coupled to rotational angular momentum), by

$$c_{PT}(N, J, N', J') = (2N + 1)(2N' + 1)(2J' + 1) \\ \times \begin{pmatrix} N & L & N' \\ 0 & 0 & 0 \end{pmatrix}^2 \begin{Bmatrix} N & L & N' \\ J' & S & J \end{Bmatrix}^2 \tag{11}$$

where J is the total angular momentum, S is the electronic spin angular momentum (1 for O_2 and 0 for N_2), and L is the component of the 2nd rank polarizability tensor. $L = 0$ for average polarizability (The Cabannes component) and $L = 2$ for the present Raman scattering. The standard definitions for 3-j and 6-j coefficients are used. Near equivalents to this equation are given in Renschler *et al.* [1969] and in Loëte and Berger [1977] (both give the formula for "line strengths" which include the initial state degeneracy). For $S = 0$ (*i.e.*, N_2), eq. 11 reduces to the result of Penney *et al.* [1974], eq. 7:

$$\begin{aligned} c_{PT}(J \rightarrow J+2) &= \frac{3(J+1)(J+2)}{2(2J+1)(2J+3)} \\ c_{PT}(J \rightarrow J) &= \frac{J(J+1)}{(2J-1)(2J+3)} \\ c_{PT}(J \rightarrow J-2) &= \frac{3J(J-1)}{2(2J+1)(2J-1)}. \end{aligned} \tag{12}$$

This derivation gives correct Placzek-Teller coefficients for N_2, but approximates those for O_2 by treating it as a pure Hund's case b molecule. At low N, J the departures from the pure coupling case due to the electron spin-rotation interaction are enough to significantly affect the spectrum, as noted by Renschler *et al.* [1969] and Rich and Leppard [1971]. In the classic study of the O_2 ground state, Tinkham and Strandberg [1955] include the correct eigenvectors for levels up to $J = 26$ in the case b basis set (their Table V and equation 54). Above this level the molecule is described by case b behavior to a very high degree of accuracy. For $J = 0$ and all odd J levels the case b description is exact. For even J levels, $J \neq 0$, the transformation from case b basis functions $\phi_{N,J}$ to eigenfunctions $\Psi_{N,J}$ is given by

$$\begin{aligned} \Psi_{J-1,J} &= b_J\phi_{J-1,J} - d_J\phi_{J+1,J} \\ \Psi_{J+1,J} &= d_J\phi_{J-1,J} + b_J\phi_{J+1,J}. \end{aligned} \tag{13}$$

The b_J and d_J values from Tinkham and Strandberg [1955] are used here to calculate correct Placzek-Teller coefficients for values up to $J = 10$, above which the corrections become completely negligible. The database calculated using the corrected eigenvectors is prepared with an intensity cutoff to include all rotational Raman lines with intensities at 296 K within 0.1% of the strongest line. Because of the mixing of states, this now includes two $\Delta N = 4$ transitions. An almost identical result was determined by Altmann *et al.* [1972] who calculated eigenvectors for the secular determinant and molecular parameters given in the slightly earlier work of Mizushima and Hill [1954].

3.5 Pressure broadening coefficients

Γ is used here for the full-width at half-maximum pressure broadening coefficient to distinguish it from the γ used for anisotropy of polarizability. The best existing measurements of pressure broadening for the rotational Raman lines are from Jammu *et al.* [1966]. These authors note some evidence that the unresolved Q branches of vibrational Raman bands seem to broaden less than lines due to ordinary dipole transitions, but that the rotational Raman lines broaden comparably to dipole transitions. They present self-broadening measurements for N_2, O_2, CO_2, and CO, as well as He and Ar broadening of N_2, O_2. All measurements were made at room temperature. Given the experimental conditions (very high pressures, modest spectral resolution) and the lack of air-broadening measurements, temperature dependences, and a tabulation of the J-dependent N_2 broadening coefficients, it was decided not to use these measurements as the basis for broadening in the present data set. Instead, for O_2 the HITRAN92 values corresponding to rotational transitions of the same ΔN are initially adopted [Rothman *et al.*, 1992]. Where multiple corresponding transitions exists, the pressure broadening coefficients are averaged. For the two $\Delta N = 4$ transitions, the average of the values for lines connecting the upper and lower states is taken. The resulting pressure broadening coefficients are multiplied by 1.185, which is the average result for the ratio of measured air pressure broadening coefficients for O_2 magnetic dipole rotational transitions to those given in HITRAN (see Chance *et al.* [1991b] for an explanation of this correction). For N_2, pressure broadening values for the corresponding quadrupole lines of the vibrational fundamental are adopted. Values listed for the pressure broadening coefficients of both O_2 and N_2 are at 296 K. The temperature dependence should be calculated using the recommended HITRAN92 coefficient of $n = 0.5$ for N_2 lines [Rothman *et al.*, 1992] and a value of $n = 0.72$ for O_2 lines [Chance *et al.*, 1991b], where

$$\Gamma_T = \Gamma_{296} \times \left(\frac{296}{T}\right)^n. \tag{14}$$

4. SOLAR REFERENCE AND RING SOURCE SPECTRA

A solar reference spectrum for the range 230-800 nm, at 0.01 nm resolution has been determined by combining ground-based measurements [Kurucz *et al.*, 1984] and balloon measurements [Hall and Anderson, 1991] and re-calibrating in wavelength. The spectrum is given at 0.01 nm resolution, in vacuum wavelengths accurate to better than 0.001 nm above 305 nm and 0.002 nm below 300 nm. It will be described more fully in a future publication. The purposes for constructing such a spectrum include GOME wavelength calibration studies and calculating Ring effect contributions to GOME measurements. The solar spectrum has been convolved with the rotational Raman cross sections described here to create a source spectrum for fitting of GOME data. The solar spectrum and solar-rotational Raman convolved spectra, with and without the GOME slit function, are available from the authors.

5. CONCLUSIONS

The complete rotational Raman scattering database as described in the previous sections is available from the authors. This is a summary of the best available data that were found in the present investigation, and subsequent calculations. It provides a substantial improvement in the ability to model the atmospheric Ring spectrum, particularly when it is combined with the updated values of the wavelength dependent polarizability anisotropies also included in this study. One item not included here is the additional broadening due to Rayleigh-Brillouin scattering [Kattawar *et al.*, 1981]. For the rotational Raman lines, this will provide an extra source of broadening, although the extent of the broadening is within the uncertainties in the pressure broadening for scattering in the troposphere. The effect of Rayleigh-Brillouin scattering for the filling in of the central Cabannes line for narrow Fraunhofer lines might be significant for some satellite measurement conditions, although it has been found to be negligible for SBUV measurements [Joiner *et al.*, 1995]. During the course of the study, several references relating to vibrational Raman scattering were uncovered. These are included in the references with appropriate notation.

6. REFERENCES

K. Altmann, G. Strey, J.G. Hochenbleicher, and J. Brandmüller, Simulation des intensitätsverlaufs im Raman-spektrum von sauerstoff unter berücksichtigung der spinaufspaltung, *Z. Naturforsch.* **27a**, 56-64, 1972.

D.R. Bates, Rayleigh scattering by air, *Planet. Space Sci.* **32**, 785-790, 1984.

J.P. Burrows, K.V. Chance, A.P.H. Goede, R. Guzzi, B.J. Kerridge, C. Muller, D. Perner, U. Platt, J.-P. Pommereau, W. Schneider, R.J. Spurr, and H. van der Woerd, *Global Ozone Monitoring Experiment Interim Science Report*, ed. T. D. Guyenne and C. Readings, Report ESA SP-1151, ESA Publications Division, ESTEC, Noordwijk, The Netherlands, ISBN 92-9092-041-6, 1993.

M. Bussemer, Der Ring-effekt: Ursachen und einfluß auf die spektroskopische messung stratosphärischer spurenstoffe, Diplomarbeit, Universität Heidelberg, 1993.

K.V. Chance, J.P. Burrows, and W. Schneider, Retrieval and molecule sensitivity studies for the Global Ozone Monitoring Experiment and the SCanning Imaging Absorption spectroMeter for Atmospheric CHartographY, *Proc. S.P.I.E., Remote Sensing of Atmospheric Chemistry,* **1491**, 151-165, 1991a.

K. V. Chance, W. A. Traub, K. W. Jucks, and D. G. Johnson, On the use of O_2 spin-rotation lines for elevation angle calibration of atmospheric thermal emission spectra, *Int. J. IR-MM Waves* **12**, 581-588, 1991b.

D.J. Fish and R.L. Jones, Rotational Ramån scattering and the Ring effect in zenith-sky spectra, *Geophys. Res. Lett.* **22**, 811-814, 1995.

J.F. Grainger and J. Ring, Anomalous Fraunhofer line profiles, *Nature* **193**, 762, 1962.

L.A. Hall and G.P. Anderson, High-resolution solar spectrum between 200 and 3100 Å, *J. Geophys. Res.* **96**, 12,927-12,931, 1991.

D.M. Hunten, Surface albedo and the filling-in of Fraunhofer lines in the day sky, *Astrophys. J.* **159**, 1107-1110, 1970.

K.S. Jammu, G.E. St. John, and H.L. Welsh, Pressure broadening of the rotational Raman lines of some simple gases, *Can. J. Phys.* **44**, 797-815, 1966.

J. Joiner, P.K. Bhartia, R.P. Cebula, E. Hilsenrath, R.D. McPeters, and H. Park, Rotational Raman scattering (Ring effect) in satellite backscatter ultraviolet measurements, *Appl. Opt.* **34**, 4513-4525, 1995.

J. Joiner and P.K. Bhartia, The determination of cloud pressures from rotational Raman scattering in satellite backscatter ultraviolet measurements, *J. Geophys. Res.* **100**, 23,019-23,026, 1995.

G.W. Kattawar, A.T. Young, and T.J. Humphreys, Inelastic scattering in planetary atmospheres. I. The Ring effect, without aerosols, *Astrophys. J.* **243**, 1049-1057, 1981.

L.V. King, On the complex anisotropic molecule in relation to the dispersion and scattering of light, *Proc. Roy. Soc. A* **104**, 333-357, 1923.

R.L. Kurucz, I. Furenlid, J. Brault, and L. Testerman, Solar Flux Atlas from 296 to 1300 nm, National Solar Observatory, Sunspot, New Mexico, 240 pp., 1984.

A. Kuze and K. V. Chance, Analysis of cloud-top height and cloud coverage from satellites using the O_2 A and B bands, *J. Geophys. Res.* **99**, 14,481-14,491, 1994.

M. Loëte and H. Berger, High resolution Raman spectroscopy of the fundamental vibrational band of $^{16}O_2$, *J. Molec. Spectrosc.* **68**, 317-325, 1977.

M. Mizushima and R.M. Hill, Microwave spectrum of O_2, *Phys. Rev.* **93**, 745-748, 1954.

J. Noxon and R. Goody, Noncoherent scattering of skylight, *Izv. Atmos. Ocean. Phys.* **1**, 163-166, 1965.

C.M. Penney, R.L. St. Peters, and M. Lapp, Absolute rotational Raman cross sections for N_2, O_2, and CO_2, *J. Opt. Soc. Amer.* **64**, 712-716, 1974.

G. Placzek and E. Teller, Die rotationnstruktur der Ramanbanden mehratomiger moleküle, *Z. Physik* **81**, 209-258, 1933.

D.L. Renschler, J.L. Hunt, T.K. McCubbin, Jr., and S.R. Polo, Triplet structure of the rotational Raman spectrum of oxygen, *J. Molec. Spectrosc.* **31**, 173-176, 1969.

N.H. Rich and D.W. Lepard, Spin structure in the Raman spectrum of oxygen, *J. Molec. Spectrosc.* **38**, 549-551, 1971.

S. Solomon, A.L. Schmeltekopf, and R.W. Sanders, On the interpretation of zenith sky absorption measurements, *J. Geophys. Res.* **92**, 8311-8319. 1987.

M. Tinkham and M.W.P. Strandberg, Theory of the fine structure of the molecular oxygen ground state, *Phys. Rev.* **97**, 937-951, 1955.

A.T. Young, Rayleigh scattering, *Appl. Opt.* **20**, 522-535, 1981.

7. ACKNOWLEDGEMENTS

This research was supported by NASA grant NAGW-2541 and by ESA contract 10996/94/NL/CN.

TABLE 1. Relative Rayleigh and Raman Scattering Intensities Mostly from Kattawar *et al.*, 1981

V polarization in	H polarization in	Sum (natural light in)
	Rayleigh-Brillouin	
$^VC_V = 180 + 4\epsilon$	$^HC_V = 3\epsilon$	$^0C_V = 180 + 7\epsilon$
$^VC_H = 3\epsilon$	$^HC_H = 3\epsilon + (180 + \epsilon)\cos^2\theta$	$^0C_H = 6\epsilon + (180 + \epsilon)\cos^2\theta$
$^VC_0 = 180 + 7\epsilon$	$^HC_0 = 6\epsilon + (180 + \epsilon)\cos^2\theta$	$^0C_0 = (180 + 13\epsilon) + (180 + \epsilon)\cos^2\theta$
		$\rho_0^C = 6\epsilon/(180 + 7\epsilon)$
	Raman	
$^VW_V = 12\epsilon$	$^HW_V = 9\epsilon$	$^0W_V = 21\epsilon$
$^VW_H = 9\epsilon$	$^HW_H = 9\epsilon + 3\epsilon\cos^2\theta$	$^0W_H = 18\epsilon + 3\epsilon\cos^2\theta$
$^VW_0 = 21\epsilon$	$^HW_0 = 18\epsilon + 3\epsilon\cos^2\theta$	$^0W_0 = 39\epsilon + 3\epsilon\cos^2\theta$
		$\rho_0^W = 6/7$
	Sum	
$^VT_V = 180 + 16\epsilon$	$^HT_V = 12\epsilon$	$^0T_V = 180 + 28\epsilon$
$^VT_H = 12\epsilon$	$^HT_H = 12\epsilon + (180 + 4\epsilon)\cos^2\theta$	$^0T_H = 24\epsilon + (180 + 4\epsilon)\cos^2\theta$
$^VT_0 = 180 + 28\epsilon$	$^HT_0 = 24\epsilon + (180 + 4\epsilon)\cos^2\theta$	$^0T_0 = (180 + 52\epsilon) + (180 + 4\epsilon)\cos^2\theta$
		$\rho_0^T = 6\epsilon/(45 + 7\epsilon)$

UARS SOLSTICE Data as a Calibration and Validation of GOME

P. Peeters[1], P.C. Simon[1], G. Rottman[2] & T.N. Woods[2]

[1]Belgian Institute for Space Aeronomy
Brussels, Belgium
[2]High Altitude Observatory/NCAR
Boulder, Colorado; USA

Abstract

The GOME instrument consists of a spectrometer and scan mechanism to provide spectral radiance measurements of the earth's atmosphere over the entire spectral range 240 to 790 nm. The photometric calibration of the instrument is accomplished with a separate calibration unit including both calibration lamps and a diffuser to direct solar radiation into the spectrometer. In this report we concentrate on a calibration activity using the solar irradiance as a well calibrated source of known illumination, and from the GOME instrument response we derive the sensitivity of the instrument and changes in the instrument response with time. As the "known" solar input we use daily observations of the SOLSTICE instrument on NASA's Upper Atmosphere Research Satellite (UARS). SOLSTICE covers the spectral range from 120 to 420 nm, and the overlap with GOME spectral range provides a calibration of channels 1 and 2. The 2σ absolute calibration of the SOLSTICE data is ±4%, a value that can be transferred to the GOME observations by direct comparison of the two data sets. In addition, the 2σ relative accuracy of the SOLSTICE data set is approximately ±2%, and helps to determine trends and changes in the GOME instrument response. The GOME/SOLSTICE comparison establishes characteristics of the GOME instrument in the solar irradiance configuration only, and additional and ancillary information on the solar diffuser and scan mirrors is also required to establish the calibration of GOME for radiance observations.

1. INTRODUCTION

The Global Ozone Monitoring Experiment (GOME) was launched onboard the ERS-2 spacecraft in April 1995. This instrument is a nadir-viewing spectrometer that observes solar radiation backscattered by the Earth's atmosphere and scattered from its surface. Because the input solar radiation is absorbed along its path through the atmosphere, the returned spectra recorded by GOME contain detailed information of the atmosphere's content of ozone, nitrogen dioxide, water vapor, as well as other trace gases. Knowledge of the solar radiation input is also usually required to establish the amount of absorption, although there are differencing techniques that to first order are independent of the incoming solar radiation because they use two or more wavelengths. In order to extract reliable quantitative information on the atmospheric constituents, we require precise knowledge of the sensitivity of the GOME instrument. Moreover, in order to detect changes in time of these atmospheric constituents, we will require an additional precise understanding of how the GOME instrument sensitivity has evolved and varied in time.

The GOME instrument can directly measure the Earth's radiance scattered into its spectrometer, or in an alternate mode, using a slightly different optical path, it can measure the solar irradiance arriving at the instrument. In both configurations, the optics of the spectrometer are the same, only a scanning mirror and diffuser are inserted for the direct solar measurement. In order to extract the desired geophysical unit of observed radiance, we must establish the efficiency of the instrument to transfer and convert the incoming radiation to a recorded instrument signal. This efficiency is determined in the pre-launch calibration, but then it needs to be validated once the GOME is operating on-orbit, and furthermore, it must be continually monitored as the mission proceeds. From a long history of space observations, there is every reason to believe that in time the GOME efficiency will change and, in fact, the efficiency will usually decrease with time. This aging process is likely a complicated combination of contamination of optical elements coupled with the exposure to radiation, especially very energetic ultraviolet radiation of the Sun. By limiting exposure and taking every precaution to avoid contamination, both in the preparation and testing of the instrument prior to launch and in the outgassing environment of the satellite on orbit, the instrument degradation can be minimized to perhaps only a few percent per year of operation.

In the research project described here, we use a priori information of the solar radiation to establish the GOME instrument response and to evaluate how this in-flight efficiency compares with the pre-launch calibration of the instrument. We are using the ultraviolet irradiance measurements of the SOLSTICE instrument, one of two UV irradiance instruments on the Upper Atmosphere

Research Satellite (UARS). These measurements extend back to the launch of UARS late in 1991 and are expected to continue for at least another three to five years. Therefore the SOLSTICE will provide a continuous data set for the cross-calibration of the GOME instrument. Although details of its optical design are quite different from the GOME design, the SOLSTICE is also a spectrometer with spectral coverage overlapping the GOME channel 1 and channel 2 and with comparable spectral resolution. The SOLSTICE measurements have their own inherent uncertainties with respect to both absolute calibration and with respect to drifts in the instrument response over time, and these factors are considered in this report. We rely on the independence of the two observations to gain an important insight into the validity of the measurements and our confidence in the respective calibration techniques, with special emphasis on an improved understanding of the GOME performance.

The SOLSTICE instrument is described below in Section 2. Its observations have been validated by comparison with the SUSIM instrument on UARS and with the SSBUV and SUSIM instruments on the first two ATLAS missions, and the resulting solar irradiance scale is believed to be accurate to ±4%. Section 3 discusses the GOME observations and compares channel 1 (240 to 295 nm) and 2 (290 to 405 nm) with the SOLSTICE measurements. We discuss three aspects of the comparison: the wavelength registration, the irradiance validation (differences in absolute calibration), and trends that can be established in the GOME instrument response. Finally, in Section 4 we give our conclusions and our recommendations for future activities.

2. OVERVIEW OF THE SOLSTICE MEASUREMENTS

The Solar Stellar Irradiance Comparison Experiment (SOLSTICE) is one of ten instruments on the Upper Atmosphere Research Satellite (UARS). The primary scientific objective for the SOLSTICE program is to make precise and accurate measurements of the solar spectral irradiance, over the spectral range 119 to 420 nm. Moreover, it has a goal of measuring solar variability over arbitrarily long time periods, for example, over the duration of the UARS mission that may exceed ten years. The requirement for absolute accuracy is on the order of ±10% (2-σ value), but the requirement for relative accuracy between any two measurements spaced throughout the UARS mission is ±2% (2-σ value). To achieve these goals the instrument response is determined from both preflight calibrations and from in-flight calibration and validation programs. The SOLSTICE has been designed with the unique capability of monitoring a number of bright blue stars (those with O and B spectral type) using the same optical elements and detectors employed for the solar observations. These stars, which vary by only small fractions of a percent over long time periods, provide a stable reference for deriving the SOLSTICE instrumental degradation rates.

A second instrument, the Solar Ultraviolet Irradiance Monitor (SUSIM) (Brueckner et al., 1993), is also aboard UARS measuring the solar UV irradiance with basically the same spectral coverage and resolution as SOLSTICE. However, SOLSTICE and SUSIM have quite different optical designs and, moreover, employ dramatically different in-flight calibration techniques.

The reader is referred to papers by Rottman et al. (1993), Woods et al. (1993), and Woods et al. (1996) for details of the SOLSTICE instrument design, measurement technique, calibrations, and validations. Briefly, SOLSTICE is a three channel grating spectrometer which uses the same optical elements for both the solar and stellar observations but uses interchangeable entrance apertures, bandpasses, and integration times to accommodate the 10^8 : 1 dynamic range between the solar and stellar irradiances. The three overlapping channels are the G channel from 119 to 190 nm ($\Delta\lambda$=0.1 nm), the F channel from 170 to 320 nm ($\Delta\lambda$=0.25 nm), and the N channel from 280 to 420 nm ($\Delta\lambda$=0.35 nm). Only the SOLSTICE F and N channel data are included here for comparisons with the GOME solar irradiances at wavelengths longward of 240 nm.

For the solar irradiances, the SOLSTICE data are corrected for scattered light, detector linearity, detector dark counts, detector gain changes, instrument sensitivity and degradation. The stellar irradiances undergo similar processing, but the degradation factors are treated as free parameters and are adjusted to make the mean stellar irradiance invariant in time. The resulting degradation factors are then the same ones applied to the solar data. The wavelength scale is referenced in vacuum wavelength units to high resolution solar spectra above 200 nm (Anderson and Hall, 1989; Kurucz, 1991) and to atomic or ionic transition levels below 200 nm (Sandlin et al., 1986; Kelly and Palumbo, 1973; Kelly, 1987). Each spectrum's wavelength scale is also adjusted to the SOLSTICE reference wavelength scale to account for small wavelength shifts related to temperature changes and to pointing offsets. The primary science requirement is to provide one full solar spectrum per calendar day, and to achieve this, the data processing algorithm combines typically 15 individual observations to form the single daily spectrum, adjusted to 1 AU. This daily SOLSTICE spectrum, called the Level 3BS product, is reported for each 1.0 nm interval (centered on the half nm) between 119 to 420 nm and is available from the NASA Goddard data center (its Web address is http://daac.gsfc.nasa.gov).

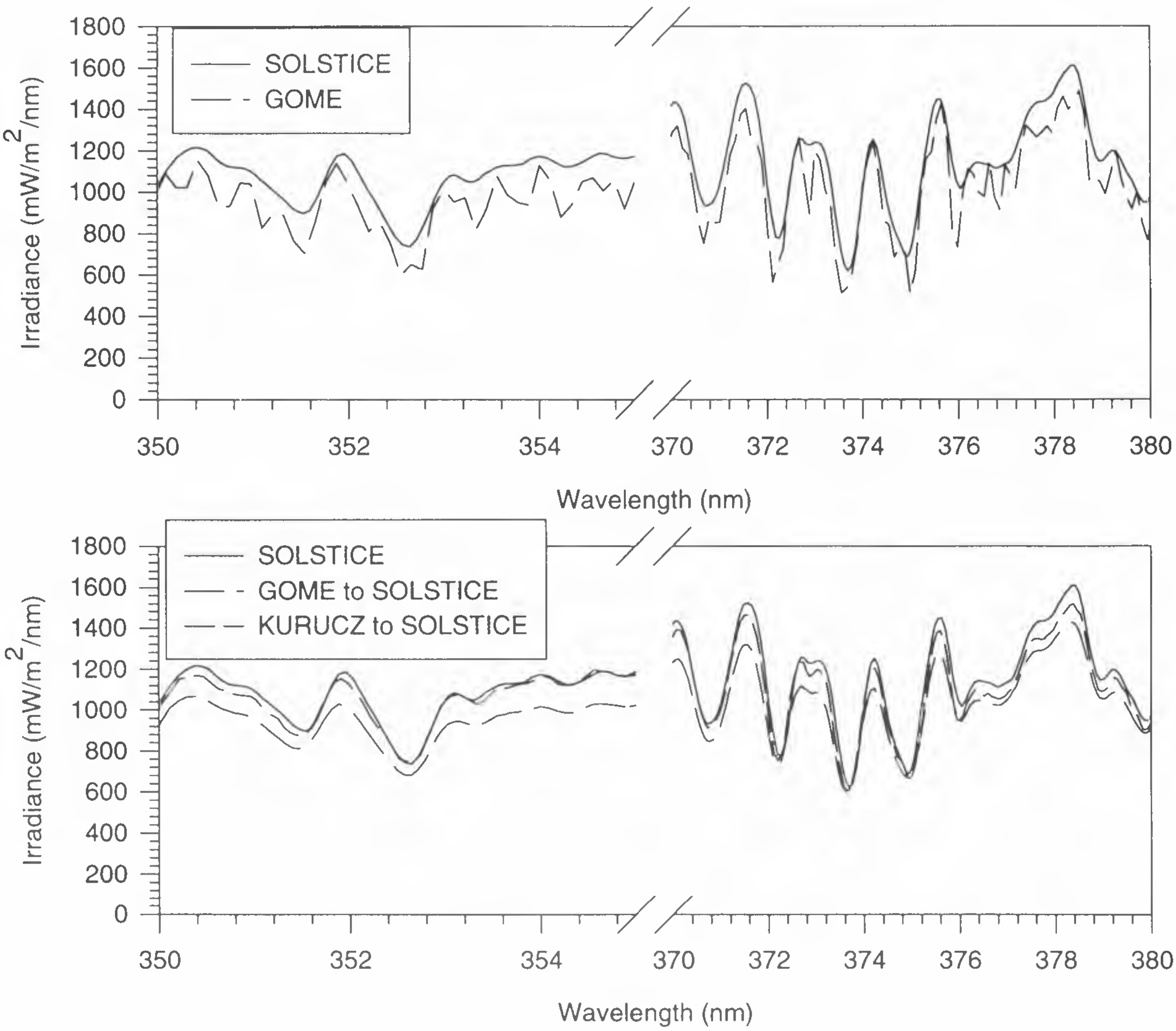

Figure 1. *(a) Two wavelength regions of SOLSTICE and GOME irradiance at instrumental resolution showing the differences in resolution. (b) SOLSTICE at instrumental resolution compare to GOME and high resolution ground based spectra convolved with the SOLSTICE effective bandpass.*

The validation of the SOLSTICE solar irradiances was a joint effort of four solar UV irradiance programs (Woods et al., 1996). The measurements of the solar ultraviolet spectral irradiance made by the two UARS solar instruments, SUSIM and SOLSTICE, are compared with same-day measurements by two other solar instruments on the Shuttle Atmospheric Laboratory for Applications and Science (ATLAS) missions, ATLAS SUSIM and Shuttle Solar Backscatter Ultraviolet (SSBUV) experiment. Measurements from the four instruments agree to better than the 2-σ uncertainty of any one instrument, which is ±5-10% for all wavelengths above 160 nm, as well as for strong emission features below 160 nm. Additionally, the long-term relative accuracy of the two UARS data sets is better than the original 2% goal, especially at wavelengths greater than 160 nm. This level of agreement is credited to accurate pre-flight calibrations coupled with comprehensive in-flight calibrations to track instrument degradation. Because the agreement of the SOLSTICE solar irradiance with the other three measurements is better than the SOLSTICE absolute accuracy of ±10%, the SOLSTICE uncertainty presented in this report (e.g. Section 3 and fig 2) is the SOLSTICE relative accuracy (~2%) plus the average of the differences between the four solar irradiance measurements from UARS and ATLAS (Woods et al., 1996).

3. GOME INSTRUMENT PERFORMANCE

The GOME instrument performs daily observation of the solar irradiance during its Sun Observation Timeline (SOT), a 42 seconds timeline inserted into the Normal Observation Timeline (NOT) when the satellite is close to the earth's north pole. Prior to launch the sensitivity of GOME was evaluated using radiance standards, namely 1000 Watt FEL lamps calibrated by NIST (ESA, 1995). Although carefully checked on the ground, in-flight validation of the solar irradiance is necessary to detect changes or drift in the response of the instrument. This is particularly important for solar irradiance measurements since they are performed using a diffuser plate and mirror inserted between the sun and the detector. Furthermore, changes in the response of the instrument are to be expected, especially early in the mission when the satellite has been put into orbit and first exposed in vacuum to highly energetic solar radiation. The diffuser and other optical elements will likely change during the satellite lifetime, and their performance will evolve with respect to preflight calibration. For these reasons, external and independent sources of solar irradiance are essential for monitoring of the in-flight performance. The SOLSTICE daily solar irradiance measurements provide an accurate and validated reference for this purpose.

Up to now, only limited GOME solar irradiance spectra have been provided by DLR and included in this work: July 22 to 25, August 24 to 27, September 1 to 3 and 14 to 17, October 4 to 7 and 29 to 31 and November 8 to 11. As far as possible, time coincident SOLSTICE irradiance spectra are retrieved from the NCAR database, and we have used the "level 3BS merged" high resolution products.

It is important to note that only SOLSTICE data up to September 1994 are fully validated and released. Data used in this work are preliminary and provisional. More specifically, new calibration parameters taking into account revised stellar pointing information are now being applied to the 1995 data.

3.1. Wavelength validation

Since July 22nd, all GOME wavelength values are reported in vacuum, as is the case for SOLSTICE wavelengths. Therefore there is no need to convert from one scale to another as was the case for the first two GOME spectra (30 May and 6 June).

The spectral resolution of GOME and SOLSTICE are somewhat different. Although the theoretical SOLSTICE resolution is 0.2 nm for channel F and N, the "effective" bandpasses are larger. The SOLSTICE spectrometer design (Monk-Gilleson) only permits a single wavelength to be in perfect focus and other wavelengths will have a slightly broader effective bandpass. This effect is about 10% over the spectral range if the best focus is in the center of the spectral range. If the best focus is not centered in the spectral range, then the effective bandpass becomes even larger. The effect is about 1.1 for the F channel ($\Delta\lambda$~0.25 nm) and 1.8 for the N channel ($\Delta\lambda$~0.35 nm). The differences between SOLSTICE and GOME resolution can be seen in Figure 1a where both irradiances are plotted at instrumental resolution for 22 July 1995. One can clearly identify in the GOME spectrum features missing in the SOLSTICE spectrum. Note that the displayed wavelength region correspond to channel N of SOLSTICE where the effective bandpass is the largest. Figure 1b depicts both GOME and high resolution ground based spectra (Kurucz et al, 1991) convolved with the SOLSTICE effective bandpass. The different features and structures now match very well between the two spectra.

3.2. Irradiance validation

The SOLSTICE irradiance are reported adjusted to one astronomical unit and GOME is adjusted accordingly using the formula:

$$I_0 = I\left(\frac{d}{d_0}\right)^2 \qquad (1)$$

where

$$\left(\frac{d_0}{d}\right)^2 = 1.000110 + 0.034221\cos\Gamma$$
$$+ 0.00128\sin\Gamma + 0.000719\cos 2\Gamma \qquad (2)$$
$$+ 0.000077\sin 2\Gamma$$

and $\begin{matrix}\Gamma = 2\pi(J-1)/365 \\ 1 \le J \le 365\end{matrix}$,d_0 correspond to 1 AU. Hence.

The procedure used to adjust both spectra to a common wavelength scale is the same that has been defined for the UARS/ATLAS irradiance comparison (Woods et al., 1996). Each spectrum is first interpolated to a common 0.025 nm scale.. The resulting spectrum is then convolved to a common 1 nm grid, centered at half nm, ranging from 240 to 420 nm using a triangular convolution kernel of 1 nm FWHM. This procedure removes many (but not all) of the discrepancies most notable near the strong absorption lines. The relative irradiance difference is defined as

$$\Delta(\lambda) = \left(\frac{I_{GOME}(\lambda)}{I_{SOLSTICE}(\lambda)} - 1\right) \qquad (3)$$

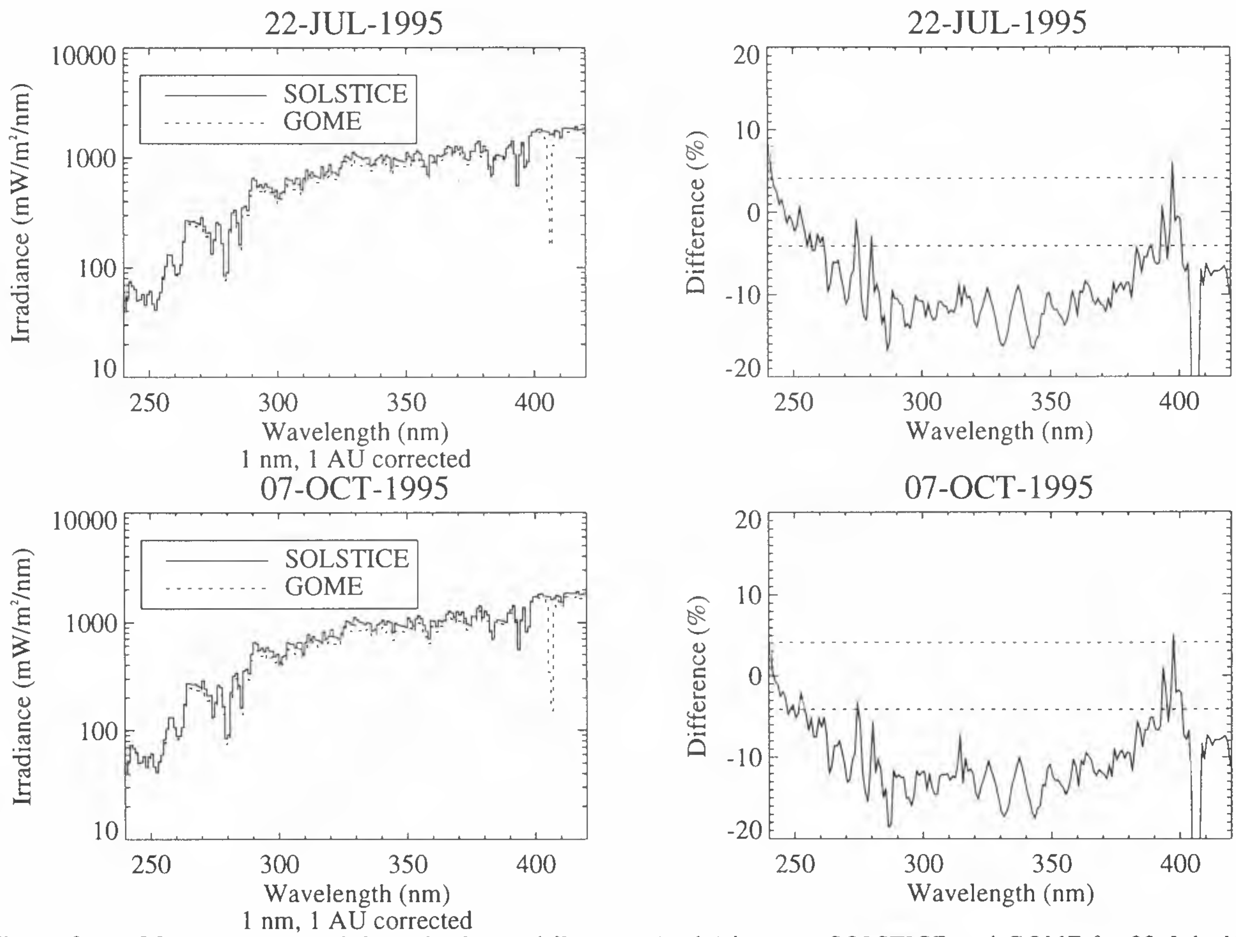

Figure 2a and b. *Raw spectra (left) and relative differences (right) between SOLSTICE and GOME for 22 July 1995 (a) and 7 October 1995 (b). Both spectra* are *reduced to 1 nm intervals and normalized to 1 AU. The dashed lines in the difference plots indicate the SOLSTICE 2-σ uncertainty (±4%) based on the recent UARS/ATLAS comparison (Woods et al., 1996).*

These wavelength dependent differences are compute for each pair of coincident SOLSTICE/GOME spectra. However, the most striking differences are identified on the first comparison and are reasonably constant in each subsequent comparison. Figure 2a and 2b display both the raw spectra and the relative difference between GOME and SOLSTICE expressed in percent for 22 July 1995 (a) and 7 October 1995 (b). SOLSTICE average $\pm 2\sigma$ uncertainty is indicated by a pair of dashed lines on the difference plots. This uncertainty is approximated as the average over that specified wavelength range from the recent UARS/ATLAS comparison (Woods et al., 1996).

The discrepancies at the overlap region between channels 2 and 3 (around 400 nm) show up immediately. On the other hand, the matching between channel 1 and 2 (307 nm) is rather successfully controlled. The (2-3) overlap problem has been recognized from the beginning and will be addressed in the future.

The agreement between SOLSTICE and GOME is reasonably good around 250 nm and above 390 nm. However, there is a marked deviation with a characteristic parabolic shape between 300 and 370 nm that can be as high as 13%. According to TPD, the disagreement may originate from changes in the instrument response between air and vacuum operation (Zoutman et al., 1995). Studies are in progress at TPD to resolve this problem. The average deviations can be summarized in the following table:

	Average differences w.r.t. SOLSTICE (%)			
Date	240-250	250-300	300-370	370-400
22 July	1.9	-8.1	-11.8	-6.2
24 Aug	-2.0	-8.3	-12.1	-6.3
14 Sept	-0.5	-9.4	-12.5	-6.6
7 Oct	-1.7	-10.2	-12.8	-6.9

We are encouraged that the deviation has globally increased between these two different times by only 1 to 2%. We discuss this behavior in the section 3.3.

The last feature that we consider on these plots is the so-called "etalon effect". This effect is caused by constructive and destructive interferences of light that falls on the detector arrays. The light is first internally reflected in the passivating SiO_2 layer and possibly in a thin layer of ice that is formed on the cooled detector arrays. During the preflight investigations, it was found that the etalon structure shifted considerably in time due to the forming and increasing of an ice layer on the detector. It was predicted that the shift of the etalon structure in flight would be much smaller due to the almost perfect vacuum conditions in the in-flight

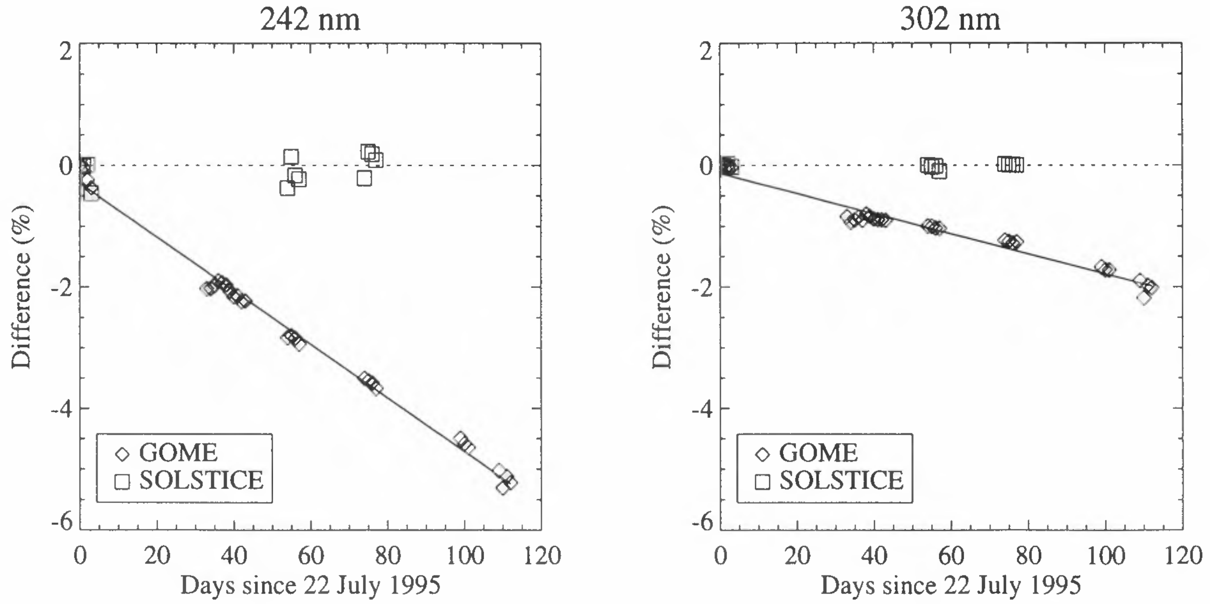

Figure 3. *Difference of the integrated irradiance within 4 nm relative to 22 July 1995 at 242 nm (left) and 302 nm (right). Both SOLSTICE (square) and GOME (diamond) are displayed as well as a linear fitting of the GOME values.*

condition. This etalon structure can be easily identified on the GOME/SOLSTICE ratio and is characterized by a long wavelength modulation beginning around 340 nm. This structure shows up also at longer wavelengths (440 and 640 nm) but is not displayed here since it is beyond the common SOLSTICE-GOME wavelength window. It is hoped that the etalon structure will reach a stable condition in order to be accurately accounted for in the radiance response function.

3.3. GOME degradation analysis

We have seen previously that the GOME/SOLSTICE ratio increases with time. We expect the GOME instrument response to slowly evolve and degrade in time, a common behavior of spaceborne instruments.

To quantify this degradation, we continually compute the ratio with respect to an average reference spectrum. We select the spectrum of 22 July 1995 as our reference spectrum and evaluate the evolution of the ratio:

$$D(\lambda,t)=\left(\frac{I_t(\lambda)}{I_{ref}(\lambda)}-1\right) \qquad (4)$$

Each irradiance value is averaged over 4 nm band (λ±2nm) and plotted against time. The same procedure is applied to the SOLSTICE irradiance taking the spectrum for UARS day 1410 (referenced to the launch date of UARS) as reference.

The results are displayed in figure 3 for λ=242 nm and λ=302 nm. The most striking feature is the linear decrease of the GOME irradiance for the period considered. At 242 nm, the irradiance decreases at a rate equal to -0.044 %/day, and -0.016 %/day at 302 nm. Thanks to its reliable stellar calibration, SOLSTICE does not exhibit any significant drift over that period. We are reasonably confident in the fact that SOLSTICE measures the "real" solar flux. However, several SOLSTICE values have been removed from this comparison. They correspond to the days when the UARS satellite is in a configuration such that the solar arrays may significantly (about 1%) enhance straylight in the SOLSTICE spectrometer and corrupt those measurements. The SOLSTICE data processing algorithms are now being improved to remove these corrupted values.

We are particularly surprised by the very low spread of the GOME measurements, and the data fit very well the linear regression. The day-to-day measurements exhibit a very good accuracy. Removing the linear trend, the residual "noise" for 242 nm is significantly below 1% and likely a true solar variability.

To compare the GOME degradation to SOLSTICE, we have plotted in figure 4 the stellar correction coefficient of SOLSTICE from the beginning of its operation (October 3, 1991). We have overlaid the measured GOME degradation. The GOME degradation rate is surprisingly close to the stellar correction applied to SOLSTICE instrument in its early days of operation. The observed degradation rate of GOME is quite reasonable and similar in magnitude instruments as SOLSTICE's degradation rate. Note however that the time scale is defined as the real calendar day and not the total exposure time. SOLSTICE exposure time is 8 hours per day while GOME operates in solar measurement mode only for 40 seconds per day.

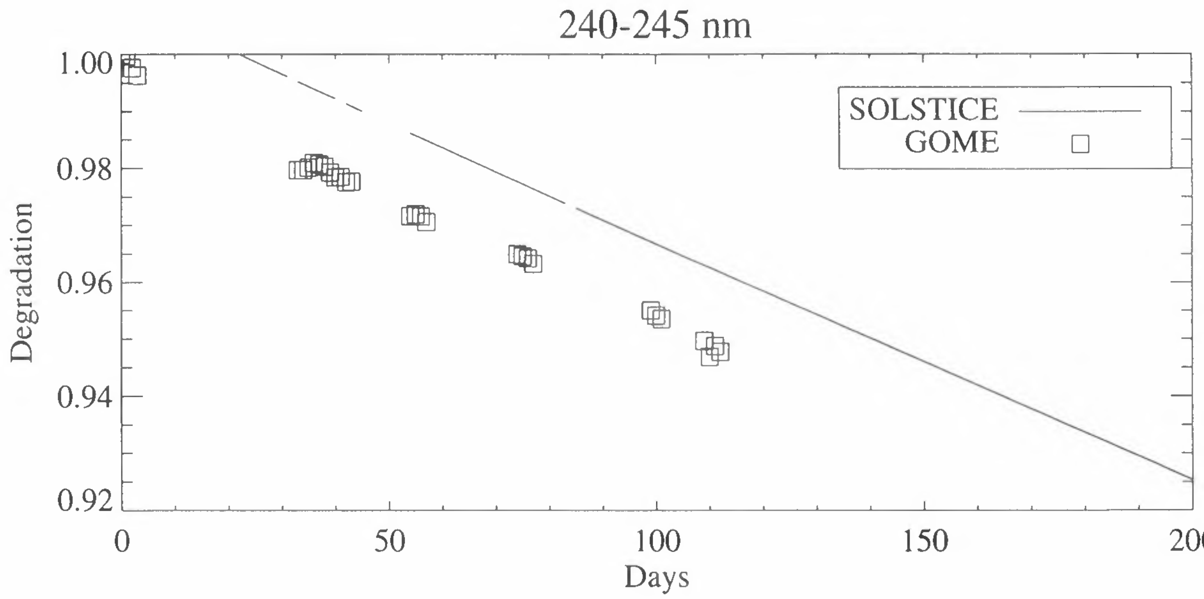

Figure 4. *Stellar degradation rate of the SOLSTICE instrument in the 240-245 nm range (solid line) during its first 200 days of measurement compared to the degradation of the GOME instrument at 242 nm.*

Not surprisingly, the highest degradation rate is found in the UV short wavelength region (≈250 nm). The higher energy of this radiation is perhaps more efficient to degrade the optical coatings or the diffuser. However, the whole wavelength range from 240 to 790 nm show degradation at different rates as depicted in figure 5a and 5b. Figure 5a displays the degradation rate for wavelength in the GOME-SOLSTICE window (240-420 nm). The maximum (in absolute value) is found at 240 nm and the degradation gets smaller for longer wavelengths. Unfortunately, the etalon effect prevents us from distinguishing between the degradation rate and the etalon modulation. Applying a rough smoothing, one can eventually identify the overall degradation rate for the whole GOME wavelength range (Fig. 5b).

4. CONCLUSIONS

So far, 30 GOME solar irradiance spectra have been received and analyzed. These include spectra from July, August, September, October and November 1995. SOLSTICE level 3BS merged spectra have been used for calibration and validation of wavelength, irradiance and instrument degradation. As far as possible, the most recent SOLSTICE calibration files have been used for the year 1995. Though possible modifications may be provided in the future, we anticipate a maximum change of 1 or 2% near 250 nm and much less for longer wavelength.

Wavelength consistency has been checked in the common GOME-SOLSTICE wavelength window of 240 to 420 nm. There are no significant discrepancies between GOME and SOLSTICE when the two data sets are intercompared at the same effective spectral resolution.

Irradiance validation shows that GOME displays a systematic offset with respect to SOLSTICE. Since we are reasonably confident in SOLSTICE uncertainty based on previous UARS/ATLAS validation, this discrepancy likely originates in the changes of pre-flight/in-fly calibration of GOME, probably due to changes in the diffuser and component optical coating characteristics. This offset needs to be further studied. The deviation shows a characteristic parabolic shape curve between 260-370 nm.

The instrument degradation is analyzed by comparing selected wavelength integrated irradiance with respect to an arbitrary reference date (22 July 1995). In the UV, the GOME instrument irradiance exhibits a marked linear decrease of the absolute irradiance. The maximum decreasing rate is found at short wavelength (240 nm) and is of -0.04%/day. The degradation decreases (less degradation) for increasing wavelength. However, the degradation analysis is perturbed by the etalon structure around 350 nm. Compared to SOLSTICE's early instrumental degradation, GOME degradation rates are of similar magnitude. These rates are reasonable for satellite-borne optical instruments subjected to highly energetic solar fluxes. Furthermore, comparing day-to-day irradiance, the GOME instrument displays a very good precision of less than 0.5%.

5. REFERENCES

Anderson, G.P. and L.A. Hall, Solar irradiance between 2000 and 3100 Angstroms with spectral band pass of 1.0 Angstroms, J. Geophys. Res., 94, 6435-6441, 1989.

Brueckner, G.E., K.L. Edlow, L.E. Floyd, J.L. Lean, and M.E. VanHoosier, "The Solar Ultraviolet Spectral Irradiance Monitor (SUSIM) Experiment on Board the Upper Atmospheric Research Satellite (UARS)", J. Geophys. Res., 98, 10695-10711, 1993.

Kelly, R.L., and L.J. Palumbo, Atomic and ionic emission lines below 2000 Angstroms, NRL Report., No. 7599, 1973.

Kelly, R. L., Atomic and ionic spectrum lines below 200 Angstroms: hydrogen through krypton, J. Phys. Chem. Ref., 16, (S1), 1-1678, 1987.

Kurucz, R.L., The solar spectrum, in Solar Interior and Atmosphere, eds. A.N. Cox, W.C. Livingston, and M.S. Matthews, University of Arizona Press, Tucson, 1991.

Rottman, G. J., T. N. Woods, and T. P. Sparn, Solar Stellar Irradiance Comparison Experiment 1: 1. instrument design and operation, J. Geophys. Res., 98, 10667-10678, 1993.

Sandlin, G.D., J.-D. F. Bartoe, G.E. Brueckner, R. Tousey, and M.E. VanHoosier, The high-resolution solar spectrum, 1175-1710 Å, Ap. J., Suppl., 61, 801-898, 1986.

Woods, T. N., G. J. Rottman, and G. J. Ucker, Solar Stellar Irradiance Comparison Experiment 1: 2. instrument calibration, J. Geophys. Res., 98, 10679-10694, 1993.

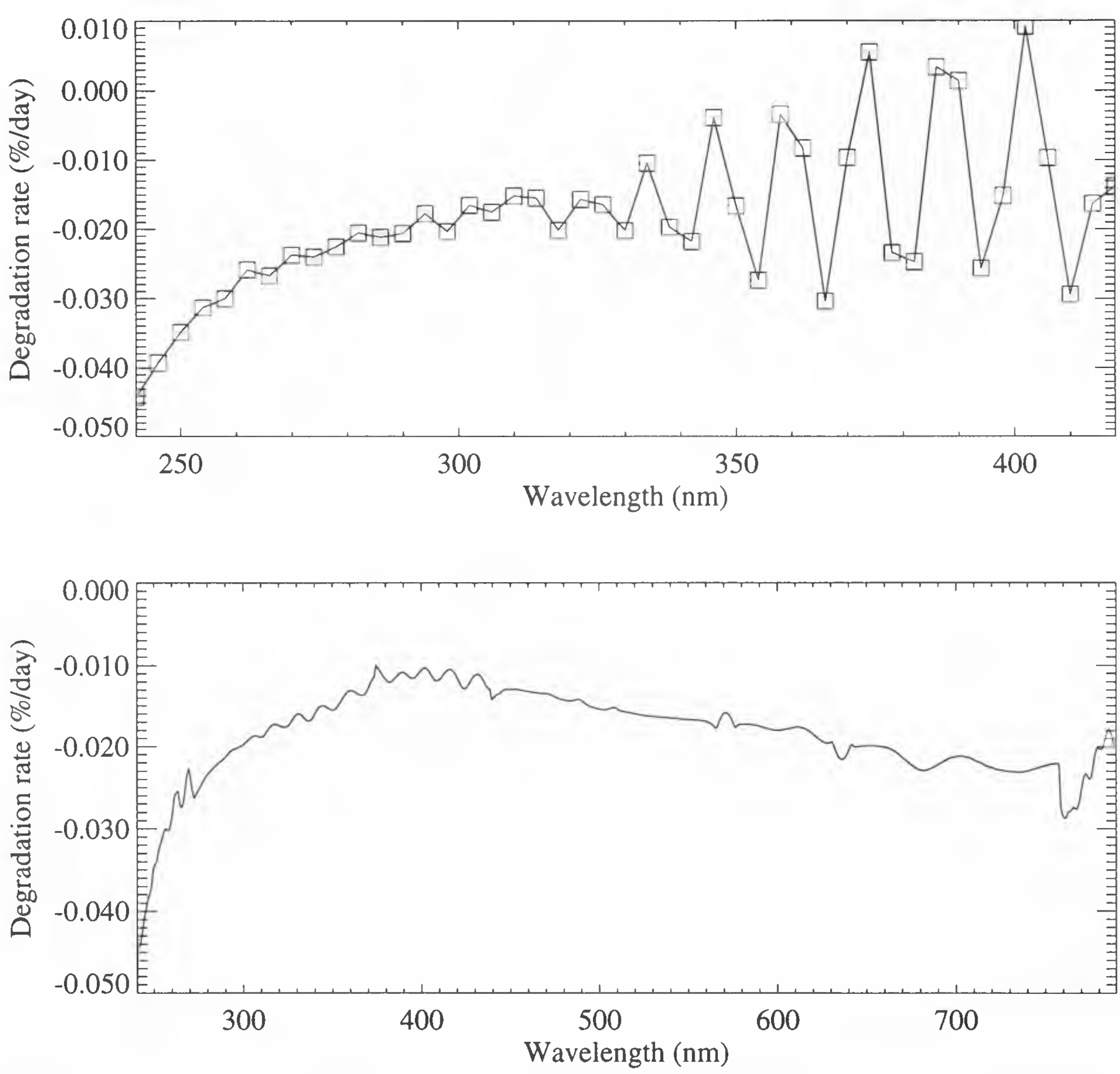

Figure 5. *(a) GOME degradation rate for the 240-420 nm range estimated from the linear regression of the integrated irradiance over 100 days of measurements. (b) Degradation rate for the whole GOME spectral range. Etalon structure and dichroic structure have been smoothed out.*

Woods, T. N., D. K. Prinz, J. London, G. J. Rottman, P. C. Crane, R. P. Cebula, E. Hilsenrath, G. E. Brueckner, M. D. Andrews, O. R. White, M. E. VanHoosier, L. E. Floyd, L. C. Herring, B. G. Knapp, C. K. Pankratz, and P.A. Reiser, "Validation of the UARS Solar Ultraviolet Irradiances: Comparison with the ATLAS-1, -2 Measurements", J. Geophys. Res., in press, 1995.

ESA Publication Division, GOME Users Manual, ESA (ESTEC), SP-1182, September 1995

Zoutman, E, A. Bos, M. Le Kluse, GOME Commissioning phase 2 results, TPD Space Instrumention, TPD-ERS-GO-MIR-42, 1 November 1995

Acknowledgment

We thank B. Knapp, O.R. White and C. Pankratz (HAO/NCAR) for helpful discussions and support in using HAO SOLSTICE database. This work has been supported by PRODEX-UV A.O. ERS2-Project 2 (151903).

GOME Calibration and Validation Using Backscatter UV Techniques

E. Hilsenrath[1], J. Gleason[1], S. Janz[2], X-y Gu[3], R.P. Cebula[3], K. Chance[4], and R. Hoekstra[5]

1. NASA/Goddard Space Flight Center
2. IDEA Corporation
3. Hughes-STX Corporation
4. Smithsonian Astrophysical Society
5. TNO/TPD

Abstract

GOME radiance, irradiance, and ozone products were validated by NASA, Goddard Space Flight Center through three tasks which included, pre-launch calibration comparisons with SBUV and TOMS radiometric standards, validation of GOME Level-1 irradiance and radiance and Level 2 total ozone data products using SBUV/2 and TOMS algorithms and data, and studies of GOME data using the Goddard radiative transfer code. The pre-launch calibration using the NASA large aperture integrating sphere was checked against that provided by TPD. Agreement in the calibration constants, derived in air, between the Goddard and TPD system were better than 3%. Validation of Level-1 irradiance data included comparison of GOME and SSBUV and the UARS solar irradiances measurements. Large wavelength dependent differences, as high as 10%, were noted between GOME and the US instruments. This discrepancy has now been attributed to radiometric sensitivity changes experienced by GOME when operating in a vacuum. GOME Earth radiance data were then compared to the NOAA-14 SBUV/2 radiances. These results show that between 340 and 400 nm the differences in GOME and SBUV/2 data are less than 5% with some wavelength dependence. At wavelengths shorter than 300 nm, differences are of the order of 10% or more where the GOME radiances are larger. To test GOME DOAS retrieved total ozone values, these values were compared with ozone amounts retrieved using GOME radiances in the TOMS version-7 algorithm. The differences showed a solar zenith angle dependence ranging from 0 to 10% where the TOMS algorithm values were higher. GOME radiances below 300 nm were further validated by selecting radiances at wavelengths normally used by SBUV and processing them through the SBUV ozone profile algorithm and then compared to climatological values. The GOME ozone profiles ranged from 10-30% lower over altitude compared to climatological values. This is consistent with the offsets detected in the SBUV/2 radiance comparisons at wavelengths shorter than 300 nm.

Introduction

NASA Goddard Space Flight Center has participated in the GOME validation through an ESA announcement of opportunity. The proposed validation investigation included three tasks: 1) Pre-launch calibration evaluation, 2) Post launch data validation, and 3) Algorithm studies using GOME data. The validation effort focused primarily on GOME data from Channels 1 and 2. These channels cover the wavelength range 240 to 405 nm which overlap wavelengths covered by NASA's SBUV and TOMS instruments. Our overall goal is to develop a consistent, long term, global ozone data set through better understanding of instrument performance and radiative transfer properties of the atmosphere. A description of the methodology for pre- and post-launch calibration, validation, and of producing long term data sets from US BUV instruments has been reviewed by *Hilsenrath et al.*, 1994.

In this progress report we describe briefly results from the pre-launch calibration activity using NASA calibration standards, post-launch validation of Level 1 irradiances and radiances from comparisons with SSBUV and NOAA-14 SBUV/2 modeled radiances and Level 2 DOAS ozone retrievals compared with BUV ozone retrievals using the Level 1 GOME radiance in the TOMS version 7 and SBUV profile algorithms. Finally we have conducted very preliminary algorithm research using GOME radiance to study the Ring effect and the effect of absorbing aerosols on the GOME radiances. The GOME Level 1 and Level 2 data used in this first phase of validation was received from the DLR up until December, 1996 on CD-ROMs.

1. Pre-launch Calibration Intercomparison

Backscatter measuring instruments such as TOMS, SBUV, and GOME require careful calibrations to determine sensitivity to both Earth radiance and the Solar irradiance. Irradiance calibrations are derived by illuminating the instrument with an irradiance standard provided by a national laboratory such as the US National Institutes for Standards and Technology. However, there are no standards for radiance applicable for remote sensors with extended fields of view, therefor flat diffuser plates illuminated by an irradiance source are used as a radiance target. Traditional flat plate calibrations have been subject to large uncertainties due to the difficulty in the measurement of the angular distribution of the diffuse scattering from the targets. Inconsistencies in bidirectional reflectance distribution function (BRDF) measurements on the order of 10% were not uncommon in the past [*Heath, et al.*, 1993]. The sphere based calibration technique was developed to enhance the accuracy of extended source radiance based calibrations, and to provide a baseline for the continuing improvement in BRDF measurements. The sphere technique is inherently less prone to systematic errors due to the simplicity of the calibration set-up, and requires only that one can measure accurately the sphere port area and the distance to the target. Additionally, the sphere is easily transportable allowing for on-site inter-calibrations to be performed. Recent results from comparisons of this technique with flat plate calibrations on the SSBUV, TOMS, and SBUV/2 yield agreement on the 2-3 % level. [*Janz et al.*, 1996].

Calibration of GOME has been reviewed by *Hahne et al.*, [1994]. The cross-calibration of SSBUV with both the GOME FSM and FM instruments using NASA's integrating sphere as a transfer was performed at TPD in the fall of 1994, [*Heath et al.*, 1994]. The results indicated very good consistency (2-3 % level) between the sphere based radiance sensitivity and the flat plate based sensitivity over the wavelength range that the sphere was calibrated, 250 nm - 450 nm. There was also good consistency between flat plate techniques using targets measured both by TPD and the Goddard BRDF facility. The good agreement among the various calibration techniques and set-ups provides a large degree of confidence that the GOME instrument and SSBUV are on a common radiometric scale, traceable to NIST standards, and provide a solid baseline for inter-comparisons of these instruments while in space. Further details of the ground calibration are reported elsewhere in this volume.

2. Post-launch Validation of Level 1 Data

Plans for Level-1 validation of GOME included comparison of GOME solar irradiance and Earth radiance data with the TOMS, SBUV/2, and SSBUV. The eighth flight of SSBUV was conducted in January 1996 for which there are no GOME data yet available. The Earth Probe TOMS launch has been postponed until mid 1996. The SBUV/2 on NOAA-14 was launched in December, 1995 but has only recently become operational because of numerous spacecraft and instrument problems. Therefor, Level 1 radiance comparisons has been limited to a few number of comparisons using specially processed data for this validation effort. GOME solar irradiances have been compared to earlier SSBUV flights as well as the UARS instruments. The detailed UARS comparisons, particularly the SOLSTICE is being reported elsewhere in this volume however comparisons with SSBUV are summarized below.

Solar irradiance

GOME solar irradiance comparisons with SSBUV and the UARS SOLSTICE and SUSIM instruments show

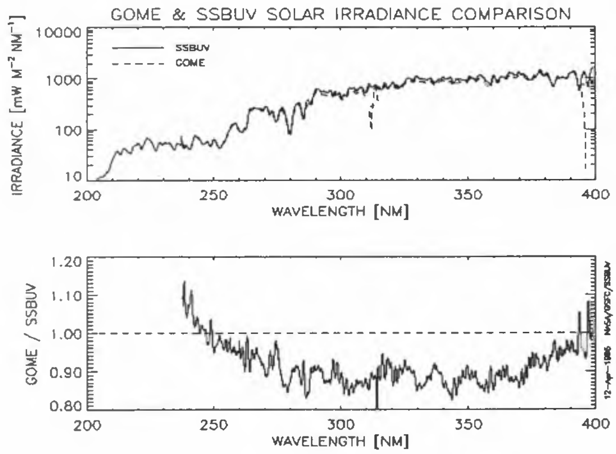

Figure 1. GOME SSBUV Solar irradiance comparison

significant differences (10-20%) particularly at wavelengths between 260 and 290 nm. A comparison with SSBUV data is shown in Figure 1 and is very similar to the comparisons of GOME and the UARS instruments. Comparisons among the US solar irradiances show agreement to better than 3% over wavelength with nearly zero systematic differences (*Woods et al.*, 1996, *Cebula, et al.*, 1996). Therefor the difference seen in figure 1 are primarily due to errors in GOME. These differences have now been explained to result from air-to-vacuum changes in GOME sensitivity. Similar changes have been observed in SBUV/2 instruments and are attributed to out-gassing from protective coating used on the GOME instrument's optical surfaces. ESA, TPD, and the University of Bremen are developing correction a factor to account for this sensitivity change. As GOME irradiances are refined additional comparisons will be made with the SSBUV-8, the UARS instruments and SBUV/2 on NOAA-14

Earth Radiances Comparisons

Comparisons of GOME radiances with SBUV/2, TOMS, and SSBUV have been limited for reasons mentioned above. To enhance the validation with limited data, a radiative transfer model was developed to compute radiance from SBUV/2 ozone data anywhere in the vicinity of a GOME observation. The model is particularly useful since SBUV observations are only made at 12 discrete channels with 1.1 nm resolution. Therefor the model affords a comparison over all wavelengths at the GOME wavelength resolution. In addition, special NOAA-14 SBUV/2 and GOME data sets were compiled for the period August 25-27 over Mauna Loa, Hawaii during a Network for Detection of Stratospheric Change (NDSC) ground based ozone intercomparison campaign. This campaign provided independently validated total ozone and profile ozone data from NOAA-14 using

SBUV/2 data over Hawaii.

The model to calculate radiances applicable to GOME channels 1 and 2 radiances involves the Dave-Mateer radiative transfer code [*Dave*, 1964], which is the major tool in the BUV processing and analysis. The Earth's backscattered radiance is a function of the solar zenith angle, the ozone profile shape and the surface reflectivity which all have to be accounted for in model calculation. The model has recently been updated to include Raman Scattering (Ring effect) [*Joiner et al.*, 1995]. To model the GOME radiances for a given ground pixel, the GOME measured radiance at 380 nm is used for derivation of the surface reflectivity and includes the solar zenith angle at the GOME measurement. From these parameters the theoretical radiance, which is the sum of the single scattered (SS) and the multiple scattered and reflected (MSR) radiances, are computed. For radiance calculations shorter than 340 nm the ozone profile measured independently, e.g. SBUV/2, is included to compute the theoretical radiances. The MSR component depends primarily on the total column ozone and the surface reflectivity. For practical applications of the model and GOME comparisons, the normalized radiances (the ratio of the Earth radiance to solar irradiance which is proportional to the directional albedo, (hereinafter simply called 'radiances') are employed.

Based on these principals, the GOME radiances are calculated using Bass and Paur cross sections at about 0.05 nm steps. As the last step in the calculation of the GOME radiances, an integration is implemented to take into account the GOME slit width, including the GOME slit function in its integrand. Since the integration needs to be computed in wavelength (λ) space, a partial derivative of λ with respect to the pixel number p was applied to convert Δp into $\Delta\lambda$ in the form of the GOME slit function.

The GOME measured and the theoretical values are then compared by analyzing the percent differences between the measured GOME radiances with the theoretically computed radiances. This difference is called the residue. This method was successfully applied to the SBUV continuous scan data in revealing spectral anomalies in the data and validation of Dave-Mateer radiative transfer code [*Gu et al.*, 1996]. In order to minimize impact from ozone profile errors, a non-ozone absorbing wavelength range of 340 - 400 nm was first chosen for this comparison.

Figure 2 shows the residue described above and the residue due to the Ring effect. The Ring effect residue is calculated from the GOME measured solar irradiance, the solar zenith angle, and the surface pressure [*Joiner et al.*, 1995]. For this case the reflectivity was low therefor a near ground pressure was assumed. For this analysis, 22 GOME nadir ground pixels over the Arabian Sea on July 23 were used. The solar zenith angles were large enough

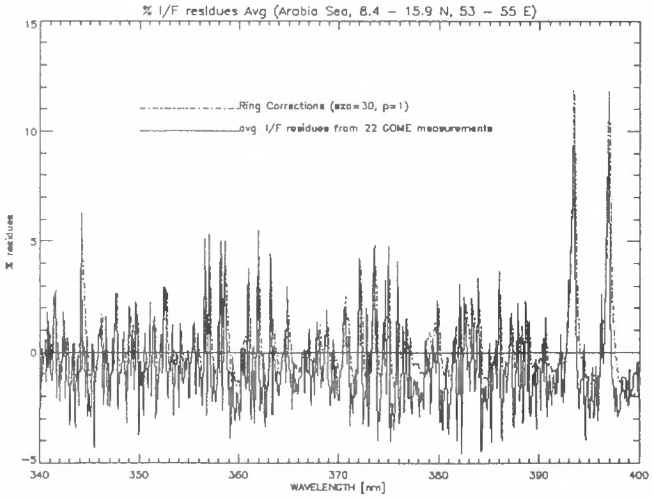

Figure 2. Residue comparing GOME and calculated radiance. Ring effect residues are also shown.

(>25°) so that sea glint is not a concern but were also small enough (<30°) that the polarization corrections are not important. On average the residues are small meaning that the GOME calibration is accurate to the order of 1% where the unaccounted for Ring effect amounts to a peak-to-peak "noise" of about 5%. Close inspection of the two curves in Figure 2 reveals a systematic wavelength misalignment of about 0.06 nm. Studies of SBUV continuous scan data, demonstrated that a small wavelength shift ($d\lambda$) between the earth radiance (I) and solar irradiance (F) may generate about ten times larger wavelength shift $\Delta\lambda$ in the normalized radiances. For example, the observed 0.06 nm misalignment might be generated by $d\lambda$ of 0.006 nm, which is smaller than the GOME tolerance of 0.0156 nm. To further refine the comparison, two additional steps were taken. The first was to account for the Ring effect and the second to adjust the wavelength to match the location of the Fraunhofer lines. Figure 3 indicates that after these adjustments the 'final' residue is about ±1% peak-to-peak with an offset or calibration error of about 1%. These results are comparable to the findings using SBUV data. Work has begun to further understand the remaining structure in the 'final' residues.

Additional residues from other geographical locations were also analyzed to understand GOME radiances compared to the model calculations. Figure 4 illustrates the 'final' (wavelength adjusted and Ring effect removed) residues for other samples of selected nadir ground pixel over the Sahara desert in August. Comparing this figure to Figure 3, several differences are seen. These features could be due to several factors such as, residual Ring effect, aerosol scattering, key data, or calibration errors.

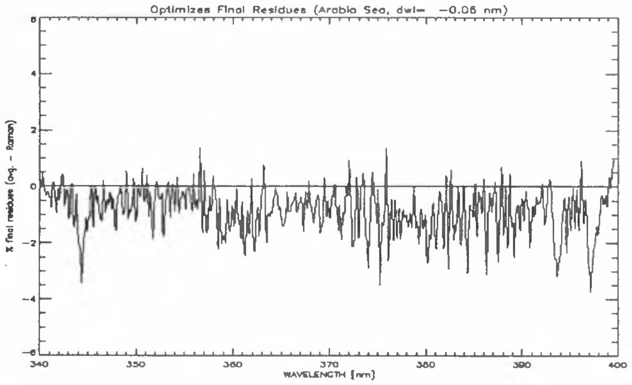

Figure 3. Final residue includes wavelength adjustment and removal of Ring effect.

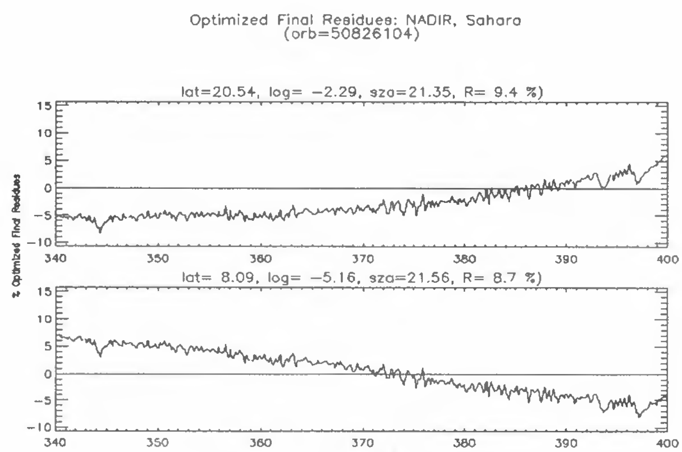

Figure 4. Final residue over Sahara desert in August.

Recent investigation of TOMS data [*Hsu et al.*, 1996] have shown reflectivity anomalies (among only two wavelengths) which could be associated with smoke and dust. These anomalies result from absorbing aerosols which cause a wavelength dependent signature in the residues. The upper curves in Figure 4 represents a 'final' residue with a clear sky (reflectivity of 9%). The polarization corrections are extremely small because of the surface property and low SZA (about 20°). Figure 4 shows both a positive (upper curve) and negative (lower curve) reflectivity anomaly with respect to wavelength. The lower curve reflects what is seen in TOMS data and our radiative transfer model (*Torres and Bhartia,* 1995) which is associated with desert dust. This is by no means a definitive study of GOME observations of the spectral signatures of absorbing aerosols. Studies of GOME data are planned with comparison to the 12 year record of TOMS data.

In order to validate GOME radiances from 250 nm to 400 nm, radiances were calculated from a special processing of NOAA-14 SBUV/2 data taken over Mauna Loa, Hawaii during an NDSC ozone intercomparison campaign conducted in August 1995. This intercomparison campaign provides an excellent opportunity to validate the SBUV/2 data used to compare with the GOME data. Figure 5 illustrates the comparability of the SBUV/2 with several ground based lidar and microwave measurements as well as Umkehr and balloon soundings for August 25, 1995.

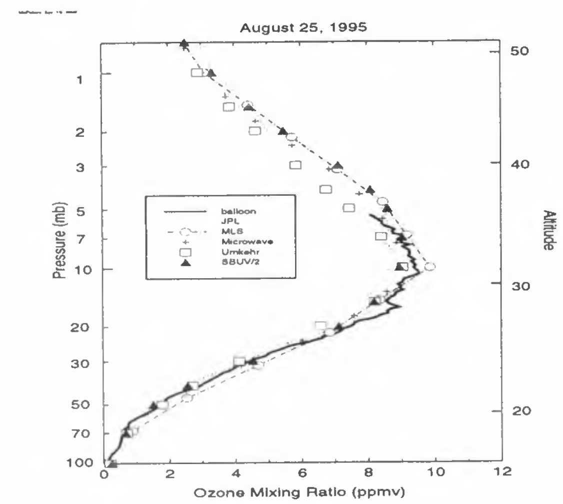

Figure 5. Ozone measurements during the NDSC campaign.

Also compared in this data set are data from the MLS on the UARS. The agreement of all the data sets with SBUV/2 is about 5% or better. Radiances were calculated using the method described above using the SBUV/2 ozone values illustrated in Figure 5. A total of six GOME observations near Mauna Loa from Channels 1a and 2 were compared to the calculated radiances of August 25. The radiance residuals are illustrated in figure 6. In

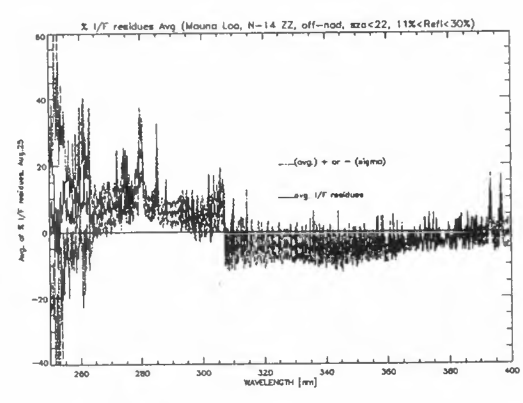

Figure 6. GOME and calculated radiances channels 1a and 2.

channel 1a, GOME measured radiances are about 10% higher on average.

The 1 sigma standard deviation grow to as large as ±20% but is likely due to GOME channel 1 detector noise. However, on average the GOME radiances are about 2% lower in channel 2 which is consistent with the results in Figure 2. The Ring effect, which was not removed in this comparison (because it was not modeled below 300 nm), results in sharp features at the Mg and Ca Fraunhofer lines seen in the Figure 6.

DOAS vs TOMS Total Ozone Retrievals

The Goddard BUV algorithms were used for calculating total column ozone using GOME radiance and irradiance data. The GOME data was slit-averaged to TOMS 1.1 nm bandpass and the radiance and irradiance values interpolated to TOMS wavelengths at 312, 317, 331, 340, 360, 380 nm. Albedos, geo-location, solar zenith angles, satellite view angles were then processed through the version 7 TOMS algorithm (McPeters, et al 1993). The TOMS results were compared with DOAS results from the same ground pixel. The TOMS results were calculated with two different sets of wavelengths, the A-triplet: 312,331,380 nm, and the B-triplet: 316,331,380 nm. The primary difference between the triplets is the 312 wavelength of the A-triplet is measured using the 1b band radiances. All of the other wavelengths are measure in the 2b band. The differences between the A-triplet and the B-triplet ozone values are a measure of the inter-band calibration.

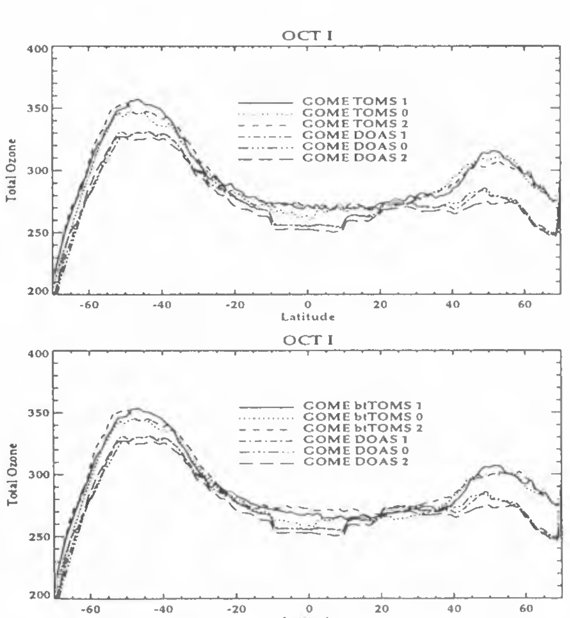

Figure 7. GOME-TOMS and GOME-DOAS ozone.

Figures 7 upper (A-triplet) and lower (B-triplet) show that the overall agreement between GOME-TOMS and the GOME-DOAS is reasonable. However the GOME-DOAS results are consistently lower than the TOMS results. The GOME-DOAS ozone values show a 'step function' behavior when plotted as a function of latitude. This behavior is probably the results of retrieval assumptions in the GOME-DOAS algorithm. Figure 8 upper (A-triplet) and lower (B-triplet) show the per-cent difference between the GOME-DOAS and the GOME-TOMS values as a function of latitude. The individual measurements have been smoothed for easier interpretation. Lower figure 8 shows a 2% positive shift compared with upper figure 8. This indicates a small calibration bias between the 312 nm radiance measured on Band 1b compared with the 317 nm radiances measured on Band 2b.

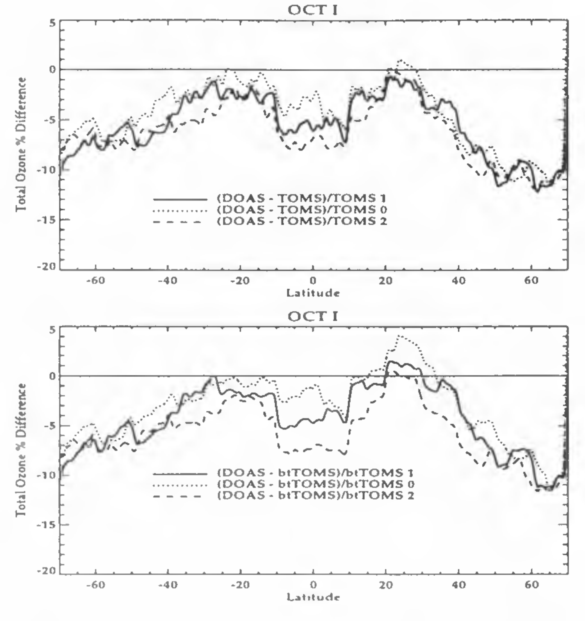

Figure 8. TOMS - DOAS differences versus latitude.

GOME-TOMS - GOME-DOAS differences show a significant (0 to 10%) latitude dependence. This is more likely a solar zenith angle dependence which is shown in figure 9 which is a replot of the data in figure 8. As the TOMS algorithm has not shown this solar zenith angle dependence using the Nimbus-7 radiance data, one must assume that this solar zenith angle (SZA) dependence is contained in the GOME-DOAS data. The other notable feature is the scan angle dependence of the GOME-TOMS results. The initial results presented at the final validation workshop in March, 1996 were calculated with incorrect SZA values. (NB: The SZA values recorded on the level 2 data records are the spacecraft SZA, not the SZA at the earth observation point!!) After this error was discovered the ozone values were recalculated and the scan bias was reduced but not removed. Further studies are required to assess the cause of this scan angle bias.

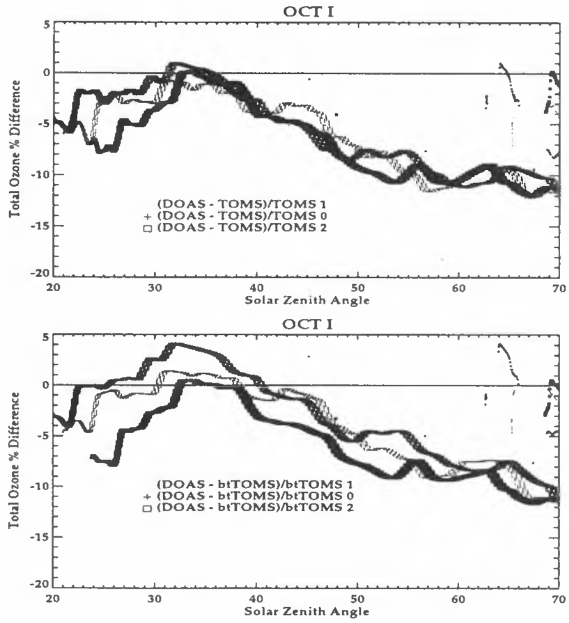

Figure 9. TOMS- DOAS differences versus SZA.

GOME Ozone Profiles Using the SBUV Algorithm

The Goddard algorithms were also used for calculating ozone vertical profiles using GOME radiance and irradiance data. The GOME data were again slit-averaged to the 1.1 nm SBUV bandpass. The radiance and irradiance data were interpolated to the 12 SBUV wavelengths; 255.5, 273.5, 283.0, 287.6, 292.2, 297.5, 301.9, 305.8,312, 317, 331, 340 nm. Albedos, geo-location, solar zenith angles, and satellite view angles were processed through the version 6 SBUV algorithm.

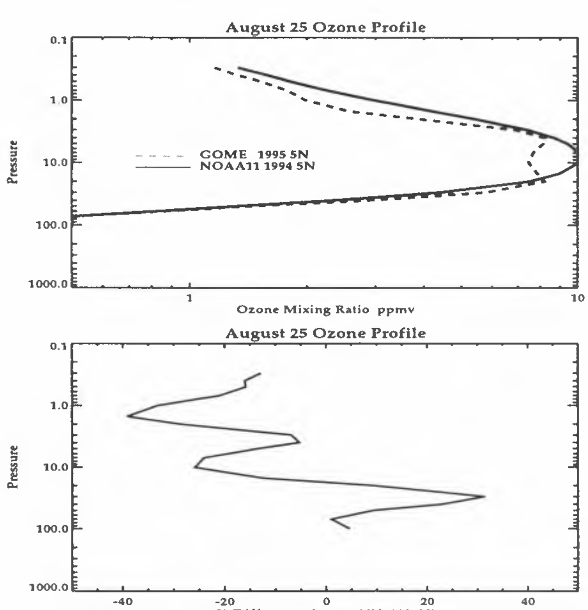

Figure 10. GOME profile results.

Approximately 130 measurements were averaged. The GOME 1996 average profile is compared to the same day in 1995 measured by the SBUV/2 instrument on NOAA-11 and illustrated in the upper panel in figure 10. The GOME ozone profiles show too little ozone indicating that the radiance levels are too high. There is a notch in the profile at 10 mb indicating a wavelength dependent calibration error. The lower panel in figure 10 illustrates the difference in the GOME average profile and the climatology. Differences increase to as much as 30% near 1 mb. These results are consistent with the results described above in the Earth Radiance Comparison section. A 1% calibration error results in 2% ozone error at 1 mb. This ratio decreases with increasing pressure [*Fleig et al.*, 1990].

Concluding Remarks

The NASA Goddard validation effort began before launch of GOME. NASA standards used for calibrating SBUV/2 and TOMS were also used to calibrate GOME. These calibrations were compared with TPD calibration and good agreement was found. The good agreement among the various calibration techniques and set-ups provides a large degree of confidence that the GOME instrument and the US BUV instruments are on a common radiometric scale, traceable to NIST standards, and provide a solid baseline for inter-comparisons of these instruments while in space.

Because TOMS Earth Probe launch is delayed, SBUV/2 has only recently become operational, and the SSBUV just completed its flight (January 11-18, 1996) after this first release of GOME data for validation, comparisons with Level 1 and 2 data has been has been limited. Nevertheless a great deal has been learned about the performance of GOME. Level 1 irradiance comparison show that GOME experienced a large wavelength dependent change in sensitivity as a result of the vacuum of space and is of the order of 15% at 300 nm. Level 1 radiances seem to agree with SBUV/2 calculated radiances on the order of a 2% at wavelengths larger than 340 nm. At wavelengths shorter than 300, GOME radiances appear to be high by as much as 10% with a large amount of noise. When comparing GOME DOAS total ozone values with GOME total ozone values using the BUV algorithm, a latitude and SZA angle dependence appears of the order of 0-10% where TOMS values are higher. GOME ozone profiles derived from the BUV profile algorithm compared with climatological values for the same season and latitude yields values about 10-30 % to low which is consistent with the Earth radiance difference discussed above. The irradiance error which results from the air-to-vacuum sensitivity change likely appears in the radiance as well. If this is the case, this error is canceled in the albedos and has no effect on retrievals. Therefor the error seen in the radiance (in reality albedo) from the SBUV comparisons below 300 does not seem to be a calibration error, but an error associated with the key data applied to radiances in channel 1a. The source of the error is still unknown.

Algorithm research using GOME radiances has begun. Initial studies included studies of Ring data and relationship to cloud top heights, but are not reported here. GOME radiances between 340 and 400 which is free from ozone absorption were used to further study reflectivity anomalies discovered in TOMS which are associated with absorbing aerosols such as smoke and dust. With this initial release of GOME data one can conclude that these signatures likely also appear in the GOME radiances however further validation is required to draw any conclusions at this time.

It is recommended that pre-launch instrument key data particularly the air-to-vacuum shift be further refined. In addition, instrument performance should be tracked and corrected over time for the duration of its lifetime. This should be the primary objective for the GOME validation community. Instrument characteristics need to be updated periodically and Level-1 data products reprocessed. These data should then be validated followed by Level-2 reprocessing. Level-2 validation may reveal additional errors on either or both Level 1 and Level 2 data. This process is highly iterative and requires a team of committed and strongly supported experts to test and validate GOME data.

References

Cebula, R. P., G. O. Thuillier, M. E. VanHoosier, E. Hilsenrath, M. Herse, G. E. Brueckner, and P. C. Simon, Observations of the solar irradiance in the 200-350 nm interval during the ATLAS-1 Mission: A comparison among three Sets of measurements - SSBUV, SOLSPEC, and SUSIM, *Geophys. Res. Lett.*, in press, 1996.

Dave, J.V., Multiple scattering in a non-homogeneous, Rayleigh atmosphere, *J. Atmos. Sci., 22,* 273-279, 1964

Fleig, A.J., R.D. McPeters, P.K. Bhartia, B.M. Schlesinger, R.P. Cebula, K.F. Klenk, and S.L. Taylor, Nimbus-7 SBUV users guide, NASA Ref. Pub. 1234, 1990.

Gu, X., R. D. McPeters, C. Seftor, C. Wellemeyer and R. P. Cebula, Spectral anomalies in the SBUV continuous scan data and validation of forward model calculation for ozone retrieval, to be submitted to *J. Geophys. Res.*, 1996.

Hahne, A., J. Callies, A. Lefebvre, B. Christensen, R. Hoekstra, L. Fontijn, C. Olij, E. Zoutman, and G. Nutzel, Calibration of the GOME instrument for ERS-2, *ESA Journal, 18*, 119-128, 1994.

Heath, D.F., Z. Wei, W.K. Fowler, and V.W. Nelson, Comparison of spectral radiance calibrations of SBUV-2 satellite ozone monitoring instruments using integrating sphere and flat-plate diffuser techniques, *Metrologia*, *30*, 259-264, 1993

Heath, D.F., R. Hoekstra, E. Zoutman, C. Olij, "NASA Sphere Calibration for GOME FM", TPD-ERS-GO-MIR-33, 1994.

Hilsenrath E., P.K Bhartia, and R.P. Cebula, Calibration of BUV satellite ozone data - An example of for detecting environmental trends, *Earth Observer,* 6, 26-33, 1994

Hsu, C., J.R. Herman, P.K. Bhartia, C.J. Seftor, O. Torres, A.M. Thompson, J.F. Gleason, T.F. Eck, and B.N. Holben, Detection of biomass burning smoke from TOMS measurements, *Geophys. Res. Lett.23,* 745-748, 1996.

Janz, S., E. Hilsenrath, J. Butler, D.F. Heath and R.P. Cebula, Uncertainties in radiance calibrations of backscatter ultraviolet (BUV) instruments, *Metrologia*, (in press), 1996.

Joiner, J., P. K. Bhartia, R. P. Cebula, E. Hilsenrath, R. D. McPeters, and H. Park, Rotational Raman scattering (RING effect) in satellite Backscatter ultraviolet measurements, *Appl. Opt., 34*, 4513-4525, 1995.

McPeters, R.D., A.J. Krueger, P. K. Bhartia, J.R. Herman, A. Oaks, Z. Ahmad, R. P. Cebula, B.M. Schlesinger, T.Swissler, S.L.Taylor, O.Torres, C.G.Wellemeyer, Nimbus-7 Total Ozone Mapping Spectrometer (TOMS) Data Products User's Guide, NASA reference Publication 1323, 1993

Torres, O. and P.K. Bhartia, Effect of stratospheric aerosol on ozone profile from BUV measurements, *Geophys. Res. Lett. 22,* 235-238, 1995.

Woods, T. N., D. K. Prinz, J. London, G. J. Rottman, P. C. Crane, R. P. Cebula, E. Hilsenrath, G. E. Brueckner, M. D. Andrews, O. R. White, M. E. VanHoosier, L. E. Floyd, L. C. Herring, B. G. Knapp, C. K. Pankratz, and P. A. Reiser, Validation of the UARS and ATLAS Solar ultraviolet irradiances, *J. Geophys. Res.*, in press, 1996.

Acknowledements

We thank Richard McPeters of Goddard Space Flight Center who provided us with advance data from the NDSC intercomparison.

Studies on the Precision of GOME Irradiance and Radiance Products and GOME Measurements of OClO and BrO over Antarctica

M. Eisinger, J. P. Burrows, A. Richter

Institute of Environmental Physics, University of Bremen, Germany

Abstract

The quality of irradiance and radiance products as delivered by the GOME Data Processor (GDP) has been assessed both by internal comparisons and by evaluating these data by means of the Differential Optical Absorption Spectroscopy (DOAS) method. Selected solar spectra as measured by GOME from June to November 1995 have been compared. Etaloning effects, changes of the dichroic transmissivity and long-term degradation have been found. These result in an error of a few percent for the irradiances and radiances if not accounted for. Wavelength stability was found to be better than 0.01 nm in most cases, both for solar irradiances and earth radiances. Validation of earth radiances focussed on the 450–500 nm region in channel 3 which is important for ozone retrieval in the visible part of the spectrum. In this region large residuals were found in the DOAS fits which can be explained by a shift of the instrumental nadir polarisation sensitivity η_{nadir} compared to the calibration data (version 5) used in the GDP. Recommendations for further improvements of the level 1 data quality are given.

The first GOME measurements of BrO and OClO over Antarctica are reported indicating high signal-to-noise ratio and excellent instrumental stability for channel 2 data. BrO and OClO have been detected in the measurements from July to September 1995. Further analysis of GOME measurements of halogen oxides is under way.

1 Introduction

The Global Ozone Monitoring Experiment is a new European sensor on board ESA's Second European Remote Sensing Satellite (ERS-2) (*Burrows et al.,* 1988; *GOME Interim Science Report,* 1993; *GOME Users Manual,* 1995). ERS-2 was launched on the 21st April 1995 and GOME was switched on after being allowed to outgas for 4 weeks at the end of May 1995. Thereafter a series of functional tests were undertaken prior to GOME entering its first Validation Phase, which ran from July 1995 to January 1996.

A number of different issues have been focussed on during GOME's first intensive Validation period. The main objective of this part of the validation was to investigate issues of relevance to the level 1 irradiance and radiance products in GOME. Issues such as etaloning, periodic noise and shifts or drifts in the dichroic mirror wavelength selection have been studied. These impact on the accuracy or potential accuracy of level 1 and level 2 products and need to be understood. Finally as test of GOME's performance, an attempt was made to observe over the Antarctic the trace gases BrO and OClO from GOME data. Both these species play significant roles in the anthropogenic reduction of stratospheric ozone known as the Ozone Hole (*WMO,* 1994).

2 Solar irradiances

Solar irradiances are measured by GOME once a day within the Sun Observation Timeline (SOT). During this timeline which is carried out around one of the 14 sunrises GOME sees each day GOME observes the sun via its diffuser plate. While the sun is passing the field of view several solar spectra are recorded. In the following only spectra averaged over one timeline, as given in the extracted level 1 product, are used.

The solar irradiance, normalized to an earth-sun distance of 1 Astronomical Unit (AU) is expected to be quite stable. It should vary by not more than a few percent between 210 and 300 nm, and by less than one percent above 300 nm, the remaining variability being related, for example, to the 27 day solar rotation and the 11 year solar cycle (*Brasseur and Solomon,* 1986). Therefore, the daily GOME irradiance measurements provide a powerful tool for monitoring instrumental stability and enable at least some aspects of level 0 to 1 data processing to be investigated. In the following the normalized irradiance is assumed to be stable, in other words: all changes in the measured spectra are treated as instrumental effects.

Results from a comparison of GOME solar irradiances obtained during the Validation Campaign are presented. In total 23 solar spectra (6 June, 22–25 July, 25–27 and 29–31 August, 15–17 September, 5–7 and 29–31 October, 9–11 November 1995) have been investigated. Irradiances have been extracted by the DLR program gdp01_ex (Version 1.71) and normalized to 1 AU using routines from *Montenbruck and*

Pfleger (1994) to calculate the earth-sun distance. In most cases ratios of solar spectra measured on different days are investigated. As the wavelength grids on which the spectra are given differ slightly from day to day, the spectra have been interpolated linearly onto one wavelength grid before ratioing.

This study has focussed on the use of comparison of solar spectra in order to establish the precision of the measurements made by GOME. The absolute accuracy of the solar irradiance has been assessed elsewhere and requires the comparison with measurements by other instruments such as SSBUV and SOLSTICE.

2.1 Etaloning 1

The Reticon photodiode array detectors employed in the GOME instrument are protected by a 3 μm SiO_2 coating. This coating already acts as interference layer. In addition, as even under vacuum conditions cooled photodiode array detectors function as an effective cold trap for molecules from the rest gas, thin interfering ice layers may form. This is well known from ground-based measurements using photodiode arrays (*Mount et al.,* 1992). These layers modulate the instrumental radiance response with a sinusoidal function. Its period is determined by the thicknesses of the individual layers. In the GOME instrument the detector arrays are cooled to 235 K by two-stage Peltier elements. Deposition of material is expected from the ERS–2 satellite's or GOME's "atmosphere" in space.

A stable interference would cancel in ratios of solar irradiances. However, if the interference layer is changing with time, sinusoidal features can be observed in the ratios. This change is expected to be largest when the detector coolers have to be switched off. In GOME operation, a temporary cooler switch-off is sometimes necessary to recover from instrumental errors. In this case detectors are not cooled for typically a few hours, reaching temperatures between 260 and 270 K.

Observations

An etalon effect varying with time is observed in GOME channels 2–4. It is largest in channel 2. The day-to-day change which is important for evaluation by means of the Differential Optical Absorption Spectroscopy (DOAS) method seems to be slowly stabilizing, especially when related to the time since last cooler switch-off. In channel 2 the peak-to-peak change was for example 0.1% from the 23rd July to the 24th July (1 week after a cooler switch-off) but only less than 0.05% from the 6th October to the 7th October (7 weeks after a switch-off). The overall peak-to-peak change for the period from the 26th August to the 6th October when detectors were cooled continuously is 1% in channel 2 (Figure 1). Larger changes occur during cooler switch-offs, leading e.g. to a 4.5% peak-to-peak change from 6 to 29 October at the end of channel 2. The etalon structure observed in the ratios has a period of about 13 nm in channel 2 and 55 nm in channel 4. In channel 3 etalon and dichroic effects (see below) are mixed so that a period for etaloning alone cannot readily be observed.

Impacts and recommendations

For irradiances (level 1 products): At present a constant interference layer is assumed for the level 0 to 1 processing. Therefore absolute irradiances may be in error by several percent as a result of the changing etalon effect.

It is recommended to take into account the varying etalon structure by monitoring the in-orbit etalon change and introducing a time-dependent calibration. A possible recipe for deducing a time-dependent etalon correction would be to switch off coolers, allow the detectors to warm up, switch on the coolers again, and perform sun measurements whenever possible for some time after the cooler switch-on. The changing etalon should then readily be observable in subsequent sun spectra. Time after cooler switch-on might parametrize the necessary etalon correction. Since only etalon *changes* can be observed by simply ratioing irradiances the most difficult part of this exercise will be the determination of the *absolute* etalon correction which serves as a reference for all subsequent time-dependent corrections. It has to be checked how far the radiance response given with the Version 8 keydata, which should reflect the in-orbit situation as from the 2nd July 1995, can serve as reference for the case of warm detectors.

For DOAS (level 1 to 2 processing): In level 1 to 2 processing irradiance/radiance ratios are calculated. Usually solar irradiance and earth radiance are measured within 24 hours. The effect of a changing etalon on trace gas columns as determined by DOAS is therefore expected to be small under most circumstances. There are, however, some situations where the DOAS fits might be disturbed by the varying etalon:

- in the very first months of GOME operation;
- when too much time has elapsed between solar and earthshine spectrum;
- when coolers were switched off/on between solar and earthshine spectrum;
- during the first hours or days after cooler switch-on;
- when absorbances resemble the etalon features, as can be the case with the wide absorption bands of ozone in the visible;
- for very low absorbances (e.g. BrO).

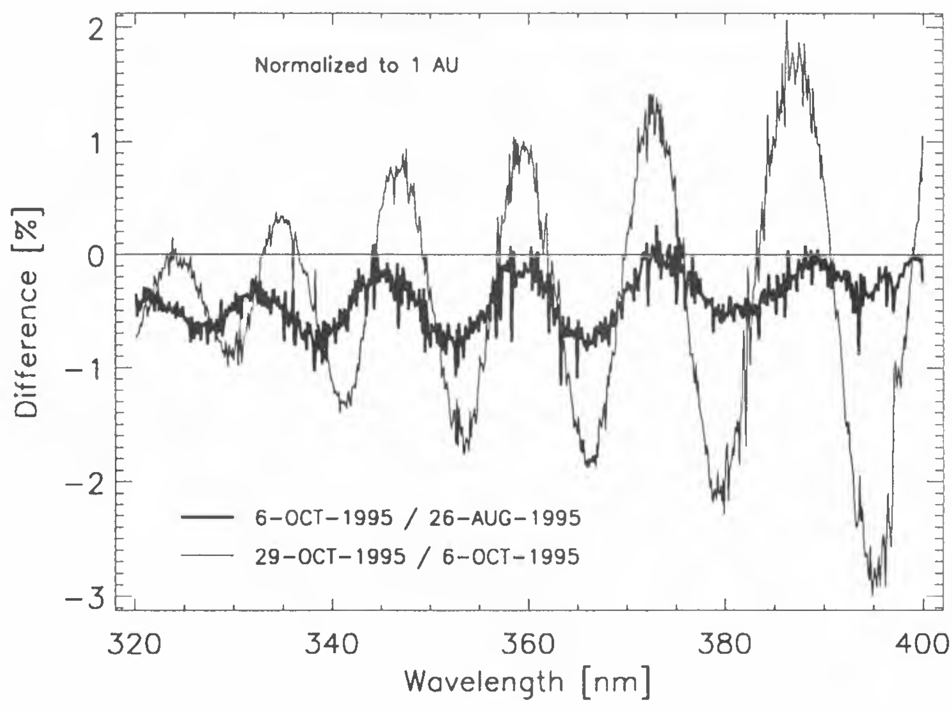

Figure 1: Etalon changes in GOME channel 2. Solar spectra are normalized to an earth-sun distance of 1 Astronomical Unit and then ratioed. Plotted are the deviations of solar ratios from unity. Detectors were cooled continuously between the 18th August and the 25th October 1995. Detector coolers were switched off for 1.5 hours on the 25th October 1995. In addition to the etalon a general downward trend in the measured signals is seen (cf. section 2.5).

It is therefore recommended for level 1 to 2 processing to use always the solar spectrum nearest in time to the current earthshine spectrum as background spectrum, even if it is recorded *after* the earthshine spectrum. Care has to be taken that a solar spectrum is not used when there was a cooler switch-off/on between earthshine and solar spectrum. Information about the cooling status of the detectors will be necessary to assess both level 1 and level 2 data quality.

2.2 Etaloning 2

Observations

In addition to the "normal" etalon, in channels 3 and 4 sinusoidal features having a period of 5–6 nm and an amplitude of 10^{-3} peak-to-peak can be observed in the solar ratios (Figure 2). They are not related to cooler switch-offs and are also observed in ratios of single (unaveraged) solar spectra. Interference at the dichroic mirror separating the light between channels 3 and 4 is most likely the cause of these "small-scale oscillations" since their period increases somewhat with wavelength, and is continuous over the border between channels 3 and 4.

Impacts and recommendations

For *irradiances* only a small (0.1%) additional error is introduced. However, concerning *DOAS* the oscillations might present a significant error for NO_2 fits since they could interfere with NO_2 bands. It is recommended to identify the exact source of the effect and to investigate whether it can be eliminated in the measurements. Any remaining structures might be removed by a software filter in the level 0 to 1 processing, if necessary.

2.3 Dichroic drift

The transmissivity of the dichroic beam splitter mentioned in the previous section has a pronounced wavelength dependence between 400 and 500 nm (low-wavelength half of channel 3). This is reflected by the radiance response function of GOME (*GOME Users Manual,* 1995).

Observations

In the 400–500 nm region features which are steeper than normal etalon structures and not influenced by cooler switch-offs are observed in the solar ratios (Figure 3). The changes of measured irradiances are large early in the GOME mission (cf. 6th June and 22nd July). They decrease rapidly (cf. 26th August and 6th October). This effect can be explained by a

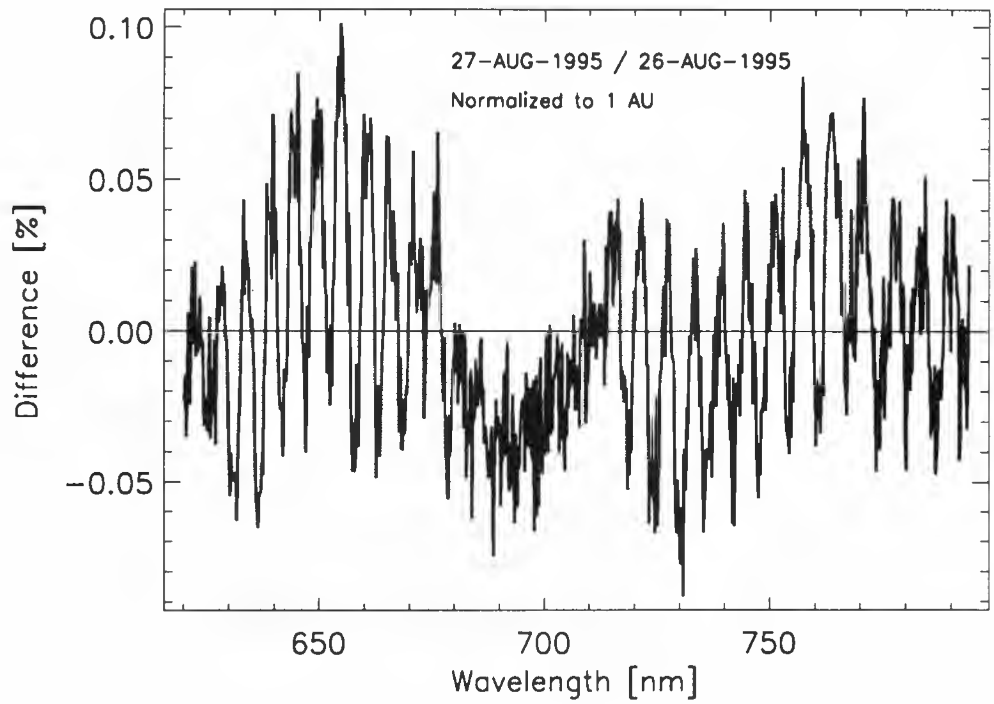

Figure 2: Small-scale oscillations in channel 4.

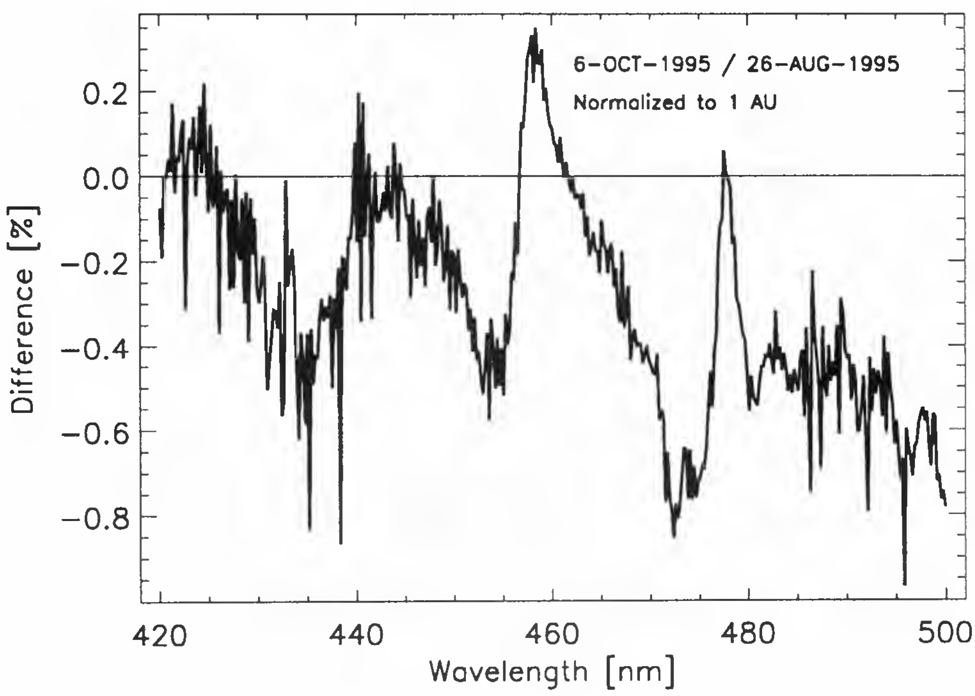

Figure 3: Dichroic features in channel 3.

changing transmissivity of the dichroic mirror, possibly due to outgassing.

Impacts and recommendations

The impacts of the dichroic structure on the data quality are similar to those of the Etalon (1). Furthermore, as radiance response and polarisation sensitivity are intimately linked, the polarisation sensitivity has also to be corrected (see section 3.1). For the radiance response a strategy for separating etalon and dichroic effects has to be developed. It is hoped for that dichroic transmissivity finally stabilizes. Until then – which might even be late in GOME's life – a time dependent radiance response has to be applied in level 0 to 1 processing.

2.4 Wavelength stability

In order to provide a wavelength calibration of GOME during the mission, Pt/Cr/Ne hollow cathode lamp spectra are measured daily. In 0 to 1 processing, 4th order polynomial coefficients are calculated from the (measured) pixel positions of selected lamp lines at known (vacuum) wavelengths. The polynomial is then used to convert detector pixels to wavelengths in nanometers.

Observations

Solar spectra recorded on different days have been plotted and compared visually[1]. Although the general agreement of the wavelength scale is rather good, sometimes shifts between 0.005 and 0.01 nm (corresponding to 0.05 to 0.1 detector pixels in channels 1 and 2) were observed over regions of several nanometer width. Figure 4 depicts an example. The fact that individual Fraunhofer lines are much narrower than the sampling of GOME (the latter is 0.11 nm in channels 1 and 2) can explain only random shifts. The observed non-random, i.e. systematic shifts are real discrepancies in wavelength calibration and not caused by undersampling. Wavelength shifts are observed in all 4 GOME channels.

Impacts and recommendations

As a result of the pronounced Fraunhofer features *irradiances* are incorrect by up to several percent (looking at a fixed wavelength) by even minute wavelength shifts. In practice, the problem looks somewhat different because in most applications interpolation between wavelength grids will be necessary, for example, to match earthshine and solar grids in order to calculate reflectivities.

In *DOAS* shifts are treated (and at least partially compensated) by the "shift and squeeze" process. However, GOME has a pixel resolution somewhat smaller than the effective Nyquist limit. This implies that during a software shift of the recorded spectra some information may be lost or falsely distributed at the subpixel resolution. By this, additional errors are introduced.

It is recommended to directly compare uncalibrated (raw) lamp spectra and solar spectra for the days on which shifts were observed in order to understand their origin and to be able to change the wavelength calibration algorithm in a way that shifts are further minimised.

2.5 Broadband degradation

Observations

The ratio of solar spectra, normalized to 1 AU, from 11th November and 24th July 1995 (Figure 5) shows in addition to the features already discussed a downward trend in solar irradiances measured by GOME in all 4 channels, largest (−4.5%) at the beginning of channel 1, but also significant (−1.5%) in channels 2 and 3.

Impacts and recommendations

This translates, if not taken into account, directly into an additional systematic error for the *irradiances*. The effect on *DOAS* should be negligible because it is both a broadband and longterm effect.

Degradation was to be expected in the harsh radiation environment of space. The reasons for long-term degradation have to be studied in more detail. It is necessary to separate between changes of the diffuser plate's Bidirectional Reflectance Distribution Function (BRDF) which affect only the solar irradiances, and all other changes which affect both irradiances and radiances. The BRDF and radiometric response functions then have to be corrected, possibly again with time as parameter.

Preliminary information about the degradation of the BRDF of the diffuser plate in space, measured from the ratio of the intensity of the Pt/Cr/Ne lamp with and without diffuser, indicates that its degradation is much smaller than that observed for the whole instrument. This necessitates the determination of the sun/moon ratios to quantify this result because the moon observations are obtained directly using the scan mirror.

3 Earth radiances

Earth radiances are highly variable depending on measurement geometry, ground albedo, cloud cover, and atmospheric composition. Validation of radiances is therefore much more difficult than validation of irradiances and by no means straightforward.

[1] During the Validation Campaign ratios of solar spectra were also investigated, but, as was pointed out by J. Callies and A. Türk, substantial errors are introduced by the necessary interpolations. This means from the ratios alone wavelength shifts cannot be unambiguously detected. Interpolation errors do not impair the conclusions drawn in all other sections since the effects discussed there are observed on a scale of many detector pixels.

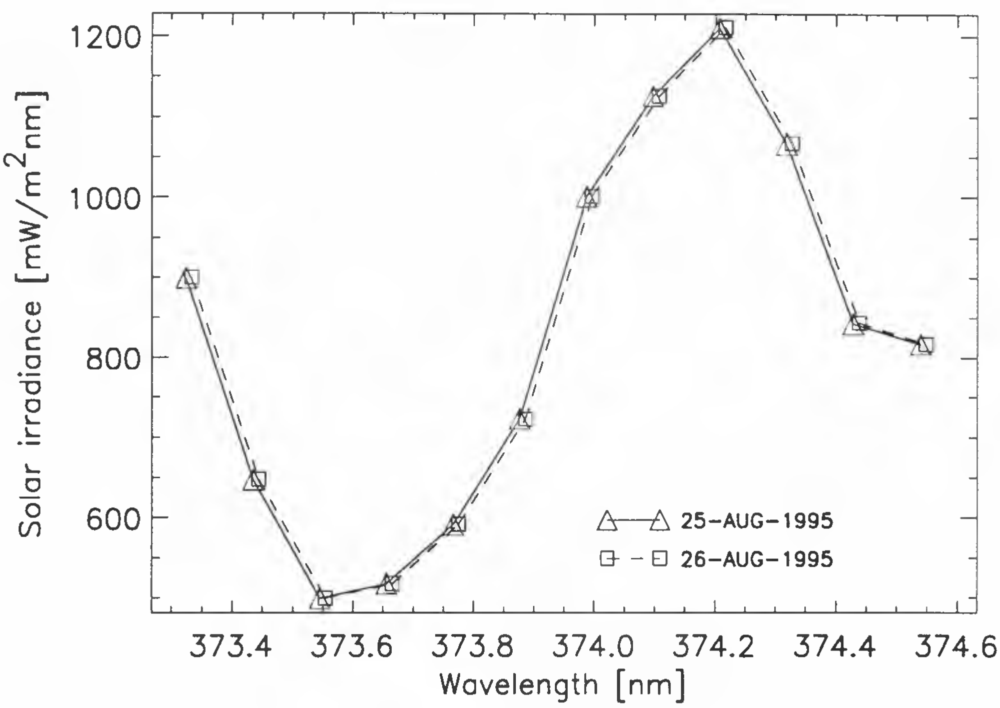

Figure 4: Wavelength shift of 0.01 nm in channel 2.

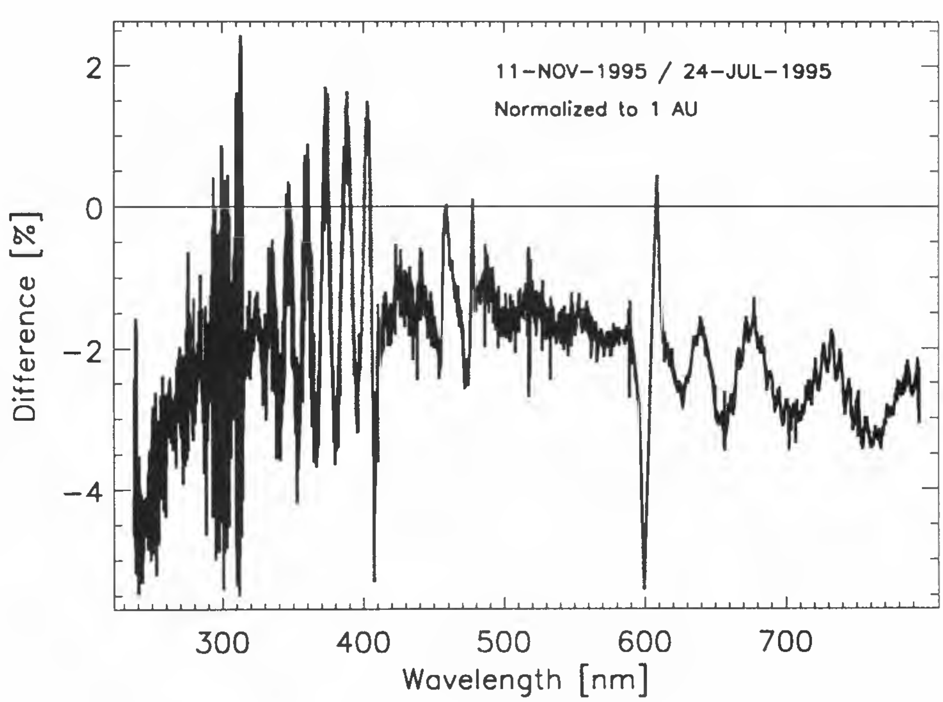

Figure 5: Long-term behaviour

All findings for the irradiances can be applied also to the radiances (with the stated exception for a possible BRDF change.) In particular, the accuracy of wavelength calibration is confirmed to be better than 0.01 nm in most cases by the shifts which are necessary in DOAS fitting to align solar and earthshine spectra.

One possibility to validate radiances is to apply some algorithm (as the SBUV/TOMS or the DOAS algorithm) on them. Certain algorithms will be sensitive to certain errors. The DOAS algorithm employed in the following is sensitive to errors on a "differential" scale (typically some nanometers wide). It cannot detect broadband deviations or a wrong scaling factor.

3.1 Polarisation correction in the 450–500 nm region

To retrieve ozone columns from GOME visible measurements, DOAS fits have been performed on several windows including the 450–500 nm window (window "B"). In ground-based zenith-sky measurements accurate ozone columns are calculated from this window. Details on the fitting using GOME level 1 data can be found elsewhere (*Eisinger et al.,* this issue). The tests described in this section were first carried out using GOME channel 3 data from orbit 1322 (22nd July 1995), the first GOME orbit available for validation studies. The analysis was later repeated on orbit 1053 (3rd July 1995) and the findings from orbit 1322 could be confirmed. In the following only results from orbit 1053 will be presented since during this orbit GOME was in static nadir viewing mode (no scanning). This simplifies interpretation. As polarisation correction in channels 1b–4 cannot yet be applied for integration times above 1.5 s, analysis has to be restricted to solar zenith angles below 85°.

Ozone fit errors turned out to be moderate in window B, at least when solar zenith angles were not too low. However, large residuals were found in virtually all spectra. Figure 6 depicts an example. As a result of these residuals ozone slant columns retrieved in this region are expected to be in error. A short digression on the GDP polarisation correction algorithm (PCA) has to be made before the residuals can be explained (for details see *GOME Data Processor Level 0 to 1 Algorithms Description*).

Polarisation correction in the GDP

Polarisation correction of the signal measured by GOME is necessary because reflectances have to be calculated from (unpolarised) solar irradiances and (polarised) earth radiances. Sensitivities of GOME, however, are different for light polarised parallel and perpendicular to the entrance slit. The polarisation sensitivity ratio η depends on wavelength λ and scan mirror angle α:

$$\eta(\lambda, \alpha) = \eta_{\mathbf{nadir}}(\lambda) \cdot \chi(\lambda, \alpha)$$

where $\chi(\lambda, \alpha)$ is the scan mirror part of the polarisation sensitivity. The nadir part η_{nadir} has, as a function of wavelength, some pronounced "ripples" between 450 and 500 nm (unfortunately) arising from the optical properties of the dichroic beam splitter separating the light between GOME channels 3 and 4 (Figure 7). It is these "ripples" which occur again in the fit residuals. In this study only nadir pixels are investigated so that $\eta = \eta_{\mathrm{nadir}}$ and the index can be dropped.

The incoming light (scattered from Earth's surface and atmosphere) has a certain wavelength-dependent fractional polarisation $p(\lambda)$. In the PCA the measured signal has to be transformed to the signal GOME would have seen if $p = 0.5$ (unpolarised light). Fractional polarisations are calculated from the signals of the three Polarisation Measurement Devices (PMDs) and the "7th point" (a theoretical value for the UV end of the spectrum, assuming single scattering. Originally, having also three p values from the channel overlap regions it really was the "*7th* point".). Note that already in this step η has to be used. From these 4 values p is interpolated for all detector pixels. The measured signal is then multiplied by a correction factor

$$c(\lambda) = \frac{1}{2} \cdot \frac{1 + \eta(\lambda)}{p(\lambda)(1 - \eta(\lambda)) + \eta(\lambda)}.$$

Analysis of residuals

To study in detail the reason for the large fit residuals analysis was repeated using the same level 1 data but *without* polarisation correction in level 0-1 extraction. As expected ozone fit errors and fit residuals were much larger. The fit residuals, however, can now be interpreted as some "empirical" polarisation correction factors. Apart from a lot of noise, their overall shape is quite stable during the orbit.

The residual from the same groundpixel as in Figure 6 is compared to two versions of η (made differential) in Figure 8. Note that in this comparison both the wavelength dependence of p and the functional form of c are neglected. The figure should therefore be interpreted with great care. Nevertheless, the overall shapes can be compared. The two versions of η shown in Figure 8 refer to the humid-air (version 0) and vacuum (version 5) situation, respectively. The steep decrease between 472 and 475 nm in version 5 was moved by 9 nm towards longer wavelengths in version 0. This feature is also present in the residual, but shifted by 1.1 nm towards longer wavelengths compared to version 5. It can be concluded that the in-orbit η lies between the humid-air η and the vacuum η, but nearer to the vacuum η.

In order to check whether there is a slow transition of η between the humid-air case and the vacuum case (caused mainly by outgassing of the dichroic mirror), orbit 2123 (nadir-static, 16th September) was analysed in the same way. Interestingly, residuals from July and September look very similar. No sig-

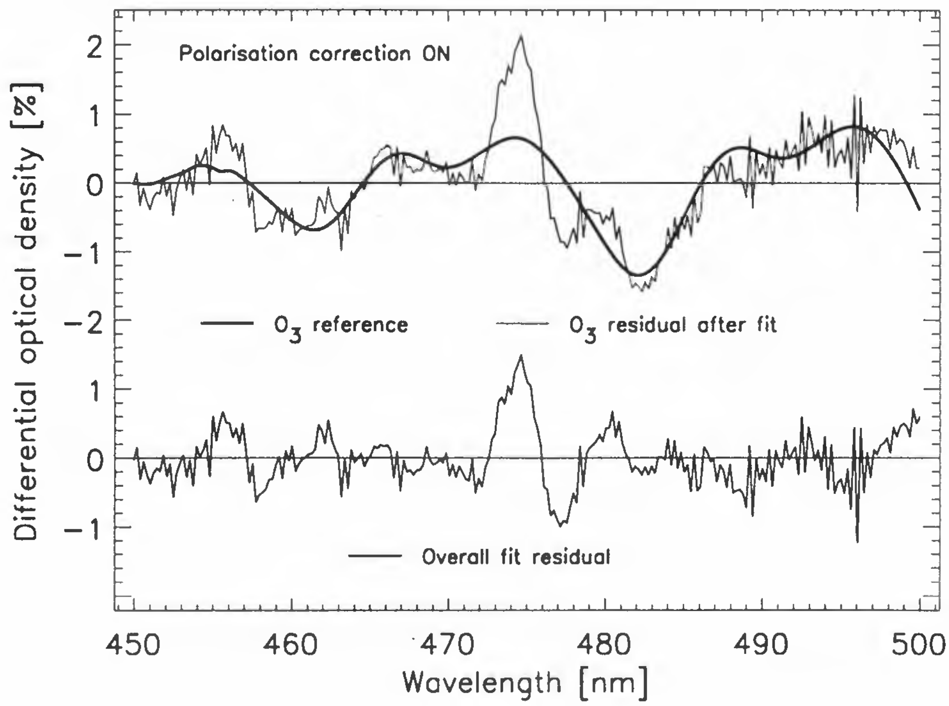

Figure 6: Fit results in the 450–500 nm window for ground pixel 1839 from orbit 1053 (nadir-static, 3rd July 1995, 17:07:57 UT, integration time 1.5 s, solar zenith angle 80.22°). Polarisation correction has been applied in level 0-1 extraction.

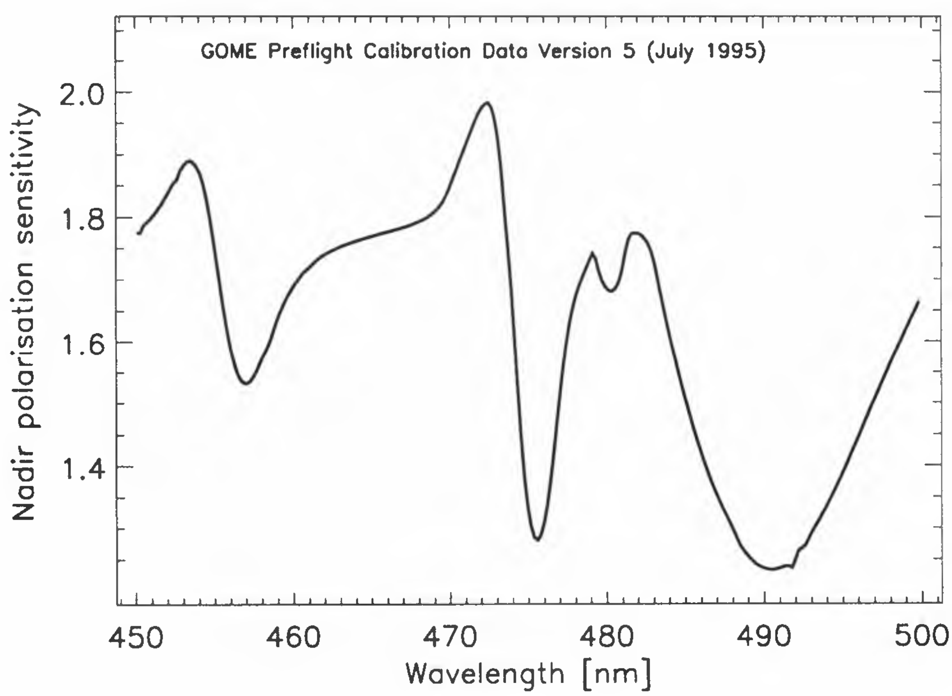

Figure 7: GOME nadir polarisation sensitivity η_{nadir}, keydata version 5 (July 1995), as established by TPD during the GOME preflight calibration campaign.

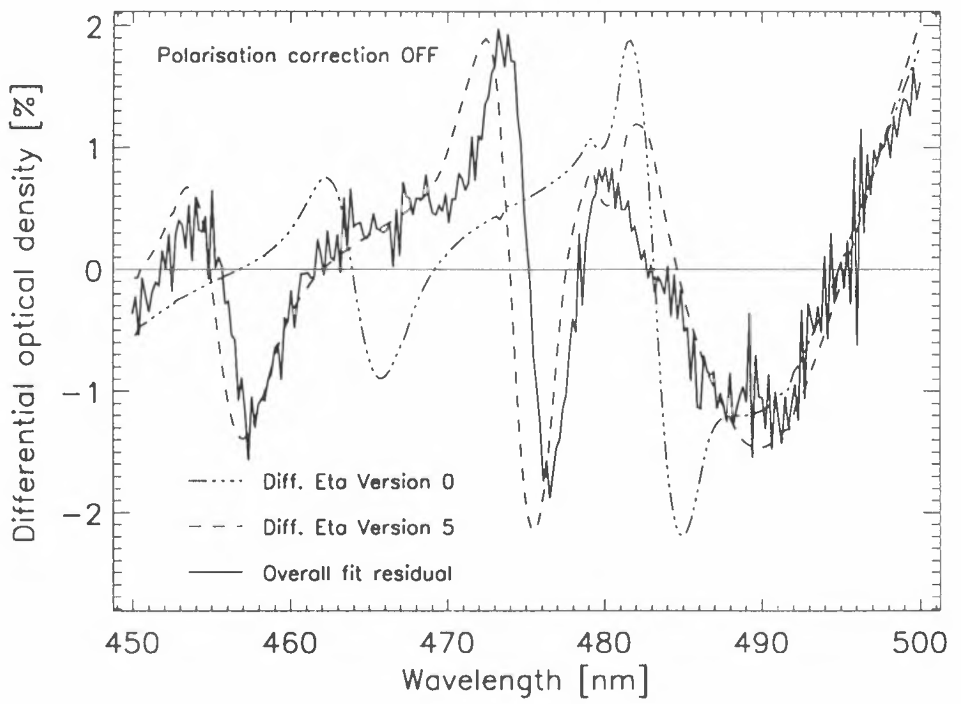

Figure 8: GOME nadir polarisation sensitivity η, version 0 and version 5, compared to fit residual from the same ground pixel as in Fig. 6, but without polarisation correction being applied in the level 0-1 processing. η has been made "differential" (by subtracting a 2nd order polynomial) and scaled arbitrarily. For further discussion see text.

nificant shift in wavelength is found (not shown). If there is any, it is much less than one detector pixel (0.2 nm) during these 2.5 months.

In summary, there are strong indications from the DOAS fit residuals in the 450–500 nm region that the real nadir polarisation sensitivity η is significantly different from η as given with the version 5 keydata[2]. The most important difference seems to be an overall wavelength shift of about 1 nm (the real η being shifted to longer wavelengths) in the 450–490 nm region. No drift of the real η was found between the 3rd July and the 16th September 1995.

Recommendations

Improving polarisation correction in this wavelength region is worthwhile because it is considered well suited for ozone retrieval.

As a first step the nadir polarisation sensitivity η has to be corrected to actual in-orbit conditions. Residuals from DOAS fits using nadir-static data without polarisation correction can be helpful in establishing the new η. Using the corrected η in the GDP the residuals have again to be investigated. If they are still substantial (compared to ozone absorption) modifications of the PCA have to be considered. η has to be monitored and, if necessary, adapted during the lifetime of GOME.

[2]No comparisons have been made to later versions (6–8) of the keydata but to our knowledge η was not changed in these versions.

The influence of the "dichroic residuals" on ozone and NO_2 retrieval using GOME channel 3 data has to be investigated.

Finally, nadir-static measurements are an invaluable tool for monitoring both instrument performance and data processing. It is recommended to carry out nadir-static measurements during at least one orbit in the monthly calibration timeline.

Outlook

The accuracy of η provided, η can be included in the DOAS fitting for some off-line tests using nadir pixels. (Including η, however, is *not* recommended for the GDP level 1-2 processing.) This can be done only in regions where $\eta(\lambda)$ has sufficient "differential" structure (mainly channel 3).

- Using polarisation-corrected level 1 data this "η fitting" serves as quality check for the PCA. η should not be found by the fit if the PCA works perfectly.

- Using level 1 data *without* polarisation correction "η fitting" should allow determination of a (mean) fractional polarisation value p for the fitting window independent of PMD measurements. This might be interesting for further studies on GOME polarisation measurements.

4 Detection of BrO and OClO over Antarctica

Although it is named Global *Ozone* Monitoring Experiment the GOME was conceived to measure a variety of other trace gases of atmospheric relevance. At the time GOME was proposed, first observations of BrO and OClO in zenith-sky measurements over Antarctica had just been made (*Solomon et al.,* 1987 and 1989, *Carroll et al.,* 1989). These gases are both ideal candidates for the DOAS method because of their characteristic banded absorption spectra between 280 and 450 nm. BrO plays an important role in catalytic ozone destruction via its reaction with ClO

$$BrO + ClO \longrightarrow Br + Cl + O_2.$$

A second channel of the same reaction is OClO formation:

$$BrO + ClO \longrightarrow OClO + Br$$

Although it is suspected that the latter is not the only production mechanism for OClO, simultaneous measurements of BrO and OClO yield also important information on ClO chemistry.

While another group is reporting on GOME BrO measurements over Greenland (*Hegels and Perner,* this issue), in this study first results on GOME measurements of BrO and OClO over Antarctica during July–September 1995 are presented. No attempt will be made to calculate vertical column densities or to compare the GOME measurements to groundbased measurements of BrO and OClO.

4.1 Data analysis

GOME level 1 data from channel 2 have been evaluated with the DOAS method. Focus was on solar zenith angles between 80° and 95° because BrO and OClO differential optical densities are expected to be largest in this range. In addition to the reference spectra used for ozone and NO_2 analysis, BrO and OClO spectra measured by *Wahner et al.* (1987, 1988) at $T = 228$ K (BrO) and $T = 204$ K (OClO) have been used. These have been checked by measurements in our laboratory. Some window optimisation on GOME data led to the choice of a 345–359 nm window for BrO analysis, and a 356–383 nm window for OClO analysis.

Using solar irradiances as background spectra for the analysis it turned out that the differential optical densities due to the Ring effect were about by an order of magnitude larger than the expected optical densities of BrO and OClO. Nevertheless, BrO and OClO fits using GOME data with a solar reference were possible, when a calculated Ring reference spectrum was included in the fit (*Rozanov,* 1996.) This study, however, followed the approach traditionally used in ground-based analysis. An earthshine spectrum was chosen as background, reducing the Ring signal by about a factor 5. The earthshine spectrum "contains" an unknown slant column amount of the absorbers. The DOAS fits yield now differential instead of absolute slant column densities. In this study, earthshine spectra measured by GOME in the Northern Hemisphere at a solar zenith angle around 80° were used as background. The slant column amount of OClO in the background spectra is expected to be negligible, so that differential and absolute slant column densities can be equated. However, this is certainly not true for BrO.

4.2 First results

Both BrO and OClO were detected in GOME measurements from the Southern Hemisphere during July–September 1995. Examples are shown in Figures 9 and 10. In addition to the OClO bands depicted in Figure 10 the bands at 387 and 397 nm could readily be identified using GOME data.

In all cases the slant column densities are in the expected range. Remarkably, no averaging over ground pixels was necessary but single spectra (integration time 6 s) could be used for analysis. This reflects the high signal-to-noise ratio in channel 2. OClO fits having comparably low residuals were possible up to a solar zenith angle of 95°. The few exceptions found were in most cases affected by "hot pixels". Figure 11 depicts the slant column density of OClO as a function of solar zenith angle for an orbit on 27th August 1995. Even without having calculated air-mass factors in order to convert the slant columns to vertical columns it looks like the slant column increases more rapidly than the air-mass factor indicating an increase of the vertical column with increasing solar zenith angle which is to be expected for OClO. This is because OClO is rapidly photolysed.

OClO has been detected as early as on the 28th July in Southern Hemisphere data, possibly indicating very early chlorine activation in 1995. Further analysis is under way.

5 Conclusions and Recommendations

Several time-dependent instrumental effects such as etaloning, drift of the dichroic transmissivity and longterm degradation have been described which affect the precision of both irradiances and radiances by several percent if not accounted for in GOME data processing. Therefore it is recommended

- to monitor all these effects during the lifetime of GOME, both by internal (GOME vs. GOME) and external (GOME vs. other instruments measuring irradiances) comparisons;
- to develop a dynamic calibration database where these effects are properly parametrized.

Even if wavelength accuracy is already high there is some potential for further improvements which

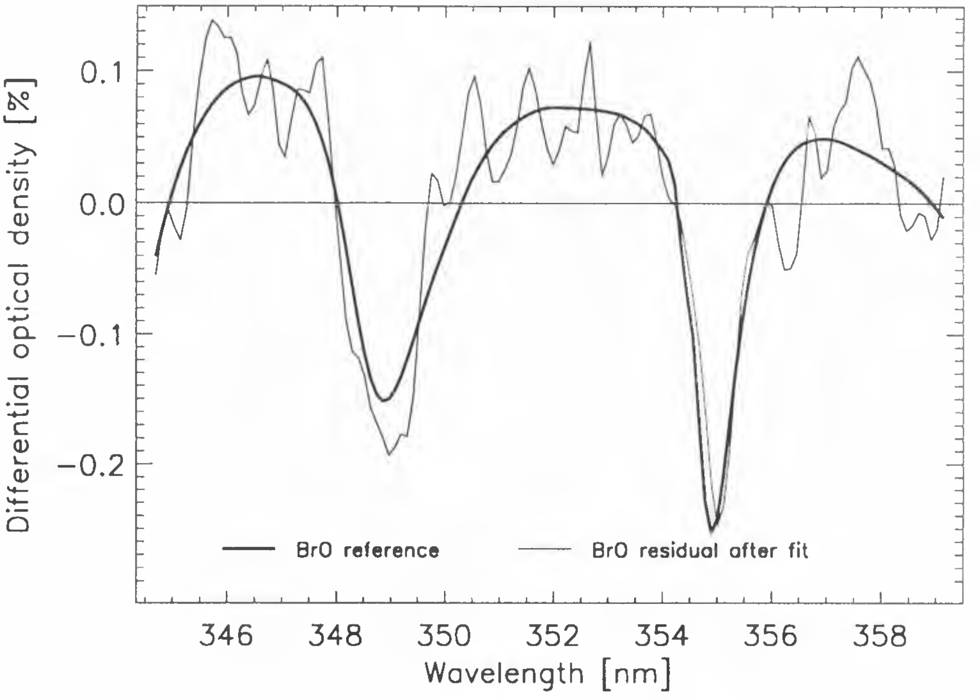

Figure 9: BrO fit results for groundpixel 1870 from orbit 1835 (27th August 1995, 7:25:42 UT, integration time 6 s, solar zenith angle 86.47°, latitude 70.17°S, longitude 21.54°E). An earthshine spectrum measured during the same orbit, but in the Northern Hemisphere, at a solar zenith angle 78.0° has been used as background. A BrO differential slant column density of $3.67 \cdot 10^{14}$ cm^{-2} and a linear fit error of 4.5% were found.

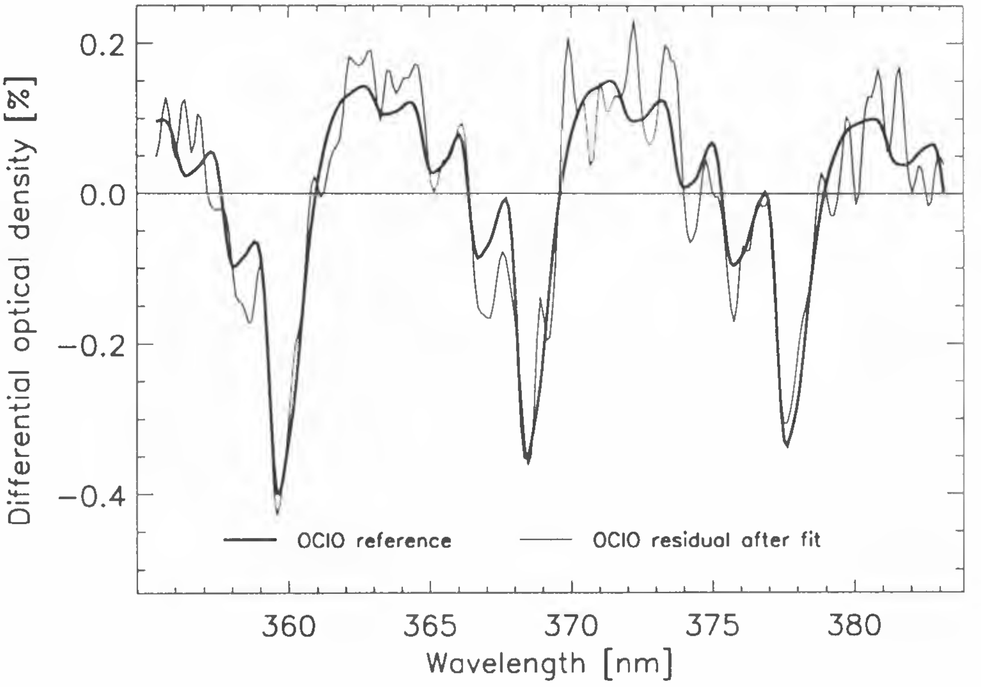

Figure 10: OClO fit results for groundpixel 1918 from orbit 1835 (27th August 1995, 7:26:54 UT, integration time 6 s, solar zenith angle 90.51°, latitude 73.90°S, longitude 14.54°E). Background spectrum as in Figure 9. OClO slant column density was $4.10 \cdot 10^{14}$ cm^{-2}, linear fit error for OClO 2.8%.

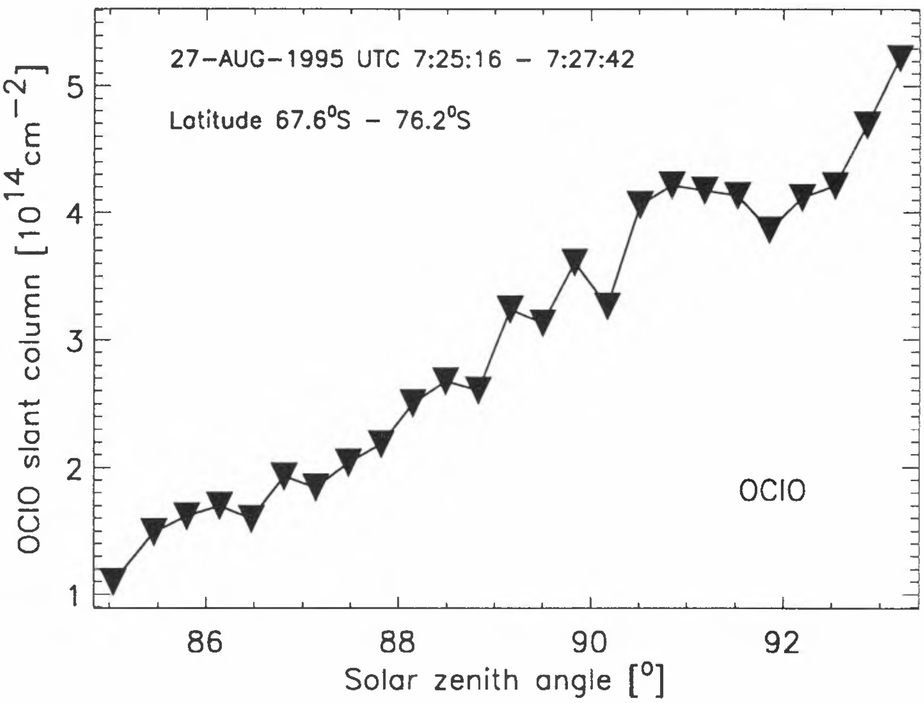

Figure 11: (Differential) slant column densities of OClO measured by the GOME during orbit 1835 (27th August 1995) over New Schwabenland, Antarctica. Each triangle represents a single 6 s measurement. GOME moves about 1000 km (along-track) during the time period shown in this plot. Errors of the linear fit were between 2.8% and 9.4% for OClO.

should help to minimize unnecessary noise due to interpolation errors.

Radiances: Polarisation correction is erroneous at present in the 450–500 nm region due to a 1 nm shift in the in-orbit polarisation sensitivity η compared to the version 5 keydata. This prevents reliable ozone retrieval in this window. It is strongly recommended do correct η to the in-orbit situation and to aim at ozone retrieval in this window.

The DOAS approach used in determination of trace gas column amounts from the GOME irradiance/radiance products is very "forgiving" in that many of the named effects simply cancel when ratioing irradiances and radiances. This was proven by the quality of the GDP *main* product (Ozone vertical columns) throughout the Validation Campaign. Another nice proof is that it is possible to detect the trace gases BrO and OClO which have only small absorptions from GOME data.

Acknowledgements

We thank J. Callies, A. Türk (ESTEC), R. Hoekstra, C. Olij, E. Zoutman (TPD), S. Slijkhuis, I. Aben (SRON), W. Balzer, D. Loyola (DLR), and M. Buchwitz (IUP) for helpful discussions. Parts of this work have been funded by the German Space Agency (DARA, contract No. 50EE9439) and the University of Bremen.

References

Brasseur, G., and S. Solomon, Aeronomy of the middle atmosphere, 2nd ed., Dordrecht: Reidel, 1986.

Burrows, J. P., *et al.*, SCIA-Mini, Proposal to ESA, Max-Planck-Institut für Chemie, Mainz, 1988.

Carroll, M. A., *et al.*, Visible and near-ultraviolet spectroscopy at McMurdo station, Antarctica. 6. Observations of BrO, *J. Geophys. Res.*, **D94**:16633–16638, 1989.

Eisinger, M., *et al.*, Studies on DOAS ozone column retrieval from the UV and visible measurements of GOME, this issue.

Global Ozone Monitoring Experiment: Interim Science Report, European Space Agency (ESA), SP-1151, 1993.

GOME Data Processor Level 0 to 1 Algorithms Description, Deutsche Forschungsanstalt für Luft- und Raumfahrt (DLR), ER-TN-DLR-GO-0022, 1995.

GOME Users Manual, European Space Agency (ESA), SP-1182, 1995.

Hegels, E., and D. Perner, Validation of GOME BrO measurements in Søndre Strømfjord, Greenland, this issue.

Montenbruck, O., and T. Pfleger, Astronomie mit dem Personal Computer, 2nd ed., Berlin: Springer, 1994.

Mount, G. H., *et al.*, Interference effects in reticon photodiode array detectors, *Appl. Opt.*, **31**:851–858, 1992.

Product Specification Document of the GOME Data Processor, Deutsche Forschungsanstalt für Luft- und Raumfahrt (DLR), ER-PS-DLR-GO-0016, 1995.

Rozanov, V., private communication, 1996.

Solomon, S., *et al.*, Visible spectroscopy at McMurdo station, Antarctica. 2. Observations of OClO, *J. Geophys. Res.,* **D92**:8329–8338, 1987.

Solomon, S., *et al.,* Visible and near-ultraviolet spectroscopy at McMurdo station, Antarctica. 5. Observations of the diurnal variations of BrO and OClO, *J. Geophys. Res.,* **D94**:11393–11403, 1989.

Wahner, A., *et al.,* Absorption cross sections for OClO as a function of temperature in the wavelength range 240–480 nm, *J. Phys. Chem.,* **91**:2734–2738, 1987.

Wahner, A., *et al.,* Absorption cross sections of BrO between 312 and 385 nm at 298 K and 223 K, *Chem. Phys. Lett.,* **152**:507–512, 1988.

World Meteorological Organization (WMO), Scientific assessment of ozone depletion, Global Ozone Research and Monitoring Project, **37**, 1994.

M. Eisinger, present address: Alfred Wegener Institute for Polar and Marine Research, D-14401 Potsdam.

J. P. Burrows and A. Richter, Institute of Environmental Physics, University of Bremen, D-28334 Bremen.

GOME Validation Project D-131

VALIDATION OF OZONE TOTAL COLUMN MEASUREMENTS (LEVEL 2 PRODUCTS)

Validation of GOME BrO Measurements in Søndre Strømfjord, Greenland

E. Hegels, D. Perner

Max-Planck-Institut für Chemie, Saarstr. 23, D-55122 Mainz, Germany

Abstract

The validation of the Global Ozone Measuring Experiment (GOME) on-board ESR2, the European Space Agency's new environmental satellite launched in April 1995 is well under way now and has resulted in the first observation of the stratospheric BrO radical by remote sensing from space. During July/August 1995 BrO was detected by groundbased DOAS experiments in Greenland which data validate the GOME data during its overpasses. The groundbased remote sensing experiments were performed mainly for the purpose of calibrating GOME by observation of zenith scattered sunlight.

1 Introduction

BrO has been detected before by remote spectroscopic sensing (Caroll et al., 1989; Wahner et al., 1990; Arpag et al., 1994; Fish et al., 1995) as well as by in situ measurements (Brune et al., 1989; Toohey et al., 1990).

Bromine as a potential ozone depleting agent has been pointed out by McElroy et al., 1986 and Wofsy et al., 1975.

While the majority of inorganic chlorine in the stratophere is tied up in relatively long lived reservoirs, HCl and $ClONO_2$, the lifetimes for HBr and $BrONO_2$ are much shorter making BrO the predominant inorganic bromine species there. As a result of this partitioning, bromine is much more efficient than chlorine on a per atom basis at destroying ozone (WMO/UNEP, 1994).

In contrast to chlorine elementary bromine is returned by reactions (1) and (2).

$$BrO + BrO \rightarrow Br + Br + O_2 \qquad (1)$$
$$\rightarrow Br_2 + O_2 \qquad (2)$$

In addition the reaction of HO_2 and BrO lead to another important destruction channel for O_3. At midlatitude the lower stratospheric ozone is consumed via that reaction at a rate comparable to or even exceeding those of chlorine alone (Poulet et al., 1992, Avallone et al., 1993, Garcia and Solomon, 1993).

A key reaction of BrO is its synergistic coupling with ClO to destroy ozone (Yung et al., 1980; McElroy et al., 1986). About half of the net reaction of ClO with BrO leads to ozone loss and during the antarctic ozone hole formation accounts for approximately 15 to 30 % of the ozone loss in the polar stratospheric vortex (Jones et al., 1989; Anderson et al., 1989, Solomon et al., 1990).

2 Measurements

2.1 Ground Based DOAS

Spectra were taken by an UV-VIS spectrometer using DOAS (Differential Optical Absorption Spectroscopy) in the wavelength region from 316 to $518nm$. The instrument was placed in Greenland at 270m above sea level on Tacan Hill ($50.62°W$, $66.99°N$) near Søndre Strømfjord (SS).

A bundle of $50\mu m$ diameter fibres arranged circularly at one end and in a rectangle ($2.5mm \times 150\mu m$) at the other end serves as the entrance slit to the spectrometer. This entrance slit provides oversampling for the $25\mu m$ wide diodes in the array. The resolution is $1.1nm$.

The observations were made with zenith scattered sunlight. Twilight BrO was identified by its absorption bands at 349, 355 and $361nm$.

A nonlinear multiparameter procedure fitted simultaneously up to seven laboratory spectra (here BrO, NO_2, O_3, O_4 and a Ring-spectrum) to the differential spectrum (Perner et al., 1991). This procedure yielded differential slant columns because the measured spectra were divided by a reference spectrum which contained a certain amount of the compound's absorption.

2.2 GOME DOAS

The evaluation of GOME spectra is done with the same algorithm. A set of labratory spectra taken with a different spectrometer (resolution $0.6nm$) are used. To achieve the same resulution the GOME spectra are smoothed.

Figure 1 shows the BrO absorption spectrum in nadir scattered sunlight collected by GOME in the 2nd

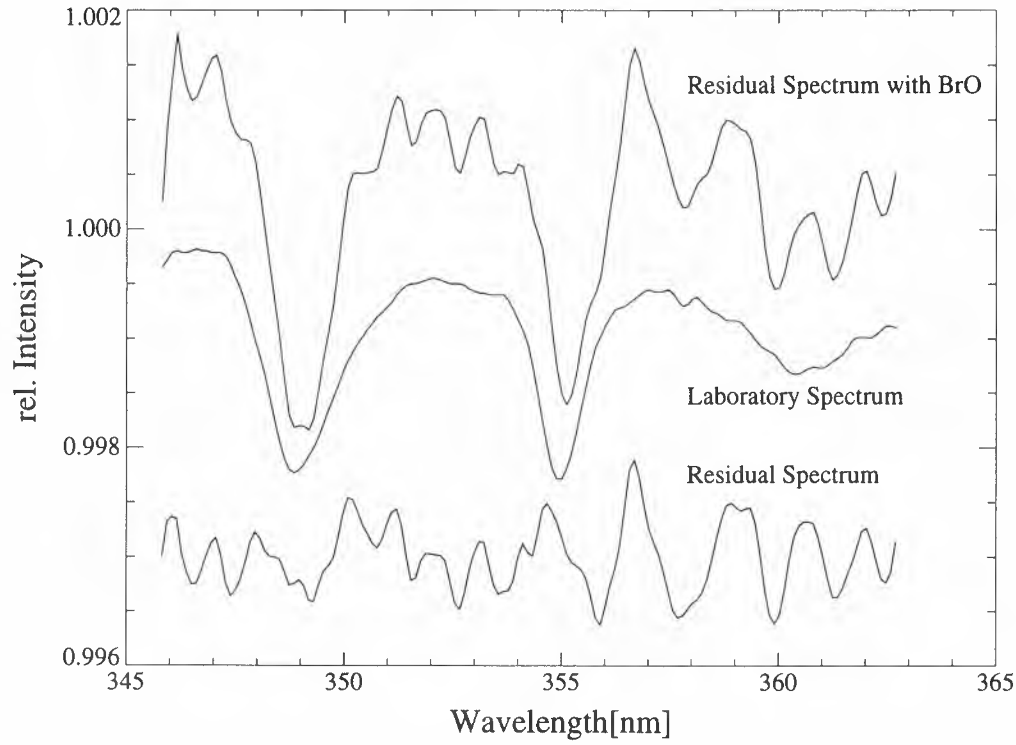

Figure 1: GOME spectrum with BrO absorption after correction for Fraunhofer and Ring structures and elimination of NO_2 and O_3 absorptions in nadir scattered sunlight on 950728, SZA 84.8°, 00:36:04 UT, Lat. 69.82°, Long. 304.37°

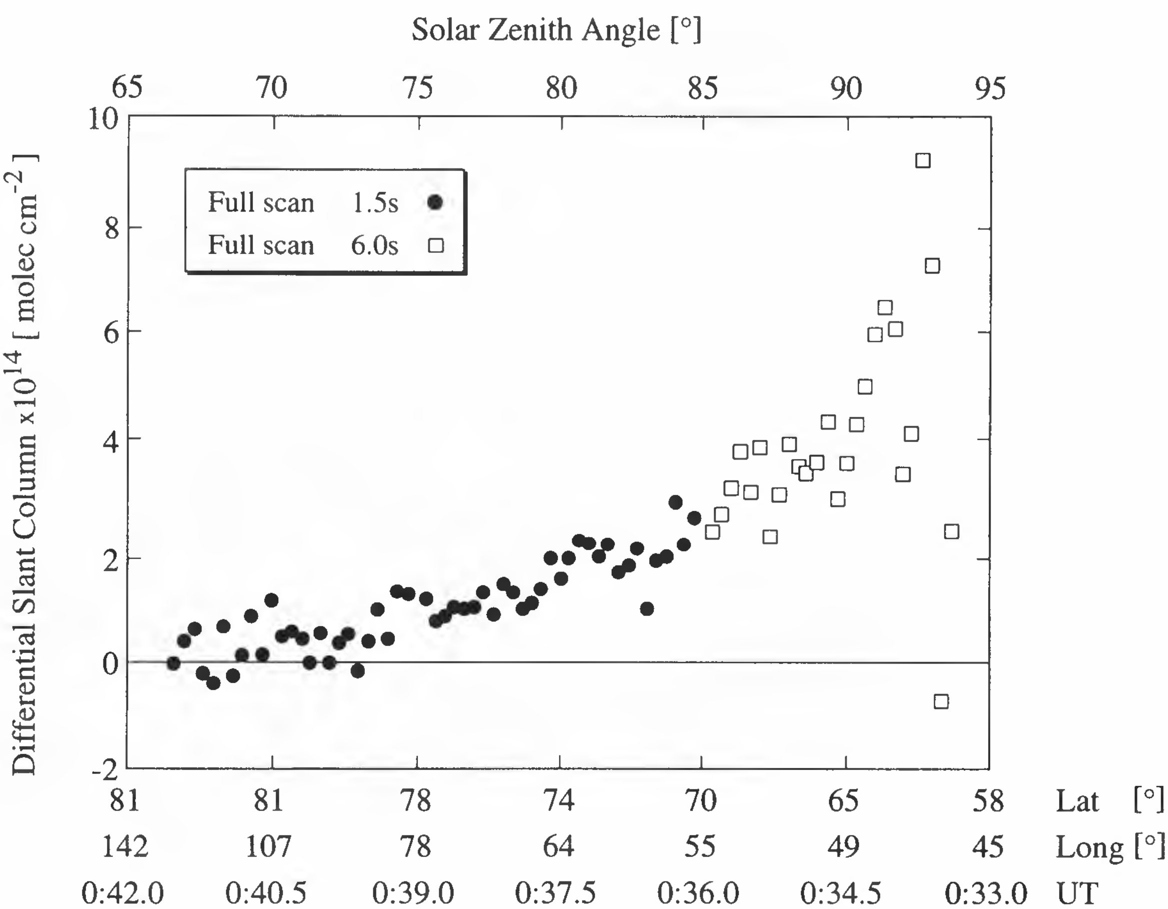

Figure 2: Differential slant column of BrO as a function of solar zenith angle, universal time, latitude and longitude. 6 s integration time for full scan width 960 km on the ground (open circles), fly back 1.5 s (closed circles), Groundpixel size 40x960 km^2 (full swath width).

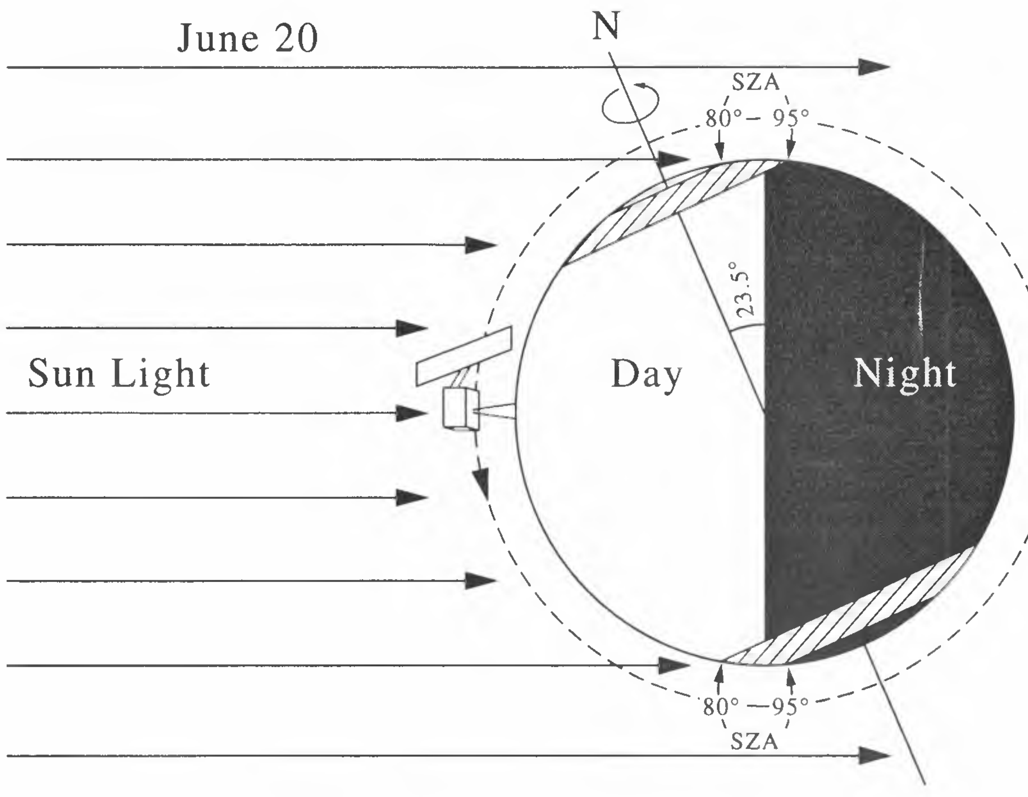

Figure 3: Regions of high sensitivity detection of stratospheric trace gas absorptions by GOME on ESR2 (hatched area).

spectral channel from 290 to 400nm. This orbit went over Søndre Strømfjord. The weak differential slant column absorption by stratospheric BrO is obtained by using a nadir reference spectrum at a solar zenith angle (SZA) of 70° from the same orbit. Light references of direct sun illumination of a scattering plate gave rise to much larger noise levels.

3 Validation

Figure 2 shows the BrO diffential slant columns along part of the orbit. Due to the small vertical column abundances of BrO the absorptions are only pronounced for long pathlengths of sunlight in the stratosphere. Large SZAs yield the most accurate results.

The groundbased remote sensing experiments were performed from 950727 to 950808 mainly for the purpose of calibrating GOME by observation of zenith scattered sunlight. During that period ERS2 overpassed Søndre Strømfjord at a SZA of about 88°. During July/August 1995 BrO was detected also by groundbased DOAS experiments in Greenland which data validate the GOME data during its overpasses. Table 1 shows the differential slant column densities of BrO as observed by nadir and by zenith observation.

Conclusions

The presently achieved sensitivity restricts the detection of BrO by single scans generally to latitudes 57°-90° N and S. Furthermore there are some limitations according to season. Figure 3 gives the global area for a sensitive observation of trace species in the stratosphere (high SZA) around summer solstice.

In the beginning of 1996 validation by the Greenland based DOAS was resumed again this time to study vortex events above Søndre Strømfjord. At that time also validation of OClO is possible, so that essentially two important inorganic halogen compounds can be followed by ERS2 based GOME.
Therefore the remote observation from space of this key halogen species demonstrates not only the excellent performance of GOME but offers to map the global distribution of this important radical. In the future studies of seasonal, interannual and hopefully decadal variations will be carried out.

Acknowledgment

The support of the groundbased measurements by the Danish Meteorological Institute is highly appreciated. We acknowledge the release of ESR GOME spectra to us by the DLR according to the ERS Announcement of Opportunity by ESA.

	GOME					GBO				
	SZA	Time	DSC	Lat.	Long.	SZA	Time	DSC	Lat.	Long.
	[°]	UT	$\frac{molec}{cm^2} \times 10^{14}$	[°]	[°]	[°]	UT	$\frac{molec}{cm^2} \times 10^{14}$	[°]	[°]
SZA ref.			70°/80°					70°/80°		
950728	88.8	0:34:56	3.9 / 3.9	66.0	50.7	88.3	0:38:00	5.0 / 3.7	67.0	50.6
	88.5	0:35:02	4.5 / 3.8	66.3	51.0	88.6	0:43:00	4.1 / 3.4	67.0	50.6
	88.2	0:35:08	3.5 / 2.8	66.7	51.4	88.8	0:47:00	4.6 / 3.3	67.0	50.6
950730	90.5	1:11:57	4.4 / 4.3	64.8	58.8	89.8	0:54:00	3.2 / 2.7	67.0	50.6
	90.1	1:12:04	8.6 / 4.6	65.1	59.1	90.1	1:02:00	3.5 / 3.8	67.0	50.6
	89.8	1:12:10	5.4 / 3.6	65.5	59.5	90.6	1:12:00	3.9 / 3.6	67.0	50.6

Table 1: Comparison of differential slant columns (DSC) of BrO measured by GOME and by ground-based observation (GBO) in the region of Søndre Strømfjord, SS, Greenland. Evaluations were made with reference spectra taken at 70° and 80° SZA, respectively. The observations immediately preceeding the overpass over SS on day 950728 served as reference in GOME evaluation. For GBO the corresponding pm spectra of the particular day were used. Differential cross section at 355nm: GOME 7.9×10^{-18} cm^{-2} (0.5nm resolution), GBO 6.2×10^{-18} cm^{-2} (1.1nm resolution)

Bibliography

Anderson J.G., W.H. Brune, S.A. Lloyd, D.W. Toohey, S. P. Snader, W. L. Starr, M. Loewenstein, and J.R. Podolske, Kinetics of O_3 destruction by ClO and BrO within the Antarctic vortex; an analysis based on ER-2 data, J. Geophys. Res., 94, 11480, 1989

Arpag K.H., P.V. Johnson, H.L Miller, R.W. Sanders and S. Solomon, Observations of the stratospheric BrO column over Colorado, J. Geophys. Res., 99, D4, 8175-8181, 1994

Avallone, L.M., D.W. Toohey, W.H. Brune, R.J. Salawitch A.E. Dessler, and J.G. Anderson, In situ measurements of ClO and ozone: Implications for heterogeneous chemistry and mid-latitude ozone loss, Geophys. Res. Lett., 17, 1795, 1993

Brune W.H., J.G. Anderson, and K.R. Chan, In situ observation of BrO over Antarctica: ER-2 aircraft results from 54°S to 72°S latitude, J. Geophys. Res., 94, 16639, 1989

Fish D.J., R.L Jones and E.K. Strong, Mid-latitude observations of the diurnal variation of stratospheric BrO, J. Geophys. Res., 100, 18863, 1995

Garcia, R.R., and S. Solomon, A new numerical model of the middle atmosphere, 2, Ozone and related species, J. Geophys. Res., 99, 12937, 1994

Jones, R.L., et al., Lagrangian photochemical modeling studies of the 1987 Antarctic spring vortex, 1, Comparison with AAOE observations, J. Geophys. Res., 94, 11529, 1989

McElroy, M. B., R. J. Salawitch, S. C. Wofsy and J. A. Logan, Antarctic ozone: Reductions due to synergistic interactions of chlorine and bromine. Nature, 321, 759, 1986

McElroy, M. B., R. J. Salawitch, and K. Minschwaner, The changing stratosphere, Planet. Space Sci., 40, 373-401, 1992

Perner D., T. Klüpfel, U. Parchatka, A. Roth, and T. Jörgensen, Groundbased UV-VIS spectroscopy: Diurnal OClO profiles during January 1990 above Søndre Strømfjord, Greenland, Geophys. Res. Lett., 18, 787-790, 1991

Perner D., A. Roth, and T. Klüpfel, Groundbased measurements of Stratospheric OClO, NO_2 and O_3 at Søndre Strømfjord in Winter 1991/92, Geophys. Res. Lett., 21, 1367-1370, 1994

Poulet, G.M., M. Pirre, F. Magain, R. Ramaroson, and G.le Bras, Role of the BrO + HO_2 reaction in the stratospheric chemistry of bromine, Geophys. Res. Lett., 23, 2305, 1992

Solomon, S., R.W. Sanders, and H.L. Miller, Visible and near-ultraviolet spectroscopy at McMurdo Station, Antarctica, 7, OClO diurnal photochemistry and implications for ozone destruction, J. Geophys. Res., 95, 13807, 1990

Toohey, D.W., J.G Anderson, W.H. Brune, and K.R. Chan, In-situ measurements of BrO in the Arctic Stratosphere, Geophys. Res. Lett., 17, 513, 1990

Yung, Y.L., J.P. Pinto, R.T. Watson and S.P. Sander, Atmospheric bromine and Ozone perturbations in the lower stratosphere, J. Atm. Sci., 37, 339-353, 1980

Wahner A., J. Callies, H.P. Dorn, U. Platt, and C. Schiller, Near UV atmospheric absorption measurements of column abundances during the Airborne Arctic Stratospheric Expedition, January-February, 1989, 3, BrO observations, Geophys. Res. Lett., 17, 517, 1990

Wofsy, S.C., M.B. McElroy, and Y.L. Yung, The chemistry of atmospheric bromine, Geophys. Res. Lett., 2, 215-218, 1975

World Meteorological Organization (WMO), Global Ozone Research and Monitoring Project, Scientific assessment of ozone depletion: 1994, WMO Rep. No. 37, Geneva 1994

Product Specification Document of the GOME Data Processor, Deutsche Forschungsanstalt für Luft und Raumfahrt (DLR), ER-PS-DLR-GO-0016, 1995

GOME OZONE TOTAL AMOUNTS VALIDATION BY GROUND-BASED OBSERVATIONS PERFORMED AT THE NDSC/ALPINE STATIONS

J.-C. Lambert[1], M. Van Roozendael[1], P. Peeters[1], P.C. Simon[1], M.-F. Merienne[2], A. Barbe[2], H. Claude[3], J. de La Noë[4], J. Staehelin[5]

1. Belgian Institute for Space Aeronomy, Brussels, Belgium
2. Université de Reims, France
3. Deutscher Wetterdienst, Hohenpeißenberg, Germany
4. Observatoire de Bordeaux, Université de Bordeaux, France
5. ETH, Atmosphärenphysik, Zurich, Switzerland

Abstract
The first results of the GOME geophysical validation campaign obtained by means of ground-based observations performed at the NDSC/Alpine and secondary stations are summarised. For validation purpose, the accuracy of the ground-based instruments is analysed and quantified. A special care is given to the retrieval of total ozone with the ground-based DOAS/SAOZ instrument. A methodology of comparison is defined, emphasising the optimisation of the co-location of the air masses probed by the satellite and the ground-based instruments. The 45 days of GOME data processed during the commissioning phase are compared to the total ozone measurements provided by two Brewer, four Dobson and one SAOZ instruments. The relative differences between the GOME and the correlative ground-based total ozone are analysed with respect to the solar zenith angle. In average, the GOME ozone total amounts underestimate the ground-based measurements, between 2 and 8%. Using ground-based data, a test case study is carried out on the fitting window which could be used for ozone retrieval in the visible, demonstrating the importance of O_4 interferences when defining the window spectral range.

1. INTRODUCTION

The Global Ozone Monitoring Experiment (GOME) on board the Earth Remote Sensing (ERS-2) satellite was launched by ESA on 21 April 1995 onto an heliosynchronous polar orbit. Its main scientific objective is the study of trace constituents in the lower and the middle atmosphere. GOME is a combination of four grating spectrometers observing the solar radiation scattered from the atmosphere or from the Earth's surface, covering the spectral range 240-790 nm. The instrument is operated in the nadir-viewing geometry and the current 960 km swath width is divided into three 80x40 km pixels. Atmospheric constituents are detected by means of the Differential Optical Absorption Spectroscopy technique (DOAS). In particular, the GOME ozone total amounts retrieved during the commissioning phase were obtained by using the DOAS method in the Huggins bands.

This work reports the first results of the geophysical validation campaign of the GOME ozone total amount measurements, obtained by means of ground-based observations performed at the NDSC (Network for the Detection of Stratospheric Changes) Alpine and complementary stations. Preliminary results of the validation of nitrogen dioxide total amounts are reported in the paper related to the SAOZ Network (Lambert et al., 1996). The following results are based upon only the limited set of 45 days of GOME ozone data processed during the commissioning phase (22 July - 13 December 1995), without fully adequate corrections for multiple scattering and Earth's sphericity in the air mass factors. Hence the conclusions given here are still preliminary and have to be confirmed by the validation of expanded time series of data.

2. GROUND-BASED INSTRUMENTS

The NDSC/Alpine Stations

The NDSC is a set of high-quality remote sensing research stations for observing and understanding the physical and chemical state of the stratosphere. The mid-latitude reference NDSC site in the northern hemisphere consists of the *International Scientific Station at the Jungfraujoch* (ISSJ, Switzerland), the *Observatoire de Haute Provence* (OHP, France) and the *Observatoire de Bordeaux - Plateau de Bure* (France). These stations combine measurements of total vertical columns of ozone and of other key constituents such as NO_y, ClO_y or CH_4, and vertical profiles of ozone, aerosols and ClO. In addition, complementary measurements are performed at two secondary stations, namely Arosa in Switzerland and Hohenpeißenberg in Germany. The validation results reported here are focused on the GOME ozone total amounts and rely on the observations performed with the Dobson, Brewer and SAOZ instruments listed in Table 2-1. Additional informations on the vertical profiles of ozone density were given by Brewer-Mast ozone sondes launched at Payerne (Switzerland).

Table 2-1 Correlative measurements at the NDSC/Alpine stations

Stations	Instruments
Arosa (46°N, 9°E)	Brewer, Dobson
Bordeaux (46°N, 1°W)	Dobson
Hohenpeißenberg (48°N, 11°E)	Brewer, Dobson
Jungfraujoch (47°N, 8°E)	SAOZ
O.H.P. (44°N, 5°E)	Dobson
Payerne (46°N, 7°E)	Ozone Soundings

Ground-based Instruments

Since 1958, *Dobson* spectrophotometers have been deployed in a world-wide network and measure the ozone total vertical amount from the ground. The Dobson instrument is a double-monochromator based upon the differential absorption method in the UV range where ozone exhibits strong absorption features (Huggins bands). The measurement principle relies on the ratio of the direct sunlight intensities at two standard wavelengths. The most widely used combination, recommended as the international standard, is the couple of pairs of wavelengths referred to as the AD pair (305.5-325.4; 317.6-339.8 nm).

The *Brewer* grating spectrophotometer is similar in its principle to the Dobson, but it has an improved design. The determination of the ozone total amount is obtained from a combination of five wavelengths in the region between 306 and 320 nm.

The *SAOZ* instrument (Système d'Analyse par Observation Zénithale) is a UV-visible grating spectrometer looking at the sunlight scattered at the zenith during the twilights (Pommereau and Goutail, 1988). Narrow absorption features due to ozone, NO_2, O_4, H_2O, OClO and BrO are detected by means of the DOAS technique, based on the fit of the calculated differential optical thickness with the observed one. In particular, ozone slant amounts are derived from the absorption in the Chappuis bands, between 470 and 540 nm. They are converted into total vertical columns by using a standard air mass factor (AMF), which is calculated by a validated radiative transfer model (Sarkissian et al., 1995), assuming given vertical distributions of the atmospheric constituents controlling the penetration of the solar radiation in the atmosphere.

3. ACCURACY OF THE GROUND-BASED DATA

The accuracy and precision budgets of the Dobson, Brewer and SAOZ measurements are analysed with respect to various critical parameters.

Absorption Cross-sections

The measurement with the Dobson and Brewer spectrophotometers is based on the absorption of ozone in the Huggins bands. The ozone absorption cross-sections in these bands are known to be temperature dependent. Using the temperature corrections of the Dobson ozone absorption coefficients determined by Komhyr et al. (1993) and the stratospheric temperature at 50 hPa above the sites, the temperature effect was found to account for a 2% systematic difference between the SAOZ and the Dobson measurements at mid-latitude (Van Roozendael et al., 1995). This systematic bias is introduced by the difference between the mean 50 hPa temperature and the reference temperature selected for the Dobson ozone absorption coefficients (226.85 K).

The SAOZ measurement is based upon the ozone absorption in the Chappuis bands. In this spectral range, the absorption cross-sections are almost temperature independent. The uncertainty associated to the spectral analysis comes from the fit between the observed and the calculated optical thicknesses, and from the laboratory cross-sections used in the fitting procedure. The fit generates a pseudo-random noise lower than 1% while the uncertainty on the absorption cross-sections introduces a systematic error of about 3% in the Chappuis bands.

SAOZ Air Mass Factor

The SAOZ AMF used to convert the observed slant total amount into vertical total amount depends on the scattering geometry and is sensitive to fluctuations in pressure, temperature and ozone vertical distributions. To estimate the contribution of the fluctuations of the scattering geometry to the accuracy of the SAOZ total ozone, the data obtained at the ISSJ with the standard SAOZ AMF were compared to those retrieved with an AMF calculated with ozone vertical profiles measured at Payerne by means of Brewer-Mast ozone sondes. Figure 3-1 depicts the relative differences between the SAOZ data obtained with the standard SAOZ AMF and those retrieved with the AMF calculated with measured ozone profiles. It also illustrates the effect of the residual ozone amount in the SAOZ reference spectrum (see below). The time-serie shows that the daily fluctuations might account for ± 1% of scatter in the SAOZ total ozone. The seasonal variation of the vertical distributions introduces in the SAOZ data a seasonal systematic bias of about 3% from July to November 1995.

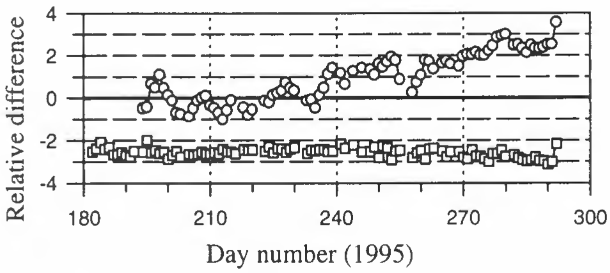

Figure 3-1 Relative differences (in per cent) between the SAOZ total ozone obtained with the standard and with the corrected SAOZ AMF calculated with measured ozone profiles (open circles), and relative differences between SAOZ total ozone obtained with two different reference spectra (open squares).

The SAOZ data obtained with the two methods were compared to the total ozone measured with the Dobson located at Arosa. Only the morning values of the SAOZ data were used for this intercomparison, to optimise the spatial coverage of the two measurements. The differences between the morning values of the SAOZ total ozone obtained with different AMF and/or reference spectra and the Dobson data from Arosa are displayed in Figure 3-2. This figure shows that the SAOZ total ozone retrieved with a corrected AMF (open circles) is closer to the Dobson measurements than the SAOZ data obtained with the standard AMF (shaded squares). The use of the corrected AMF cuts down the mean difference between the SAOZ and the Dobson total ozone from 1.6±2.8% down to 0.6±2.1%. The SAOZ AMF is also sensitive to the altitude of the site. For the Jungfraujoch station (3580 m a.s.l.) the standard AMF at sea level underestimates by 5% the AMF calculated for the altitude of the station.

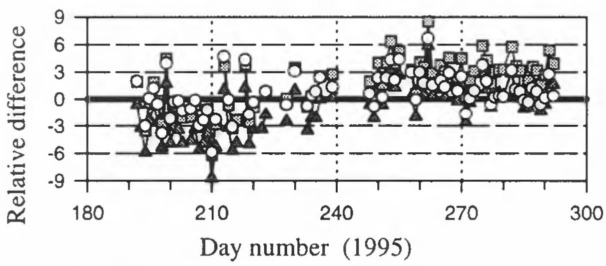

Figure 3-2 Relative differences (in per cent) between the SAOZ and the Dobson total ozone. SAOZ data are obtained with: (1) standard AMF and high SZA reference spectrum (dark triangles); (2) standard AMF and low SZA reference spectrum (dark squares); (3) corrected AMF and low SZA reference spectrum (open circles).

Residual Ozone in the SAOZ Reference Spectrum

The observed optical thickness consists in the logarithm of the ratio between the observed and a reference spectrum. The uncertainty on the residual ozone amount contained in the reference spectrum introduces a constant offset in the retrieved total ozone. This offset depends on the method used to estimate the residual ozone (Vaughan et al., 1996). Figure 3-1 (open squares) depicts the relative differences between the SAOZ data obtained with a reference spectrum recorded at high solar zenith angle (SZA), and those retrieved with a reference spectrum recorded at lower SZA. When the residual ozone amount is estimated with the classical methods using a reference spectrum recorded in the zenith viewing mode, the uncertainty on this residual ozone leads to a systematic offset in the total ozone of about 3% (Figure 3-1, open squares). This uncertainty can be attributed to the error on the SAOZ AMF at low SZA, error that can be significantly reduced by using a reference spectrum recorded in the direct Sun viewing mode, since the error on a direct Sun AMF is negligible at low SZA.

Tropospheric Perturbations of the SAOZ Data

At twilight, the tropospheric part of the effective optical path of the sunlight reaching the SAOZ is one order of magnitude smaller than the stratospheric part. In addition, the tropospheric amount of ozone is usually lower than 10% of the total column. Hence, the tropospheric contribution to the total absorption seen at twilight by the instrument is lower than 4%. However, the tropospheric contribution could occasionally increase due to the overpass of polluted air masses with high tropospheric ozone concentrations. Moreover, fog and snow showers could increase the tropospheric contribution of the observed total amount by enhancing the tropospheric multiple scattering and consequently the light path. Multiple scattering, normally negligible, is not taken into account in the SAOZ AMF calculation. In addition, absorptions by O_4 and H_2O are enhanced by tropospheric multiple scattering as well. Since O_4 and H_2O interfere with ozone, the retrieved ozone amounts can be biased (Van Roozendael et al., 1994). The statistical analysis of the differences between total ozone measured by the SAOZ at the ISSJ and the Dobson at Arosa shows that the scatter of this differences correlates with the observed O_4 slant amount, that is with the occurrence of multiple scattering events. On long time series, this random error should not exceed 1%.

Quality Control of the Ground-based Data

Most of the instruments operated at the NDSC/Alpine stations recently participated to intercomparison campaigns in order to control their quality, to assess their accuracy and to examine their consistency with other types of instruments. Comparisons between Dobson and Brewer data over long periods indicate that these instruments might suffer from long term drift associated to calibration changes and need to be corrected for. The day-to-day fluctuations in the differences between the Dobson and Brewer total ozone are usually small (± 1.5% in average). Calibration changes should not exist for SAOZ instruments since they are self-calibrated in wavelength with the solar Fraunhofer lines. The four Dobson used in the GOME validation exercise participated to the WMO Dobson Intercalibration Campaign held at Arosa in July-August 1995. The Brewer #40 (Arosa) and the SAOZ #13 (OHP) were operated at the same site for intercomparison purposes. The mean agreement between the various Dobson, the Brewer #40 and the SAOZ #13, was found to be better than 1.6% RMS. Another intercomparison campaign was held in September 1994 at Camborne (UK) for UV-visible DOAS zenith-sky spectrometers. The agreement between four SAOZ and two other DOAS spectrometers was within 3% for total ozone, as well as for the co-located Dobson measurements and ECC ozone soundings (Vaughan et al., 1996). During the GOME validation campaign, the co-location of the Brewer and Dobson spectrophotometers at Arosa and Hohenpeißenberg gave a permanent quality control. The consistency with measurements performed at the other sites has also been studied (e.g., Figure 3-2).

In summary, the following improvements have been implemented in the retrieval of the SAOZ data at the ISSJ, especially in the frame of the GOME validation exercise: (i) the calculation of a daily AMF by means of ozone profiles measured at Payerne; (ii) the most accurate method for the ozone residual amount estimation in the reference spectrum by using a direct Sun spectrum as reference; (iii) the rejection of erroneous data by using the slant amounts of O_4 and H_2O measured by the SAOZ at the ISSJ to detect tropospheric multiple scattering events. The error budgets for the direct Sun (Dobson and Brewer) and the zenith-sky (SAOZ) ground-based instruments are summarised in Table 3-1.

Table 3-1 Accuracy (in per cent) of the direct Sun (Dobson and Brewer) and zenith-sky (SAOZ) ozone measurements at the NDSC/Alpine stations

Error source	**Dobson, Brewer**	**SAOZ**
Cross-sections	± 2	< 3
Measurement	± 1.5	± 1
Multiple scattering		± 1
AMF		± 1
Residual O_3		< 1
Total Error (RMS)	**2.5**	**3.5**

4. METHODOLOGY OF COMPARISON

This section describes the methodology defined for comparing the GOME and the ground-based total ozone. Some potential sources of discrepancies between the different instruments, due to their own observing mode, are highlighted.

The total ozone observed at the Alpine stations from July to December 1995 ranged only from 240 up to 360 DU. Therefore, all the conclusions given here are valid only for the observed range of total ozone.

Geometry of the Ground-based Observations

Direct Sun measurements with the Dobson and the Brewer spectrophotometers are performed at SZA lower than 75°. When the cloud cover prevents from making direct Sun observations, the two instruments can be operated in the zenith-sky mode. In this case, the observed slant amount is converted into a vertical column by using empirical tables of correlation between the two observation modes. Nevertheless, data obtained within the direct Sun geometry are known to be more accurate by a few per cent than those obtained with the zenith-sky method (e.g., De Backer and De Muer, 1991). Therefore, only direct Sun data will be considered here. For the SAOZ, the most accurate measurements are obtained at twilight for SZA between 86° and 91°.

Temporal Coincidence of the Probed Air Masses

For validation purpose, the air masses probed by GOME and by the correlative ground-based instruments should be as similar as possible. Since the Dobson and the Brewer are usually operated several times a day, it is sometimes possible to obtain correlative total ozone for ERS-2 overpasses within a time window of two hours. Correlative data within a larger time window are also taken into account if the temporal variability in the ozone field is lower than the measurement accuracy. This can be checked by looking at the variability of the ozone data obtained during the day. The TOVS (TIROS Operational Vertical Sounder) ozone maps delivered by the KNMI (Royal Dutch Meteorological Institute) can also give some informations on the homogeneity of the ozone field in the line-of-sight of the instruments. The zenith-sky measurements (SAOZ) are always performed during twilight while ERS-2 overpasses the mid-latitude sites around noon. Therefore, a significant difference in time exists between the air masses probed by GOME and by the SAOZ, varying from 5 hours in winter up to 8 hours in summer for the Alpine stations.

Geometrical Coincidence of the Probed Air Masses

The differences in the geometry of observation between the nadir, the direct Sun and the zenith-sky viewing instruments can also introduce some scatter in the comparison. From a crude calculation of the ozone gradients using the TOMS (Total Ozone Mapping System) total ozone maps, within a spatial extent of several hundred kilometres, the spatial gradients of the ozone field might contribute by ± 2.5% to the scatter (Van Roozendael et al., 1995). For the GOME validation, the viewing geometry of the ground-based instrumentation has been taken into account.

Optimisation of the Co-location of the Measurements

The absorption light path related to the viewing geometry has been investigated for the ground-based ozone monitoring instruments in order to estimate the geolocation of the air masses effectively probed. For the direct Sun viewing instruments, the estimation is straightforward. For the zenith-sky measurements (DOAS/SAOZ), the estimation needs a radiative transfer model assuming given vertical distributions of the atmospheric constituents controlling the penetration of the solar radiation in the atmosphere. The GOME pixels are selected when presenting an intersection with the absorption light path of the correlative ground-based measurement.

The Brewer and Dobson spectrophotometers operated in the direct Sun mode sample air masses up to 200 km from the station, depending on the SZA, and hence on the season. The effective geolocation of the air mass probed by the SAOZ at twilight extends up to several hundred kilometres from the ground-based site within an azimuth range varying with the season. The horizontal projection of the air mass sampled by the SAOZ extends from 100 up to 350 km at 87° SZA and from 150 up to 550 km at 91° SZA.

The same radiative transfer model used for the ground-based instruments has been applied to the nadir viewing geometry. The effective geolocation of the GOME measurement is calculated to extend from the ground pixel up to 30 km in summer and up to 100 km in winter. This is not taken into account in this first validation exercise, mainly because of the 30 km difference between the pixel geolocation given in the GOME data files and by the ESA orbit propagator.

5. RESULTS OF TOTAL OZONE VALIDATION

Since the work reported here is based upon only the 45 days of GOME ozone data processed during the commissioning phase, the conclusions are still preliminary and have to be confirmed by a validation based on expanded time series of data and an upgraded version of the processing algorithm. The SZA of the GOME measurement never reaches 75° for latitudes lower than 52°. Therefore the lack of AMF corrections for multiple scattering and Earth's spherical geometry for SZA larger than 75° does not preclude the GOME data validation at mid-latitude. Moreover, the proximity of the NDSC/Alpine stations prevents from any disturbance introduced by the use in the GOME AMF calculation of latitude-band climatologies without interpolation. The ozone total amounts measured by GOME and the ground-based instruments generally exhibit a similar behaviour.

Validation by the Brewer spectrophotometer

The relative difference between the GOME and the correlative Brewer total ozone at Arosa (solid circles) and at Hohenpeißenberg (open squares) is depicted in Figure 5-1. For both stations, the GOME total ozone underestimates in average those measured by the Brewer: -2.5±2.4% at Arosa and -3.8±2.3% at Hohenpeißenberg. This underestimation might depend on the SZA of the GOME measurement. This assumption has to be confirmed by a validation study with expanded time series of measurements. The difference in total ozone does not seem to depend on the latitude of the centre of the GOME pixel, as shown in Figure 5-2. In Figure 5-3, the correlation plot between the total ozone measured by GOME and the Brewer indicates that the sensitivity of GOME to ozone might be lower than the Brewer one for ozone total amounts ranging from 240 to 360 DU. At Arosa, this difference is currently 16% (r^2=0.82) and at Hohenpeißenberg only 5% (r^2=0.91).

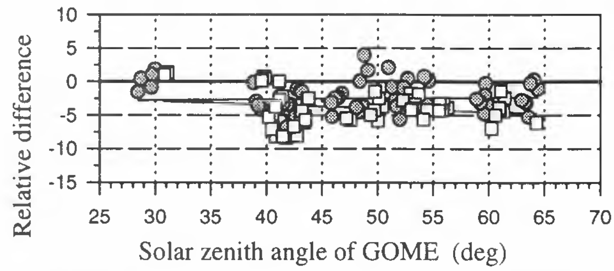

Figure 5-1 Relative difference (in per cent) between the GOME and the Brewer total ozone at Arosa (dashed circles) and at Hohenpeißenberg (open squares), as a function of the solar zenith angle of the GOME measurement.

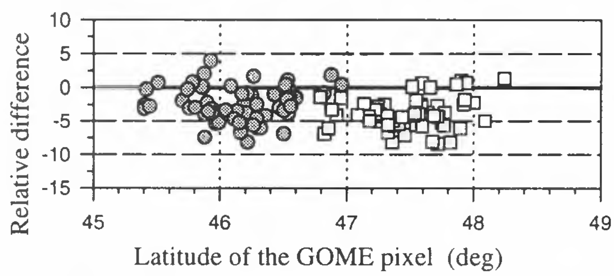

Figure 5-2 Relative difference (in per cent) between the GOME and the Brewer total ozone at Arosa (dashed circles) and at Hohenpeißenberg (open squares), as a function of the latitude of the GOME pixel.

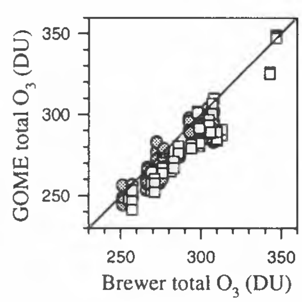

Figure 5-3 Correlation plot between the total ozone measured by GOME and by the Brewer at Arosa (dashed circles) and at Hohenpeißenberg (open squares), in Dobson units.

Validation by the Dobson spectrophotometer

Figure 5-4 and Figure 5-5 display the relative differences (in per cent) between the ozone total amounts measured by GOME and the different Dobson instruments of the Alpine stations, respectively versus the GOME SZA and the latitude of the GOME pixel. Similarly to Figure 5-1, Figure 5-4 shows that in average the GOME total ozone underestimates the Dobson measurements, whatever the location of the instrument:

-5.6±3.1% at Arosa, -5.3±3.4% at Bordeaux, -5.1±3.9% at Hohenpeißenberg and -2.7±4% at the OHP. The number of comparison points is too scarce to reveal any SZA dependence in the differences which, in addition, do not depend significantly on the latitude of the GOME pixel.

Validation by the SAOZ spectrometer

The relative difference between the total ozone measured by GOME and by the SAOZ instrument at the ISSJ station is displayed in Figure 5-6. The mean difference is -4±3%. This result confirms the lower total ozone observed by GOME by comparison with the ground-based measurements. In average, the difference displays a significant SZA dependence: -2±4% at SZA lower than 45°, -4±4% between 45° and 60° SZA, and -8±3% between 60° and 75° SZA. The SAOZ total ozone is corrected for the seasonal variation of its AMF, and should be consequently independent on the GOME SZA. The discrepancy between the GOME and the SAOZ total ozone does not depend significantly on the latitude of the centre of the GOME pixel, as shown in Figure 5-7. The SZA dependence of the discrepancy prevents from seeing any difference in the ozone sensitivity between GOME and SAOZ observations. A method to solve this problem has been applied in the results of the GOME validation with the SAOZ network (Lambert et al., 1996), but the number of observations available in this study is too scarce to proceed for a single station.

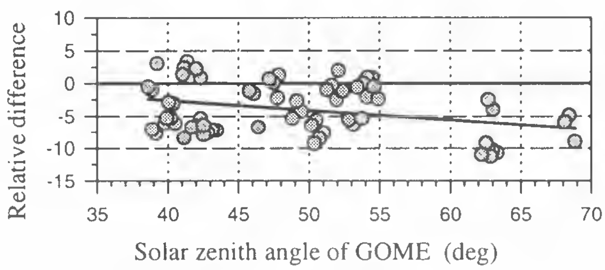

Figure 5-6 Relative difference (in per cent) between the GOME and the SAOZ total ozone at the ISSJ, as a function of the SZA of the GOME measurement.

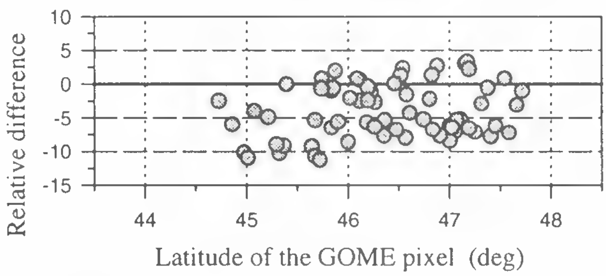

Figure 5-7 Relative difference (in per cent) between the GOME and the SAOZ total ozone at the ISSJ, as a function of the latitude of the GOME pixel.

6. TOTAL OZONE DETERMINATION FROM VISIBLE SPECTRA: A TEST CASE STUDY ON THE FITTING WINDOWS USING GROUND-BASED DATA

The GOME ozone vertical column amounts retrieved during the commissioning phase were obtained by application of the DOAS method in the UV region (Huggins bands of ozone). It is anticipated that GOME would be able to retrieve ozone total amounts from the visible range (Chappuis bands) as well. The choice of the most relevant visible windows is still a matter of discussion. Except for the differences in observation geometry, the retrieval of total ozone in the visible region is rather similar for GOME and the DOAS ground-based instruments. Hence an additional interest of the ground-based instruments in the context of the GOME validation is the potential for test case studies using ground-based data analysed in different fitting windows. In this work, two different windows were selected for processing the SAOZ data recorded at the ISSJ during the commissioning phase: (1) the usual DOAS/SAOZ window for ozone (470-540 nm) and, (2) an ozone window recently suggested for GOME (510-550 nm). Figure 6-1a shows the percentage relative differences in total ozone obtained when comparing the time series determined in both windows.

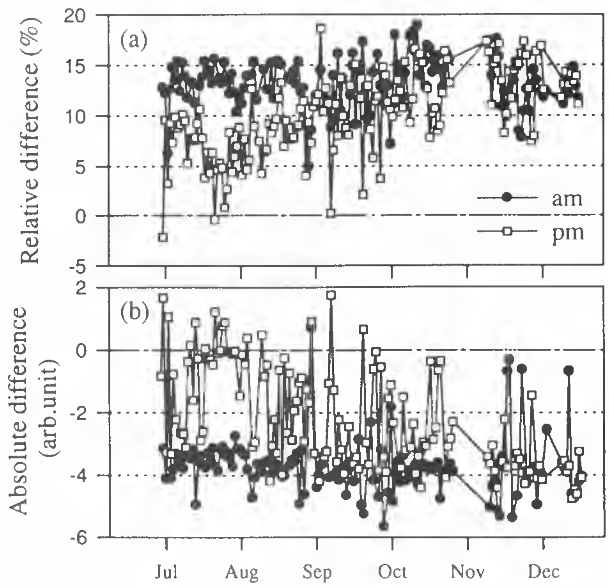

Figure 6-1 Comparison of O_3 and O_4 retrievals using two different spectral windows (see text): (a) relative difference in total ozone, and (b) absolute difference in O_4 slant amounts.

The results show large differences in the retrieved ozone values (between 0 and 20%) which are anticorrelated with differences in the O_4 amounts (Figure 6-1b). The origin of the problem appears clearly when looking at the differential structures (Figure 6-2) for both species in the two windows.

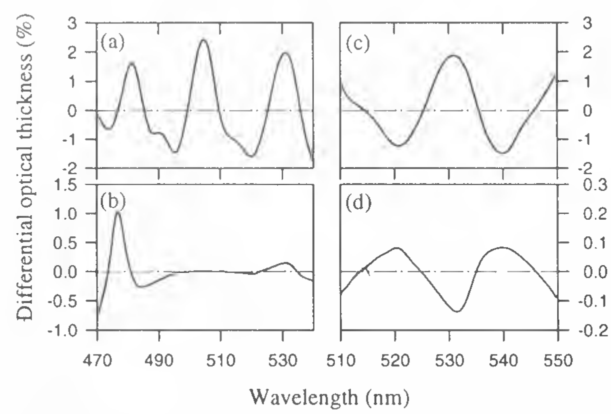

Figure 6-2 Differential optical thicknesses (in per cent) of O_3 (a,c) and O_4 (b,d) derived from least-squares analysis of SAOZ data (25.07.95, 88° SZA, PM) in two different spectral windows (see text).

For the 510-550 nm window (Figure 6-2c,d), the correlation coefficient between ozone and O_4 is larger than 0.9. Additional tests using a slightly enlarged window (510-565 nm) give similar results. Consequently, the 510-550 nm window appears to be not suitable to fit ozone in the visible, at least for ground-based measurements. This conclusion might be extended to GOME observations as well, although the contribution of O_4 to the optical thickness in the GOME geometry (nadir) is expected to be smaller.

7. CONCLUSIONS

Within the scope of the validation of the GOME ozone total amounts, the accuracy and the precision of the ground-based measurements have been discussed and quantified for the Dobson and Brewer spectrophotometers and for the SAOZ instrument. The seasonal variation of the SAOZ AMF, the estimation of the residual ozone amount in the reference spectrum and the tropospheric multiple scattering have been taken into account in the retrieval of total ozone with the SAOZ spectrometer. A methodology of comparison has been developed, emphasising the problem of the coincidence of the air masses probed by the satellite and the ground-based measurements. In particular, a selection criterion of the GOME pixel, based on the modelisation of the instrument line-of-sight, has been defined. The comparison of the 45 days of GOME data processed during the commissioning phase with the ground-based total ozone has shown that GOME ozone data are in average lower than the ground-based measurements. The mean discrepancies with the Dobson and the Brewer total ozone are given in Table 7-1. The comparison also pointed out the SZA dependence of the differences between the GOME and the SAOZ data, which is summarised in Table 7-2. The number of observations with the Brewer and the Dobson to be compared with GOME is too small to see any significant SZA dependence. According to the correlation plot between the GOME and the Brewer observations, the total ozone sensitivity of GOME between 240 and 360 DU might be lower than the Brewer one, by 16% at Arosa and by 5% at Hohenpeißenberg.

Table 7-1 Relative difference (in per cent) between the GOME and the Dobson and Brewer total ozone at the NDSC/Alpine and secundary stations.

Station	Dobson	Brewer
Arosa	-5.6±3.1	-2.5±2.4
Bordeaux	-5.3±3.4	-
Hohenpeißenberg	-5.1±3.9	-3.8±2.3
OHP	-2.7±4.0	-

Table 7-2 Relative difference (in per cent) between the GOME and the SAOZ total ozone at the ISSJ, as a function of the GOME SZA.

GOME SZA	Relative Difference
45°	-2±4
55°	-4±4
70°	-8±3

As, in addition to its retrieval in the UV range, GOME total ozone is intended to be derived from the visible, a test case study on the 510-550 nm and 510-565 nm fitting windows has been applied to the SAOZ data from the ISSJ, leading to the conclusion that interferences between ozone and O_4 can dramatically alter the retrieval of ozone total amounts in these windows, and that the 510-550 nm fitting window might be inadequate for GOME processing.

8. REFERENCES

De Backer, H., and D. De Muer, *Intercomparison of Total Ozone Data Measured with Dobson and Brewer Ozone Spectrophotometers at Uccle (Belgium) from January 1984 to March 1991, Including Zenith-sky Observations*, J. Geophys. Res., 96, 20711-20719, 1991

Komhyr, W.D., C.L. Mateer, and R.D. Hudson, *Effective Bass-Paur 1985 Ozone Absorption Coefficients for Use with Dobson Ozone Spectrophotometers*, J. Geophys. Res., 98, 20451-20465, 1993

Lambert, J.-C., M. Van Roozendael, P.C. Simon, M. De Mazière, F. Goutail, A. Sarkissian, J.-P. Pommereau, L. Denis, V. Dorhokov, P. Eriksen, E. Kyro, J. Leveau, H.K. Roscoe, G. Vaughan and C. Wahlstrom, *Validation of the ERS-2 GOME Products with the SAOZ Network*, Proceedings of the GOME Validation Campaign Final Results Workshop, Frascati, Italia, 24-26 January 1996, this volume

Pommereau, J.-P., and F. Goutail, *Ground-based Measurements by Visible Spectrometry during Arctic Winter and Spring 1988,* Geophys. Res. Lett., 15, 891, 1988

Sarkissian, A., H.K. Roscoe, D.J. Fish, M. Van Roozendael, M. Gil, H.B. Chen, P. Wang, J.-P. Pommereau and J. Lenoble, *Ozone and NO2 air-mass factors for zenith-sky spectrometers: Intercomparison of calculations with different radiative transfer models*, Geophys. Res. Lett., 22, 1113-1116, 1995

Van Roozendael, M., M. De Mazière and P.C. Simon, *Ground-based Visible Measurements at the Jungfraujoch Station since 1990*, J. Quant. Spectrosc. Radiat. Transfer, 52, 231-240, 1994

Van Roozendael, M., P. Peeters, P.C. Simon, H.K. Roscoe and A. Jones, L. Bartlett and G. Vaughan, F. Goutail, J.-P. Pommereau, E. Kyro, C. Wahlstrom, G. Braathen, *Absolute Calibration of SAOZ Measurements of by Comparison with Dobson and Brewer Instruments*, Proceedings of the Third Annual Symposium on Polar Stratospheric Ozone, Schliersee, Bavaria, 18-22 September 1995, in press

Vaughan, G., H.K. Roscoe, L.M. Bartlett, F. O'Connor, A. Sarkissian, M. Van Roozendael, J.-C. Lambert, P.C. Simon, K. Karlsen, B.A. Kaestad Hoiskar, D.J. Fish, R.L. Jones, R. Freshwater, J.-P. Pommereau, F. Goutail, S.B. Andersen, D.G. Drew, P.A. Hughes, D. Moore, J. Mellqvist, E. Hegels, T. Klupfel, F. Erle, K. Pfeilsticker, U. Platt, *An intercomparison of ground-based UV-Visible sensors of ozone and NO_2*, J. Geophys. Res., 1996, in press

9. ACKNOWLEDGEMENTS

The authors address all their acknowledgements to the different co-investigators of the B103 Proposal for providing high quality data in real time.

This work has been supported by the PRODEX-GOME A.O. ERS-2 Project 1, by the Belgian State-Prime Minister's Service - Science Policy Office (contract GC/35/002), and by the EC contracts EV5V-CT93-0334 and EV5V-CT93-0348.

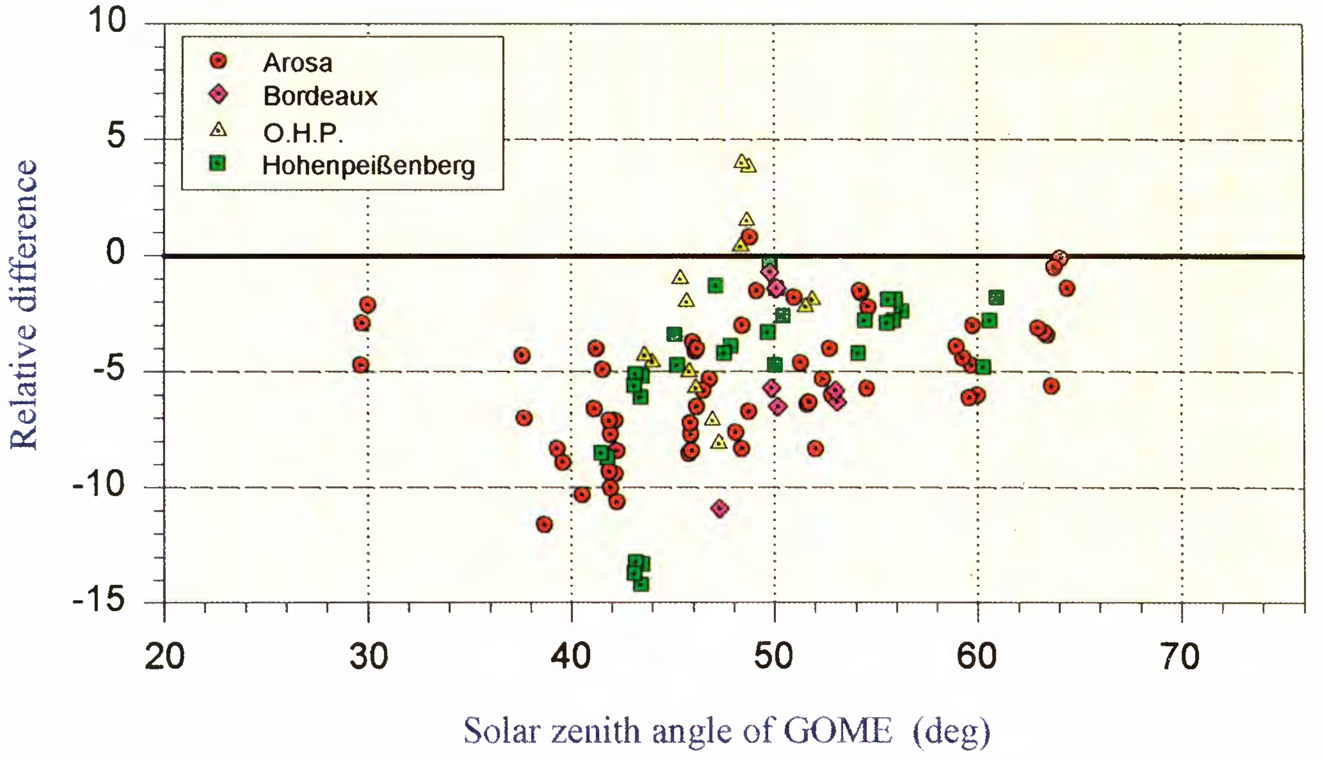

Figure 5-4 Relative difference (in per cent) between GOME and Dobson total ozone, as a function of the GOME solar zenith angle

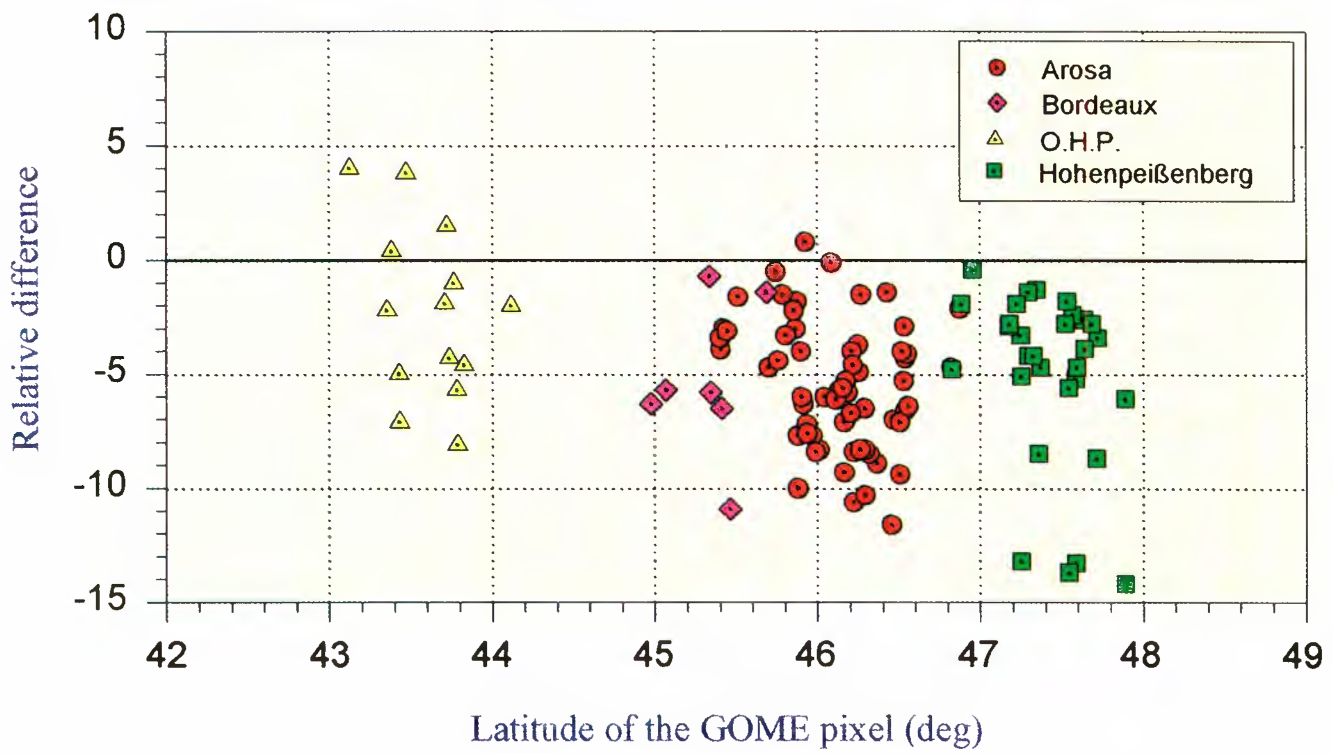

Figure 5-5 Relative difference (in per cent) between GOME and Dobson total ozone, as a function of the latitude of the centre of the GOME pixel

GOME PRODUCTS VALIDATION WITH THE SAOZ NETWORK

J.-C. Lambert[1], M. Van Roozendael[1], P.C. Simon[1], M. De Mazière[1], J.-P. Pommereau[2], F. Goutail[2], A. Sarkissian[2], L. Denis[2], V. Dorokhov[3], P. Eriksen[4], E. Kyro[5], J. Leveau[6], H.K. Roscoe[7], G. Vaughan[8] and C. Wahlstrom[9]

1. Belgian Institute for Space Aeronomy, BIRA-IASB, Brussels, Belgium
2. Service d'Aéronomie du CNRS, Verrières-le-Buisson, France
3. Central Aerological Institute, Dolgoprudny, Russia
4. Danish Meteorological Institute, Copenhagen, Denmark
5. Finnish Meteorological Institute, Sodankyla, Finland
6. Faculté des Sciences, Université de la Réunion, France
7. British Antarctic Survey, Cambridge, UK
8. University College of Wales, Aberystwyth, UK
9. Norwegian Institute for Air Research, Kjeller, Norway

Abstract
The first 45 days of GOME total ozone and nitrogen dioxide measurements have been compared to those provided by the SAOZ ground-based network over a wide range of latitudes from the Arctic to the Antarctic. It is concluded that total ozone provided by the current GOME retrieval algorithm is already accurate within ±5% for all seasons at the tropics, from spring to fall at northern mid-latitudes and during summer up to 60°N. During other seasons and up to 75° SZA, the difference with the ground-based instruments does not exceed 12%. Below 75° SZA, the comparison demonstrates a SZA dependence of the GOME measurements as well as a relatively lower sensitivity. At high latitude in summer, GOME seems to overestimate the ozone column by 10-20%, as well as in the ozone hole in Antarctica at spring. At high latitude and SZA larger than 75° where multiple scattering and the sphericity of the Earth are not taken into account in the GOME retrieval, the ozone data are not yet reliable. Finally, compared to those of the SAOZs, the preliminary NO_2 measurements show an extremely large spread which indicates that the current retrieval of this species needs improvement.

1. INTRODUCTION

The SAOZ (Système d'Analyse par Observation Zénithale) is a UV-visible spectrometer which measures total ozone and nitrogen dioxide twice daily at twilight by looking at the sunlight scattered by the atmosphere at the zenith. Since identical instruments are deployed world-wide, it was proposed to use the data of this network to investigate the performances of GOME over a wide range of latitudes from the Arctic to the Antarctic. A first comparison with GOME ozone measurements in the Huggins bands was conducted at northern mid-latitude using a variety of instruments including a SAOZ spectrometer, part of the NDSC/Alpine station (Lambert et al., same issue). This first exercise concluded to a small underestimation of total ozone by GOME of 2 to 8% and to a significant Solar Zenith Angle (SZA) dependence when compared to SAOZ. Here, the comparison is extended to all latitudes using the methodology already described by Lambert et al., which will not be repeated. The only difference, unless specified, is the use of preliminary SAOZ results transmitted in real time from the remote stations. However, changes between preliminary and final SAOZ data are generally small, and therefore are not expected to modify significantly the conclusions drawn from the present analysis. The largest limitation of the comparison to date consists in the limited time period of the validation: 45 days, from July to December 1995. It is anticipated that more precision will be gained in the future when longer time series of data will be available.

2. THE SAOZ NETWORK

The SAOZ instrument is a grating spectrometer which looks at the sunlight scattered at zenith (Pommereau and Goutail, 1988). The UV-visible part of the zenith-sky spectrum is recorded during twilight periods for SZA ranging from 86° up to 91°. Column densities along the line of sight, or slant columns, are retrieved by the Differential Optical Absorption Spectroscopy method (DOAS) applied in the visible Chappuis bands (450-580 nm) for ozone and in the 406-526 nm window for nitrogen dioxide. Slant columns are converted into vertical columns by using a standard Air Mass Factor (AMF), calculated with a radiative transfer model which has been validated by comparison (a) with other calculations following a variety of numerical schemes (Sarkissian et al., 1995) and (b) with integrated balloon profiles (Sarkissian et al., 1996).
A number of SAOZ are currently operating. There are listed in Table 1. The SAOZ of Oslo is the one of Ny-Ålesund which was operated at Oslo for a limited period in August 1995. In addition, a DOAS UV-visible zenith-sky spectrometer of BIRA-IASB design, described in Van Roozendael et al. (1995[a]), is operated at Harestua (60°N, Norway). Since the GOME products were not available in the Pacific sector, the data of Dumont d'Urville and Tarawa were not used in the present analysis. The station of Kerguelen started in December 1995 only.

3. SAOZ ACCURACY

In the visible range, between 400 and 630 nm, slant total amounts of O_3, NO_2, $(O_2)_2$, O_2 and H_2O are retrieved by a least squares iterative procedure using high resolution absorption cross-sections published in the literature and convolved with the SAOZ slit function. The precision of the measurements is given by

Location	Lat	Long	Institute
Ny-Ålesund	79N	12E	NILU
Thule	77N	69W	DMI
Scoresbysund	70N	22W	CNRS/DMI
Zhigansk	67N	123E	CNRS/CAO
Sodankylä	67N	27E	CNRS/FMI
Harestua (UV-vis)	60N	9E	BIRA-IASB
Oslo	60N	11E	NILU
Aberystwyth	52N	4W	U. of Wales
Jungfraujoch	47N	8E	BIRA-IASB
O. Haute Provence	44N	6E	CNRS
Tarawa	01N	172E	CNRS/NIWA
Reunion	21S	55E	U. Reunion
Bauru	22S	48W	CNRS/UNESP
Kerguelen	49S	70W	CNRS
Faraday	65S	66W	BAS
Dumont d'Urville	67S	142E	CNRS

Table 1 The SAOZ network.

the one sigma confidence level of the least squares fit calculated for each spectrum. On average at twilight, the precision is better than 0.5% for ozone and 1.5% for NO_2. The high resolution ozone absorption cross-sections used are those of Brion et al. (1993), scaled by -1.9% to those of Anderson and Mauersberger (1992), the most accurate data published so far (0.5% accuracy) but available at discrete wavelengths only. As shown by Brion et al., the temperature dependence of the ozone cross-sections in the visible is not significant (<1%). The overall accuracy of the SAOZ ozone slant total amounts is better than 2%. For NO_2, the uncertainty of the absorption cross-sections (Merienne et al., 1994) is of the order of 5%, but a rather large temperature dependence was shown by Harwood and Jones (1994) and Coquart et al. (1995), and is not taken into account in the present analysis. If corrected for this temperature dependence, the NO_2 stratospheric columns would have to be reduced by about 15%.
The conversion of the slant column into a vertical or total column requires the use of an AMF dependent on the vertical distributions of the atmospheric constituents controlling the penetration of the solar radiation in the atmosphere. According to Sarkissian et al. (1996), the use of an average standard AMF at mid-latitude instead of an AMF calculated from daily ozone soundings, introduces a deviation smaller than 3%. In addition, as shown by Van Roozendael et al. (1995[b]), Hoiskar et al. (1995) and Denis et al. (1995), the seasonal cycles of density and ozone profiles would introduce a systematic seasonal AMF variation of 5-6% amplitude at 67°N, 3-4% at 44°N and negligible at the tropics. Compared to the standard SAOZ AMF, it also introduces an average latitudinal dependence of -3% at 67°N to +2.8% at the tropics (Denis et al., 1995). Since a standard AMF is used for the real time preliminary analysis, the above systematic errors need to be kept in mind in the discussion.
Finally, the ozone and NO_2 data do show some dispersion because of the multiple scattering in the lower tropospheric layer in presence of dense clouds or haze combined with the local pollution (Van Roozendael et al., 1994). This contribution varies from one station to another depending on their location with respect to sources of pollution. Long time series of comparisons with Dobson and Brewer measurements show that this contribution does not exceed 1% on average for ozone. For NO_2, it is negligible at a remote location, but can introduce large spikes in the data in populated regions like Europe, which must be removed by adequate criteria.
The SAOZ instruments have been intercompared at several occasions in the field to other DOAS UV-visible spectrometers, SAOZ, Dobson, Brewer and ozone soundings: during the NDSC UV-visible intercomparison held in New Zealand in 1992 for NO_2 (Hofmann et al., 1995), at Camborne (UK) in September 1994 in the frame of the SESAME campaign for ozone (Vaughan et al., 1996), and within the NOAA/WMO Dobson Intercalibration Campaign held at Arosa (Switzerland) in July-August 1995. At Camborne, four SAOZ and the UV-visible spectrometer of BIRA-IASB were intercompared, and their results were consistent within 3% (10 DU) for ozone and 5% for NO_2 and consistent also with Dobson measurements and ozone soundings within 3% (Vaughan et al., 1996). Long time series of SAOZ total ozone measurements were also compared with those of the TOMS-Nimbus 7 and TOMS-Meteor 3, showing a scatter of ±2.5%, but with a systematic seasonal dependence at high latitude attributed partly to the inversion of the TOMS nadir measurements at large SZA and partly to changes in the shape of the ozone profiles compared to the climatology used in the TOMS inversion procedure (Pommereau et al., 1995).

4. SELECTION OF CO-LOCATED EVENTS

Since the ozone field may display large horizontal gradients and high day-to-day variability in total amounts, particularly at high latitudes, the real locations of the measurements of both the nadir viewing GOME and the zenith viewing ground-based spectrometers must be taken into account.
The viewing geometry and the light path were modelled for the zenith-sky observations. The effective geolocation of the stratospheric part of the air mass sampled by a ground-based zenith-sky instrument at twilight, is located in the direction of the Sun between 100 and 350 km from the instrument at 87° SZA and between 150 and 550 km at 91° SZA. Its azimuth varies from sunrise to sunset as well as with the season. Therefore, the GOME pixel is selected at the geolocation calculated by the model. The effective geolocation of the GOME measurements, which can move up to 30 km from the ground pixel in summer and up to 100 km in winter, is not taken into account in this first validation exercise, because of the 30 km discrepancy between the location of the pixel in the GOME data files and that provided by the ESA orbit propagator.

5. TOTAL OZONE COMPARISONS

The 45 days of relative differences between GOME and SAOZ total ozone at all stations are depicted in Figure 1-a versus the latitude of the centre of the selected GOME pixel and in Figure 1-b versus the SZA of the GOME measurement. At SZA<75°, the comparison is reasonably good, although there is on average a significant SZA dependence of the relative differences. The GOME total ozone is larger than that of SAOZ by 5% at high Sun and for low ozone in the tropics and becomes smaller at high latitude, -12% at 60°N and 70° SZA. At SZA>75° where the GOME retrieval does not take into account the multiple scattering and the Earth's sphericity, the GOME total ozone is on average larger by 15% and the deviation from SAOZ becomes rapidly negative after 90° SZA.

The plot versus latitude in Figure 1-a shows that the scatter increases on average from ±5% at the tropics and mid-latitudes, to ±20% at high latitude and for SZA larger than 75°. Although total ozone varies rapidly there, the increasing scatter largely exceeds that observed with TOMS (Pommereau et al., 1995).

The correlation between the GOME and SAOZ total ozone for a variety of stations distributed from the tropics up to 60°N, is shown in Figure 2. There is a large spread due to the SZA dependence already identified. For removing partly this contribution from the correlation, the data have been sorted into four SZA classes. The regression coefficients for each class of SZA (GOME = a + b x SAOZ (DU)) are shown in table 2. The similar slopes for the four classes (between 0.6 and 0.77) indicate some systematic lower sensitivity of GOME compared to SAOZ, for ozone total amounts ranging from 250 up to 340 DU.

The spread of the data combining all the stations shown in Figure 1 is thus the result of several factors: a SZA dependence and a smaller relative sensitivity of GOME, the temporal variability of the ozone field, and a latitudinal/seasonal dependence of the SAOZ AMF.

Table 2 Regression coefficients between the GOME and SAOZ total ozone measurements sorted into four classes of SZA and for seven sites distributed from the tropics up to 60°N.

SZA	(a)	(b)	r^2
< 45°	81	0.71	0.55
45° < SZA < 55°	103	0.6	0.5
55° < SZA < 65°	75	0.66	0.63
65° < SZA < 75°	33	0.77	0.6

5.1 Northern Mid-latitudes

This latitude belt has already been investigated by Lambert et al. (same issue). The results obtained with SAOZ, Dobson and Brewer observations at the NDSC/Alpine sites show a good agreement. After taking properly into account the 3-4% seasonal cycle of the SAOZ AMF and the altitude of the station of the Jungfraujoch (47°N), it is concluded that on average GOME underestimates total ozone by about 3%. In addition the comparison demonstrates a smaller relative sensitivity of GOME compared to the ground-based measurements and probably also a SZA dependence, but less evident because of the relatively limited range of SZA. The results obtained with the SAOZ data at Aberystwyth (52°N) and at the Observatoire de Haute Provence (44°N) confirm these results.

5.2 Summer Northern Latitudes

At Harestua (60°N), where the final data of the BIRA-IASB UV-visible spectrometer were corrected for the 5-6% AMF seasonal dependence, the comparison with GOME does show a SZA dependence of 6% between 50 and 75° SZA, as shown in Figure 3.

Further north at the polar circle, the preliminary data of Sodankylä and Scoresbysund show a systematic offset compared to Harestua, partly due to the underestimation of large ozone columns by GOME, partly to the use of standard AMF and perhaps also partly to the residual ozone amount in the reference spectrum used in the SAOZ real time processing. However, these plots confirm the SZA dependence of GOME. At the very high latitude stations of Thule (77°N) and Ny-Ålesund (79°N), the GOME total ozone is larger than that measured by the SAOZ by 10 to 20% and the reason for this has not yet been identified. It exceeds by far the 5-6% anticipated from the use of a standard AMF not corrected for the season. It can be noticed that the spread increases also at high latitude, which can be attributed partly to the large differences in time between the SAOZ measurements around midnight in summer and that of the GOME about local noon.

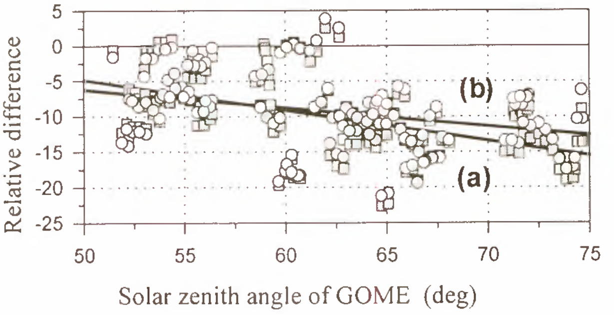

Figure 3 Relative differences between the GOME and UV-vis total ozone ([GOME - UV-vis] / UV-vis, in per cent) at Harestua (60°N) as a function of the GOME SZA. Dark squares and the regression line (a) stand for the UV-vis total ozone retrieved with the SAOZ standard AMF while open circles and the regression line (b) are obtained with an AMF calculated by means of ozone soundings.

5.3 Antarctic: Ozone Hole Conditions

The SAOZ #06 operated by the British Antarctic Survey is located at Faraday (65°S) in the Antarctic Peninsula. In August-October 1995, the station was often inside the polar vortex and ozone total columns as low as 130 DU were observed, in addition to the large day-to-day variations in total ozone occuring usually during this season at the stations located near the edge of the vortex. According to Figure 4, the relative difference between GOME and SAOZ within a limited range of SZA (69°-75°) is correlated with the ozone total amount, which is overestimated by GOME at very low values and the opposite when ozone increases rapidly outside the vortex. These findings are confirmed by the measurements of the co-located Dobson spectrophotometer.

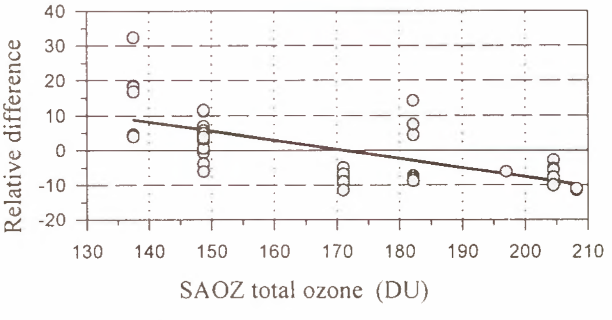

Figure 4 Relative differences between the GOME and SAOZ total ozone ([GOME - SAOZ] / SAOZ, in per cent) at Faraday (65°S) as a function of the ozone total amount.

5.4 Southern Tropics

In the tropics, the number of available co-located events is relatively scarce due to the large spacing between the consecutive satellite swaths. At Reunion Island, the SAOZ preliminary data show a spurious systematic difference between morning and evening. Since this disappeared later after resetting the instrument, it might be due to a drift of the clock which will be easily corrected in the final data.

For the moment, if a daily average is used (which is insensitive to clock drift), GOME and SAOZ measurements agree within a few per cent. This is confirmed by the new station of Bauru in Brazil installed on 24 November 1995, where the GOME data obtained on 11, 12 and 13 December at 6° SZA, are consistent with those of the SAOZ within ±3%.

5.5 Overall GOME - SAOZ Consistency

From the average differences between the two instruments (less than 5 per cent at 45° SZA and 10 per cent at 60° SZA), a first estimate of the period during which GOME results will be better than a given uncertainty can be derived for each latitude belt (Figure 5). It can be concluded that the current GOME retrieval algorithm already provides ozone columns within an accuracy of 5% at all seasons at the tropics, from April to October at mid-latitudes and from May to September at 60°N. At other seasons and up to 75° SZA, the difference with the ground-based instruments does not exceed 12% except at high latitude in the Arctic or in the ozone hole in Antarctica, where GOME overestimates the ozone column. At SZA > 75°, further algorithm developments, currently in progress, are needed to increase the accuracy of the winter measurements.

6. NITROGEN DIOXIDE

Although the first objective of the validation of the GOME products during the commissioning phase was limited to the ozone total amounts, it was thought useful to have a first look at the preliminary NO_2 data. However, since NO_2 exhibits a diurnal increase between sunrise and sunset and the GOME measurements are performed around local noon, the comparison with dawn and dusk SAOZ data is not straightforward. The first option would be to interpolate linearly the morning and evening SAOZ measurements at the local time of the ERS-2 overpass. Since the diurnal change of NO_2 is not linear but fast in the morning and slower in the afternoon after the complete photolysis of N_2O_5, an alternative approach would be to validate GOME with the evening SAOZ data. If needed, a small correction might be added in the future based on a photochemical model simulation.

The preliminary GOME and the SAOZ NO_2 total columns are compared in Figure 6. The quantification of the discrepancies between both sets of measurements is currently irrelevant. Although some SZA dependence seems to show off, the extremely large scatter between the current GOME and the SAOZ NO_2 data does not allow to conclude, whatever the comparison method. Since long time series of ground-based measurements at remote locations far away from pollution sources, do not show such large dispersion, improvements in the preliminary GOME NO_2 retrieval, currently in progress, are expected to increase significantly the agreement between the satellite and the ground-based data.

7. REFERENCES

Anderson, S. M. and K. Mauersberger, Laser Measurements of Ozone Absorption Cross-sections in the Chappuis Bands, *Geophys. Res. Lett.*, 19, 933-936, 1992.

Brion, J., A. Chakir, D. Daumont, J. Malicet and C. Parisse, High Resolution Laboratory Cross-sections of O_3, Temperature Effect, *Chem. Phys. Lett.*, 6, 612, 1993.

Coquart, B., A. Jenouvrier and M. F. Merienne, The NO_2 Absorption Spectrum II. Absorption Cross Sections at Low Temperature in the 400-500 nm Region, *J. Atm. Chem.*, 21, 251, 1995.

Denis, L., J. P. Pommereau, F. Goutail, T. Portafaix, A. Sarkissian, M. Bessafi, S. Baldy, J. Leveau, P.V. Johnston and A. Matthews, SAOZ Total O_3 and NO_2 at the Southern Tropics and Equator, *Proc. 3rd Europ. Symp. on Polar Ozone*, in press, 1995.

Harwood, M. H., and R. L. Jones, Temperature Dependent Ultraviolet Cross-sections of NO_2 and N_2O_4: Low Temperature Measurements of the Equilibrium Constant $2NO_2$ <--> N_2O_4, *J. Geophys. Res.*, 9, 922, 1994.

Hofmann, D., J., P. Bonasoni, M. De Mazière, F. Evangelisti, A. Sarkissian, G. Giovanelli, A. Goldman, F. Goutail, J. Harder, R. Jakoubek, P. Johnston, J. Kerr, T. McElroy, R. McKenzie, G. Mount, J. P. Pommereau, P. Simon, S. Solomon, J. Stutz, A. Thomas, M. Van Roozendael, E. Wu, Intercomparison of UV/Visible Spectrometers for Measurements of Stratospheric NO_2 for the Network for the Detection of Stratospheric Change, *J. Geophys. Res.*, 16, 765-16,791, 1995.

Hoiskar, B.A.K., A. Dahlbak, G. Vaughan, G.O. Braathen, F. Goutail, J.P. Pommereau and R. Kivi, Seasonal Variations in Air Mass Factors for Ozone Computations Based on Climatology Data, *Geophys., Res. Lett.*, submitted, 1995.

Lambert, J.-C., M. Van Roozendael, P. Peeters, P.C. Simon, M.-F. Merienne, A. Barbe, H. Claude, J. de La Noë and J. Staehelin, GOME Ozone Total Amounts Validation by Ground-based Observations Performed at the NDSC/Alpine Stations, *Proceedings of the GOME Geophysical Validation Final Results Workshop, 24-26 January 1996, Frascati, Italy*, this issue.

Merienne, M.F., A. Jenouvrier and B. Coquart, The NO_2 Absorption Spectrum I: Absorption Cross-sections at Ambient Temperature in the 300-500 nm Region, *J. Atm. Chem.*, 20, 281, 1994.

Pommereau, J.-P., and F. Goutail, Ground-based Measurements by Visible Spectrometry during Arctic Winter and Spring 1988, *Geophys. Res. Let.*, 891, 1988.

Pommereau, J.-P., F. Goutail, H. Le Texier and T.S. Jorgensen, Stratospheric Ozone and Nitrogen Dioxide Monitoring at Southern and Northern Polar Latitudes, *Proc. 28th Liège International Astrophysical Colloquium "Our Changing Atmosphere"*, 141, 1989.

Pommereau, J. P., F. Goutail and A. Sarkissian, SAOZ Total Ozone Measurements in Antarctica. Comparisons with TOMS Versions 6 and 7, *Proc. 3rd Europ. Symp. on Polar Ozone,* EC Ed., in press, 1995.

Sarkissian, A., H.K. Roscoe, D.J. Fish, M. Van Roozendael, M. Gil, H.B. Chen, P. Wang, J.-P. Pommereau and J. Lenoble, Ozone and NO_2 air-mass factors for zenith-sky spectrometers: Intercomparison of Calculations with Different Radiative Transfer Models, *Geophys. Res. Lett.*, 22, 1113-1116, 1995.

Sarkissian, A., G. Vaughan, H.K. Roscoe, L.M. Bartlet, F.M. O'Connor, D.G. Drew, P.A. Hughes and D.M. Moore, Accuracy of Measurements of Total Ozone by a SAOZ Ground-based Zenith Sky Spectrometer, *J. Geophys. Res.*, in press, 1996.

INTRODUCTORY PAPERS

Van Roozendael, M., M. De Mazière and P.C. Simon, Ground-based Visible Measurements at the Jungfraujoch Station since 1990, *J. Quant. Spectrosc. Radiat. Transfer*, 52, 231-240, 1994.

Van Roozendael, M., C. Hermans, Y. Kabbadj, J.-C. Lambert, A.-C. Vandaele, P.C. Simon, M. Carleer, J.-M. Guilmot, R. Colin, Ground-Based Measurements of Stratospheric OClO, NO_2 and O_3 at Harestua, Norway (60°N, 10°E) during SESAME, *Proceedings of the 12th ESA Symposium on European Rocket and Balloon Programmes & Related Research, Lillehamer, Norway, 29 May - 1 June 1995*, ESA SP-370, 305-310, 1995[a].

Van Roozendael, M., P. Peeters, P.C. Simon, H.K. Roscoe and A. Jones, L. Bartlett and G. Vaughan, F. Goutail, J.-P. Pommereau, E. Kyro, C. Wahlstrom, G. Braathen, Absolute Calibration of SAOZ Measurements by Comparison with Dobson and Brewer Instruments, *Proc. 3rd Europ. Symp. on Polar Stratospheric Ozone*, EC Ed., in press, 1995[b].

Vaughan, G., H.K. Roscoe, L.M. Bartlett, F. O'Connor, A. Sarkissian, M. Van Roozendael, J.-C. Lambert, P.C. Simon, K. Karlsen, B.A. Kaestad Hoiskar, D.J. Fish, R.L. Jones, R. Freshwater, J.-P. Pommereau, F. Goutail, S.B. Andersen, D.G. Drew, P.A. Hughes, D. Moore, J. Mellqvist, E. Hegels, T. Klupfel, F. Erle, K. Pfeilsticker, U. Platt, An intercomparison of ground-based UV-Visible sensors of ozone and NO_2, *J. Geophys. Res.*, in press, 1996.

8. ACKNOWLEDGEMENTS

The authors would like to thank the staff of the SAOZ stations and J. Hottier for collecting daily the data and making them available. This work was supported by the PRODEX A.O. ERS-2 Project 1 and the OSTC contract GC/35/002 in Belgium, the Programme National de Chimie de l'Atmosphère in France, and the Environmental Programme of the European Commission in the frame of SCUVS-II, contract EV5V-CT93 0334.

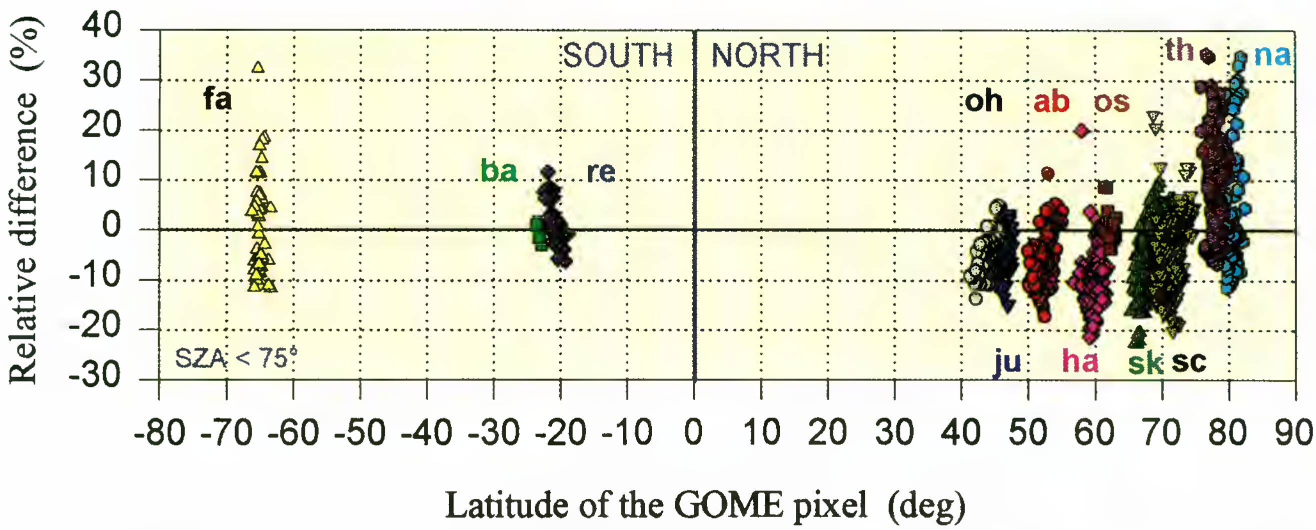

Figure 1-a Relative differences ([GOME-SAOZ]/SAOZ, in per cent) between the GOME and SAOZ total ozone, as a function of the latitude of the centre of the GOME pixel. Results are depicted only for SZA < 75°.

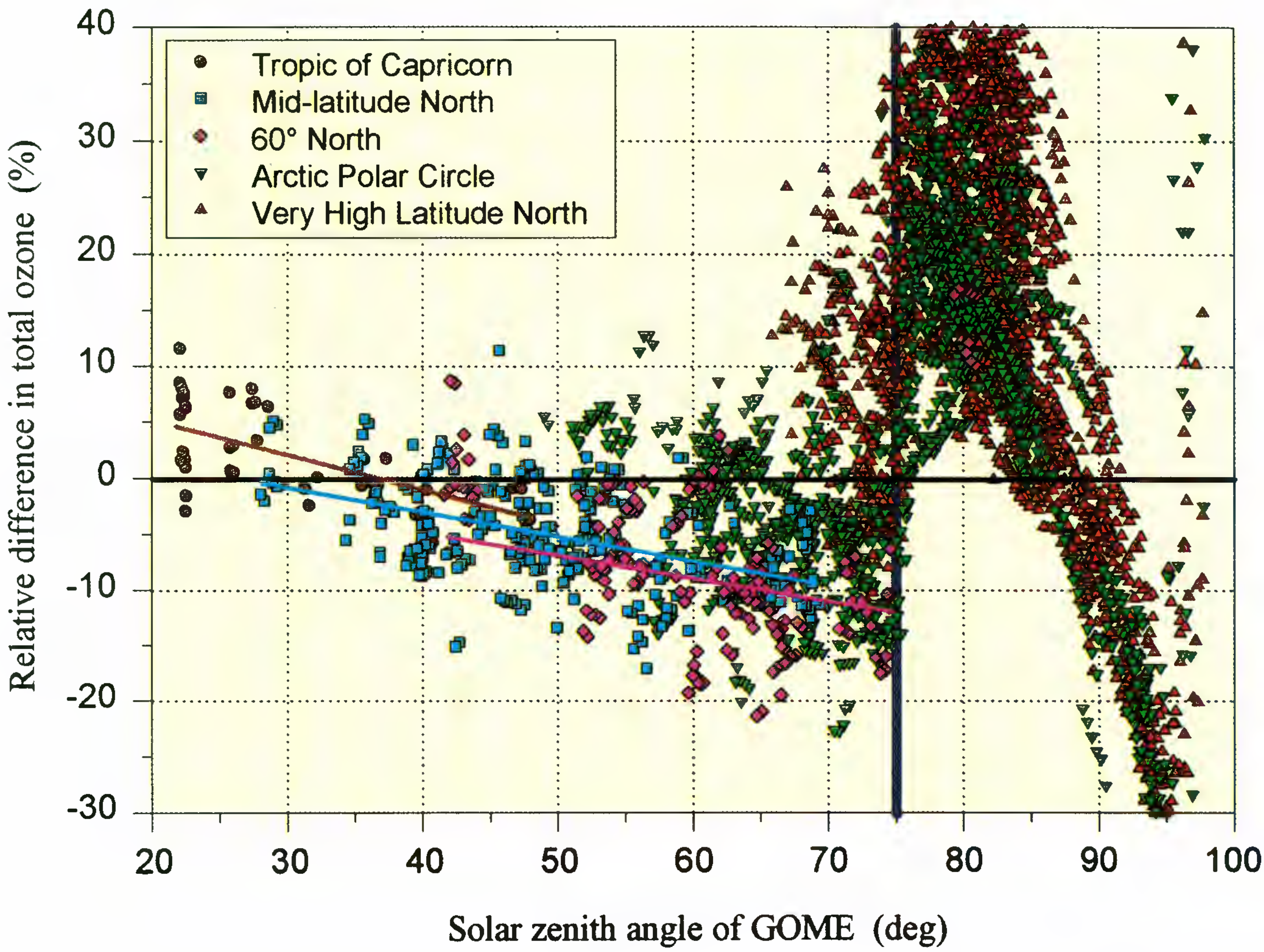

Figure 1-b Relative differences ([GOME-SAOZ]/SAOZ, in per cent) between the GOME and SAOZ total ozone, as a function of the GOME solar zenith angle. SAOZ sites are grouped into five latitude belts.

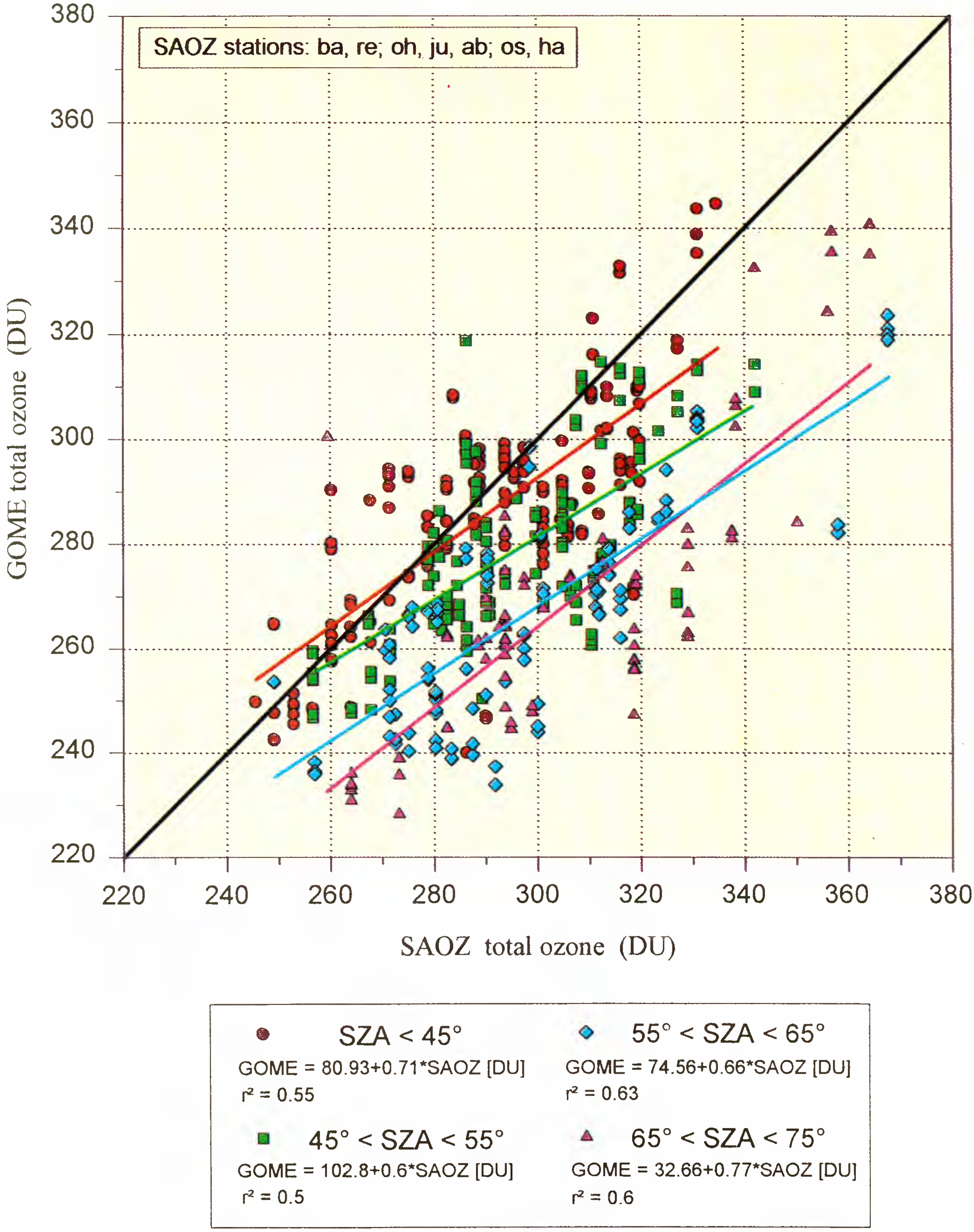

Figure 2 Regression plot between GOME and SAOZ total ozone (Dobson units) for southern tropical, northern mid-latitude and 60° north stations. Data are sorted into four ranges of GOME SZA.

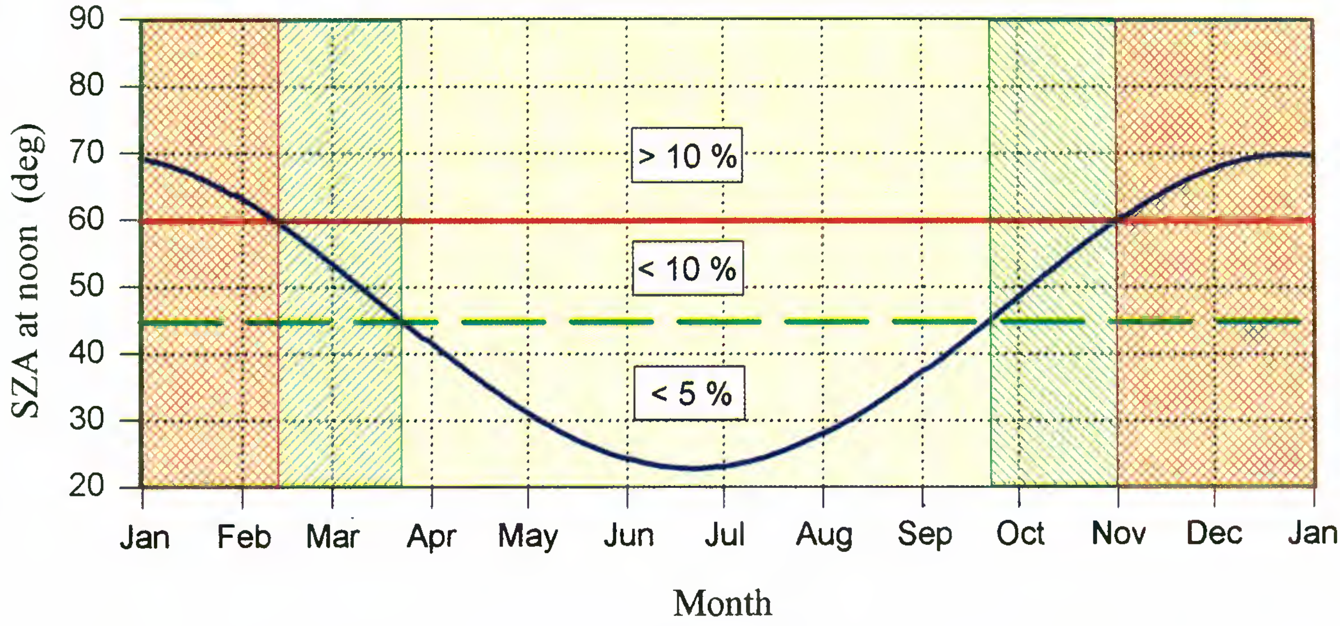

Figure 5-a Seasonal variation of the solar zenith angle at noon at 45° north. Dashed areas indicate the periods when the consistency between GOME and SAOZ total ozone is expected to be better than 5 % (SZA < 45°), 10 % (green area, SZA < 60°), or worse than 10 % (red area, SZA > 60°).

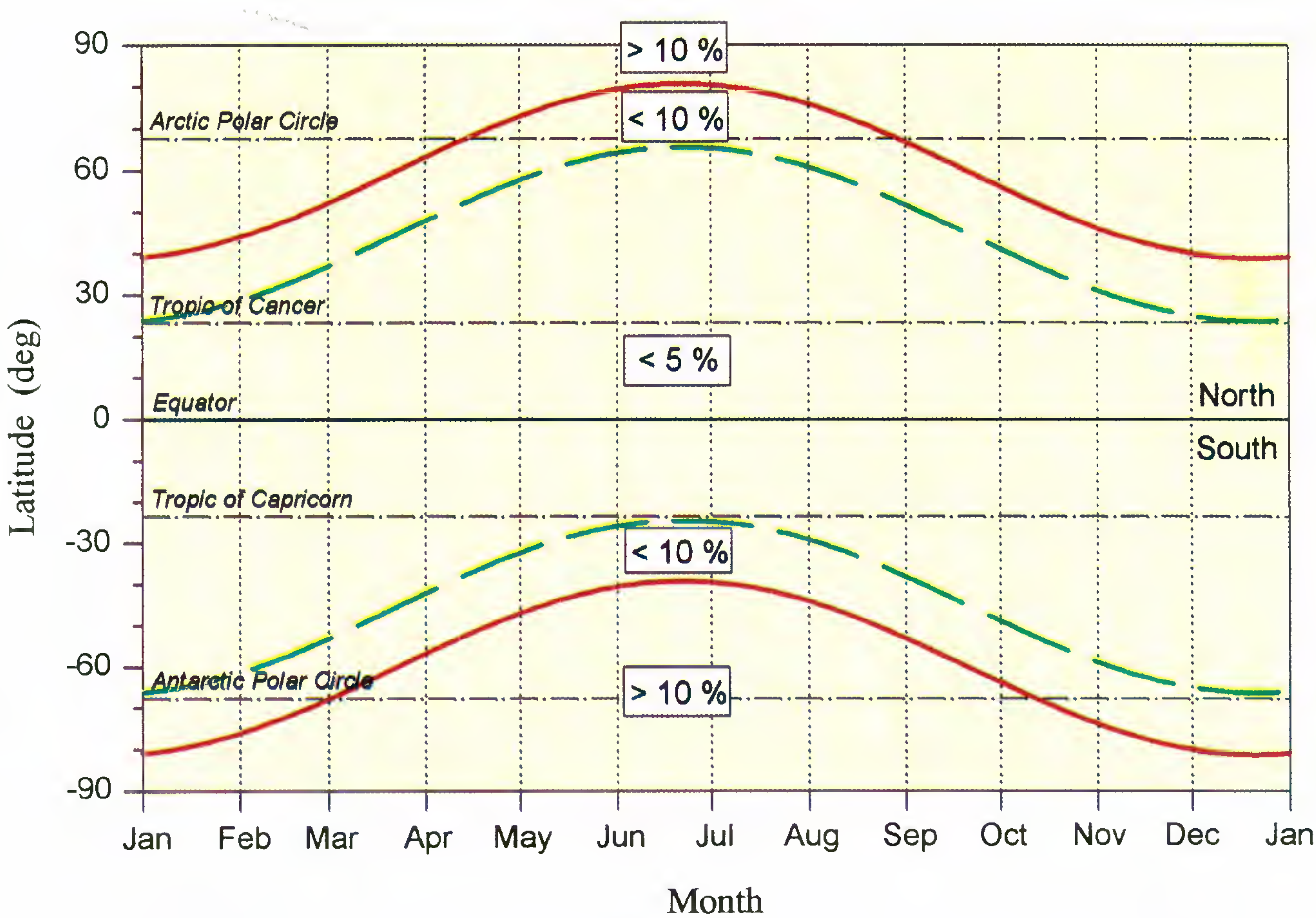

Figure 5-b Seasonal variation of the consistency between GOME and SAOZ total ozone, as a function of the latitude, assuming that the consistency is better than 5% at SZA < 45° and 10% at SZA < 60°.

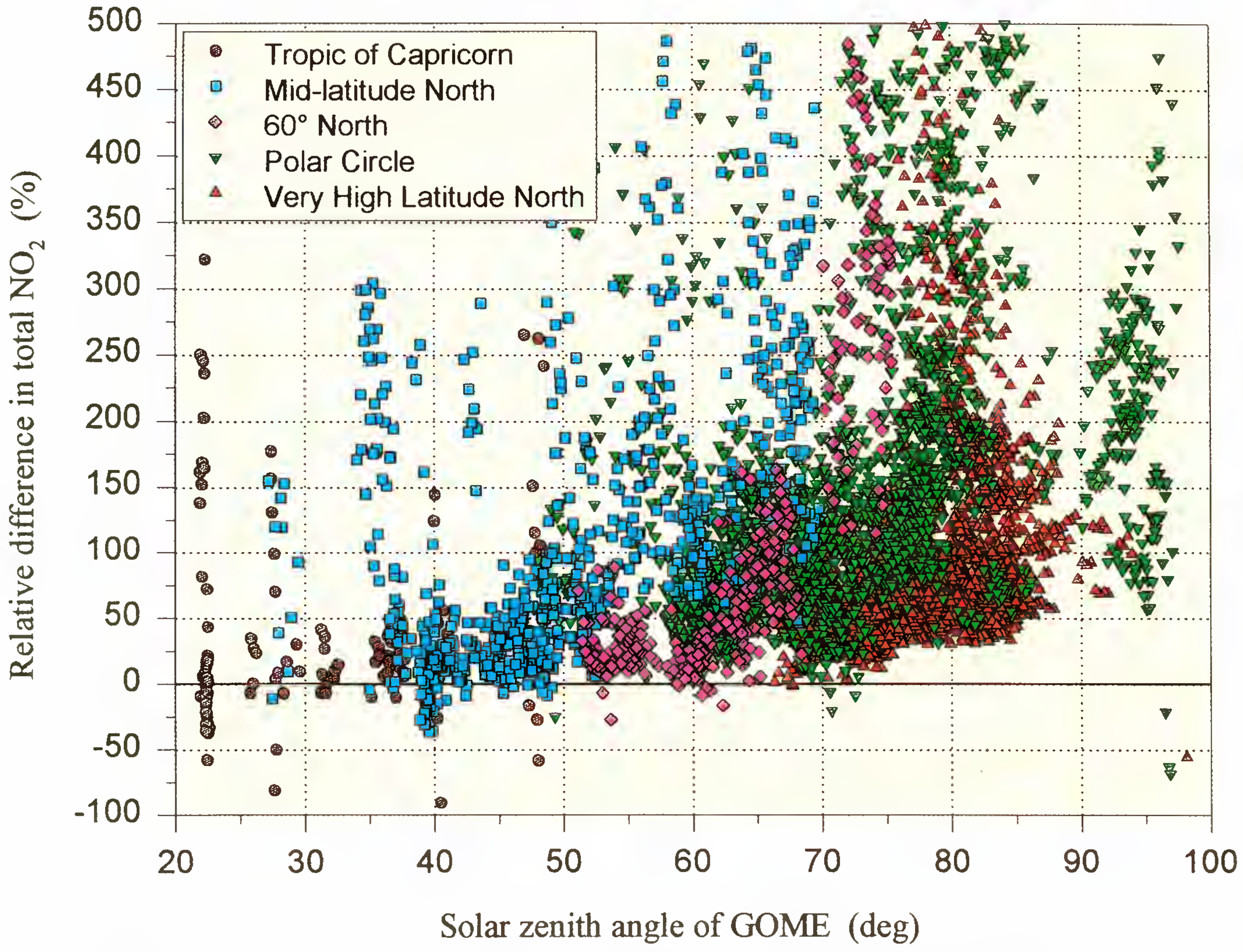

Figure 6-a Relative differences ([GOME-SAOZ]/SAOZ, in per cent) between GOME and SAOZ NO_2 total amounts, as a function of the GOME solar zenith angle. SAOZ sites are grouped into five latitude belts.

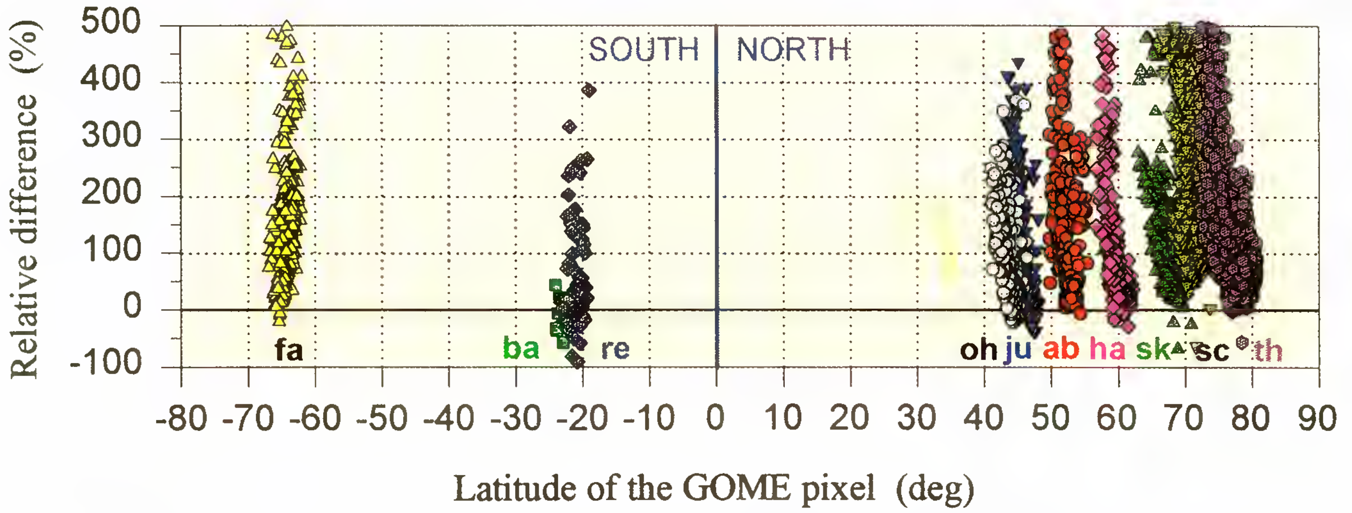

Figure 6-b Relative differences ([GOME-SAOZ]/SAOZ, in per cent) between GOME and SAOZ NO_2 total amounts, as a function of the latitude of the centre of the GOME pixel.

VALIDATION OF ERS-2 GOME OZONE DATA BY GROUND-BASED OBSERVATIONS AT UCCLE (BELGIUM)

E. Schoubs and D. De Muer

Royal Meteorological Institute of Belgium
Ringlaan 3, B-1180 Brussels, Belgium

Abstract

The Royal Meteorological Institute of Belgium participated in the GOME validation campaign making use of a Dobson and Brewer spectrophotometer as well as electrochemical Brewer-Mast ozone soundings. The institute has already a long experience in measuring total ozone amounts and ozone profiles.

The quality of the ground-based ozone column measurements at Uccle (50°48'N, 4°21'E) with a Dobson and Brewer spectrophotometer (independently calibrated) is adequate to be used as ground-truth measurements for GOME. Electrochemical ozone sondes give the opportunity for validation of the ozone vertical column densities below the cloud cover.

Within a time window of 3 hours and a horizontal distance of 500 km between the ERS-2 overpasses and Uccle, the vertical column density of ozone measured by GOME and ground-based data was compared.

The mean difference between GOME and the Brewer respectively Dobson ozone values amounts to -1.7±2.9% respectively -2.5±2.6%. There seemed to be no statistically significant dependence on the air mass factor of the ground-based data, the solar zenith angle at the GOME pixels and the kind of GOME pixel (west, nadir, east and backscan). A small dependence of the mean difference on the ground-based ozone amount was found.

As distinct from this a highly significant dependence of the mean difference on the cloud cover fraction (CCF) of the GOME pixels was found ranging from 0 (CCF=0) up to -6 to -9% (CCF=1). Comparison of the cloud top height used in the GOME algorithm and the one deduced from Meteosat images together with temperature and humidity profiles of correlative ozone soundings were made. It was found that the systematic overestimation of the GOME cloud top height resulted in an ozone vertical column density that was on average 2.6% too high with respect to the values deduced from ozone soundings.

1. INTRODUCTION

The Royal Meteorological Institute of Belgium (KMI/IRM) has a long tradition in ozone monitoring. The routine total ozone measurements at Uccle (50°48'N, 4°21'E) with Dobson spectrophotometer no. 40 started in 1971. In 1983 the Brewer spectrophotometer no. 16 was installed at the same station. Measurements of the vertical column density (VCD) of ozone are performed several times per day with both instruments.

In 1969 a program of regular ozone soundings with electrochemical (Brewer-Mast) ozone sondes was started. In general three soundings per week (on Monday, Wednesday and Friday) are made. This resulted in one of the longest and most complete time series of ozone profiles in the world. The ozone soundings at Uccle were already used in the past for the validation of satellite ozone data [*De Muer et al.*, 1990] or Lidar ozone data [*De Backer et al.*, 1994].

The calibration history and the error budget of all these routine ozone measurements is very well documented (see next section). The combination of high-quality ozone measurements with two spectrophotometers (which allows a continuous check for a drift of either of the two instruments) and ozone profiles performed at the same location offer a good opportunity for the validation of GOME ozone data.

The present validation study includes 45 days of ERS-2 overpasses within a horizontal distance of 500 km from Uccle during the period from 23 July to 13 December 1995. A comparison of direct sun column ozone amounts from Dobson and Brewer spectrophotometers, with GOME data has been performed in a time window of 3 hours. A study of the correlative data as a function of horizontal distance, time difference, air mass factor, solar zenith angle of the GOME pixel, column ozone amount and cloud fraction has also been made. In addition the GOME ozone vertical column density under the cloud top is compared with corresponding ozone amounts from our soundings.

2. QUALITY CONTROL OF THE GROUND-BASED OZONE DATA SET AT UCCLE

The calibration of the Dobson and Brewer spectrophotometer which are operated at Uccle were described in detail by *De Backer and De Muer* [1991] and *De Muer and De Backer* [1992]. From these two papers we mention the following conclusions which are of relevance for the present study:

- The so called "extraterrestrial constant" of the Brewer spectrophotometer was determined in such a way as to eliminate any mean diurnal variation and hence any dependence of the calculated ozone VCD's on the air mass factor (AMF) of ozone.
- The weighting function of the ozone absorption coefficients used in the algorithm for calculation of the ozone VCD from Brewer measurements, was adjusted in such a way as to yield the same mean ozone VCD as from the Dobson spectrophotometer over the year 1984; from 1985 on the calibration of the two instruments is kept completely independent.
- The mean differences of quasi-simultaneous observations of ozone VCD with both instruments show no dependence on the AMF.
- The mean differences between quasi-simultaneous zenith sky and direct sun measurements are virtually zero at both instruments; the overall standard deviation of the differences is 1.3% with the Brewer spectrophotometer and 1.5% with the Dobson instrument.

In September 1994 the Brewer spectrophotometer was compared with Brewer no. 17 (a travelling standard). The difference between the two instruments was virtually zero, which means that no noticeable drift occurred in our Brewer instrument since the initial comparison in 1984.. The Dobson spectrophotometer was recently compared with the world standard at the International Dobson Spectrophotometer Intercomparison organised by WMO/GAW at Arosa (Switzerland) in August 1995. A small difference (<1%) between the two instruments has been taken into account

Figure 1 gives an indication of the quality of our ground-based ozone data. Over the period 1984 through 1995 the mean value as well as the long-term trend of the differences between direct sun (DS) measurements with the Brewer and Dobson spectrophotometer, are virtually zero. The standard deviation of the individual differences shown in Figure 1 is 1.0%. This means that the accuracy of the DS measurements of the Brewer and Dobson instrument with respect to the standard instruments, expressed in terms of the 95% confidence limits, amounts to 2% at most.

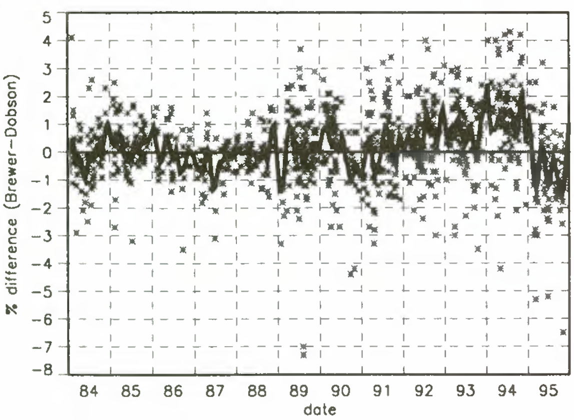

Fig. 1. Time series of percentage differences of individual VCD's of ozone calculated from DS measurements with Brewer no. 16 and Dobson no. 40 at a maximum time difference of 30 minutes, over the period 1984 through 1995. The full line is a running mean of the individual percentage differences, using a normally distributed weighting function with a 2σ value of 60 days.

From Figure 1 we also see that there is no systematic annual variation of the differences. Taking into account the above-mentioned calibration method of the Brewer instrument, we may conclude that both spectrophotometers show no noticeable dependence on the AMF. This also appears from the results as represented in Figure 2.

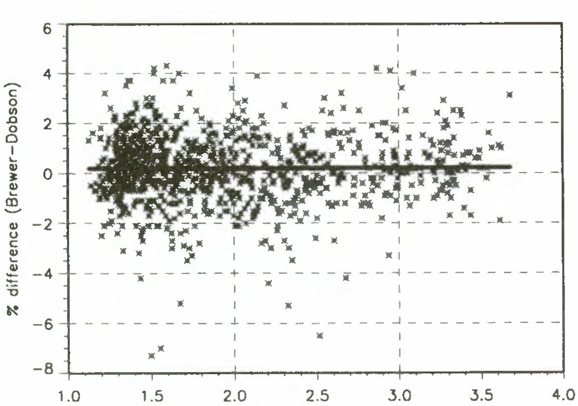

Fig. 2. Plot of the percentage differences shown in Figure 1, as a function of the AMF of the ozone layer. A linear least square regression line is fitted to the data.

A great deal of effort was put in an error analysis of the ozone sounding data, such as studies of interference of other minor constituents, influence of the response time of the ozone sensor, pump efficiency, pump temperature and altitude uncertainty (see e.g. *De Muer et al.* [1995]. Recently the ozone profiles obtained with our Brewer-Mast electrochemical ozone sondes have been compared with those measured at KNMI (Royal Meteorological Institute of the Netherlands, Debilt) (52°6'N, 5°11'E) with ECC sondes. A study of the effect of the pump-efficiency on the measured ozone profile has led to a better calibration of the ozone soundings [*De Backer et al.*, 1996].

TABLE 1. Overview of the Correlative Measurements

DATE	DOBSON		BREWER		DIST. (km)
	DS	ZS	DS	ZS	
July 23			x	x	316
July 24			x	x	79
July 25			x	x	9
Aug. 25				x	18
Aug. 26		x		x	96
Aug. 27		x		x	316
Aug. 29.		x		x	13
Aug. 30		x		x	216
Aug. 31	x	x	x	x	171
Sept. 1	x	x	x	x	99
Sept. 2		x		x	116
Sept. 3			x	x	265
Sept. 4	x	x	x	x	98
Sept. 5		x	x	x	436
Sept. 6		x	x	x	356
Sept. 7		x	x	x	8
Sept. 8		x		x	83
Sept. 9			x	x	447
Sept. 15		x		x	266
Sept. 16				x	124
Sept. 17		x		x	53
Sept. 20		x	x	x	147
Sept. 21		x	x	x	68
Sept. 22		x	x	x	310
Sept. 23		x	x	x	50
Sept. 27		x		x	133
Sept. 28		x	x	x	415
Oct. 1				x	315
Oct. 2		x	x	x	79
Oct. 3		x	x	x	7
Oct. 5		x	x	x	172
Oct. 6	x	x	x	x	99
Oct. 7		x	x	x	117
Oct. 11		x		x	357
Oct. 12		x		x	6
Oct. 13	x	x	x	x	85
Oct. 29	x	x	x	x	36
Oct. 30	x	x	x	x	403
Oct. 31		x		x	49
Nov. 9		x		x	171
Nov. 10		x		x	99
Nov. 11		x		x	116
Dec. 11		x			96
Dec. 12		x			6
Dec. 13		x			215

Dates of ERS-2 overpasses in 1995 are given. The symbol x indicates the availability of a direct sun (ds) and zenith sky (zs) measurement with the Dobson and Brewer instruments in a time window of 3 hours. Dist. is the horizontal distance in km between the centre of the closest GOME pixel and Uccle.

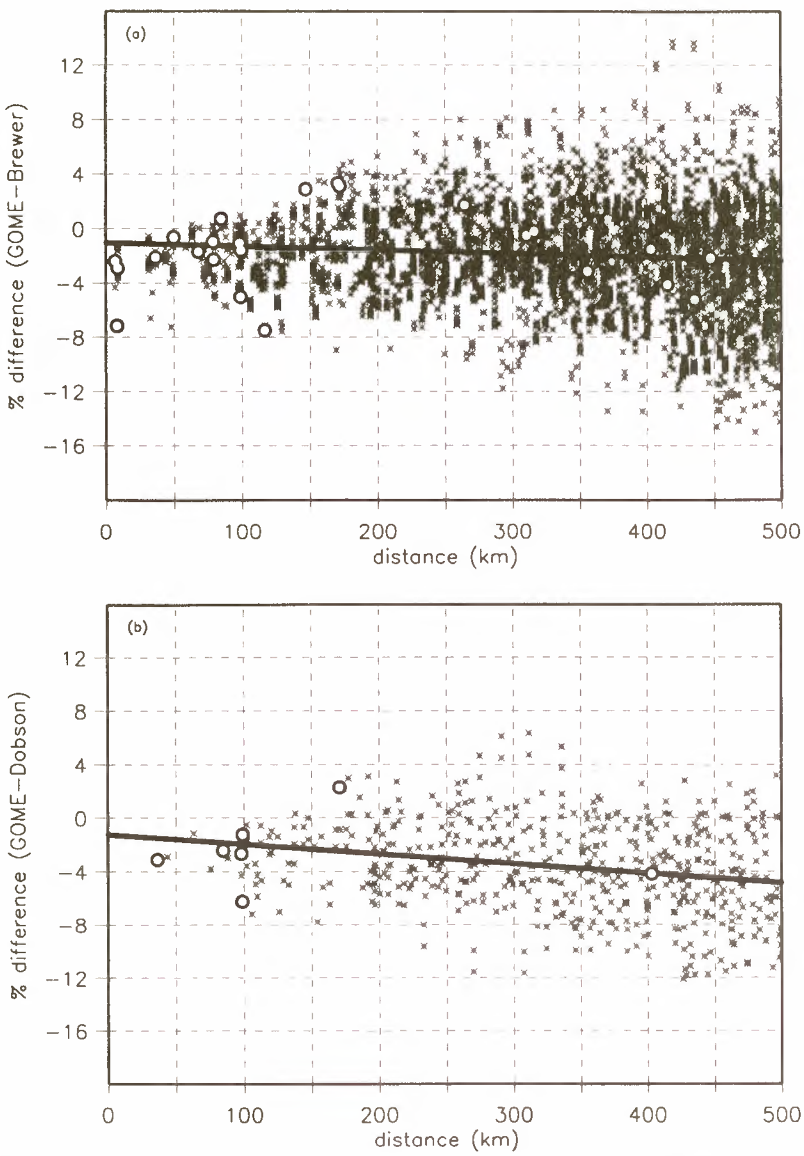

Fig. 3. Plot of percentage differences between GOME and direct sun Brewer (a) or Dobson (b) VCD's of ozone as a function of horizontal distance between Uccle and the centre of the GOME-pixel. The circles indicate the closest pixels. The least squares linear regression curve is fitted through the data. The slopes (± standard deviation) are given by: (a) -0.003% (± 0.0005%) and (b) -0.007% (± 0.001%)

3. DATA SET DESCRIPTION

For the validation a data set was considered including all GOME ground-pixels within 500 km horizontal distance from our test-site. Every GOME total ozone data point was compared with the closest in time DS Dobson and Brewer ozone value. The time limit was set to 3 hours before and after the ERS-2 overpass.

Table 1 shows an overview of the dataset. From July to mid August no Dobson data are available due to the participation of our spectrophotometer at the International Dobson Spectrophotometer Inter-comparison in 1995. We see that with the Brewer instrument more DS measurements are available as compared to the Dobson. This is due to the fact that the Brewer instrument is completely automated, which allows frequent measurements at regular time intervals.

4. MEAN DIFFERENCE BETWEEN GOME AND GROUND-BASED MEASUREMENTS

In Figure 3a respectively 3b the percentage differences of VCD's of ozone, calculated from GOME and DS Brewer respectively Dobson measurements for the whole data set (described earlier), are plotted as a function of horizontal distance. The circles represent the differences derived from the closest (in distance) GOME pixel. The solid line is the least squares linear regression line through the data points.

The mean difference between GOME and the Brewer ozone values amounts to -1.7%, with a standard deviation of 2.9%. For the Dobson we have found a slightly lower mean difference of -2.5% with a standard deviation of 2.6%. From Figure 3 we also see that the spread around these mean values increase with increasing horizontal difference. When we limit the horizontal distance to 100 km the standard deviation around the mean value becomes 1.6% for the Brewer and 1.4% for the Dobson. This can be attributed to instrumental effects. At larger horizontal distances real ozone differences are superimposed on these instrumental uncertainties, which leads to a larger spread. A smaller time window would not decrease the spread around the mean value, as can be seen in Figure 4, where the percentage differences between GOME and Brewer ozone VCD's are plotted as a function of time difference between correlative measurements. For the Dobson measurements the same conclusion can be taken.

Special attention has been given to the dependence of the mean difference (between the VCD of ozone measured at Uccle and the GOME data) on the airmass factor (AMF) and the VCD of the ground-based data, the solar zenith angle (SZA) of the GOME pixels and the kind of GOME pixel (west, nadir, east or backscan). For the latter, no statistically significant dependence was found.

Figure 5 shows the differences between GOME and Brewer (a) as well as between GOME and Dobson (b) VCD's of ozone, as a function of AMF of the ground-based data. In the caption of the figure the coefficients (± Their standard deviations) of the least squares linear regression line are given. Although the slopes of the fit lines are marginally significant (at the 95% significance level), we consider that there is no clear dependence since the slope can change drastically if only GOME overpasses during a randomly chosen subperiod are considered.

We also found no clear-cut dependence on the solar zenith angle of GOME (see Figure 6) ranging from 28 to about 70 degrees for the comparison with the Brewer data and from 40 to 70 degrees when we make the comparison with the Dobson values. The spread around the mean difference is remarkably low for small SZA's (up to 40 degrees). This conclusion can however

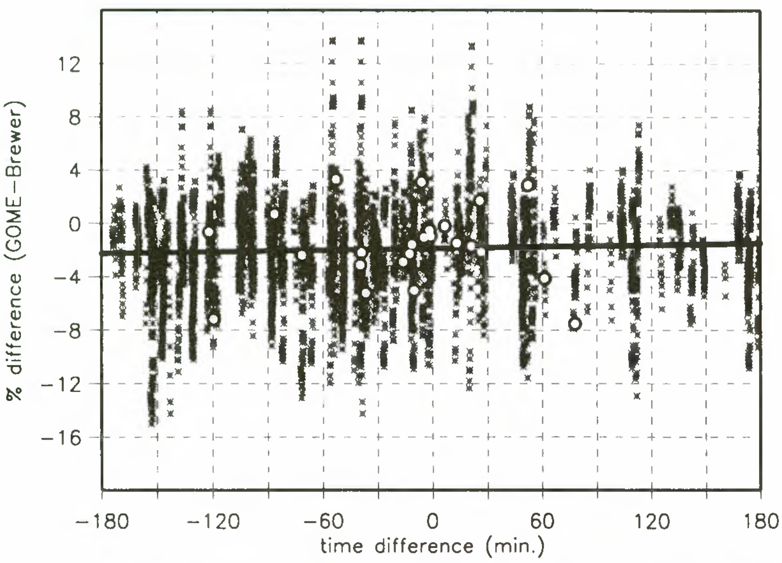

Fig. 4. Percentage differences between GOME and direct sun Brewer VCD's of ozone as a function of time difference between correlative measurements. The circles indicate the closest pixels.

change if we could do the comparison over a larger range of solar zenith angles.

From Figure 7 a small but statistically significant dependence of the mean difference on the ozone VCD of the ground-based measurements was found. With increasing Brewer values, the mean difference increases with about 4% per 100 DU. It should be mentioned that for this comparison only a small range of ozone values was considered (between 260 and about 323 DU for the Brewer and between 270 and 323 DU for the Dobson). So this dependence clearly needs to be confirmed for a larger range of the VCD's.

As distinct from the above mentioned statements, a highly significant dependence of the mean difference on the cloud cover fraction (CCF) of the GOME pixel was found (see Figure 8). For cloud-free pixels (CCF=0) the mean difference is virtually zero, while for completely cloudy pixels (CCF=1) the mean difference is -6% respectively -9% for the comparison with the Brewer respectively the Dobson spectrophotometer. The same behaviour was found when we restricted the data-set to intercomparisons within 100 km horizontal distance. Also the zenith sky Brewer and Dobson measurements show the same dependence.

5. VALIDATION OF THE GOME GHOST VERTICAL COLUMN DENSITY

Since the GOME instrument can not look down through the clouds, the effective slant column (ESC) from the DOAS algorithm should be corrected for the ozone amount under the cloud-top. This amount is called the Ghost Vertical Column (GVC) density. We deduced the GVC from the GOME level 2 intermediate result record, using the following equation:

$$GVC = VCD + \frac{(1 - CCF).VCD.AMFg - ESC}{CCF.AMFc},$$

with AMFg and AMFc the air mass factor to the ground and the cloud top. If the mean cloud top height or pressure (CTP) is known, we can calculate from our soundings the amount of ozone below the cloud top and compare this with the GOME GVC.

On 23 days of ERS-2 overpasses also correlative ozone soundings at Uccle were performed (see Table 2). From these soundings the GVC was determined as follows. As a first step the range of temperatures of the cloud top within the GOME pixel was determined, making use of infrared Meteosat images around the time of the ERS-2 overpasses. With the assumption that the temperature profile at the closest GOME pixel did not differ significantly from the temperature profile from our ozone sounding, the corresponding range of cloud top pressures was determined (fifth column in Table 2). In general these values agreed well with the cloud top as determined from the humidity profiles, which offered an independent check.

From Table 2 it is obvious that the CTP used in the GOME cloud algorithm is systematically too low i.e. that the cloud top height is too high. The mean cloud top pressure used in the ICFA algorithm was 486.1 hPa while from Meteosat and temperature soundings a mean value of 683 hPa was determined. The overestimation of the cloud top height in the GOME algorithm resulted in a GVC

TABLE 2. Comparison of Ghost Vertical Columns and Cloud Top Pressures

DATE	CCF (G)	CTP (G) (hPa)	GVC (G) (DU)	CTP (M+S) (hPa)	GVC (S) (DU)
July 24	.12	448.5	18.4	725	15.1
Aug. 25	.41	486.4	18.2	888→713	1.8→7.3
Aug. 29	.78	487.1	18.1	617→589	8.4→9.6
Aug. 30	.36	483.9	17.9	777→737	9.1→11.0
Sept. 1	.11	488.4	18.6	986→967	.4→1.0
Sept. 4	.24	485.6	17.9	736→665	7.7→10.7
Sept. 6	.42	493.3	18.1	748→593	6.9→12.5
Sept. 8	.93	488.0	18.6	449→336	14.9→20.1
Sept. 15	.26	485.0	17.9	735→682	6.9→8.6
Sept. 20	.43	483.8	17.7	702→670	9.3→10.7
Sept. 21	.30	486.7	17.9	554	16.3
Sept. 22	.26	491.9	18.2	722→654	7.9→10.1
Sept. 23	.25	485.5	18.3	730→600	8.5→13.6
Sept. 27	.38	488.3	18.6	800→775	6.4→7.3
Oct. 2	.47	488.6	18.9	500→390	16.9→22.3
Oct. 3	.39	486.3	18.5	850→496	2.5→14.7
Oct. 6	.16	487.9	18.9	850	4.9
Oct. 11	.33	493.2	18.4	925	3.6
Oct. 13	.26	487.9	18.9	927→828	1.8→5.2
Oct. 30	.34	494.2	18.4	662	10.5
Nov. 10	.30	487.4	19.0	500→426	15.0→17.6
Dec. 11	.50	485.0	19.4	674→519	10.8→16.3
Dec. 12	.41	486.3	19.0	659→640	10.8→11.4
mean	.37	486.1	18.4	683	9.9
st. dev.			0.4		5.2

Dates of ozone soundings correlative with ERS-2 overpasses are given. Only the closest GOME pixels are considered. CCF (G) and CTP (G) are the cloud cover fraction and the cloud top pressure of the GOME pixel. CTP(M+S) represents the cloud top pressure derived from Meteosat images and temperature profiles of ozone soundings. GVC(G) and GVC(S) are the ghost vertical column densities of ozone calculated from GOME data and our ozone soundings. In the last two rows mean values and standard deviations are shown.

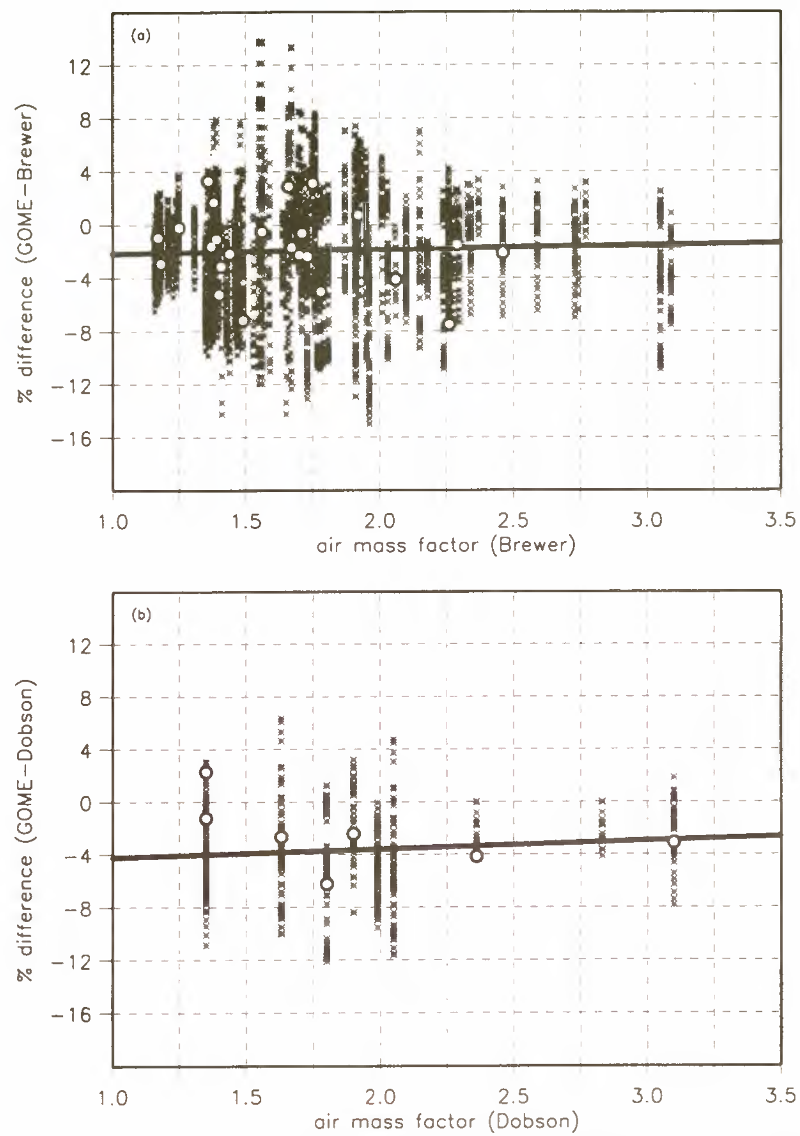

Fig. 5. Plot of percentage differences between GOME and direct sun Brewer (a) or Dobson (b) VCD's of ozone as a function of air mass factor of the ground-based data. The circles indicate the closest pixels. The coefficients (± standard deviation) of the least squares linear regression curve (the solid line) $y=C_0 + C_1x$ are given by:
(a) $C_0 = -2.47$ (± 0.21) and $C_1 = 0.31$ (± 0.12)
(b) $C_0 = -4.85$ (± 0.60) and $C_1 = 0.63$ (± 0.31)

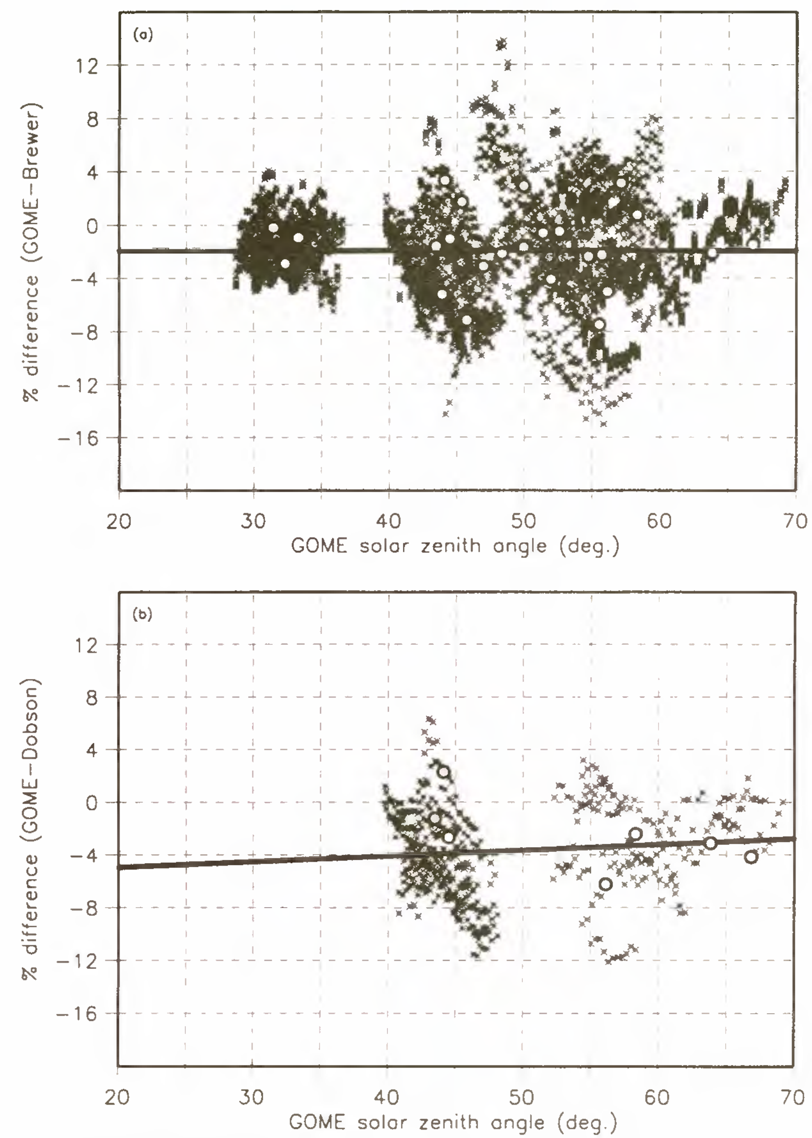

Fig. 6. Plot of percentage differences between GOME and direct sun Brewer (a) or Dobson (b) VCD's of ozone as a function of the solar zenith angle at the GOME pixel. The circles indicate the closest pixels. The coefficients (± standard deviation) of the least squares linear regression curve (the solid line) $y=C_0 + C_1x$ are given by:
(a) $C_0 = -1.90$ (± 0.24) and $C_1 = -0.001$ (± 0.005)
(b) $C_0 = -5.83$ (± 0.89) and $C_1 = 0.044$ (± 0.018)

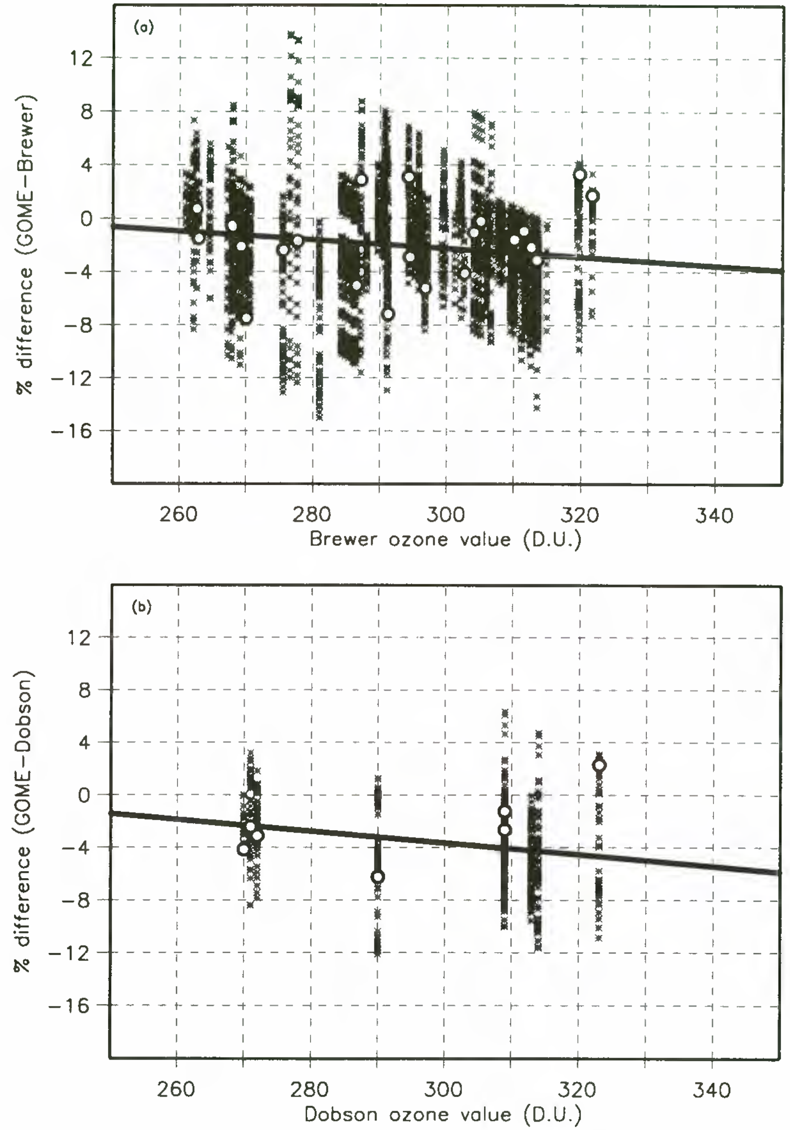

Fig. 7. Plot of percentage differences between GOME and direct sun Brewer (a) or Dobson (b) VCD's of ozone as a function of the ground-based ozone amount. The circles indicate the closest pixels. The coefficients (± standard deviation) of the least squares linear regression curve (the solid line) $y=C_0 + C_1x$ are given by:
(a) $C_0 = 10.73$ (± 0.84) and $C_1 = -0.041$ (± 0.003)
(b) $C_0 = 12.36$ (± 1.77) and $C_1 = -0.058$ (± 0.006)

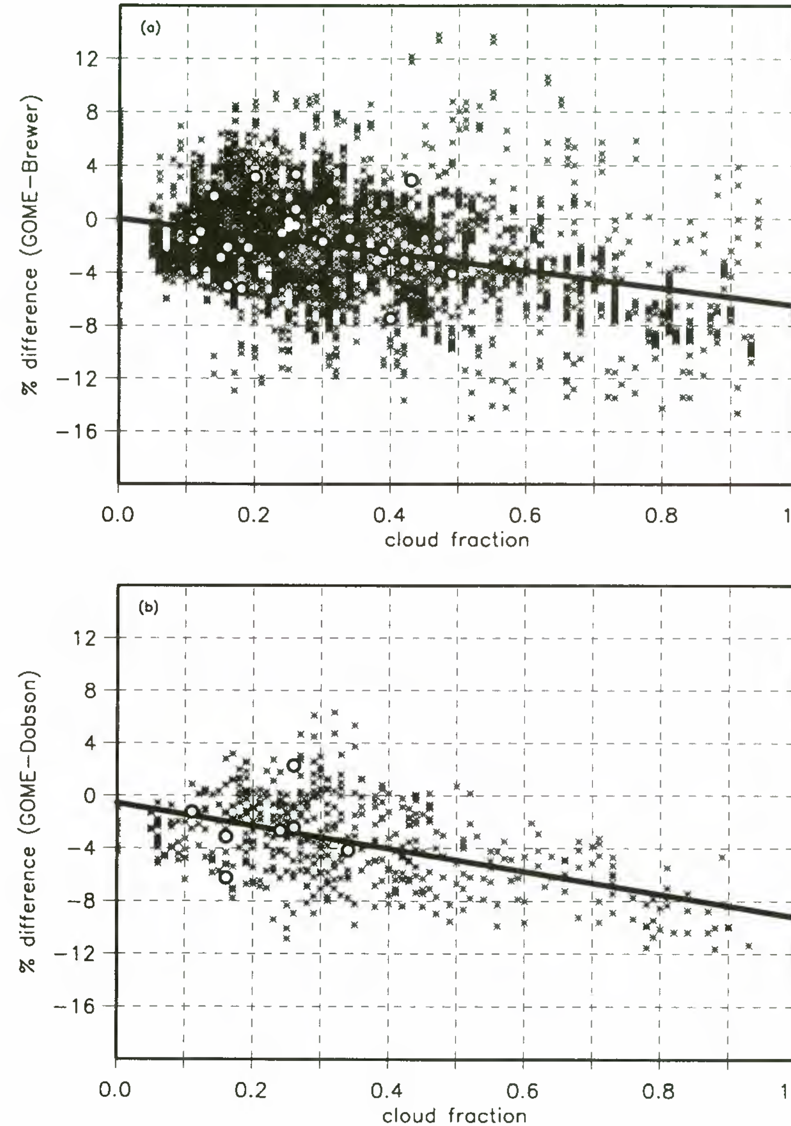

Fig. 8. Plot of percentage differences between GOME and direct sun Brewer (a) or Dobson (b) VCD's of ozone as a function of cloud cover fraction of the GOME pixels. The circles indicate the closest pixels. The coefficients (± standard deviation) of the least squares linear regression curve (the solid line) $y=C_0 + C_1x$ are given by:
(a) $C_0 = 0.80$ (± 0.15) and $C_1 = -7.36$ (± 0.35)
(b) $C_0 = -0.32$ (± 0.09) and $C_1 = -6.68$ (± 0.27)

density of ozone that was on average 8.5 DU too high. If this overestimation is taken into account, the mean difference between the VCD of ozone measured at Uccle and the GOME data, would even increase by 2.6% at a CCF=1.

6. CONCLUSIONS

1. GOME ozone measurements from a set of 45 days within a horizontal distance of 500 km and with a time difference less then 3 hours, were compared with ground-based Brewer and Dobson data. The mean difference between GOME and Brewer respectively Dobson amounts to -1.7%±2.9% respectively -2.5%±2.6%, the GOME data being the lowest.
2. There seemed to be no statistically significant dependence of the mean difference on the air mass factor of the ground-based data and the kind of GOME pixel (west, nadir, east and backscan). Also no clear-cut dependence was found on the solar zenith angle of the GOME pixel when a range from 28 to 70 degrees (40 to 70 degrees) was considered in the comparison with the Brewer (Dobson) instrument. In a relatively narrow range from about 260 and 323 DU, there was a small but statistically significant dependence of the mean difference on the ground-based ozone amount (about 4% per 100 DU). This needs to be confirmed for a larger range of VCD's.
3. A highly significant dependence of the mean difference on the cloud cover fraction (CCF) of the GOME pixel was found, ranging from 0 (CCF=0) up to -6 to -9% (CCF=1).
4. From Meteosat cloud images combined with temperature and humidity profiles from corresponding ozone soundings, it was found that the cloud top height used in the GOME algorithm was too high. This resulted in an overestimation of the GOME ozone vertical column density of about 2.6%, what implicates that the dependence of the mean difference (see 3) would even be stronger by the same amount.

7. RECOMMENDATIONS

1. The database of cloud top reflectances in the GOME level 1 to 2 algorithm needs to be adjusted.
2. The estimated value of the mean cloud top pressure over mid-latitudes needs to be increased.
3. The GOME validation needs to be continued over at least one annual cycle to verify whether or not the dependence of the mean difference (between GOME ozone data and ozone measured at Uccle) on the magnitude of the VCD is confirmed over a larger range of ozone values.

8. REFERENCES

De Backer, H., and D. De Muer, 1991, Intercomparison of total ozone data measured with Dobson and Brewer ozone spectrophotometers at Uccle (Belgium) from January 1984 to March 1991, including zenith sky observations, *J. Geophys. Res.*, 96, 20711-20719.

De Backer, H., E. P. Visser, D. De Muer, and D. P. J. Swart, 1994, Potential for meteorological bias in lidar ozone data sets resulting from the restricted frequency of measurement due to cloud cover, *J. Geophys. Res.*, 99, 1395-1401.

De Backer, H., D. De Muer, E. Schoubs. and M. Allaart, 1996, A New Pump Correction Profile for Brewer-Mast Ozonesondes. *To be presented at the XVIII Quadrennial Ozone Symposium-96* (12-21 September 1996).

De Muer, D., H, De Backer, R. E. Veiga, and J. M. Zawodny, 1990, Comparison of SAGE II ozone measurements and ozone soundings at Uccle (Belgium) during the period February 1985 to January 1986, *J. Geophys. Res.*, 95, 11903-11911.

De Muer, D., and H. De Backer, 1992, Revision of 20 years of Dobson total ozone data at Uccle (Belgium); Fictitious Dobson total ozone trends induced by sulfur dioxide trends, *J. Geophys. Res.*, 97, 5921-5937.

De Muer, D., H. De Backer, and Ph. Van Haver, 1995, Analysis of 25 years of regular ozone soundings at Uccle (Belgium), *Atmospheric ozone as a Climate gas*, edited by W. Wang and I. Isaksen, 113-129, Springer-Verlag Berlin.

9. ACKNOWLEDGEMENTS

This study was supported by the European Space Agency and the Belgian Services for Scientific Policy under PRODEX-GOME Cal/Val A.D. ERS2-Project 1 (151902).

PRELIMINARY VALIDATION OF GOME OZONE MEASUREMENTS BY COMPARISON WITH TOTAL OZONE DATA FROM AROSA (SWITZERLAND)

J. Staehelin and A. Renaud

Institute for Atmospheric Science, Federal Institute of Technology, ETH-Hönggerberg, CH-8093 Zürich, Switzerland

Abstract

Total ozone measurements from two Dobson spectrophotometers (D62 and D101) and one Brewer spectrophotometer (B40) at Arosa are compared with 34 GOME (Global Ozone Monitoring Experiment on board satellite ERS-2) overpasses from the July to December period 1995. Total ozone from GOME was found, on average, to be lower than ground based measurement by -3.03 ± 2.64 %, -2.80 ± 2.69 % and -1.34 ± 2.94 % compared with D101, D62 and B40 respectively. The differences are not statistically significant within the small available sample. The data analysis revealed that the differences between GOME and ground based measurements are dependent on total ozone amount, the air mass factor of the satellite measurements and distance of the satellite measurement from Arosa. This must be regarded as somewhat preliminary analysis since the representativeness of the sample is questionable and also only low total ozone values could be compared.

1. INTRODUCTION

The ozone shield prevents harmful solar UV-B radiation from penetrating the earth's atmosphere and is therefore crucial for any life on our planet. Stratospheric ozone has begun to decline noticably over midlatitudes and Antarctica since the beginning of the 70s the main reason for which being the anthropogenic release of substances that deplete stratospheric ozone such as chlorofluorocarbons (CFCs) and bromine containing volatile organic gases such as halons (WMO, 1995). It is important to know the exact amount of depletion of the global ozone shield in order to assess the extent of the problem and also to compare these data with numerical models which describe the anthropogenically induced disturbances on stratospheric ozone.

Ground based ozone measurements using sun photometry are useful for measuring total ozone and its long term trends at single stations. However, this method is hardly suitable for obtaining global coverage of the total ozone field. This information can be obtained from satellite measurements. Instrument TOMS (Total Ozone Mapping Spectrometer) on board of satellite NIMBUS 7 provided the most extended data set which could be used to quantify ozone trends with almost global coverage (Stolarski et al., 1991 and 1992). However, history has shown that the evaluation of satellite total ozone measurements using data from carefully maintained ground based stations is crucial in deducing reliable trends. TOMS measurements suffered from the degradation of the diffuser plate and other technical problems which lead to the development of different highly sophisticated inversion algorithms such as version 6 (Herman et al., 1991) and version 7. On the other hand, satellite data are useful to indicate possible instrumental problems associated with ground based total ozone measuring stations.

Satellite measurements also provide reliable trends for upper and middle stratospheric ozone (WMO, 1995). However, the most significant trends for atmospheric total ozone amount have been obtained for the lower stratosphere where reliable and precise measurements of ozone are difficult to obtain from instruments in space. The trends derived from SAGE1 and 2 instruments are controversial (WMO, 1995). Thus, the potential of instruments such as GOME (Global Ozone Monitoring Experiment) to measure ozone profiles in the troposphere is of great interest. However, profile measurements from GOME in the troposphere have to be validated with measurements performed from the ground such as ozone balloon measurements.

Satellite instruments have limited lifetimes and the replacement of space borne instruments will allways cause problems in homogenisation of the series. Thus, in order to ensure more composite satellite series for the future, it will be necessary to compare these data with those obtained from carefully maintained ground-based total ozone stations.

In this paper we compare total ozone measurements from the GOME instrument (Global Ozone Monitoring Experiment) on board the second European Remote Sensing Satellite (ERS-2) with those of Arosa from the period of July to December 1995. ERS-2 was launched in April 21. 1995 by ESA (European Space Agency).

2. TOTAL OZONE MEASUREMENTS AT AROSA

Total ozone measurements by sun photometry started at Arosa in 1926 and a continuous series is available since the beginning of the 30s. Ozone measurements at Arosa are performed by the Swiss Meteorological Institute since 1988. The world longest series at Arosa is very valuable in assessing total ozone trends for Northern midlatitudes since it covers many solar cycles in the anthropogenically unperturbed stratosphere (Staehelin et al., 1994).

However, reliable trend determination from ground based measurements is a challenging problem as annual long term trends since the beginning of the 70 have shown a decrease in total ozone of several percent per decade for midlatitudes. Five Dobson spectro-photometers employing partially different detection devices were used at Arosa (Staehelin et al., 1995). The reevaluation of the long series total ozone series was described briefly (Hoegger et al., 1994) and will be discussed in a forthcoming paper. In recent times this problem has been addressed by using several instruments which measure total ozone simultaneously. Presently, two Dobson spectrophotometers (D101 and D62) and two Brewer spectrophotometers (B40 and B72) are in operational use at Arosa. Only direct sun observations are currently performed at Arosa because their accuracies are higher than zenith sky total ozone measurements. Weather conditions at Arosa allow us to obtain a representative sample for the entire year. The stability of the Dobson spectrophotometers are checked at least twice per month by using standard lamps. Standard lamp readings can also be used to deduce corrections for possible instrumental drifts. The measurements used in this analysis were slightly adjusted by the readings of the standard lamp tests.

The instruments of the world-wide Dobson network are intercompared every four to five years with a world standard instrument. The primary world standard instrument (D83) is maintained by a group at the Climate Monitoring and Diagnostics Laboratory at NOAA in Boulder, Colorado, USA. The instrument is calibrated by the Langley plot method every summer at the Mauna Loa observatory at Hawaii, where the tropical weather conditions allows a precise determination of the extraterrestrial constants necessary in Dobson spectrophotometry. D83 has proven its extraordinary long-term instrumental stability (Komhyr et al., 1989). The accuracy of the calibration of the standard instruments is believed to be in the order of ± 1 % or better for the entire operational μ-range (R.D. Evans, personal commun.). The Brewer spectrophotometers are calibrated also by the Langley plot method at the Mauna Loa Observatory. The standard consists of a triade of Brewer spectrophotometers which are simultaneously operated by AES Canada at Toronto.

The Dobson spectrophotometers were compared with the standard instruments at Arosa in 1986, 1990 and 1995. The intercomparison of the Dobson spectrophotometers with the standard instruments are usually based on simultaneous measurements over half a day, thus introducing some additional uncertainty in the calibration of the individual instruments.

Figure 1 indicates that the quasi-simultaneous measurements from the two Dobson spectrophotometers employed during 1995 show some scatter in the single data and that the dependence on the air mass, μ, is only weak, though statistically significant. Dependencies of the difference of the Dobson and Brewer spectrophotometers on the air mass, μ, were found to be larger which is similar to our earlier findings (Staehelin et al., 1995; Högger et al., 994).

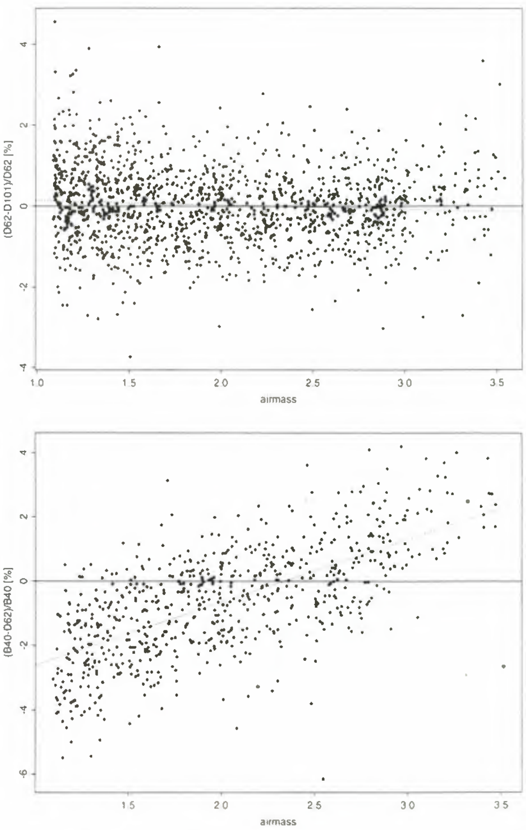

Figure 1: Relative Differences in quasi-simultaneous measurements (maximal difference in time: 5 min.) as a function of μ for Dobson and Brewer total ozone measurements of Arosa for 1995.

In February and March 1993 total ozone was also determined by spectral measurements of direct solar irradiance at Arosa by a group from the University of Innsbruck (Huber et al., 1995). With this instrument, total ozone is calculated by using extraterrestrial UV-measurements from satellites, which is a different approach to that of the Langely plot method used in Dobson and Brewer spectrophotometry. On 21 days 657 spectra of solar irradiance were measured during completely uncovered sun and 231 spectra were made when the sun was uniformly covered by thin clouds but still visible. During the same period a sample of 105 Dobson and of 890 Brewer quasi-simultaneous measurements was available. On average, the total ozone amount from the spectral instrument is lower by 0.4 ± 0.7 % compared to the Brewer instrument and by 1.1 ± 0.9 % compared to the results from the Dobson spectrophtotometer. This reafirms the conclusion that total ozone results from Arosa are expected to have an average accuracy in the order of ± 1.5 %.

3. COMPARISON OF TOTAL OZONE AMOUNT OF AROSA WITH GOME MEASUREMENTS

The sample of available GOME data allows a comparison with Brewer measurements from Arosa for 34 days and with Dobson measurements for 33 days. GOME measurements are believed to be suitable for comparison with ground based data as long as the distance of the light path of the satellite passes within from 600 km of Arosa. However, large fluctuations of the measurements of one overpass over Arosa were found, possibly because of the difference in the east, west and central pixels of the satellite measurements. Because of the small duration of the overpass we generally used the ground based data with closest correspondence in time and GOME overpass averages for the comparison.

Figure 2 and Table 1 show the results of the comparison of the GOME total ozone data with the total ozone values measured at Arosa. Table 2 contains the correlation matrix of the readings for the GOME data and the ground based measurements (single values with closest correspondence in time), the values using daily means from Arosa are almost identical. The correlation between GOME and ground based measurements is higher for the Dobson than the Brewer measurements, although the average total ozone amount is closer between Brewer and GOME than between Dobson and GOME measurements. Total ozone amounts from the ground-based instruments were generally somewhat higher than the values reported from GOME, but the differences for the entire sample were not statistically significant on the basis of two σ values.

Table 1: Total ozone values from the GOME validation: Relative differences between GOME and Arosa ground-based measurements (GOME-groundb. instr.)/groundb. instr * 100, sample of 34 (33) measurements) and relative differences between Arosa ground based measurements for comparison. The table includes the standard deviation (1σ values).

in %	mean	median	min./max.
GOME-D101:	- 3.03 ± 2.64	-3.12	-7.39/+ 4.37
GOME-62:	- 2.80 ± 2.69	- 2.76	- 7.28/+ 3.34
GOME- B40:	- 1.34 ± 2.94	- 1.51	- 6.86/+ 5.33
D62-D101	- 0.23 ± 0.90	- 0.32	- 2.71/+ 2.03
B40-D62	- 1.54 ± 1.52	- 1.88	- 4.82/+ 1.39

Table 2: Correlation matrix for comparison between GOME and ground-based total ozone measurements for Arosa (values with closest correspondence in time) obtained for 34 (33) values from the end of July to the beginning of December, 1995.

	GOME	D101	D62	B40
GOME	1	0.92	0.92	0.88
D101	0.92	1	0.99	0.97
D62	0.92	0.99	1	0.98
B40	0.88	0.97	0.98	1

Table 3: Results of the statistical analysis including measurements of GOME (all single measurements suitable for comparison with ground based station, in DU) and differences between GOME measurements (averages of the overpasses) and total ozone measurements of Arosa (single measurements with most closest correspondence in time). p-value: error probability (0: value smaller than 10^{-5}); d: distance of the overpass of GOME, in km; AMF: air mass factor of the GOME measurements. Cl_{fr}: cloud fraction from GOME measurements.

	equation	p-value
statistics GOME data for Arosa overpasses		
GOME	294.63- 10.54 · error GOME	0
GOME	dependence on distance d: not statistically significant	
GOME	394.24 - 41.97 AMF	0
GOME	285.00 - 18.52 Cl_{fr}	0
statistics GOME in comparison with data from Arosa		
GOME-D101	47.36 - 0.19 D101	0.003
GOME-D62	50.61 - 0.21 D62	0.002
GOME-B40	50.81 - 0.19 B40	0.019
GOME-D101	-26.31 + 0.044 d	0.034
GOME-D62	-28.08 + 0.050 d	0.017
GOME-B40	not statistically significant with d	
GOME-D101	- 39.25 + 10.73 AMF	0.012
GOME-D62	- 38.08 + 10.55 AMF	0.015
GOME-B40	not statistically significant with AMF	
GOME-total ozone Arosa: not statistically significant with Cl_{fr}		

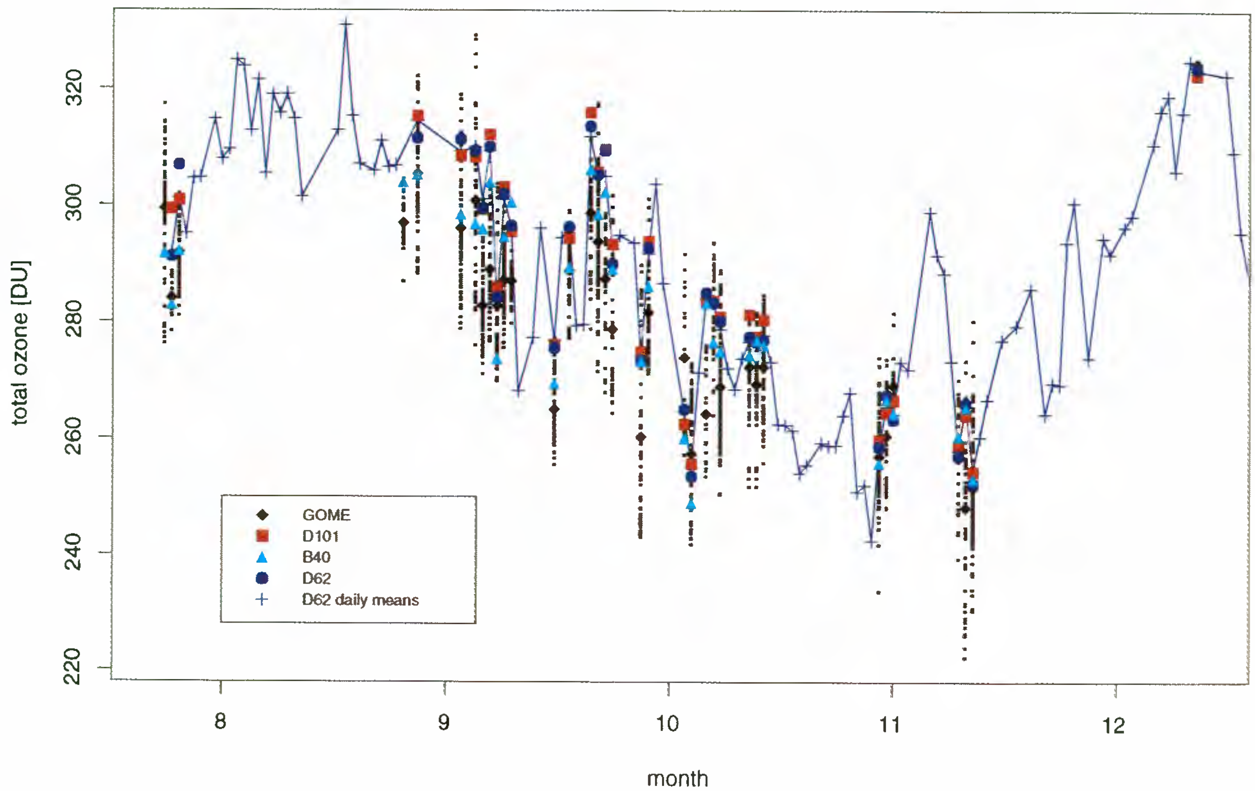

Figure 2: Comparison of total ozone values from GOME and ground-based instruments for Arosa.

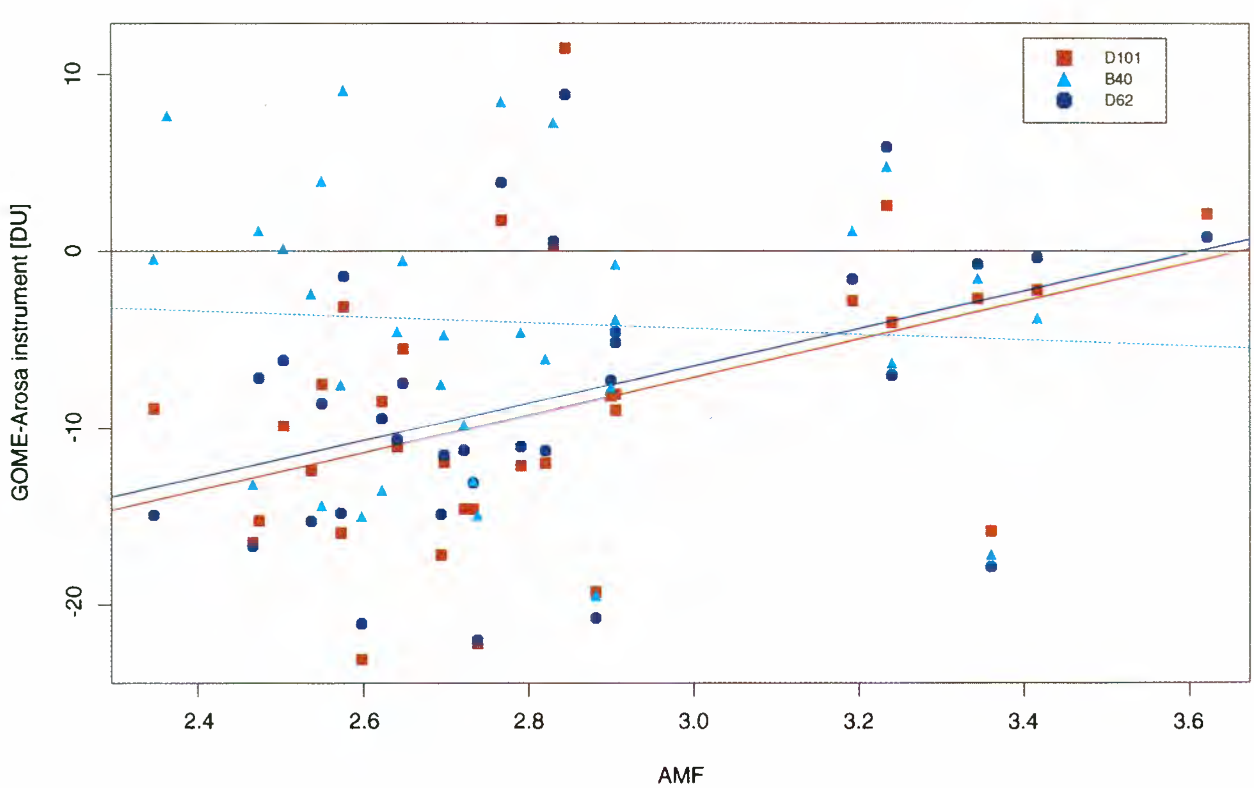

Figure 3: GOME (daily means) minus ground-based measurements at Arosa (single values with closest correspondence in time) as function of the air mass factor (AMF) of GOME measurements.

4. STATISTICAL ANALYSIS OF THE DIFFERENCE BETWEEN GOME AND AROSA MEASUREMENTS

The closer agreement found for the different total ozone instruments at Arosa compared to the GOME measurements is not surprising, since the GOME measurements refer to air paths through the atmosphere which differ from those of the ground-based instruments. In a further analysis we tested the statistics for the GOME overpass data for Arosa and considered the differences between the GOME measurements and the Arosa ground-based measurements most closely related in time to the GOME overpasses. The results of the analysis are summarised in Table 3.

The highly significant dependence found for AMF within the sample of GOME measurements for Arosa is due to a positive trend from summer to early winter in the AMF (GOME tracking) corresponding to a total ozone decrease with a typical seasonal variation between summer to early winter (correlation coefficient between AMF and total ozone: -0.70). Thus, we can't determine the influence of the inadequate AMF (Fig. 3) calculation in the current GOME retrieval but is expected this will be improved in the next version of GOME retrieval. Furthermore, a significant correlation between the GOME sample and cloud fraction is believed to be due to the current simple algorithm of GOME based on constant cloud top altitude. The statistically significant correlation between the difference of GOME and the Dobson measurements of Arosa with the distance of the GOME measurements with closer agreement with larger distances seems surprising (Fig. 4). The complex orography over the Alpine area may possibly be part of the answer, but the problem should be further investigated when a larger data set of GOME data becomes available.

Significant correlations were found between GOME minus ground based measurements and total ozone amount (Fig. 5). Substantial differences between ground based measurements and GOME values would be expected by extrapolating this relation to large total ozone amounts typical for spring in northern midlatitudes. However, the available sample does not allow to verify this assumption.

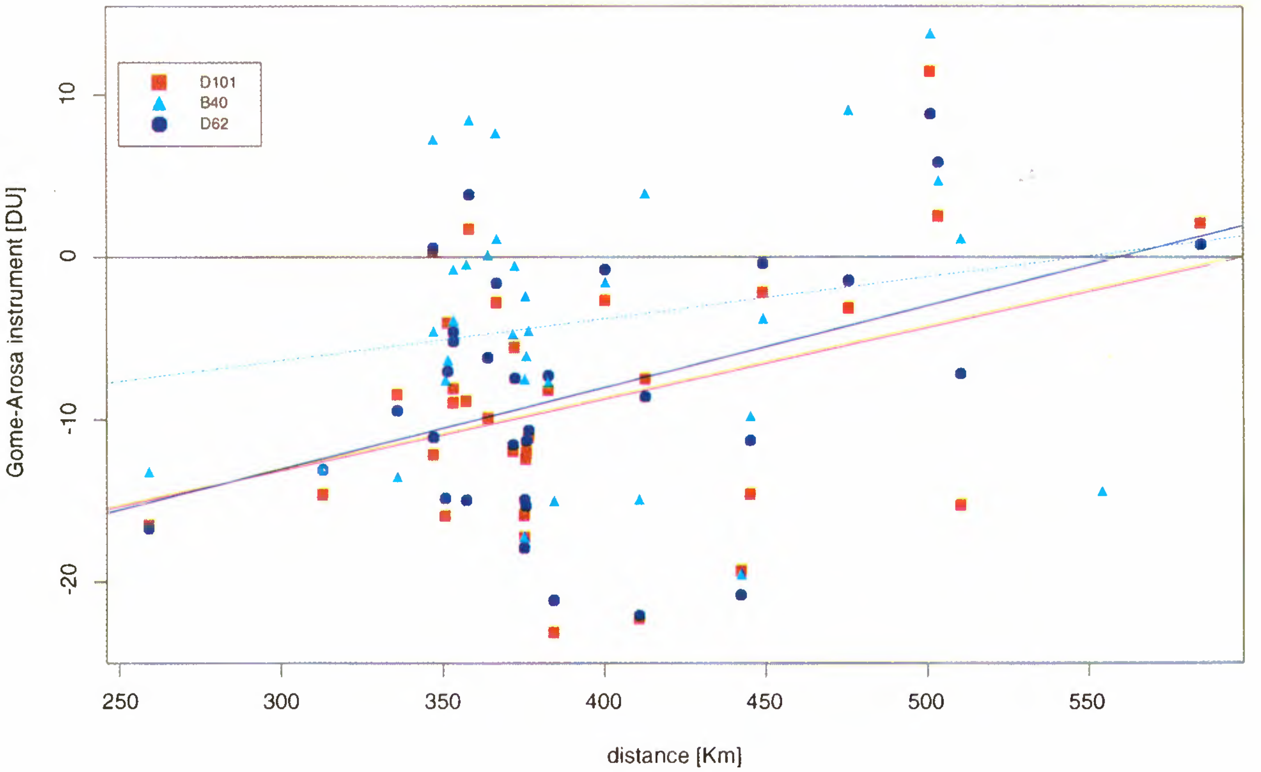

Figure 4: GOME (daily averages) minus ground-based measurements at Arosa (single values with closest correspondence in time) as function of distance of the GOME measurements.

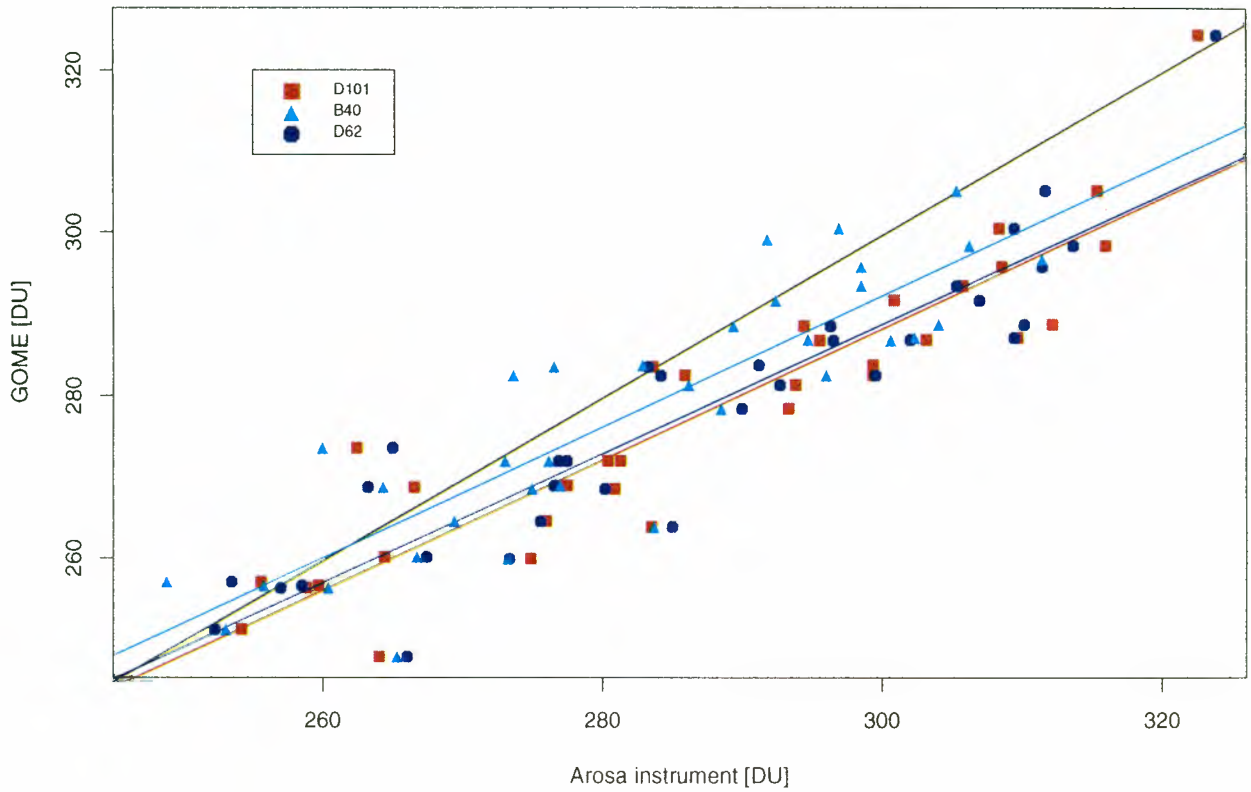

Figure 5: GOME measurements at Arosa as a function of total ozone amount from ground-based instruments at Arosa (averages of GOME overpasses and single values from Arosa with closest correspondence in time).

5. CONCLUSIONS

GOME measurements from 35 days are available for comparison with ground-based total ozone measurements at Arosa but the small available sample does not allow us to validate the GOME measurements on a scientifically sound basis. The results of a preliminary GOME total ozone validation leads to the following observations:

1. Because of the lack of a randomised sample the results of the GOME validation are questionable.

2. The comparison indicated that GOME data are generally lower than those determined by the ground-based instruments, but the differences are not statistically significant in the small available sample.

3. The differences between GOME and Dobson measurements at Arosa depend on the distance of the GOME measurements from Arosa for D101 and D62, the air mass factor of GOME for D101 and D62, and total ozone amount (for all three instruments).

4. The differencies between GOME and ground based measurements could be possibly attributed to known deficiencies in the current version of GOME total ozone retrieval algorithm.

5. After improvement of GOME algorithm the validation of GOME data must be repeated to explore whether this accounts for the observed inconsistencies.

6. Only by including the measurements of one entire annual cycle can GOME data be validated by ground-based total ozone measurements on a scientifically sound basis, and again, the number of available measurements has to be increased dramatically.

7. GOME data must be validated over a longer time scale (approximately every year) to assess the problem of a possible temporal calibration drift.

8. Information on the ozone profile is scientifically more relevant than total ozone. No ozone profile data from GOME are presently available, but they must be retrieved to make use of the inherent possibilities of GOME's instrumental design. Profile information needs to be validated using ozone profile measurements of known quality such as ozone balloon measurements before they can be used in scientific investigations.

5. REFERENCES

Herman, J.R., Hudson, R. et al. 1991. A new self-calibrating method applied to TOMS/SBUV backscattered ultraviolet data to determine long-term global ozone change. *J. Geophys. Res.*, Volume 96, pp. 7531-7545.

Hoegger, B., Viatte, P. et al., 1994. Quality control concept and recent development of the Light Climatic Observatory at Arosa - ozone measuring station of the Swiss Meteorological Institute (LKO) in Ozone in the Troposphere and Stratosphere, Part 2, NASA conference publication 3266, R.D. Hudson, Ed., Goddard Space Flight Center, Greenbelt, Maryland, pp. 711-713.

Huber, M., Blumthaler, M. et al., 1995. Total atmospheric ozone determined from spectral measurements of direct solar UV irradiance. *Geophys. Res. Lett.*, Volume 22, pp. 53-56.

Komhyr, W.D., Grass, R.D et al. 1989. Dobson spectrophotometer 83: a standard for total ozone measurements. *J. Geophys. Res.*, Volume 94, pp. 9847-9861.

Staehelin, J., Bader J. et al. 1994. Trend analysis of the long-term Swiss ozone measurements, in Ozone in the Troposphere and Stratosphere, Part 1, NASA conference publication 3266, R.D. Hudson, Ed., Goddard Space Flight Centre, Greenbelt, Maryland, pp. 186-189.

Staehelin, J. and Schill, H. et al. 1995. Total ozone observation by sun photometry at Arosa, Switzerland. *Opt. Engin.* Volume 34, pp. 1977-1986.

Stolarski, R., Bloomfield, R.D et al. 1991. Total ozone trends deduced from NIMBUS 7 TOMS data. *Geophys. Res Lett.*, Volume 18, pp. 1015-1018.

Stolarski, R., Bojkov, R. et al. 1992. Measured trends in Stratospheric Ozone. *Science*, Volume 256, pp. 342-349.

WMO 1995. Scientific Assessment of Ozone Depletion: 1994. *World Meteorological Organization, Global Ozone Research and Moitoring Project* - Report 37, WMO, Geneva.

ERRORS OF STRATOSPHERIC DOAS-MEASUREMENTS DUE TO THE WAVELENGTH DEPENDENCE OF THE AIR MASS FACTOR AND THE INCORRECT REMOVAL OF THE FRAUNHOFER LINES

T. Wagner, H. Haug, L. Marquard, E. Scheer, U. Platt

Institut für Umweltphysik, University of Heidelberg,
INF 366, 69120 Heidelberg, Germany

Abstract
The special quality of the sun as a light source and the properties of the radiation transport through the atmosphere are pecularities of Zenith-Scattered-Light DOAS measurements of stratospheric species. Both can lead to large errors in the data evaluation for groundbased and satellite measurements. Due to Rotational-Vibrational-Raman scattering so called 'Fraunhofer ghosts' may lead to structures in the scattered light spectra which need to be taken into account. Here we present an estimate of the magnitude of these errors and show possible correction procedures.

1. INTRODUCTION

The light path through the atmosphere for different wavelengths is not the same, because of the wave-length dependence of Rayleigh- and Mie-scattering and molecular absorption. This leads to a wavelength dependence of the Air Mass Factor (AMF) [Frank, 1991].

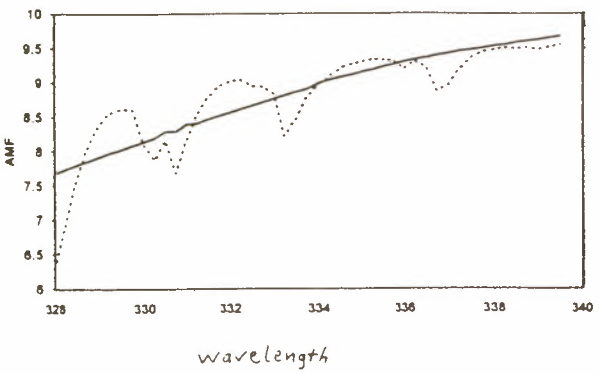

Figure 1: UV-O_3-AMF, calculation for a SZA=90°, high resolution and smoothed O_3-cross-sections, respectively.

In particular due to the strong change of the O_3-cross section over the range of the Huggins bands the AMF shows the inverse structure of the O_3-cross-section (Fig. 1).

Thus the determined O_3-absorptions underestimate the true value systematically if an averaged AMF is used for the evaluation. This error is calculated for the O_3-absorption at 333.5 nm in dependence of the solar zenith angle (SZA).

The solar spectrum shows characteristic Fraunhofer lines which are much stronger than the absorptions of atmospheric trace gases. This Fraunhofer lines can be removed in principle taking into account in the fit procedure a spectrum measured at small solar zenith angle and thus with small trace gas absorptions and a Ring spectrum. The trace gas absorption of the so called Fraunhofer spectrum (REF) has to be added after the determination of the absorption of the measured spectrum (SCD).

The absorption corresponding to the vertical column (VCD) is derived by dividing this sum by the AMF.

$$VCD = (SCD + REF) / AMF \qquad (1)$$

For many cases the fit coefficient (SOL) of the Fraunhofer spectrum differs from unity. This leads to errors in the determination of the trace gas absorptions, because not the true amount of REF is subtracted from the measured spectrum in the fit procedure. Additionally spectral interferences between trace gas absorptions and the Fraunhofer structures can lead to strong errors in particular of weak absorbers, if the Fraunhofer structures are not removed exactly.

A possible reason for an incorrect removal of the Fraunhofer lines is Vibrational-Raman-scattering.

SITE DESCRIPTION

The error determination was performed for spectra taken from groundbased DOAS-measurements at Kiruna (68.8°N, 21.8°E) in the winter 1993/94 [Wagner, 1994].

Two temperature stabilized grating spectrographs, one for the visible (375 nm - 688 nm, flat-field holographic grating) and one for the UV-range

(318 nm - 384 nm, Czerny-Turner), were used to measure zenith scattered sunlight. The incomming light is focussed by two lenses onto quartz fibre bundles and fed into the spectrographs. The dispersed light is detected by cooled photo-diode-arrays, which allow simultaneous light detection over the whole spectral range [Stutz, 1991].

RESULTS

Wavelength dependence of the AMF:

The calculation of the error due to the fine structure of the AMF at the Huggins bands was performed in the following way:

The wavelength dependent O_3-absorption corresponding to a fixed vertical O_3-column (VCD_{true}) is calculated for the wavelength range of the UV-O_3-evaluation (328 nm - 340 nm). For the calculations the high resolution O_3-cross sections of Bass and Paur were used [Bass, 1985].

$$A_{VCD}(\lambda) = VCD_{true} * \sigma_{ozone}(\lambda) \qquad (2)$$

This absorption is multiplied with the wavelength dependent AMF for different SZA to simulate the O_3-absorption for measured spectra:

$$A_{SCD}(\lambda, SZA) = AMF(\lambda, SZA) * A_{VCD}(\lambda) \qquad (3)$$

The O_3-cross-section is fitted to these spectra to determine the apparent O_3 slant column SCD_{app}. The apparent vertical O_3-column VCD_{app} is calculated by deviding by the averaged AMF:

$$VCD_{app}(SZA) = SCD_{app}(SZA) / AMF(SZA) \qquad (4)$$

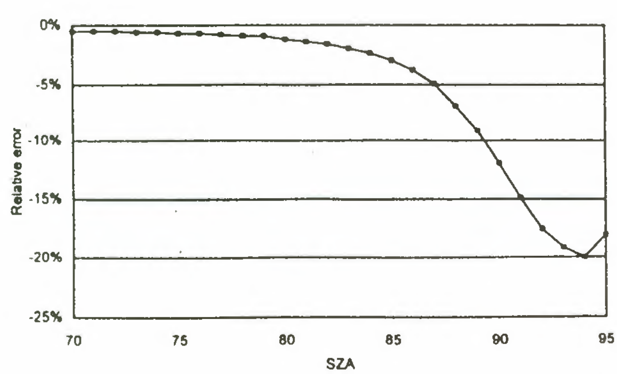

Figure 2: Relative error due to the fine structure of the O_3-AMF in the spectral region of 328-340nm as a function of solar zenith angle.

This VCD_{app} (SZA) is compared to the original O_3-column VCD_{true} to derive the respective error.

Figure 2 shows the relative error in dependence of the SZA. The relative deviation increases towards higher SZA with maximum deviation of about -20 %.

In Fig. 3 a typical diurnal variation of the O_3-VCD for ground-based UV-measurements is shown obtained by using the averaged AMF. While for smaller SZA's the VCD's are nearly constant, for higher SZA's there is a systematic decrease in the VCD's in agreement with the calculations.

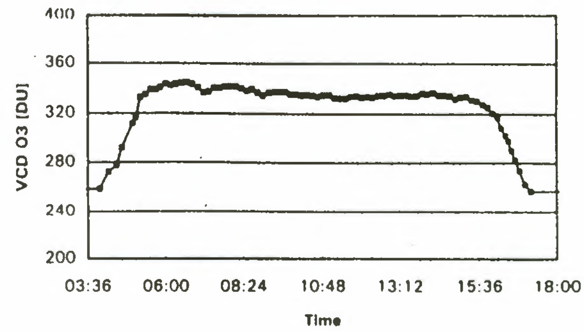

Figure 3: Diurnal variation of the measured O_3-VCD, Kiruna, March 18, 1994.

Although AMF for satellite geometry differs in principle from those for ground based observations a similar effect for the fine structure of the AMF in the O_3-Huggins bands was found for a single scattering radiation transfer model [Frank, 1991] (Figure 4). The difference of the AMF in the middle of the O_3-absorption band (333.8 nm) from the AMF beside (332.7 nm, 336 nm) is even larger for satellite geometry. Therefore a relative error up to 20 % for the O_3-evaluation in the UV is expected for the GOME-measurements at high SZA. This is in particular important for the observation of the O_3-VCD in the polar winter.

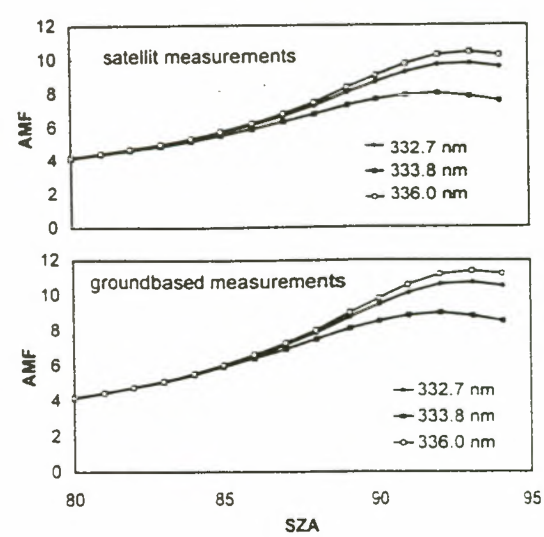

Figure 4: Comparison of the SZA-dependence of the UV-O_3-AMF for satellite and ground based measurements.

Correction of the Fraunhofer lines:

Several effects can cause a deviation of the fit coefficient of the Fraunhofer spectrum, SOL, from 1 if it is not fixed:

A) The Ring effect was not corrected exactly (e.g. because of a wrong or a missing Ring spectrum).

B) The spectral resolution of the measured spectrum and the Fraunhofer spectrum are different.

C) In the spectral region for the evaluation a spectrum contains large trace gas absorptions (e.g. at the Huggins bands or in the case of large H_2O- and O_4-absorptions).

D) The broad band structure of the measured spectrum and the Fraunhofer spectrum differs strongly (e.g. when clouds appear).

E) Possible SZA-dependent straylight in the spectrograph changes the depth of the measured Fraunhofer bands.

Examples for Case A), C) and D) are shown in Figure 5 to 7. The upper parts of the diagrams show the variation of the fit coefficient of the Fraunhofer spectrum and the lower part shows the correspondent error for the trace gas evaluations. The errors are calculated from the differences between the trace gas evaluations with unfixed SOL compared to the same evaluation with SOL = 1. Especially for large absorption enhancements of H_2O and O_4 due to tropospheric clouds [Erle, 1995] large errors up to 15 % have been detected.

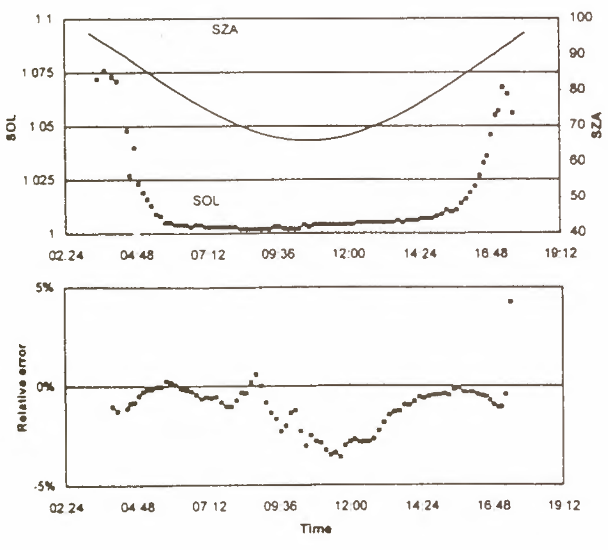

Figure 5: Top: Diurnal variation of SOL for the UV-O_3-evaluation, Kiruna, March 25, 1994.
Bottom: Relative deviation of the O_3-VCD.

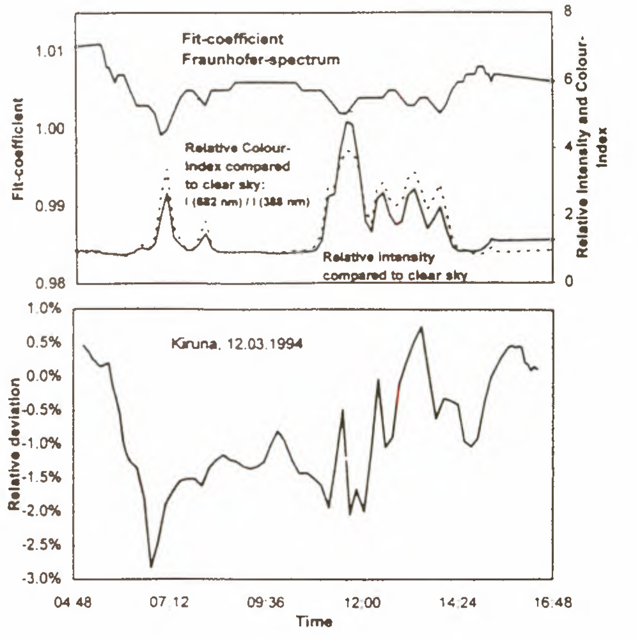

Figure 6: Top: Variation of SOL due to changes of the broad band signal of the measured spectra (Kiruna, March 12, 1994) when clouds appear. The periods of cloudy sky are indicated by enhanced light intensity and enhanced colour-index (ratio of intensities at 682 nm and 388 nm) compared to clear sky measurements [Wagner, 1995].
Bottom: Relative deviation of the O_3-VCD as determined by the fitting algorithm .

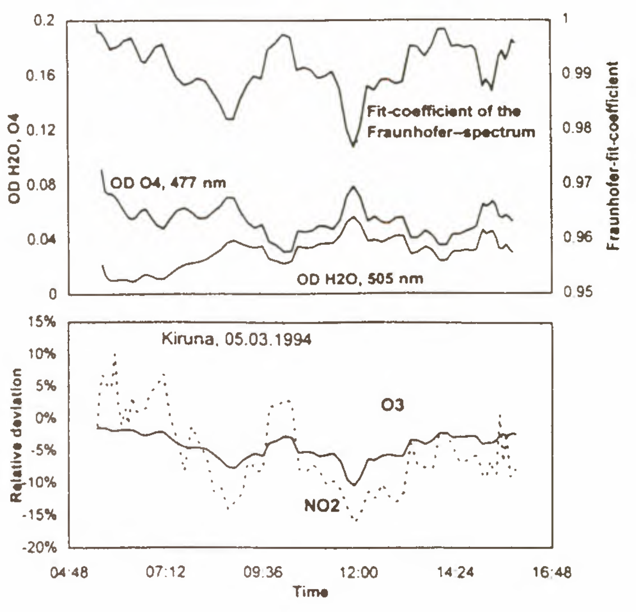

Figure 7: Variation of SOL for largely enhanced absorptions of tropospheric absorptions of H_2O and O_4 under cloudy skies.
Bottom: Relative error of the O_3-VCD and the NO_2-VCD.

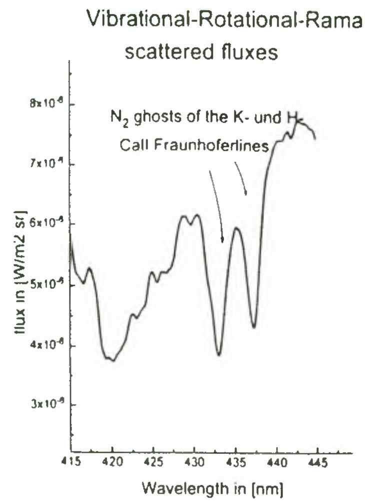

Figure 8: Vibrational-Raman-scattered light for ground based geometry and SZA=10°. The Fraunhofer ghosts of the CaII-K and H lines are calculated with a radative transfer model.

Although there is a consensus in literature of Rotational-Raman-scattering being the major cause of the Ring effect, there are other contributors like e.g Vibrational-Raman Scattering (VRS) [ESA,1996]. VRS leads to so called 'Fraunhofer ghosts' in scattered light spectra shifted by several nanometers (e.g 40nm) from the original Fraunhofer line in the solar spectrum (Figure 8). For example the differential optical densitiy of a ghost is expected to be around 0.1 % for a CaII-K Fraunhofer ghost at a resolution of 1.5 nm. These 'Fraunhofer ghosts' show a slight SZA dependence and lead to different structures in the Frauhofer reference spectra, taken at small SZA, and the spectrum taken and evaluated at the larger SZA. Especially when using a direct solar spectrum as the Fraunhofer reference which doesn't contain these ghosts, an additional error in the retrieval of the VCD's is made.

CONCLUSIONS

Due to the fine structure of the O_3-AMF for the UV large systematic errors up to 20 % are expected. This is confirmed by groundbased O_3-measurements in the UV. The SZA dependent deviation from the true O_3-VCD is qualitatively and quantitatively similar to the calculated values. Calculations of single O_3-AMFs for satellite geometry show that the error is expected to be at least of the same magnitude as for ground based measurements. This is in particular of great importance for the O_3-observations during the polar winter.

Because of its systematic behavior this error can be corrected by multiplying the derived O_3-VCD by the SZA dependent ratio VCD_{true} / VCD_{app} (equations 2, 4).

The same effect as in the UV is expected also for the Chappuis bands in the visible. Although it is about one order of magnitude smaller it should be corrected because of its systematic behavior.

Although there can occur smaller residuals if the fit coefficient of the Fraunhofer spectrum is not fixed to 1 there is no physical reason for a deviation of SOL from 1. The data evaluation of ground based DOAS measurements shows that SOL differs from 1 because of several reasons. The biggest errors of about 15 % occur when the absorptions of the tropospheric trace gases H_2O and O_4 are largely enhanced under cloudy skies.

Fraunhofer ghosts due to Vibrational-Raman-scattering lead to additional structures in scattered light spectra. Especially when using a direct solar spectrum as a Fraunhofer reference these ghosts may lead to an additional error in the retrieval of VCD's.

REFERENCES

[Bass, 1985] A. M. Bass, R. J. Paur, The ultraviolet cross-section of ozone: I. Measurements, *Atmospheric Ozone, Proc. Quadrenial Ozone Symp. 1985.*

[Erle, 1995] F. Erle, K. Pfeilsticker, U. Platt, On the Influence of tropospheric clouds on zenith-scattered-light-measurements of stratospheric species, *Geophys. Res. Lett., 22, 1995.*

[ESA,1996] J.Burrows, U.Platt, M.Vountas, H.Haug, K.Chance, L.Marquard, A.Richter, V.Rozanov, K.Muirhead, Study of the Ring Effect, ESA 10996/94/NL/CN, 1996.

[Frank, 1991] H. Frank, Ein Strahlungstransport-modell zur Interpretation von spektroskopischen Spurenstoffmessungen in der Erdatmosphäre, Diplomarbeit, Institut für Umweltphysik Heidelberg, 1991.

[Stutz, 1991] J. Stutz, Charakterisierung von Photodiodenzeilen zur Messung stratosphärischer Spurenstoffe, Diplomarbeit, Institut für Umweltphysik Heidelberg, 1991.

[Wagner, 1994] T. Wagner, Spektroskopische Messung stratosphärischer Spurenstoffe im arktischen Winter 1993/94: Abweichungen von der normalen Spurenstoffzusammensetzung, Diplomarbeit, Institut für Umweltphysik Heidelberg, 1994.

[Wagner, 1995] T. Wagner, T. Senne, F. Erle, C. Otten, J. Stutz, K. Pfeilsticker, U. Platt, Determination of Cloud properties and Cloud Type from DOAS-Measurements, *Poster at the Third European Symposium on Polar Stratospheric Ozone Research, Schliersee, Bavaria, 18-22 September 1995.*

ACKNOWLEDGEMNTS

We want to thank the ESRANGE-team from the measuring site at Kiruna for their friendly help.

Validation of GOME O_3 and NO_2 Measurements in Bremen, Ny-Ålesund, and Neumayer

A. Ladstätter-Weißenmayer, J. P. Burrows, A. Richter, F. Wittrock, M. Buchwitz, M. Weber

Institute of Environmental Physics, University of Bremen, Germany

M. Eisinger and R. Neuber

Alfred Wegener Institute for Polar and Marine Research, Potsdam, Germany

Abstract

During the commissioning phase of GOME, groundbased DOAS (Differential Optical Absorption Spectroscopy) measurements from the University of Bremen in Ny-Ålesund, Spitsbergen (79°N), and Bremen, Germany (53°N), combined with ozone sonde data from the Alfred Wegener Institute taken at the Neumayer Station in Antarctica (71°S) were compared with GOME retrieved O_3 and NO_2 vertical columns as part of the GOME validation effort between July 1995 and December 1995. It was found that GOME ozone values in Bremen and Ny-Ålesund tend on average to be 3–6% below the ground based results, while the sonde data at Neumayer were in good agreement with GOME. Coincident data sets from GOME and Neumayer sondes were unfortunately limited to three days in October 1995. The comparison between Ny-Ålesund, Bremen, and Haute Provence, France (44°N), did not show a clear dependence of the GOME ozone vertical columns on the solar zenith angle.

NO_2 vertical columns measured by GOME over Bremen and Ny-Ålesund deviate up to about +60% from the ground based measurements. It was concluded that large uncertainties in the airmass factor (AMF) due to uncertain tropospheric NO_2 content and the choice of reference spectra in the DOAS fitting are considered the major cause for the observed discrepancy. Based on our experience with the DOAS technique applied to both ground based and GOME measurements recommendations for future improvements of GOME data products are proposed.

1 Introduction

The Global Ozone Monitoring Experiment (GOME) is the first European passive remote sensing instrument operating in the ultraviolet, visible, and near infrared wavelength regions whose primary objective is the determination of the amounts and distributions of trace atmospheric constituents (Burrows *et al.* 1988, 1993).

The objective of this study was to validate the currently available GOME Data Processor (GDP) O_3 and NO_2 data products by comparison with ground based measurements and balloon borne sonde measurements. After the successful launch of GOME on the ERS-2 satellite on 21 April 1995 in Kourou, the first data products with O_3 and NO_2 vertical columns (level 2 products) were available at the end of July 1995. Ground based DOAS experiments of the University of Bremen using several UV and visible grating spectrometers in Bremen (53.1°N,8.9°E) and Ny-Ålesund (78.9°N,11.9°E) have been carried out on a routine basis since June 1994 (Richter *et al.* 1995, Wittrock *et al.* 1995). Between July and December 1995 daily mean values of vertical columns of O_3 and NO_2 retrieved from GOME ground pixels located within a 500km radius of each measurement site were cross-validated with the University of Bremen DOAS results. A total of forty-four days of GOME data were available for this study.

Polar ozone sonde experiments on balloon platforms are regularly carried out by the Alfred Wegener Institute in Ny-Ålesund and at Neumayer Station, Antarctica (70.6°S,8.4°W). Due to the limited availability of correlative measurement sets with GOME for the north polar region during the validation campaign, validation activities are only reported here for the Neumayer sonde experiments.

Section 2 briefly summarizes the setup of the University of Bremen DOAS spectrometers and ozone sonde experiments of the Alfred Wegener Institute. A brief description of the data analysis techniques employed in the different experiments is presented as well. The results of the comparison of our ground based DOAS and balloon-borne sonde measurements with O_3 and NO_2 vertical columns retrieved from GOME are reported in Section 3, followed by a discussion of the status of GOME validation (Section 4). Recommendations concerning improvements of the GOME vertical column retrieval of O_3 and NO_2 are given in Section 5.

2 Measurement Techniques

2.1 Ground Based DOAS

In Bremen two grating spectrometers in the Czerny-Turner configuration are employed for zenith sky measurements between 325–405 nm and 400–700 nm, respectively. Spectral resolution of the instruments is 0.25 and 0.9 nm, respectively. This is slightly worse than the 0.2–0.4 nm spectral resolution of the GOME instrument. The University of Bremen employs a third spectrometer of similar design in Ny-Ålesund (325–400 nm). All spectrometers are thermostated for improved wavelength stability and are equipped with Reticon diode array detectors which are cooled by Peltier elements to −40° C. A HgCd lamp is used for absolute wavelength calibration.

First trace gas measurements in Bremen were carried out in the winters of 1993 and 1994 and since June 1994 both instruments have been operated continously. Experiments in Ny-Ålesund were initiated in February 1995. At both locations trace gases such as O_3, NO_2, BrO, and $OC\ell O$ have been successfully measured (Richter *et al.* 1995, Wittrock *et al.* 1995, Eisinger *et al.* 1996).

O_3 slant columns are retrieved from the spectral window between 450 and 500 nm and NO_2 slant columns between 425 and 450 nm using the DOAS fitting technique. A description of the origin of DOAS and its approach is provided elsewhere (see Eisinger *et al.* in this issue). Laboratory spectra of ozone and nitrogen dioxide measured with the field instruments were used as references. Ring spectra, which have been recorded with the cross-polarizer method as described by Solomon *et al.* (1987), and an O_4 reference spectrum from Greenblatt *et al.* (1990) were included in the fitting procedure. Airmass factors needed for the conversion to vertical column densities were determined using the single scattering version of the AMFTRAN radiative transfer program written by H. Frank, University of Heidelberg. It has been shown that differences between single and multiple scattering are negligible for measurements carried out from the ground (Perliski and Solomon, 1993).

The University of Bremen DOAS spectrometers were cross-validated with other existing observation programmes such as TOVS, SAOZ (Jungfraujoch, 46.5°N, 8.0°E), Brewer (De Bilt, 52.1°N, 5.2°E), and GUV filter instrument. The validation of the ground based DOAS is summarized in Table 1. The percentages given in the table represent values of the standard deviation (1σ).

Table 1. Ground Based DOAS Validation

	Date	O_3	NO_2
	Bremen (53°N)		
SAOZ (47°N)	6/95–8/95	±8%	±10%
Brewer (52°N)	5/95–11/95	±6%	–
TOVS	5/95–12/95	±4%	–
	Ny-Ålesund (79°N)		
GUV	8/95–9/95	±1%	–

2.2 Sonde Measurements

The Alfred Wegener Institute carries out regular ozone soundings at its two polar stations, Koldewey in Ny-Ålesund, Spitsbergen, and Neumayer, Antarctica. Since correlative measurements from Koldewey sondes and GOME are available for only one day during this phase of the Validation Campaign, Koldewey sonde measurements are not considered further. The instruments used are balloon-borne electrochemical concentration cell (ECC) ozone sondes where an iodine-iodide redox reaction is used to transform the *in-situ* ozone concentration to an electrical current. The sondes are launched from ground and reach their maximum height of 30–35 km within about 2 hours. Ozone concentrations are measured with a height resolution of 100 m and an accuracy of ±5% in the lower stratosphere and ±10% elsewhere. This was established by several intercomparison campaigns (see e.g. *Hilsenrath et al.*, 1986).

Balloon trajectories are calculated by integrating the measured horizontal wind data. To determine vertical ozone columns the measured ozone number densities are integrated up to the balloon burst height. An estimated value for the column above the sonde is added assuming constant mixing ratio above burst height. Since the estimated columns amount to about only 10 % of the total column, the additional error on the total column introduced by this assumption is believed to be small. The accuracy of the total ozone column as determined from the sonde measurements is estimated to be ±5%.

An ozone profile measured at Neumayer on 7 October is compared to a profile from 5 August in Figure 1 illustrating the nearly complete ozone depletion in 14–18 km height in October.

3 GOME Validation

3.1 Bremen and Ny-Ålesund

GOME determines vertical columns of ozone and NO_2 with the DOAS technique and the validation of GOME also permits a comparison of this technique with different viewing geometries. Selection criteria for GOME data to be included in this study were that ground pixels are within a radius of 500 km of each observation site and that the solar zenith angle (SZA) is below 75° since the multiple scattering correction in the GOME Data Processor (GDP) is only applied for SZA< 75°. GOME usually passes over Bremen at around 10 am and the comparison was limited to daily morning mean (am) values from the ground based measurements. Due to more frequent overpasses in the polar region, Ny-Ålesund is covered by GOME at different times throughout the day (between noon and 8 pm) so that daily mean values of O_3 vertical columns are calculated for the entire day. Figures 2 and 3 depict GOME daily ozone values and measurements with the DOAS spectrometers in Bremen and Ny-Ålesund, respectively. The error bars

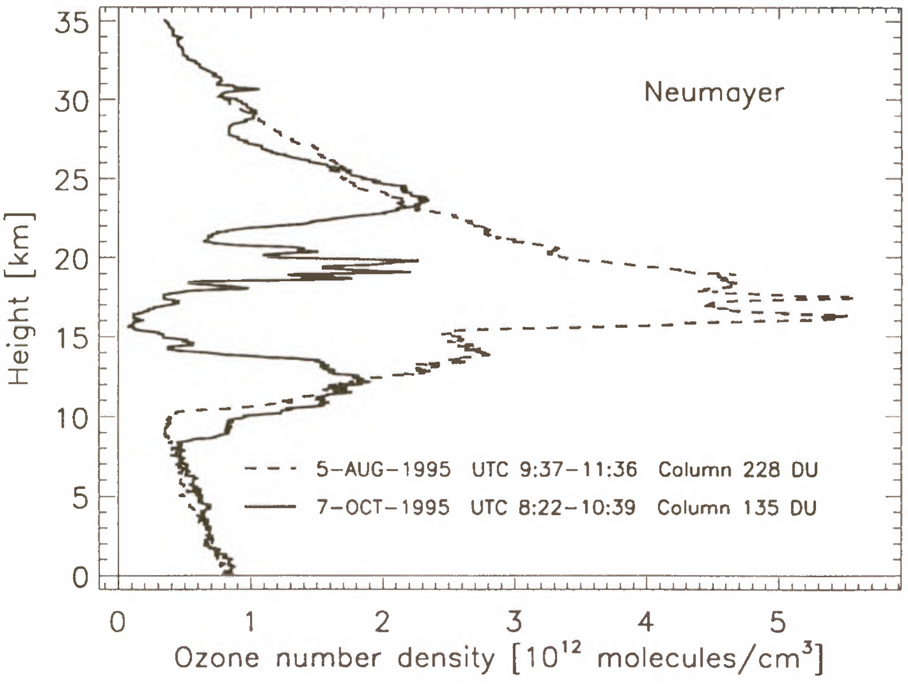

Figure 1: Ozone profiles as measured by ECC ozone sondes over Neumayer, Antarctica, on 5 August and 7 October 1995, the latter being near the annual "Ozone Hole" minimum. The two other profiles used in the comparison with GOME (1 October and 11 October) are very similar to the profile from 7 October.

indicate the spread (one standard deviation) of the GOME O_3 values within the chosen 500km radius.

For both locations the GOME ozone values tend to be on average 3 to 6% below our ground based results. In order to check whether a solar zenith angle dependence exist for GOME O_3, mean ozone ratios of Bremen and Ny-Ålesund are plotted in Fig. 4 along with the GOME ratios obtained at Haute Provence (43.6°N, 5.5°E) with the GOME breadboard model (BBM) (see also Türk *et al.* in this issue). The comparison with Haute Provence was chosen since the experimental setup and the DOAS fitting techniques used were similar to that of the University of Bremen. A consistent solar zenith angle dependence of the GOME deviations from ground based ozone measurements, as seen in Fig. 4 from the comparison between Ny-Ålesund, Bremen, and Haute Provence, is not observed. However, the limited data set available in the comparison is not sufficient to derive firm conclusions.

Figure 5 compares GOME NO_2 values in September 1995 with ground based DOAS measurements in Bremen. Only GOME NO_2 vertical columns which were derived from the 425–450 nm spectral range are shown. At both locations the NO_2 values from GOME exceed the ground based values by about 60%. A similar behavior is shown for Ny-Ålesund in Figure 6.

In order to explain the large differences observed for NO_2 the DOAS analysis of selected GOME spectra in September (Bremen) was repeated using the ground based DOAS routines in the same spectral window from 425 to 450 nm. Preflight GOME flight model (FM) reference spectra of O_3 and NO_2 at about 240 K and GOME FM Ring reference spectra were used in the DOAS fit. Airmass factors were determined using the latest version of the radiative transfer model GOMETRAN++ with implemented solar ray spherical geometry and multiple scattering (Rozanov *et al.* 1996). AMFs for cloudy ground pixels were determined assuming a cloud height of 4 km and cloud albedo of 0.8. The fractional cloud cover (ICFA) values provided with the GOME level 2 products were linearly interpolated between cloudless pixel AMF (albedo 0.33) and cloudy pixel AMF. In addition, a ghost vertical column below the assumed cloud top was added to obtain the total column as outlined in the GOME Level 1 to 2 Algorithms Description (1994). The NO_2 total columns retrieved from GOME spectra using the University of Bremen DOAS approach agreed now to within 20% with the ground based measurements (see Figure 5). The implications from this exercise are discussed in Section 4.

3.2 Neumayer

At Neumayer ozone sondes were launched twice a week yielding a total of 26 sonde measurements between 20 July and 31 October 1995. GOME data were available for selected days. Since in the present version of the level 1 to 2 processing software multiple scattering correction for the air mass factors has been applied for solar zenith angles below 75° only, GOME

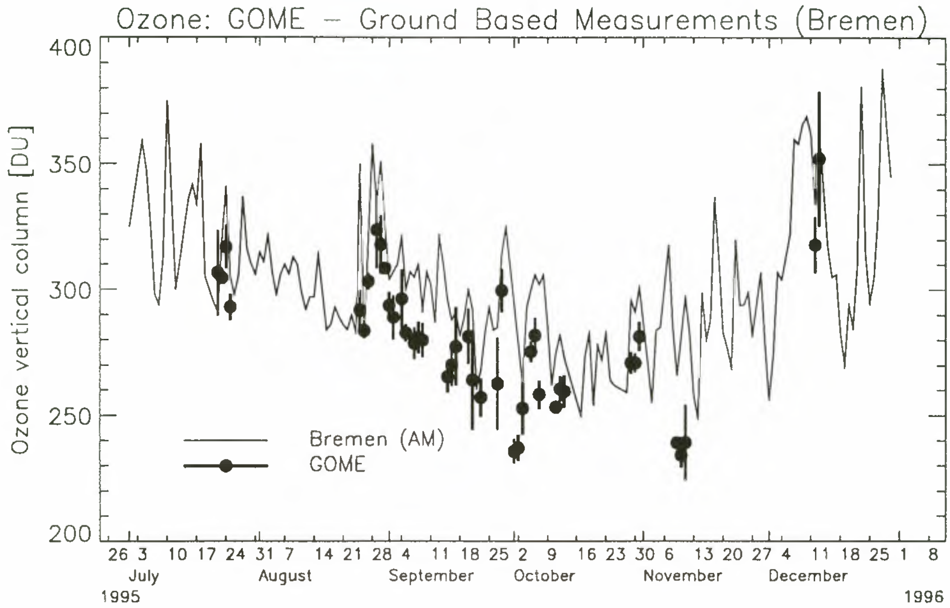

Figure 2: Comparison of O_3 vertical columns between ground based DOAS and GOME in Bremen (53°N). Diurnal and seasonal variation are well observed with GOME. In most cases GOME vertical columns lie slightly below the ground based values by a few percent.

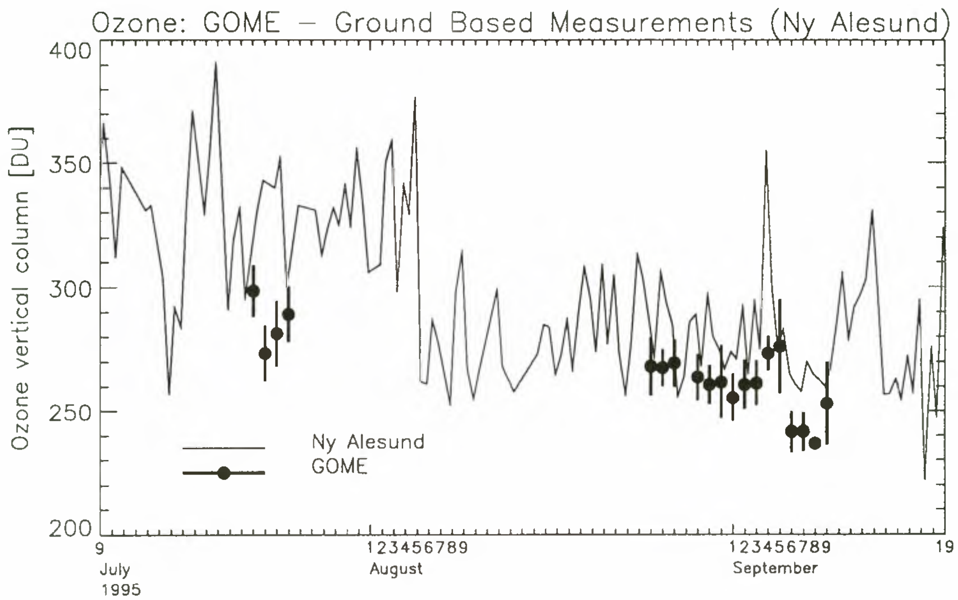

Figure 3: Comparison of O_3 vertical columns between ground based DOAS and GOME in Ny-Ålesund (79°N). Similar to Bremen (see Figure 2), GOME ozone values generally lie slightly below the ground based values. Comparison is not possible after mid September because of the missing multiple scattering correction for GOME data having solar zenith angles larger than 75°

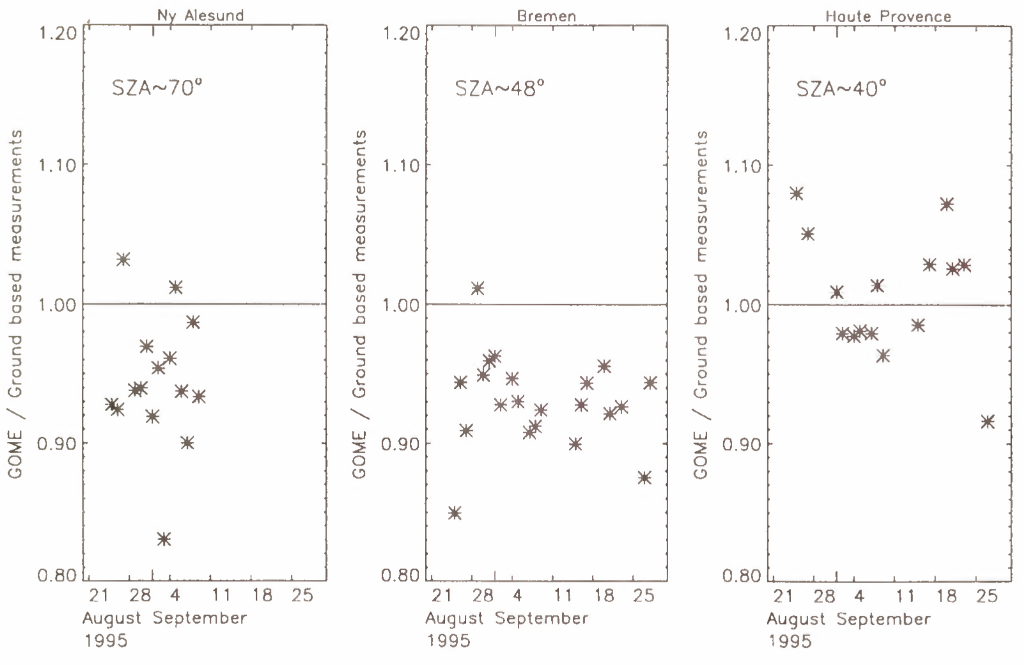

Figure 4: Comparison of O_3 vertical column ratios (GOME/ground based DOAS) in Ny-Ålesund (79°N), Bremen (53°N), and Haute Provence (44°N). A consistent solar zenith angle dependence of the GOME vertical column deviations can not be derived from this figure.

data before mid September have to be excluded from comparison with Neumayer. Three days are left for comparison: 1, 7, and 11 October 1995. At this time ozone columns within the Antarctic spring "Ozone Hole" reached their annual minimum.

The temporal coincidence has been optimized by adjusting the sonde launch times so that the sondes were within the lower stratosphere during the GOME overpass. To achieve best possible spatial coincidence only GOME ground pixels nearest to the sonde trajectory have been included in the comparison. The horizontal distance between GOME footprint and sonde trajectory is less than 300 km in all cases. Figure 7 shows the situation for 7 October.

Results for the three days are given in Table 2. Errors stated for GOME are the standard deviations for the selected ground pixels and for the sondes the ±5% intervals.

Table 2. Neumayer Sonde Comparison with GOME

Date	O_3 vertical column [DU] GOME	Sonde
1 Oct 1995	152 ± 5	151 ± 8
7 Oct 1995	147 ± 2	135 ± 7
11 Oct 1995	131 ± 4	130 ± 7

4 Discussion

Ground based DOAS: The agreement of the ozone vertical columns between GOME and ground based DOAS is generally satisfactory. The fairly large spread of GOME ozone values (up to 20% depending on the day) within the 500km radius may be explainable by spatial gradients in the atmospheric ozone distribution. Despite this fact a systematic trend of the mean GOME values being a few percent below the ground based results is observed. Sources of error may be, for instance, related to uncertainties in the calculated UV airmass factors. Improvements are expected to be achieved when the new version of the GDP software will be introduced and optimized based on recommendations by the GOME Science Advisory Committee. A critical review on the status of DOAS ozone retrieval in the UV and visible with GOME can be found elsewhere (see Eisinger *et al.* in this issue).

GOME NO_2 columns retrieved by the GDP exceed ground based values by up to 60%. A critical issue for NO_2 is the proper determination of airmass factors, which in turn depends on the right choice of NO_2 vertical profiles. In ground based measurements using the DOAS techniques, the large tropospheric content of NO_2 is generally neglected due to cancelling effects by ratioing spectra with a reference spectrum recorded at a nearby fixed solar angle. However, such cancellation effects do not exist for GOME since solar spectra are used as reference and, therefore, the tropospheric NO_2, its seasonal and diurnal variation as well as the climatology has a large influence on the GOME retrieved vertical columns of NO_2.

Radiative transfer calculations with GOMETRAN++ show differences up to 100% in the cal-

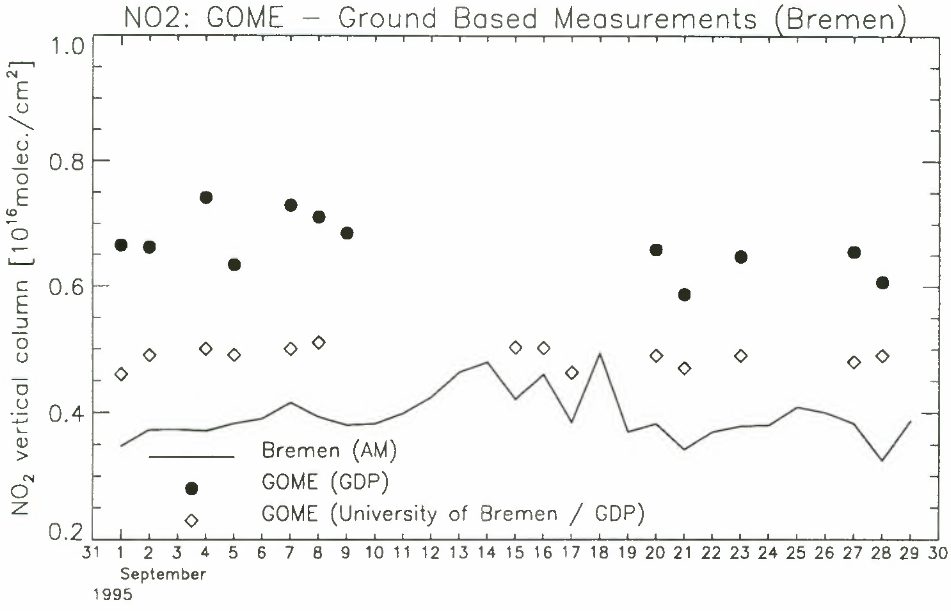

Figure 5: Comparison of NO_2 vertical columns between ground based DOAS and GOME in Bremen (53°N). The solid points are the daily averages from vertical columns (425–450 nm) as determined by the GOME Data Processor (GDP). The diamonds depict the daily mean values from GOME which were reanalyzed using the University of Bremen DOAS algorithm and the GOMETRAN++ radiative transfer model. Possible explanations for the discrepancies in the GOME values from the GDP and University of Bremen analysis are given in the text.

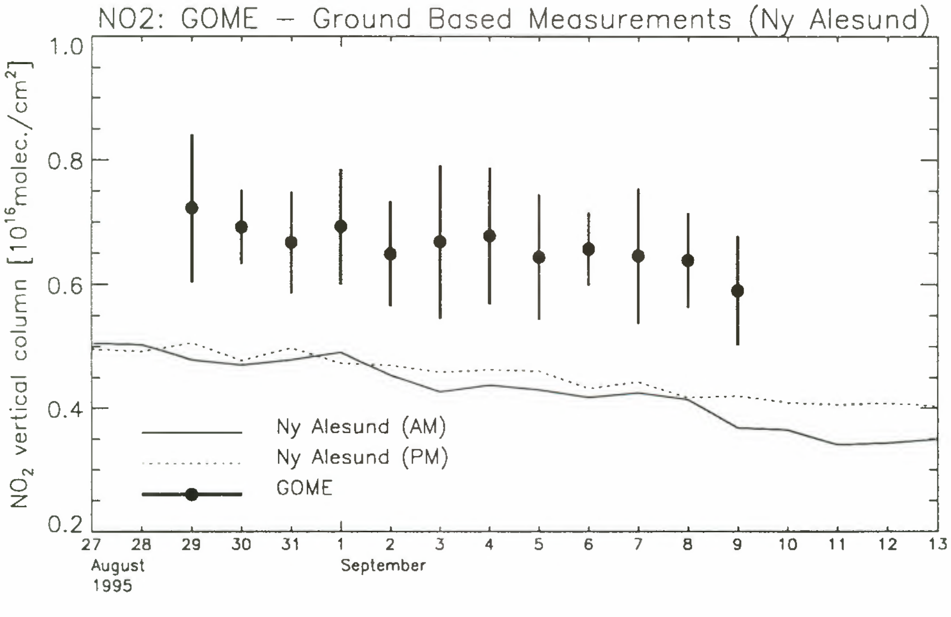

Figure 6: Comparison of NO_2 vertical columns between ground based DOAS and GOME in Ny-Ålesund (79°N). As in Figure 5, GOME values processed in the 425–450nm region are displayed. Only GOME spectra processed after 27. November 1995 were analyzed using the new spectral window. Comparison is not possible after middle of September because of the missing multiple scattering correction for GOME data with solar zenith angle larger than 75°. Note that Ny-Ålesund data were not subjected to the reanalysis as described in Fig. 5.

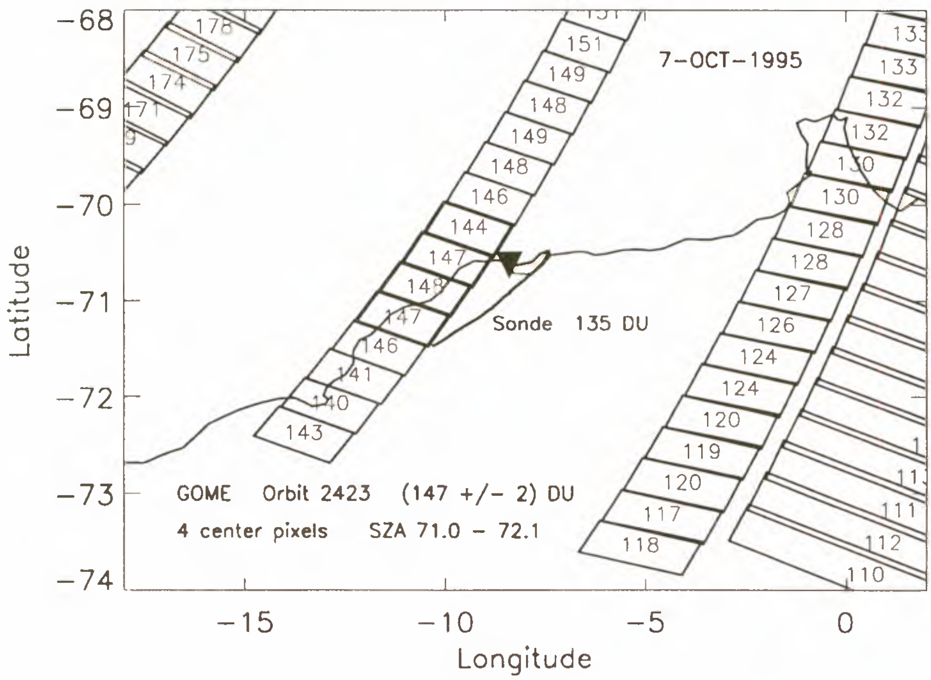

Figure 7: GOME overpass at Neumayer, Antarctica, on 7 October 1995, 9:18 UT. The thick line starting from the station (triangle) indicates the sonde trajectory. For each GOME ground pixel the ozone vertical column density from the GDP level 2 product is given. For comparison only the nearest pixels (emphasized) were selected. Note that the agreement between sonde and GOME measurement is somewhat better when the horizontal ozone gradient (which is believed to be real) is taken into account.

culated AMF if the surface albedo varies between 0 and 1. In addition, the height of a cloud layer (assumed as a boundary layer and Lambertian reflector) can be crucial in the AMF determination since cloud height determines how much of the tropospheric NO_2 is cut off from the radiative transfer. Even with the improvement achieved in our reanalysis, the errors in the vertical columns are still estimated to be large because of uncertainties in the diurnal variation of tropospheric NO_2. In our analysis a mid latitude vertical profile for 53°N and September was assumed and taken from the MPI Mainz 2-D chemo-dynamical model (Crutzen and Gidel, 1983; Brühl, 1992). For cloudy scenarios, the correction added to the measured vertical column in form of a ghost vertical column is substantial. Assuming our September profile and a cloud top height of 4 km, 55% of the total NO_2 column will be below the cloud top height. It is obvious that the measured vertical column is extremely sensitive to the variation in climatology. In general it is agreed that ground based DOAS measurements primarily determine stratospheric NO_2 vertical columns due to the cancellation effects of tropospheric NO_2 as mentioned earlier. For this reason NO_2 values retrieved with GOME are expected to be higher than the ground based values as observed in Figure 5.

Using reference spectra measured with the GOME FM at lower atmospheric temperatures (as in our DOAS analysis) rather than room temperature spectra from Schneider *et al.* 1987 (GDP analysis) has the effect of lowering the NO_2 slant columns derived from GOME spectra by about 15%.

Neumayer: Sonde and GOME measurements agree very well. Obviously, firm conclusions cannot be drawn from this 3-day comparison because of the limited amount of data covering only solar zenith angles between 70.8° and 74.7°, only center (near-nadir) pixels and only one climatological situation (described in the present GDP by latitude band and month). In fact, as O_3 profiles are strongly deviating here from the climatological profiles used for airmass factor calculation in the GDP it is expected that for non-ozone-hole situations the deviations of GOME from ground based measurements will be larger.

5 Conclusion and Recommendations

This comparative study has demonstrated that ozone values can be retrieved reliably from GOME. Some systematic trends in the GOME data have been observed when compared with the ground based DOAS measurements. Recommendations to improve the accuracy of the GOME ozone vertical columns using the DOAS technique are summarized elsewhere (see Eisinger *et al.* in this issue) and will not be repeated here.

It was shown that NO_2 vertical columns critically depend on the AMF and ghost column correction and, to less extent, on the proper choice of reference spectra. A better understanding of the vertical NO_2 profile, particularly, in the troposphere and the diurnal variations of tropospheric NO_2 is needed. The NO_2 AMF as well as the ghost vertical column correction strongly depend on the cloud top height and climatology assumed. The updated cloud climatology database planned for the new GDP release may improve the NO_2 retrieval. In many cases NO_2 may be only sufficiently determined at relative large solar zenith angles even in the 425–450 nm spectral window currently considered the optimum window for NO_2. It is recommended that GOME FM NO_2 reference spectra at atmospheric temperature be used in the GOME DOAS retrieval. The retrieval of NO_2 from GOME data is currently in an early stage and additional studies are required before routine retrieval of reliable NO_2 vertical columns will be possible in the near future. However, it was demonstrated that GOME is sensitive to tropospheric NO_2 which opens the intriguing possiblity to study separately tropospheric and stratospheric NO_2 amounts, ultimately leading to a better understanding of the dynamics and chemistry of this important atmospheric constituent.

GOME validation by comparison with ground based measurements in the polar regions has to be continued in order to cover all seasons and meteorological situations. It is planned to improve the comparison by calculating the ground pixels GOME actually "sees" based on the solar angles and the most probable scattering height. GOME data can then be interpolated from the "true" ground pixels to the sonde trajectories. Furthermore, the polar validation activities will be extended on other instruments such as Fourier transform spectrometer and filter measurements.

Acknowledgements

We thank A. Türk (ESA/ESTEC) for providing us with preliminary data obtained at Haute Provence with the GOME BBM. We also thank A. Piters (KNMI) and M. Rex (AWI) for helpful discussions during this project. We are grateful to S. Hofinger and T. Schmidt from Neumayer Station for their willingness to get up earlier than usual for the sonde launches. This study has been financed in part by the German Space Agency (DARA, FZK 50EE9439), the University of Bremen, the State of Bremen, and the European Space Agency (ESA).

References

Brühl, C., MPI Mainz, private communications, 1992.

Burrows, J. P., *et al.*, SCIAMINI, ESA Proposal, Published by Max-Planck-Institut für Chemie, Mainz, Germany, 1988.

Burrows, J.P., *et al.*, GOME Interim Science Report, ESA Special Publication 1151, 1993.

Crutzen, P.J., and L.T. Gidel, A Two-Dimensional Model of the Atmosphere. 2: The Tropospheric Budget of the Anthropogenic Chlorocarbons, CO, CH_4,$CH_3C\ell$ and the Effect of Various NO_x Sources on Tropospheric Ozone, *J. Geophys. Res.*, **88**, 6641–6661, 1983.

Eisinger, M., *et al.*, I. BrO Measurements over Bremen (53°N) 1993-1994, submitted to *J. Atm. Chem.*, 1996.

Gome Level 1 to 2 Algorithms Description, Technical Note ER-TN-DLR-GO-0025, Issue 1A, DLR Oberpfaffenhofen, Germany, 1994.

Greenblatt, G.D. *et al.*, Absorption Measurements of Oxygen between 330 and 1140 nm, *J. Geophys. Res.*, **D95**, 18577–18582, 1990.

Hilsenrath, E., *et al.*, Results from the Balloon Ozone Intercomparison Campaign (BOIC), *J. Geophys. Res.*, **D91**, 13137–13152, 1986.

Perliski, L.M., and S. Solomon, On the Evaluation of Air Mass Factors for Atmospheric Near-Ultraviolet and Visible Absorption Spectroscopy, *J. Geophys. Res.*, **D98**, 10363–10374, 1993.

Richter, A., *et al.*, Ground Based UV/Vis Measurements of O_3, NO_2, BrO, and $OC\ell O$ over Bremen (53°), *Proc. 3rd Europ. Symposium on Stratospheric Ozone 1995, Schliersee* in press.

Rozanov, V., *et al.*, GOMETRAN: A Radiative Transfer Model for the Satellite Project GOME - The Plane-Parallel Version, submitted to *J. Geophys. Res.*, 1996.

Schneider, W., *et al.*, Absorption Cross Sections of NO_2 in the UV and Visible Region (200-700nm) at 298 K, *J. Photochem. Photobiol. A*, **40**, 195–217, 1987.

Solomon, S., *et al.*, On the Interpretation of Zenith Sky Absorption Measurements, *J. Geophys. Res.*, **D92**, 8311–8319, 1987.

Wittrock, F., *et al.*, Ground Based UV/Vis Measurements of O_3, NO_2, BrO, and $OC\ell O$ over Ny-Ålesund (79°N,12°E), *Proc. 3rd Europ. Symposium on Stratospheric Ozone 1995, Schliersee* in press.

A. Ladstätter-Weißenmayer, J. P. Burrows, A. Richter, F. Wittrock, M. Buchwitz, and M. Weber, Institute of Environmental Physics, University of Bremen, PO Box 330440, D-28334 Bremen.

M. Eisinger and R. Neuber, Alfred Wegener Institute for Polar and Marine Research, D-14401 Potsdam.

GOME Validation Project D-131

Studies on DOAS Ozone Column Retrieval from the UV and Visible Measurements of GOME

M. Eisinger, A. Richter, J. P. Burrows

Institute of Environmental Physics, University of Bremen, Germany

A. Piters

Royal Dutch Meteorological Institute, De Bilt, The Netherlands

Abstract

Various aspects of ozone column retrieval from GOME channel 2 and 3 spectra by the Differential Optical Absorption Spectroscopy (DOAS) method have been investigated. DOAS evaluation has been performed on GOME level 1 data. In the UV some sensitivity tests have been undertaken and improvements for the GOME Data Processor (GDP) are suggested. In the visible region the suitability of four different wavelength windows for ozone column retrieval has been investigated. Ozone columns retrieved by the GDP both in the UV and the visible have been compared. The results indicate a good potential for the visible but still columns on average 30% higher than from the UV. The largest deviations occur at small ICFA cloud fractions. Finally, it is recommended to modify the calculation of air-mass factors in the GDP. For the future a combination of UV (for low solar zenith angles) and visible (for high solar zenith angles) ozone is proposed.

1 Introduction

The remote sensing of atmospheric gases from ground-based, balloon-borne, aircraft or satellite platforms utilizes the characteristic absorption or emission features of a particular gas. Remote sensing of ozone has been shown to be possible from the UV to the microwave spectral regions. Each part of the electromagnetic spectrum, coupled with a particular viewing geometry has specific advantages and disadvantages for the retrieval of ozone for different parts of the atmosphere (*Ozone Measuring Instruments...*, 1989).

The GOME (Global Ozone Monitoring Experiment) is a new instrument launched aboard ERS-2 in April 1995. GOME observes the spectral region from 240 to 790 nm (*Burrows et al.*, 1988; *GOME Interim Science Report,* 1993).

In the wavelength range covered by the GOME instrument both the Hartley-Huggins bands in the near UV and the Chappuis bands in the visible can be utilized to determine atmospheric ozone columns. Traditionally, ozone has been retrieved from the UV spectral information by the SBUV/TOMS satellite instruments and by ground-based Dobson, Brewer, and several filter instruments. Alternatively in ground-based zenith-sky measurements ozone columns are usually calculated from the visible absorption bands.

Currently the ozone columns in the GDP *main* product are derived from the UV (GOME channel 2) via the DOAS method. A major advantage of the UV is the high signal-to-noise ratio for the absorbances because differential absorptions are more than ten times larger in the Huggins bands than in the Chappuis bands. However, the retrieval of ozone from the UV has several disadvantages as well. The most important are the temperature dependence of differential absorption cross sections and the wavelength dependence of air-mass factors (AMFs) by which the slant column densities from the DOAS fits have to be divided in order to get vertical column densities.

The objective of this study was to investigate a number of aspects of relevance to the DOAS ozone retrieval in both the UV and visible spectral regions. This is of great importance for the GOME data interpretation and usage. In the following sections several aspects of DOAS ozone retrieval in both the UV and the visible bands are discussed. Section 2 describes tests performed using level 1 data (radiances/irradiances). Section 3 compares ozone vertical columns retrieved from the UV and visible as given by the GOME Data Processor (GDP) in the level 2 product.

2 DOAS studies using GOME level 1 data

Measurements of atmospheric trace gas columns employing the difference in absorption at different wavelengths date back to the time of *Dobson* (1926), who used wavelength pairs to derive ozone columns. *Noxon* (1975) derived NO_2 columns from the depth of absorption bands in continuous spectra. The differential absorption technique became a standard method for zenith sky measurements (e.g. *Noxon et al.,* 1979, *Solomon et al.,*, 1987). The term DOAS (Differential Optical Absorption Spectroscopy) was first applied to long-path measurements of tropospheric trace gases (e.g. *Perner and Platt,* 1979). DOAS was chosen as the method for operational retrieval of trace gas columns from GOME measurements. It is the first time this method has been applied to measurements from space-borne instruments.

DOAS evaluation was performed on GOME level 1 data as extracted by the DLR program gdp01_ex (version 1.71) with all options[1] set "on" except unit conversion. The DOAS fit runs presented in this study were performed with the program which is used for analysing the ground-based zenith-sky measurements of the Bremen group (e.g. *Richter et al.,* 1995). (From this program the operational DOAS routine in the GDP was developed.) Given the solar irradiance $I_0(\lambda)$ and the earth radiance $I(\lambda)$ measured by GOME, and the differential absorption cross sections $\sigma_i'(\lambda)$ of the relevant species, their slant column densities L_i are fitted together with polynomial coefficients c_j according to the Lambert-Beer law

$$\ln I(\lambda) = \mathrm{SOL} \ln I_0(\lambda) - \sum_i L_i \sigma_i'(\lambda) + \sum_j c_j \lambda^j .$$

For a discussion of the additional fit parameter "SOL" see below. "SOL" is set to 1 unless otherwise stated.

2.1 Reference spectra

Absorption cross sections of ozone and NO_2 have been measured as a function of temperature with the GOME flight model (FM) (*Dehn,* 1995; Final Report to ESA in preparation). In this study O_3 cross sections measured at $T = 221$ K and NO_2 cross sections measured at $T = 241$ K have served as references.

The empirical spectrum used to account for the Ring effect, the partial filling-in of Fraunhofer lines in earthshine radiances by inelastic (mainly Raman) scattering, was also measured with the GOME FM (*Burrows et al.,* 1995).

It is recommended to use the ozone, NO_2, and Ring spectra measured with the GOME FM for operational processing. This was already substantiated in detail during the Validation Campaign. Tests on GOME level 1 data showed that the fit using the GOME FM O_3 and NO_2 data was superior (i.e. resulted in less residual error) to any literature spectra available (*Bass and Paur,* 1985; *Schneider et al.,* 1987; *Harwood and Jones,* 1994). The main advantage of using the GOME FM reference spectra for DOAS analysis of GOME FM in-orbit data arises from their having appropriate spectral resolution so that convolution with the instrumental slit function is not necessary.

For O_4 the measurements by *Greenblatt et al.* (1990) with some corrections to the wavelength axis proposed by *Burkholder* were used. The spectrum of H_2O was calculated (*Chance,* 1994) from the HITRAN database and convoluted with the GOME slit function.

Since GOME spectra are given in vacuum wavelengths all trace gas references were converted to vacuum wavelengths according to the *Edlén* (1953) formula.

[1]These options are controlling the calibration steps to be applied on the raw (level 0) data: Leakage / fixed pattern noise / straylight correction, normalisation (Binary Units (BU) $\rightarrow$ BU/s), polarisation correction, radiometric calibration (BU/s $\rightarrow$ mW/m^2.nm.sr), unit conversion (mW/m^2.nm.sr $\rightarrow$ photons/s.m^2.nm.sr).

2.2 Ultraviolet window tests

The UV fitting window used in the present GDP, 325–335 nm, was chosen for the tests described below. They were performed on a set of 57 ground pixels from orbits 1351 and 1352 (24th July 1995) covering the complete solar zenith angle range from 19° to 93°. O_3 was the only trace gas fitted (with the exception of the tests described in the next paragraph).

NO_2

Fit runs were performed with and without NO_2 as species in addition to ozone. For most ground pixels negative, i.e. unphysical, NO_2 slant columns with large fit errors were found. This is explained by the small absorbance of NO_2 compared to O_3 in the UV window. NO_2 normally cannot be found because uncertainties in the ozone cross sections and the wavelength dependence of the AMFs (which are neglected) are of the same order of magnitude as the NO_2 differential spectrum in this region.

Including NO_2 in the fitted species, however, leads to a reduction of the retrieved ozone slant columns of up to 4% for solar zenith angles above 80°. (For smaller zenith angles the effect on ozone is quite small.) It is therefore recommended to use only ozone as trace gas reference for the UV fits.

A quality control test is however also recommended. This involves the determination of the NO_2 slant column in the window 425–450 nm and subsequently estimation of the UV NO_2 differential absorption. Provided the latter is less than 1% of the O_3 absorption then NO_2 can be neglected in the UV window.

Solar irradiance in linear fit

Comparison of fits where the factor "SOL" is a free parameter and fits with "SOL" fixed to 1 were made. The only trace gas considered was ozone. Note that "SOL" is an exponent for the solar irradiance I_0 and that there is no physical reason for it to have a value other than 1. If "SOL" is included as a fit parameter its value ranges between 0.86 and 0.96 and ozone fit errors are drastically reduced. The reason is that a "SOL" factor less than 1 at least in part accounts for the Ring effect, because "Ring(λ)" correlates strongly to $(I_0(\lambda))^{-1}$. However, including the solar irradiance in the linear fit can have quite a strong impact on the ozone slant columns. Ozone slant columns where "SOL" was fitted were up to 12% higher than with "SOL"= 1. The proper way to take account of the Ring effect is fitting an empirical (i.e. measured) or theoretical "Ring spectrum" in addition to ozone and to fix "SOL" to 1, i.e. to exclude the solar irradiance from the linear fit. This strategy is strongly recommended, both for the UV and the visible region.

Temperature dependence

The differential absorption cross sections in the Huggins bands decrease with increasing temperature (Figure 1). For the "classical" DOAS fitting an ozone spectrum at a certain temperature has to be chosen, thereby neglecting the real temperature profile of the atmospheric ozone. In the GDP the temperature at the ozone concentration maximum from climatology is selected. To estimate the error introduced by deviations of the actual temperature from climatology, fits were performed with ozone reference spectra measured by the GOME flight model at $T = 202$ K, $T = 221$ K, and $T = 241$ K.

It was found that raising the temperature of the ozone reference by 20 K increased the ozone slant column density calculated by the DOAS fit (and thereby the vertical column) by 6%. This implies a temperature effect of 0.3%/K or, put into a simple rule of thumb, assuming an ozone vertical column of 330 DU: 1 K temperature deviation means 1 DU ozone deviation[2]. In this simple estimation the atmospheric temperature profile has been neglected.

In conclusion it is vital in GOME ozone validation to regularly check the deviations of the actual temperature profile from the climatology used in the GDP because these deviations might lead to systematic errors of a few percent in the retrieved ozone column. For example, in winter 1995/96 stratospheric temperatures over the Arctic have been unusually low for several weeks (*von der Gathen,* 1996). The GDP, assuming climatological values, is expected to somewhat overestimate ozone columns in this situation.

Air-mass factors

Air-mass factors for scattered light observations depend on a large number of parameters, e.g. the measurement geometry (solar zenith angle, line-of-sight zenith angle, relative azimuth), wavelength, air and ozone density profiles, aerosol loading and the density profile of the molecule considered. For the ozone Huggins bands the situation is special because of their large absorption. The atmosphere cannot be considered optically thin at these wavelengths. At ozone absorption minima the light penetrates deeper into the atmosphere, leading to a lowering of the most probable scattering height compared to absorption maxima. Thus UV AMFs are significantly dependent on wavelength (much more than VIS AMFs). An example is shown in Figure 2.

The AMF follows the shape of the ozone absorption bands, being lowest in the absorption maxima. It varies between 4.69 and 4.87 or by 3.8% over the fitting window in this example[3]. In the present GDP the "classical" DOAS approach is implemented. The AMF is calculated for the window center wavelength, i.e. 330 nm, where the AMF is near its upper limit. Thereby systematic errors are introduced which possibly lead to ozone columns which are too low. Since the wavelength dependence of the AMF is larger for larger slant columns, these errors are expected to increase with increasing solar zenith angles.

Furthermore, the AMFs in the UV are more sensitive to the ozone total column, the ozone vertical profile, and the stratospheric aerosol loading, than the AMFs in the visible. In addition, the temperature profile influences absorption and thereby also the AMF. More detailed AMF sensitivity studies for "real" GOME situations are clearly needed, but it is safe to say that, considering the atmospheric variability, there are large uncertainties in the UV AMFs due to (at present necessary) simplifications in level 1 to 2 processing, and that these uncertainties are largest for large solar zenith angles. AMFs will be a key issue both in understanding GOME deviations from ground-based measurements and in future improvements of the algorithm. It is recommended that in the long run "classical" DOAS where ozone absorption cross sections (at a certain temperature) are fitted, is replaced in the UV by "modified" DOAS where the wavelength dependence of the AMF is taken into account by fitting optical densities calculated by a radiative transfer model.

2.3 Visible windows tests

In the visible wavelength range several wavelength windows within GOME channel 3 were tested in order to derive an optimum for ozone retrieval. These tests were performed on orbits 1322 (22nd July 1995, the first GOME orbit available) and 2123 (16th September 1995).

Based on *Diebel et al.* (1995) the following criteria have to be applied for window optimisation:

1. strong differential ozone absorption structures;

[2]Note that this number depends on the fitting window. It is given for the 325–335 nm window.

[3]The AMF can be evaluated at any wavelength within the fitting window since the center wavelength is not *a priori* suited better than other wavelengths. [For the 325–335 nm window the center wavelength is probably even a bad choice. Note that at 330 nm the temperature dependence of the absorption cross section (and thereby of the AMF) is relatively large.] Choosing another AMF wavelength can result in vertical columns shifted by a few percent. However, it is recommended to refer to physical reasons for choosing the AMF wavelength(s) rather than to fine-tune vertical columns by adjusting the AMF wavelength.

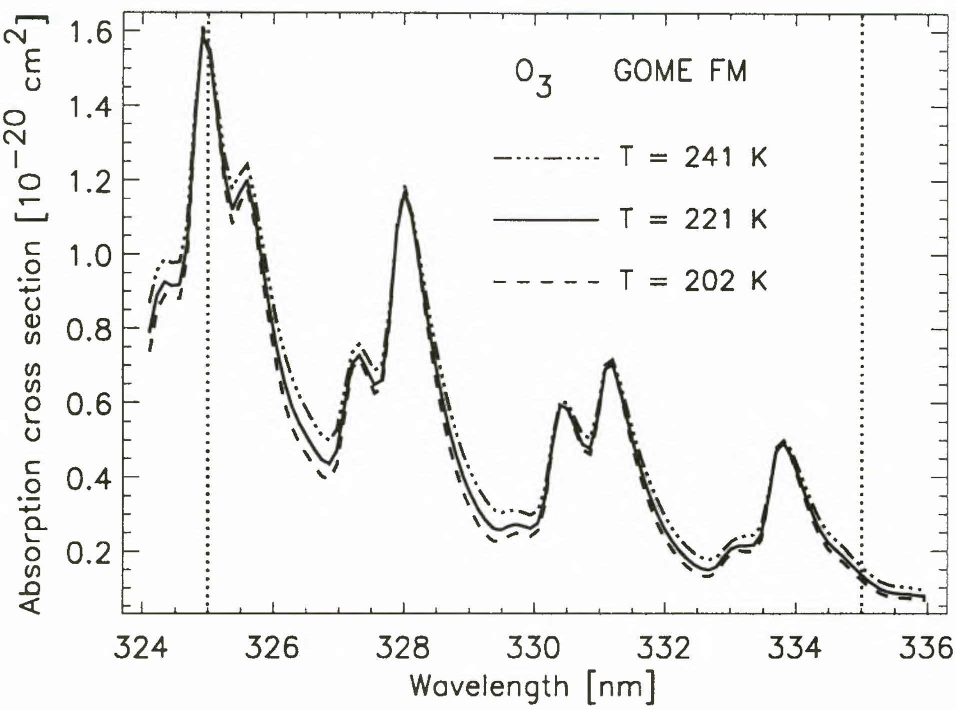

Figure 1: Absorption cross sections of the ozone Huggins bands as measured with the GOME flight model at $T = 202$ K, $T = 221$ K, and $T = 241$ K. The vertical dotted lines denote the present UV fitting window in the GOME Data Processor.

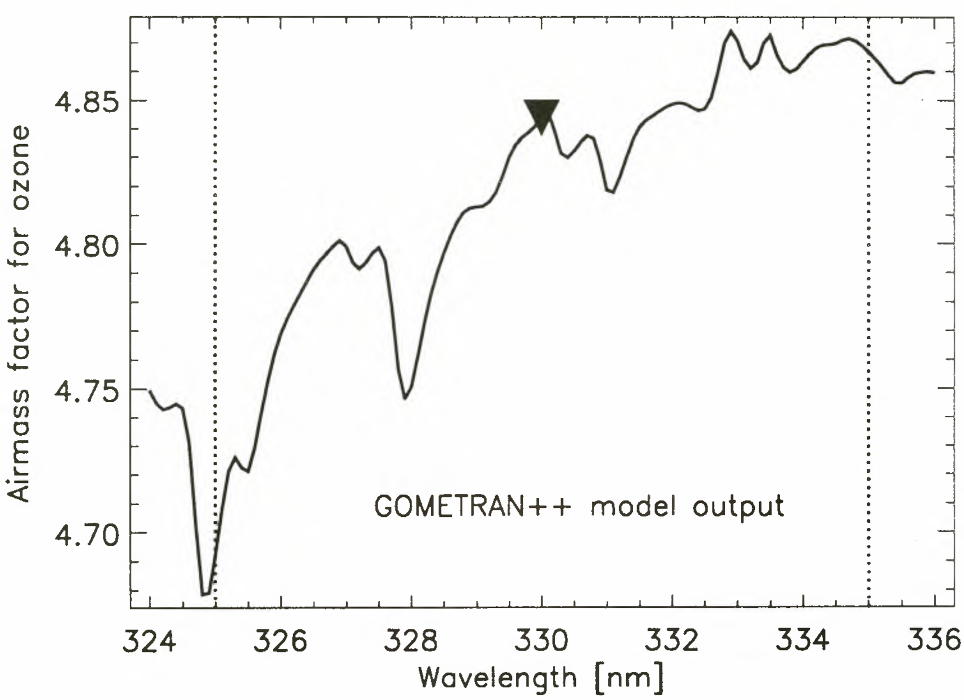

Figure 2: Air-mass factor for ozone as calculated by the radiative transfer model GOMETRAN++. Scenario: solar zenith angle 77°, line-of-sight zenith angle 0.5°, relative azimuth 119°, January, latitude band 50–60°N, ozone vertical column 348 DU. Trace gas reference spectra as described in section 2.1. The triangle indicates the air-mass factor at window center which is used in the GOME Data Processor for conversion to vertical columns.

2. minimal interference by O_4, H_2O, and by strong Fraunhofer lines;
3. window size between 100 and 300 pixels (20–60 nm in the visible);
4. moderate variations of the air mass factor across the window;
5. high signal-to-noise ratio;
6. no crossing of GOME channel boundaries;
7. minimal interference by instrumental features such as etaloning and polarisation sensitivity effects.

The last item has been added to the *Diebel et al.* list after the experience with the GOME data (see below). Differential absorptions of the relevant species are shown in Figure 3. Ozone differential absorptions are largest above 490 nm while interference by O_4 and H_2O is smaller below 500 nm, so that the first two criteria compete against one another and a compromise has to be found.

Three wavelength windows were studied in detail:

- 425–450 nm (A);
- 450–500 nm (B);
- 500–565 nm (C).

Window A (425–450 nm, fit: O_3, NO_2, Ring)

This window is well suited for NO_2 retrieval (Figure 4). However, the differential absorption cross sections of ozone are only about $6 \cdot 10^{-23}$ cm^2 peak-to-peak in this region. Assuming for example an ozone vertical column of 300 DU and an AMF of 4 (corresponding to a solar zenith angle around 70°), a differential optical density of only $2 \cdot 10^{-3}$ results. (For comparison: The UV differential optical density around 328 nm for the same slant column would be near 0.3 which is larger by a factor 150.) Additional errors can easily be introduced by a changing etalon effect. As a result ozone fits are not recommended to be used from this window.

Window B (450–500 nm, fit: O_3, NO_2, O_4, Ring)

This or a similar window is commonly used for determining ozone columns from ground-based DOAS measurements. Ozone differential absorptions are about five times higher than in window A. It includes only weak water absorption bands and an O_4 band which does not correlate with ozone. However, the GOME measurements are compromised by residuals dominated by "dichroic ripples" (Figure 5). These are introduced by the wavelength dependence of the instrumental nadir polarisation sensitivity η, which is dominated in this wavelength region by the behaviour of the dichroic mirror separating the light between GOME channels 3 and 4. (For details see *Eisinger et al.*, this issue.) Until the η issue in the key parameters is resolved, this window is also not to be recommended for O_3 retrieval.

Window C (500–565 nm, fit: O_3, NO_2, O_4, H_2O)

As ozone absorption cross sections are comparable to those in window B ozone fit errors are expected to be relatively small in this window. The polarisation sensitivity η is smooth (no small-scale structure) and should not disturb the fits. Indeed, when solar zenith angles are not too low, ozone can be fitted with low residuals (Figure 6). However, an O_4 band at 530 nm and (although to a less extent) two H_2O bands at 500–513 nm and 537–554 nm are interfering with ozone absorption bands. Interference is confirmed by the differences in the fitted O_3 slant columns if O_4 (or H_2O) are also fitted in addition to O_3. The differences can be 10–20%. The ozone columns from this window are also sensitive to the order of the fitted polynomial. They are higher for a 4th order polynomial than for a 2nd order polynomial. This means the polynomial might interfere with ozone absorption.

For operational processing it is important to note that windows B and C are large (containing 240–310 detector pixels), thus increasing the computer time per DOAS fit considerably.

Summary

It is clear that window A is not suited for ozone fits in the visible. The choice between window B and C depends mainly on the evolutionary status of the GDP. In the long run improvements in the polarisation correction should result in reliable ozone fits using window B. In the meantime window C represents a good alternative. Interference by O_4 and H_2O, however, has to be carefully investigated. In the next section some GDP results from a window similar to C will be discussed. This window (C') has been made somewhat smaller than C to reduce processing time. Unfortunately, thereby also O_4 interference is increased (compared to C).

3 Validation of ozone columns retrieved in the VIS window

In this section the total ozone vertical columns retrieved from the 510–560 nm (VIS) window (C') are compared with the total ozone column retrieved from the 325–335 nm (UV) window. Both ozone columns were derived with the GDP level 1–2 software (version 1.20). The DOAS fitting included the following species: O_3, NO_2, and BrO in the UV window and O_3, NO_2, and O_4 in the visible window. The solar spectrum was included in the linear part of the

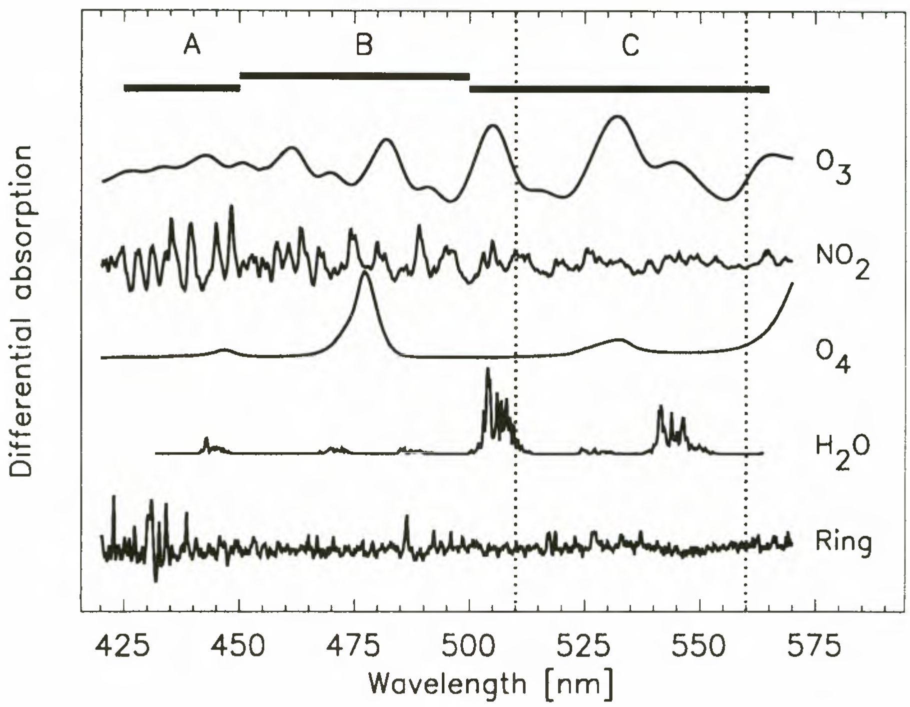

Figure 3: Differential absorptions of the most important gases and empirical "Ring spectrum" in the visible part of the spectrum (GOME channel 3). Note that the amplitudes are not to scale. The bars indicate the three test windows used in this study. The vertical dotted lines are the borders of the VIS fitting window C' used by the GDP in version 1.20 (until November 1995). Results from this window are discussed in section 3. In Version 1.21 the GDP moved to window A.

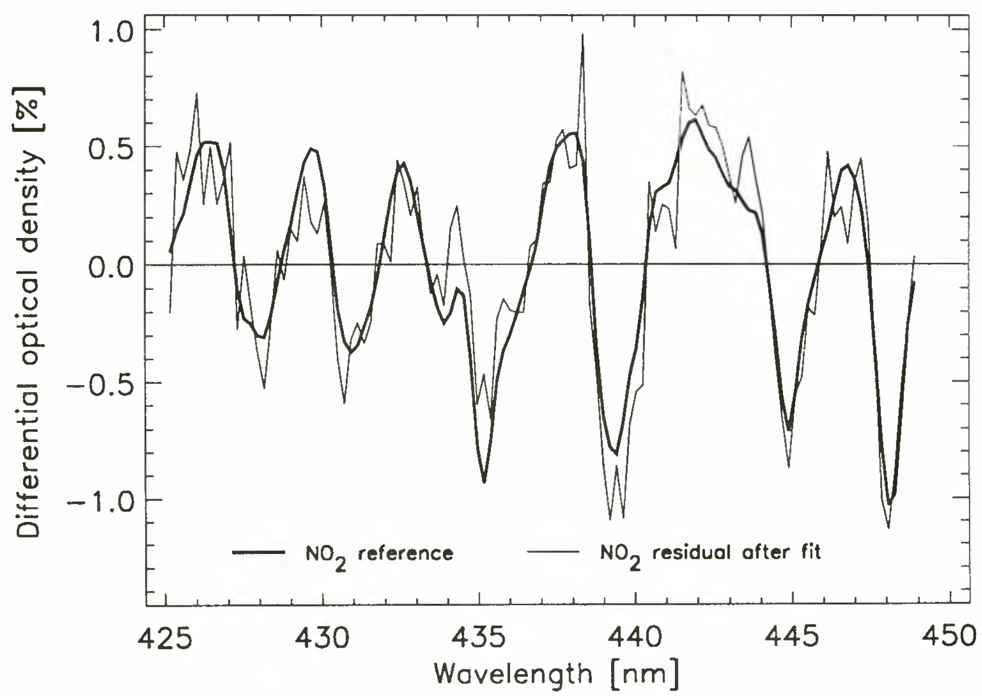

Figure 4: Window A: NO_2 fit results for groundpixel 3206 from orbit 2123 (16th September 1995, 11:12:42 UT, integration time 6 s, solar zenith angle 86.97°, latitude 81.04°N, longitude 99.27°E).

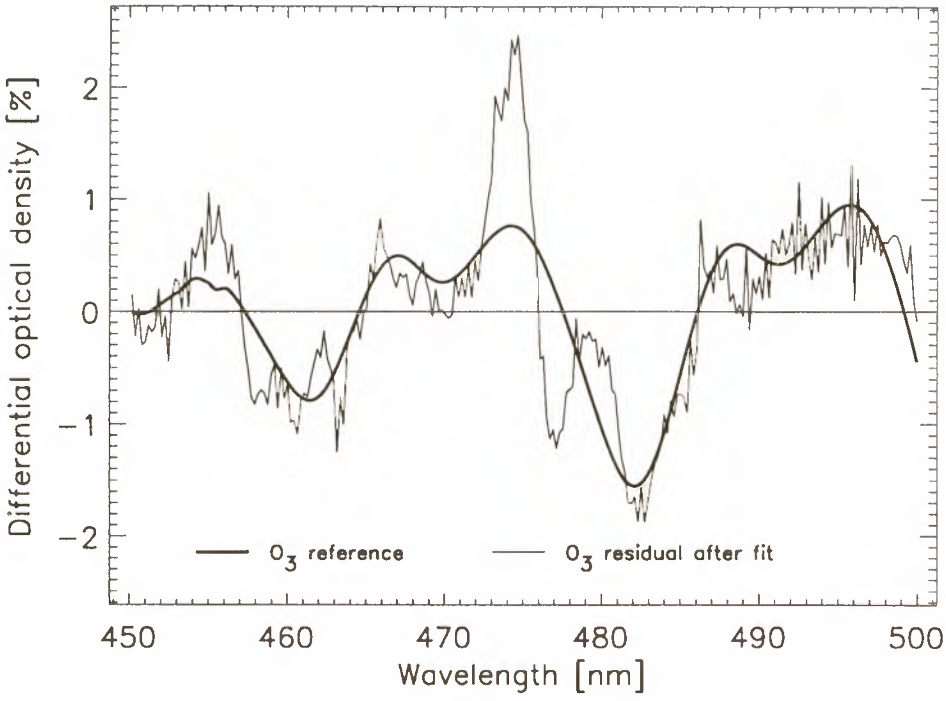

Figure 5: Window B: O_3 fit results for groundpixel 3236 from orbit 2123 (16th September 1995, 11:13:29 UT, integration time 1.5 s, solar zenith angle 84.37°, latitude 84.23°N, longitude 80.23°E). The large residuals around 457 nm and 477 nm are mostly introduced by an inadequate polarisation correction.

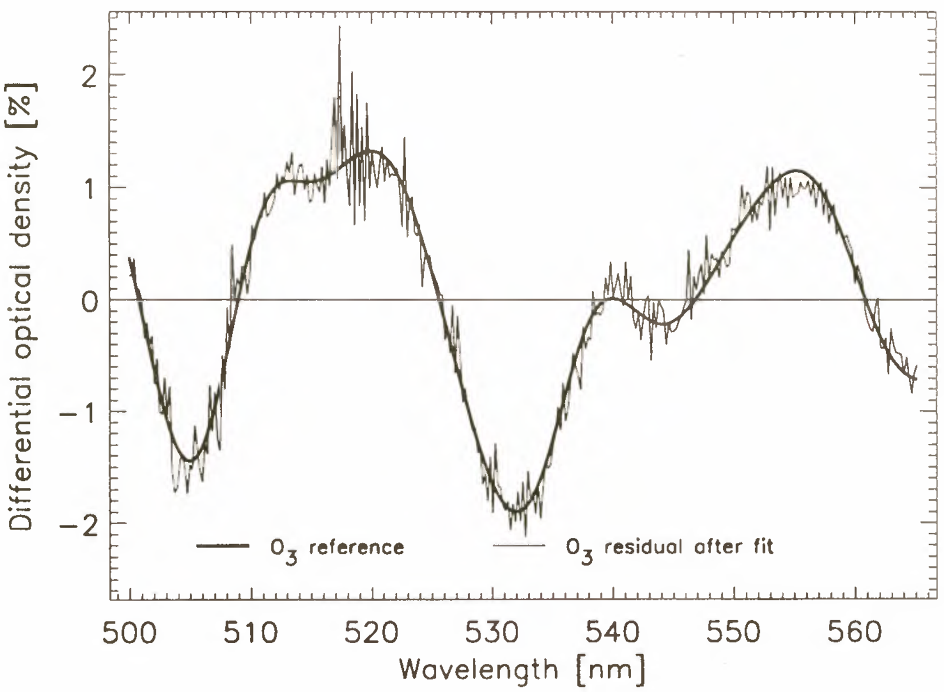

Figure 6: Window C: O_3 fit results for groundpixel 3236 from orbit 2123. The residuum is somewhat larger between 515 and 520 nm due to the Ring effect. Fit results: Ozone slant column 2640 DU, fit error 2.4%.

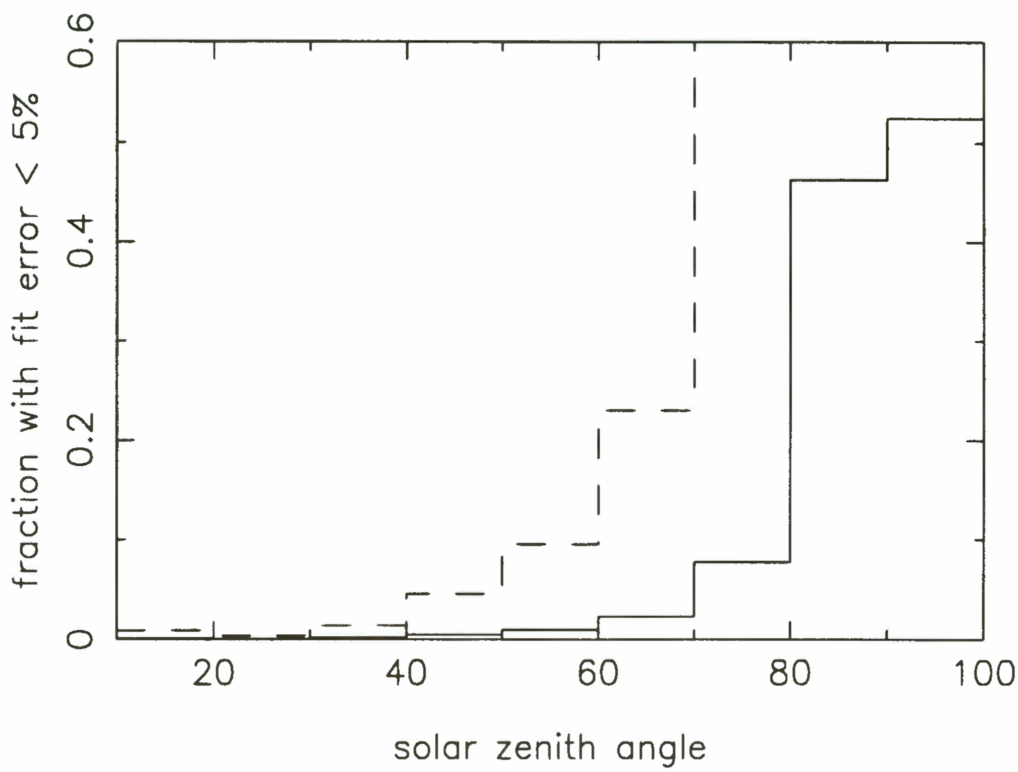

Figure 7: The fraction of VIS ozone values with fit errors less than 5% (solid line). The dashed line is the same, but enhanced by a factor 10.

fitting process, but the Ring spectrum was not included. A total of 15 days of GOME data (between approximately 6 UT and 22 UT) have been used in this comparison: 23–25 July, 25–27 August, 15–17 September, 5–7 and 29–31 October.

In the level 1–2 software version considered in this study, AMFs for the visible window were calculated assuming single scattering, while the AMFs for the UV window (for solar zenith angles less than 74.6°) were calculated assuming multiple scattering. Since single scattering AMFs normally are lower than multiple scattering AMFs the total ozone columns retrieved from the visible window are expected to be a few percent higher than the UV values. For a first comparison of total ozone columns retrieved from the visible window with those from the UV window, all values having solar zenith angles less than 74.6°, with ozone fit errors (both UV and VIS) less than 5%, and with viewing angles less than 7° ("nadir" pixels) were selected.

3.1 Comparison of UV and VIS ozone from the GDP

Only a relatively small number of the ozone values retrieved from the visible window by the current version of the GDP have fit errors less than 5%. In general fit errors are smaller for larger values of the slant ozone column, so the number of values with fit errors smaller than 5% increases with increasing solar zenith angle (Figure 7).

Figure 8 shows the comparison of the two O_3 retrievals for the 514 selected values. The majority of the ozone total column values retrieved from the visible window correlate well with values retrieved from the UV window, however the columns from the visible window are about 30% higher. These values have a range of about 8%. The latter arises in part from the errors associated with individual ozone values (the average fit error in the VIS values is 4.5%, and in the UV values 1.9%).

About 15% of the selected VIS values are more than 60% and up to a factor 4 larger than the corresponding UV values. The DOAS fit errors, however, are smaller than 5% (the selection criterium). In order to understand why the VIS values are so high in some cases, one GOME orbit was examined in more detail as described in the next subsection.

Dependence on ICFA cloud cover fraction

In Figure 9 an example is given of the behaviour of the total ozone column retrieved from the visible window compared to that retrieved from the UV window. Shown are the GOME data of the 16th September, 1995, between 9:56 and 10:23 UT (orbit 2123, Southern Hemisphere). This orbit is nadir static (the scan mirror was fixed to the nadir-looking position) so subsequent values are only about 10 km apart for solar zenith angles below 75°. The error bars plotted are the DOAS fit errors. Note that in this plot all values are shown (i.e., not only those with fit errors smaller than 5%, as in the previous subsection). The UV values show the expected relatively smooth be-

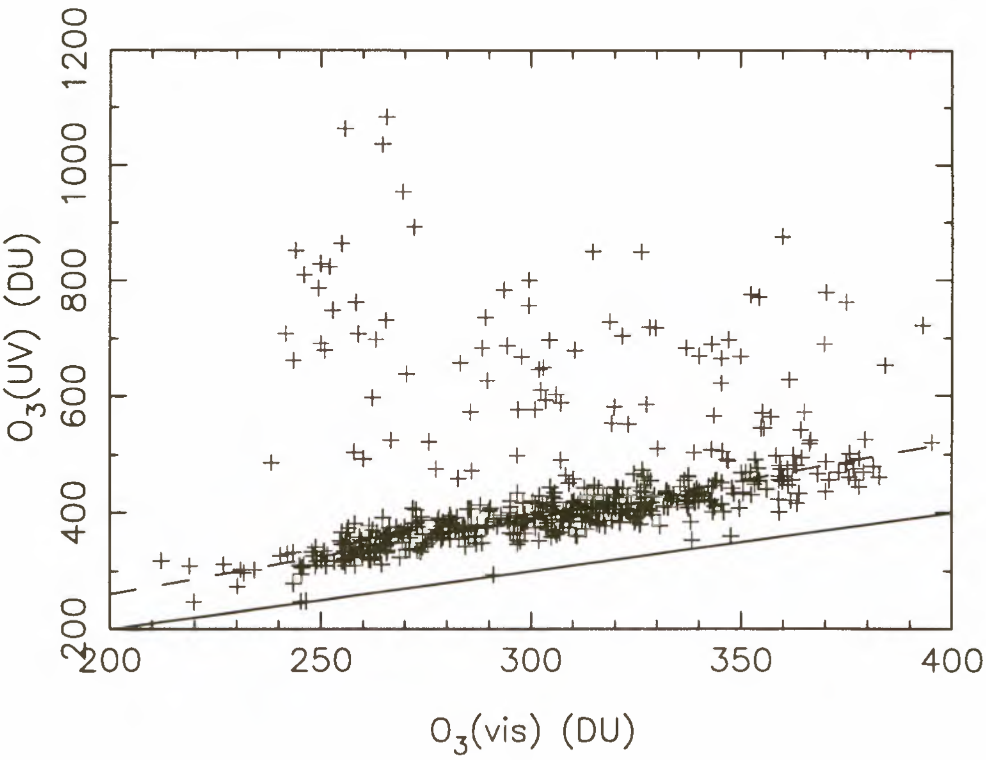

Figure 8: The total ozone (vertical) column as retrieved from the visible window, O_3(vis), versus the ozone column from the UV window, O_3(UV). The solid line is the line O_3(vis) = O_3(UV). 85% of the data is distributed around the line $O_3(\mathrm{vis}) = 1.30 \cdot O_3(\mathrm{UV})$ (dashed), with a spread of about 8%.

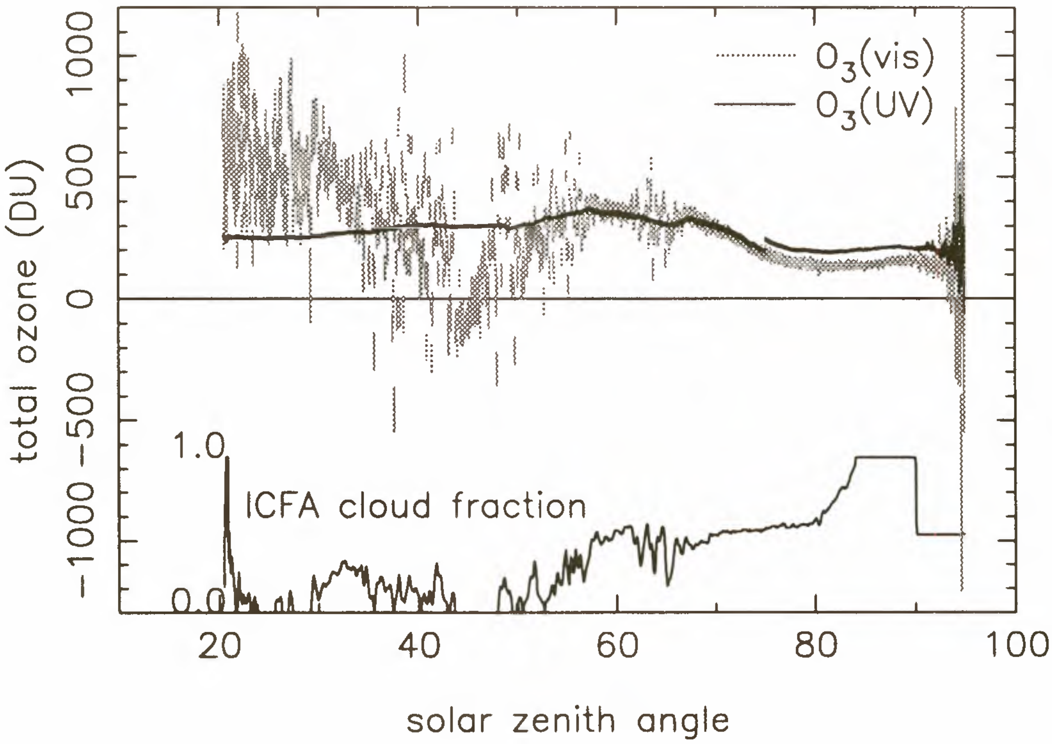

Figure 9: The total ozone columns for 16th September 1995, between 9:56 UT and 10:23 UT as a function of the solar zenith angle (Southern hemisphere). The error bars are the DOAS fit errors: UV values in black, and VIS values in grey. The solid line at the bottom indicates the corresponding ICFA cloud-cover fraction. The jump in the UV values at a solar zenith angle of 74.6° is caused by the assumption of single scattering used for the calculation of AMFs above this solar zenith angle. This will be changed in future versions of the GDP.

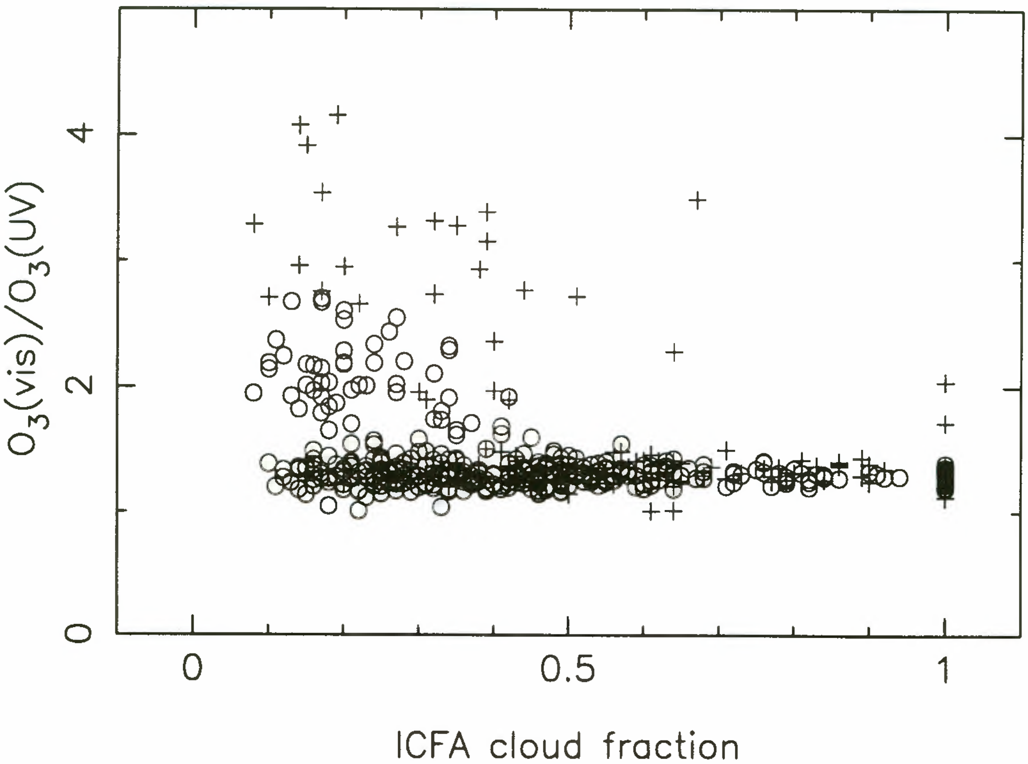

Figure 10: The ratio of the vertical ozone column retrieved from the visible window and that retrieved from the UV window as a function of the ICFA cloud-cover fraction. Included are only those values for which the DOAS fit errors are less than 5%. Circles indicate (UV) ozone values larger than 280 DU, crosses indicate smaller ozone values.

haviour. The VIS values show a smooth behaviour for a few restricted time intervals (= solar zenith angle intervals). In other time periods the VIS values are widely spread around the UV values. The cloud-cover fraction as calculated by the initial cloud fitting algorithm (ICFA) is plotted in the same figure. It appears that regions with high cloud-cover (> 0.5) result in a "better" behaviour of the VIS values than regions with low cloud-cover. This hypothesis was tested by studying the behaviour of the ratio of the VIS value and the UV value with respect to the ICFA cloud-cover fraction (Figure 10). The data used are the same as in the previous subsection (solar zenith angles less than 74.6°, fit errors less than 5%, only "nadir" pixels). It appears that large deviations between UV values and VIS values occur mostly in pixels with small cloud-cover fractions. Furthermore, it appears that the deviations can be larger (both absolute and relative) for smaller (UV) ozone values (< 280 DU). Also it is clear from Figure 10 that most of the VIS values are comparable to the UV values (apart from a small systematic difference as discussed earlier). Even for very small cloud-cover fractions (< 0.2) half of the VIS values correlate well with the UV values.

In summary, the total ozone column retrieved from the visible window (510–560 nm) is often larger than the column retrieved from the UV window, more often at lower ICFA cloud-cover fractions, and with (on average) larger deviations for smaller (UV) ozone columns.

3.2 Discussion

DOAS fit errors for ozone retrieved from the visible window are in general much larger than those retrieved from the UV window. But the (relatively few) VIS values with small fit errors (< 5%) are in most cases (85%) comparable to the corresponding UV values, apart from a systematic offset.

The 30% systematic offset (the VIS values being higher than the UV values) can at least partly be caused by the assumption of single scattering in the calculation of the VIS AMFs. However, AMF calculations performed at KNMI (*Koelemeijer*, 1996) and at IUP Bremen (*Buchwitz*, 1996) show that the differences between single scattering AMFs and multiple scattering AMFs in the visible are probably not much larger than about 10%. There are therefore other contributions to this behaviour.

In addition, further 15% of the VIS values with small fit errors are much larger (60% up to a factor 4) than the corresponding UV values.

The tests done in section 2.3 show that there is strong *interference* of the ozone reference spectrum with the reference spectra of O_4 and H_2O. Leaving one (or both) of these latter species out of the fitting process results in ozone deviations of 10–20%. Although this is a considerable amount it does not account for the large deviations found in section 3.1

(e.g., Figure 8).

Etalon structures, which can appear in the differential spectrum if the solar and the earth spectrum are observed with a relatively long time gap, can interfere with the ozone structures. This would, however, result in an alternating in time of "wrong" and "right" VIS values on a rather long timescale. This is not observed.

In the previous subsection it was shown that the large deviations occur more often at low ICFA cloud-cover fractions. Clouds play an important role in the visible window: the intensity of the backscattered solar radiation, is usually higher for a cloudy sky than for a clear sky. This is less significant in the UV range. This suggests that the retrieval of ozone in the VIS is sensitive to the signal level. High radiances mean high *signal-to-noise* ratio. However, it is difficult to understand why the VIS value is not in all cases affected by this sensitivity. Still most of the VIS values appear to be o.k.

It might be that the wavelength dependence of the *surface albedo* interferes with the ozone reference spectrum. This effect can only show up when the pixel is not fully cloudy. And it might be different for different types of surfaces.

Another possibility is that it has something to do with the *polarisation* of the radiance, because clouds (and ice surfaces) tend to depolarise the radiation. In window C' the polarisation sensitivity is a relatively smooth function of wavelength (no differential structures), but it is not yet clear whether this polarisation sensitivity is fully accounted for by the fitted polynomial, or whether a residual can still be in the spectrum which then can interfere with ozone.

Since VIS window C' is quite large the possibility of *spatial aliasing* should at least be mentioned. The systematic offset observed can however not be explained by spatial aliasing which should result in symmetrical deviations.

3.3 Conclusions

In section 3.1 it was stated that the relative ozone fit error in the visible window is smaller for larger solar zenith angles, caused by the increasing *slant* columns as a function of solar zenith angle. Furthermore, the spatial variability of the VIS values is much smaller at large solar zenith angles than at small solar zenith angles (Figure 11). This is possibly related to the behaviour of the VIS values as a function of the reflectivity or the cloud-cover fraction (section 3.1). For solar zenith angles larger than 70° the average ICFA cloud-cover fraction for the 15 days studied is larger than 0.5. Note that the pixel-to-pixel variation of the UV values *increases* with solar zenith angle, from about 3 DU for angles smaller than 50° to 16 DU for angles larger than 90°. The small fit error and small spatial variability of the VIS ozone values for large solar zenith angles, indicates that ozone columns from the absorption in the visible should be of high precision. That there are some VIS ozone values with small fit errors which deviate strongly from the UV values should be a reminder not to equate fit errors and total errors of the vertical columns.

After changes to the GDP (e.g. AMFs with multiple scattering, GOME FM reference spectra) it is anticipated that the VIS ozone values might change by 10-50% from the present values.

Finally, it is of importance that the VIS ozone can be derived for larger solar zenith angles than the UV ozone. This is especially important in spring in both polar regions when the depletion of ozone becomes important.

4 Conclusions and Recommendations

4.1 Slant column fitting (DOAS)

It is recommended for the level 1–2 processing to use O_3, NO_2, and "Ring" spectra measured with the GOME flight model as reference spectra. For the UV window from which the GOME *main* product is calculated at present, it is recommended to exclude NO_2 and BrO from the fit and to include fitting of a Ring spectrum. The solar irradiance has to be excluded from the linear fit. These and some other recommendations have already been discussed and will be implemented in the next version of the GOME Data Processor.

Concerning the VIS window the situation is more complicated. In the tests described in section 2.3 were only slant columns were calculated. However, fit quality is only one criterion. Accuracy of vertical columns has to be the final criterion. During the Validation Campaign in the GDP first a window 510–560 nm (C'), then 425–450 nm (A, the "NO_2 window") was used. The comparison between ozone vertical columns retrieved from C' and those retrieved from the UV (section 3) indicates a good potential for window C' but the columns are still systematically too high. Furthermore, interference by O_4 and H_2O cannot be neglected above 500 nm. The 450–500 nm (window B) fits were shown to be disturbed by "dichroic residuals" due to an non-perfect polarisation correction. Their influence on ozone vertical columns retrieved from window B, however, still has to be estimated. Therefore, it is suggested to test also window B in the GDP by choosing it as the visible window for some time of the operational processing (e.g., to process with window B the same days which were already processed with window C', which would allow a direct comparison between both VIS windows.) The results can then again be compared to the results from the UV window which should enable a "final" decision on the optimal fitting window in the visible. Of course, in parallel the keydata (and possibly the polarisation correction algorithm) will have to be modified in such a way that the "dichroic residuals" in window B are minimised.

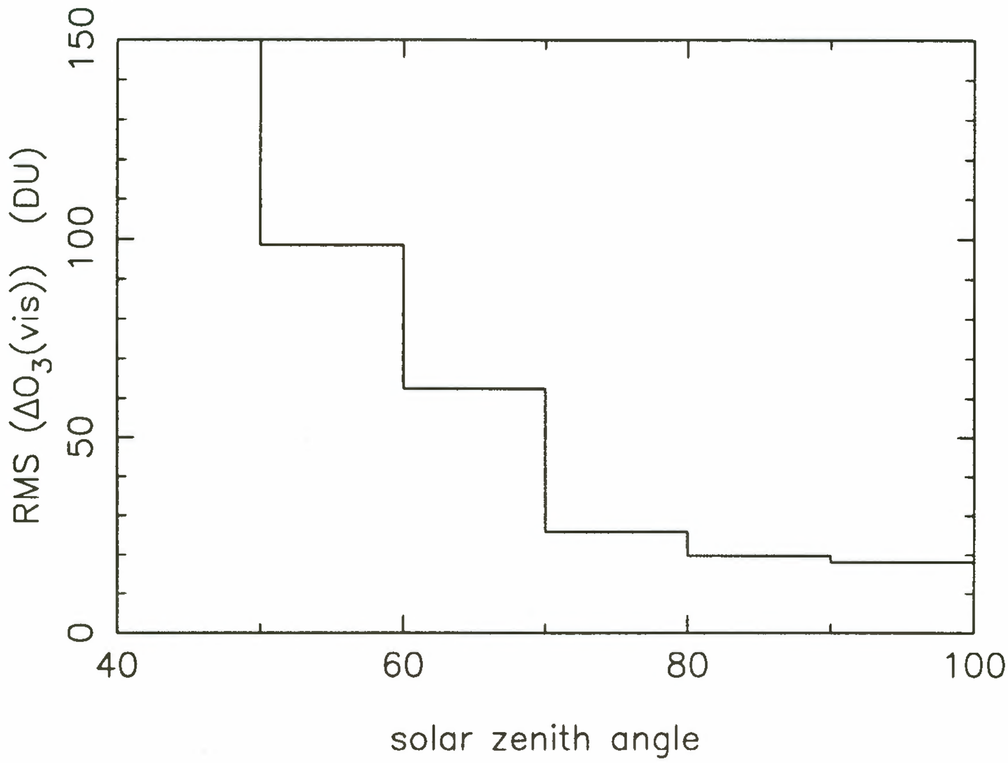

Figure 11: Pixel-to-pixel variation of the ozone columns retrieved in the visible, expressed in rms difference between the VIS values from neighbouring pixels (maximum distance 40 km) as a function of solar zenith angle.

4.2 Air mass factors

We believe that most of the remaining discrepancies between GOME and ground-based measurements are caused by air mass factors. On the one hand, there are principal limitations because the knowledge of the state of the atmosphere is always less than what is required for "exact" calculations, so that climatological profiles have to be assumed. However, there is still a lot of potential for improvements in the current AMF algorithm. Due to historical reasons at present single scattering AMFs are calculated by one radiative transfer model (**AMFTRAN**) and afterwards corrected for multiple scattering with factors calculated by another model (**GOMETRAN++**). This separation is not only artificial but inconsistent because the two models are known to yield somewhat different results in their single scattering modes. It is strongly recommended for future versions of the GDP to calculate *only* multiple scattering AMFs. If this is not possible *on-line* for each ground pixel (which is expected due to processing time limitations) look-up tables for the multiple scattering AMFs have to be created from which the actual values can then be interpolated.

4.3 Outlook

It was pointed out that ozone columns retrieved from the UV have their strength at low solar zenith angles because AMFs are best known there. Ozone columns from the visible region are most reliable at large solar zenith angles since absorbances are high there. For very large zenith angles retrieval from the VIS is superior compared to the UV because the UV radiation will not reach the lower atmosphere any longer (the UV sun has already set). It is therefore natural to envisage a "smart" combination of UV and visible for the main ozone product, thereby taking full advantage of the enormous wealth of spectral information from the multi-channel instrument GOME.

Acknowledgements

We thank W. Balzer, D. Loyola, E. Mikusch, W. Thomas (DLR-DFD), and R. Spurr (DLR/SAO) for their patience in putting up with and thinking over our numerous and long lists of wishes for "improvements" of the GOME Data Processor. We are grateful to M. van Roozendael (IASB) for redrawing our attention to the O_4 interference in the visible region and to M. Weber (IUP) for helpful comments. This work was funded in part by the University of Bremen, the State of Bremen, DARA (contract No. 50EE9439), and SRON, The Netherlands.

References

Bass, A. M., and R. J. Paur, The ultraviolet cross-sections of ozone, *Proc. Quadr. Ozone Symp. 1984, Halkidiki, Greece*, 1985.

Buchwitz, M., private communication, 1996.

Burkholder, J. B., private communication.

Burrows, J. P., *et al.*, SCIA-Mini, Proposal to ESA, Max-Planck-Institut für Chemie, Mainz, 1988.

Burrows, J. P., *et al.*,, Study of the Ring Effect, ESA Contract No. 10996/94/NL/CN, 1995.

Chance, K., private communication, 1994.

Dehn, A., Temperaturabhängige Absorptionsspektroskopie bedeutender Spurengase der Atmosphäre im ultravioletten und sichtbaren Spektralbereich, Thesis, University of Bremen, 1995.

Diebel, D., *et al.*, Tracegas study: Detailed analysis of the retrieval algorithms selected for the level 1-2 processing of GOME data. Final progress report, 1995.

Dobson, G. M. B., and D. N. Harrison, *Proc. Roy. Soc. London,* **A110**:660, 1926.

Edlén, B., The dispersion of standard air, *J. Opt. Soc. Am.,* **43**:339–344, 1953.

Eisinger, M., *et al.*, Studies on the precision of GOME irradiance and radiance products..., this issue.

von der Gathen, P., private communication, 1996.

Greenblatt, G. D., *et al.*, Absorption measurements of oxygen between 330 and 1140 nm, *J. Geophys. Res.,* **D95**:18577–18582, 1990.

Global Ozone Monitoring Experiment: Interim Science Report, European Space Agency (ESA), SP-1151, 1993.

Harwood, M. H., and R. L. Jones, Temperature dependent ultraviolet-visible absorption cross sections of NO_2 and N_2O_4, *J. Geophys. Res.*,, **D99**:22955–22964, 1994.

Koelemeijer, R., private communication, 1996.

Noxon, J. F., Nitrogen dioxide in the stratosphere and troposphere measured by ground-based absorption spectroscopy, *Science,* **189**:547–549, 1975.

Noxon, J. F., *et al.*, Stratospheric NO_2. 1. Observational method and behavior at mid-latitude, *J. Geophys. Res.,* **C84**:5047–5065, 1979.

Ozone Measuring Instruments for the Stratosphere, ed. by W. B. Grant, Opt. Soc. Am., 1989.

Perner, D., and U. Platt, Detection of nitrous acid in the atmosphere by differential optical absorption, *Geophys. Res. Lett.,* **6**:917–920, 1979.

Product Specification Document of the GOME Data Processor, Deutsche Forschungsanstalt für Luft- und Raumfahrt (DLR), ER-PS-DLR-GO-0016, 1995.

Richter, A., *et al.*, Ground based UV/vis measurements of O_3, NO_2, BrO, and OClO over Bremen (53°N), *Proc. 3rd European Symposium on Polar Stratospheric Ozone Research, Schliersee, Germany, 1995.*

Schneider, W., *et al.*, Absorption cross sections of NO_2 in the UV and visible region (200–700 nm) at 298 K, *J. Photochem. Photobiol.,* **A40**:195–217, 1987.

Solomon, S., *et al.*, On the interpretation of zenith sky absorption measurements, *J. Geophys. Res.,* **D92**:8311–8319, 1987.

M. Eisinger, present address: Alfred Wegener Institute for Polar and Marine Research, D-14401 Potsdam.

A. Richter and J. P. Burrows, Institute of Environmental Physics, University of Bremen, D-28334 Bremen.

A. Piters, Royal Dutch Meteorological Institute, NL-3730 AE De Bilt.

GOME Validation Projects D-131 and NL-112

COMPARISON OF GOME COLUMN OZONE WITH GROUND-BASED MILLIMETER WAVE MEASUREMENTS AT NY-ÅLESUND, SPITSBERGEN

B.M. Sinnhuber, J. Langer, U. Raffalski, and K.F. Künzi

Institute of Environmental Physics
University of Bremen, Germany

D131

Abstract
Profiles of stratospheric ozone and chlorine monoxide were measured with a ground-based millimeter wave radiometer at the arctic NDSC station Ny-Ålesund, Spitsbergen. Stratospheric ozone column densities were calculated from the retrieved ozone profiles and compared with total ozone measured by the GOME instrument.

1. INTRODUCTION

The Radiometer for Atmospheric Measurements (RAM) has been developed by the Institute of Environmental Physics of the University of Bremen as an instrument for ground-based millimeter-wave observations of trace gases in the stratosphere and lower mesosphere in the frequency range from 100-300 GHz. As part of the European Stratospheric Monitoring Stations (ESMOS/arctic) and the german ozone research program this instrument is operated continuously at the artic station of the Network for the Detection of Stratospheric Change (NDSC) Ny-Ålesund, Spitsbergen.

2. THE INSTRUMENT

The RAM is a heterodyne receiver consisting of two front-ends for the observation of ozone at 142 GHz and chlorine monoxide (ClO) at 204 GHz, respectively, which are operated in a time-sharing mode. Both front-ends consist of a rotatable mirror for calibration, a quasi-optics and a mixer-HEMT pre-amplifier stage with Potter horn antenna which is cryogenically cooled to ~12 K. The quasi-optics is based on ellipsoidal and plane aluminum mirrors and grid polarisers as optical elements. It includes an optical path-length modulator, a Martin-Puplett-Interferometer (MPI) as single-sideband filter and a cooled sideband load. A dichroic plate acting as a low-pass filter is mounted in the ozone front-end to decrease baseline effects due to higher harmonic response of the detector.

At 142 GHz a waveguide is used for the injection of the local oscillator (LO) signal into a finline fundamental mixer equipped with planar diodes. At 204 GHz the local oscillator signal is quasi-optically coupled into a single-ended whisker-contacted fundamental mixer via a MPI diplexer.

The back-end consists of a 2048 channel acousto-optical spectrometer (AOS) with a center frequency of 2.1 GHz, a bandwidth of 945 MHz and a frequency resolution of ~1.3 MHz. This allows to retrieve trace gas volume mixing ratio (VMR) profiles in the altitude range from 15 to 60 km from the shape of the observed signal.

The whole system is computer controlled and can operate automatically. Critical parameters, like room temperature, the temperatures of the internal calibration loads the outside air temperature and other important system data are measured continuously, digitized and stored together with the atmospheric data on digital-audio tapes (DAT). Dependent on the observing mode the data can add up to 30 MBytes per day. The only maintenance necessary for the receivers is the daily calibration of the internal cold loads, the refill of the liquid nitrogen dewars (if external cold loads are used for calibrating the receiver) and changing the DAT. Since 1995, the RAM is connected to the internet. This allows near real time processing of ozone VMR profiles and permit to remotely control the instrument.

In a first stage of development the radiometer was operated in a winter campaign in Ny-Ålesund from January to March 1993 only measuring ozone. From January to April 1994 the radiometer was successfully tested at the same location in a time sharing mode, measuring both, ozone and chlorine monoxide, yielding ozone profiles throughout the entire period. From the ClO spectrum for March, 13, a profile has been inverted.

In the most recent configuration as it is installed and operated presently in the NDSC-station the radiometer consists of two quasi-optical front-ends measuring chlorine monoxide at 204 GHz and ozone at 142 GHz. In March 1995 we obtained two ClO spectra, in two breif periods showing unperturbed and slightly perturbed conditions.

3. THE PRINCIPLE OF OPERATION

As a passive device the mm-wave radiometer detects radiation coming from the atmosphere. The radiation in the mm-wave region (wavelenght of 1 - 10 mm, corresponding to frequencies of 300 - 30 GHz) is due to molecular rotational transitions. The frequencies of interest which are characteristical for certain species are chosen with respect to minimize the contaminating contribution of other molecules being too close to the interesting frequency.

The principle of operation is based on the fact that in the microwave region the width of a molecular line is proportional to the pressure and the integral over the line is proportional to the total column of the observed molecule. Since the atmospheric pressure exponentially decreases with increasing altitude, the line observed by a ground-based radiometer is a superposition of the line contributions from different altitudes with the outer wings of the line dominated by the low altitude contribution and the line center dominated by the high altitude contribution. The vertical resolution of this method is mainly limited by the scale height of the atmosphere (6 - 10 km). The advantage of millimeter-wave radiometry is, that for strong lines like ozone the signal is only weakly perturbed by clouds. Thus, for ozone the RAM complements other techniques in that it provides nearly weather independent VMR profiles with high time resolution (one profile per hour, if needed) in the altitude range from 15 - 60 km.

With respect to chlorine monoxide the RAM is the only permanent ground based sensor providing information on the total column and the vertical distribution of this species in the arctic region.

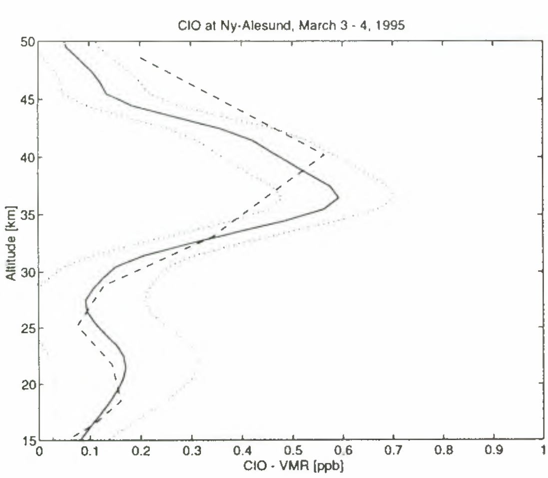

Fig. 1. ClO profile from March 3-4, 1995 as measured by the RAM (solid line), compared with data from the SLIMCAT 3D chemical transport model (dashed), showing slightly perturbed chemistry at 20-25 km. The dotted lines show the error bars of the profile retrieved from millimeter wave data.

However, the measurements of chlorine monoxide are possible only for good troposheric conditions, i.e. low tropspheric opacity.

Besides ClO- and ozone profile a by-product of the RAM is to permanently deliver data about the tropospheric opacity, which can be used to derive total tropospheric water vapor content.

4. MEASUREMENTS OF CHLORINE MONOXIDE

Measurements of emission spectra at 204 GHz have been made permanently in winter/spring 1994 and since the operational mode of the RAM started in December 1994 in the NDSC station. We obtained three spectra of chlorine monoxide from this period which have been inverted showing no perturbed chemistry in the altitude range from 18 to 25 km at March 18 and an only slightly perturbed situation March 3-4, respectively.

Concerning the instrumental limits the spectra we obtained clearly show that the signal to noise ratio can be reduced to the minimum of approximately 20 mK which is sufficient to detect strong ClO abundance as can be found during perturbed chemistry (values of 100 mK are expected from forward calculations). For unperturbed chemistry the calculated ClO-value is approximately 40 mK which is also detectable with the RAM. Therfor the main limiting factor for ClO measurements is tropospheric attenuation.

5. MEASUREMENTS OF OZONE

Ozone profiles were retrieved from the millimeter wave measurements during the two campaigns in late winter 1993 and 1994 and continuously since fall 1994. Due to some technical problems, unfortunately no measurements were performed between end of September 1995 and mid ofgg December 1995. A time series from mid of February 1995 to August 1995 is given in fig. 7, showing a typical seasonal cycle with a maximum in spring.

Strong variations in the ozone VMR in all three winters can be seen. They are strongly dominated by dynamical effects, especially the presence or absence of the polar vortex. In 1995, low ozone values are measured when Ny-Aalesund was inside the polar vortex, while higher ozone VMR was measured outside the vortex. This is unusual, since in previous years at lower levels (around 475 K) inside the polar vortex higher ozone mixing ratios were measured than outside. The fact that there was less ozone inside the vortex than outside is probably a result of large ozone depletion inside the polar vortex in January 1995, which was reported by several investigators..

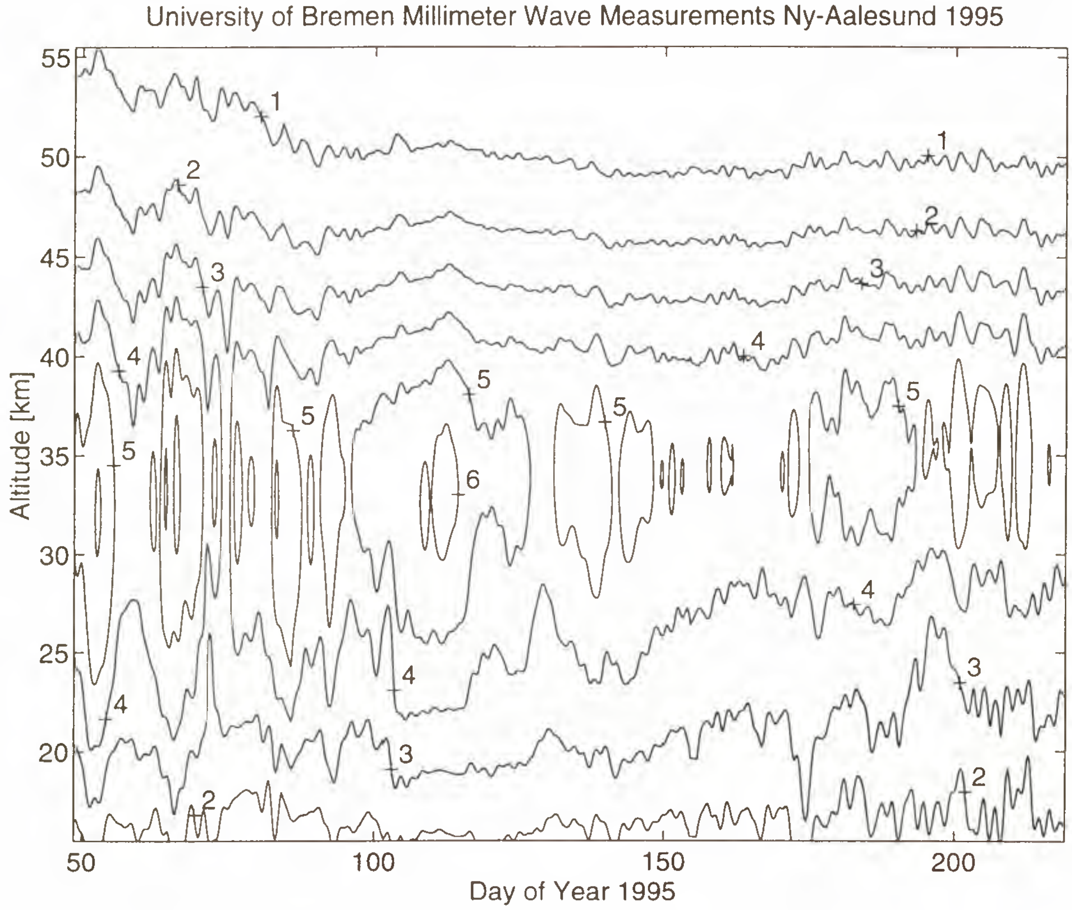

Fig. 2. Time-height cross section of the ozone volume mixing ratio (in ppm) from February to August 1995 as measured by the RAM at Ny-Ålesund. It shows a typical seasonal cycle with the maximum in spring.

6. COMPARISON OF OZONE COLUMN DENSITIES WITH GOME DATA

For comprison with total ozone from the GOME instrument, ozone column densities were calculated from the RAM ozone volume mixing ratio profiles. Temperature and pressure profiles used for this calculation are the same as used for the profile retrieval itself,namely the daily Ny-Ålesund radiosondes, which are completed with CIRA standard profiles above the maximum sonde altitude.

For the data of 1995 ozone column densities calculated from the microwave measurements were also compared to total ozone of the UV/visible DOAS instrument. The DOAS was installed in Ny-Aalesund in February 1995 and is operated by the University of Bremen. Figure 3 shows the daily mean values of total ozone, as measured by the DOAS together with ozone column densities above 15 km, calculated from RAM measurements (lower curve). The considered period ranges from end of February 1995 to the end of May 1995. After this period, the DOAS measurements are quite uncertain, since the airmass factors become to small. A good correlation can be seen, which seems to be better in March than in May. The overall correlation is seen in fig. 4, with a correlation coefficient of 0.89.

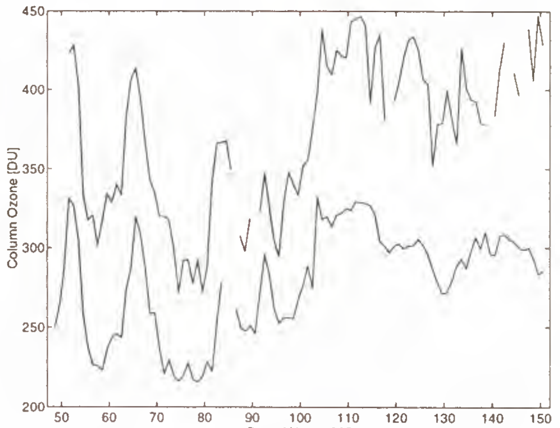

Fig. 3. Column ozone above 15 km calculated from RAM profiles together with total ozone from the DOAS instrument.

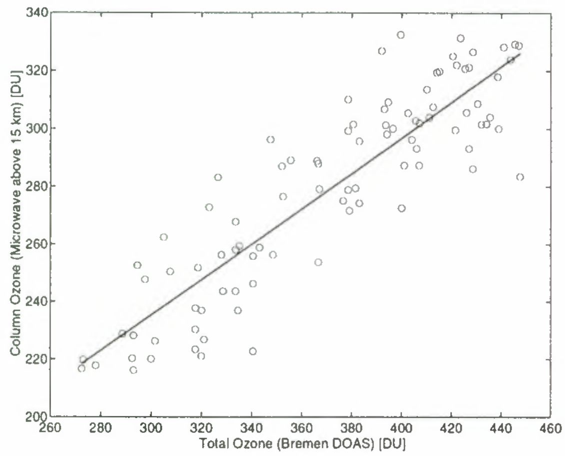

Fig. 4. Correlation of ozone column densities above 15 km from the RAM with total ozone of the DOAS instrument.

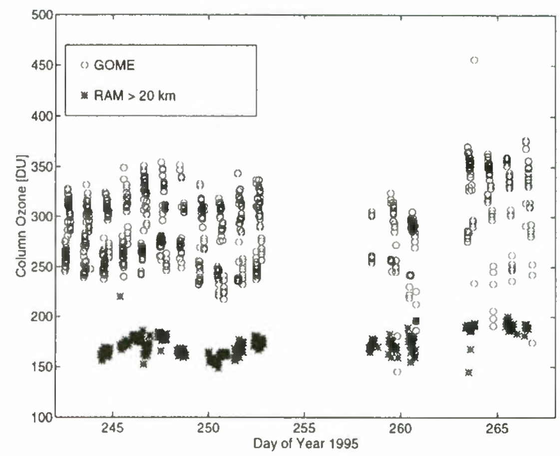

Fig. 5. Ozone column densities as measured by GOME (circles) together with column densities above 20 km measured by the millimeter wave radiometer (stars).

For September 1995, ozone column densities measured by the RAM were compared with total ozone measurements by GOME. During this period a relative strong baseline contribution in the millimeter wave data, due to a technical problem which has been fixed in the mean time, do not allow resonable retrievals below approximately 20 km. Therefor ozone column densities were calculated above an altitude of 20 km.

Figure 5 shows the ozone column densities, calculated from the RAM profiles above 20 km, compared to GOME total ozone within a radius of 500 km to Ny-Ålesund (78.9°N, 11.9°E). The source of the very strong variation of the GOME data is not yet known. A restriction of the radius to be compared to much less than 500 km does not reduce the variations of the GOME data significantly.

The restriction of the calculated ozone column densities to altitudes above 20 km not only reduces the absolute values, but of course also reduces the observed variations in column ozone. Within the period considered here, two ozone sondes were launched at Ny-Ålesund: at September 6 and September 20. Ozone column densities from the ground up to 20 km, calculated from the ozone sonde measurements are 127 DU and 161 DU, respectively. The resulting total ozone values (from ozone sondes below 20 km plus RAM data above 20 km) are in quite good agreement to averaged GOME data.

7. SUMMARY

Measurements of stratospheric ozone and chlorine monoxide profiles were performed with a ground-based millimeter wave radiometer at Ny-Ålesund, Spitsbergen. Ozone column densities above an altitude of 15 km were computed. These ozone column densities are well correlated with the DOAS UV/visible instrument. Total ozone values calculated from ozone sondes below 20 km and millimeter wave measurements above 20 km are in quite good agreement with averaged GOME data.

8. ACKNOWLEDGMENTS

Part of this work was supported by the Alfred Wegener Institute for Polar Research, by the German Bundesministerium für Bildung und Forschung and by the Commission of the European Comunity.

BALLOON MEASUREMENTS OF AEROSOL EXTINCTION, OZONE AND NO_2 PROFILES FOR THE VALIDATION OF THE GOME ALGORITHMS AND PRODUCTS

C. Brogniez, R. Ramananahérisoa and J. Lenoble

Laboratoire d'Optique Atmosphérique, Université des Sciences et Technologies de Lille, France

J.P. Pommereau, C. Phillips and L. Denis

Service d'Aéronomie, Verrières le Buisson, France

Abstract
Profiles of aerosol extinction and size distribution and ozone and nitrogen dioxide number density, required for the GOME retrieval algorithms and the validation of its inversion process, were measured in October 1995, during the commissioning phase of the satellite instrument, by a combination of balloon borne instruments at Aire sur l'Adour, France.

1. INTRODUCTION

The aim of the GOME measurements is the retrieval of ozone and NO_2 total columns as well as ozone profiles from nadir viewing observations. Since the algorithm is sensitive to atmospheric scattering by stratospheric aerosols which need to be included explicitly in the calculations, it was proposed to carry out simultaneous measurements of profiles of aerosol extinction, ozone and NO_2 during the commissioning phase, in order to provide the necessary information for case studies for testing the validity of the GOME retrieval process.
The measurements were carried out in October 1995 at Aire sur l'Adour (44.7°N, 0.25°W) in south-western France using several balloon borne instruments: the RADIBAL photo-polarimeter, the BALLAD limb radiometer and the BOCCAD sun-radiometer of the Laboratoire d'Optique Atmosphérique de Lille (LOA), and the SAOZ uv-visible spectrometer of the Service d'Aéronomie (SA). Five flights were performed in near-coincidence with GOME overpasses above the station; their preliminary results are described below.

2. BALLOON-BORNE INSTRUMENTS

2.1. RADIBAL (RADIomètre BALlon) designed by LOA in 1983, is a small FOV (2°) photopolarimeter which measures the radiance and the polarization degree of the sunlight scattered by the atmosphere at 1650 and 850 nm during the ascent and/or the descent of the balloon. The rotation of the gondola around its vertical axis (1 rpm) allows the measurement of the azimuth dependence of the radiance and polarization at several altitudes (Herman et al., 1986).
The atmosphere slant optical depth is estimated by the reflectance (normalised radiance) at 30° scattering angle. The aerosol size distribution is retrieved by fitting the measured reflectance and polarization degree diagrams with diagrams computed with MIE routines for log normal distribution (LND) models, assuming a spherical shape for the aerosols and a fixed refractive index (Santer et al., 1992, Brogniez et al., 1992). The accuracy of the RADIBAL absolute calibration is ~ 10%, and the polarisation is measured within 2%. When retrieving the aerosols from the measurements, the contribution of the molecular scattering and of the troposphere illumination leads to additional errors (Brogniez et al., 1996). The effective radius is then retrieved within ~ 8% and the refractive index within ~ 2%; the effective variance is defined within 20%.

2.2. BALLAD (BALloon Limb Aerosol Detection), is a linear CCD detector (1728 diodes oriented vertically) radiometer allowing the measurement of the vertical distribution of the limb radiance as well as of the limb polarized radiance. As for RADIBAL, the rotation of the gondola around its vertical axis (1/3 rpm) allows to determine the azimuth dependence of the radiance and polarization measurements. Rotating interferential filters and polaroids allow the estimation of the wavelength dependence of the reflectance and polarization. BALLAD is a new instrument developed in 1993, which requires extensive modelling for being interpreted. Its measurements are not yet analysed.

2.3 BOCCAD (Balloon OCCultation for Aerosol Detection) operates also at the balloon ceiling level, approx. 32 km. It is a solar occultation instrument, designed in 1994, set up on the same gondola as RADIBAL and BALLAD, but which performs at sunset only, after the measurements of BALLAD are completed. The gondola stops rotating and the instrument points toward the sun.
An objective forms the sun's image on a CCD matrix of 244 x 550 pixels. The vertical and horizontal FOV of the instrument are 10° and 7.5° respectively and the optical axis of the instrument is pointing ~ 2° below the balloon horizon so that the whole occultation event can be observed. A filter-wheel between the objective and the detector, allows to perform multi-spectral measurements. Three interferential filters centred at 850, 780 and 443 nm are dedicated to aerosol study, a fourth centred at 600 nm is dedicated to ozone. A large number of images are formed successively in each channel during the flight (typically 150 to 300 depending on the event). Radiance measurements are converted into transmission by using a reference image obtained nearly outside the atmosphere. Then the ephemeris allow to convert the time-transmission data into tangent altitude-transmission data taking into account atmospheric refraction. The inversion is conducted in the same way as we use to do with satellite occultation data (Chu et al., 1989). After correction from molecular attenuation, the inversion is conducted following a Chahine's procedure leading to an extinction coefficient for each channel from which the ozone and aerosol contributions are discriminated.

2.4 SAOZ is the balloon borne version (Pommereau et al., 1991, Pommereau et al., 1994, Pommereau and Piquard, 1994) of the ground-based uv-visible diode array spectrometer designed for total ozone, NO_2 and PSC measurements in polar areas also used for the validation of the GOME total ozone measurements (Lambert et al., this issue). It is a 1024 diodes, 50 µm entrance slit, 300-630 nm range, spectrometer with a resolution of 0.6 nm and an oversampling of about a factor 4. Its field of view of 360° in azimuth and +10°, -6° in elevation is defined by a conical mirror and circular baffles. Three stages of diffusers in front of the entrance slit allow to get a response independent of the orientation of the gondola in respect to the direction of the sun. Slant columns of O_3, NO_2, $(O_2)_2$ and tropospheric H_2O are retrieved by a least squares iterative procedure using high resolution absorption cross-sections published in the literature and convoluted with the SAOZ instrument function. Slant columns are inverted into vertical profiles by onion peeling. The residual amount of absorbent above the maximum altitude of the balloon is determined by comparison of the measurements performed during ascent and occultation. The location and altitude of the balloon are measured with an accuracy of ±150 m with a GPS receiver and pressure and temperature with a set of Vaisala radiosonde sensors. The vertical coordinate used in the presentation of the results is therefore geometric altitude. One standard deviation random errors shown in the profiles are those estimated by the least squares fit, propagated in the inversion process. The ozone absorption cross-sections used are those of(Brion et al. (1993). After normalisation by -1.9%, they are consistent with the most accurate ones (0.5% accuracy) of Anderson and Mauersberger (1992) but available at few discrete wavelengths only. Acording to Brion et al., they are independent of temperature in the visible range. The accuracy of ozone concentrations woudl be therefore better than 2%. For NO_2, the uncertainty of the absorption cross-sections (Merienne et al., 1994) is of the order of 5% only, but in addition there is a rather large temperature dependence as shown by Harwood and Jones (1994) and Coquart et al., (1995), not taken into account in the present analysis. If corrected for this temperature dependence, the NO_2 stratospheric concentrations would have to be reduced by 12-15%.

3. BALLOON FLIGHTS

Five flights were performed in October from Aire sur l'Adour. The date, UT time of measurements, instrument and location of tangent point (at mean altitude ~ 20 km) or balloon location (for RADIBAL), are given in table 1.

The October 2 flight, dedicated to SAOZ, was a sunset flight released at 16:30UT in the afternoon performed in presence of large thunderstorms above Northern Spain. Measurements were performed during ascent and occultation down to -6° solar elevation. RADIBAL was flown on Oct 5 and operated during the slow descent of the balloon between 27 and 14 km. Three flights were performed on the 12th : a first SAOZ launched by the end of the night for sunrise occultation followed by measurements during the descent below the parachute; BALLAD and BOCCAD released at 15:00UT which both operated at the balloon float altitude of 32 km, BALLAD first in the afternoon down to ~+2° solar elevation, then BOCCAD, from ~+2° to ~-6°; and finally, a second SAOZ was launched at 17:00UT for simultaneous sunset occultation measurements.

Date	UT	Instr.	location
Oct 2	17-19	SAOZ	43.8N - 2.0W
Oct 5	16-18	RADIBAL	43.9N - 0.1E
Oct 12	06-07	SAOZ	43.7N - 2.1E
Oct 12	17-18	BOCCAD	43.3N - 4.6W
Oct 12	17-19	SAOZ	43.7N - 2.7W

Table 1. Sequence of balloon flights performed at Aire sur l'Adour in October 1995 for the validation of GOME.

4. RESULTS

The results of the above flights, currently available, are shown below. Figure 1 displays the SAOZ ozone and NO_2 profiles with their the one standard deviation uncertainties, at sunset on October 2, obtained by averaging the late afternoon ascent measurements starting at 2 km and the more precise occultation observations ending at 15 km. Since the profile shown is a weighted average and the ascent measurements are less precise because of the smaller sun zenith angle, there is a discontinuity of precision between 14 and 15 km.

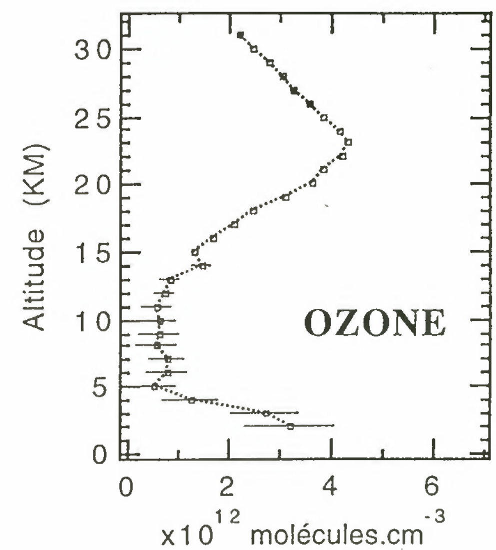

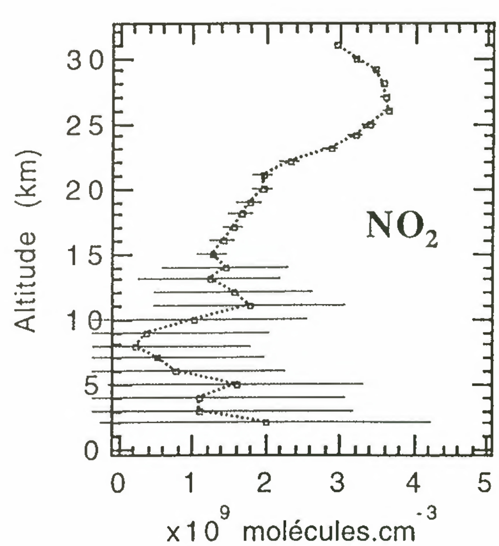

Figure 1. Ozone and NO_2 density profiles measured at sunset by SAOZ on October 2.

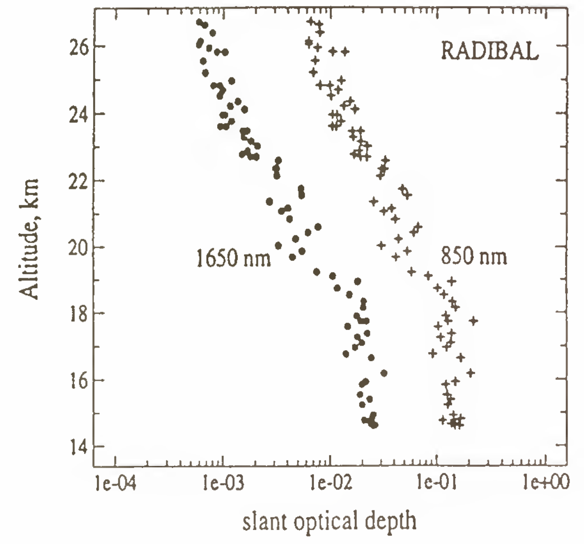

Figure 2. RADIBAL slant optical depth at 1650 nm (dots) and 850 nm (plusses) for October 5.

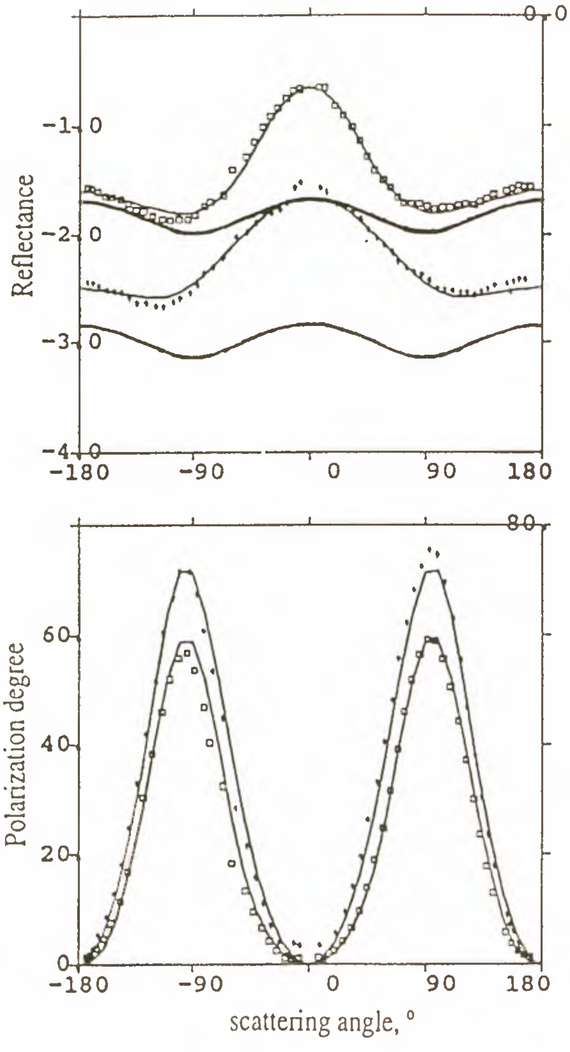

Figure 3. Example of reflectance (upper curves) and polarization degree (lower) versus scattering angle observed at ≅ 17 km on October 5: squares for 850 nm and crosses for 1650 nm; simulations in full lines and Rayleigh reflectance in thick lines

The RADIBAL slant optical depths at 850 and 1650 nm measured on October 5 are shown in figure 2; the aerosol layer is mainly located below 20 km and the aerosol loading is relatively small. An example of reflectance and polarization diagrams measured by RADIBAL at both wavelengths, at ~ 17 km, is shown in fig. 3 together with the results of simulations. Particle effective radius and variance derived by fitting the model parameters at each altitude step, are shown in fig. 4. The effective radius of the aerosol particles in the main layer is ≅ 0.35 μm and the variance is small.

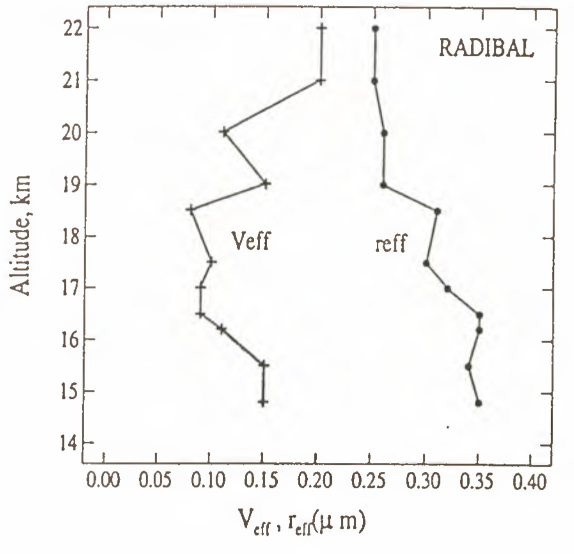

Figure 4. Vertical profiles of effective radius (dots) and of retrieved effective variance (plusses) on October 5.

The BOCCAD profile of aerosol extinction at 850 nm measured on October 12 is shown in fig. 5. The maximum extinction is small: ~5×10^{-4} km^{-1}. Assuming an exponential decrease of the extinction coefficient at altitudes higher than 22 km, the total vertical aerosol optical depth at 850 nm above the tropopause at 13 km would be ~ 0.0032.

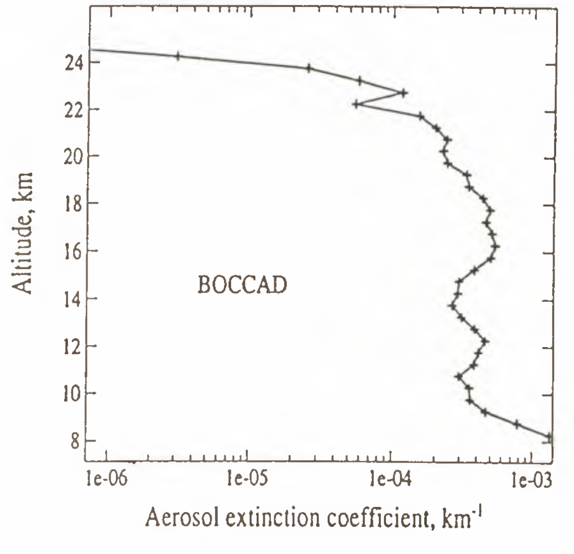

Figure 5- Aerosol extinction coefficient at 850 nm measured by BOCCAD on October 12.

Ozone number density profiles retrieved by BOCCAD and SAOZ are shown in figure 6a. There are four profiles shown : SAOZ at sunrise looking 300 km east of the balloon, SAOZ ascent in late afternoon starting at 2 km altitude, BOCCAD and SAOZ measurements looking 300 km west during the sunset occultation. All profiles do show the same maximum concentration at about 24 km. Except for the lowermost points, the two sunset profiles are consistent within their error bars.

Figure 6b shows three NO_2 profiles recorded during the SAOZ flights with their respective error bars: sunrise occultation above 9 km, late afternoon ascent above 2 km and sunset above 12 km. Above 18 km, the NO_2 concentration is larger at sunset after the daytime photolysis of N_2O_5. One can note also a significant NO_2 peak of 3 10^9 mol.cm^{-3} around the tropopause in the morning measurements looking east that is above south France. This is a feature commonly observed in light easterlies anticyclonic conditions as was the case on October 12. The NO_2 maximum at 11- 12 km is thought to be the consequence of accumulation of aircraft exhaust.

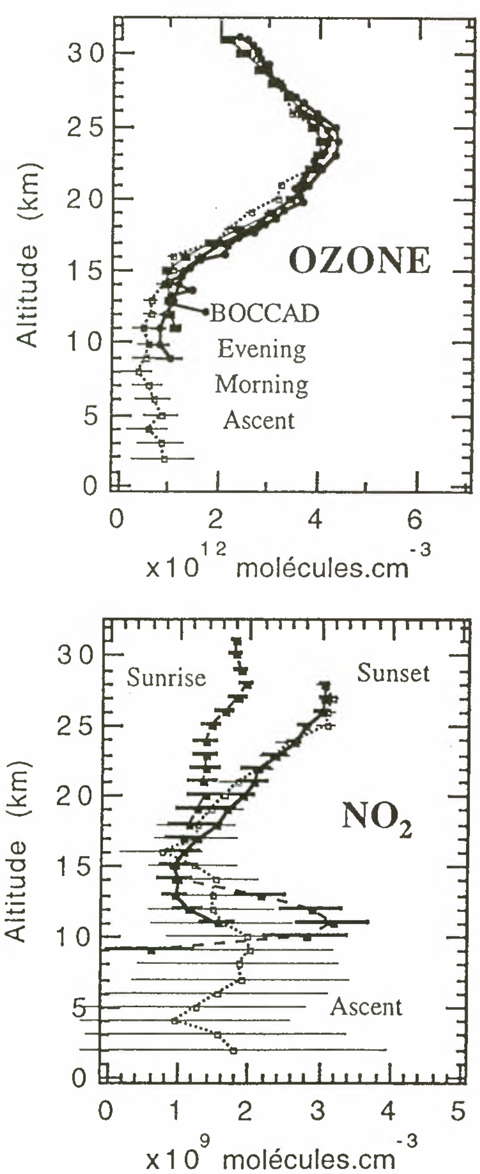

Figure 6. Ozone and NO_2 number density profiles measured on October 12.

5. CONCLUSIONS

The balloon-borne experiments RADIBAL, BALLAD, BOCCAD and SAOZ were flown in combination in October 1995 from Aire sur l'Adour in south western France, during the GOME validation phase. Altogether, they provided a complete set of profiles of aerosol extinction, effective radius, ozone and NO_2 densities, collocated with the GOME observations. Additional Mie calculations will allow to derive the spectral aerosol contribution, needed for inclusion in the GOME retrieval algorithm. The ozone and NO_2 profiles combined with the profile of the aerosol extinction, can be used for testing and validating the GOME profile inversion procedure when it will become available.

6. REFERENCES

Anderson, S. M. and K. Mauersberger, Laser measurements of ozone absorption cross-sections in the Chappuis band, 1992, *Geophys. Res. Lett.*, 19, 933.

Brion, J., A. Chakir, D. Daumont, J. Malicet and C. Parisse, 1993, High resolution laboratory cross-sections of O_3, temperature effect, *Chem. Phys. Lett., 6*, 612.

Brogniez, C., Santer, R., Diallo, B. S., Herman, M., Lenoble, J. and Jager, H.,, 1992. Comparative observations of stratospheric aerosols by ground-based lidar, balloon-borne polarimeter and satellite solar Occultation. *J. Geophys. Res.*, vol. 97, pp. 20805.

Brogniez, C., Lenoble , J., Herman, M., Lecomte, P. and Verwaerde, C., 1996. Analysis of two balloon experiments in coincidence with SAGE II in case of large stratospheric aerosol amount: Post-Pinatubo period, *J. Geophys. Res.*, vol..101, pp. 1541-1552.

Chu., W. P., McCormick, M. P., Lenoble, J., Brogniez, C. and Pruvost, P., 1989, SAGE II inversion algorithm, *J. Geophys. Res.*, vol. 94, pp. 8339-8351.

Coquart, B., A. Jenouvrier and M. F. Merienne, 1995, The NO_2 absorption spectrum II. Absorption cross sections at low temperature in the 400-500 nm region, *J. Atm. Chem.*, 21, 251.

Harwood, M. H., and R. L. Jones, 1994, Temperature dependent ultraviolet cross-sections of NO_2 and N_2O_4: low temperature measurements of the equilibrium constant $2NO_2$ <--> N_2O_4, J. Geophys. Res., 9, 922.

Herman, M., Balois, J. Y., Gonzalez, L., Lecomte, P., Lenoble, J., Santer, R. and Verwaerde, C., 1986. Stratospheric aerosol observations from balloon-borne polarimetric experiment. *Appl. Opt.*, vol. 25, pp. 3573.

Merienne, M.F., A. Jenouvrier and B. Coquart, 1994, The NO_2 absorption spectrum I: absorption cross-sections at ambient temperature in the 300-500 nm region, *J. Atm. Chem.*, 20, 281.

Pommereau, J.P., J. Piquard and F. Goutail, 1991, A light uv-visible spectrometer for atmospheric composition measurements by solar occultation, *Proc. 10th ESA Symposium on European Balloon Programmes and Related Research*, 215, ESA-SP 317.

Pommereau, J. P. and J. Piquard, 1994, Ozone, Nitrogen dioxide and Aerosol vertical distributions by UV-visible solar occultation from balloons, *Geophys.*

Res. Lett., 13, 1227-1230.

Pommereau, J.P., F. Goutail, J. Piquard, L. Denis et C. Phillips, 1994, The SAOZ balloon optical sonde for atmospheric chemistry study, *Proc. 11th ESA Symp. Europ.. Rocket & Balloon Prog.*, ESA SP 355, 87.

Santer, R., Brogniez, C., Herman, M. Diallo, B. S. and Ackerman, M., 1992. Correlative measurements of the stratospheric aerosols, *J. Geophys. Res.*, 97, 20825.

7. ACKNOWLEDGEMENTS

Balloon flights were operated by the Balloon division of the Centre National d'Études Spatiales (CNES) which is acknowledged as well as the support given to both laboratories by the French Programme National de Chimie Atmosphérique (PNCA).

OZONE CONCENTRATION OVER NORTHERN ITALY (MODENA AREA) BY MEANS OF DOBSON MEASUREMENTS AND OZONE-SOUNDINGS COMPARISON WITH GOME OBSERVATIONS

R. Santangelo, S. Pugnaghi, S. Teggi, A. Loria, P. Frontero, L. Lombroso
Dip. Sci. Ing. - Sez. Osservatorio Geofisico - Univ. di Modena, Italy

T. Colombo, R. Santaguida
Serv. Met. dell'Aeronautica - Sestola, Modena, Italy

Abstract
This paper gives the preliminary conclusions about GOME geophysical validation based on the activities carried out by our group and in particular on the results of the measurements performed in the Modena area (Northern Italy).
During the ERS-2 commissioning phase we carried out ozone-soundings, Dobson measurements and other related activities. In this period (August - December 1995) 19 ERS-2 orbits with GOME observations were available above Northern Italy.
Total ozone column data seem quite well measured by GOME at this latitude. Nevertheless they seem slightly underestimated if compared with Dobson measurements (about 3.5%). The number of comparisons available up to now is considered not enough and therefore a longer time series to confirm the results (taking into account winter and spring periods too) is needed.

1. INTRODUCTION

As part of GOME [ESA SP-1151 1993, ESA SP-1182, 1995] geophysical validation team we carried out ozone profile measurements at the meteorological station of the University of Modena, Dobson measurements at the base of the Italian Meteorological Service at Sestola, on the mountains near Modena and other measurements like UV-B and aerosols optical thickness at the base of Sestola.
The following results are based upon quoted measurements and GOME observations available above Northern Italy during the commissioning phase (end of July- December 1995). During this period 45 days of GOME level 2 product were analyzed, among them 19 are above Northern Italy and these are considered here.
Last summer a great number of fronts crossed all Europe, and weather was unusually cloudy in Italy. Among the considerd 19 days only a few were sunny, mainly during the end of September and October. Therefore direct sun observation was not always possible.

2. OZONE-SOUNDINGS

Atmospheric soundings were carried out using AIR-3A-RT radiotheodolite [Call et al. 1987] and AIR-4A-OZ-1680 sondes. The system works at 1680 MHz and is a completely movable instrument. Sensors data are digitally transmitted every three seconds with an error checking code with high precision and reliability.
The sondes measure atmospheric pressure, temperature and relative humidity (PTU). Wind speed and direction are determined from the balloon trajectory. Ozone profile is obtained using an Electrochemical Concentration Cell (ECC) originally developed by NOAA/ERL (USA) laboratories. The ECC produces a current proportional to ozone concentration. Cell current and other associated parameters are precisely measured and transmitted [A.I.R. 1991].
Range and accuracy of AIR-4A-OZ-1680 sondes are reported in Tab. 1.

Tab. 1	P (hPa)	T (°C)	R.H. (%)	O_3 (ppm)
Range	1050 to 3	50 to -90	5 to 100	0 to 1000
Accuracy	±1 hPa	±0.5 °C	±3 %	±5 %

The ozone-soundings for the GOME geophysical validation were performed about 10 km apart the town of Modena where the Geophysical Observatory has its rural meteorological station located in the Po valley towards Apennines mountains. Station coordina-tes are: Longitude 10.77°E, Latitude 44.64°N, Altitude 53 m (m.s.l.).
Ozone profiles were successfully carried out on 11th and 30th of August and again on 4th of October; on 15th of September two sondes lost signal at an altitude lower than 17 km.

Figg. 1a, 1b and 1c show the ozone profile measured on 11th of Aug., 30th of Aug. and 4th of Oct. respectively. The solid line is the ozone partial pressure (mPa), dash and dot and dash lines are the ozone volume mixing ratio (ppm) and ozone mass mixing ratio (ppm) respectively. The dot line is the vertical temperature profile in kelvin degrees. In each plot integrated ozone from the sonde measurements and Dobson daily mean are reported (DU).

Ozone profiles are available at NILU data-base, according to NASA Ames format [Gaines and Hipskind, 1992], in the directory /o3sondes/modena.

The upper part (above 28 km) of the ozone density profiles was extrapolated with a decreasing exponential function. The integral of the extrapolating function gives an estimation of the residual ozone concentration at altitudes above the balloon burst level. In Tab. 2 computed residual ozone is reported.

Tab. 2	burst level	residual ozone
day	km	D.U.
11th Aug 1995	33.2	43.4
30th Aug 1995	33.1	42.1
4th Oct 1995	30.7	57.5

The correction factors to normalize total ozone soundings, including residual ozone, to Dobson measurements are quite close to 1 (see next Tab. 3).

Tab. 3	Total ozone	Corr. Fact.
day	DU	---
11th Aug 1995	287	1.037
30th Aug 1995	326	1.001
4th Oct 1995	257	0.970

Atmospheric soundings permit to obtain the Cloud Top Pressure values which are compared with CTP extracted from GOME level 2 product [ER-PS-DLR-GO-0016 1995, ER-TN-IFE-GO-0018 1995, ER-TN-DLR-GO-0025 1995] as shown in Tab. 4.

Tab. 4	sounding	GOME
day	hPa	hPa
30th Aug 1995	870	454
15th Sep 1995	no clouds	454
4th Oct 1995	680	455

3. DOBSON MEASUREMENTS

Dobson measurements were performed at Sestola (Modena). In Sestola there is a base of the Italian Meteorological Service and the WMO-GAW station #201. Its coordinates are: Longitude 10.77°E, Latitude 44.22°N, Altitude 1030 m (m.s.l.). In this station Dobson spectrophotometer #48 (since 1975) and Brewer instrument #063 (since 1992) [Colombo & Santaguida, 1995] are installed. Because of its altitude the station is usually in a clear atmosphere. Brewer measurements show no sulfur dioxide at the station level. This is a good condition for Dobson measurements beacause SO_2 absorbs ultraviolet at the wavelengths used by Dobson and therefore no SO_2 means that no false increase of total ozone is added [WMO Report 37, 1995].

During July-August 1995 Dobson #48 was calibrated in an intercomparison field measurements at Arosa, Switzerland. During this period calibration tables giving differences of 0.05% between our Dobson #48 and Dobson #65 (Boulder, USA) were obtained. Finally, a standard procedure is used during measurements. This permits to have a set of measurements with homogeneous instrumental precision.

During GOME overpass a large number of measurements were perfomed during sunny days. Of the three types of measurements: Direct Sun (DS), Zenith Blue Sky (ZBS) and Zenith Cloud (ZC), the direct sun are of course the most reliable. To compare level 2 GOME product in cloud covered days Dobson zenith cloud measurements have been used too. Algorithm used to estimate total ozone by means of zenith blue sky and zenith cloud has been optimized taking into account the local situation and the existing direct sun measurements perfomed in near times.

GOME observations close to the station (i.e. GOME pixel whose center longitude and latitude differs less than 1.5° from station longitude and latitude) have been extracted from level 2 GOME product files. From the 19 orbits above Modena area, 153 GOME measurements were available.

Fig. 2a shows all GOME observations considered (black points), closest GOME measurements (white squares), days of ozone sonde launch (black arrows), Dobson daily mean using all types of Dobson measurements (triangles downward) and Dobson daily mean using only Dobson DS measurements (triangles upward). The numbers indicate the days of the month. Fig. 2b is part of the previous Fig. 2a and shows only GOME observation closest the station and Dobson DS daily mean trend. This plot highlights that usually GOME underestimates total ozone.

Tab. 5 shows Dobson daily mean of the considered day, Dobson nearest to the time of GOME observation, the closest GOME observation of the station and the Cloud Cover Fraction (CCF) in percent. On the right of the Dobson nearest measurement the type of Dobson measurement (DS or ZC) is reported. Dobson nearest in time ranges from some minutes up to one hour and a half.

Fig. 3a is the distribution of the percent differences between GOME data and Dobson daily mean. Mean value is -2.8% and the standard deviation ±3.5%. which expresses the validity of the obtained results over a day time period.

Fig. 3b is the distribution of the percent differences

between GOME data and Dobson measurements nearest the time of the satellite overpass. Mean value is -3.5% and the standard deviation is ±3.6% which shows the GOME underestimation.
Figg 4a and 4b show the distributions of the percent differences between GOME and Dobson measurement (nearest correspondence in time) for ZC and DS respectively. In the figures, distribution mean values and standard deviations are shown too.

Tab. 5 **day**	**Dobson mean** **Dobson nearest**	**GOME** **CCF (%)**
11 Aug. 95	297.6±0.8	not available
26 Aug. 95	292.4±9.6 292.8 (DS)	292.3 14
27 Aug. 95	303.3±14.6 321.5 (ZC)	312.9 21
30 Aug. 95	326.4±8.8 330.0(ZC)	310.7 14
02 Sep. 95	305.8±14.4 315.7 (ZC)	307.7 25
03 Sep. 95	306.4±11.3 323.4 (ZC)	303.7 14
06 Sep. 95	314.3±17.3 307.8 (ZC)	295.3 21
08 Sep. 95	312.3±13.2 310.3 (ZC)	279.7 49
15 Sep. 95	270.7±11.4 265.9 (DS)	261.7 15
21 Sep. 95	293.4±17.1 315.1 (ZC)	290.7 17
22 Sep. 95	299.7±3.3 302.9 (ZC)	290.8 21
27 Sep. 95	286.6±8.8 282.5 (DS)	282.9 15
01 Oct. 95	281.4±10.4 282.6 (DS)	273.3 12
04 Oct. 95	249.2±2.1 250.4 (ZC)	242.2 100
07 Oct. 95	261.0±6.9 273.9 (ZC)	257.7 13
13 Oct. 95	295.3±23.9 279.5 (DS)	280.4 14
29 Oct. 95	251.9±7.5 247.2 (DS)	252.5 45
30 Oct. 95	not available	260.8 50
11 Nov. 95	not available	261.5 40
13 Dec. 95	not available	322.5 100

In principle Dobson measurements performed at Sestola (about 1 km height) need a further correction, due to the first km of tropospheric ozone, for a precise comparison with GOME observations. Ozone soundings (Tab. 6) show in any case that such correction is rather small with a seasonal dependence (1÷5 DU).

Tab. 6 day	Total ozone first km DU
11th Aug 1995	3.7
30th Aug 1995	4.5
15th Sep 1995	3.3
4th Oct 1995	1.4

4. OTHER ACTIVITIES

Other activities carried out in this framework are UV-B (290-320 nm) broadband measurements, sunphotometric measurements (aereosols optical thickness), infrared atmospheric spectral measurements (2.5-14.5 μm) and UV-VIS-NIR (240-800 nm) atmospheric spectral measurements. These data are being fully analyzed and only some preliminary results are reported here.
Fig. 5 shows the atmospheric radiance in the quoted infrared range. The three curves are for three different instrumental zenith angles. Ozone peak at 9.6 μm is evident.
Fig. 6 shows UV-B trend measured at Sestola during the first ten days in November 1995. The number above each peak is the Dobson daily mean of the considered day. On the 2nd of November a front crossed our area, followed by a Northern advection (mA air mass type) which lasted three days. During these days total aereosols optical thickness was very low, ozone increased and UV-B decreased. From the 7th of November a high pressure field took place: tropospheric aereosol increased very quickly even at the station of Sestola in the nearby mountains.

5. CONCLUSIONS

When no cloud cover exists, so that direct sun is observable by Dobson, GOME level 2 product appears to agree rather well with observations. The data show a certain underestimation by GOME. However the mean percentage deviation is very small and within the standard deviation -0.4±2.5%. The slight underestimation is strengthened if a further small correction for the first km of tropospheric ozone is included. Moreover calibration might also depend on the intensity of the signal, so that a calibration for a complete year would be preferable.
When cloud cover exists and, in particular, when only zenith cloud measures are possible by Dobson, GOME level 2 product appear to underestimate the total ozone concentration -5.3±3.0%.
In these meteorological conditions GOME seems to overestimamate the real height of cloud top if compared with that observed by soundings. Since similar results have been obtained by other validation teams [GOME Validation Campaign workshop, 24-26

Jan. 1996, ESRIN, Frascati, Italy] an improvement of GOME algorithm is recommended.
A calibration for a complete year, in order to cover Winter and Spring periods, is also suggested.
The availability of direct vertical ozone sounding obtained by radiotheodolite suggests the validation of GOME ozone profile.

6. REFERENCES

AD-A167 000 Part 2 of 2 1985, Handbook of Geophysics and the Space Environment, *U.S. Air Force Geophysics Laboratory, Hanscom Air Force Base, MA.*

A.I.R. 1991, *Intellisonde Rawin/Ozonesonde System, Operations Manual*, AIR Inc., CO (USA).

Burrows J., Diebel D., Frank H., Muirhead K., Munro R., Kerridge B., Pemberton D., Platt U. 1994, A Study of Methods for Retrieval of Atmospheric Constituents, *ESA Report ref.: ESA CR (P) 3882, July 1994.*

Call D.B., Lassman S.J., Whitaker S.D., Horn R.D., Lovelace L. 1987, Digital radiosondes received by digital radiotheodolite provides fully automated upper air soundings, *Sixth Symposium Meteorological Observations and Instrumentation, New Orleans, La, January 12-16, 1987.*

Colombo T., Santaguida R. 1995, Misure di inquinamento atmosferico di fondo a Monte Cimone (background atmospheric measurements at Mt. Cimone) *Rivista di meteorologia aeronautica, anno 55°, N. 1-2, pp 59-70, gennaio-giugno 1995.*

ER-PS-DLR-GO-0016 1995, Product Specification Document of the GOME Data Processor, *DLR-DFD, Oberpfaffenhofen Germany.*

ER-TN-IFE-GO-0018 1995, GOME Software Databases for Level 1 to 2 Processing, *DLR-DFD, Oberpfaffenhofen Germany.*

ER-TN-DLR-GO-0025 1995, GOME Level 1 to 2 Algorith Description, *DLR-DFD, Oberpfaffenhofen Germany.*

ESA SP-1151 1993, The GOME Interim Science Report, *ESA Publications Division, 1993.*

ESA SP-1182 1995, Global Ozone Monitoring Experiment, *ESA Publications Division, Sep. 1995.*

Gaines A.E. and Hipskind 1992, Format Specification for Data Exchange, *Earth System Science Division at NASA Ames Research Center.*

WMO - Report N. 37 Published in February 1995: Scientific Assessment of Ozone Depletion: 1994, p 1.7, other contributions in the same rep.

Fig. 1a) O_3 Profile - Modena - 1995 Aug. 11 - 9:30 GMT

Station coordinates: Longitude 10.77E, Latitude 44.64N, Altitude 53 m

Dobson daily mean: 297.6 ± 0.8 D.U.
Integrated ozone of the sonde: 287 D.U.

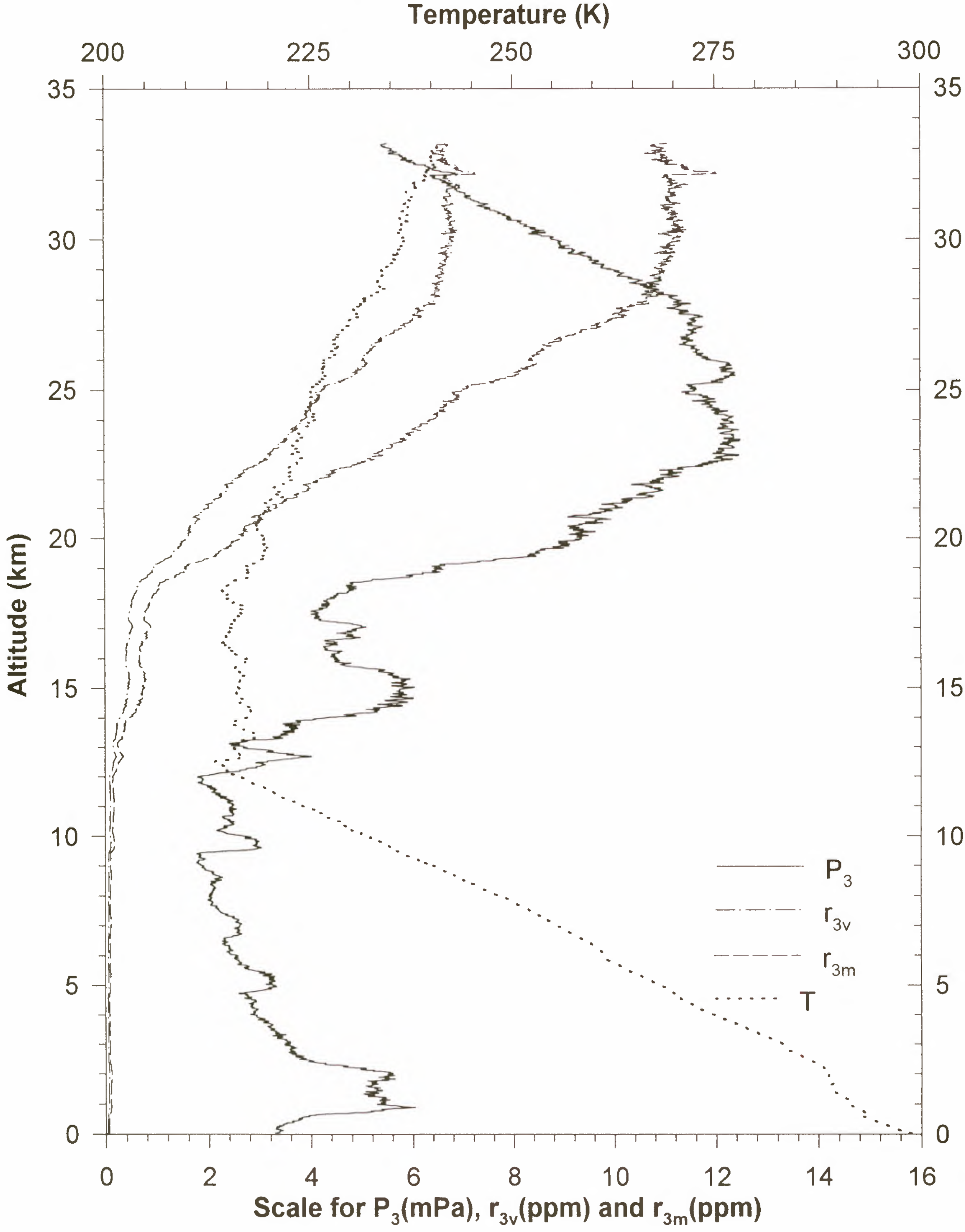

Fig. 1b) O_3 Profile - Modena - 1995 Aug. 30 - 10:30 GMT

Station coordinates: Longitude 10.77E, Latitude 44.64N, Altitude 53 m

Dobson daily mean = 326.4 ± 8.8 D.U.
Integrated ozone of the sonde: 326 D.U.

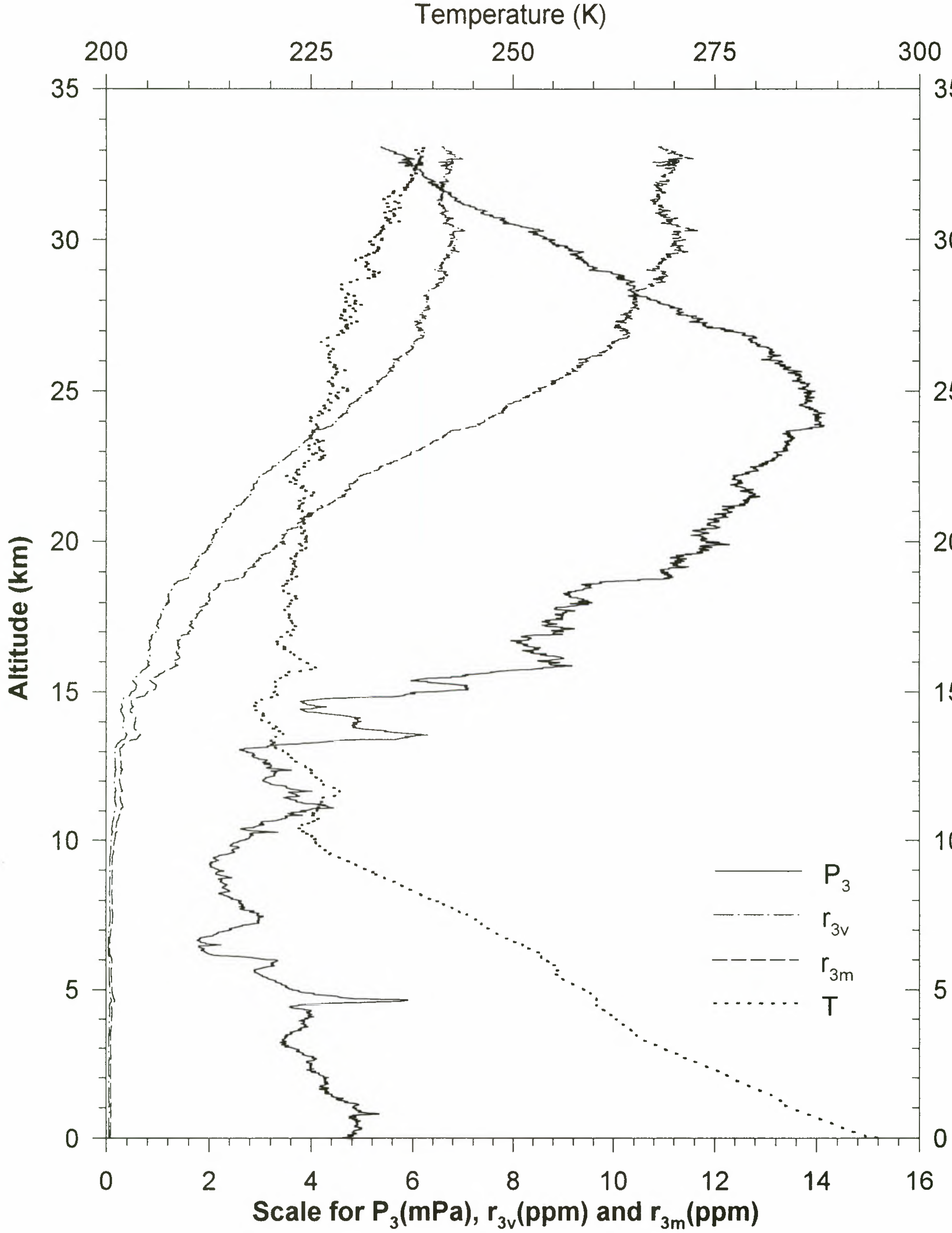

Fig. 1c) O_3 Profile - Modena - 1995 Oct. 4 - 9:30 GMT

Station coordinates: Longitude 10.77E, Latitude 44.64N, Altitude 53 m

Dobson daily mean: 249.2 ± 2.1 D.U.
Integrated ozone of the sonde: 257 D.U.

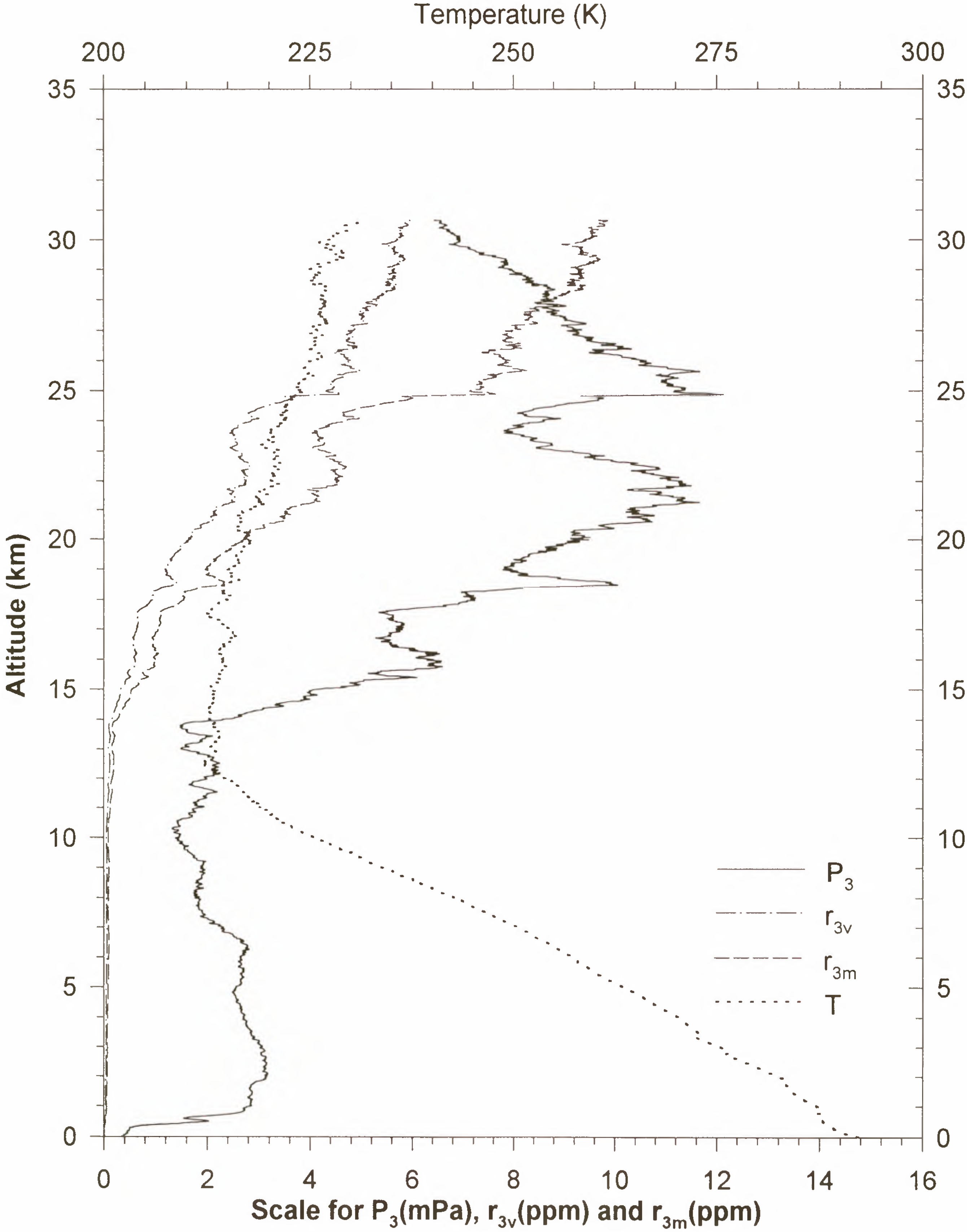

Fig. 2a) GOME & Dobson daily mean - Total ozone near Modena (1995)

Sestola (Modena) WMO station N. 201: Lat. 44.22°, Long. 10.77°, Alt. 1030 m (Dobson N. 48)

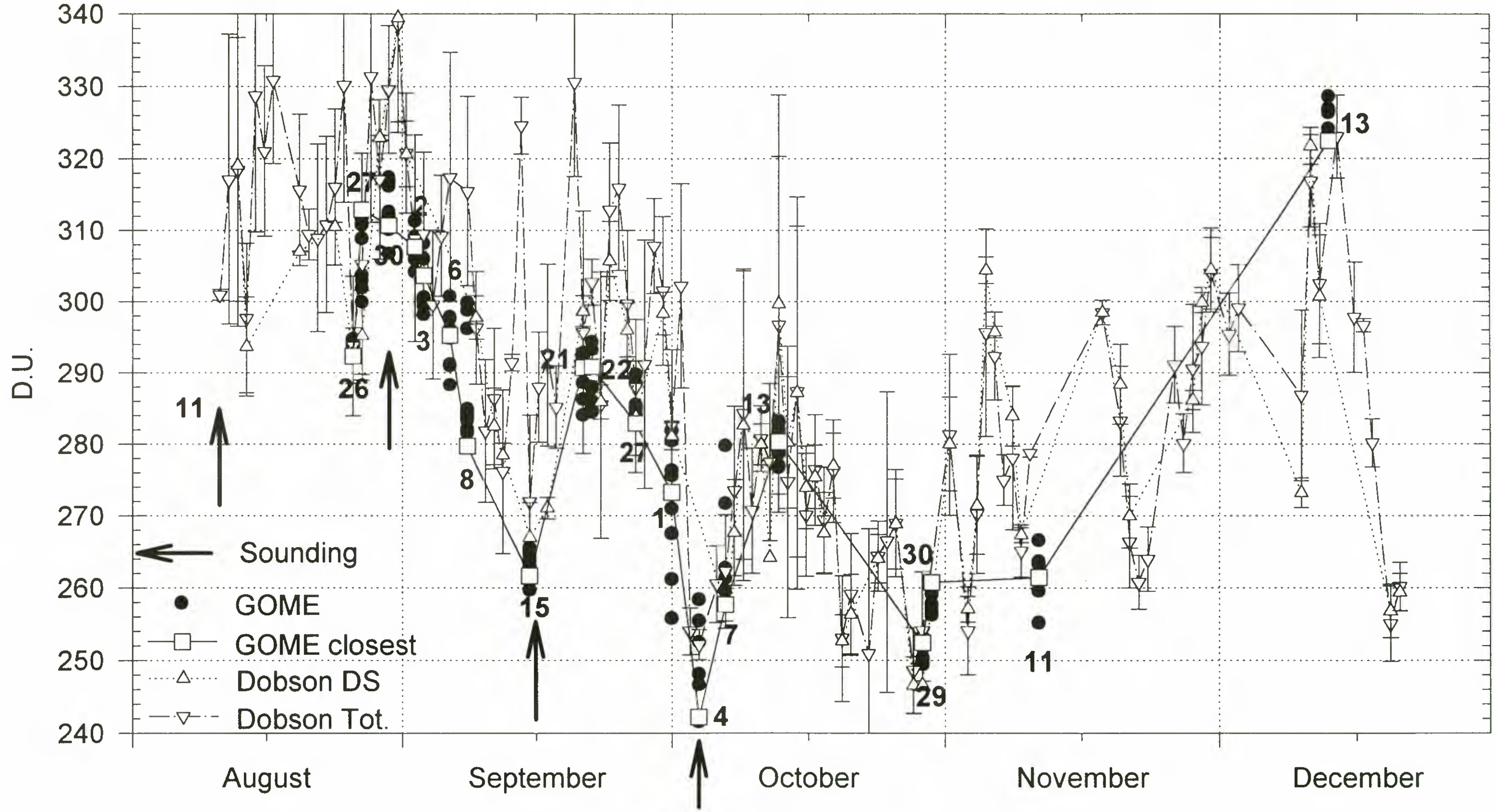

Fig. 2b) GOME & Dobson daily mean (DS) - Total ozone near Modena (1995)

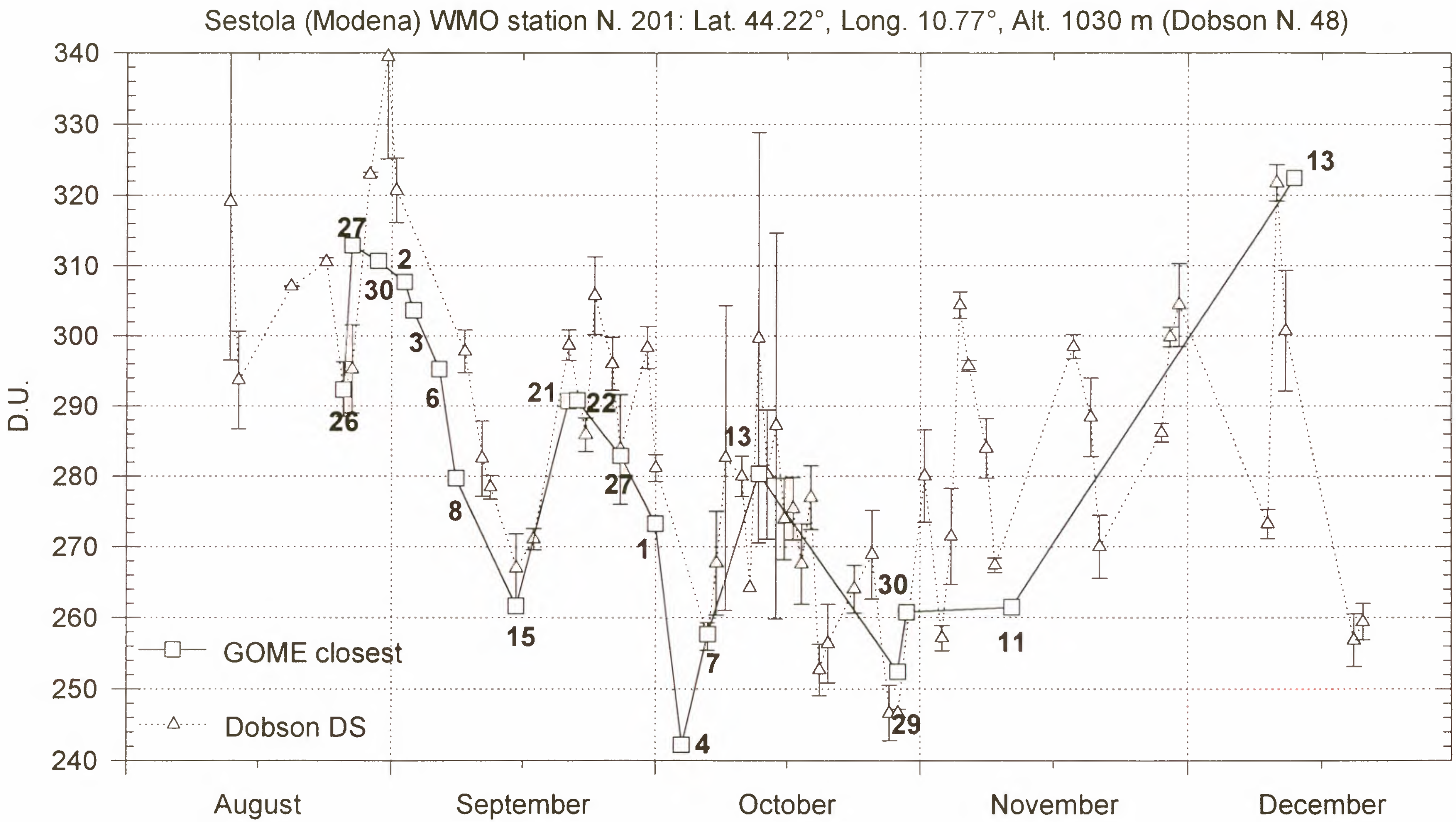

Fig. 3a) (GOME-Dobson)/GOME [mean]

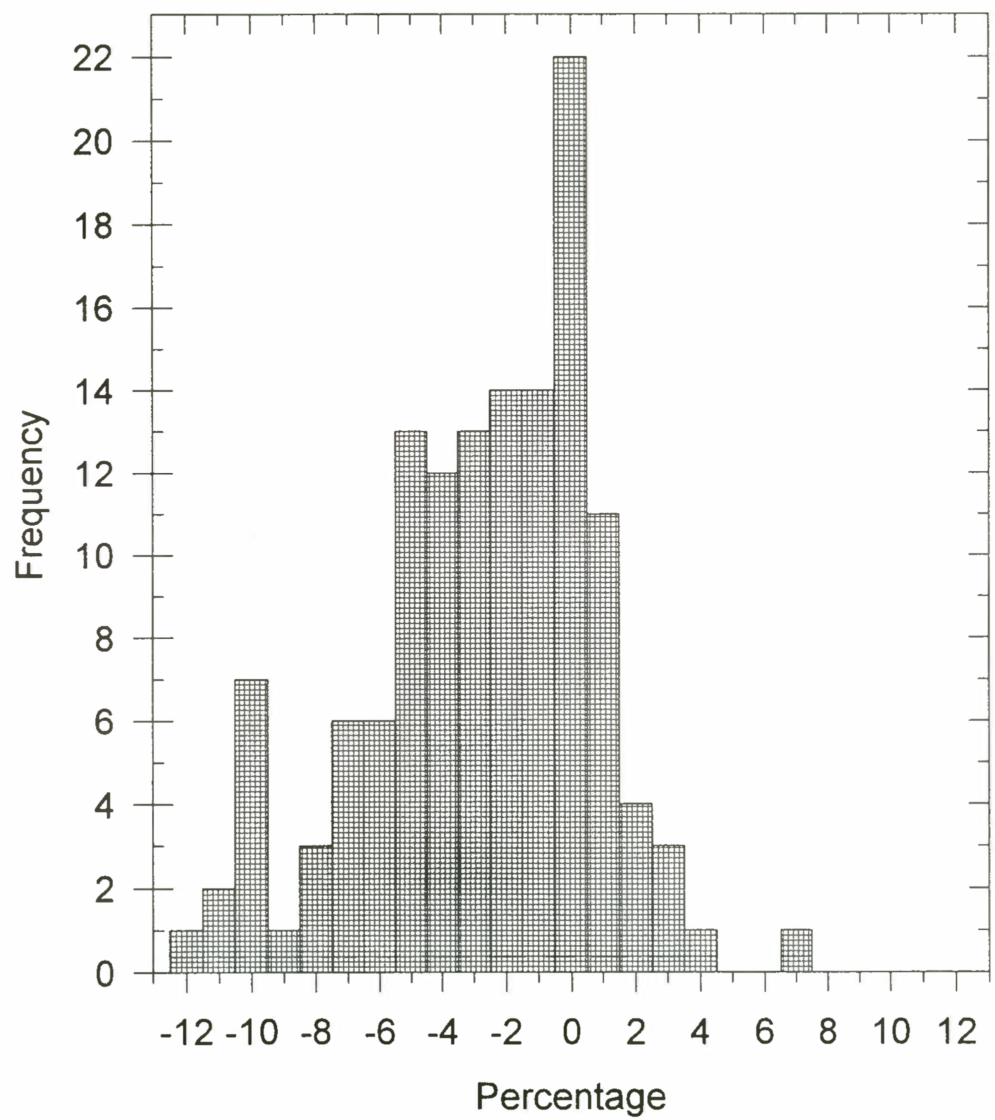

Fig. 3b) (GOME-Dobson)/GOME [nearest]

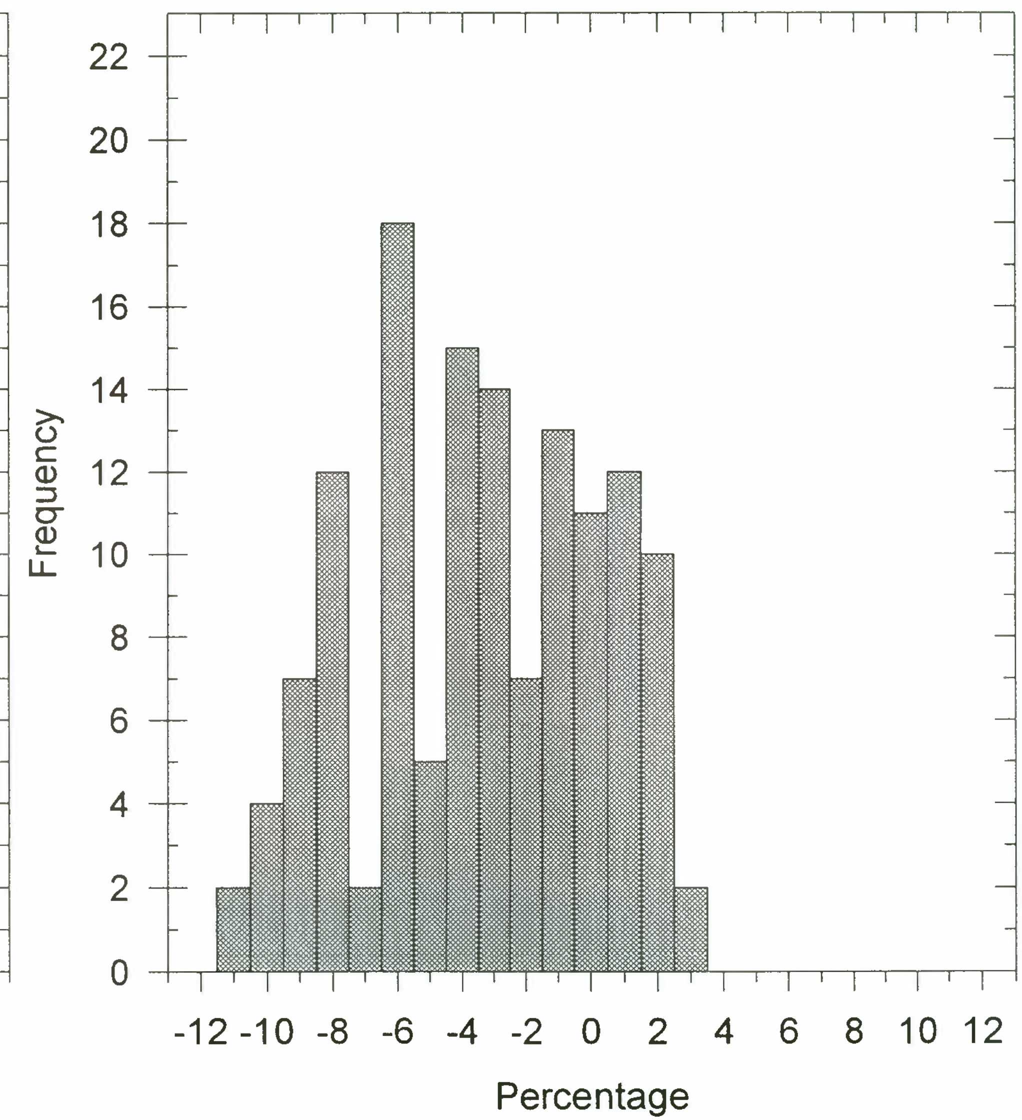

Fig. 4a) (GOME-Dobson)/GOME [ZC]

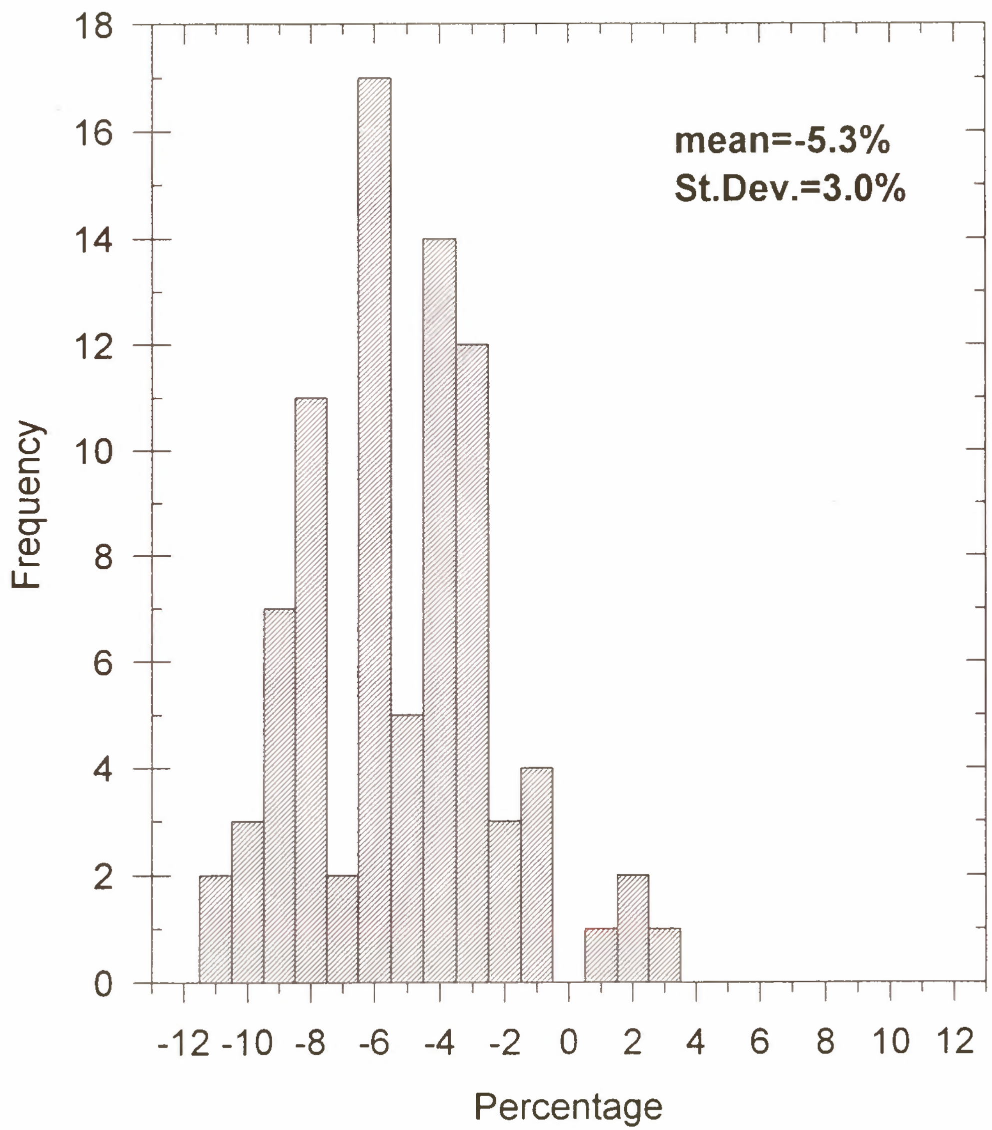

Fig. 4b) (GOME-Dobson)/GOME [DS]

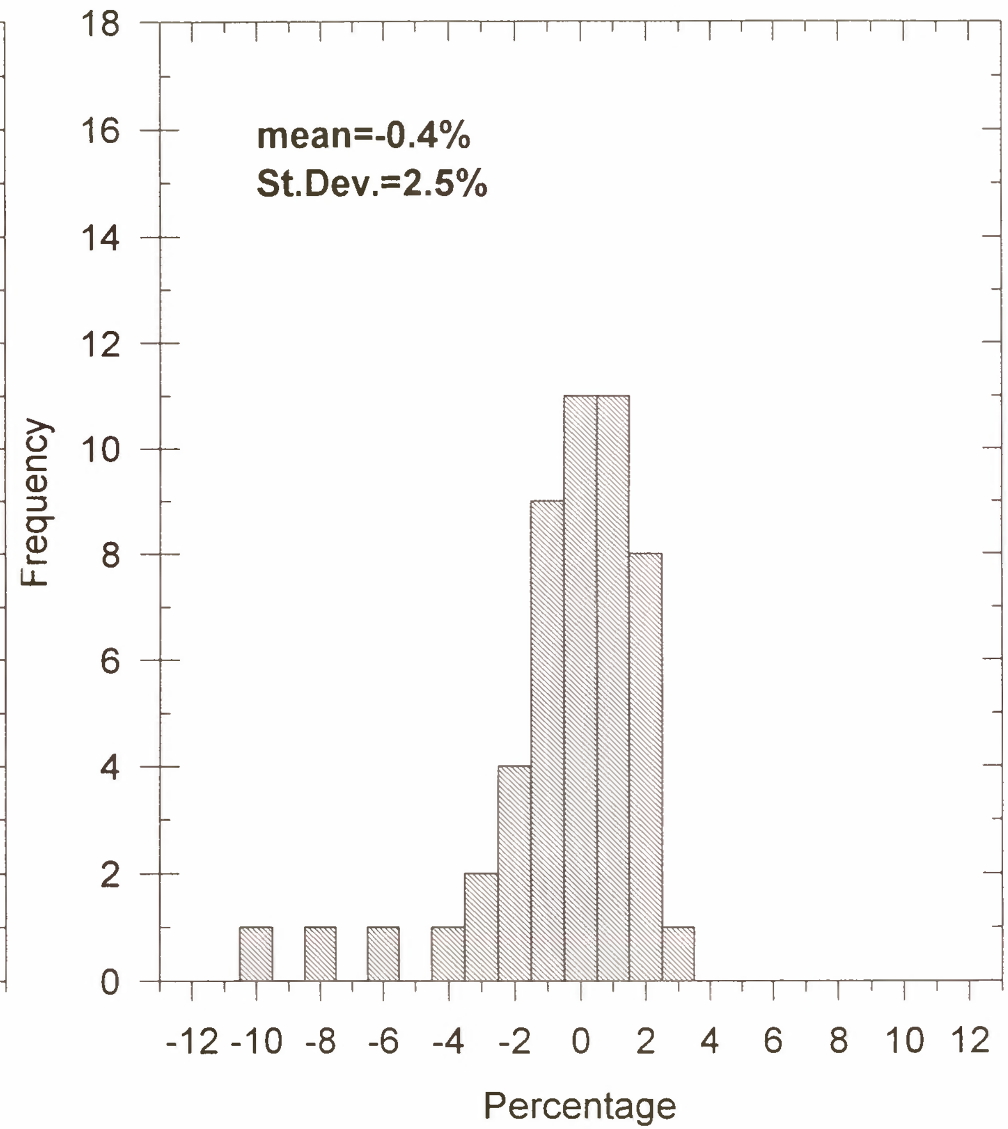

Fig. 5) Modena - Infrared atmospheric radiance - Zenith angles: 64°, 74°, 77°

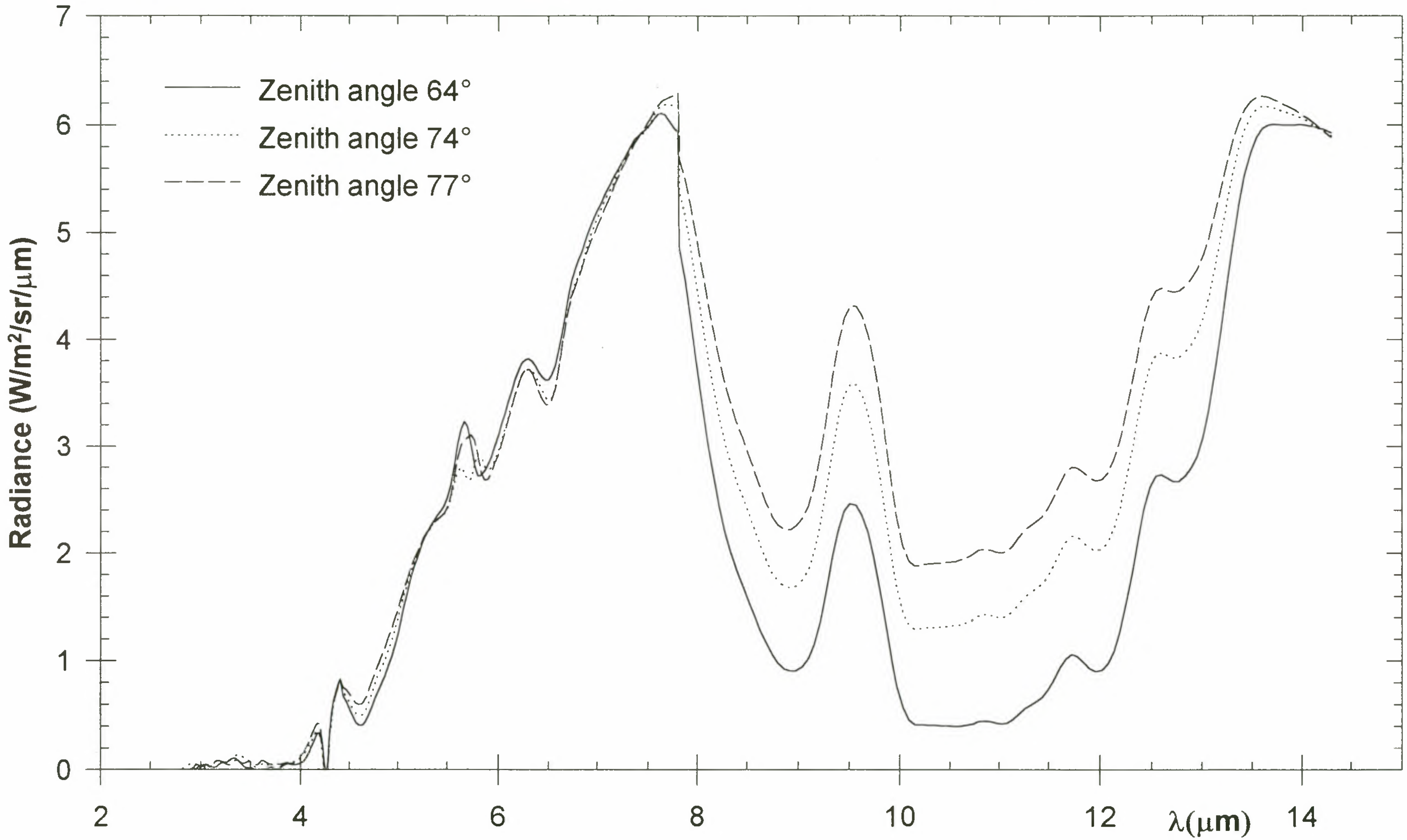

Fig. 6) UV-B Irradiance - Sestola Nov. 95 - Stat.: Long. 10.77°, Lat. 44.22°, Alt. 1030 m

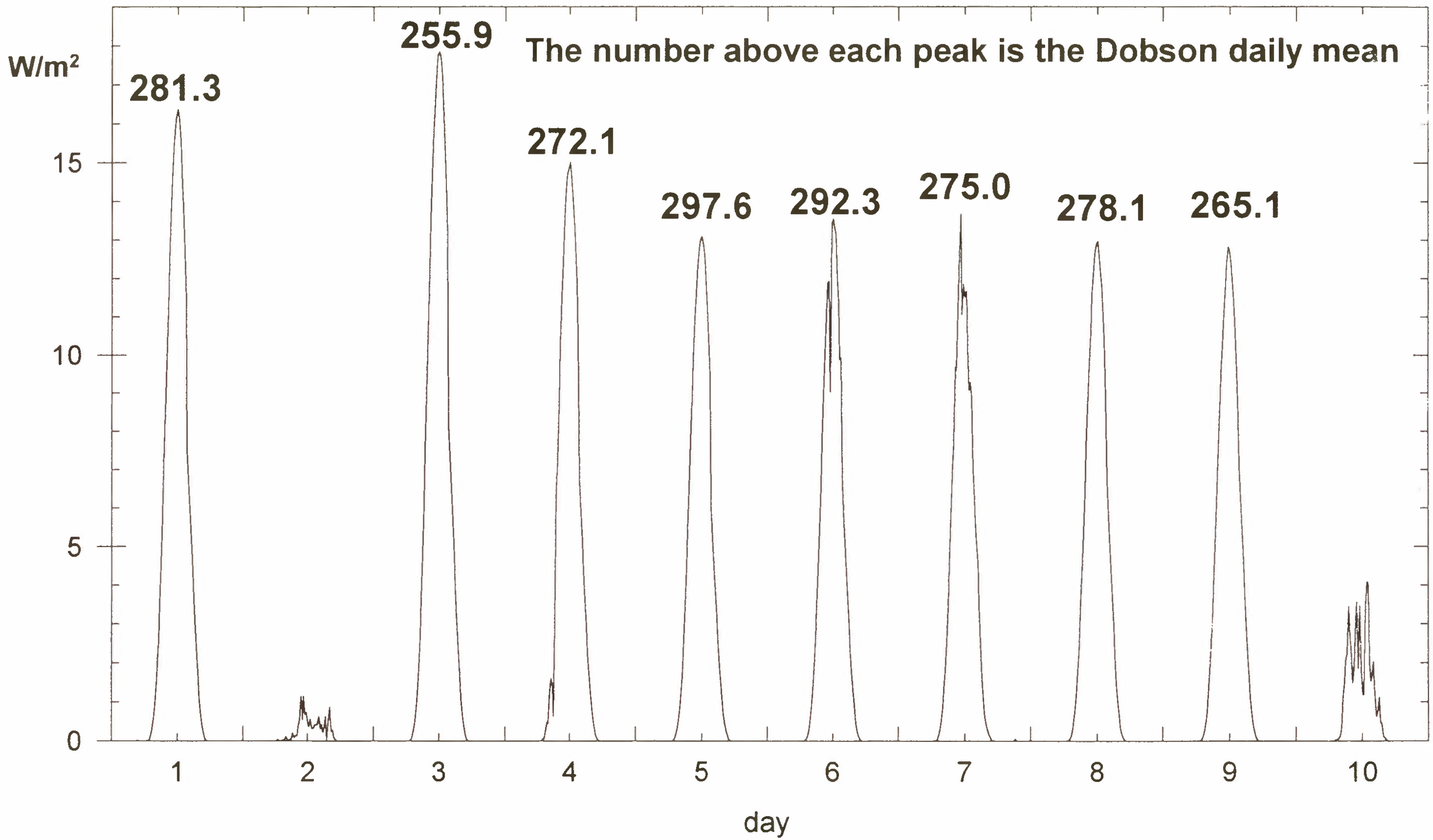

Validation of total ozone measurements with GOME during the main validation phase: the Norwegian project

G. Hansen & A. Dahlback.

Norwegian Institute for Air Research, Tromsø / Kjeller, Norway

Abstract

The Norwegian GOME validation project aimed at validating GOME total ozone measurements by comparing GOME data with ground-based measurements gathered with Brewer, Dobson, SAOZ and UV multi-channel filter (GUV, NILUV) instruments. The validation of ozone vertical profiles by means of ozonesondes and ozone lidar was postponed due to the non-availability of respective GOME data. The validation of total ozone data revealed a general underestimation of total ozone by GOME in the order of 3 to 12% compared to ground-based measurements. The size of the deviation is clearly dependent on the cloud fraction and - less clearly - on solar zenith angle (SZA). At SZA < 50° and a cloud fraction < 0.2 the deviation is in the order of 10 DU (~3%), increasing to about 35 DU (10-14%) for a cloud fraction of 1. At small (< 0.2) and large (> 0.8) cloud fractions there is no significant SZA dependence of the total ozone deviation, while at intermediate cloud fraction values the deviation is rather constant up to SZA values of 65 ° and then increases significantly.

1. INTRODUCTION

The Norwegian GOME validation/calibration project is based on a **PRODEX** contract between the European Space Agency (ESA) and the Norwegian Institute for Air Research (NILU). The objectives, the time frame and the budget of the project were defined in a **statement of work** agreed upon by the participating parties. The project was officially started in April 1995.

The Norwegian GOME validation/calibration project mainly aimed at the validation of total column ozone measurements by comparing GOME data with ground-based measurements achieved with various techniques: Brewer, Dobson, SAOZ, UV multi-channel filter instruments (GUV, NILUV), ozonesondes and ozone lidar. A second - optional - aim was to validate vertical density profiles of ozone if provided by GOME by comparing them with ground-based profiles taken with ozonesondes and ozone lidar. The latter aim was not achieved in the main validation phase due to the non-availability of such GOME data.

The main validation phase was started as scheduled, i.e. three months after the launch of ERS-2, on July 20, 1995. However, due to problems with the conversion algorithms for the GOME products these were not available until end of October. As a consequence of this, the main validation phase was extended until end of December 1995. This interim validation report contains the results of the Norwegian GOME validation as presented on the GOME validation workshop on January 24-26, 1996, at ESRIN, Frascati (Italy).

2. VALIDATION PREPARATIONS

As agreed upon in the Statement of Work, a 3-month-period after the ERS-2 launch was used to develop a couple of software tools both for the Norwegian validation and for common use in the validation community.

The routine ***PASS*** calculates passovers / passbys of the ERS-2 satellite (with GOME onboard) for a list of selected ground-based sites within a chooseable horizontal range. The routine uses ESA's official orbit propagator software, the provision of which is gratefully acknowledged. Its main purpose is to schedule ground-based measurements optimally with respect to GOME measurements. A modified version of ***PASS***, called ***DOBRGOM***, is used in connection with the validation software package ***DOBSGOME***. It provides a list of passovers/passbies for a list of selected stations in chronological order.

The software package ***DOBSGOME*** was developed in cooperation with R. Koopman, RIVM, The Netherlands. It purpose is to extract both relevant GOME data and ground-based data for a specified time interval and for specified frame conditions (maximum spatial and temporal separation between the two data sets) which then can be used in a further evaluation procedure.

Furthermore, the package provides postscript files with a graphical display of the selected GOME measurements.

All software mentioned above was installed at the NADIR database at NILU and was available to all participants of the GOME validation/calibration.

3. GROUND-BASED MEASUREMENTS

The original ground-based instrument set to be used was completely based on standard techniques (Brewer, Dobson, SAOZ, ozonesondes) which have been described before. The ozone differential absorption lidar at Andøya, intended to validate vertical ozone profiles, has been established recently; a description of the system is given by Hoppe et al. (1995). Shortly before the start of the main validation the possibility to include multi-channel moderate bandwidth UV filter instruments (GUV, NILUV) arose, and in fact it turned out that this technique was the most valuable one as it yields total ozone values under much worse weather conditions and at lower sun elevations than any other technique. A detailed description of this instrument and results of a

Name	Latitude (N)	Longitude (E)	Instruments
Oslo	59.91	10.72	Brewer, GUV, Dobson, SAOZ
Tromsø	69.66	18.97	Brewer, Dobson, GUV
Ny-Ålesund	78.91	11.88	Dobson, GUV, SAOZ
Punta Arenas	-53.20	-70.90	GUV (,Brewer)
Andøya	69.29	16.02	ozonesondes, lidar, NILUV
Gardermoen	60.12	11.06	ozonesondes
Bear Island (Bjørnøya)	74.51	19.02	ozonesondes
Ørlandet	63.42	9.24	ozonesondes
Takvatn	69.12	19.08	NILUV

Table 1: List of stations involved in the Norwegian validation project

first intercalibration with standard techniques is given by Dahlback (1995).
The stations involved in the validation, their coordinates and the instruments available there are listed in Table 1.

3.1 **Oslo**

Brewer measurements were performed on 91 days (76%) in the period July 17 through November 13, 1995; only direct-sun measurements were taken into account. GUV measurements are available from 147 days (89%) in the period July 19 through December 31. A SAOZ instrument was run at Oslo in the period July 19 through August 23; data are available from all days. The Dobson instrument was run throughout the validation period, and at the moment data from 20 days in the period July 25 - September 15 are available, mainly with only one value per day. An example of ground-based data gathered during a 10-day period in August 1995 is shown in Fig. 1. It reveals that on most days Brewer, Dobson and GUV measurements agree very well. The SAOZ values are generally around 10 DU lower than the other measurements; they were excluded from this analysis by the choice of selection criteria.

3.2 **Tromsø**

Due to the location of Tromsø (3° north of the polar circle) total ozone measurements with Brewer, Dobson and GUV are limited in time; after November 3 the sun does no longer exceed an elevation angle of 5°. Brewer measurements were performed on 65 days (72%) in the period July 18 through October 15. After that date, no more measurements were taken due to low sun elevation. Furthermore, on many of these days only few measurements were taken due to very bad weather conditions during most of the validation period. For the same reason, Dobson measurements are available for only 20 days (22%) in the period mentioned above. With the GUV instrument, measurements were made on 92 days (87%) in the period July 20 through November 3, but also here both quality and number of single measurements were strongly affected by the weather conditions. Fig. 2 shows the GUV and Brewer measurements taken in the period August 29 - September 7, 1995.

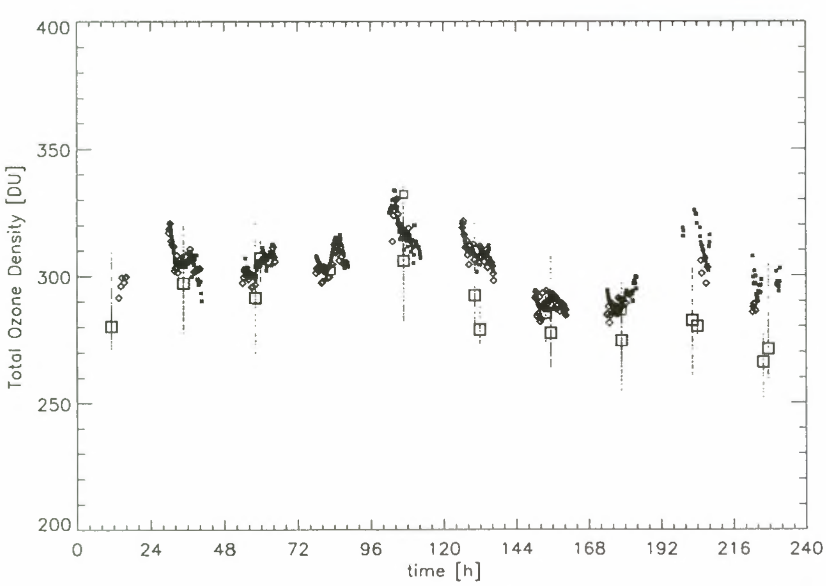

Fig. 1. Groundbased measurements at Oslo in the period August 25 - September 3, 1995. Stars: GUV data; diamonds: Brewer data; squares: Dobson data; large squares: distance-weighted GOME pixel averages (see text).

3.3 **Ny-Ålesund**

Ny-Ålesund is about 12° north of the polar circle which results in midnight sun until end of August and polar night already from end of October. This restricts Dobson measurements to mid of September, GUV measurements to about October 10 and SAOZ measurements to about October 20.
GUV measurements were performed on 77 days (94%) in the

period July 19 through October 8. The SAOZ instrument first installed at Oslo was operational from September 1; it took measurements on all days (51) in the period September 1 through October 21. Dobson measurements are available for 21 days (33%) in the period July 19 - September 15. Fig. 3 shows a sequence of nearly continuous GUV measurements and sporadic Dobson measurements at this site in the the second half of July.

3.4 **Punta Arenas**

At Punta Arenas, a Brewer, a GUV and a NILUV are operated. The Brewer data are not available for this campaign but have been used to calibrate both the GUV and the NILUV. For the GOME main validation GUV data from the period October 17 - December 13 are available.

3.5 **Andøya**

10 ozonesondes were launched at the Andøya Rocket Range in the period August through October: on August 3, 9, 28, September 1, 7, 13, 20, 29, October 9, and 12. Eight of these yielded reliable total ozone values, one (September 29) gave a value with a large uncertainty as it only reached a maximum altitude of 25 km, and one (August 28), gave no total ozone value as it only reached 20 km maximum altitude.

Lidar measurements at the nearby ALOMAR facility were strongly inhibited by the unfavourable weather conditions in Northern Norway this summer. Measurements were taken on 31 days (19%) of the main validation period. So far, 15 runs have been evaluated 8 of which yielded usable ozone profiles (August 13, September 1, 2, 3, 4, 6, 7, 8, 9).

The NILUV instrument was installed at ALOMAR on August 9 and has been running until mid of November except in periods with extremely bad weather conditions (storm), 64 days in total. The total ozone evaluation was started recently, and first results from early September 1995 - together with lidar data - are shown in Fig. 4. These data agree very well both with total ozone derived from ozonesondes on September 1 and 7, and lidar data from the same period.

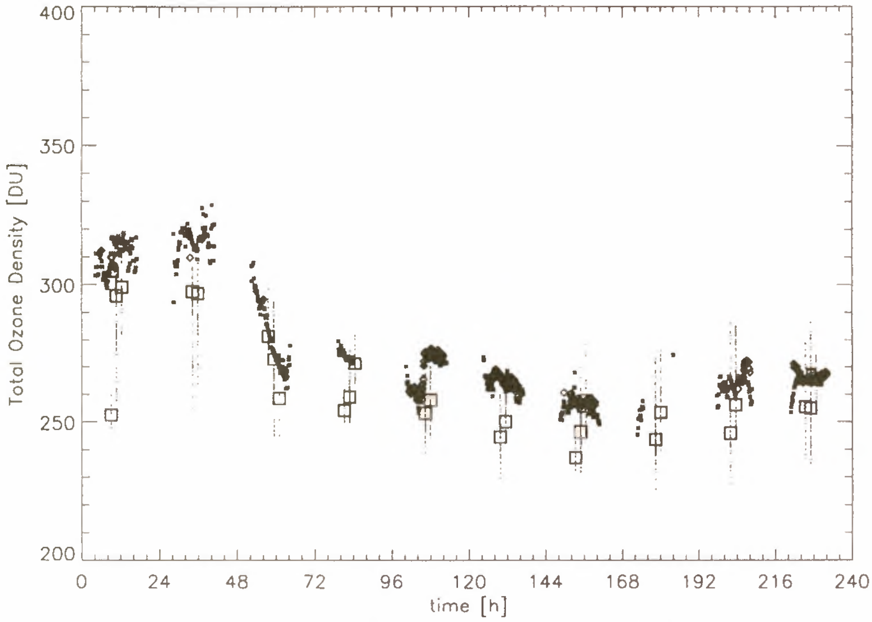

Fig. 2. Groundbased measurements at Tromsø in the period August 29 - September 7, 1995. Stars: GUV data, diamonds: Brewer data, squares: Dobson data, big squares: distance-weighted GOME orbit averages of selected pixels (see text).

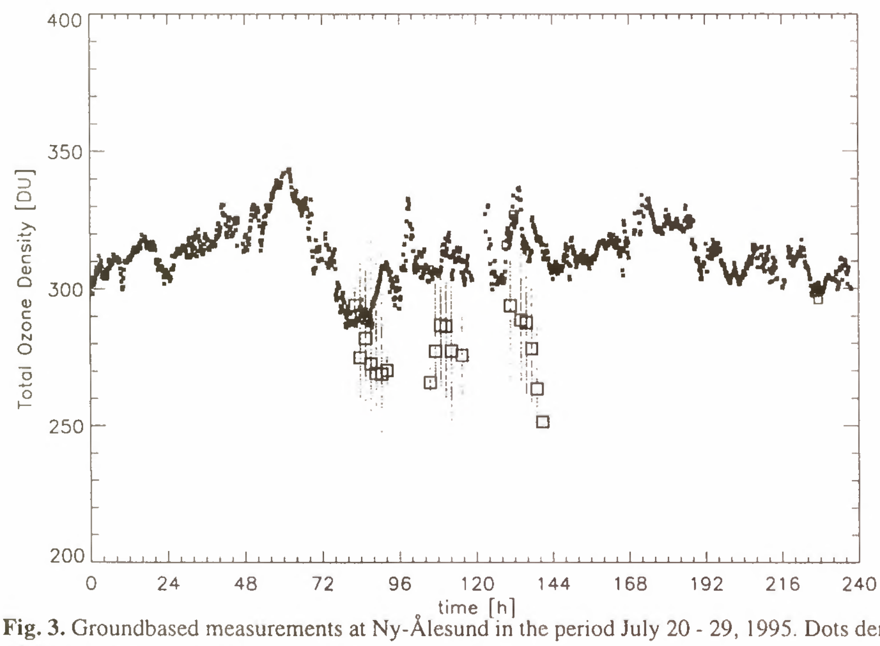

Fig. 3. Groundbased measurements at Ny-Ålesund in the period July 20 - 29, 1995. Dots denote GUV data, squares Dobson data, big squares and dots: as above.

3.6 **Other ozonesondes**

12 ozonesondes were launched at Gardermoen (July 26; August 23; September 6, 20; October 4, 18, 25; November 1, 22, 29, December 13, 27) 11 of which can be evaluated with respect to total ozone (not July 26).

At Ørlandet, 6 ozonesondes were launched (August 9; September 6; October 4; November 1, 29, December 27); all have been evaluated with respect to total ozone.

At Bear Island 11 ozonesondes were launched (August 16, 23; September 6, 13, 20, 27; October 4, 11, 18, 25; November 1) eight of which yielded total ozone values. One sonde (October 25) only reached 22 km; in two cases (September 6, October 11) ozone data were lost due to technical problems.

3.7 **Other measurements**

Before being installed at ALOMAR, the NILUV instrument was run at Takvatn, about 100 km southeast of Tromsø in the period July 20 -August 3. These data are not yet evaluated with respect to total ozone.

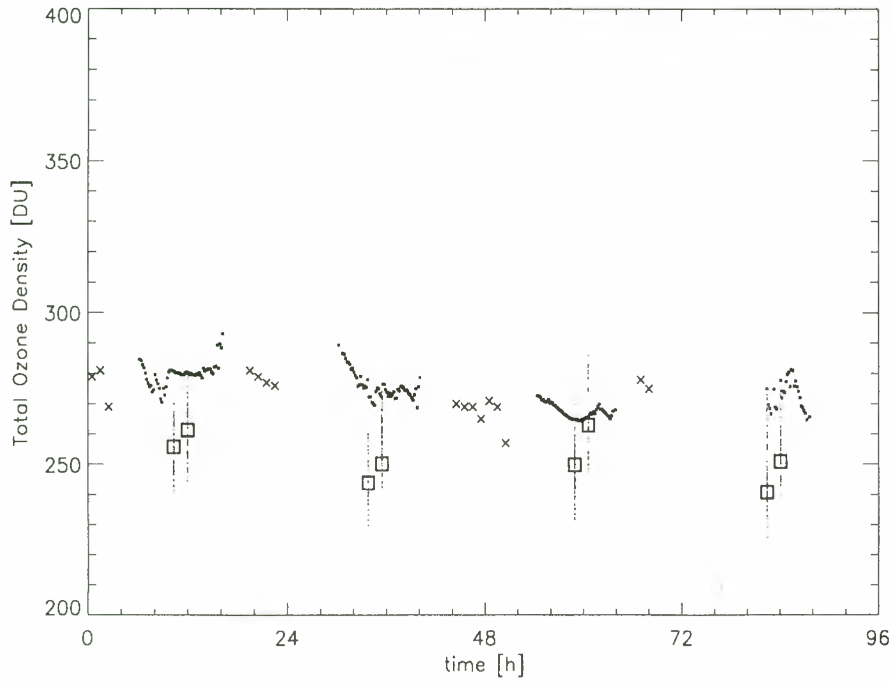

Fig. 4. Measurements at Andøya in the period September 2 - 5, 1995. Small stars: NILUV data, x'es: ozone lidar data, big squares and dots: GOME data as in previous plots.

Data from 6 other Norwegian GUV stations are not available at the time being. NILUV instruments owned by NILU have also been running throughout the validation period in Southern Chile but data from these are not available so far, either.

4. COMPARISON OF GROUND-BASED DATA WITH GOME DATA

Due to the delay in the GOME data processing only a limited set of GOME data was delivered until beginning of January 1996 and included in the main validation:

- July 23 - 25,
- August 25 - 27, 29 - 31,
- September 1 - 9, 15 - 17, 20 - 23, 27, 28,
- October 1 - 3, 5 - 7, 11 - 13, 29 - 31,
- November 9 - 11,
- December 11 -13.

For these periods the following ground-based data are available:

- Brewer, GUV and SAOZ at Oslo,
- NILUV at Andøya,
- Brewer and GUV at Tromsø,
- Dobson, GUV and SAOZ at Ny-Ålesund,
- GUV at Punta Arenas,
- in total 10 ozonesonde from the 4 ozonesonde sites.

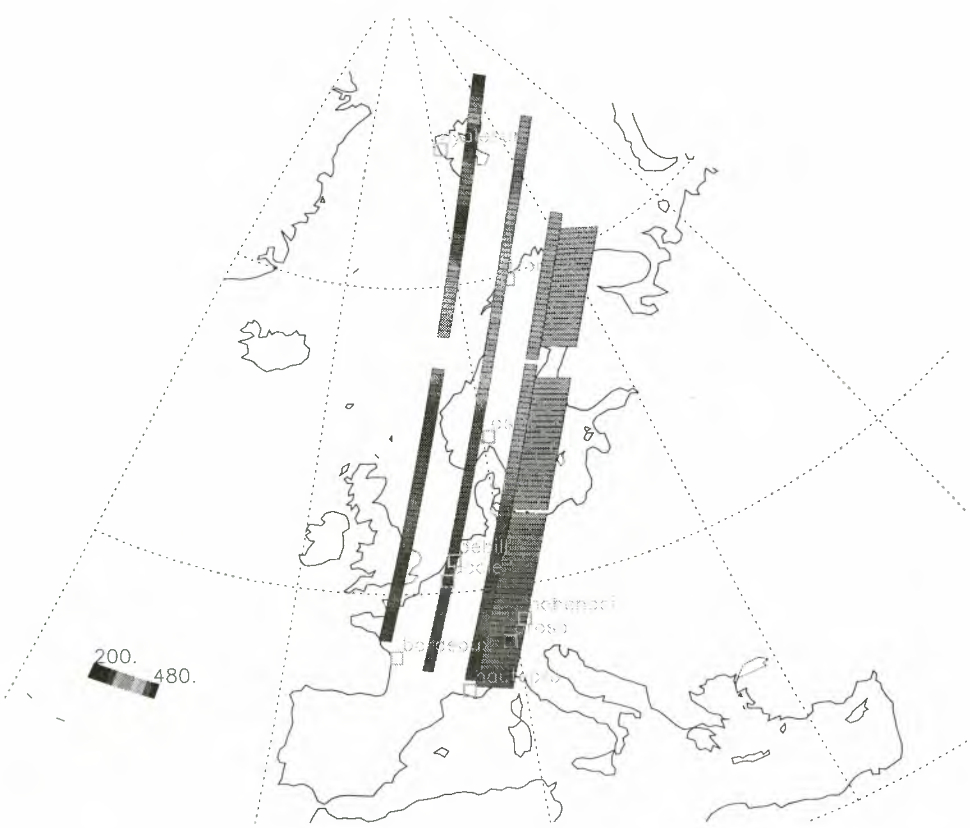

Fig. 5. GOME pixels selected with the *DOBS-GOME* routine from GOME data file 50725091.lv2 with a maximum horizontal distance of 600 km to ground-based stations (Brewer, Dobson, GUV).

Both ground-based and GOME data were pre-selected by use of the *DOBSGOME* routine. The output files *dgYYMMDD.dif* only contain GOME pixels with a horizontal distance between the pixel center nadir point and the ground station of **less than 600 km** and ground-based data taken **within 6 h** with respect to the average measuring time of the selected GOME pixels. An example of GOME pixels selected from the most favourable orbit on July 25, 1995, is shown in Fig. 5.

In the further evaluation, both ground-based and GOME data to be considered were reduced by the use of more restrictive criteria. Because of the considerable variations of total ozone within few hours at all stations (see, e.g., Fig. 3) only ground-based data taken in a ±2-h window with respect to the average GOME measuring time were regarded. Of the GOME data, only those with an air mass factor < 10, a relative error < 5% and a solar zenith angle < 73.5° were taken into account.

The validation procedure consisted of the following steps:

- calculation of an average ground-based total ozone value for each orbit of a day;
- calculation of the total ozone difference between each selected GOME-pixel value and the respective average ground-based value;
- calculation of linear regression coefficients for each day from all selected pixels weighted with the reciprocal horizontal distance squared (hereafter called version A); two examples are shown in Fig. 6;
- determination of the dependence of the total ozone difference on solar zenith angle (SZA) and cloud fraction (CF), using days with no significant dependence on the distance;
- calculation of total ozone differences between average ground-based total ozone and the closest pixel of each GOME orbit considered;
- calculation of linear regression coefficients from the latter data set using all orbits included in the analysis (hereafter called version B);
- determination of average deviations for the 3 stations, and their dependence on SZA and CF.

The validation with ozonesonde measurements was only evaluated with method B.

Fig.s 1 - 3 show - besides the respective groundbased data - GOME total ozone values as selected by the *DOBSGOME* routine: all single pixel values are marked by small dots (which appear in an almost vertical line because of the high velocity of GOME), while the big squares are the distance-weighted averages of the selected single values per orbit and station. The number of dots indicates whether the respective orbit passed close to the site (many points, e.g., at Oslo on August 29, 10 UT) or at a large distance (few points, e.g., at Ny-Ålesund on July 23, 10 UT and 20 UT). These examples already show significant features which will be further discussed on a statistical basis below:

- at Oslo in most cases the averaged GOME values are close to average ground-based values but in general smaller;
- the agreement at Oslo and Tromsø is worst under bad weather conditions (Sept. 2, 3 at Oslo, August 30, Sept. 1 at Tromsø);
- at Ny-Ålesund the GOME values of total ozone are in general significantly lower (more than 20 DU or 8%) than ground-based values.

Evaluation version A, i.e., extrapolating the deviation at the site by applying linear regression to all pixel values selected from single days, and then taking a (error-) weighted average of all daily values, yields deviations as given in Table 2; two examples of single-day analyses are shown in Fig. 6.

From Table 2 it is evident that the GOME values are

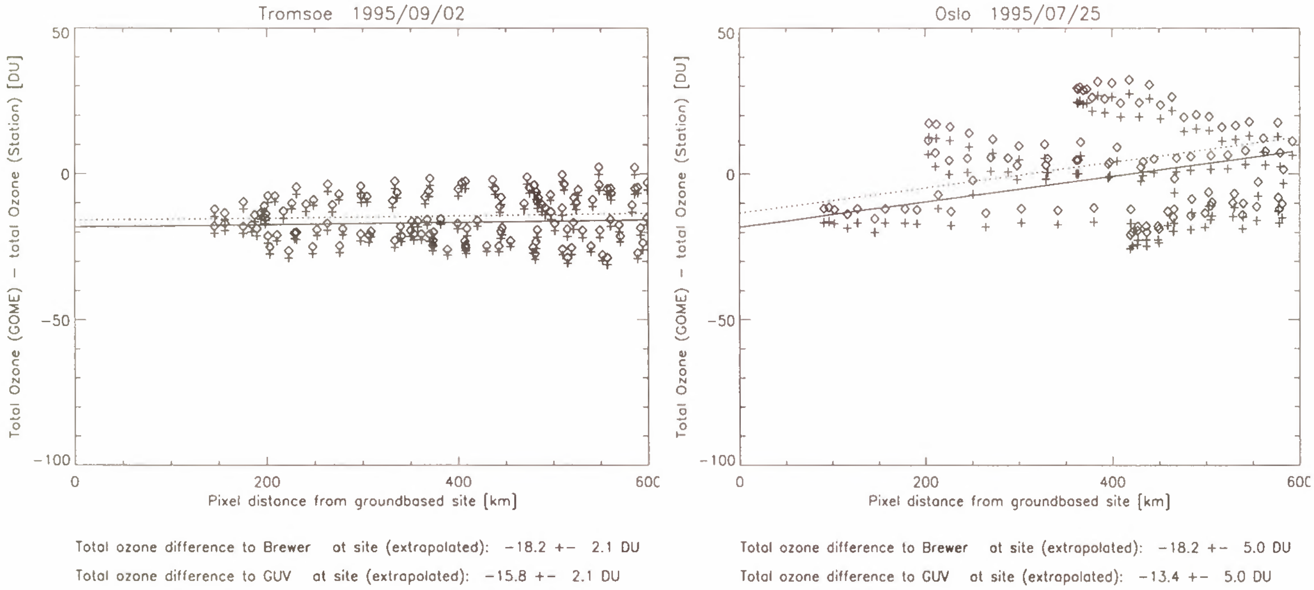

Fig. 6. Deviation between all GOME pixel values and their respective ±2-hour window ground-based average value on September 2 at Tromsø (left panel) and on July 25 at Oslo (right panel). Diamonds denote GOME deviations from GUV and crosses deviations from Brewer. Solid line: linear (distance-weighted) fits through Brewer deviations, dotted line: linear (distance-weighted) fits through GUV deviations.

Station name	Instrument	number of values	total ozone diff. [DU]
Oslo	Brewer	26	-15.1
Oslo	Dobson	6	-24.4
Oslo	GUV	37	-15.7
Tromsø	Brewer	25	-16.6
Tromsø	GUV	31	-17.2
Ny-Ålesund	Dobson	10	-28.3
Ny-Ålesund	GUV	20	-27.3
Punta Arenas	GUV	6	+6.4

Table 2. Mean total ozone deviations derived by method A

generally lower than ground-based measurements at the Northern stations. Furthermore, the differences are similar at Oslo and Tromsø, but clearly larger at Ny-Ålesund. After re-calibration of the GUV instruments in November/December 1995, there is no a systematic offset between GUV and Brewer measurements at Oslo and Tromsø, and between Dobson and GUV measurements at Ny-Ålesund. The Dobson at Oslo, on the other hand, reveals a significantly larger deviation from GOME than the other two instruments. This can be caused by the much smaller measurement statistics and the fact that there is usually only one Dobson measurement per day. Still one would not expect such a significant deviation, and, therefore, a case-by-case analysis should be performed.

At the only Southern hemisphere station, Punta Arenas, the extrapolated GOME total ozone values are slightly larger than those of the ground-based instrument. However, the number of validation days here is still too small to speak of a hemispheric (or seasonal) dependence of the total ozone difference.

Evaluation version A also reveals - as to be expected - a scattering of the total ozone differences increasing with distance (seen nicely on the left panel of Fig. 6), but in many cases this is not random but structured, as for example in the right panel of Fig. 6. Here, the total ozone values obviously vary considerably between the different pixel paths (west, center, east, back). This is either due to real horizontal structures in the total ozone distribution also at scales much smaller than 600 km, or to insufficiencies in the GOME algorithm not accounting for the differences in scattering geometry for the different pixel paths.

To identify a possible dependence of the total ozone deviations on solar zenith angle and cloud fraction, only pixels within a radius of less than 200 km were considered; data from Punta Arenas were not included due to a possible seasonal effect. Furthermore, only GUV measurements were chosen as a comparison data set, as they cover a wider range of cloud fraction and solar zenith angle conditions than Dobson, Brewer, and SAOZ.

Fig.7 shows the dependence of the total ozone deviation on the cloud fraction for three different SZA regimes. Measurements from Oslo are marked with diamonds, those from Tromsø with triangles and those from Ny-Ålesund with crosses. At SZA values < 50° the deviations concentrate around -10 DU at small cloud fractions (up to values of 0.4) and then increase - apparently linearly - to values of -40 DU at a cloud fraction of 1. There are, however, too few points to confirm a real linear dependence. At SZA values between 50 and 65°, with much more data points, a similar behaviour is seen. Up to cloud fraction values of about 0.3, the deviation is

Station	Date (YYMMDD)	time between sonde launch and GOME [h]	distance [km]	SZA [°]	cloud fraction	ozone difference [DU]
Gardermoen	950906	0.85	266.8	52.47	0.51	-36.94
Gardermoen	950906	-0.81	263.1	55.94	0.66	-26.28
Gardermoen	950920	-0.10	80.6	59.01	0.11	-24.57
Ørlandet	950906	-0.48	17.1	57.90	0.44	-19.27
Andøya	950907	-0.87	9.8	60.45	0.55	- 9.59
Andøya	950920	-0.71	39.8	67.89	1.00	-25.89
Bear Island	950920	0.07	121.2	72.58	0.25	+20.69
Bear Island	950927	0.49	194.4	73.30	0.80	-50.00

Table 3: Validation of closest GOME pixels with coinciding ozonesonde launches (all days available).

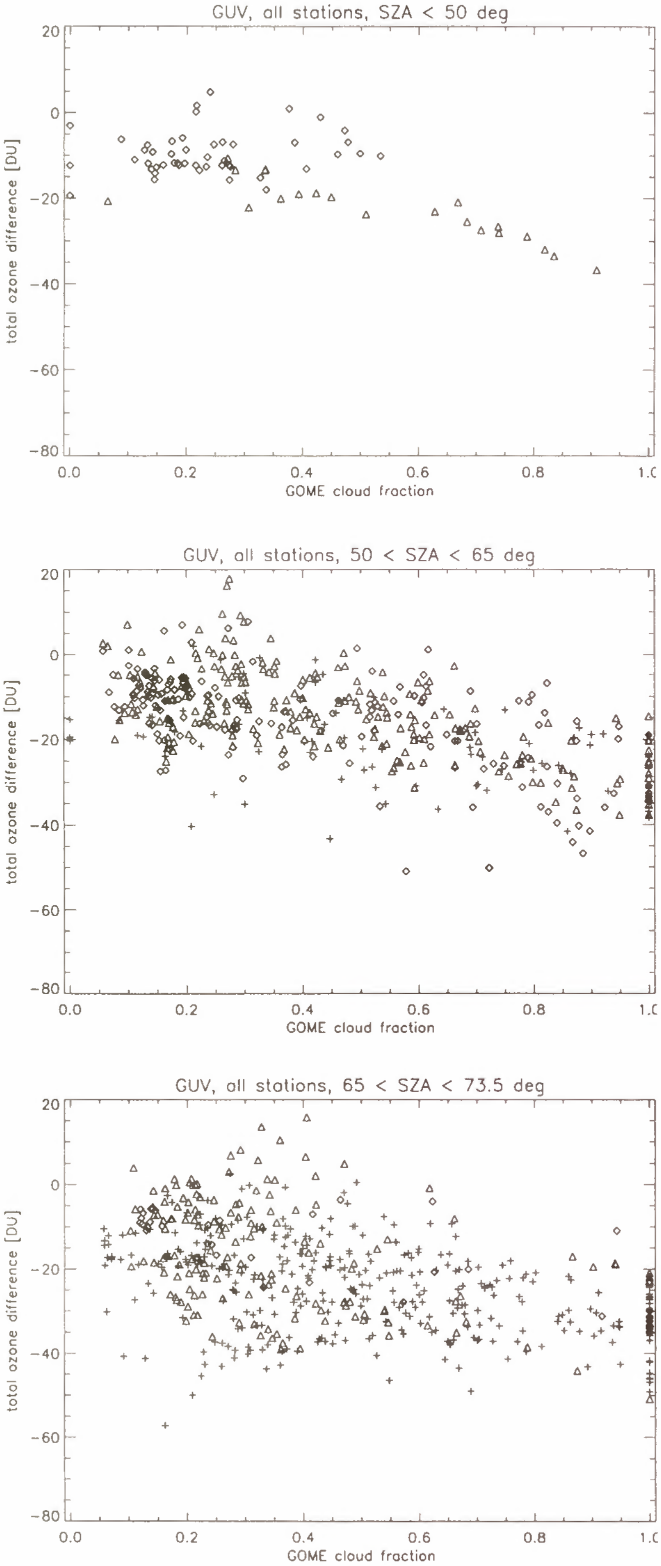

Fig. 7. Total ozone deviation between GOME and ground-based (GUV) data as a function of cloud fraction for solar zenith angles < 50° (upper panel), 50° < SZA <65° (central panel), and 65° < SZA < 73.5° (lower panel). Diamonds denote Oslo data, triangles Tromsø data, and crosses Ny-Ålesund data. Only pixels closer than 200 km to ground-based station are considered.

rather constant (-10 ± 15 DU), and then begins to increase, reaching -30 ± 10 DU at a cloud fraction of 1. The scattering of the single points is consider-ably larger than at smaller SZA. It increases further for SZA values between 65 and 73.5°. Despite the large scattering it is obvious that the deviation is larger already at small cloud fractions (-15 to -20 DU at cloud fractions < 0.2) and that it further increases to -30 ± 20 DU at cloud fractions of 0.5. At larger cloud fractions, however, the deviation remains almost constant at the latter value while the scattering of the values is reduced. Note that in all SZA regimes the scattering is largest for cloud fractions between 0.2 and 0.5!

The differences between the three plots in Fig. 7 already imply that there is also a dependence of the deviation on the solar zenith angle. Fig. 8 shows this dependence for 4 cloud fraction regimes. In the upper left panel all data with cloud fractions < 0.2 are displayed. There is no clear dependence of the average deviation on SZA, but the scattering increases with increasing SZA. There is an indication of a second-order effect: points with positive deviations are exclusively found between SZA of 55 and 70°, while negative deviations of more than 25 DU are almost only found at SZA > 65°. The upper right panel, containing all data with cloud fractions between 0.2 and 0.5 reveals a very similar pattern: an average deviation of about -10 DU at SZA < 65° and a scattering increasing with SZA. The secondary effect of the first panel , however, is much more pronounced, in particular the increasing negative deviation at SZA > 65°, reaching about -30 ± 15 DU at an SZA of 73.5°. The lower left panel containing data with cloud fractions between 0.5 and 0.8 reveals one significant change compared to the upper panels: the average deviation at SZA < 65° has increased to -15 to -20 DU, but is still rather constant. At larger SZA it drops , reaching a maximum deviation of -30 ± 10 DU at an SZA value of 73.5° as in the previous regime. In the lower right panel with cloud fractions > 0.8, almost exactly the same pattern is found as for the previous cloud fraction regime, but with an offset of another -5 to -10 DU: at SZA < 65° the deviation is about -25 ± 10 DU while at larger SZA it drops to about -35 ± 10 DU. The sudden rise to positive deviations at

Station name	estimated total ozone difference, CF < 0.5 [DU]	estimated total ozone difference, CF > 0.5 [DU]
Oslo	-10	-25
Tromsø	-14	-25
Andøya	-17	-36
Ny-Ålesund	-27	-35
Punta Arenas	+10	(-3)

Table 4. Average GOME total ozone deviations asderived with method B.

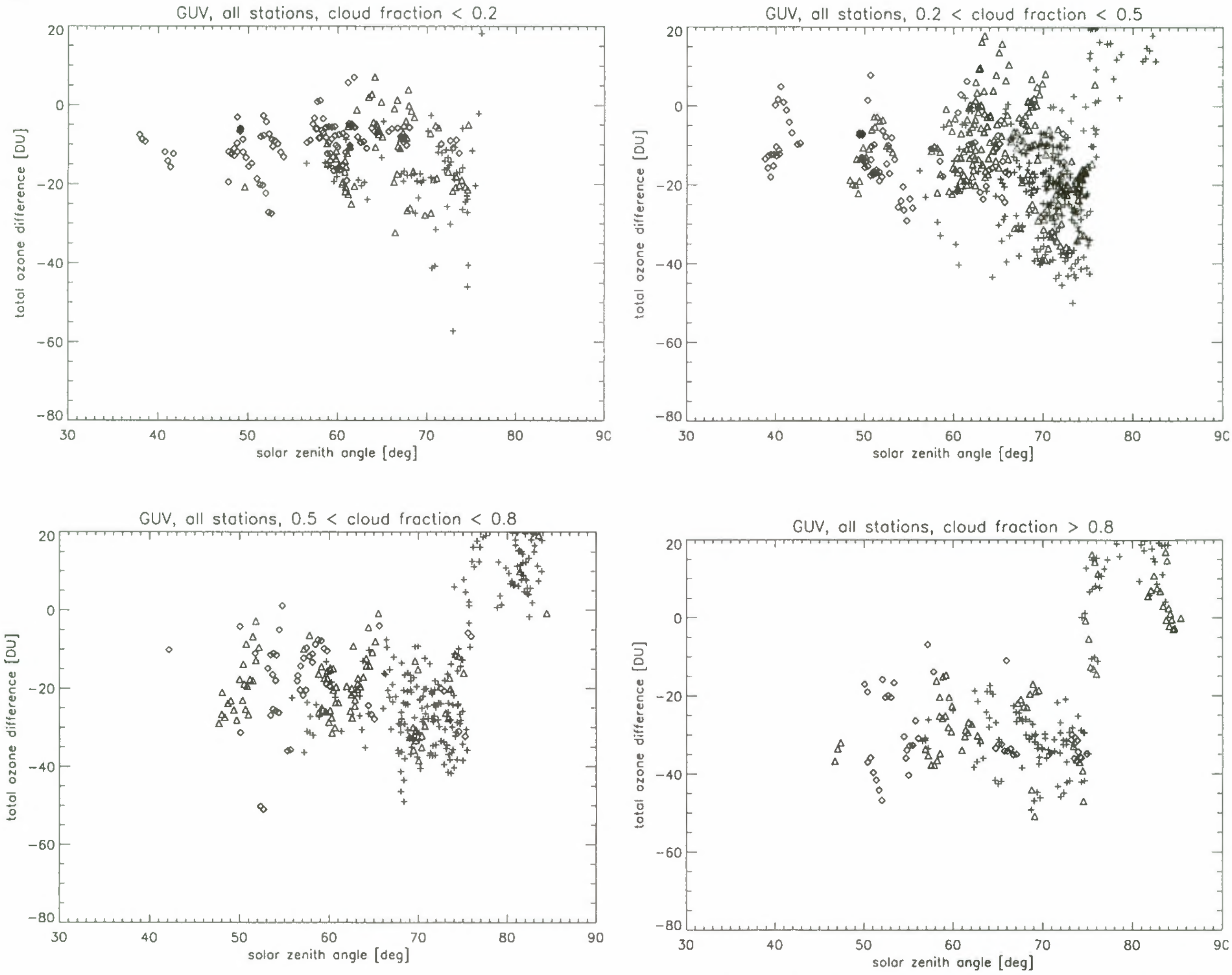

Fig. 9. Deviation of GOME total ozone from GUV measurements as a function of solar zenith angle: for cloud fractions < 0.2 (upper left panel), 0.2 < cloud fraction < 0.5 (upper right panel), 0.5 < cloud fraction < 0.8 (lower left panel), and cloud fraction > 0.8 (lower right panel). Data from Oslo are marked with diamonds, data from Tromsø with triangles, and data from Ny-Ålesund with crosses.

SZA values > 73.5° is due to the lack of a multiple scattering correction in the presently used GOME algorithm; this will be included in the next version.

Test investigations were made with even more restrictive selection criteria, namely a maximum pixel - site distance of 100 km and a ground-based averaging window of only ±1 h. Both cases led to a reduction of data points but not to a significant reduction of the scattering. This indicates that there are probably inherent factors which cause a scattering of ±10 DU under "good" conditions (small SZA, small CF), and ±20 DU under bad conditions (large SZA, large CF).

The total ozone deviation between GOME and ground-based measurements, and its dependence on SZA and CF was also analyzed by applying the closest-pixel evaluation method (B) to the GUV data set. Taking only closest pixels with distances < 200 km for the three stations (without discriminating according to cloud fraction), the result is very similar to that of method A: about -15 DU deviation at small SZA, increasing to about -40 DU at SZA > 70°. The dependence of the deviation on CF is seen in method B when the deviation as a function of distance is plotted for CF < 0.5 and CF > 0.5 separately (Fig. 9). The values deduced by this method are given in Table 4; they confirm the results already presented above from another point of view:

- at Oslo where most SZA values are smaller than 65° the data show a clear difference between small- and large-CF conditions; small-CF data reveal rather small scattering;
- the Tromsø data have similar average deviations as the Oslo data as well as similar differences between small-CF and large-CF data; however, the scattering is much larger due to the wider range of SZA values;
- the Ny-Ålesund data reveal significantly larger negative deviations than the first two stations, but less difference between small-CF and large-CF values; this is due to the SZA generally > 60°;
- the Punta Arenas data show positive deviations at small CF values; the two large-CF values are slightly negative, i.e. deviate from small-CF values in the same way as at the other stations.

Similar values are deduced from the analysis of the closest pixels for all ozonesonde launches where GOME data are available (with the exception of one Bear Island sounding); these data are listed in Table 3. They also confirm the significant scattering of deviations even at very close distances between GOME pixel and ground-based measurement volume.

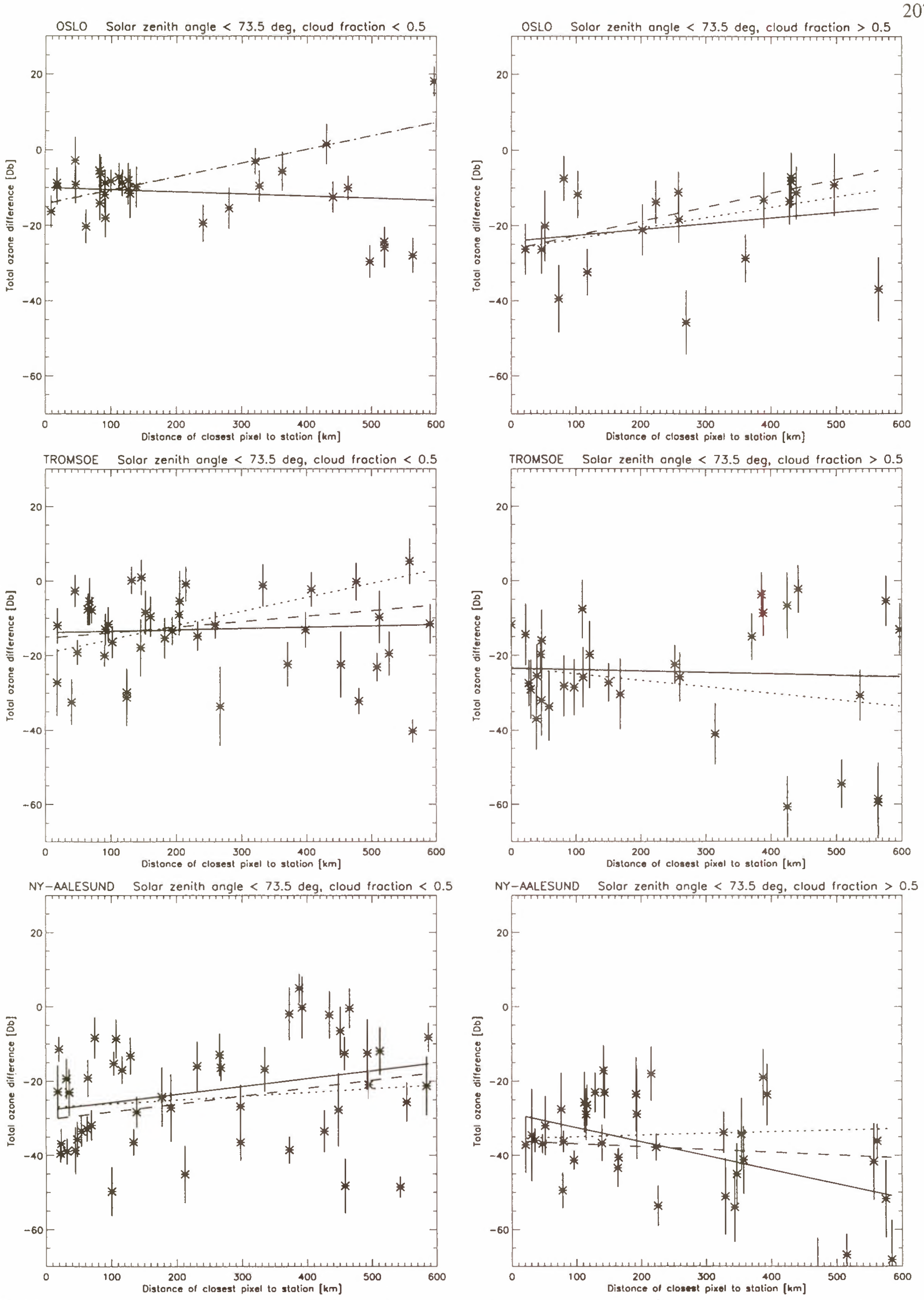

Fig 10. Summary plots of all closest pixels at Oslo (upper row), Tromsø (center row) and Ny-Ålesund (lower row). Left column: pixels with cloud fraction < 0.5, right column: pixels with cloud fraction > 0.5. Solid lines: unweighted linear regression fits, dotted lines: distance-weighted fits, dashed lines: distance- and ozone-error-weighted fits.

4. DISCUSSION AND CONCLUSIONS

The GOME main validation campaign was based on 30 days with GOME level-2 data (total ozone) which were compared with ground-based measurements (Brewer, Dobson, UV filter intruments, ozonesondes) at Oslo, Tromsø, Andøya, Ny-Ålesund and Punta Arenas. Only ground-based data recorded within a ± 2-h window

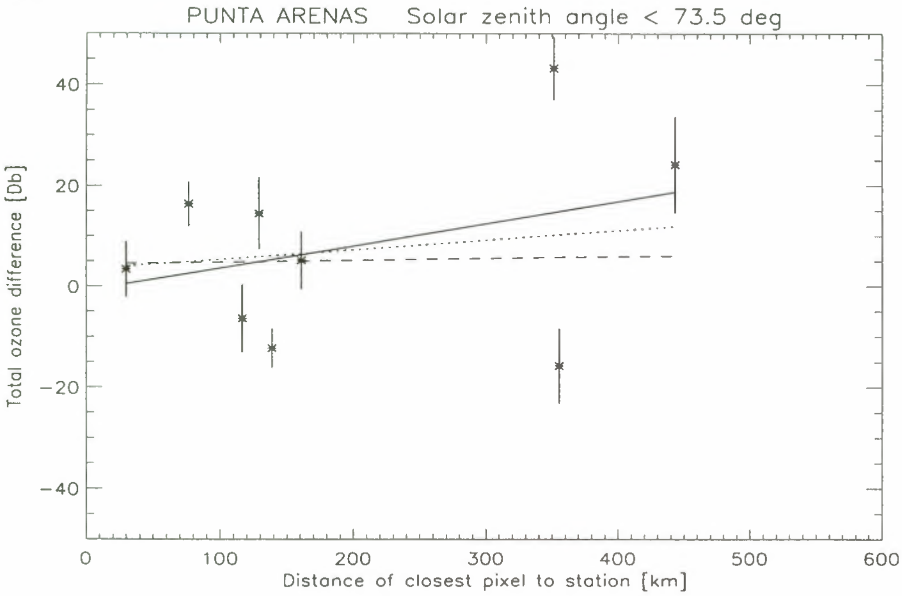

Fig. 11. Summary plot of closest pixels at Punta Arenas including all cloud fraction values. Lines: as in Fig. 10.

around the GOME pass-over were regarded, as well as GOME data within a horizontal range of 600 km from the ground-based station and with uncertainties < 5% and SZA < 73.5°. The GOME total ozone values turn out to be generally lower than ground-based values, with deviations ranging from -10 to -40 DU at the Northern stations, depending both on solar zenith angle and cloud fraction. The deviation between GOME and ground-based total ozone data is in the order of -10 to -15 DU at solar zenith angles < 60° and cloud fractions < 0.5; it increases to about -40 DU for SZA ≈ 73.5° and CF > 0.5. At the only Southern station, Punta Arenas, GOME measures slightly larger values than the ground-based instrument.

These findings agree with results presented by other validation teams on the recent GOME validation workshop at ESRIN, Frascati. The latter show a good agreement between ground-based and GOME data at mid-latitudes, but with the GOME values generally being 1 - 4 % lower than ground-based values. This is also seen at Oslo and Tromsø, while at Ny-Ålesund the situation is obviously worse. The dependence of the deviation on SZA and CF was confirmed by measurements with the SAOZ network. Almost all other stations are located at midlatitudes thus having no data with high SZA on the selected days. Besides that the measurements are mostly made under good weather conditions, i.e. at rather small CF values for close GOME pixels.

A couple of possible reasons for the SZA/latitude and cloud fraction effects have already been identified and discussed at the workshop: use of a plain atmosphere, general use of a mid-latitude winter ozone profile in the model, inaccurate determination of cloud top height and, as a consequence, wrong vertical ghost columns etc. These effects will be taken into account in a new version of the level-2 algorithm, but according to first estimates the corrections do not seem to be sufficient. It is, therefore, recommended to repeat the validation with a selected set of already processed data as soon as the new data are available.

The difference between the Northern and the Southern stations indicates that there might be a seasonal / climatological effect in the deviation, which is, for example, also found in another DOAS-based technique (SAOZ) when being compared with Brewer and Dobson measurements. For this reason it is highly recommendable to continue the validation throughout the spring and summer 1996. It would also be of great advantage to include more ground-based measurements from the Southern hemisphere in the validation.

5. REFERENCES

Dahlback, A.,Measurement of biological effective UV-doses, total ozone abundance and cloud effects with multi-channel moderate bandwidth filter instruments, submitted to *Appl. Optics*, 1995.

Hoppe, U.-P., G. Hansen, and D. Opsvik, Differential absorption lidar measurements of stratospheric ozone at ALOMAR: First results, *Proc. 12th ESA Symp. on Europ. Rocket & Ballon Res.*, Lillehammer, 1995.

6. ACKNOWLEDGEMENTS

Trond Svenøe, University of Tromsø, and Finn Tønnessen, University of Oslo, provided data from Brewer and Dobson instruments at these sites. Britt Ann Kåstad Høiskar provided the SAOZ data from Oslo and Ny-Ålesund. The support by Cathrine Wahlstrøm Tellefsen during the main validation is gratefully acknowledged. Last not least the authors would like to thank Dr. Rob Koopman for the excellent cooperation in developing the DOBSGOME evaluation software. This project was supported by ESA PRODEX funding.

VALIDATION OF GOME TOTAL OZONE COLUMN WITH THE ASSIMILATION MODEL KNMI

Ankie J.M. Piters, Pieternel F. Levelt, Marc A.F. Allaart, and Hennie M. Kelder
KNMI, PO Box 201, 3730 AE De Bilt, The Netherlands

Abstract

The two-dimensional global Assimilation Model KNMI (AMK) is used to validate GOME total ozone columns. A method is developed to derive an upper limit on the intrinsic (random) uncertainty in the GOME ozone values. This method makes use of the information on the model reliability. It is found that the intrinsic (random) uncertainty in GOME total ozone columns is rather small: less than 6 DU (or about 2%). Furthermore, a systematic error is identified which depends on the viewing direction.

1. INTRODUCTION

The Global Ozone Monitoring Experiment (GOME) on board the European satellite ERS-2 measures the spectrum of solar radiation scattered from the Earth's atmosphere between 240 and 790 nm (GOME Interim Science Report, 1993). Apart from ozone, several other trace gas densities can be derived from this spectrum. The technique used by the GOME Data Processor (GDP) to derive these trace gases on an operational basis is Differential Optical Absorption Spectroscopy (DOAS). The DOAS method fits the ratio of the scattered solar radiation (radiance) and the direct solar radiation (irradiance) to reference spectra of the trace gases absorbing in this wavelength region. The *slant* column densities derived in this way are then divided by an effective air mass factor in order to obtain the *vertical* column densities. The air mass factors — which account for the light path of the solar radiation through the atmosphere — are calculated by the GDP with radiative transfer models, developed at the Institutes for Environmental Physics of Heidelberg and Bremen (see other papers in this issue).

In this paper the Assimilation Model KNMI (AMK; Levelt et al., 1996), which is initially developed for imaging of global ozone maps, is used to validate ozone vertical column densities as retrieved by the GDP from GOME observations. The AMK calculates two-dimensional global ozone maps at any given time, using observations of total ozone columns and observations of horizontal wind fields.

Data assimilation as performed by, for instance, the AMK is an essential tool for the validation of satellite data (for several methods of data assimilation see, e.g., Daley, 1991). GOME overpasses are often at large distances from the different ozone measuring ground stations used in the validation campaign. Furthermore, it is not always possible to obtain a ground-based measurement simultaneously with a GOME overpass. Since the ozone column is highly variable in time and space, a lot of ground-based measurements are not suitable for direct comparison. However, data assimilation presents a tool to use these measurements for comparison with GOME, because it takes into account the knowledge about the dynamical behaviour of ozone. Future plans at KNMI, The Netherlands, include combining the AMK with the ground-based measurements gathered by many institutes during the validation period (see other papers in this issue).

Another way of using the AMK for validation is the comparison of GOME observations with predicted ozone values based on *previous* GOME observations, the main topic of this paper. Differences between the ozone columns directly observed by GOME and the predicted AMK ozone columns gives information on the self-consistency of GOME. An important point to be considered here are the uncertainties in the model itself.

Section 2 describes the AMK and discusses its uncertainties, Section 3 presents the GOME data used for the present study, and Section 4 discusses the results.

2. MODEL DESCRIPTION

The AMK is a two-dimensional (latitude, longitude) global model. It advects the ozone column using the horizontal wind at a single pressure level. The wind fields are obtained from the European Centre for Medium-range Weather Forecast (ECMWF). Observations of total ozone columns are assimilated into the model with the single-correction method. For details on the advection and assimilation methods see Levelt et al. (1996).

The three main assumptions in the model are: (*i*) The total ozone column variability is dominated by the variability in a relatively thin vertical layer; (*ii*) Chemical processes have much larger timescales than dynamical processes; (*iii*) The wind fields transporting the ozone are approximately horizontal.

The first assumption is based on observations of ozone profiles. In normal atmospheric conditions the variability is largest around the tropopause. For ozone-hole conditions the assumption still holds, but here the altitude of the largest variability is much higher. The second assumption is usually valid for the upper troposphere and the lower stratosphere, where the chemical lifetime of ozone varies from weeks to months. However, it is not valid under ozone-hole conditions. The third assumption is based on the knowledge that wind tends to flow along isobaric surfaces, which are in first order approximation horizontal. For a more detailed discussion on the validity of these assumptions we refer to Levelt et al. (1996).

Model uncertainties introduced by making these assumptions can stay relatively small, as long as the AMK is continuously fed with observations. Experiments with TOVS data show that the (root mean square) difference between observations and model output is dominated by the uncertainty in the TOVS data. If the assimilation of new observations is turned off, this difference increases with approximately a factor of two in two days (see Levelt et al., 1996). In general, the reliability of the AMK predicted ozone column at a given time and place decreases as a function of the elapsed time after the last contributing assimilated observation.

The AMK has been optimized for the assimilation and advection of NOAA-TOVS data (Levelt et al., 1996). The assimilation technique makes use of empirically determined coefficients, which are sensitive to the uncertainties in both the model and the observations (in

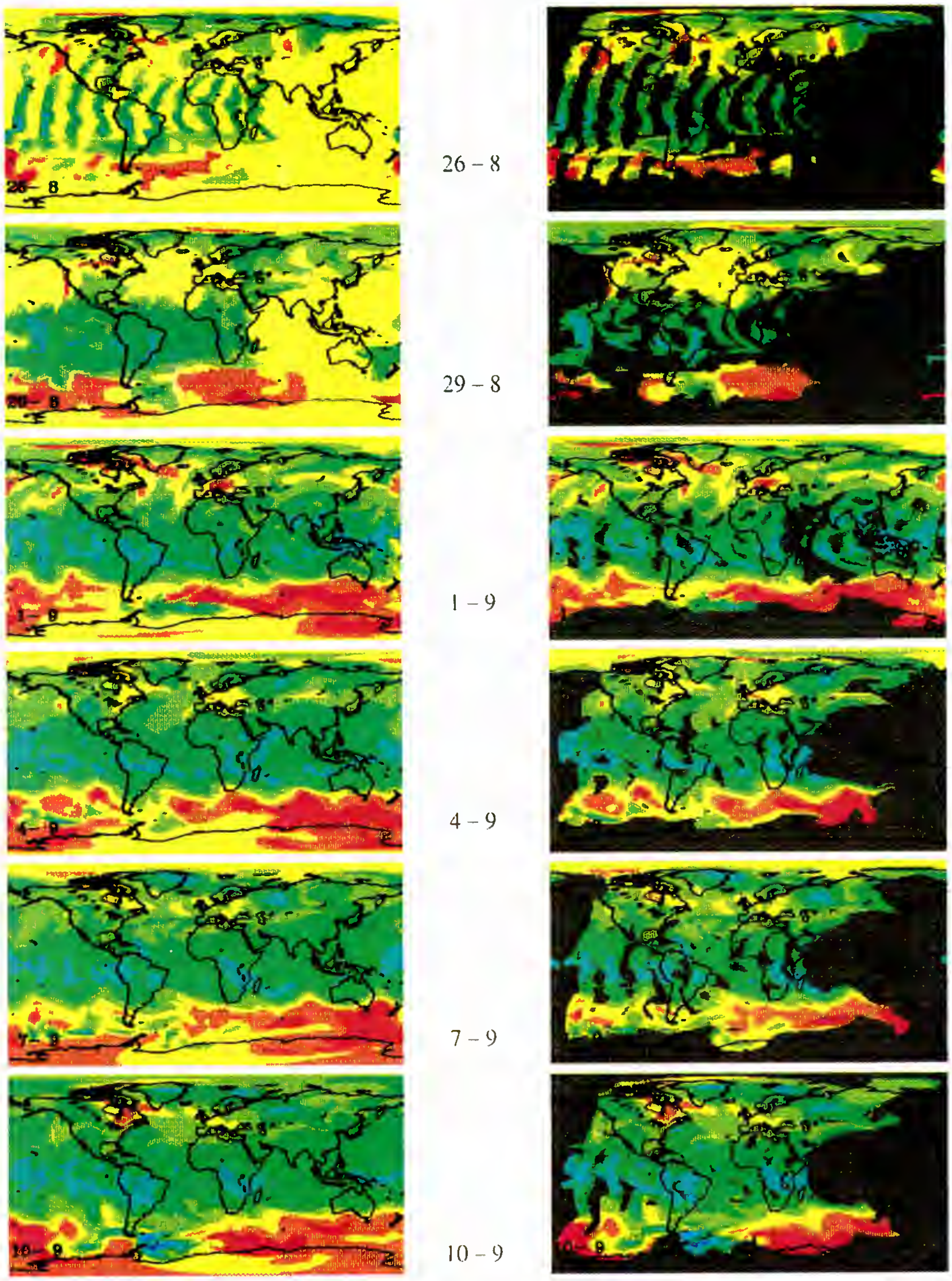

Figure 1: The global ozone fields resulting from the AMK run of 16 consecutive days in August and September (left hand panels). The right hand panels display the same results, but now the 'uncertain' ($q < 0.5$, see Section 4.1) regions of the model output are coloured brown. Different ozone values are indicated by different colours, red for high ozone values (~ 350 DU), light blue for low ozone values (~ 200 DU). Time goes from top to bottom, the 6 panels are from 26 and 29 August, 1, 4, 7, and 10 September, all at 0 UT, respectively. The stripe-like structures after the first day of the model run, at 26 August 0 UT (upper left panel), show the satellite orbits of 25 August, deformed by the wind field. Inbetween the orbits, no information exists on the ozone values, therefore the start field of 300 DU (yellow) is still visible here. The relatively large 'uncertain' (brown-coloured) regions in the right hand panels (Indian Ocean and Australia) result from the data gaps near the date line. The South Pole is not observed (hence ozone values there are indicated 'uncertain'), because the Sun is not illuminating this part of the Earth in the time period studied here.

Table 1: The GOME data used in the present study. Listed are for every day the start and end time of the available observations (columns 2 and 3), and the GDP level 1–2 software version (column 4).

day in 1995	start time	end time	version
25 August	6:03:23	21:50:08	1.20
26 August	5:31:52	21:18:37	1.20
27 August	6:40:57	20:47:07	1.20
28 August	—	—	—
29 August	0:36:13	23:05:10	1.21
30 August	0:04:43	23:59:58	1.21
31 August	0:00:00	23:42:45	1.21
1 September	5:44:07	21:30:38	1.21
2 September	5:12:35	20:59:07	1.21
3 September	6:21:40	20:27:37	1.21
4 September	5:50:10	21:36:42	1.21
5 September	5:18:39	21:05:11	1.21
6 September	6:27:46	20:33:41	1.21
7 September	5:56:14	21:42:47	1.21
8 September	5:24:44	21:11:17	1.21
9 September	6:33:51	20:39:47	1.21

this case TOVS observations). Using GOME data in the model instead of TOVS data, in principle requires other coefficients. These coefficients can be calculated after running the model with at least one month of consecutive observations. Since the present study only uses 15 days of observations (and for most days only 9 out of 14 orbits), we will use as a first order approximation the TOVS coefficients. Tests with TOVS data show that the model output is not very sensitive to small changes in these coefficients (ibid).

The present advection scheme of the AMK uses wind fields at a single pressure level. The specific pressure level used is again empirically determined on TOVS data (ibid), for a time period without an ozone hole. Since this level (200 hPa; comparable to results of Riishojgaard and Lary, 1994) approximately equals the level where the ozone variability is observed to be largest (the tropopause, except under ozone hole conditions), we believe that the best pressure level will not be very different for the GOME data studied here (no ozone hole present). This will be verified when more consecutive GOME data are available. Future versions of the AMK will be using wind fields at different pressure levels, to account for the different altitudes of highest ozone variability, which is clearest in the presence of an ozone hole.

3. THE GOME DATA

The GOME data used in the present paper cover the period between 25 August and 9 September 1995. This period is selected because it is the largest (semi-)consecutive period of processed observations in the validation data set. However, this time period still has some gaps: one day (28 August) was not processed and for most of the other days only 9 out of 14 orbits were processed (those received at the Kiruna ground station). Table 1 shows for every day the start and end time of the processed data used in this study.

Note that during the time period studied here ozone values are relatively low and the ozone variability is relatively small when compared to other seasons. Therefore, the conclusions drawn in this paper might only be valid for these relatively quiet periods.

From the data listed in Table 1 we used only the ozone values with DOAS fit errors less than 5%, with solar zenith angles at the time of observation less than 74.6°, and for which no errors were reported (according to the flags in the 'Intermediate Results Record' of the GDP level 2 product). The threshold for the solar zenith angles is chosen, because in the GDP software version 1.20 and 1.21 (used here) the air mass factors for larger solar zenith angles (> 74.6°) are still calculated using the first order approximation of single scattering, while for smaller solar zenith angles multiple scattering has been included in the calculations. For large solar zenith angles, ozone values are expected to be 20 – 30% too high. In future releases the air mass factors will all be calculated with the multiple scattering included.

4. RESULTS

4.1. The experiment

The start field at 25 August 1995 at 0 UT is chosen to be a field with ozone values of 300 DU everywhere.[1] In the present experiment, AMK runs from 25 August, 0 UT, until 10 September 1995, 0 UT, and is fed by the GOME observations listed in Table 1. Figure 1 (left column) shows the resulting ozone fields every third day, at 0 UT.

Due to the time gaps in the GOME data, a large part of the Earth (containing Australia and Sout-East Asia) is not fed with observations. So the ozone values predicted by the AMK will be uncertain in this region. Furthermore, even if the AMK *would* be continuously fed with observations, it still needs a spin-up period in the order of a few weeks, before the ozone column values are reliable.

Therefore, we define a 'reliability flag' $q_i \in [0, 1]$ for each grid cell i, which depends on the time elapsed after the last observation contributing to the ozone value in this grid cell. The 'flag field' q_i is advected in the same way as the ozone field, so that the reliability information on the ozone values keeps attached to it. However, the flag is 'devaluated' in time: it is assumed to decline exponentially as $\exp\{-0.01\Delta t\}$, where Δt is in hours. This means that, starting with a fully reliable ozone field (i.e., $q_i = 1$ for every i), after 2 days without any observations the flag would be 0.6 everywhere, and after 3 days it would be 0.5 everywhere. For the start field we take $q_i = 0$, for all i, and every time an ozone observation is assimilated in the ozone field, the value $q = 1$ is assimilated in the 'flag field' q_i, at the same location and with the same assimilation coefficients as for the ozone (see Section 2 and Levelt et al., 1996).

In the right column of Figure 1 the regions with flag $q_i < 0.5$ (corresponding to about three days without observations) are coloured brown. The spin-up period of the model and the missing data regions are clearly visible.

4.2. GOME intrinsic uncertainty

The self consistency of the GOME observations is tested by looking at the root mean square value of the differences between the observations and the predicted model output (based on *previous* GOME observations, and the observed wind field) at the same time and location as the observation. This root mean square value would be equal to the random uncertainty in the GOME observations, in the ideal case of a perfect model and in the case

[1] Another possibility would be to start with a more realistic field, e.g., the assimilated TOVS data on 25 August. However, possible systematic differences might exist between TOVS and GOME, which are unknown yet. We prefer the *known* bias introduced by a constant start field.

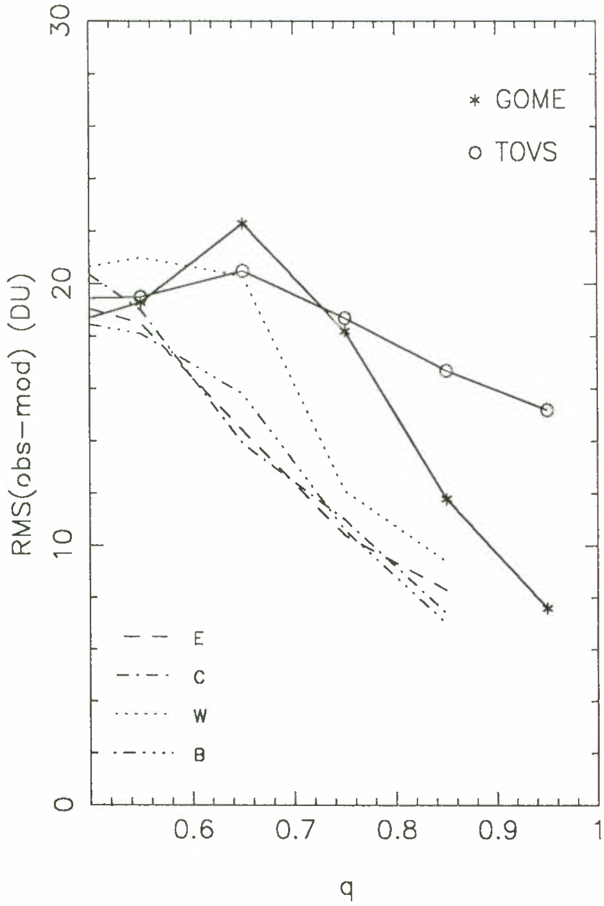

Figure 2: The root mean square of the difference between the observations and the model-output for the last three days of the AMK run, as a function of the reliability flag q. The data is binned in bins of $\Delta q = 0.1$. The stars indicate the results for the AMK run with GOME data, the circles indicate the results for the AMK run with TOVS data (see Section 4.2). The four dashed and dotted lines indicate the results for the AMK runs 'East', 'Centre', 'West' and 'Backscan' (see Section 4.3). The number of points contributing to the root mean square is more than 1600 per q-bin for the solid lines, and more than 160 per q-bin for the dashed and dotted lines.

that the GOME observations would have no systematic dependencies on for instance the solar zenith angle or the surface albedo or the viewing direction. In more realistic cases the root mean square value gives an *upper limit* to the intrinsic (random) uncertainty in the GOME ozone values. By plotting the root mean square value of the differences between observations and model output as a function of the reliability flag q (Figure 2, solid line with stars), the influence of model uncertainties (caused both by the relatively large periods without observations and by the simplifying assumptions underlying the model, see Section 2) can largely be ruled out. The model is perfect if $q = 1$, so the asymptotic value of the root mean square for $q \to 1$, gives the tightest constraint on the intrinsic uncertainty in the GOME total ozone value. From Figure 2 we conclude that this intrinsic uncertainty is less than 7 DU, which is very accurate ($\sim$ 2%): the zenith sky observations of ground-based Brewer instrument, for instance, have a larger uncertainty (5%, see Piters et al., 1996).

For comparison a similar experiment is done with an AMK run using only TOVS total ozone data. We used 15 consecutive days in April 1992[2], starting with the same start field as in the GOME experiment. The root mean square of the differences between the TOVS observations and the model output for the last three days of the run is plotted in Figure 2 (solid line with circles). The asymptotic value of the TOVS root mean square value for $q \to 1$ is about 15 DU, corresponding to the intrinsic uncertainty usually attributed to the TOVS data (Planet et al., 1984).

Note that when the systematic dependencies of GOME total ozone value on for instance solar zenith angle (as observed by the GOME validation team, see other papers in this issue) will become less in future processing of the GOME data, the upper limit to the intrinsic uncertainty will become even smaller than 7 DU. In the next subsection we identify another systematic dependence of the GOME total ozone column, and find a tighter constraint on the intrinsic uncertainty.

4.3. Dependence on viewing direction

Here, we study the possible dependence of the GOME total ozone column on the viewing direction or line-of-sight zenith angle. In normal operational mode, the GOME scan mirror moves every 6 seconds in 4.5 seconds from left to right over approximately 60° and in 1.5 seconds back again. During the validation period the instrument integrated 0.375 seconds at the end of every 1.5 seconds, resulting in four ground pixels per scan, the so-called 'East', 'Centre', 'West', and 'Backscan' pixel. The scan mirror velocity together with the integration time determine the size of the ground pixels: the 'East', 'Center' and 'West' ground pixels are approximately $80 \times 40\text{km}^2$, the 'Backscan' pixel is approximately $240 \times 40\text{km}^2$. The corresponding average line-of-sight zenith angles for these ground pixels are $-13°$, $+7°$, $+27°$, and $-23°$.

The experiment described in Section 4.1 is repeated here four times, each time assimilating only the observations with the same viewing direction. The four different AMK runs are called 'East','Center','West', and 'Backscan', to their corresponding GOME ground pixel types. Figure 2 also shows the root mean square value of the differences between the observations and the model output for the four different AMK runs as a function of the reliability flag q. The root mean square value is in all these cases smaller than that for the AMK run using all observations as described in Section 4.2. This suggests that the intrinsic uncertainty in the GOME total ozone values is even smaller than 6 DU, and that there is a systematic error on the GOME total ozone value depending on viewing direction.

The magnitude of this systematic error is found by comparing the four different model outputs at the end of the AMK runs, on 10 September, 0 UT. If there would be no systematic errors with respect to the viewing direction, these four model outputs are expected to look the same, at least for the regions where the model uncertainties are small (i.e., q large). We have calculated the difference between two model outputs for each grid cell, and averaged over the grid cells for which $q > 0.6$ for both AMK runs. In Figure 3 these mean differences of each AMK run with AMK run 'Centre' are plotted. The error bars indicate the uncertainty in the mean. From this figure, it appears that significant systematic differences exist between ozone values corresponding to different pixel types.

[2]Note that the variability of the ozone field in April is larger than in September. This might influence the results presented here. However, the root mean square differences for the TOVS experiment are expected never to be smaller than the intrinsic TOVS uncertainty, i.e., approximately 15 DU.

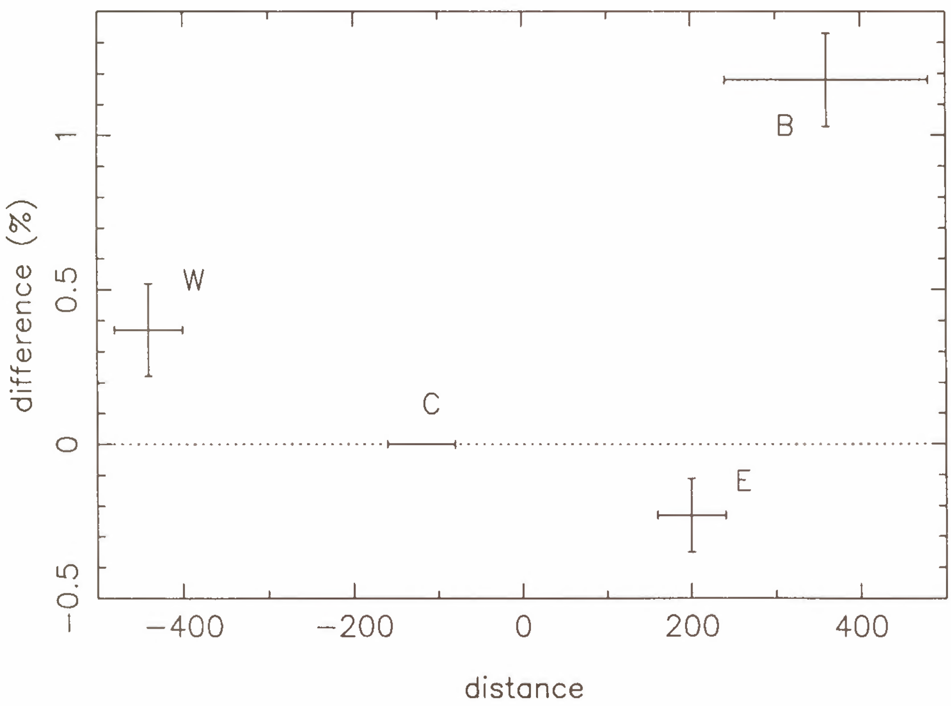

Figure 3: The average deviation of the model output of AMK runs 'West', 'Center', 'East' and 'Backscan' with respect to the output of AMK run 'Center' (see Section 4.3). The average has been taken over the set of grid cells with flag $q > 0.6$. The error bars denote the uncertainty in the mean. The horizontal axis indicates the position and extend of the different ground pixel types used in the different AMK runs, expressed in the distance (in km) from the projected nadir viewing direction. Negative distances refer to West.

The magnitude of the differences found here between the ozone values from the 'West', 'Centre' and 'East' pixels appears to be consistent with the dependence of the air mass factor on the differential azimuth angle [3], which is *not* taken into account in the GOME retrieval algorithms (Thomas, 1996).

The large systematic offset of the 'Backscan'-pixel values can not be explained by the air mass factor dependence on the azimuth angle (in this case, the offset would be expected to be somewhat lower than the 'East' pixel offset in Figure 3). The explanation might have something to do with the size of the 'Backscan' ground pixel. This pixel is three times as large as the other three ground pixels, due to the higher scanning velocity of the scan mirror while moving from right to left. The air mass factor, ozone vertical column, polarization and cloud cover can vary considerably along the pixel. Although in the present GDP software some first order corrections are made for (known) variations, there might still be some bias due to the inevitable averaging over the extended 'Backscan' pixel.

5. CONCLUSIONS

In the previous sections, the Assimilation Model KNMI proved to be of value in the validation of GOME total ozone values. Although the data set available for this study is very limited (15 consecutive days with large data gaps), we are able to derive the following conclusions.

For the period considered here (25 August – 9 September 1995) and for the GOME data processing software versions 1.20 and 1.21, the intrinsic (random) uncertainty of GOME total ozone columns is less than 6 DU, or approximately 2%, (Sections 4.2. and 4.3).

For this same period and software versions there appears to be a systematic error in the total ozone column depending on the viewing direction or pixel type (Section 4.3). The magnitude of this systematic error with respect to the 'Centre'-pixel observations is $0.37 \pm 0.15\%$ for the 'West'-pixel observations, $-0.23 \pm 0.12\%$ for the 'East'-pixel observations, and $1.18 \pm 0.17\%$ for the 'Backscan'-pixel observations. The magnitude of the differences found here between the ozone values from the 'West', 'Centre' and 'East' pixels appears to be consistent with the expected difference due to the dependencies of the air mass factor on the differential azimuth angle. But the systematic difference between the ozone values from the 'Backscan' pixels and those from the other pixels is too large to be explained by these air mass factor dependencies.

[3] Azimuth angles are defined in a plane parallel to the Earth's surface at the point observed by the instrument. The differential azimuth angle is defined as the difference between the azimuth angles of the radiation reflected towards the instrument and the incident radiation.

Acknowledgements

We gratefully acknowledge the members of the GOME Validation Group for fruitful discussions on the topics discussed in this paper. Especially, we would like to thank John Burrows (IUP, Bremen) and Piet Stammes (KNMI) for their helpful comments. We are grateful to Wolfgang Balzer and the data processing team at DLR for helping us to understand the GDP product. Ankie Piters is funded by SRON, The Netherlands, Pieternel Levelt is funded by BCRS, The Netherlands.

References

Daley R., Atmospheric Data Analysis, Cambridge University Press, Canada, 1991

Global Ozone Monitoring Experiment, Interim Science Report, European Space Agency (ESA), SP-1151, 1993

Levelt P.F., Allaart M.A.F., Kelder H.M., On the Assimilation of Total ozone satellite Data, *accepted for publication*, Annales Geophysicae, 1996

Piters A.J.M., Levelt P.F., Kuik F., Allaart M.A.F., Kelder H.M., Ground-based measurements at KNMI used for GOME validation, this issue, 1996

Planet W.G., Crosby D.S., Lienisch J.H., Hill M.L., Determination of total ozone amount from TIROS Radiance Measurements, J. Clim. Appl. Meteorol. 23, 308, 1984

Proceedings of the GOME validation workshop, Frascati, 24–26 January, 1996 (this issue)

Riishojgaard L.P., Lary D.J., Short range simulations of extratropical total ozone with ASPERGE/-IFS, Proceedings of ECMWF Workshop on the stratosphere and numerical weather prediction, ECMWF, 1994

Thomas W., DLR, private communication, 1996

GROUND-BASED MEASUREMENTS AT KNMI USED FOR GOME VALIDATION

Ankie J.M. Piters, Pieternel F. Levelt, Foeke Kuik, Marc A.F. Allaart, and Hennie M. Kelder
KNMI, PO Box 201, 3730 AE De Bilt, The Netherlands

Abstract

During the validation campaign of GOME, ground-based measurements of total ozone and of ozone profiles have been performed at KNMI, The Netherlands. Total ozone columns have been measured with a Brewer instrument around the GOME overpass times. Sondes, measuring the ozone profiles, were launched when it was most likely that the sonde would measure the same air mass as GOME at the overpass time. The retrieved GOME total ozone columns are on average 4–5% lower than the corresponding Brewer values.

1. INTRODUCTION

During the 6 months validation campaign (21 July 1995 – 23 January 1996) of the Global Ozone Monitoring Experiment (GOME) on board the European satellite ERS-2, KNMI (De Bilt) performed ground-based measurements of total ozone and ozone profiles. The total ozone measurements, obtained with a Brewer instrument, are used for direct comparison with the total ozone columns retrieved from GOME observations. The first results of this comparison are presented here. The ozone profiles, obtained with ECC sondes, will be used for validation of (future) GOME ozone profiles. The development of profile retrieval algorithms using forward modelling methods will also benefit from these ozone sonde profiles. The retrieval algorithms will be used for validation of GOME ozone profile retrieval.

In Section 2 we shortly describe the instruments used. Section 3 discusses the selection criteria used for the comparison of the total ozone columns measured with the Brewer instrument with those retrieved from GOME observations. In the same Section we present the strategy used for launching the ozone sondes. In Section 4, we show the first results of the comparison of GOME total ozone with the Brewer measurements.

2. THE INSTRUMENTS

2.1. Brewer spectrophotometer

The Brewer instrument is a double monochromator type MK III. Brewer #100 is operational at KNMI since 1 January 1994. The Brewer derives total ozone, using the measurement of solar radiation at four wavelengths (310.1 nm, 313.5 nm, 316.8 nm, and 320.1 nm). The radiance calibration and wavelength stability of the Brewer are checked several times a day with an internal tungsten halogen lamp and an internal mercury lamp, respectively. In normal operational mode total ozone is measured roughly every 15 minutes from sunrise to sunset. When the sun is visible, direct solar radiation is measured. These 'direct sun measurements' have a precision (i.e., due to measurement uncertainties) of 1%. When the sun is not visible, the Brewer measures the solar radiation scattered from the zenith. These 'zenith sky measurements' have a precision of 5%. However, the *accuracy* (i.e., due to systematic errors) can be larger than these measurement uncertainties. Comparison of the observations from the Brewer #100 and those from the Brewer in Uccle (#16; 50.8 N, 4.35 E) show that a possible systematic offset between these two instruments is less than 2%, part of this offset may even be caused by a ('real') average ozone gradient over the distance between De Bilt and Uccle ($\sim$ 170 km). Near-simultaneous zenith sky and direct sun ozone values can differ up to 8%.

2.2 Ozone sondes

The ozone sondes used at KNMI are Electrochemical Concentration Cell (ECC) sondes, which measure profiles up to an altitude of approximately 30 km, with a resolution of about 100 m. Also measured are the pressure, temperature, humidity, and position of the sonde. The accuracy of the measured ozone partial pressure is estimated to be better than 10%. Ozone sondes are normally launched once a week, more often during the GOME validation campaign (see Section 3). The quality checks performed on the observed profiles include the comparison of the Brewer total ozone column with the integrated profile. If the integrated profile differs from the Brewer total ozone column by more than 30 DU, the profile is marked unreliable.

3. DATA SELECTION AND MEASUREMENT STRATEGY

3.1 Total ozone

The data used for the validation of the total ozone column is listed in Table 1. For the comparison of Brewer total ozone values with GOME values we used only Brewer direct sun measurements, because of the larger uncertainties in the zenith sky measurements (see Section 2.1). From the GOME data we selected one ground pixel per day, the one closest to De Bilt (52.1 N, 5.18 E). The value retrieved from this GOME pixel was compared with the Brewer (direct sun) measurement closest in time to the GOME overpass time. Due to possible strong gradients in the ozone field, e.g. during front passages, total ozone amounts can differ up to 50–100 DU for distances in de order of 200 km and a time interval of about two hours. The distances of the closest GOME pixel to De Bilt can still be as large as 400 km, and the difference in time between the two measurements can be as large as 4 hours (for cloudy days; see Table 1). In these cases, a direct comparison with the Brewer measurement, in the presence of strong gradients in the ozone fields, will be of less value than when the GOME pixel co-incides with the De Bilt measurement, both in time and in place. Therefore, we classified the Brewer data used for the comparison in Section 4 with respect to their distance to the closest GOME pixel centre, and with respect to their time difference with the GOME observing time.

Table 1: The data used for the validation of the total ozone column. Column 1 gives the day of the observation; columns 2 and 3 the time (UT) and value (DU) of GOME total ozone; columns 4 and 5 the time (UT) and value (DU) of Brewer (direct sun) total ozone; column 6 lists the difference ΔO_3 in DU between GOME and Brewer total ozone value; column 7 gives the distance ('dist') in km from the GOME pixel centre to De Bilt; column 8 the pixel-type (B, E, N, C, W, corresponding to five different scanning angles of the instrument mirror: approximately $-23°$, $-13°$, $0°$, $+7°$, $+27°$, respectively); column 9 gives the solar zenith angle ('sza'); column 10 the cloud cover fraction as calculated by the GOME Data Processor.

day	GOME time	GOME O_3	Brewer time	Brewer O_3	ΔO_3	dist	type	sza	cloud fraction	day	GOME time	GOME O_3	Brewer time	Brewer O_3	ΔO_3	dist	type	sza	cloud fraction
23–7	10:12:23	302	10:16	304	−2	278	W	32.2	0.19	16–9	11:23:31	298	11:37	293	5	123	B	51.0	0.20
24–7	11:20:47	310	11:17	311	−1	80	B	34.2	0.10	17–9	10:52:19	295	10:51	302	−7	67	C	50.0	0.18
25–7	10:49:29	287	10:53	294	−7	20	C	33.5	0.14	20–9	10:58:03	287	10:42	300	−13	133	E	51.2	0.41
25–8	11:15:01	300	10:45	294	6	16	B	42.9	0.43	21–9	10:26:39	265	10:25	284	−19	40	W	50.9	0.40
26–8	10:43:43	280	10:47	286	−6	78	C	42.2	0.27	22–9	11:34:50	253	9:12	266	−13	303	B	53.8	0.27
27–8	10:12:18	306	10:22	309	−3	278	W	41.9	0.43	23–9	11:03:43	257	9:44	269	−12	39	E	52.6	0.54
29–8	10:49:23	299	10:52	305	−6	26	C	43.4	0.32	27–9	10:37:59	294	10:37	289	5	157	W	53.7	0.19
30–8	10:18:03	320	10:09	316	4	182	W	42.8	0.30	28–9	10:06:38	300	10:46	323	−23	375	W	53.2	0.19
31–8	11:26:21	320	10:58	326	−6	168	B	45.3	0.20	1–10	10:12:24	235	15:00	245	−10	278	W	54.3	0.57
1–9	10:55:09	306	10:15	317	−11	114	C	44.4	0.00	2–10	11:20:47	233	11:20	254	−21	80	B	56.7	0.45
2–9	10:23:43	280	12:43	310	−30	85	W	44.1	0.69	3–10	10:49:29	274	9:38	284	−10	20	C	56.0	0.45
3–9	11:32:00	313	11:44	334	−21	259	B	46.6	0.30	5–10	11:26:27	303	11:49	308	−5	170	B	58.1	0.11
4–9	11:00:47	294	11:04	311	−17	87	E	45.7	0.39	6–10	10:55:09	276	10:50	301	−25	114	C	57.4	0.06
5–9	10:29:30	283	10:20	302	−19	407	N	45.0	0.16	7–10	10:23:49	259	8:35	287	−28	85	W	56.8	0.53
6–9	11:37:43	310	11:36	324	−14	347	B	48.2	0.21	29–10	10:32:22	273	10:40	284	−11	64	W	64.8	0.13
7–9	11:06:27	266	10:35	299	−33	15	E	47.0	1.00	30–10	11:40:27	262	11:38	280	−18	393	B	68.2	0.53
15–9	10:15:13	266	9:37	295	−29	230	W	48.4	0.35	11–11	10:23:40	243	10:21	271	−28	86	W	68.9	0.41

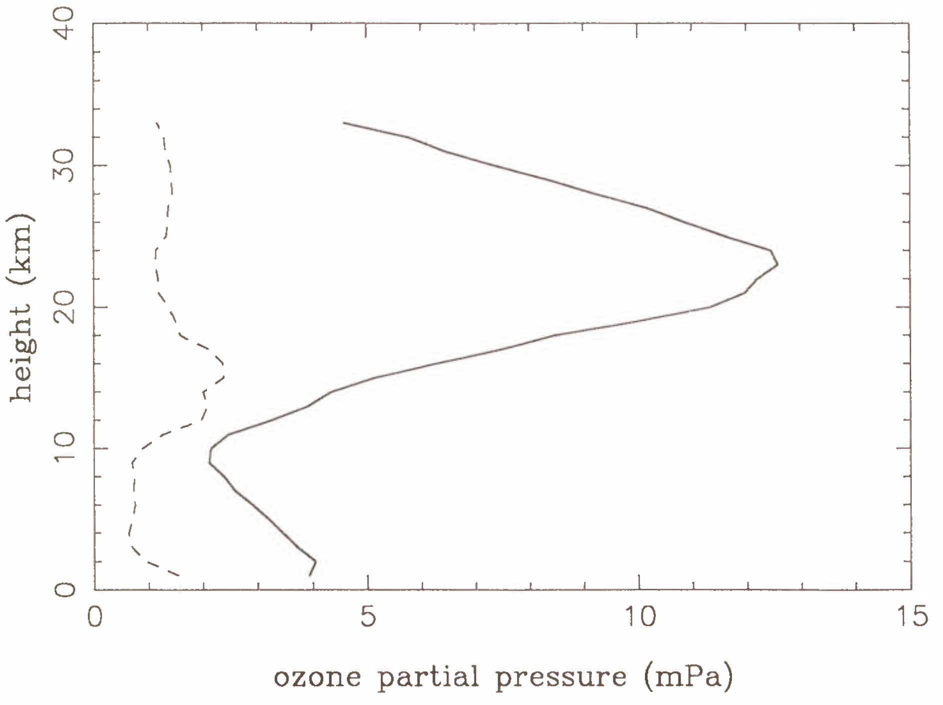

Figure 1: The average ozone profile of the 26 ozone sondes launched during the GOME validation period (solid line), and the standard deviation (dashed line).

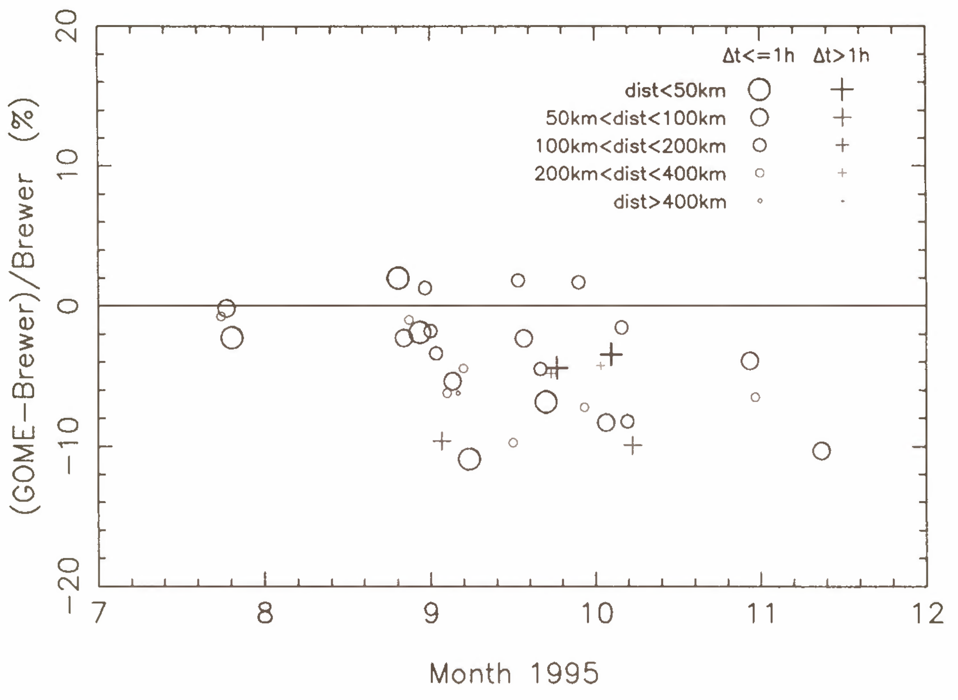

Figure 2: The relative difference between the GOME ozone column and the ozone column measured by the Brewer instrument as a function of time. Plusses denote values which have been measured with more than 1 hour time difference, circles denote values which have been measured with less than 1 hour time difference. The size of the symbols indicate the distance of the GOME pixel centre to De Bilt (large is close by, small is far away, see Table 1).

3.2 Ozone profiles

The ozone sondes have been launched only on those days for which the sonde was expected to fly through roughly the same air mass as that observed by GOME. This was estimated using the information on the movements of previous sondes. High priority was given to the launch of sondes which were expected to pass the ozone maximum (at an altitude between 15 and 20 km) at a (projected) position co-located with a GOME ground pixel. A total of 26 sondes resulted in reliable ozone profiles, and can be used for validation of future GOME ozone profiles. The average and standard deviation of these profiles is plotted in Figure 1. [1]

4. RESULTS AND DISCUSSION

The differences between the GOME total ozone columns and the Brewer values range from $+2\%$ to -11% (see Figure 2). The average offset of the GOME values with respect to the Brewer values is $-4.4 \pm 0.6\%$ with a standard deviation of 4%. This standard deviation is partly caused by differences in time and space between the GOME and the Brewer observations. But even if the Brewer observation would be simultaneously measured and co-located with the GOME ground pixel, some scatter is expected due to the averaging of GOME over a $40 \times 80\mathrm{km}^2$ (or $40 \times 240\mathrm{km}^2$) ground pixel. The standard deviation of the differences between total ozone columns of GOME and Brewer is relatively small (4%) when compared to the variation in ozone itself ($\sim 7\%$ for the studied period, Table 1). If we select only the values with a distance less than 100 km and a time difference less than 30 minutes, the average offset is $-4.5 \pm 1.1\%$, which is not significantly different from the average offset including all observations from Table 1, and the standard deviation is 3%. On the basis of this relatively limited data set (34 measurements) we cannot find a significant dependence on solar zenith angle or on the cloud cover fraction calculated by the GOME Data Processor or on the GOME viewing direction (as reported in several papers in this issue), but we cannot rule out such a dependence either. Sensitivity studies of this kind should be done using the total data set obtained by Brewer and Dobson instruments participating in the validation campaign (see also Koopman and Van der Woerd 1996).

Acknowledgements

We gratefully acknowledge Hugo de Backer and Els Schoubs (KMI, Uccle, Belgium) for their cooperation in the comparison of the Brewer instruments. We would like to thank R. Agterberg, P. van der Veer, and R. Rothe for the preparation and launching of the ozone sondes. Ankie Piters is funded by SRON, The Netherlands, Pieternel Levelt is funded by BCRS, The Netherlands.

References

Koopman R.M., Van der Woerd H.J., Validation of GOME ozone columns using DOBSGOME and GOME ICFA cloud cover using ATSR-2, this issue, 1996

Piters A.J.M., Levelt P.F., Allaart M.A.F., Kelder H.M., Validation of GOME total ozone column with the Assimilation Model KNMI, this issue, 1996

[1] The ozone variability is largest in a small vertical layer around 16 km, just above the tropopause. The total ozone column variability is dominated by the ozone variability in this vertical layer. This principle is used in the two-dimensional assimilation model developed at KNMI (see Piters et al. 1996).

OZONE PROFILES AND OZONE FIELDS FOR VALIDATION OF THE ERS-2 GOME OZONE COLUMN

H.J. van der Woerd, F. Alkemade, A. Apituley, R.M. Koopman, E.P. Visser & R. de Winter-Sorkina
Air Research Laboratory, RIVM, P.O. Box 1, 3720 BA Bilthoven, The Netherlands

Abstract

During the GOME commissioning phase the RIVM ozone and aerosol lidar systems were deployed. A set of observations with detailed information on the vertical, and temporal distribution of ozone, clouds and aerosol in the troposphere is available for validation. The ozone column below the clouds was found to introduce errors in the order of a few DU in the total ozone column. The observed temperature profiles were used to calculate the corrections on the absorption cross sections used in the DOAS UV-window. The resulting uncertainty was also in the order of a few DU. These errors are much smaller than the difference found between the GOME and ground-based observations. Interpolation methods to reconstruct the daily global ozone fields from GOME observations show that the coverage by GOME is somewhat sparse.

1. INTRODUCTION

During the GOME commissioning phase a comprehensive set of regular measurements of the ozone column and other essential parameters to validate the DOAS algorithm were collected in Belgium and The Netherlands. This NL-114 proposal concentrated not only on the total ozone column amount, but also on the profile of ozone, temperature and aerosol backscatter and cloud characteristics. All these atmospheric parameters play a role in the algorithm for derivation of the ozone vertical column (OVC). Here we report on the lidar observations and use of ozone and temperature profiles in the GOME validation campaign. In addition, a first attempt of a global ozone field reconstruction is presented.

2. RIVM LIDAR MEASUREMENTS

At RIVM two operational lidar systems monitor the ozone profile in the free troposphere and the aerosol backscatter profile plus cloud-base height in and just above the planetary boundary layer (PBL).

The RIVM tropospheric ozone lidar (Sunesson et al., 1994) is used for routine measurement of vertical ozone distributions. The system uses the DIAL technique to calculate ozone concentrations from recorded elastic backscatter signals at 289 nm and 299 nm. The characteristics of the system are given in Table 1. During routine operation, measurements are made on a daily basis, provided there is no precipitation or fog and that the cloud base is above about 2 km. Ozone measurements are also made under broken cloud conditions (De Backer et al., 1994).

Table 1. Characteristics of the RIVM ozone lidar

Product	Tropospheric Ozone Concentration Profile
Location	Bilthoven (52°07′ N, 5°12′ E)
Observation time	± 1 hour around overpass
Duration	1 to 2 hours measurement
Frequency	3 times a week (typical)
Total profiles	30 in NILU database
Vertical Range	1 km to 10 km
Resolution	0.5 km near to 1.5 km far
Precision	1 % near to 20 % far
Accuracy (overall)	Better than 10 %

Recently, the receiver geometry was improved and a fast mechanical shutter was included. This new configuration allows the lowest altitude from which backscattered light is detected to be chosen at will. The measurement upper range varies from about 4 km to around 10 km, depending on actual atmospheric conditions (e.g. the aerosol content of the PBL, the ozone concentration profile and cloud conditions).

Lidar signals at the measurement wavelengths are recorded in series of "bursts" of laser shots. Many bursts are recorded that can be averaged during post processing to obtain a sufficient signal to noise ratio for the ozone retrieval. Depending on the signal levels, 15 to 30 minutes of measurement time is needed for one profile. Bursts containing clouds below a certain altitude are marked and rejected. Bursts free of clouds are averaged and an ozone profile is computed. This is illustrated in Fig. (1) and Fig. (2). In Fig. (1), on the next page, an example of the time series of lidar signals show a complex cloud situation with different cloud layers at various heights ranging from 0.6 km to 11 km. By careful selection of lidar data an ozone profile could be constructed up to about 10 km. This ozone concentration profile is presented in Figure 2 (following pages). The noise (indicated by dots) in the higher part of the profile is quite large due to the limited measurement time given by the cloud conditions. The result from a balloon sounding of the ozone profile performed by KNMI in De Bilt is also shown (broken line).

The tropospheric ozone lidar was operated on as many occurrences as possible on the pre-calculated time of overpass of GOME with location of one of the pixels over Bilthoven (see Table 2). It was attempted to take data as closely in time as possible to the overpasses. In those instances that ozone sondes were scheduled to be launched from de Bilt (at 2 km distance from Bilthoven) the data takes of the lidar were linked to the launch time of the balloons.

Table 2. Available RIVM tropospheric ozone profiles. Also indicated is the availability of ozone sondes.

Month	Day	Begin (hr)	Max (km)	De Bilt	Uccle
Jul	21	9.1	6.0	db	--
	22	10.8	8.1	--	uc
	24	9.5	4.7	--	uc
	25	9.6	9.0	db	--
	26	11.5	4.5	--	uc
	31	13.0	6.0	db	uc
Aug	1	8.2	8.5	--	--
	3	10.4	7.0	db	--
	4	10.6	9.4	--	uc
	23	13.3	4.5	db	--
	26	10.4	9.5	--	--
	30	13.4	11.3	--	uc
Sep	1	10.9	10.6	--	uc
	5	10.6	4.9	--	--
	7	11.7	3.9	db	--
	11	12.5	4.5	db	uc
	14	10.5	4.6	--	uc
	28	17.5	11.9	--	--
	29	14.3	12.8	--	uc
	29	19.6	12.7	--	uc
Oct	3	16.9	3.5	db	uc
	4	9.4	11.0	db	uc
	5	21.1	13.5	--	--
	6	10.2	13.5	--	uc
	8	15.3	11.0	--	--
	9	11.2	10.0	db	uc
	10	11.1	9.0	db	uc
	12	13.8	9.1	--	--
	14	12.9	7.8	--	--
	18	15.2	8.9	--	uc

Not all overpasses were covered. The weather conditions were the main cause of this. In total 30 tropospheric ozone profiles were collected during the validation campaign. The profile maxima range between about 4 km to 13 km in height. The precision ("noise") level in the profiles ranges from a few $\mu g/m^3$ ozone (1 %) at about 1 km to 10 - 20 $\mu g/m^3$ ozone ($\geq$20 %) towards the upper limit of the profile. The magnitude of this error is determined by the remaining noise level after averaging of the recorded signals on the one hand and the spatial resolution set during processing on the other hand. The accuracy is expected to be better than 10 %, with possibly larger values within and at the top of the PBL due to aerosol scattering effects. A detailed analysis of lidar tropospheric ozone vertical distributions and balloon carried sensor measurements using this dataset will be carried out in the near future.

The automated RIVM lidar system for aerosol and PBL measurements uses a pulsed Nd:YAG laser at 1064 nm pointing vertically. The wavelength of 1064 nm (instead of 532 or 355 nm) was chosen because of its high sensitivity for aerosol versus molecular backscatter. Averaged lidar profiles are stored with a time resolution of $\approx$4.5 min, which is sufficient to monitor the typical diurnal course of the mixed layer height. From these profiles the cloud base up to 4 km in height with an accuracy of 40 m could be retrieved. The automated aerosol lidar has operated flawlessly throughout the campaign. Cloud-base height data and backscatter profiles were submitted for 42 days.

3. GOME GHOST VERTICAL COLUMNS

Examples of the tropospheric ozone profiles obtained are shown in Fig (3). Especially during the summer large variations in the profile are observed near the PBL due to photochemical smog formation. These profiles deviate from the tabulated ozone profile that is used to correct for the ozone column that can not be observed by GOME due to clouds. This 'Ghost Vertical Column (GVC)' is in the order of 20 DU.

We have analysed 16 ozone profiles that were obtained near a GOME overpass. The true GVC, given by the integrated ozone concentration between ground and the ICFA cloud-top pressure (typically 490 hPa), was found to range between 12.0 and 28.4 DU, compared to an average 18 DU for the standard profile. Subsequently we have calculated the effect on the ozone vertical column (OVC) by substitution of the truly observed GVC in :

$$OVC. AMF_{tot} = SC + CF. GVC_{true} . AMF_{cloud}$$

where

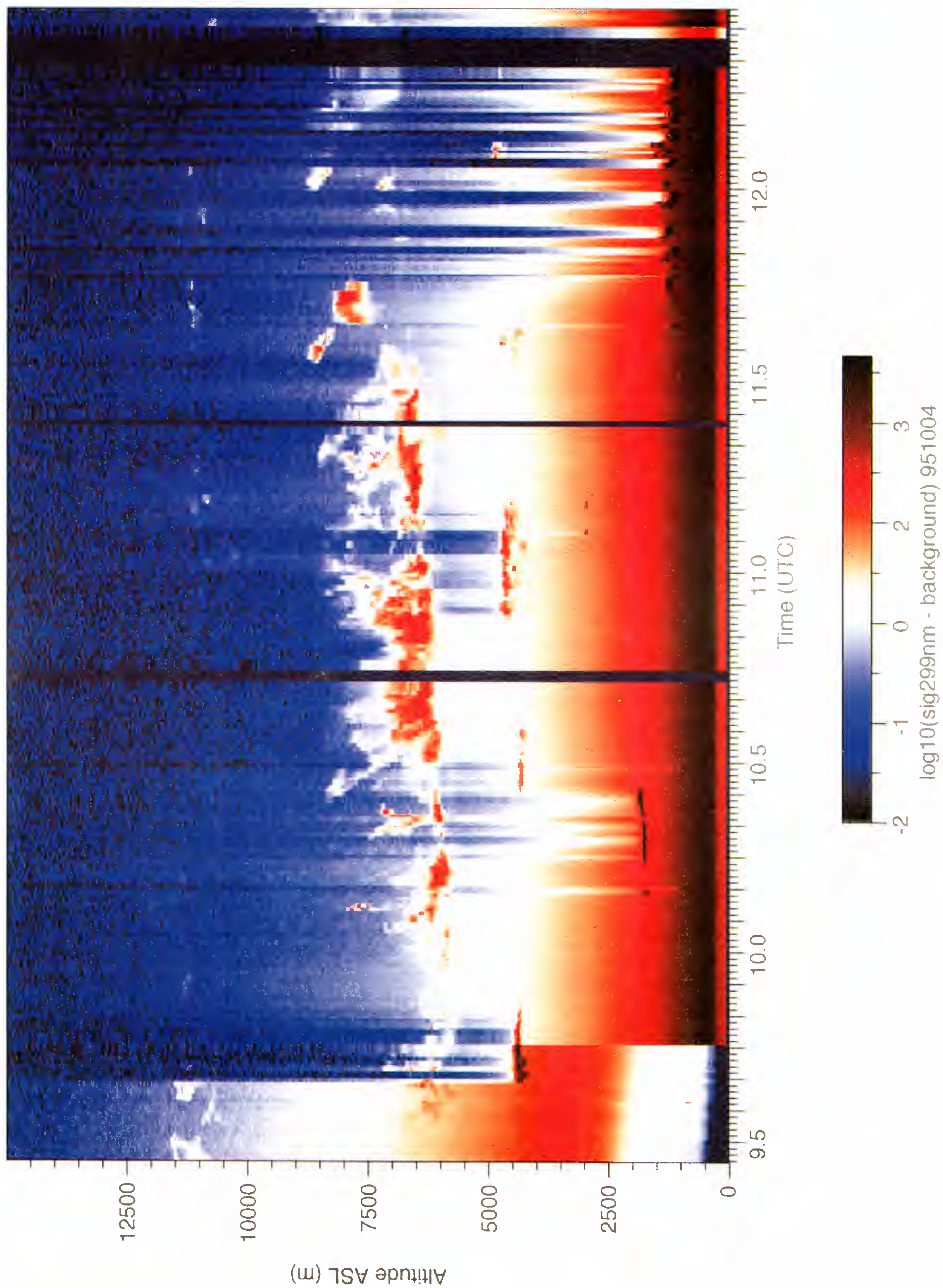

Altitude ASL (m)
0
2500
5000
7500
10000
12500
9.5
10.0
10.5
11.0
11.5
12.0
Time (UTC)
log10(sig299nm - background) 951004
-2
-1
0
1
2
3

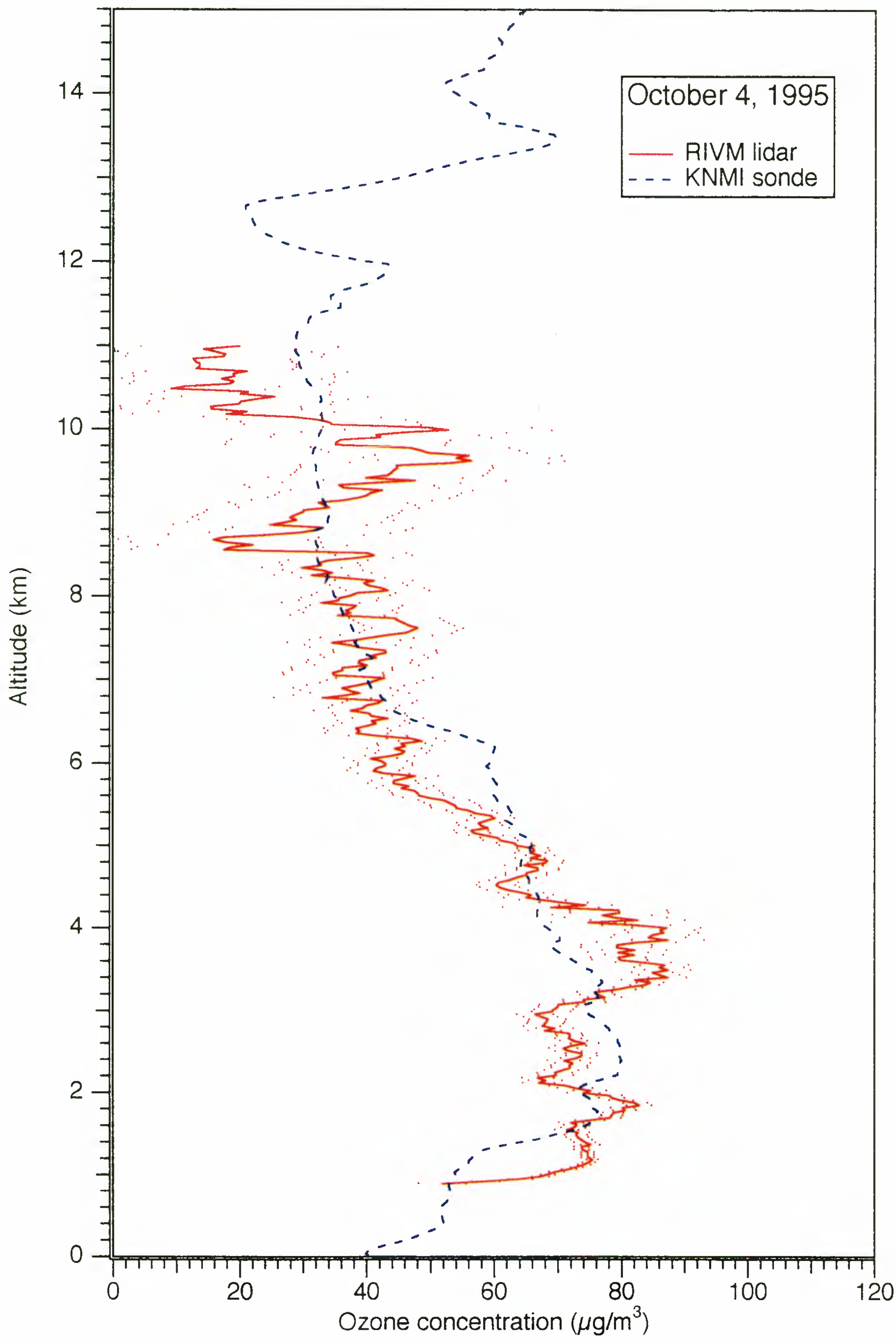

October 4, 1995
RIVM lidar
KNMI sonde
Altitude (km)
0
2
4
6
8
10
12
14
0
20
40
60
80
100
120
Ozone concentration (μg/m3)

$$AMF_{tot} = CF.\ AMF_{cloud} + (1\text{-}CF).\ AMF_{clear}$$

Here we have taken the Air Mass Factor (AMF) under clear and cloudy conditions, the DOAS Slant Column (SC) and the ICFA Cloud Fraction (CF) from the intermediate results record. Because the cloud fraction is less or equal to 1.0 the error in the OVC is smaller than the error in the GVC. A notable example is the summer smog situation which gives a large difference in the GVC but a much smaller correction in the OVC because smog generally occurs under clear-sky conditions.

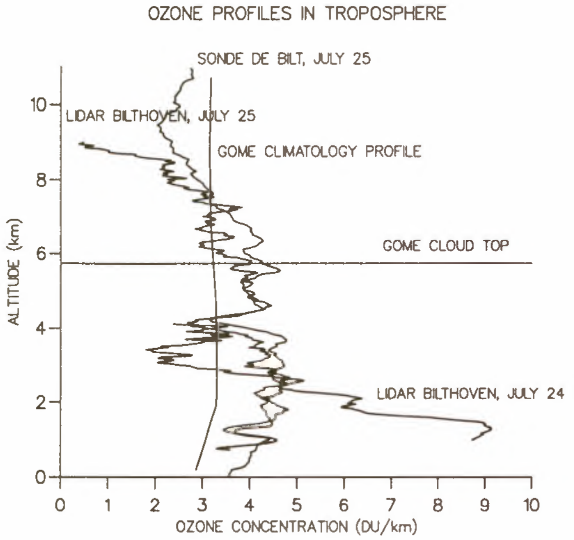

Figure 3. Ozone profiles in the troposphere as measured by lidar and sonde. Note the smog layer at July 24 below 3 km. For clarification the GOME climatology profile and the cloud-top height of the ICFA algorithm are plotted.

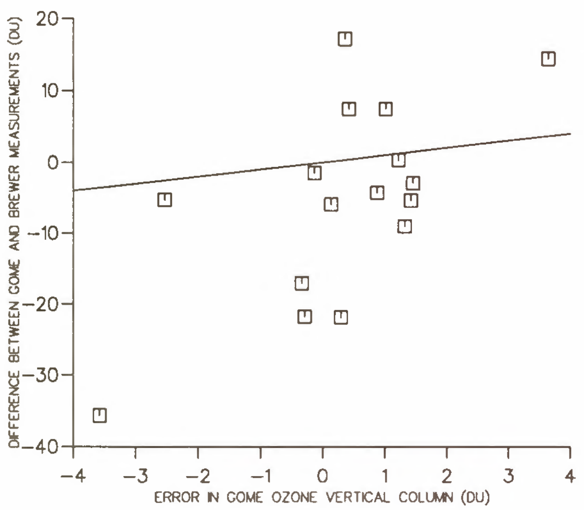

Figure 4. The error in the OVC derived from the difference between observed and tabulated ozone column below the ICFA cloud-top height. The corrections are small.

The OVC corrections for 16 profiles in the period July - October in Western-Europe were found to be small (range -4 to + 4 DU). The observed differences between ground-based and GOME total ozone column observations are plotted as function of these corrections in Fig. (4) There is no correlation. Also no correlation with the ICFA cloud fraction was found.

4. GOME DOAS TEMPERATURE-DEPENDENCE

A second application of the use of ozone profiles in the ozone column validation is to check whether ozone- and temperature profiles are consistent with the assumed climatology. Because the ozone absorption cross sections in the Huggins bands are temperature dependent the fitted DOAS slant column might be off by a few % due to difference in the T-profile around ozone maximum. The average changes in the UV-window (325 - 335 nm) ozone cross sections were calculated as function of the difference between the observed- and climatological-temperature profile and the an estimate of the change in the OVC was made. We found that in a linear approximation around 221 K, a change of +1 K results in a change by -1.2 ± 0.3 Dobson Unit in the OVC.

We have analysed 11 ozone and temperature profiles that were obtained near a GOME overpass. In the period July - October the stratospheric temperature was somewhat lower but fairly consistent with the GOME climatology. The derived errors in the OVC were found to range between -4.4 to +2.3 DU (see Fig. 5). There is no obvious correlation with the GOME total column error, which shows much larger variations.

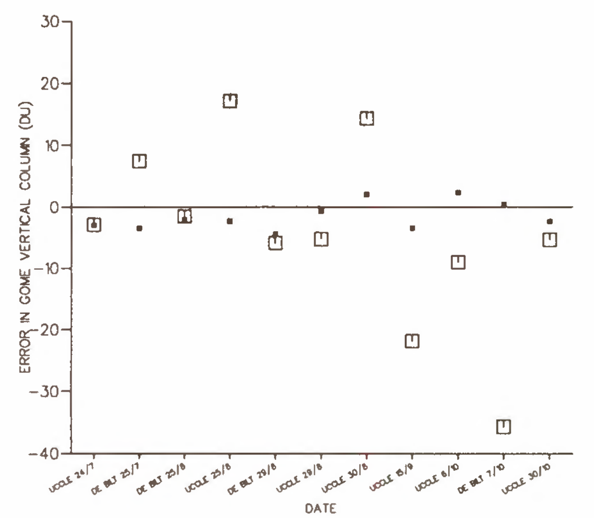

Figure 5. Estimate of the error induced by a difference between the true temperature at ozone maximum and the GOME climatological temperature. For reference the much larger difference between the simultaneously obtained GOME and Brewer ozone column is shown.

5. GOME LEVEL -2.1

The GOME orbit, repetition cycle and pixel size give a very restricted sampling of the global ozone distribution. Although GOME is expected to give reliable ozone distributions on a monthly and yearly basis, it is not obvious that with the present orbit and pixel configuration reliable ozone maps can be constructed on a daily basis.

We have tested three interpolation methods to reconstruct the ozone fields from the GOME information: Empirical Orthogonal Functions (EOF), Minimal Curvature Interpolation (MCI) and Quintic Surface Fitting (QSF). This reconstruction was tested by taking TOMS ozone fields as input for simulated GOME data. The TOMS field was sampled with the GOME orbit and pixel tracks. This sample was the input for he reconstruction of the whole field. After reconstruction the created fields were compared with the original field. This exercise was done on a continental (European region) and global scale, but with the polar regions excluded.

First, three years of daily TOMS ozone-fields were analysed to search for a set of independent geographical patterns, called EOF's, which successively describe as large an amount of the variation in the ozone field as possible (Alkemade, 1995). This set of EOF's represents some knowledge about the climatology of the ozone layer that can be 'fitted' to the simulated GOME values to yield a reconstruction of the field. Also a spline surface fitting routine (MCI) and a smooth interpolation with Akima's quintic polynomials (QSF) was applied for comparison (see Figures 6 and 8 on the next pages).

As the GOME pixels are densely spaced in latitude, the error in the interpolated fields is presented as a function of the longitudinal distance to the nearest GOME pixel. For local interpolations at latitudes between 30 and 60 degrees N, the MCI-method typically gives the best results. The mean error is less than 5 DU for distances up to 2 degrees (150 km) , rising to about 15-20 DU at 500 km. The EOF-fitting reaches similar precision as MCI only for distances greater than about 350 km (Fig. 7). Note however, that EOF sometimes reconstructs features that the MCI-interpolation misses (Fig. 6).

For interpolations on a global scale (Fig. 8) the mean errors are slightly smaller due to the easy-fitting of the smooth tropical ozone field. At short distances (5 to 10 degrees) the MCI- and EOF-method yield similar results (Fig. 9). At distances greater than 15 degrees the EOF gives the best reconstruction, mainly due to a better description of the field at the missing 4 orbits above the Pacific. The QSF gives an inferior reconstruction both on a local and global scale.

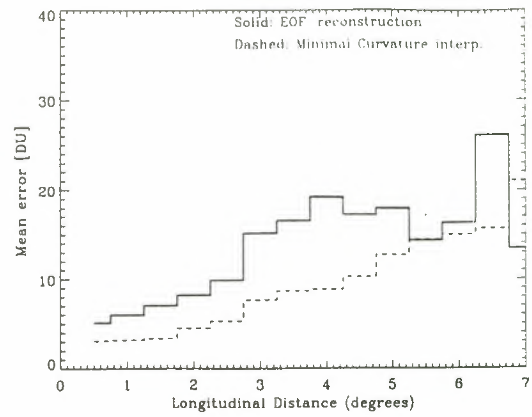

Figure 7. Mean error of the difference between the interpolated and original TOMS field over Europe (see previous figure) as function of the longitudinal distance to the nearest GOME-pixel.

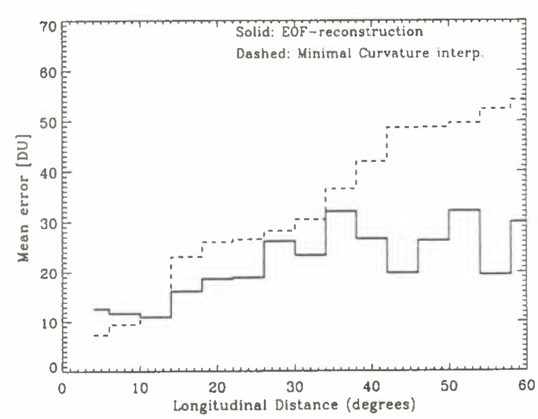

Figure 9. Mean error of the difference between the interpolated and original global TOMS field (see previous figure) as function of the longitudinal distance to the nearest GOME-pixel.

Figure 6. Colour page. Comparison of interpolation methods for the West-European region. The original TOMS field (a) was sampled with the GOME-pixel resolution. The other fields (b-d) are the reconstructed fields.

Figure 8. Colour page. Comparison of interpolation methods for the daily global ozone distribution. The original TOMS field (a) was sampled with the GOME-pixel resolution. The other fields (b-d) are the reconstructed fields.

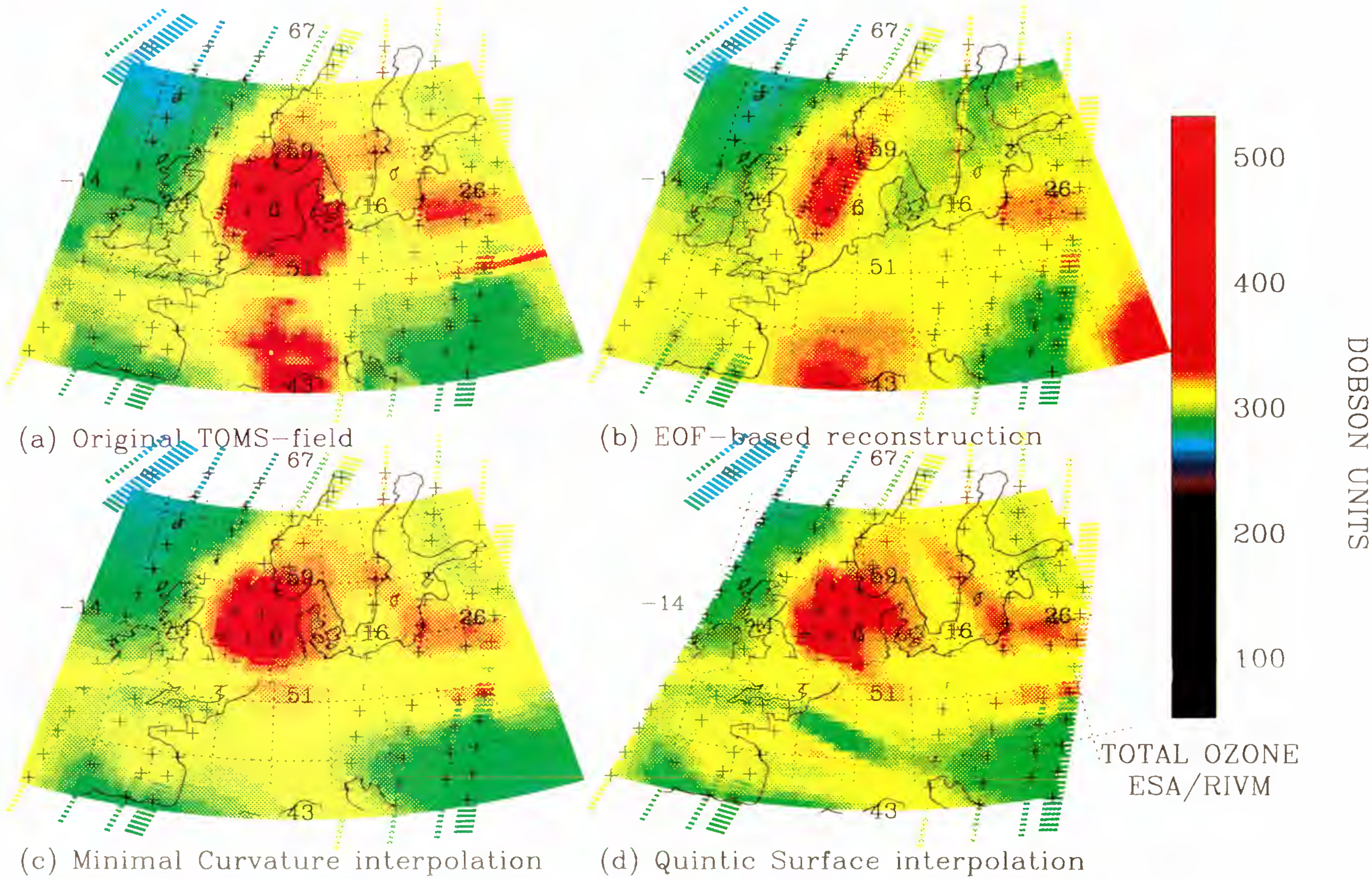
DOBSON UNITS
500
400
300
200
100
TOTAL OZONE
ESA/RIVM
67
-14
59
51
43
26
16
(a) Original TOMS-field
(b) EOF-based reconstruction
(c) Minimal Curvature interpolation
(d) Quintic Surface interpolation

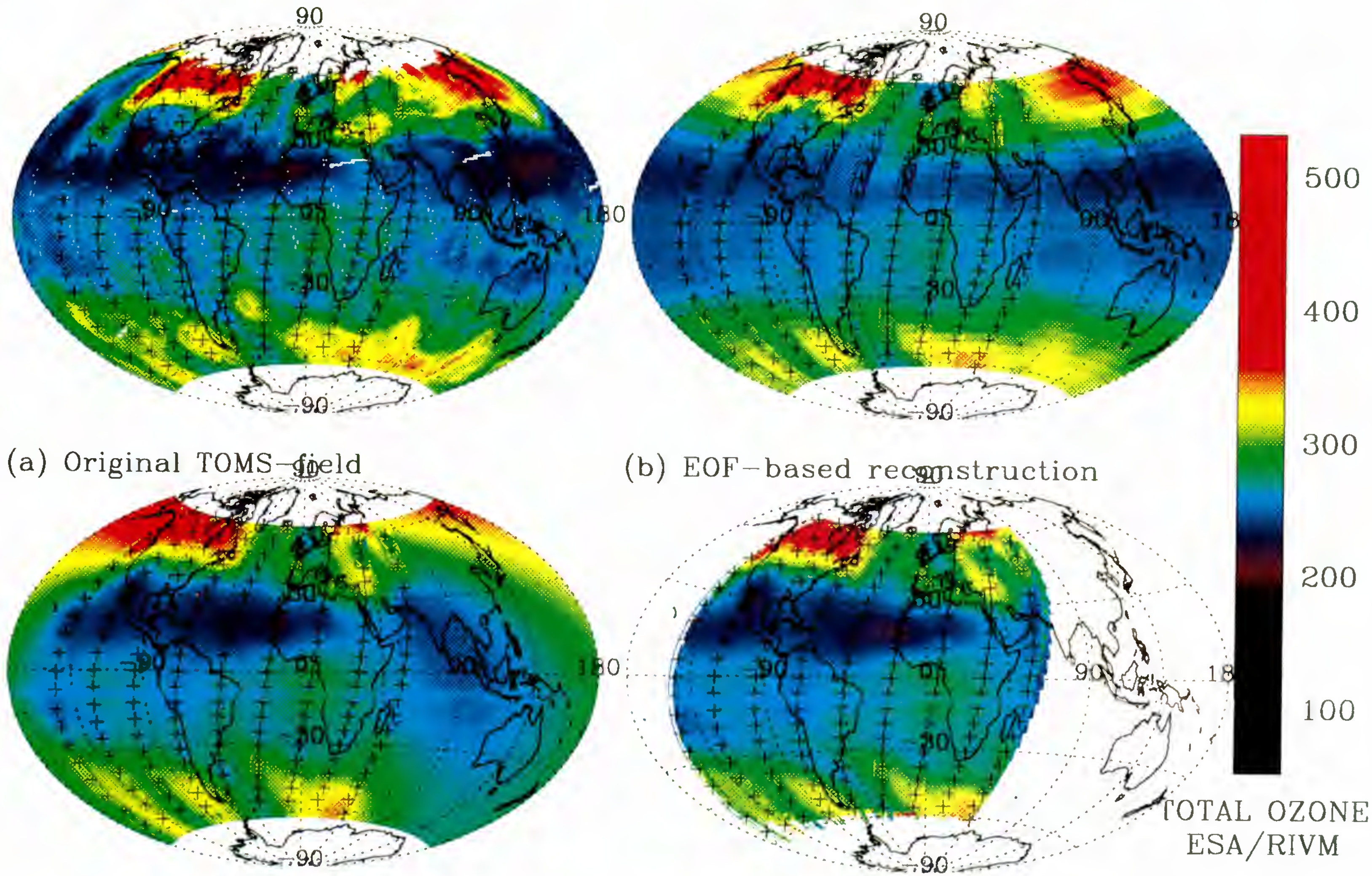

(a) Original TOMS-field
(b) EOF-based reconstruction
(c) Minimal Curvature interpolation
(d) Quintic Surface interpolation

6. CONCLUSIONS

Both RIVM lidar systems that were deployed in the GOME validation campaign have performed well. A qualitatively good dataset with detailed information on the distribution of ozone, clouds and aerosol in the troposphere and PBL is available for validation. These observations will become very valuable when operational algorithms will be developed for the derivation of the tropospheric ozone content from GOME spectra.

However, we have shown that the ozone profiles can be used already to validate some parameters that are used as input in the algorithms for derivation of the ozone vertical column. First, the total column amount below the cloud-top height or ghost vertical column was validated. Second, the observed ozone / temperature vertical distribution was used to estimate the error due the temperature sensitive ozone cross sections that are used in the DOAS fitting. Both errors turn out to be small, typically 1-2 percent of the total ozone column. This is much smaller than, and not correlated with, the GOME/Brewer differences in ozone column.

The GOME observations seem to undersample the ozone field for reconstruction of the daily dynamical changes. Field reconstruction on a daily basis is possible, but with limited accuracy. Typical mean errors for reconstruction with the MCI- or EOF-fitting are 5 DU within 150 km locally or 20 DU on a global scale.

7. RECOMMENDATIONS

From the experience during the commissioning phase we recommend to extend the validation of GOME. In particular we suggest to: - Process more orbits, - cover all seasons, - process all 14 orbits per day for global information, - validate the new co-adding mode, - give feedback on the improved algorithms, - Include more stations at other latitudes (Lauder in NZ) and -focus attention on the polar regions.

8. REFERENCES

Sunesson, J.A., Apituley, A., and Swart, D.P.J. 1994. Differential absorption lidar system for routine monitoring of tropospheric ozone. *Applied Optics*, Vol. 33, pp. 7045-7058.

DeBacker, H., Visser, E.P. et al. 1994. Potential for meteorological bias in lidar ozone data sets resulting from the restricted frequency of measurement due to cloud cover. *J. Geophys. Res.*, Vol. 99, pp. 1395-1401.

Alkemade, F.J.M. 1995. Empirical Orthogonal Function (EOF) Analysis of Ozone Variability. *Climate Change Research, Evaluation and Policy Implications*, Eds. S. Zwerver et al., Elsevier, pp. 275-278.

9. ACKNOWLEDGEMENTS

We like to acknowledge the KNMI and KMI for making available part of their sonde information on ozone and temperature. This work was partly supported by the Space Research Organisation Netherlands (SRON).

Validation of GOME ozone columns using DOBSGOME, and of GOME ICFA cloud cover using ATSR2

Rob M. Koopman and Hans J. van der Woerd

Abstract

This paper describes part of the RIVM contribution to proposal NL114, and consists of three parts.

First, systematic differences between pixels as a function of pixel type are investigated. Marginally significant systematic differences were found for the entire dataset available. However, slightly larger random variations are found when comparing averages for different months. Further investigation is required to determine whether these variations are entirely due to variations in the actual ozone distribution, or partially reflect more complex systematic errors.

Second, differences between GOME and ground-based measurements and their dependencies on measurement conditions and parameters are studied, using an enhanced version of the DOBSGOME tool. The observed differences increase strongly with increasing air-mass factor, to such an extent that other potential dependencies are obscured.

Third, preliminary results are presented of an ongoing investigation comparing cloud properties derived from ATSR-2 data to those from ICFA. Although the study has not reached the stage in which statistically significant conclusions can be drawn, the results show deviations of up to 0.7 in cloud fraction.

1 Intercomparison of GOME DOAS data records

1.1 Introduction

Conclusions on the quality of total ozone column measurements by GOME can already be drawn by studying systematic differences between averages of subsets of the entire set, which are theoretically expected to yield identical means. In the equatorial latitude regions, ozone concentrations remain relatively stable, and the remaining random ozone gradients accross the GOME tracks are expected to cancel when measurements from all 437 orbits that are currenlty available are averaged (170×10^3 pixels with latitudes between -18° and 18°). Remaining differences are thus likely to be due to systematic errors. For the first data product (orbit 1322, file 50722102.lv2), a correlation of total measured ozone as a function of line of sight (LoS) was found (see Figure 3). The line of sight is the zenith angle of the line from ERS-2 to the centre of the ground pixel. In this paper, lines of sight are labeled according to Table 2 for further reference. "East" and "West" reflect the relative location of the ground pixels during the descending part of the orbit. In order to investigate the cause of the above correlation, zonal averages of total ozone as a function of line of sight were studied. Both monthly averages and averages over the entire set of available data have been calculated.

1.2 Selection of GOME data

Two selection criteria were applied to the individual orbits and to the monthly and total datasets, namely:

- Only solar zenith angles of less than 74.6° were considered acceptable, since no Multiple Scattering correction has been applied to GOME measurements beyond this value.
- In order to eliminate "spikes" from the dataset, only observations with errors less than 2% were included in this study.

The remaining subset of the full data set was subsequently binned according to latitude (see Table 1) and line of sight (Table 2).

Table 1: Latitude bins

band 0:	-90°	-54°
band 1:	-54°	-18°
band 2:	-18°	18°
band 3:	18°	54°
band 4:	54°	90°

1.3 Averages of entire dataset

Averages of total ozone for the full currently available dataset are presented in Figure 1 and in Table 3 as a function of pixel type and latitude range. In most latitude bands, differences between the averages are in the order of a few times the estimated

Table 2: pixel types

label	pixel type	line of sight
0	Back scan	-23°
1	"East"	-13°
2	Center	7°
3	"West"	27°
4	Other	other

error of the mean σ_μ. Here $\sigma_\mu = \sigma/\sqrt{N}$; N is the number of events, and σ is the standard deviation; $\sigma^2 = \frac{1}{N}\sum x_i^2 - \mu$. ($x_i$ is measurement, μ is mean of measurements). From table 3, a generic value for the difference between averages for the pixel types of 0.5 % is found for bands 1 to 4. For these latitude regions, the differences between the pixel types are marginally significant, and could be attributed to a weak systematic effect. The aforementioned equatiorial band displays differences of about 1 σ_μ between East, Center and West pixels, but the difference between West and Back-scan pixels settles at the 5 σ_μ level.

The differences in the remaining range, [-90°:-54°], are most likely caused by the pitch of the ERS-2 orbit, which causes more Eastward pixels to sample lower ("ozone hole") values, compared to their Westerly neighbours. The typical difference as a function of pixel type for this polar region is still no greater than 1.2 %. In view of the steep gradients of the ozone distribution in this range, these differences can be explained in terms of physical ozone differences instead of systematic measurement errors.

In a similar study, averages of the ICFA cloud fraction showed differences between the pixel types as a function of latitude or solar zenith angle in the order of several σ_μ, and the magnitude of the differences in the order of 2%. Again the deviations border on significance, and systematic sources of error cannot be excluded.

Figure 1: average of Total Ozone as function of pixel type and latitude region

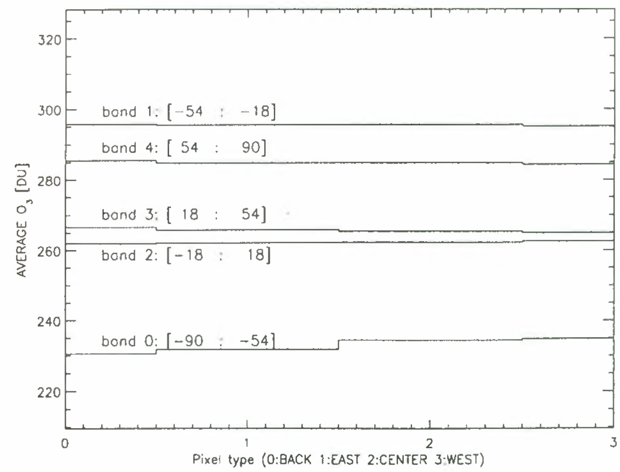

cancel out on average, and will not be detected with this method.

Figure 2: average of Total Ozone as function of pixel type and latitude region for November 1995

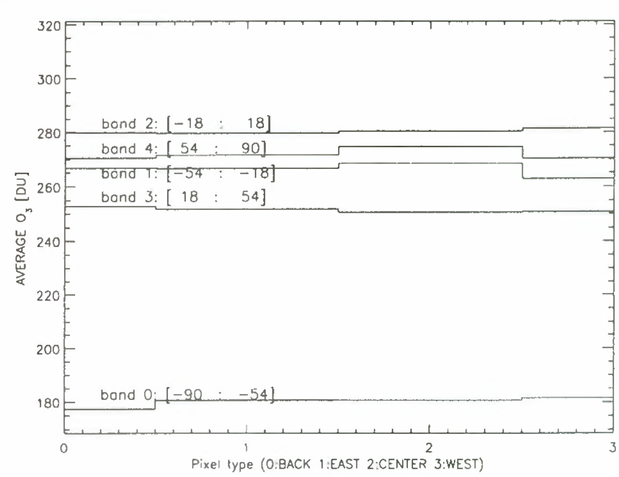

1.4 Monthly averages

The monthly averages show slightly greater differences between pixel types, but a single pattern that persists in time could not be identified. From this analysis alone, it cannot be excluded that gradients in the physical ozone distribution can account for all observed differences. The example plot in Figure 2 displays the monthly averages for November 1995. The typical differences of 1.5% are larger than those found for the entire duration of the validion campaign (Figure 1), and the sign of the differences appears to be random. The averaging method suggests that gradients of the physical ozone concentration could explain the observed differences, but does not provide evidence. More complex error patterns may

1.5 Random samples

Since only marginally significant systematic differences were found from the study of averages, a number of GOME orbits were selected at random, in an attempt to detect other deviation patterns. From the orbits in Figure 3, it can be remarked that over an 80° latitude range, the Back-scan pixel has higher values for a single orbit than the West pixel for all these random cases. From the averages it is clear that this pattern can not be persistent for the entire data set. Further investigation includes comparison with other measurements, to determine whether this difference can be explained by a large-scale gradients in the ozone distribution (see Section 2). The discontinuities in the measured ozone distribution at

Table 3: average of total ozone per pixel type per latitude band

Latitude band		Back	"East"	Center	"West"
		mean ozone values [DU] μ			
-90	-54	230.5	231.8	234.4	234.8
-54	-18	295.7	295.6	295.6	295.1
-18	18	262.0	262.2	262.3	262.6
18	54	266.6	265.8	265.3	265.0
54	90	285.6	284.7	284.8	284.3
		est. error of mean [DU] σ_μ			
-90	-54	0.60	0.60	0.65	0.63
-54	-18	0.25	0.25	0.25	0.25
-18	18	0.12	0.12	0.12	0.12
18	54	0.10	0.10	0.10	0.10
54	90	0.18	0.18	0.19	0.20
		number of points N			
-90	-54	12595	12508	10698	11766
-54	-18	40000	40065	39619	41232
-18	18	42719	42406	42095	42573
18	54	38907	38203	36563	36127
54	90	16065	16892	14787	13258

-10° and at 10° which are evident from orbit files 51005180.lv2 and 51005194.lv2 most likely reflect the gridding of the climatology data base that is used for the 1.21 Version of the level 1→2 processing algorithm.

1.6 Conclusions

Only marginally significant systematic deviations between pixel types could be identified from averages of GOME data. However, the study of data from randomly selected GOME orbits suggest that it is necessary to investigate whether systematic effects exist which are hidden by the averaging method. Our intention is to search for statistical evidence of such effects.

Figure 3: total ozone vs latitude for 4 arbitrary orbits

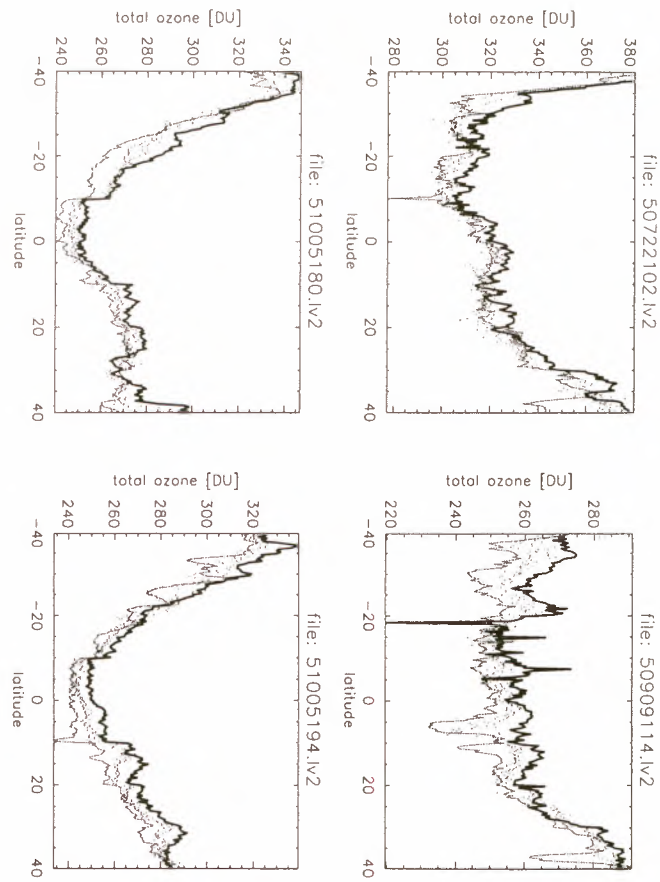

Orbit data files 50722102.lv2, 50909114.lv2, 51005180.lv2, 51005194.lv2.
Thick line: Back scan pixels, dotted line, East and Center pixels, thin line, West pixels

2 Comparison of GOME total Ozone measurements with Dobson and Brewer measurements using DOBSGOME

2.1 Introduction

In view of the limited duration of the intensive validation campaign Georg Hansen from NILU and the authors at RIVM agreed to jointly develop a tool for identification, extraction and gathering of GOME and ground-based measurements which are temporally and geographically coincident. This DOBSGOME tool is developed as a general service to all members of the validation campaign, and is aimed at reducing the workload on the validation data base server, and at prevention of redundant work by the validation groups. At RIVM, an enhanced and extended version of this tool was developed for more detailed investigations, aimed at evaluating as many overpass events as possible. In this way, sufficient data points can be obtained for the identification of statistically significant relations, in spite of the limited duration of the validation campaign. In an attempt to isolate sources of error in the GOME instrument and its data processing algorithms, deviations between GOME and ground-based measurements were investigated to find dependencies on any of the measurement parameters available from the DOAS data records.

2.2 Selection of data

2.2.1 Brewer and Dobson

Only data from the stations in Table 4 were taken into consideration for reasons of compatibility and stability of the formats used by the operators. The subset was further reduced to only include Direct Sun measurements, since these have greater accuracy than Zenith Sky measurements. After a comparison between Dobson and Brewer measurements, a choice was made to reduce the subset even further by considering only Brewer measurements, since the Brewer data appeared more consistent (see Figure 4).

Table 4: Dobson/Brewer stations

name	lat	lon
Arosa	46°.77N	9°.67E
De Bilt	52°.10N	5°.18E
Haute Provence	43°.95N	5°.71E
Ny-Alesund	78°.91N	11°.89E
Oslo	59.91N	10°.72E
Trømso	69°.66N	18°.97E
Uccle	50°.80N	4°.35E

2.2.2 GOME

Only the Total Ozone value in the DOAS Data Record(DDR) was used, which replicates the UV-Ozone value in the Intermediate Results Record. The data set was reduced by considering only measurements with Solar Zenith Angles (SZA) of less than 74.6°, since no Multiple Scattering Correction was applied beyond that value. An additional constraint was that only measurements with an error (as reported in the DDR) of less than 2% were accepted.

2.2.3 Coincidence

Each overpass event[1] with distance and time differences between the centre of a GOME measurement and a Brewer or Dobson instrument less than respective limit values has been selected for evaluation.

A preliminary study with a distance limit of 600 km revealed that, with the current level of accuracy, no strong dependance of the deviation between GOME and ground measurements was found up to 150 km and this limit was chosen as the distance limit for further investigations. When more data are available, and the accuracy of the Geolocation has improved (see section 3 on ATSR-2 and ICFA) , this selection criterion will be refined, whereby only pixels with maximum overlap of effective measurement volumes will be accepted.

A maximum acceptable time difference of 6 hours was chosen, but in practice, in 56% of the coincidences selected, the time difference was less than 1 hour. The deviation caused by large time differences was not significant compared to other sources of error. A subset of 1.1×10^3 pixels satisfied all requirements above.

Each measurement and auxiliary parameter has been plotted against the deviation between GOME and groundbased measurements of total ozone. For those cases in which a dependency was found, these plots are reproduced in section 2.3.

A disadvantage of this method is that deviations which do not systematically have the same dependence pattern for each of the different ground stations, may not be apparent from these plots, hence in-depth analysis for single stations is necessary to identify and analyse such individual patterns of dependence.

[1] An exception needs to be made for a number of overpasses in September, wich were inadvertently not evaluated due to an unexpected distribution of orbit data over validation product files, which deviates from the practice agreed for future operational files

Overpass dates

Overpasses were evaluated for each of the dates listed in Table 5

Table 5: Dates

yy	mm	dd
95	07	23-25
95	08	25-27,29-31
95	09	01-09,15-17,21-23,27-28
95	10	01-03,05-07
95	12	12

2.3 Differences betweeen GOME and Brewers

Each of the measurement parameters against which the deviation between the total ozone measurements has been compared, is discussed below.

Total Ozone Total ozone measurements by Brewer instruments have shown better correlation with GOME measurements than those by Dobson instruments, as can be seen from Figure 4. The vast majority of ground-based measurements have yielded total ozone values greater than those from GOME.

Distance No noticable correlation between the deviation of the Ozone columns and the distance between the measurements was found for the events selected, thereby confirming that 150 km is an acceptable distance limit for the current level of accuracy.

Figure 4: GOME O_3 vs Dobson/Brewer O_3

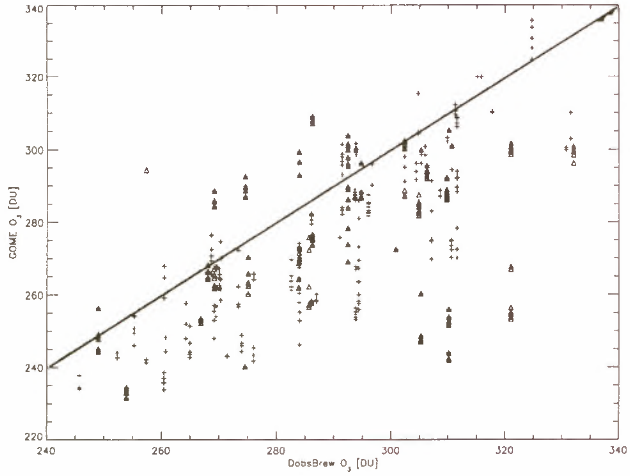

+ = Brewer, Δ = Dobson

It should be noted that the errors in the Geolocation of the GOME footprints due to the absence of Yaw Steering Mode correction in the data processing algorithm can reach values as large as 50 km.

Time difference Currently, other errors are too large to notice a (potential) correlation between the time difference between GOME and ground-based measurements and the difference in measured total ozone values.

Day of year No evidence was found for a correlation between the deviation of the Ozone measurements and the day of year for the limited range of seasons under consideration. However, indirectly seasonal effects have emerged in the dependence on SZA and total ozone amount.

ICFA cloud fraction No significant correlation was found between the deviation of GOME and Brewer Ozone measurements and GOME's ICFA. The implications of this observation are limited however, because the limitation to a subset with only Direct Sun measurements results in a subset with a strong bias towards cloud-cover fractions below 0.6. In addition, in-depth analysis is necessary to detect dependency patterns which differ between the various ground stations.

Total Air Mass Factor As can be seen from Figure 5, GOME Ozone measurements deviate strongly from Brewer measurements when the Air Mass Factor (AMF) increases beyond 3.0. This is also evident from Figure 8. A significant reduction of the deviation is expected when the data are reprocessed with the new version (**1.22**) of the Level 1→2 algorithm.

Figure 5: (GOME O_3 - Brewer O_3) vs GOME total AMF

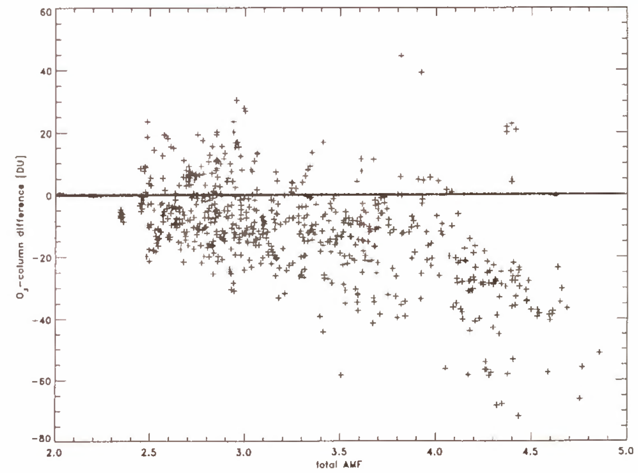

Pixel type (BECW) For this comparison, GOME pixels have been binned according to their Line of Sight zenith angle (pixel type). The differences as a function of pixel type are presented quantitatively in Table 6 and graphically in Figure 6. The estimated error of the mean is about 1 DU for each of the four distribitions, hence the differences between the pixel types are significant, the Back scan generally providing larger ozone values than the West scan. In addition, events were selected where two nearby ground stations were covered in one orbit by pixels of different type. Although the number of events is insufficient for statistical significance, it is worth noting that for three out of the four "Back - Center" coincidences, the ozone difference with the ground station is more negative for the Center pixel compared to the Back scan, which agrees with previous findings.

Solar Zenith Angle, Slant ozone column Deviations increase with increasing SZA and slant column (and therefore also with Latitude). The shape of the deviation pattern is similar to that of Figure 5, since large slant columns and large SZAs imply large AMFs. For the SZA, the dependence is plotted in Figure 7. For SZA values below 40°, deviations are only slightly greater than the typical uncertainty of the ground-based observations.

Error in GOME ozone value (lv2 product) No significant correlation was found here, suggesting that the error value provided cannot yet be used as an indication of reliability (the usual error limit of 2% was slackened to 4% for this study).

Figure 7: (GOME O_3 - Brewer O_3) vs SZA

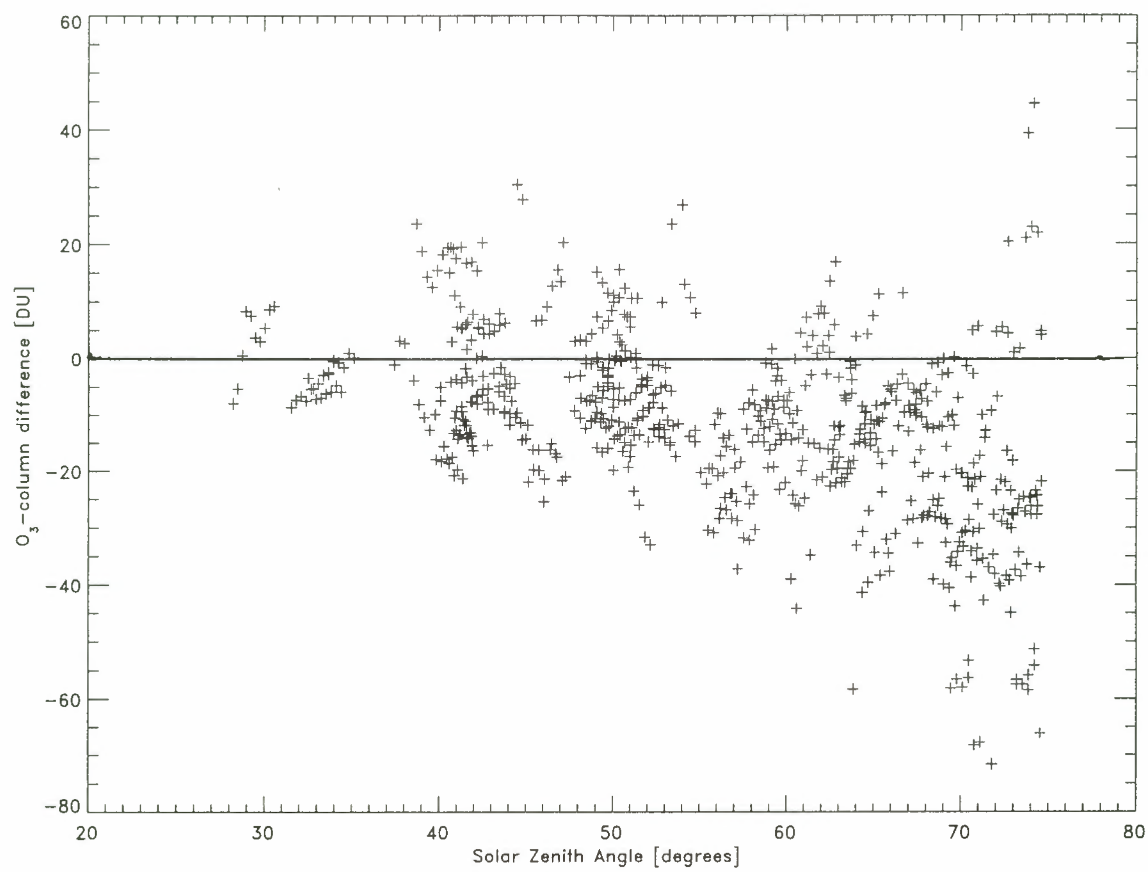

Figure 6: (GOME O_3 - Brewer O_3) vs Pixel Type

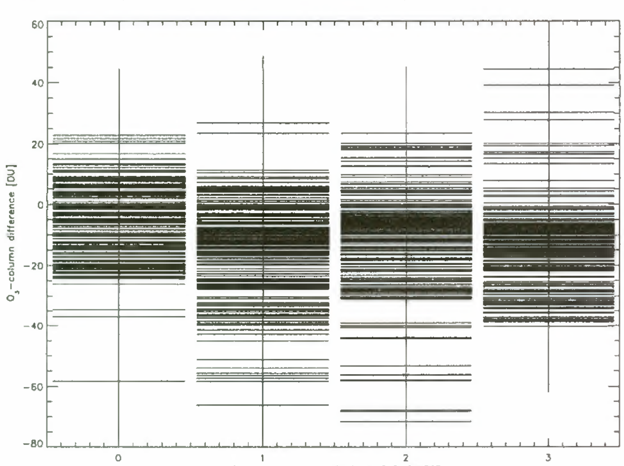

Table 6: Results for $\Delta = O_{3,\mathrm{GOME}} - O_{3,\mathrm{Brewer}}$

quantities	R	μ (DU)	σ (DU)
O_{3GOME} , O_{3Brw}	0.74		
Δ		-11.0	15.4
O_{3G} , O_{3B}(SZA<60°)	0.85		
Δ (SZA<60°)		-6.1	10.8
Δ, AMF	-0.58		
Δ, SZA	-0.59		
Δ, ICFA	-0.13		
Δ_{BACK}		-4.4	13.0
Δ_{EAST}		-17.2	17.5
Δ_{CENT}		-9.4	17.0
Δ_{WEST}		-11.0	12.4

μ = average, σ = standard deviation, R = linear correlation coefficient

AMF intensities, pixel colour, contrast These parameters are provided as diagnostics (The AMF intenisities are interim products of the AMF algorithm, the pixel colour and contrast values are derived from polarisation measurements). No significant correlation was found

2.3.1 deviations of GOME subsets with limited parameter ranges

The small deviations between GOME and Brewer instruments found for low values of the AMF suggest that the GOME instrument performs better than the overall average deviation suggests. This is convincingly demonstrated by studying the average deviation for a subset of the overpass events where the AMF was limited to a maximum value. The resulting overall average deviation as a function of this maximum value is plotted in Figure 8. For each value of the maximum AMF, the average of the differences between GOME and Brewers was calculated, plus the standard deviation of these differences (see Figure 9). For air-mass factors below 3.0, GOME and Brewer measurements agree to within 5 DU on average. Beyond AMF values of 3.5 the deviation and the average difference both increase rapidly, only to grow even faster beyond an AMF limit of 4.2. An optimal compromise would be to distribute data which are confined to a subset with AMF less than 3.0.

Figure 8: averages of AMF-limited subsets

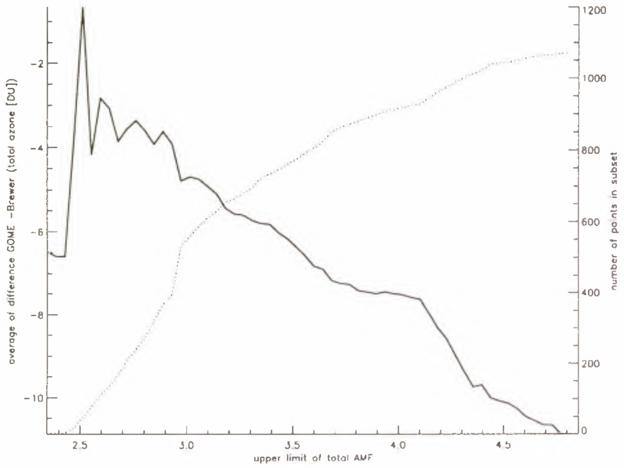

Figure 9: standard deviation of AMF-limited subsets

.

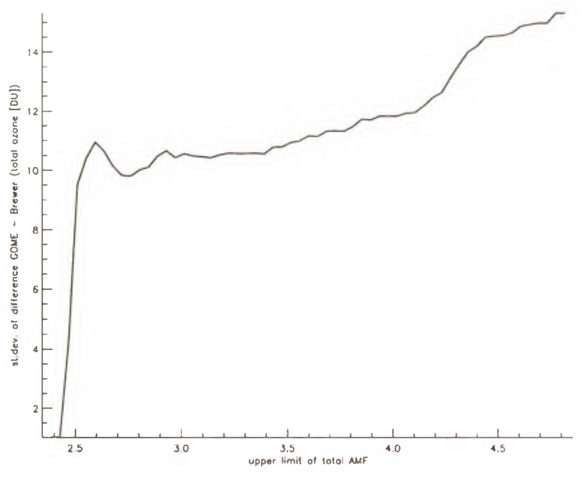

2.4 Conclusions

Differences between GOME and Brewer measurements of total Ozone columns increase with Air Mass Factor (Solar Zenith Angle). On average, the GOME instrument provides lower values than the Brewer instruments. Not only the average value of the differences, but also the standard deviation of the differences grows with increasing AMF.

Systematic differences as a function of line of sight are suspected, but further investigation of this aspect is required.

The errors introduced by the Air Mass Factor algorithm are of such magnitude that other sources of error could not be isolated.

2.5 Recommendations

We recommend not to release data processed with the current level 1→2 algorithm. Alternatively, a subset of the full dataset could be distributed which is more representative of the level of accuracy of the GOME instrument, i.e. a subsest formed by all ground pixels with Air Mass Factors below a value of 3.0.

The differences in viewing geometry between the current observation mode and the planned co-adding mode are sufficiently large to mandate a validation campaign dedicated to the co-adding mode.

In order to quickly identify potential errors in updated versions of the data processing algorithm, it is important to agree upon a reference dataset, which is to be reprocessed and analysed prior to distribution of updated data products.

3 Comparison of cloud properties derived from ATSR data with GOME ICFA

3.1 Introduction

The GOME level 1→2 algorithm, which derives total ozone columns from level 1 spectra, relies to an important extent on the Initial Cloud Fitting Algorithm. The low spatial resolution of GOME prevents accurate cloud detection, and errors in the ozone values can partially be attributed to cloud fitting errors. GOME shares its data-handling electronics with the ATSR2 instrument, and has partial overlap with its field of view. The ATSR2 instrument is much better suited for cloud detection, because of its superior spatial resolution and its viewing geometry. The cloud fraction as seen by a GOME pixel can be accurately determined by integration over the region of full overlap of GOME and ATSR2 field of views.

In addition to cloud-cover fraction (CCF), also cloud height (CTH) can be derived, in an independent manner. The independence of the determination of cloud-top height is particularly relevant to ICFA validation, since ICFA cloud-cover fraction and ICFA cloud-top height (pressure) are not independently determined. For this reason ICFA's Ghost Vertical Column (GVC) is expected to be more accurate than errors in ICFA CCF and ICFA CTH would suggest. For the above reasons, ATSR2 is an excellent tool for validation of ICFA.

This study is still in its preliminary stage, hence first results, although promising, are still sparse. Already a second application of ATSR2 data to the validation of GOME has presented itself. The relatively high spatial resolution of ATSR2 is also helpful to study the effects of the delay in the readout of the GOME detector pixels. This delay results in differences in the field of view of the various detector pixels. ATSR2 provides information on inhomogeneities in the regions that are only partially covered by the detector diode array. Inhomogeneities in these regions only affect part of the GOME radiance spectrum, and are an important cause of channel-to-channel discontinuities.

3.2 The ATSR2 instrument

The main purpose of the Along Track Scanning Radiometer is the accurate measurement of sea surface temperature (SST). The intermediate products needed for SST retrieval can be used for cloud characterisation. The instrument and its data products are briefly described below.

Spectral properties The ATSR2 is a 7 channel instrument, which measures reflected solar radiation in its 0.56μm, 0.67μm, 0.87μm and 1.6μm channels, and thermal emission in its 3.7μm,11μm and 12μm channels.

Geometric properties The scan mirror of the ATSR2 describes a circular motion around an axis which is inclined with respect to the nadir direction. This results in an elliptical footprint on the surface, and the inclination is chosen such that the ellips almost passes through nadir. At two points during the conical scan, a calibration source is observed in stead of the earth. On the surface, a forward and a nadir swath remain, which scan the same region on earth at different times and with different path lengths. The spatial resolution varies along the swath but is typically 1km$\times$1km.

Data products During the GOME validation campaign, RAL (via RSAC) supllied GBT-TVLXC products from ATSR2. "GBT" stands for Gridded Brightness Temperature, "TV" indicates that information from both Visual and Thermal channels is included. "L" and "X" imply that Longitude and Latitude grids and a piXel offset grid are provided. Finally, "C" indicates the presence of a Cloud flagging product. In the Gridding process, points from several elliptical forward or nadir scans have been combined to form one rectangular image of 512$\times$512 pixels for forward or nadir.

Figure 10: Sample ATSR2 Image:950725

3.3 Derivation of cloud properties

3.3.1 Cloud cover

Although a Cloud flagging product is available from the GBT-TVLXC data files, it is not ideally suited for determination of cloud fraction, since the cloud-flagging algorithm is aimed at rejecting pixels for which Sea Surface Temperature retreival is expected to be unreliable. The cloud-flagging algorithm is therefore rather pessimistic and frequently even sets a cloud flag for a cloud-free pixel. However, the reflectances in the Visual channels provide an excellent alternative for identification of cloudy pixels. In our analysis, we found the 0.55μm channel to be the most reliable indicator. Clouded regions are characterised by high reflectances and steep gradients at the edges. The difference between the nadir and forward view of a ground scene also provides accurate information on cloudiness. This method will be discussed in the next paragraph.

3.3.2 Cloud-top height

ATSR2 provides a unique method to derive cloud-top height, using the different viewing geometries of the nadir and forward scans. Due to the large angle (52° at the centre of the scan) between the nadir and forward directions, cloud-top height information can be retrieved from a difference image (nadir − forward) with an altitude accuracy of better than 1 km under optimal conditions. Examples of difference images are shown in Figure 14 and in Figure 15, athough reflectance differences caused by clouds have been truncated in Figure 15.

These difference views are very suitable for the detection of clouds, but test retrievals have shown that cloud-top height retrieval is often more difficult, due to changes of the shape of the clouds during the ±2 minutes between forward and nadir scans.

3.3.3 Geolocation

In order to determine the effective cloud-cover fraction for a GOME ground pixel, it is necessary to combine data from the GOME Geolocation record with the geolocation information in the **L** product. In Figure 13 a detailed view of the overlap between GOME and ATSR2 pixels is depicted. The GOME Center and East pixels are fully included within the ATSR2 field of view. After implementation of co-adding, only the GOME Center pixels will remain in full overlap.

3.4 Description of data set

3.4.1 ATSR2

GBT-TVLXC products have been provided for the entire orbit #1322 (22 July 1995). Images over selected ground sites have been provided for other orbits as well, but were not yet used in this study, except for the sample images in this paper.

3.4.2 GOME

Orbit #1322 is the first orbit for which GOME level 2 products have been made available. Recently, it has been reprocessed with version **1.21** of the level 1→2 GOME Data Processing (GDP) algorithm, but this version and older versions of GDP products suffer from inaccuracies in geolocation which are due to the absence of a yaw steering mode correction. Specifically for this study, accurate geolocation information for orbit #1322 (GOME data file 50722102.lv2) has been calculated and made available by Christophe Caspar. The uncorrected and corrected locations of pixel centres are plotted in Figure 11.

Figure 11: Yaw Steering Mode correction

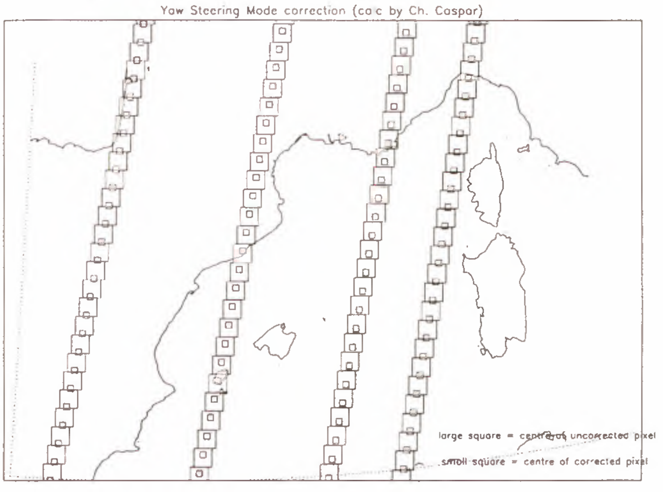

filled small squares = centres of pixels used in this study

3.5 Comparison of cloud cover fractions from ATSR2 and ICFA

Since this project is still in its early stages, only a dozen comparisons have been made thus far. Figure 12 shows, for each of these 12 GOME pixels, all ATSR pixels that are inside the boundaries of the GOME field of view. Although limited in number, this data set does cover a large range in reflectances. ATSR2 derived cloud fractions range from 0.0 to 1.0, and pixels fully over land are complemented with pixels partially over sea, and a pixel fully over sea.

Since the surface albedo is not optimally accounted for in the GDP 1.21 ICFA Algorithm, variations in surface albedo are expected to cause errors in the cloud-cover fraction For the East pixels, the variation of the ICFA values indeed appears to mimic the variation in surface albedo, in agreement with this prediction. For these cloud-free pixels, ICFA CCF is slightly greater for the two pixels over land, compared to the pixels that are partially and fully over sea.

The ICFA CCFs of the center pixels display the same lack of dynamic behaviour which is evident from a comparison with Meteosat by Robert Koelemijer which does have statistical significance. Although ATSR2 derived CCFs range from 0.3 to 1.0 for the 12 pixels that we studied, ICFA CCFs remain within the range 0.2 to 0.4.

In further stages of this study, the errors in cloud-cover fraction will be combined with information on cloud-top height, to determine the resulting error in GOME's Ghost Vertical Columns.

Figure 12: ATSR pixels within GOME pixel boundaries

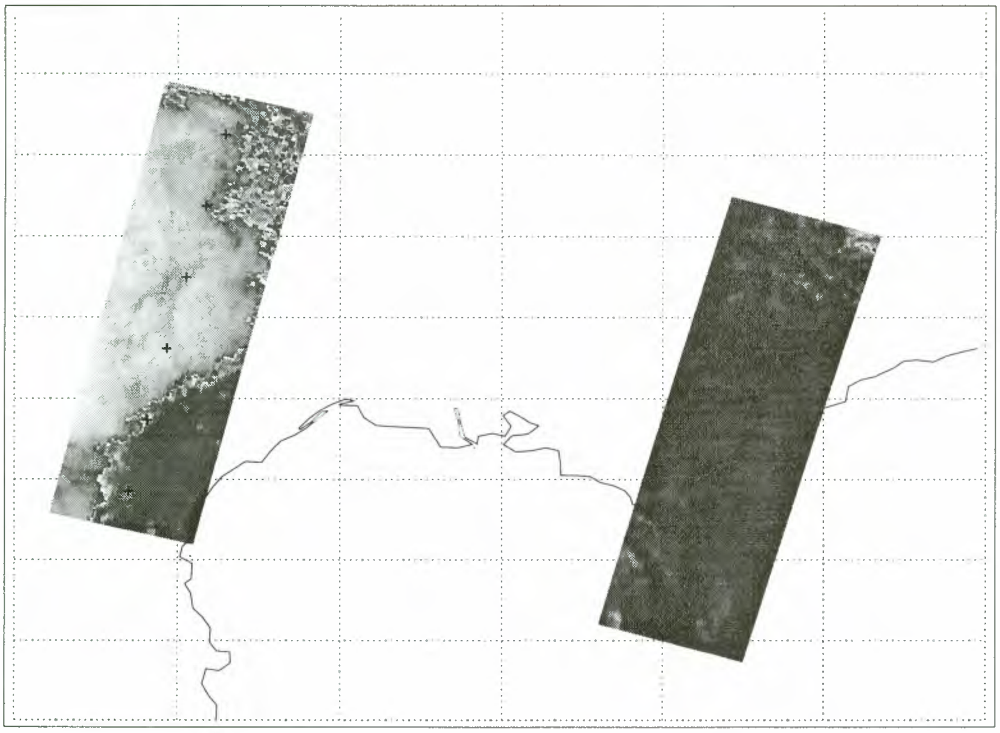

Table 7: Comparison of cloud-cover fractions from ICFA and ATSR2 for 12 GOME pixels from Figure 12

Center		East	
ICFA	ATSR2	ICFA	ATSR2
0.3	0.8	0.2	0.0
0.3	0.8	0.2	0.0
0.3	1.0	0.1	0.0
0.3	0.9	0.1	0.0
0.4	0.4	0.1	0.0
0.2	0.3	0.0	0.0

3.6 Future work: Aliasing of spatial variability

The differences in the fields of view of individual detector pixels caused by serial readout of the diode arrays adversely affect the quality of GOME spectra. In Figure 13, the fields of view of the longest-wavelength and the shortest-wavelength pixel of each channel are shown for pixel types 0 to 3. The field of view of the shortest-wavelength pixel (dark rectangle) corresponds with the geolocation as provided in the GOME DOAS data records. Inhomogeneities in the difference regions will affect only part of the specra in each channel, hence spatial variability is aliased into spectral variability. The spatial resolution of an ATSR pixel corresponds to the difference in field of view between detector diodes which are about 50 positions apart in the diode array (or 13 for the back-scan pixel). This implies that it is only possible to relate medium to broad-band features to inhomogeneities in the difference region, using ATSR2.

In addition, deviations in DOAS products caused by the differences between the fields of view of the detector pixels used by the DOAS algorithm and those used by the ICFA Algorithm (O_2 A-band) will be investigated.

3.7 Conclusions

Although our study has not yet reached a stage where statistically significant conclusions can be drawn, it is promising that the first results are in agreement with independent, statistically significant comparisons of ICFA with Meteosat. ATSR2 promises to be valuable for several aspects of the validation of GOME.

Figure 13:

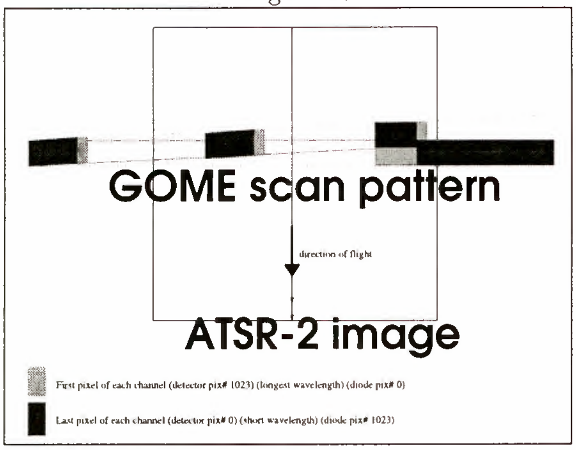

Acknowledgements

We wish to acknowledge the GOME Validation teams at BISA, KMI, KNMI and NILU for providing Brewer and Dobson data, to DLR and ESA for providing GOME data, and to RAL and RSAC for providing ATSR-2 data.

Figure 14: Difference image (2D)

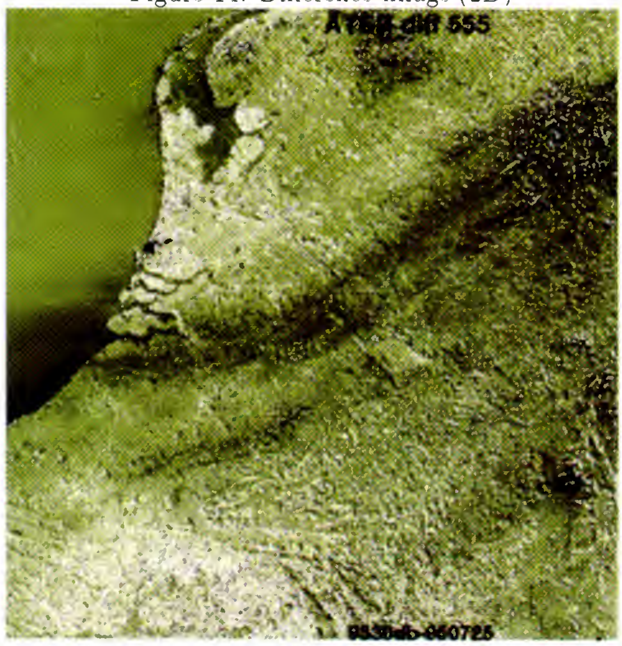

Figure 15: Difference image (3D)

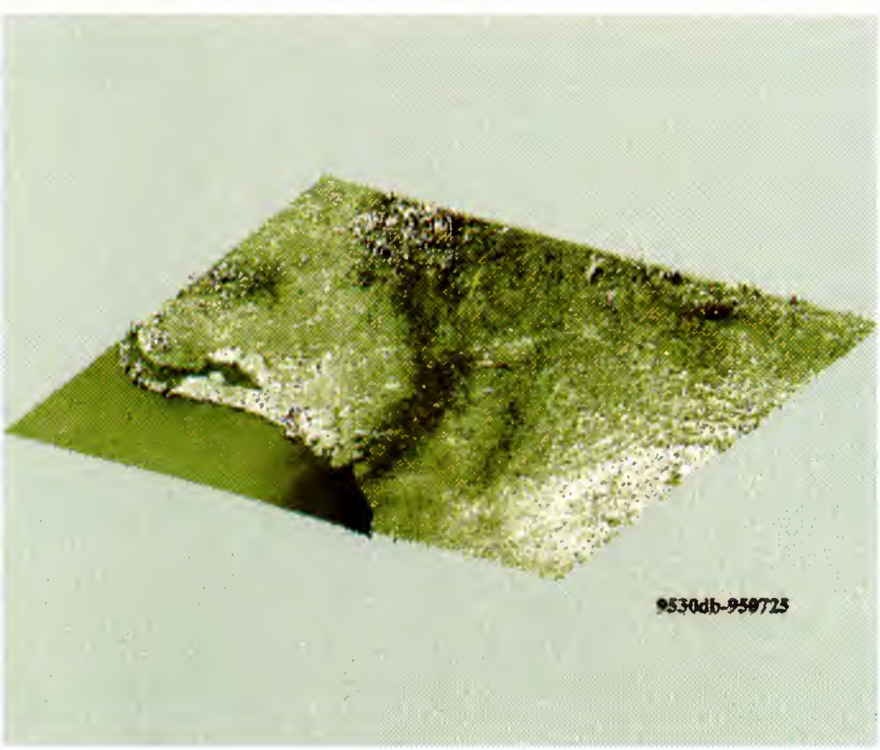

First validation of GOME cloud observations

R.B.A. Koelemeijer, P. Stammes, A.J. Feijt and A.C.A.P. van Lammeren

Royal Netherlands Meteorological Institute (KNMI)
P.O. Box 201, 3730 AE De Bilt, The Netherlands

Abstract

As a part of the ERS-2 GOME total ozone column retrieval algorithm, the Initial Cloud Fitting Algorithm (ICFA) [1] is used to account for the presence of clouds. Using ICFA, a cloud fraction is derived for each GOME pixel. This value has been compared with the cloud fraction derived from Meteosat data and ground-based lidar ceilometer measurements.

A good qualitative correlation between cloud fraction derived from ICFA, Meteosat and ground-based lidar measurements is found. However, the ICFA cloud fraction shows less variation than that derived from Meteosat and ground-based measurements. First results show that in case of *high* cloud fractions, ICFA *underestimates* the cloud fraction compared with Meteosat and ground-based measurements, especially for low clouds. In case of *low* cloud fractions over land surfaces, ICFA *overestimates* the cloud fraction. The underestimation for high cloud fraction is probably due to an underestimation of the cloud top pressure. The overestimation for low cloud fraction over land may be caused by an underestimation of the surface albedo.

It is shown that the PMD (Polarisation Measurement Device) measurements contain valuable information about cloud presence and structure. The use of the PMD cloud information could probably improve ICFA.

1. Introduction

The Global Ozone Monitoring Experiment (GOME), launched on board of the ERS-2 in April 1995, is a spectrometer measuring the terrestrial reflectivity in the UV and visible with a spectral resolution of 0.2–0.4 nm. The spatial resolution of the GOME measurements can be switched between 40×40 km^2 and 40×320 km^2. The GOME measurements contain much information on e.g. trace gas and aerosol amounts. For accurate retrievals of trace gas and aerosol amounts from GOME measurements, the retrieval algorithms must account for the presence of clouds. Cloud detection is especially important if a large part of the atmospheric constituents of interest resides in the troposphere.

The emphasis of the GOME level 1 to 2 processing so far has been on the generation of the ozone vertical column amount. In the retrieval algorithm, the measured radiances are fitted using the Differential Optical Absorption Spectroscopy (DOAS) technique [1] to yield an ozone slant column. The vertical column is derived by dividing the slant column by the appropriate airmass factor (AMF). Since the airmass factor, which represents the effective atmospheric pathlength of photons, is influenced by the presence of clouds, cloud information is a necessary input for the AMF calculations. Another effect of clouds is their screening of tropospheric ozone, which would result in an underestimation of the total column if no correction were applied. To correct for these two effects of clouds, the Initial Cloud Fitting Algorithm (ICFA) has been incorporated into the ozone retrieval algorithm.

In this study, the cloud fractional coverage, or cloud fraction, derived using ICFA has been compared with that derived from Meteosat images and from ground-based lidar ceilometer measurements (Sect. 2). In Section 3, the potential of using the PMD (Polarisation Measurement Device) measurements for cloud detection has been investigated.

2. Validation of ICFA

2.1 Initial Cloud Fitting Algorithm

The diode-array detectors of GOME measure the solar irradiance and terrestrial reflected radiance with a high spectral resolution of 0.2–0.4 nm between 240 and 790 nm. From these measurements, the reflectivity, which is defined as $\pi \times$ the reflected radiance divided by the incident solar irradiance at the top of the atmosphere, is obtained with a high degree of accuracy.

In order to derive the cloud fraction from GOME measurements, ICFA makes use of the reflectivity around the O_2 A absorption band, which is centered at about 761 nm. As an example, GOME measurements of nadir reflectivity around the O_2 A-band are shown in Fig. 1. The measurements have been performed at July 23 1995, over a cloudy scene above the Atlantic Ocean (latitude: 53.1° N, longitude: 34.1° W, solar zenith angle: 34°). The characteristic shape of the O_2 A-band is clearly visible. At wavelengths in the continuum, for which absorption is negligible, the reflectivity is high and nearly wavelength independent. Inside the O_2 A-band, the reflectivity is much lower, especially in the centre of the band near 761 nm. The shape depends on the effective pathlength of light through the atmosphere, which depends mainly on cloud top pressure, cloud fraction, cloud optical thickness, surface pressure, solar zenith angle, viewing geometry and to a lesser extent on cloud bi-directional reflectivity and surface albedo [2], [3]. Since it is not possible to retrieve all these quantities simultaneously, various assumptions are made. In the first operational version of ICFA, clouds are regarded as bi-directional reflecting surfaces; enhanced absorption by multiple scattering inside clouds is neglected. Their reflectivity is assumed to be given by asymptotic relations for optically thick clouds, with a fixed optical thickness. Consequently, the cloud top reflectivity is prescribed. For the cloud top pressure, ground pressure and surface albedo, parameterisations and climatological databases are used. Based on these assumptions, radiative transfer calculations are performed for clear and completely cloudy situations. The cloud fraction is derived using least-squares fitting of the measured radiances with calculated radiances around the O_2 A-band.

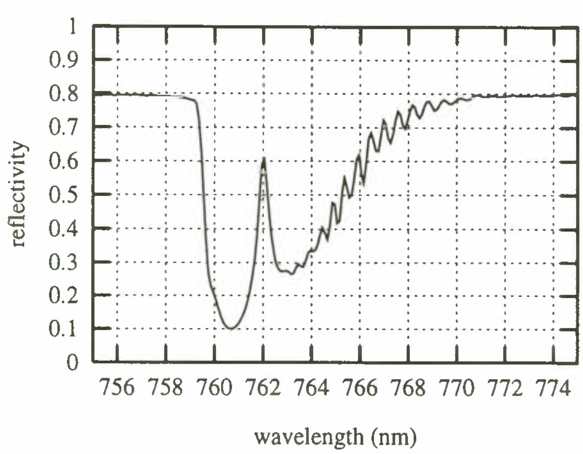

Figure 1: GOME reflectivity measurements between 755–775 nm, including the O_2 A absorption band. Data acquired at July 23 1995, over a cloudy scene above the Atlantic Ocean (latitude: 53.1° N, longitude: 34.1° W, solar zenith angle: 34°).

2.2 Cloud fraction from Meteosat

Meteosat data over NW-Europe have been archived at KNMI since January 1993. Meteosat has a high temporal resolution (measurements each half hour) and a moderate spatial resolution (9×5 km^2 for the Netherlands and surroundings) which makes it suitable for validation of ICFA cloud fraction.

Cloud fraction is derived from Meteosat data in two steps. The first step involves cloud detection; each pixel is flagged cloud-free or cloudy. The cloud detection algorithm makes use of the temporal variability of clouds and uses weather forecast model analysis to improve thresholds [4]. The cloud fraction of the cloud-free pixels equals zero. The second step is to determine the cloud fraction of the cloudy pixels. In this study, a simple linear relationship between reflectivity and cloud fraction, C, is assumed:

$$C = \frac{R - R_s}{R_c - R_s}, \tag{1}$$

in which R is the measured reflectivity, R_s is the surface reflectivity and R_c is the cloud top reflectivity. The values for R_s and R_c have been chosen em-

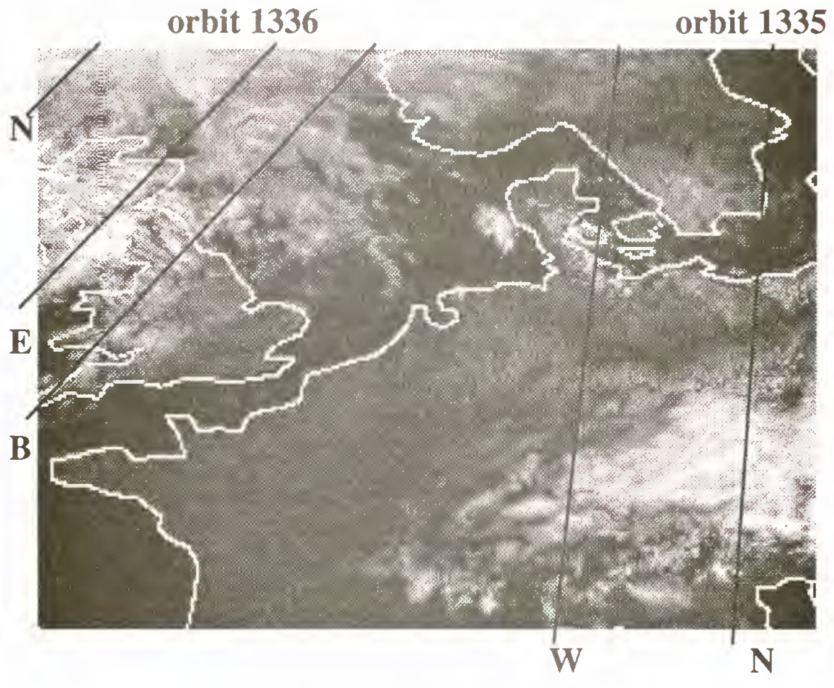

Figure 2: Meteosat visible image of NW-Europe at July 23 1995, 10:00 UT. The image is corrected for the variation of insolation. The black lines connect the centres of the different GOME pixels (East (E), Nadir(N), West(W) and Backscan(B)).

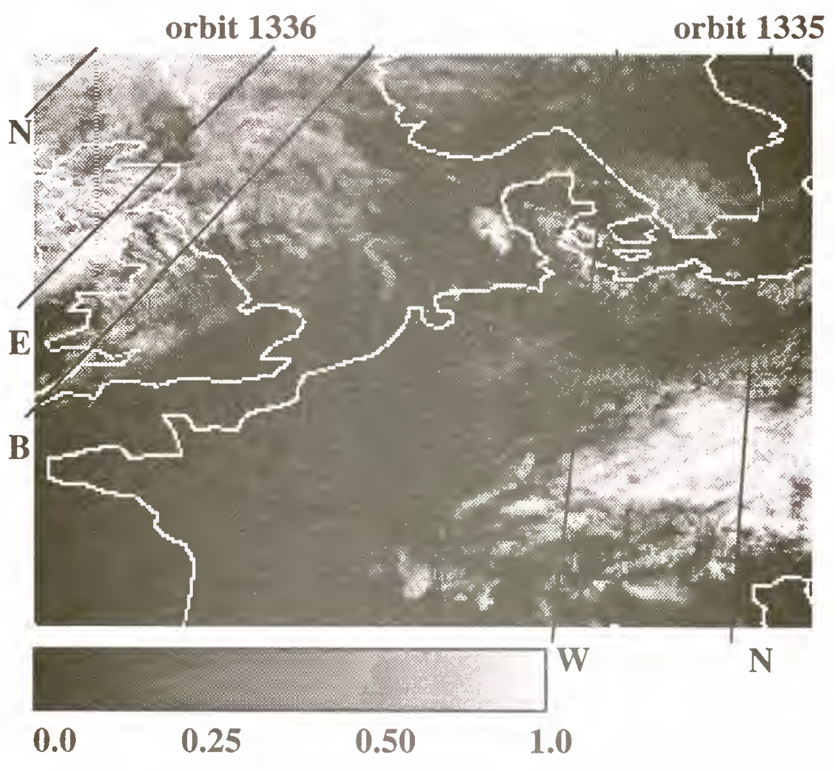

Figure 3: Grey scale plot of the cloud fraction derived from Meteosat data. Date: July 23 1995, 10:00 UT

pirically by selecting large cloud-free and completely cloudy areas. For land and sea surfaces different values for R_s have been taken. By assuming a linear relationship between reflectivity and cloud fraction, errors in cloud fraction arise in case of optically thin clouds. The cloud fraction can be interpreted as an effective cloud fraction for optically thick clouds. In this interpretation, the error in C, which is mainly due to the uncertainty in the cloud top reflectivity, is estimated to be ± 0.07.

2.3 Comparison of ICFA with Meteosat

Two GOME overpasses of July 23 1995 over NW-Europe have been analysed: orbit 1335, time of overpass about 10:10 UT, and orbit 1336, time of overpass about 11:50 UT. The time difference between the GOME overpass and the acquisition of the Meteosat data was about 10 minutes for both overpasses.

The Meteosat visible image of 10:00 UT is shown in Fig. 2. Large cloud systems can be identified over the central part of Europe and over the North Sea and the UK. The image has been corrected for the variation of insolation. In Fig. 3, the derived cloud fraction is depicted in gray scale.

GOME has four pixel-types, 'East', 'Nadir', 'West' and 'Backscan', with approximate sizes during the first period of operation, which is considered here, of 40×80 km^2 for the East, Nadir and West pixels, and 40×240 km^2 for the Backscan pixels. The centres of the GOME pixels which fell inside the Meteosat image have been connected by black lines. The orbit-numbers and pixel-types have been indicated as well. In order to compare the Meteosat cloud fraction with the ICFA cloud fraction, the Meteosat cloud fraction has been averaged to the spatial resolution of the corresponding GOME pixel. Figure 4 shows both the ICFA cloud fraction and Meteosat cloud fraction for the West and Nadir pixels of orbit 1335. For comparison, the Meteosat cloud fraction is plotted at the left of the ICFA cloud fraction. Apparently, there is a good qualitative correlation between the ICFA cloud fraction and the Meteosat cloud fraction. However, the ICFA cloud fraction shows less variation than the Meteosat cloud fraction, especially over land surfaces. In Fig. 5, the ICFA cloud fraction of orbit 1335 is shown versus the Meteosat cloud fraction. It is clear that for *high* cloud fraction, ICFA *underestimates* the cloud fraction, up to 100 %. In case of *low* cloud fraction, ICFA *overestimates* the cloud fraction.

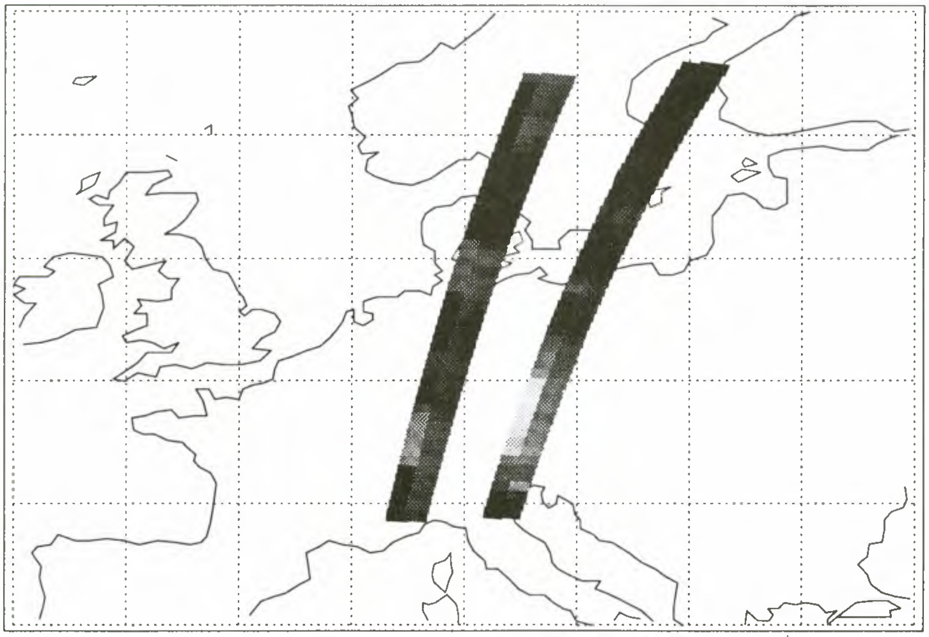

Figure 4: Cloud fraction from Meteosat (left) and ICFA (right) for the West and Nadir pixels of orbit 1335. The cloud fraction from Meteosat is averaged over a GOME pixel of 40×80 km^2.

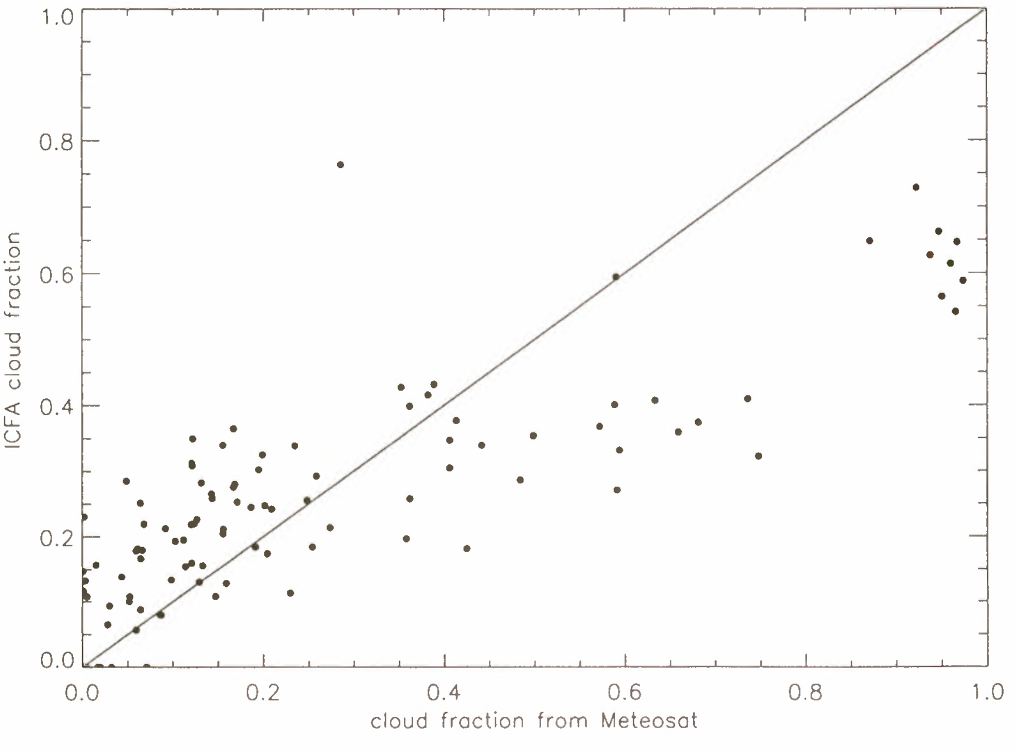

Figure 5: Correlation between ICFA cloud fraction and the cloud fraction derived from Meteosat data. Data acquired at July 23 1995, orbit 1335, 10:09 - 10:14 UT.

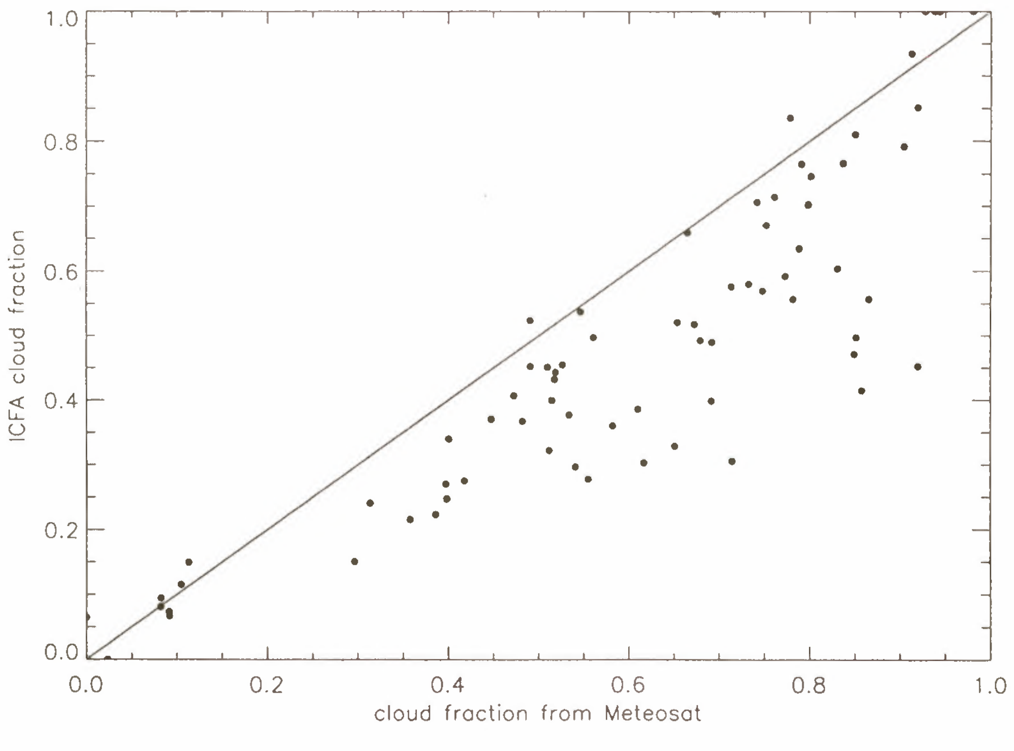

Figure 6: Same as 5, but for orbit 1336, 11:49 - 11:53 UT.

For orbit 1336, shown in Fig. 6, a better correlation between ICFA and Meteosat cloud fraction is found. The overestimation for low cloud fraction is not found in this case.

The underestimation for high cloud fraction is probably due to an underestimation of the cloud top pressure. In ICFA, the assumed cloud top pressure is about 500 hPa for the mid-latitudes, which is very low for most cases. An underestimation of cloud top pressure (= overestimation of cloud top height) leads to an underestimation of the cloud fraction. This is caused by the fact that the amount of oxygen screened by the clouds is the same for high clouds with low cloud fraction as for low clouds with high cloud fraction, and hence give the same depth of the oxygen A-band. The actual cloud top height, as estimated from the Meteosat IR images, appeared to be higher in orbit 1336 (cloud system over the North Sea and the UK) than in orbit 1335 (cloud system over the central part of Europe). If the actual cloud top height is closer to the assumed value, the error in the cloud fraction is smaller. The overestimation for low cloud fraction is especially found over land surfaces. This overestimation might be due to an underestimation of the surface albedo over land.

2.4 Comparison of ICFA with lidar measurements

At the meteorological site of Cabauw, located in the central part of the Netherlands (51.97° N, 4.93° E), lidar ceilometer measurements are performed on a routine basis. The lidar ceilometer is limited to a height of 4 km. From those measurements, cloud base height and cloud fraction have been derived. The spatial resolution of the lidar measurements due to cloud motion is much higher than that of the GOME measurements. In order to match the horizontal scale of GOME, the lidar measurements have been averaged over one hour around the GOME overpass.

In Table 1, the cloud fraction derived from the Cabauw measurements and ICFA is shown. The approximate distance between the Cabauw site and the centre of the nearest GOME pixel is given in the fourth column. In the fifth column, the cloud base height of the lowest cloud layer as measured by the ceilometer is given. In Fig. 7, the ICFA cloud fraction is plotted against the cloud fraction derived from the Cabauw measurements. Although caution should be used regarding the small number of overpasses considered here, the ground-based measurements seem to confirm that ICFA underestimates the cloud fraction for high cloud fractions. The overestimation for small cloud fractions can not be confirmed, because of the height limitation of the lidar: if the lidar does not detect any clouds, clouds may be absent, or present above 4 km height.

Table 1: Cloud fraction (CF) derived from the lidar measurements at the meteorological site of Cabauw and the ICFA cloud fraction. Fourth column: approximate distance between the Cabauw site and the centre of the nearest GOME pixel. Fifth column: cloud base height (CBH) of lowest cloud layer.

Day	CF Cabauw	CF ICFA	distance [km]	CBH [km]
Jul 22 1995	0.64	0.28	>100	1.0–1.6
Jul 25 1995	0.00	0.14	10	–
Aug 29 1995	0.75	0.47	10	0.8–2.5
Sep 17 1995	0.38	0.18	70	0.6–0.8
Oct 3 1995	1.00	0.45	10	0.4–0.5

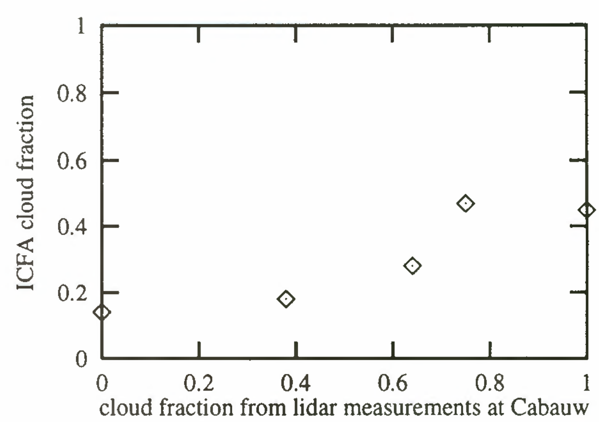

Figure 7: Correlation between ICFA cloud fraction and the cloud fraction derived from the ground-based lidar measurements at the meteorological site of Cabauw. The data are tabulated in Table 1.

3. Imaging of clouds with PMDs

To correct the GOME spectral reflectivity measurements for the polarisation sensitivity of the array detectors, Polarisation Measurement Devices (PMDs) have been added to the GOME instrument. The PMDs measure the solar irradiance and the terrestrial reflected radiance in three broad spectral bands, with effective wavelengths of 350, 490 and 700 nm for respectively PMDs 1, 2 and 3. The spatial resolution of the PMDs is 20 × 40 km^2 for a GOME swath width of 960 km, amounting to 48 PMD-pixels over the full swath. Evidently, the spatial resolution of the PMDs is much better than that of the array detectors. The polarisation sensitivity of the PMDs differs from that of the array detectors. By combining the PMD measurements and the measurements of the array detectors, the polarisation is obtained at three wavelengths for each GOME array detector groundpixel.

The PMD signal values which are supplied in the GOME extracted level 1 product, denoted by R_{PMD}, represent the ratio between the reflected radiance, I_{PMD}, and the direct solar irradiance perpendicular to the direction of propagation ($\pi F_{\odot}$). In formula:

$$R_{PMD} = \frac{I_{PMD}}{\pi F_{\odot}}. \qquad (2)$$

If polarisation correction is applied, I_{PMD} is corrected using the average polarisation of the array detector groundpixel.

Because of the better spatial resolution, the PMDs are useful for cloud detection and imaging. To illustrate this, PMD measurements of July 23 1995, orbits 1334 – 1338, over Europe, Africa and the Atlantic Ocean are shown in Fig. 8. The image is a colour composition of PMD 1, 2 and 3 measurements. The PMDs of the backscan pixels have not been used. In Fig. 9 a detail of this image is depicted, showing good correlation with the Meteosat visible image (Fig. 2). Obviously, the PMDs contain much information about cloud presence, cloud structures and surface type. The cloud information in the PMDs is presently not used in ICFA. ICFA could probably be improved by first using the PMD measurements for the estimation of cloud fraction and then using the radiances around the O_2 A-band for the retrieval of cloud top height. This method would not suffer from large errors due to climatological estimates of cloud fraction or cloud top height.

4. Discussion and conclusions

The ICFA cloud fraction has been compared with the cloud fraction derived from Meteosat images and ground-based lidar measurements. A good qualitative correlation between the cloud fraction derived from ICFA, Meteosat and the lidar measurements has been found. However, ICFA shows less variation in cloud fraction than Meteosat and ground-based measurements. First results show that for *high* cloud fractions, ICFA *underestimates* the cloud fraction compared with Meteosat and ground-based measurements, especially for low clouds. The underestimation of the cloud fraction is probably caused by the overestimation of the cloud top height. In case of *low* cloud fractions over land, ICFA *overestimates* the cloud fraction, which might be due to an underestimation of the surface albedo.

The error in the ICFA cloud fraction leads to errors in the ozone vertical column in two ways. In the first place, the error in the ICFA cloud fraction leads to errors in the airmass factor (AMF). In the operational ozone vertical column retrieval algorithm, the AMF of a partly cloudy scene is computed by computing the AMF for a cloud-free and a completely cloudy situation. Linear combination with the cloud fraction as weighting function yields the AMF of the partly cloudy scene. To estimate the error in the AMF introduced by a 100% underestimation of the cloud fraction, test calculations have been performed with the Doubling-Adding KNMI (DAK) radiative transfer model [5]. From these calculations, it is concluded that the AMF is underestimated by 2–3% for a 100% underestimation of the cloud fraction. Consequently, the total ozone vertical column is overestimated by 2–3%. In the second place, the error in the ICFA cloud fraction leads to errors in the estimated amount of ozone screened by clouds (the so-called ghost vertical column). However, the error in the

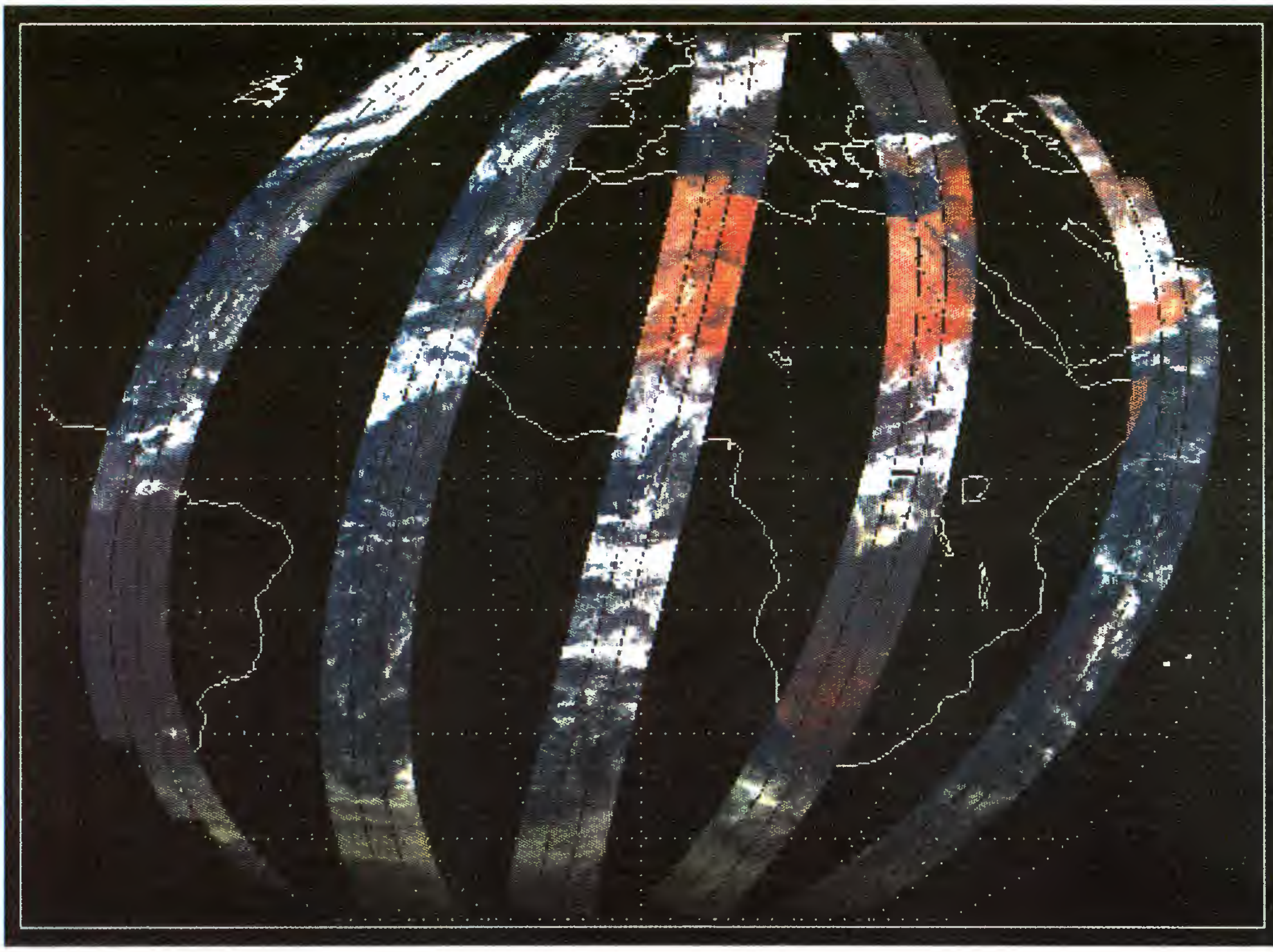

Figure 8: Colour composite of PMD 1, 2 and 3 measurements of July 23 1995, orbits 1334 – 1338. The PMD measurements provide valuable information on cloud presence, cloud structure and scene type.

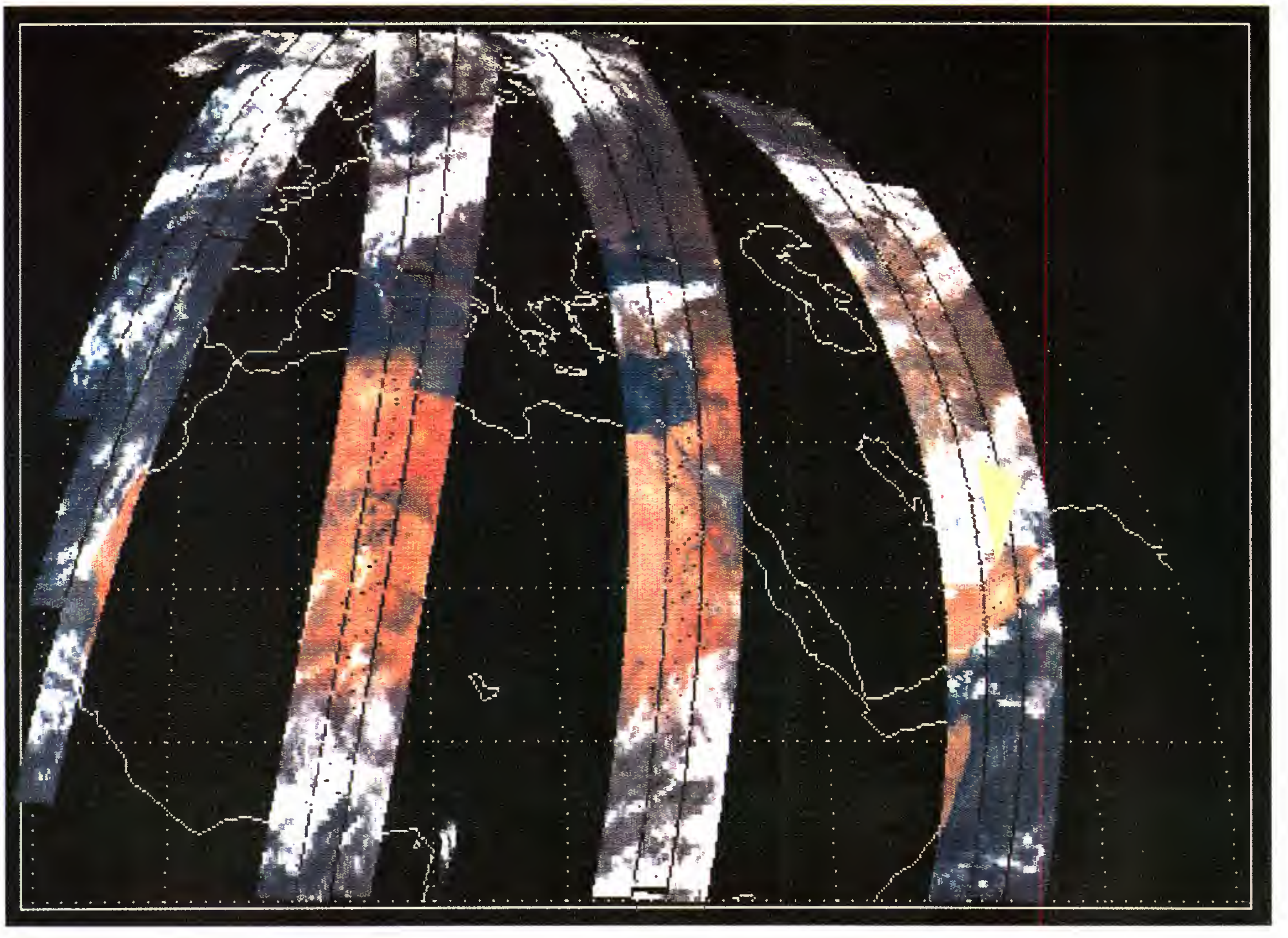

Figure 9: Detail of Fig. 8. A good correlation is found with the Meteosat visible image of Fig. 2.

ghost vertical column due to the underestimation of the cloud fraction may be largely compensated by the overestimation of the cloud top height.

It has been shown that the PMD measurements contain valuable information about cloud presence and cloud structure. This information is presently not used in ICFA. In ICFA, it is problematic to discriminate between cases of high clouds with small cloud fraction and cases of low clouds with high cloud fraction. In the current algorithm, the cloud fraction is derived assuming that the cloud top height is known in advance. ICFA could probably be improved by first using the PMD measurements for the estimation of cloud fraction and then using the radiances in the O_2 A-band for the retrieval of cloud top height.

Acknowledgements

This study was performed within the framework of the GOME validation project NL-114 of which Hans van der Woerd (National Institute of Public Health and Environmental Protection (RIVM)) was the coordinator. The GOME data were kindly provided by the European Space Agency (ESA), and processed by the Deutsche Forschungsanstalt für Luft- und Raumfahrt (DLR). The Space Research Organisation of the Netherlands (SRON) is acknowledged for the financial support of part of this work.

References

[1] Spurr, R. 1994: "GOME level 1 to 2 algorithms description", Technical Note ER-TN-DLR-GO-0025, Iss./Rev. 1/A, DLR, Oberpfaffenhofen.

[2] Fischer, J. and Grassl, H. 1991: "Detection of cloud top height from backscattered radiances within the oxygen A band. Part 1: theoretical study", J. Appl. Met., Vol. 30, pp. 1245–1259

[3] Kuze, A. and Chance, K.V. 1994: "Analysis of cloud top height and cloud coverage from satellites using the O_2 A and B bands", J. Geophys. Res., Vol. 99, No. D7, pp. 14481–14491

[4] Feijt, A.J. and van Lammeren, A.C.A.P. 1996: "Ground based and satellite observations of cloud fields in the Netherlands", Mon. Wea. Rev. (accepted)

[5] Stammes, P. 1994: "Errors in UV reflectivity and albedo calculations due to neglecting polarisation", in: Proceedings of the European Symposium on Satellite Remote Sensing, 26–30 September, 1994, Rome. EOS/SPIE volume 2311, 227–235

CO-ORDINATED GROUND-BASED OBSERVATIONS AT ARRIVAL HEIGHTS, ANTARCTICA, DURING GOME VALIDATION

G.E. Bodeker, W.A. Matthews, K. Kreher and S.E. Nichol
National Institute of Water & Atmospheric Research, Lauder, Central Otago, New Zealand

Abstract
Measurements of several atmospheric trace constituents, important for evaluating ozone depletion, were made at three sites during the Global Ozone Monitoring Experiment (GOME) validation campaign from 20 July to 31 December 1995. Instrumentation was operated at Lauder (45.04°S, 169.68°E), Campbell Island (52.55°S, 169.15°E) and Arrival Heights, Antarctica (77.83°S, 166.65°E). Of these three sites, GOME data were available only for Arrival Heights. Since the most severe ozone depletion during the past 15 years has been observed over the Antarctic, it is vital that validation of the GOME total column ozone data product is performed in this region. Measurements made by NIWA Lauder at Arrival Heights are therefore expected to provide a valuable data series against which GOME measurements may be validated. Furthermore the longer term series at this site gives an indication of the expected shorter term variations as well as the seasonal trends.

This paper presents comparisons of ground-based measurements of vertical columns of ozone and NO_2 with GOME data products at Arrival Heights. Total column ozone measurements were made using a Dobson spectrophotometer (no.17), while NO_2 measurements were made using a UV-visible absorption spectrometer. The results indicate that GOME is able to adequately measure the concentrations of both of these constituents over the Antarctic during the time period of the validation. Differences between ground-based and satellite derived data may result partially from spatial and temporal differences in the measurements.

1. INTRODUCTION

The general scientific objectives of the Global Ozone Monitoring Experiment (GOME) are:

1. To improve understanding of the processes controlling global bio-geochemical cycles in the troposphere and stratosphere.
2. To monitor natural and anthropogenic changes in the composition of the atmosphere, e.g. ozone.

Recent extratropical ozone depletion and the concomitant increase in surface ultraviolet (UV) radiation may be expected to adversely influence the biosphere. The largest decrease in total column ozone since the early 1980s has been observed over the Antarctic. If GOME is expected to play a major role in assessing the spatial and temporal characteristics of this depletion it is vital that the measurements are accurately validated over the Antarctic and mid-latitudes of the Southern Hemisphere. To this end, measurements at three sites were made by NIWA Lauder during the period of the GOME validation from 20 July 1995 to 31 December 1995.

<u>Lauder, New Zealand (45.04°S, 169.68°E)</u>

Measurements made at Lauder through 1995 include:

Measured parameter	Technique/instrument
Column ozone	UV-vis spectrometer
	Dobson no. 72
Column NO_2	UV-vis spectrometer
Column HNO_3	FTIR
Vertical ozone profiles	Ozonesonde
	RIVM ozone lidar
Vertical temperature profiles	Radiosondes
	RIVM lidar

GOME data were not available for Lauder through 1995.

<u>Campbell Island (52.55°S, 169.15°E)</u>

Measurements made at Campbell Island through 1995 include:

Measured parameter	Technique/instrument
Column ozone	UV-vis spectrometer
Column NO_2	UV-vis spectrometer

GOME data were not available for Campbell Island through 1995.

<u>Arrival Heights , Antarctica (77.83°S, 166.65°E)</u>

Measurements made at Arrival Heights through 1995 include:

Measured parameter	Technique/instrument
Column ozone	UV-vis spectrometer
	Dobson
Column NO_2	UV-vis spectrometer
	Diode array spectrometer
Column OClO	Diode array spectrometer
Column BrO	Diode array spectrometer
Column HNO_3	Bomem FTIR
Column HCl	Bomem FTIR

Measurements of column ozone and column NO_2 are part of a long-term measurement program which began in 1982 with the NO_2 spectrometer and 1988 with the Dobson spectrophotometer. GOME data were available for Arrival Heights through 1995. Comparisons of total column ozone (measured by Dobson no.17) and vertical columns of NO_2 (measured by the UV-visible absorption spectrometer) with GOME products are presented in this paper.

2. MEASUREMENT TECHNIQUES

Measurements of total column ozone were made at Arrival Heights using Dobson spectrometer no.17 from 18 September to 7 December 1995. It was then removed from the Antarctic for calibration. Direct sun observations using the AD wavelength pair were employed for the data retrieval. Dobson no.17 was referenced to the world standard Dobson (no.83) in May 1985 and to the WMO Regional RA V standard Dobson (no.105) in January 1991 and January 1996. The Regional standard has maintained its calibration with respect to the world standard Dobson to better than 1% from March 1977 to June 1992 (4 referencings). A thorough review of the Dobson spectrophotometer and its accuracy is given by *Basher* [1984]. Measurement uncertainties are estimated at 2% relative uncertainty plus 1% to 2% absolute uncertainty associated with any new standard absorption coefficients.

Measurements of slant column NO_2 were made at Arrival Heights using a ground-based UV-visible absorption spectrometer. The technique uses the distinct absorption features of NO_2 which are present in sunlight scattered from the zenith sky. Absorption spectra, between 432.0 and 484.0nm, are measured continuously between 80° and 95° solar zenith angle (SZA), typically in 1° steps, and at 15 minute intervals between 12:00 and 14:00 each day. A wavelength interval of 432.8 to 483.4nm was chosen for the NO_2 slant column retrieval. To remove the large Fraunhofer absorption features present in sunlight, the twilight measured spectra are ratioed with a selected midday reference spectrum. The retrieval makes use of a non-linear least squares fitting technique that uses laboratory absorption cross-sections of NO_2, O_3, O_4 and water vapour and accounts for temperature changes, polarization and the Ring effect. Room temperature NO_2 absorption cross-sections were used in the data retrieval to remain consistent with the GOME NO_2 retrieval. Data retrieval with more realistic, low temperature NO_2 cross-sections (-46°C) results in approximately 15% lower NO_2 slant columns. The resultant NO_2 slant column retrieval errors are less than ≈10%. Further details on the operation, calibration and sources of error of the instrument are detailed in *Johnston and McKenzie* [1989] and *Keys and Gardiner* [1991].

3. TOTAL COLUMN OZONE AT ARRIVAL HEIGHTS

Total column ozone data were extracted from the GOME level 2 data product for orbits passing within 150km of Arrival Heights. The measurement made closest to Arrival Heights was extracted from each of these orbits and are shown together with the Dobson measurements in Figure 1. Labels on each GOME data point show the distance from Arrival Heights in km. Ground-based measurements, occurring within 6 hours of a GOME measurement, were compared with the total column ozone derived from GOME. The results are summarized in Table 1.

Day no. (GOME)	Day no. (Dob)	Difference (DU)	Separation (km)
260.8286	261.0625	40.1700	143.4590
278.8523	279.0313	15.5650	8.1980
303.8621	304.0833	0.7700	147.9170
304.8404	305.0417	-11.2610	24.4110
315.8087	316.0417	-22.2200	141.5690
315.8779	316.0417	-15.9500	47.7690
285.8385	286.0521	29.8970	84.0410
285.9077	286.0521	-23.1970	31.7080
276.8958	277.0000	37.1780	44.5620
284.7910	285.0000	35.1980	102.2760
284.8602	285.0000	37.6210	36.4980
302.8839	302.9583	-2.8440	15.4090
304.9097	305.0417	-8.1610	9.4670
286.8167	287.0208	54.5270	117.2240
279.8306	280.0625	18.3600	126.1050
279.8998	280.0625	26.6070	12.7910

Table 1: Differences between GOME and Dobson total column ozone measurements for GOME overpasses within 150km and 6 hours of the measurement at Arrival Heights.

4. TOTAL COLUMN NO_2 AT ARRIVAL HEIGHTS

NO_2 vertical column densities (VCDs) were extracted from GOME orbits passing within 150km of Arrival Heights. The measurement made closest to Arrival Heights was extracted from each of these orbits.

Slant column densities (SCDs) of NO_2, measured by the ground-based spectrometer were converted to VCDs by dividing them by the appropriate airmass factors (AMFs). The AMFs were calculated with the ray tracing model of *Frank and Platt* [1990], assuming a gaussian NO_2 profile shape of width 14km centered at a height of 28km. The model also requires the vertical pressure, temperature and ozone distribution as input. A set of representative pressure, temperature and ozone profiles, from a climatology, was selected for the measurement period.

Since NO_2 exhibits large diurnal variation in concentration, an attempt has been made to minimize the temporal differences between the two intercompared data sets as follows: The SZA at the latitude and longitude of GOME, at the Earth's surface, and at the time of the GOME measurement was calculated. The ground-based measurement of the NO_2 VCD for this SZA was then extracted through exponential interpolation between VCDs at a number of SZAs spanning the GOME SZA. The two NO_2 data sets are shown in Figure 2 together with the SZA at the GOME nadir point.

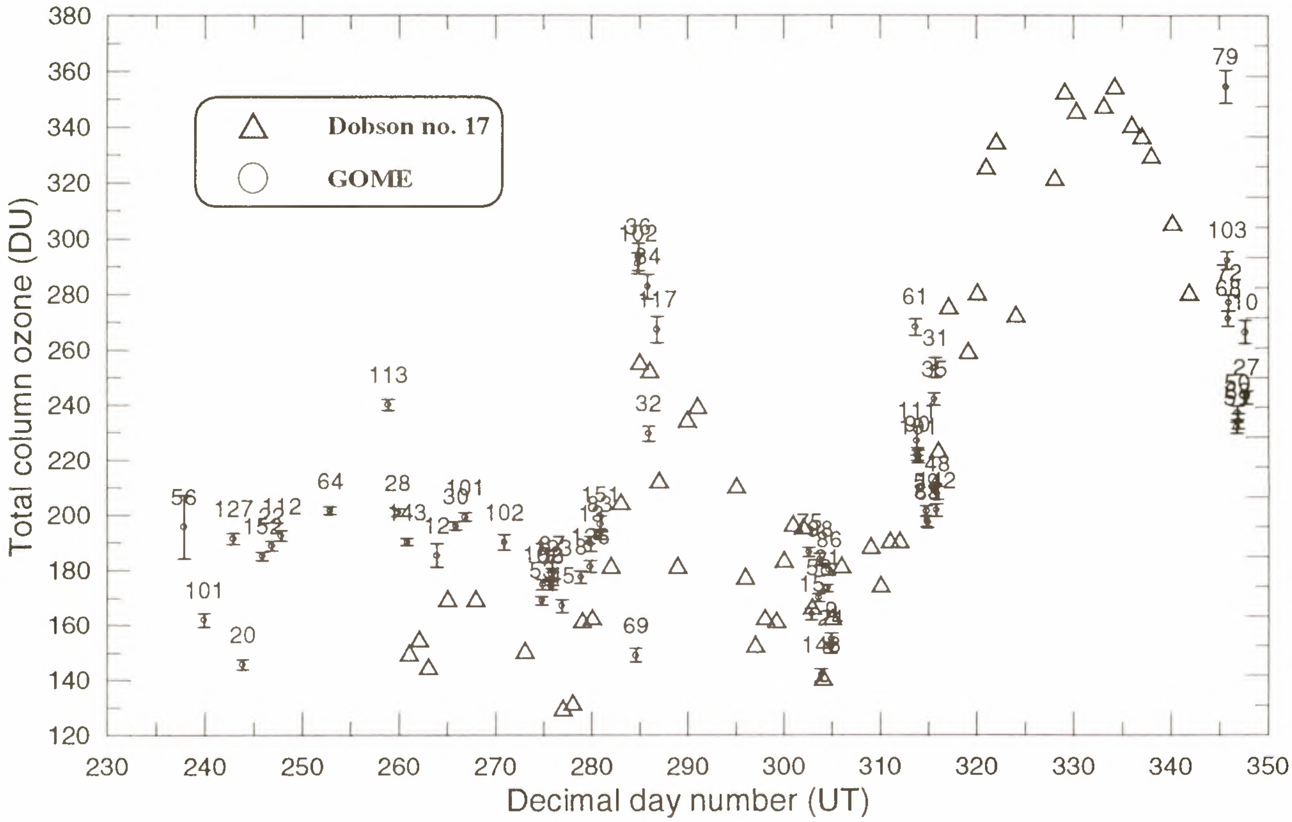

Figure 1: Total ozone at Arrival Heights (AH). The GOME measurement made closest to AH was extracted from orbits passing within 150km of AH. Labels on each GOME data point show distance from AH in km.

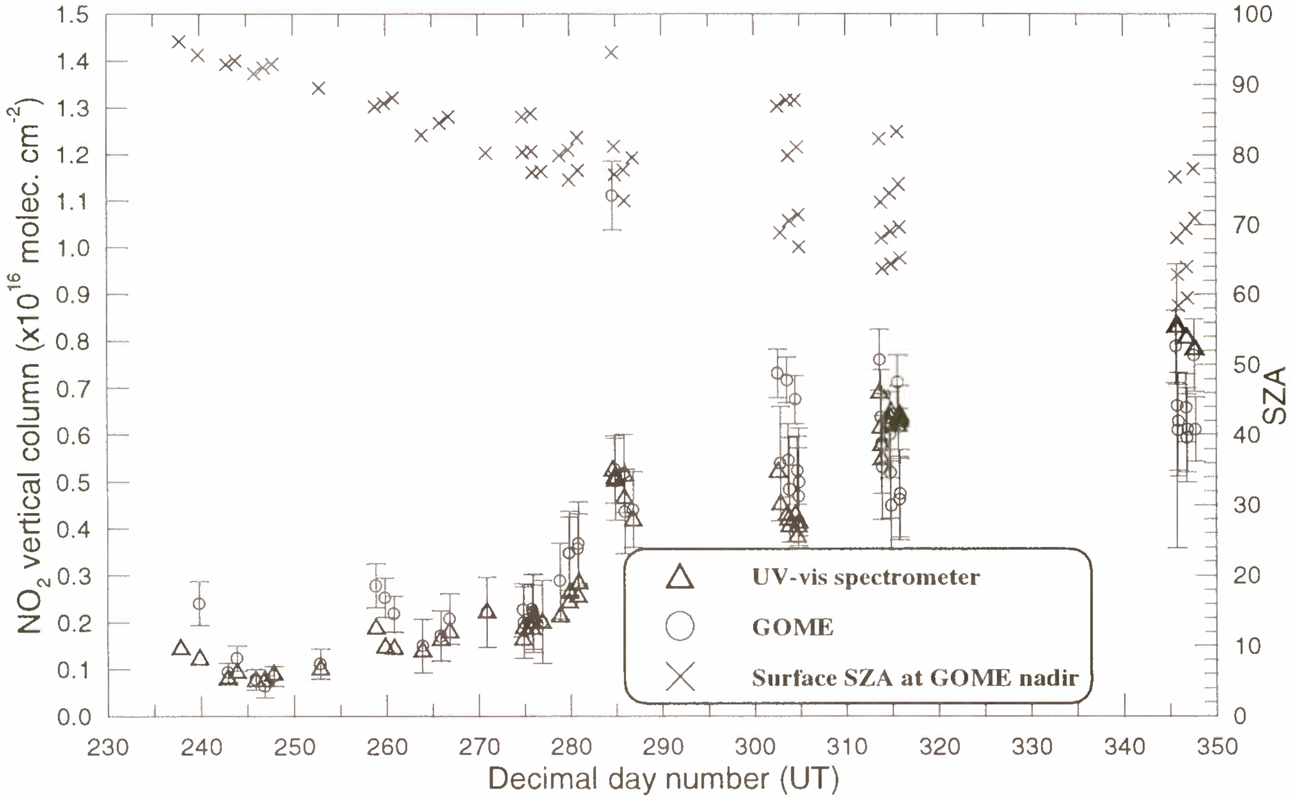

Figure 2: NO_2 at Arrival Heights (AH). The GOME NO_2 VCD measurement, from the second fit window, made closest to AH was extracted from orbits passing within 150km of AH. Ground-based vertical column measurements, made with a UV-vis spectrometer, are shown at GOME nadir SZA.

5. DISCUSSION

Even for small spatial separations, differences between GOME total column ozone and that measured by the ground-based Dobson spectrophotometer can be large, although temporal differences in a rapidly evolving Antarctic stratosphere may induce large differences e.g. at the time of the vortex breakup. Further investigation is required to determine whether there is a north/south or east/west bias in the GOME-Dobson differences. A steep meridional gradient in total column ozone at the vortex edge could result in large GOME-Dobson differences for a small spatial separation in the north-south direction.

Preliminary results suggest that GOME NO_2 VCDs are higher than those measured by the ground-based UV-visible absorption spectrometer. Although the closest GOME overpass to Arrival Heights was used for the GOME NO_2 data extraction, even co-located measurements would be expected to show small differences since the ground-based spectrometer samples a different air column when measuring the NO_2 SCD. This is further complicated by the fact that NO_2 exhibits large diurnal variation in concentration. The model used for the calculation of the airmass factors makes no attempt to account for SZA induced changes in the NO_2 concentration along the slant path. This may result in the UV-visible spectrometer slightly underestimating the NO_2 VCD. A more exact radiative transfer model is being developed which can account for this so-called "chemical enhancement". Finally the dependence of retrieved NO_2 on absorption cross-section temperatures needs to be investigated further.

OClO and BrO measurements at Arrival Heights are also available for this time period but have not been included here since there are no GOME data as yet against which they can be compared.

6. REFERENCES

Basher R.E. 1984. Review of the Dobson spectrophotometer and its accuracy, in *Atmospheric Ozone*, Proceedings of the Quadrennial Ozone Symposium held in Halkidiki, Greece, 3-7 September 1984, D. Reidel Publishing Company, pp. 387-391

Frank H. and U. Platt 1990. Advanced calculation procedures for the interpretation of skylight measurements, *Proceedings of the First European Ozone Workshop*, Schliersee, pp. 65-68.

Johnston P.V. and R.L. McKenzie 1989. NO_2 Observations at 45°S during the decreasing phase of solar cycle 21, from 1980 to 1987, *Journal of Geophysical Research*, Vol. 94, No. D3, March 1989, pp. 3473-3486.

Keys J.G. and B.G. Gardiner 1991. NO_2 Overnight decay and layer height at Halley Bay, Antarctica, *Geophysical Research Letters*, Vol. 18, No. 4, April 1991, pp. 665-668.

7. ACKNOWLEDGMENTS

We would like to thank Annette Ladstaetter-Weissenmayer for presenting these results at the final GOME validation meeting and for assistance in provide general information on GOME data retrieval. We would also like to thank Dr. Balzer of the DLR for providing the gdp12_ex software which was used to extract GOME total column ozone and NO_2 data. Finally we would like to thank Dr. Stephen Wood, Ian Boyd and Alan Thomas for operating the instrumentation at Arrival Heights.

Observations of O_3 and NO_2 with the GOME BBM during In-Orbit Validation of the ERS-2 GOME

A. Türk, J. Callies, A. Lefebvre, and A. Hahne
Earth Observation Projects Department, ESA/ESTEC, Noordwijk, The Netherlands

A. Richter and J.P. Burrows
Institute of Remote Sensing, University of Bremen, Germany

Abstract. Total column abundances of O_3 and NO_2 were measured above the Haute Provence during August and September 1995 by the GOME Breadboard Model. The instrument was operated as a zenith sky spectrometer using scattered sunlight at UV-Visible wavelengths for differential absorption spectroscopy. O_3 and NO_2 measurements are presented and compared with those from collocated instruments. For the validation of total ozone obtained by the ERS-2 GOME, 15 comparison days were available. Good agreement between both GOME instruments is observed, with mean differences of 1-3 %, but the ERS-2 GOME measurements are systematically smaller than total ozone measured by ground-based instruments.

1. Introduction

During the course of the preparation for the GOME Validation Phase [*ESA*, 1994], the GOME project team at ESTEC had decided to carry out an own measurement campaign with the GOME Breadboard Model (BBM) as a part of the overall validation campaign. For this purpose the BBM had been deployed to the Observatoire de Haute Provence (OHP; 43.94° N, 5.71° E). The choice of this observatory was driven by the need to have other ozone monitoring instruments collocated to the BBM, and to have rather "standard" atmospheric and illumination conditions for the measurements.

The present paper reports on the DOAS-type zenith sky observations which were performed with the GOME BBM during August and September 1995. The total column abundances of O_3 and NO_2 obtained during this period and their comparison to the values measured by the other OHP-located sensors and to the ERS-2 GOME data are presented. In addition, this report focuses on the difficulties encountered in evaluating total O_3 amounts from ground-based near-UV DOAS observations.

2. Experimental and retrieval methods

2.1 The GOME BBM

In early 1995 the BBM, which in fact is a fully-fledged Engineering Model, had been upgraded by Officine Galileo to a near Flight Model (FM) configuration in order to minimise differences between the two GOME instruments. This activity involved, among others, the substitution of the dichroic by one of the FM-batch, the addition of several diaphragms, the exchange of all four gratings by a set of gratings of the FM-batch, a tilt of grating #3 to avoid asymmetrical ghosts, and a new coating of the separator prism. The changes led to a geometry of the optical channels which is equivalent to the FM one. Naturally, all calibration constants acquired during the Calibration & Characterisation Phase at TPD were lost through this activity. However, this presented no problems for the DOAS measurements, as these only depend on relative radiometric stability. A detailed instrument description can be found in the *GOME Users Manual* [*ESA*, 1995a].

The experimental set-up comprised (a) the GOME BBM, (b) the Electrical Ground Support Equipment (EGSE), (c) a turbo and an ion-getter pump, (d) a cryostat, (e) a 6 m long fused-silica fibre bundle consisting of 25 single fibres of 100 μm core diametre, and (f) a small telescope. Scattered sun light is collected by the circular aperture of the fibre optic which is pointed directly at the zenith with a field-of-view (FOV) of 20°, and which is shielded such that no direct sun light can enter the fibre. The fibre is also used as polarisation scrambler to avoid the use of a polarisation correction algorithm. The circular aperture is converted to a slit-shaped exit (2.5 mm × 100 μm) which is placed in the focal plane of a small silica lens (diametre 25 mm, focal length 50 mm at 589 nm). This telescope assembly, directly attached to the BBM in the nadir direction of the scan mirror, thus nearly enables a FOV-match with GOME's FOV (2.8° × 0.14°). The atmospheric light is then dispersed and detected in the GOME instrument [*ESA*, 1995a].

The Focal Plane Assemblies (FPA), containing the Reticon diode arrays, are evacuated to a pressure of circa 10^{-6} mbar. The turbo pump is used to establish a "pre-vacuum" and is then swapped for continuous operation with the ion-getter pump. The diode arrays are cooled down to about -38° C by two-stage Peltier elements. The warm sides of the Peltiers are connected via heat pipes to the instrument's radiator cold plate which is held at a temperature of approximately 6° C by circulating destillated water from a refrigerated bath through the heat-exchanger mounted onto the cold plate.

Data are acquired and saved to disk every 1.5 sec. Depending on the integration times actually set for the detectors, the resultant data files may contain a considerable amount of "invalid" data entries. Data extraction and DOAS analysis are performed off-line on a separate

Personal Computer. The retrieved O_3 and NO_2 amounts are subsequently transferred via ftp to the NILU Validation Data Centre [*ESA*, 1995b].

2.2 Twilight zenith sky measurements

The GOME BBM/DOAS measurements were performed daily at dawn and dusk with solar zenith angles (SZA) ranging from 80° to 92°. In addition, a few spectra were acquired about noon and were initially intended to be used as the background spectra. The integration times of the detectors ranged from 3-9 sec at noon to 120-288 sec at 90°-92° SZA. Typically 140 individual measurements were taken per day; no smoothing or averaging techniques were applied to this data. As is common to all absorption spectroscopy, any particular measurement spectrum has to be ratioed with a background spectrum. The logarithm of the ratio yields the optical depth and is a measure of the effective slant column density of the various absorbers present in the atmosphere.

As the background spectra measured about 80° SZA were used. Although it was planned to use noon reference spectra, this proved to be not feasible (at least not for the retrieval of ozone in the visible spectral region where the Chappuis bands are of broad-scale nature and correlate with the detector's etalon features) due to a drifting etalon effect. The effect is most likely due to a changing ice layer thickness on the detectors and probably was caused by a combination of the rather low efficiency of the ion-getter pump and not perfectly leak-tight FPAs. It must be noted here, that if an atmospheric attenuation spectrum is used as the background (e.g., the 80° spectra) then only changes in the slant column relative to the background spectrum, rather than absolute column amounts, are measured—therefore the expression effective or differential slant column is used in this work.

The emission lines of GOME's internal hollow-cathode lamp were measured every three days for wavelength calibration of the instrument, and the detector dark signals were acquired weekly for all necessary integration times.

The DOAS analysis comprises the following steps: after subtraction of the corresponding dark currents from the measurement spectra, the atmospheric optical depth is computed. A least-squares fitting procedure is used to obtain the effective slant column densities of O_3 and NO_2 from the ratioed measurement spectra [*Richter*, 1995; *Solomon*, 1987]. This method involves the minimisation of the residual absorption features which remain when a model function of the optical depth is fitted to the measured optical depth, given the differential reference spectra of the molecular absorbers and the spectral features of the Ring effect [*Grainger and Ring*, 1962] and of Rayleigh and Mie scattering. The reference absorption spectra used in the fitting process are described in the next section. The broad-band features due to Rayleigh and Mie scattering are approximated by a low-order polynomial. Small shifts and squeezes of the reference spectra and, more importantly, of the background are allowed to improve the fitting which thereby becomes non-linear.

The least-squares fitting is performed in the three wavelength regions ("DOAS windows") 335-345 nm, 420-450 nm, and 450-500 nm. The near-UV window is only used for O_3 retrieval. The first vis-window is dedicated to NO_2 while the 450-500 nm window is used for O_3 detection in the visible. The reference spectra of O_3, NO_2 and Ring are fitted in all three windows; for the second vis-region the spectrum of the oxygen dimer O_4 is additionally included. Figure 1 shows the visible absorption cross-sections of O_3, O_4 and NO_2 and their respective residual spectra, which are obtained by subtracting the absorptions of all constituents other than the considered trace gas from the measured optical depth. The measured differential optical depth and the overall fit residual, which is of order 10^{-3}, are shown in the upper right of the figure.

The final step of the analysis scheme is the conversion of the O_3 and NO_2 slant columns to vertical columns, which are independent of the particular observing geometry. The conversion is achieved by dividing the differential slant column by the difference of air mass factors (AMF) appropriate for the considered SZAs, i.e., AMF of the measurement minus AMF of the background. This approach must necessarily assume that the vertical column abundances do not change between the two measurements. Air mass factors have to be computed by a radiative transfer model (RTM) and their evaluation is presented in section 2.4. Daily values of the vertical column abundances of O_3 and NO_2 at sunrise and sunset result from a weighted average over the vertical columns obtained at SZAs between 84.5° and 90° (O_3), and 87° and 91.5° (NO_2). These intervals are commonly used in the community, and the use of twilight averages is indeed recommended by *Sarkissian et al.* [1995a, 1996] as the best method to produce daily values of vertical columns.

2.3 Absorption cross-sections

The quality of the fitting for the effective slant columns of atmospheric absorbers can significantly be improved when reference absorption spectra are used which have been measured by the DOAS instrument itself. Therefore, the temperature-dependent cross-sections of O_3 and NO_2 have been measured with the GOME instruments as part of the GOME Calibration & Characterisation Programme [*Türk*, 1994; *Dehn*, 1995].

For the present work the O_3 spectrum measured at 221 K and the NO_2 spectrum measured at 241 K were used. Both spectra were derived from relative measurements with the GOME FM. Absolutely calibrated cross-sections were obtained by scaling the spectra to the values measured by *Bass and Paur* [1984] and *Harwood and Jones* [1994], respectively. As reference spectrum of O_4 data obtained by *Greenblatt et al.* [1990] at room temperature were used.

The Ring effect, which is most likely due to rotational Raman scattering by air molecules, is accounted for only empirically by treating it as a pseudo-absorber. By

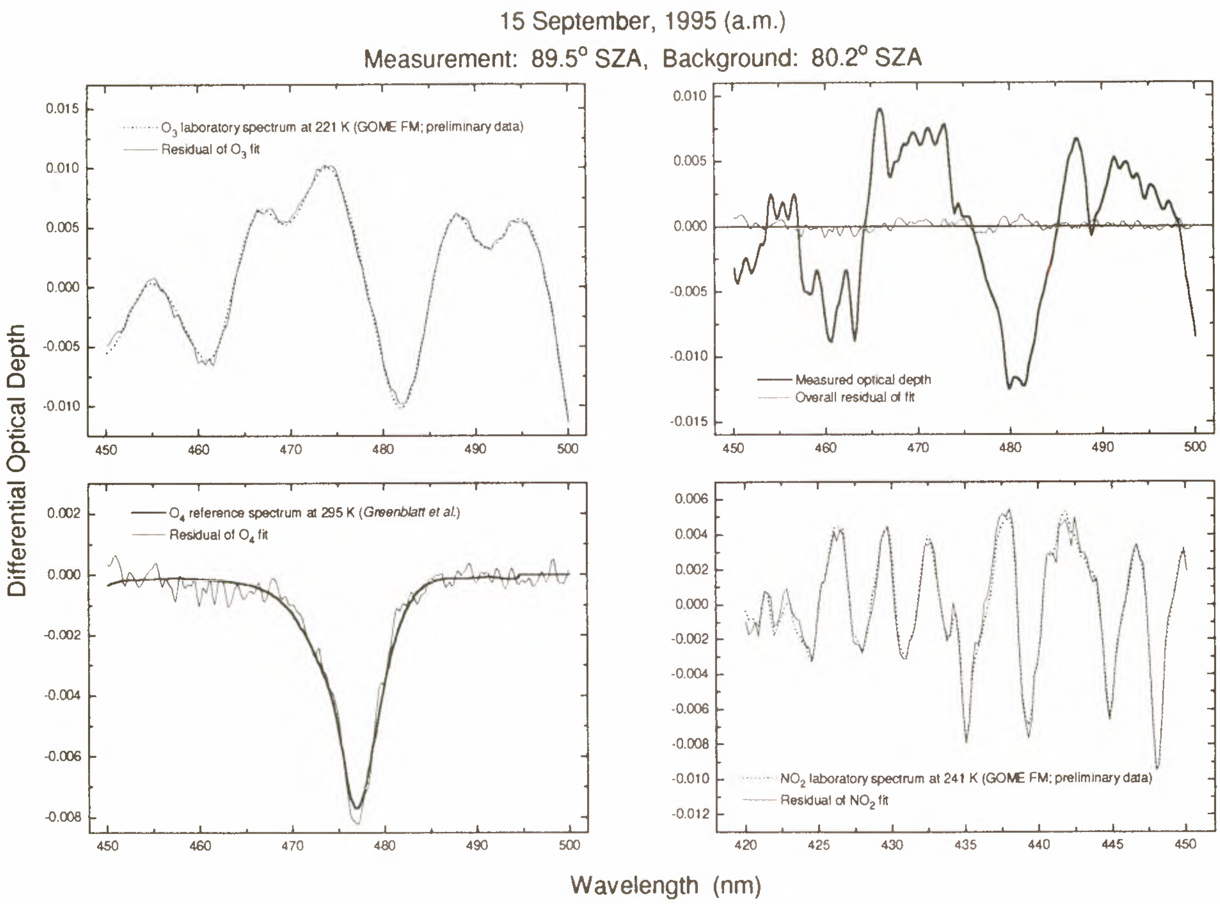

Figure 1. Residual absorptions obtained after analysis of zenith sky spectra acquired near 90° SZA on 15 September at the OHP. The statistical errors of the O_3 and NO_2 fit are 0.6 % respectively 1.1 %.

making use of the crossed-polariser method described by *Solomon et al.* [1987], such effective Ring cross-sections were measured by *Richter et al.* [1994] with the GOME instruments. It should be noted however, that the Ring effect is a complex phenomenon and further investigations on this topic are underway in order to correct for the effect on ERS-2 GOME data [*ESA*, 1996].

2.4 Evaluation of air mass factors

The computation of air mass factors (AMFs), which basically describe the enhancement in slant optical path through the atmosphere relative to the vertical optical path, is presently the most crucial part in all DOAS-related research work [*Perliski and Solomon*, 1993; *Sarkissian et al.*, 1995b], and the largest source of systematic error in the DOAS analysis is in fact associated with their evaluation. Therefore, a correct interpretation of zenith sky light measurements requires an understanding of how photons propagate through Earth's atmosphere before being detected by a zenith sky spectrometer.

In this work a single-scattering radiative transfer model (RTM), developed at the University of Heidelberg [*Frank*, 1991], is used for computing all necessary AMFs as function of wavelength and SZA. The major inputs required for this model are the climatological model profiles of pressue, temperature, densities of O_3 and NO_2, and optionally of Mie extinction. It is well-known that AMFs can show a strong dependency on the shapes of the absorber density profiles and the climatology of the atmosphere, and hence the choice of these profiles is crucial. This dependency is even more severe in the UV region. Recently, the sensitivity of AMFs of ozone to computational schemes and various geophysical parameters has been studied by *Sarkissian et al.* [1995a]. The rationale behind the AMF concept is, however, that in making sensible assumptions concerning the shapes of the climatological profiles, the errors associated with the air mass factors remain within reasonable limits. As will be shown below, this rationale seems only to apply to vis-DOAS measurements.

AMFs were determined for the centres of all three DOAS windows from 79° to 92° SZA in steps of one degree, using profile information extracted from the MPI 2D-Atmospheric Model [*Bruehl and Crutzen*, 1992]. It eventually became apparent that total ozone values obtained from the UV measurements were about 10-20 % lower than the corresponding values obtained in the visible. It is worthwhile to note that, besides the work by *Kreher et al.* [1995], virtually no publications were found in the literature where the O_3 vertical columns retrieved from ground-based scattered-UV-light observations are explicitly stated. Therefore an attempt was made in this work to understand the nature of the

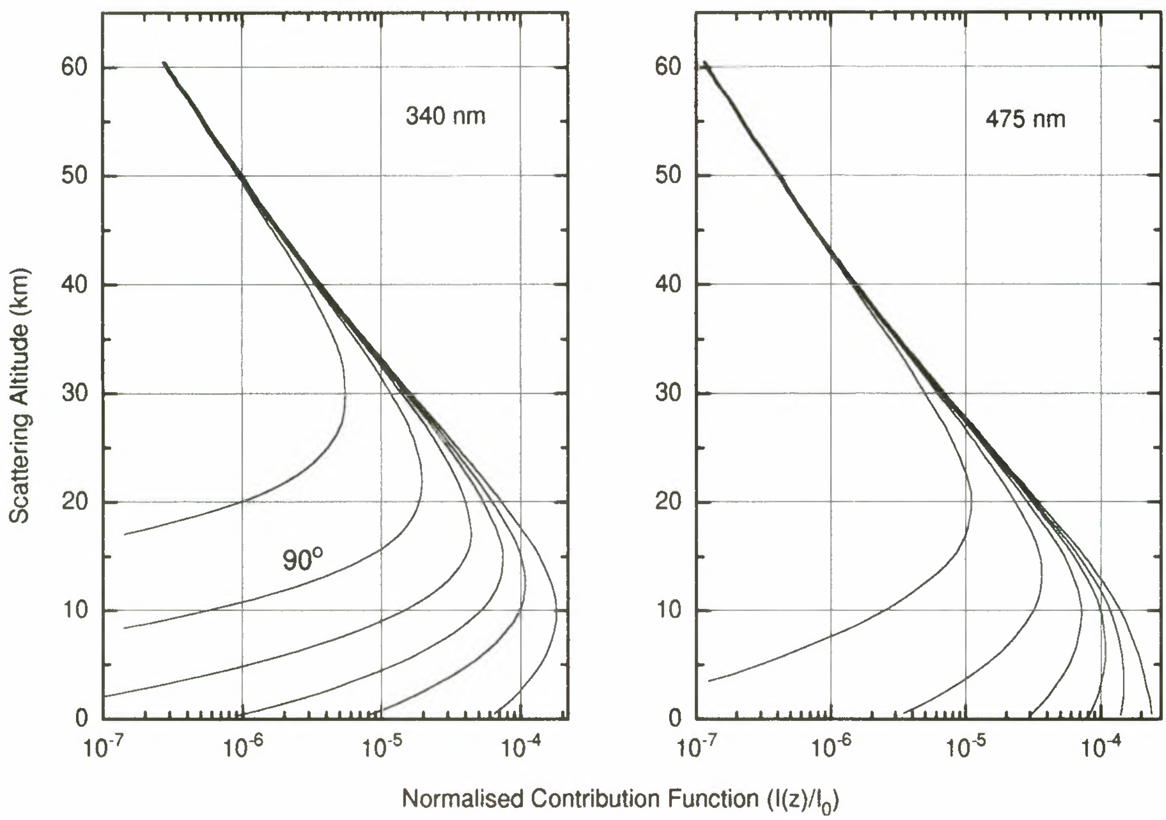

Figure 2. Relative contribution of scattered light from different altitudes to the total intensity received by a zenith-sky spectrometer. The graphs were computed for SZAs, from right to left, 80°, 84°, 86°, 88°, 90°, and 92°.

discrepancy between total ozone amounts obtained from UV and visible zenith sky observations.

A first difference between the two wavelength regions is apparent from Figure 2, where the contribution functions, as computed by the RTM and normalised with respect to the solar irradience at the top of the atmosphere, are plotted for 340 nm and 475 nm. These quantities reflect the relative contribution of scattered light from any particular altitude received by a zenith-looking spectrometer. Most of the scattering at 340 nm occurs in the lower stratosphere for all SZAs shown. In fact, there is no significant tropospheric contribution for SZAs larger than about 86°. In the visible (475 nm), by contrast, the largest contributions come from the troposphere for SZAs smaller than 88° SZA. It is important to note, however, that vis-DOAS measurements of essentially stratospheric absorbers are not dominated by this tropospheric contribution because the tropospheric air mass factors are approximately an order of magnitude smaller than the stratospheric AMFs. This means that the strong scattered-light contribution of the troposphere is effectively balanced by the contribution of the stratosphere through its associated large AMF.

The RTM derives the O_3-AMF for a given SZA by dividing the computed (simulated) slant column of ozone by the vertical column amount (which is the integrated climatological O_3 profile). As a consequence of this approach, absorber density information about the tropospheric region is included in the RTM's output although UV measurements effectively do not "see" the troposphere, and this may lead to systematic errors if the tropospheric fraction of the model ozone profile significantly deviates from the actual atmospheric conditions. An even larger source of systematic error for UV measurements can arise from the fact that at twilight the largest intensity contributions come from the 15-25 km altitude region of the atmosphere—a region where ozone mixing ratios peak sharply. Due to ozone's large absorption cross-section in the Huggins band, the twilight air mass factors are thus extremely sensitive to the profile shapes of pressure and O_3 density.

To quantitatively study the above mentioned influences on the AMF, the effects caused by replacement of the climatological O_3, pressure, and temperature profiles by measured ones was investigated. A measured Mie extinction profile was used as additional input to the RTM. Tropospheric O_3 profiles, as well as atmospheric pressure and temperature profiles, were taken from balloon soundings performed weekly during the month of August at the OHP-site [*Ancellet*, 1995]. As the tropospheric O_3 density showed strong variations, a smoothed mean profile was derived from the four measurements. It was, however, evident from all four soundings that the tropospheric O_3 abundance was considerably larger than what would have been expected from the climatological profile. The seasonal variation of tropospheric ozone has been investigated by *Beekmann*

Table 1. Changes in total ozone relative to the "pure model" (default) computation due to different inputs to the AMF algorithm.

Replaced/added input parameter	ΔAMF(90°-80° SZA)		Associated change (%) in total ozone	
	340 nm	475 nm	340 nm	475 nm
Default (only climatological profiles)	9.35	11.81	0.0	0.0
measured mean profile of tropospheric ozone	8.97	11.59	+4.1	+1.9
as above, but with measured Mie extinction profile	8.97	11.67	+4.1	+1.2
as above, but Junge exponent changed to 1.4	8.97	11.67	+4.1	+1.2
model ozone profile, measured pressure profile, Mie extinction	8.83	11.81	+5.6	0.0
measured profiles of tropsph. ozone, pressure and Mie extinction	8.49	11.58	+9.2	+1.9
as above, but with measured temperature profile	8.50	11.58	+9.1	+1.9
as above, but computational parameters changed (width of model layers and distance of rays)	8.45	11.53	+9.6	+2.4

et al. [1994] and is indeed characterised by a large maximum in spring and summer. The measured pressure profiles agreed very well with one another, and thus their mean is a good measure for the climatology of August. However, the comparison between the measured and model pressure profile revealed a deviation of up to 20 % for the lower stratosphere. During the first week in August four stratospheric O_3 profiles were measured by the OHP-based ozone lidar [*Godin*, 1995] at night-time. As these measurements also exhibited rather strong variations—it is not unusual that ozone concentrations can vary by a manifold within a few days in the lower stratosphere—it was decided not to include them as test input to the RTM, particularly because the stratospheric model profile enveloped all measured lidar profiles.

The Mie extinction profile was derived from measurements carried out on 3 August with an aerosol lidar (532 nm) based at Garmisch-Partenkirchen [*Jäger et al.*, 1995]. Using a Junge coefficient of 1.3 the profile was scaled to obtain approximate aerosol extinctions at 340 nm and 475 nm. Since stratospheric aerosol concentrations have almost reached a background level [*Jäger*, 1995], the influence of Mie extinction on the AMF was not expected to be significant.

The changes in total ozone amount, relative to the "pure model" case, are summarised in Table 1. Evidently, none of the considered climatological properties have a drastic influence on the visible air mass factors of ozone—a clear demonstration of the validity of the rationale behind the AMF concept. By contrast, the UV-AMFs decreased systematically up to nearly 10 % through inclusion of the measured profiles. For this reason the UV measurements were re-processed using new AMFs which take into account the measured mean profiles of tropospheric ozone, atmospheric pressure and temperature, and Mie extinction. The visible AMFs were not changed, seen the above results.

It should be noted that this work did not investigate the effects caused by multiple Mie scattering, a process of great importance in the troposphere. The inclusion of multiple scattering in the RTM would generally increase the air mass factors as has been demonstrated by *Perliski and Solomon* [1993], who have studied the effects of aerosol scattering on the evaluation of AMFs by comparing a single-scattering with a Monte Carlo model. Their work also implies that stratospheric AMFs are essentially independent of multiple-scattering effects for wavelengths below about 450 nm, whereas tropospheric AMFs were found to be significantly enhanced by multiple-scattering, in particular at the longer visible wavelengths. More recently, *Erle et al.* [1995] suggested a strong enhancement of the absorption of the tropospheric fractions of O_3 and NO_2 through the presence of tropospheric clouds—the additional absorptions are thought to be caused by multiple-scattering, and they may lead to considerable overestimations of the total ozone columns derived from vis-DOAS measurements.

Finally, there might exist an other effect which can lead to underestimations of total ozone derived from UV zenith sky measurements. *Fish and Jones* [1995] have shown that Raman scattering not only in-fills the solar Fraunhofer lines (Ring effect), but can also reduce the depth of narrow molecular absorption structures. Using simulated zenith sky spectra, they have demonstrated that NO_2 amounts can be underestimated by 7-8 %. This effect could therefore be similar on measured ozone columns in the UV. However, subject to further investigations must be the question whether or not the use of a measured (empirical) Ring spectrum in the DOAS analysis scheme compensates for this effect.

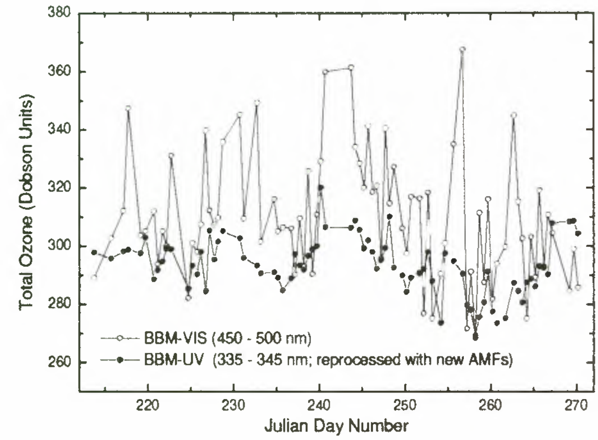

Figure 3. Total ozone measured by GOME BBM above the Haute Provence in August and September 1995.

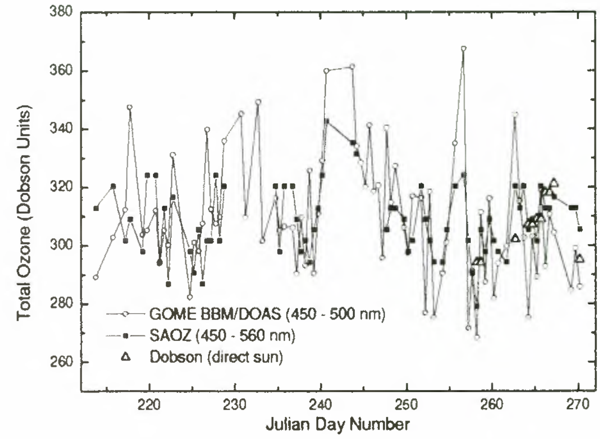

Figure 4. Comparison of total ozone amounts obtained by the OHP-based instruments.

3. Results and discussion

Figure 3 shows the observed twilight total ozone amounts obtained by the BBM as a function of the fractional Julian day. The statistical fit errors associated with the O_3 slant columns are of the order 1-2 % for the visible region and less than 1 % for the UV. The uncertainties in the AMF were estimated by a shift in the altitude of the O_3 profile by ±2.5 km. This led to an error of nearly 10 % at 90° SZA for the UV-AMF. The results presented in section 2.4 suggest that the errors associated with the vis-AMF must be less than this value. With the errors (2σ) of the O_3 absorption cross-sections (4-6 %), the absolute accuracies of the vertical column abundance of ozone were then estimated to be about 6-8 % for the visible and 10-12 % for the UV.

The agreement between total ozone columns derived from UV and visible observations is still not satisfactory, although the mean deviations have been reduced, after the re-processing, from circa 10-20 % to 5.0 ± 5.8 %, and the cautious conclusion to be drawn at this stage is that ground-based scattered-UV-light observations may not yield reliable total ozone, unless the exact climatology is known for every measurement day. If UV-AMFs were to be calculated on a daily basis, using measured O_3 profiles for each day, the agreement would probably become much better. Unfortunately, this could not be tested, since only a few balloon soundings and stratospheric lidar measurements (which happen to be performed on different days than the balloon launches) were available for August.

3.1 Comparison with OHP-based instruments

The comparison with total ozone obtained by the OHP-based SAOZ and Dobson instruments is displayed in Figure 4. Both SAOZ and Dobson data were extracted from the NILU Validation data-base. The mean deviation between the SAOZ and GOME BBM measurements (morning and evening readings treated together) amounts only to 0.4 ± 5.5 %. Despite this good agreement, the correlation between the observed day-to-day variation is not as good as would be expected from two instruments collocated to each other and observing in principle the same air masses at the same times. We believe that this disagreement can be explained by an important difference in the analysis techniques. The SAOZ method generally uses a single reference spectrum to analyse the zenith sky spectra from many days. The amount of O_3 in this reference is determined by Langley plot analysis (e.g., *van Roozendael et al.* [1994]). Vertical ozone columns are then computed by dividing the sum of slant column density and reference O_3 amount by the AMF of the measurement. By contrast, the BBM/DOAS approach records background spectra (80° SZA) every day, treating morning and evening twilights independently. As mentioned in section 2.2 the vertical columns are derived by dividing the differential slant column by the difference of two AMFs, assuming that total ozone is the same for both measurements. If, however, the total ozone amount does change by just a few DU (the time difference between 80° and 90° SZA is only about one hour), then this small change will "amplify" itself through the associated large AMFs during twilight—this effect is not accounted for in the formulae for the vertical column. Therefore, the daily variation in O_3, as observed by the BBM, is more pronounced.

Total ozone values measured by the Dobson photospectrometer (direct sun mode) are on average 2.6 ± 7.2 % larger relative to the BBM. This comparison could only be performed for the second half of September since the Dobson instrument was away on a cross-calibration campaign in August.

Figure 5 displays total NO_2 columns obtained by GOME BBM and SAOZ for both morning and evening twilights. The estimated accuracy of the NO_2 columns measured by the BBM is approximately ±10 %. The variables contributing to the total error are the same as for ozone: the slant columns of NO_2 are generally obtained with a precision of 1-2 %, the errors in the absorption cross-sections are of the order of 4 %, and the error associated with the AMF was estimated to be about 9 % at 90° SZA by shifting the Gaussian NO_2 profile (FWHM 11 km, centre altitude 28 km) by ±5 km

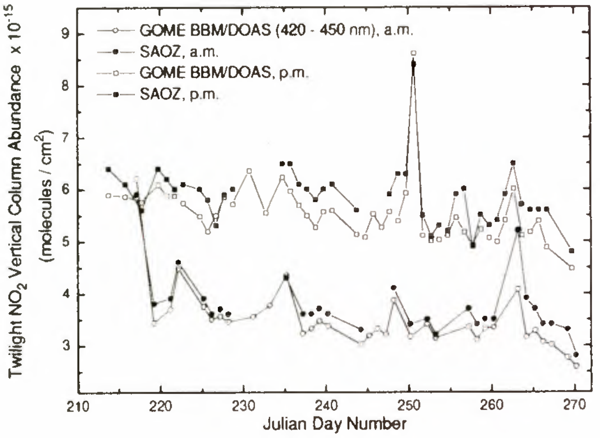

Figure 5. Vertical NO_2 amounts measured by GOME BBM and SAOZ during morning and evening twilights.

in altitude. The general good agreement between the daily variation in NO_2 as observed by the SAOZ and BBM is obvious; however, the absolute column values disagree by 7.2 ± 5.6 % on average. This can be largely explained by the fact that the SAOZ retrieval algorithm uses a NO_2 reference spectrum acquired at room temperature [*Pommereau and Goutail*, 1988], whereas the BBM uses a low-temperature spectrum.

The reason for the difference in morning and evening abundances of NO_2 is the night-time conversion of NO_2 to N_2O_5 via the reactions:

$$NO_2 + O_3 \rightarrow NO_3 + O_2$$

$$NO_2 + NO_3 + M \rightarrow N_2O_5 + M.$$

During the day the nitrate radical, NO_3, is rapidly photolysed and hence NO_2 concentrations are lower during the night [*Pommereau and Goutail*, 1988, and references there in].

3.2 Comparison with ERS-2 GOME data

For the comparison of the ERS-2 GOME data with the ground-based GOME BBM measurements the following approach was chosen. An "OHP-station pixel" is defined which extends 500 km to the East and West of the OHP, and 180 km/90 km in the North and South direction, respectively. At 90° SZA the light paths through the atmosphere, over which ozone columns are actually integrated, are typically 500-600 km in length; hence the choice of the E-W distances. The N-S distances reflect the changes in the relative sun azimuth angles during twilight for August and September; the asymmetry in this direction is introduced because in Summer the sun rises and sets north-easterly respectively north-westerly. The intercomparison of satellite and ground data is then achieved by choosing all GOME ground pixels which have their centre co-ordinates located within the defined OHP-pixel. The total ozone amounts associated with each ground pixel can then be averaged to obtain a single comparison value. This approach thus represents a straight-forward and non-weighting comparison method.

The total ozone columns observed by the ERS-2 GOME were extracted from the DLR Level 2 Product (GDP Level 2 Version 1.21, Software Database Version 1.20). At the time of the *GOME Validation Campaign Final Results Workshop*, a total of 15 comparison days was available for the period of the BBM measurement campaign. Figure 6 shows the O_3 concentrations obtained by the two GOME instruments for this period. Only the morning values of the BBM are plotted as the time of the ERS-2 overflight at the OHP is before local noon. On most days shown the ERS-2 GOME values exhibit a large spread of typically 20 DU. Considering that the chosen ground-pixels cover a rather large area, this spread is most likely explained by spatial gradients in the ozone distribution [*Piters*, 1996]. Figure 7 displays total ozone three-dimensionally above Southern France on 26 August and 17 September, and gives a good impression about the locations of the ground-pixel centres relative to the OHP-station. It is rather surprising that the largest zonal gradient in ozone distribution, i.e., versus longitude, occurs between the *Back-scan* and *East* ground-pixels, in particular because the two pixel types are located very close to one another (their centres are separated by approximately 165 km). This could possibly indicate a minor problem in the determination of the AMFs for the Back-scan pixels.

Finally, Figure 8 shows the averaged ERS-2 GOME ozone amounts together with the morning-twilight abundances obtained by the OHP-based instruments, GOME BBM, SAOZ and Dobson. It is apparent that ERS-2 GOME values are systematically smaller than total ozone measured by the ground-based instruments. The comparison yielded mean deviations of -2.4 ± 4.1 % (GOME BBM; visible), -0.8 ± 3.6 % (BBM; UV - not plotted), -5.0 ± 2.1 % (SAOZ), and -6.3 ± 2.5 % (Dobson) relative to ERS-2 GOME. The best agreement is thus achieved between the two GOME instruments. Although 15 comparison days are statistically not significant, the results of the present work suggest a good accuracy of the Level 2 products of the GOME Data Processor.

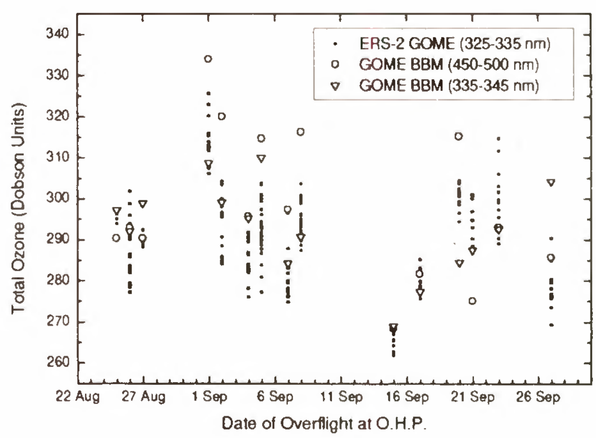

Figure 6. Total ozone amounts obtained by the ERS-2 GOME above Southern France and their comparison to the BBM measurements performed at the OHP.

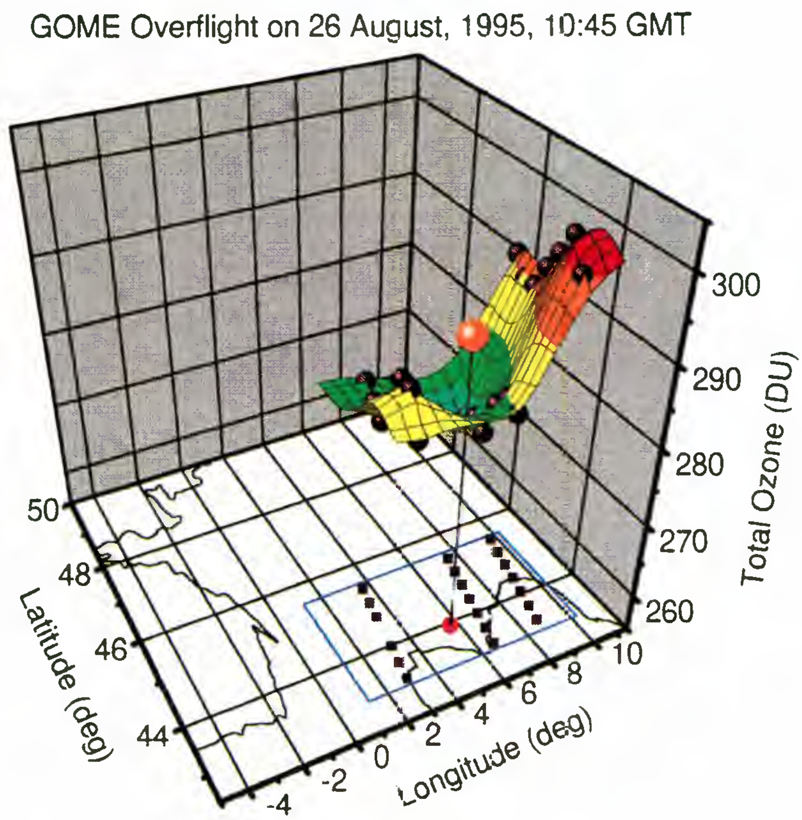

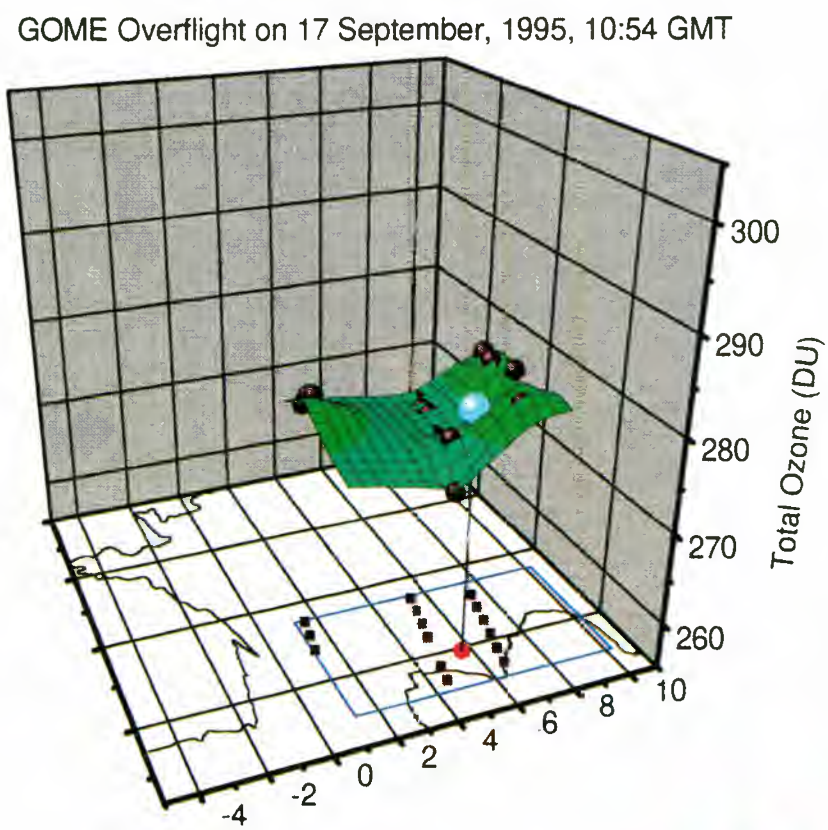

Figure 7. Total ozone amounts (black spheres) measured by the ERS-2 GOME above Southern France. The projections represent the centres of the ground pixels - shown here are the back-scan (right), East (middle) and nadir (left) pixels. On 26-Aug and 17-Sep the BBM obtained vertical columns of 293 DU respectively 282 DU (big spheres).

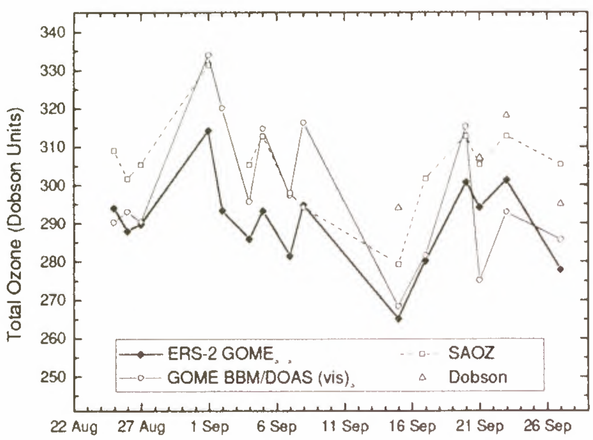

Figure 8. Ozone abundances retrieved by the OHP-based instruments and their comparison to the mean values derived for the ERS-2 GOME.

4. Summary and Conclusions

Total column abundances of O_3 and NO_2 were obtained daily with the GOME BBM during August and September 1995 at the Obseravtoire de Haute Provence. Vertical O_3 amounts, derived from DOAS measurements in the visible, are in good agreement with the values observed by the OHP-based SAOZ (mean deviation < 1 %) and Dobson (mean dev. < 3 %) instruments. Daily variations in total ozone, as measured by GOME BBM and SAOZ, show a rather poor correlation which is most likely due to different analysis approaches. By contrast, good agreement in the daily variation of NO_2 amounts was achieved with the SAOZ; however, the absolute values were presented to be about 7 % smaller on average. The difference can be explained by different NO_2 reference spectra used in the retrieval algorithms of the two instruments.

The intercomparison of total ozone obtained by the ERS-2 GOME and by the GOME BBM yielded very promising results: mean differences of 1-3 % were observed for the period of the BBM measurement campaign. For the SAOZ and Dobson instruments the mean deviations were shown to be 5-6 % for the same time period. The ERS-2 GOME measurements are systematically smaller than total ozone values obtained by the ground-based instruments. Further improvements on the accuracy of the GOME Level 2 product are expected once a new set of AMFs, using a more consistent approach for the computational schemes, have been processed at DLR; presently, there still exists a persisting discrepancy of a few percent between the AMFs as used in the GOME data processing and AMFs as calculated by GOMETRAN++. However, the results of this work already indicate a good accuracy of the ERS-2 GOME retrieval algorithms for ozone observations above mid-latitudes with "standard" atmospheric conditions.

Acknowledgements. The authors are very grateful to G. Velghe (CNRS-OHP) and G. Mégie (CNRS-Jussieu) for their support to the measurement campaign performed with the GOME BBM at the OHP station.

References

Ancellet, G., Service d'Aeronomie du CNRS, Université Paris, Jussieu, private communication, 1995.

Bass, A.M. and Paur, R.J., The ultraviolet cross-sections of ozone: I. Measurements, in *Atmospheric Ozone. Proc. of the Quadrennial Ozone Symp.*, Halkidiki, Greece, 1984.

Beckmann, M., Ancellet, G. and Mégie, G., Climatology of tropospheric ozone in southern Europe and its relation to potential vorticity, *J. Geophys. Res.*, 99, 12841, 1994.

Bruehl, C. and Crutzen, P., The MPI 2D-Atmospheric Model, MPI for Chemistry, Mainz, private communication, 1992.

Dehn, A., Temperaturabhängige Absorptionsspektroskopie bedeutender Spurengase der Atmosphäre im ultravioletten und sichtbaren Spektralbereich, Diploma thesis, Institute of Environmental Physics, University of Bremen, 1995.

Erle, F., Pfeilsticker, K. and Platt, U., On the influence of tropospheric clouds on zenith-scattered-light measurements of stratospheric species, *Geophys. Res. Lett.*, 22, 20, 2725, 1995.

ESA, GOME Validation Plan, Doc. *ER-PL-ESA-GO-0371*, ESA/ESTEC, Noordwijk, 1994.

ESA, *GOME Users Manual*, Publication ESA SP-1182, ESA/ESTEC, Noordwijk, 1995a.

ESA, GOME Validation Campaign Experimenters Handbook Version 2, ESA/ESTEC, Noordwijk, 1995b.

ESA, Study of the Ring effect, prepared under ESA Contract 10996/94/NL/CN, in press, 1996.

Fish, D.J. and Jones, R.L., Rotational Raman scattering and the Ring effect in zenith-sky spectra, *Geophys. Res. Lett.*, 22, 7, 1995.

Frank, H., Ein Strahlungstransportmodell zur Interpretation von spektroskopischen Spurenstoffmessungen in der Erdatmos phäre, Diploma thesis, Institute of Environmental Physics, University of Heidelberg, 1991.

Godin, S., Service d'Aeronomie du CNRS, Université Paris, Jussieu, private communication, 1995.

Grainger, J.F. and Ring, J., Anomalous Fraunhofer line pro files, *Nature*, 193, 762, 1962.

Greenblatt, G.D., Absorption measurements of oxygen between 330 and 1140 nm, *J. Geophys. Res.*, 95, 18577, 1990.

Harwood, M.H. and Jones, R.L., Temperature dependent ultraviolet-visible absorption cross sections of NO_2 and N_2O_4: Low-temperature measurements of the equilibrium constant for $2NO_2 \leftrightarrow N_2O_4$, *J. Geophys. Res.*, 99, 22955, 1994.

Jäger, H., Deshler, T. and Hofmann, D.J., Midlatitude lidar backscatter conversions based on balloonborne aerosol measurements, *Geophys. Res. Lett.*, 22, 13, 1729, 1995.

Jäger, H., Fraunhofer Institute for Atmospheric Research, Garmisch-Partenkirchen, private communication, 1995.

Kreher, K. et al., The latitudinal distribution (50° N-50° S) of NO_2 and O_3 in October/November 1990, *Geophys. Res. Lett.*, 22, 10, 1217, 1995.

Perliski, L.M. and Solomon, S., On the evaluation of air mass factors for atmospheric near-ultraviolet and visible absorption spectroscopy, *J. Geophys. Res.*, 98, 10363, 1993.

Piters, A., KNMI, De Bilt, private communication, 1996.

Pommereau, J.P. and Goutail, F., O_3 and NO_2 ground-based measurements by visible spectrometry during Arctic Winter and Spring 1988, *Geophys. Res. Lett.*, 15, 8, 891, 1988.

Richter, A., Ring measurements during the GOME FM Calibration, Draft Final Report submitted to ESA, 1994.

Richter, A., Institute of Environmental Physics, University of Bremen, DOAS analysis software, 1995.

Sarkissian, A., Roscoe, H.K. and Fish, D.J., Ozone measurements by zenith-sky spectrometers: an evaluation of errors in air-mass factors calculated by radiative transfer models, *J. Quant. Spectrosc. Radiat. Transfer*, 54, 3, 1995a.

Sarkissian, A. et al., Ozone and NO_2 air-mass factors for zenith-sky spectrometers: Intercomparison of calculations with different radiative transfer models, *Geophys. Res. Lett.*, 22, 9, 1113, 1995b.

Sarkissian, A. et al., Accuracy of measurements of total ozone by a SAOZ ground-based zenith-sky visible spectrometer, to be published in *J. Geophys. Res.*, 1996.

Solomon, S., Schmeltekopf, A.L. and Sanders, R.W., On the interpretation of zenith sky measurements, *J. Geophys. Res.*, 92, 8311, 1987.

Türk, A., Untersuchung der Absorptionsspektren atmosphärischer Spurengase im UV- und sichtbaren Spektralbereich, Diploma thesis, Institute of Environmental Physics, University of Bremen, 1994.

Van Roozendael, M., de Mazière, M. and Simon, P.C., Ground-based visible measurements at the Jungfraujoch station since 1990, *J. Quant. Spectrosc. Radiat. Transfer*, 52, 231, 1994.

A. Türk, J. Callies, A. Lefebvre, and A. Hahne, ESA/ESTEC, Earth Observation Projects Department, NL-2200 AG Noordwijk.

A. Richter and J.P. Burrows, Institute of Remote Sensing, University of Bremen, D-28334 Bremen.

CONCLUSIONS AND RECOMMENDATIONS

CONCLUSIONS AND RECOMMENDATIONS OF THE GOME VALIDATION WORKSHOP 24 - 26 JANUARY 1996

Evert Attema,
Manager of the GOME Geophysical Validation Campaign,
ESA/ESTEC, The Netherlands

1. Introduction

The Validation Campaign is considered very successful because it provided a very consistent picture of the quality of the GOME data products. A number of critical points were highlighted. Recommendations were made for ground processor modifications, data analysis, instrument operations, data processing and data distribution.

2. Current Data Quality of GOME Products

For the level 1 data product a very good wavelength stability was found and a high instrument precision. The polarisation measurements work well, if one discards the overlap regions between the channels. The radiance/irradiance ratio is very accurate within the ozone retrieval window and facilitates meaningful total ozone column retrieval using the DOAS technique.
A problem identified is that the radiance and irradiance levels differ from 'reference data' by up to 15% in the UV and by up to 5% in the visible part of the spectrum. Furthermore discontinuities in the radiance
measurements were detected between channels, caused by the serial readout of the detectors. Finally small time variations were found in the instrument and the diffuser as well as a slightly high noise level in channel 1 A for which corrections need to be made.

For the level 2 data product, the ozone slant column fitting works very well in the UV range. For solar zenith angles (SZA) less than 75 degrees the difference between ground validation data and DOAS results are only a few percent, the main problem being the air mass factor (AMF) used in the retrievals. Above 75 degrees SZA, the ozone total amounts were not yet considered for validation purposes because of the well identified limitation in the current AMF calculations. There is full confidence that, under "good conditions to be further analysed, NO2 can be routinely retrieved. It has also been confirmed that BrO and OClO can be retrieved at high latitudes. The fractional cloud cover determination performs quite well, although it underestimates the cloud cover fraction, which contributes to the error in the AMF.
Small but significant differences are found in the vertical ozone column between the same data processed once with the GOME algorithm and oncewith the TOMS algorithm. These differences are confirmed by ground based measurements and amount to 3-5% for mid latitudes (SZA<55 deg.) and to 10-12% for higher latitudes (55 <SZA< 75 deg.).
It was agreed that a significant part of these differences are due to the current algorithm for determining the air mass factors.
The current simple algorithm for (constant) cloud top height assignmentleads to an error in the assumed ghost column ozone amount. The current NO2 retrieval method gives values which are largely off from ground based measurements. Systematic differences in ozone values were found between East/Centre/West pixels. The retrieved total ozone shows a dependence on cloud fraction.

3. Recommendations

3.1 In order to improve the accuracy of the level 1 data products it is recommended to implement the following procedures and algorithm changes.

3.1.1 The use of the latest version of key data in the ground processor (version 8).

3.1.2 The introduction of a digital noise filter in the channel 1A processing.

3.1.3 The introduction of the co-adding patch in the satellite.

3.1.4 The use of the PMD data to remove the 'jumps' in the radiance data. This should be further investigated.

3.1.5 The use of an operational procedure to minimise the effects of etalon changes.

3.1.6 Monitoring the dichroic and air/vacuum effects.

3.1.7 Introduction of a dynamic calibration data base, if dichroic and air/vacuum effects continue to change.

3.1.8 Monitoring instrument and diffuser degradation.

3.1.9 Use of the ESA orbit propagator.

It should be noted that most of the proposed modifications have already been initiated.

3.2 In order to improve the accuracy of the level 2 data products it is recommended to implement the following procedures and algorithm changes.

3.2.1 The application of air mass factor corrections for multiple scattering and spherical geometry. Interpolation between latitude-band climatologies should be considered.

3.2.2 The use of FM measured reference spectra for O3, NO2 and Ring effect.

3.2.3 Replace the fixed cloud top height by ISCCP cloud climatology values.

3.2.4 Consider special windows optimized for NO2.

3.2.5 Use surface and cloud albedo measured by GOME in the AMFcalculation.

3.3 Regarding the next steps to be taken in the validation process the following is recommended.

3.3.1 The validation activities by the investigators should continue on a voluntary basis dependent on the available resources. A follow-up meeting should be held in approximately 6 months.

3.3.2 After the implementation of the proposed modifications to the procedures and the processor, routine processing shall be performed on the fresh data as soon as possible.

3.3.3 The system shall be re-evaluated after at least three weeks of routine operation by a 'tiger team' consisting of ESA experts and members of the validation team. For this ESA will call upon individual members of the validation team as necessary. The assessment of the effect of the implemented changes requires that a limited set of historical data (20-30 days) be quickly reprocessed and made available to all members of the validation team.

3.3.4 Priorities for investigations on the validity of the new features shall be in the following order. Total ozone/DOAS, irradiance/radiance, NO2.

3.3.5 For the time being until the start of the operational phase of the GDP with the new features some important data sets have to be processed. Sun calibration data, calibration time line data and some 3-day data sets for pre-arctic spring analysis of ozone depletion.

4. Data Release

The validation data sets currently available shall not be released to the general user but the fresh data produced during the operational phase of the GDP shall be released and hence can be used for research and publications. For the use of the current validation data sets in publications prior ESA permission should be required.
It was noted that the next ozone quadrennial was an excellent vehicle for presenting the GOME validation results to the scientific community. Abstracts should be prepared on the basis of the assumption that sufficient fresh GOME data will be available from the operational GDP by the time of preparation of the presentation. In the unlikely event that this will not be true papers might have to be withdrawn.

5. Further Observations

5.1 ESA is committed to continue with the coordination of further validation activities.

5.2 For the near future a substantial upgrade of the GDP processing power by a factor of 2 3 is considered mandatory in order to enable backlog processing, fine tuning of algorithms and fitting windows, introduction of additional windows for retrieval of NO2, SO2 and other species, as well asprofile retrieval.